Author:
Stewart, Duncan Ross McIver

Title:
Evolution of Neogene globorotaliid foraminifera and Miocene climate change

Evolution of Neogene globorotaliid foraminifera and Miocene climate change

Duncan Ross McIver Stewart

A dissertation submitted to the University of Bristol in accordance
with the requirements of the degree of Doctor of
Philosophy in the Faculty of Science.
Department of Earth Sciences, February 2003.

62500 words

For my dearest mother, who has always been there.

If we didn't learn a lot today, at least we learned a little,
and if we didn't learn a little, at least we didn't get sick,
and if we got sick, at least we didn't die;
so, let us all be thankful".

Buddha

'If we didn't learn a lot today, at least we learned a little,
and if we didn't learn a little, at least we didn't get sick,
and if we got sick, at least we didn't die;
so, let us all be thankful'.

Buddha

Abstract

The evolutionary and ecological development of the non-spinose globorotaliid planktonic foraminifera is here investigated, in the context of the changing Neogene ocean and evolutionary patterns in the planktonic foraminifera as a whole. The temperature and sea-level history of the Miocene oceans is reviewed, and additional information is introduced in two separate case studies that quantify temperature and sea-level.

A new compilation of all planktonic foraminiferal range data was constructed to study general patterns of evolution. Analysis of this range-chart data for all planktonic foraminifera, with subsets according to depth habitats and temporal divisions, show fluctuations in diversification, speciation and extinction rates through time. Preliminary results from spectral analysis of these planktonic foraminiferal speciation and extinction rates suggest the presence of periodic frequencies in the data corresponding to 36 My, 5 My and 2.4 My cycles. These findings add to the controversial extinction periodicity debate initiated by Raup and Sepkoski in the 1980s (Raup and Sepkoski, 1984, 1986).

Isotopic results suggest that the Neogene globorotaliids underwent some unexpected fluctuations in depth ecology. The Early Miocene progenitor morphospecies *Globorotalia praescitula* originated in deep, cold waters, and near the beginning of its time range appears to have had a benthic habitat, becoming planktonic later on. These findings help support the notion that foraminifera developed the planktonic habitat polyphyletically from benthic forms as supported by genetic evidence. The descendents of *Gr. praescitula* subsequently underwent an adaptive radiation occupying both near-surface and deep habitats and evolved a variety of forms. By the Late Miocene maximum diversity of globorotaliid morphospecies was reached, for which a variety of phylogenetic hypotheses have been proposed. These hypotheses are tested here.

Morphometric analysis of outline shapes is used to quantify this globorotaliid invasion of morphospace. This provides phenetic information which serves as a basis for cladistic, stratocladistic and stratophenetic analyses of the phylogeny of Neogene globorotaliids. This integrated approach to evaluating phylogeny provides a more complete picture of the evolution of this important fossil group than hitherto achieved, and presents new hypotheses in conjunction with recommended taxonomic revisions to provide a better understanding of the *Globorotalia*. These revisions include the rejection of the subgeneric nomen *Menardella* in favour of its senior synonym (*Globorotalia*) and the elevation of the subgenera *Hirsutella* and *Truncorotalia* to generic status. The principal results presented here constitute steps towards a comprehensive phylogeny and a more accurate taxonomy for *Globorotalia*, which are both central to effective biostratigraphy of Neogene marine sediments.

Acknowledgments

First and foremost, I would like to thank Professor Paul Pearson, particularly in light of the circumstances that surround the initial selection! Without Paul, this project would not have been possible. If nothing else, at least we now know that 'Pongoroa is the way to go'.

I acknowledge here the efforts of various academic colleagues. Dr. Norman MacLeod explained the intricacies of morphometrics and his correspondence was invaluable in executing eigenshape analysis and modelling/interpreting the results. Further, Dr. Heiko Pälike gave informative opinions on, and assisted with, the time series analysis of foraminiferal range data. Several other people (in no particular order) have contributed in some way to the work presented in this thesis, and for this they are duly acknowledged. They are Dr. Peter Ditchfield, Dr. Katherine Harcourt-Brown, Simon Harris, Dr. Joyce Singano, Dr. Brian Huber, Dr. William Chaisson, Dr. Edward Llewellin, Dr. Claire Horwell, Dr. George Scott, Alistair McGowan, Dr. Timothy White, Dr. Pamela Hallock, Dr. Mike Howell, the Leg 194 shipboard scientific crew and individual thanks to Matthew Carroll (the uncrowned king of grammar). All their help has been invaluable. This project was funded by NERC (grant GT 04/99/ES/21) and indirectly through the Ocean Drilling Program, so I also extend my thanks to these organisations.

There are several people in Bristol that have made my years here enjoyable ones. Ed has been 'rock' since I met him all those moons ago in Micawbers. He has provided me with countless nights out, and an equally infinite number of liquor-fuelled dialogues in which all questions were answered. It's a pity we never remembered the answers in the morning! Likewise, thanks to Jon 'effort' Wade for unparalleled gymnasium camaraderie and an endless capacity for cynicism and truth-bending! Stewart Knott and Kate HB have been there since day 1 supplying ears to bend and confirmation that all forams are in fact indistinguishable! They still continue to provide good nights out, when they make it to this side of the river. Thanks to Deborah Wharton for being seminar guinea pig, testing the delights of my research before it was ever unleashed on the general public. Thanks to Colin Walker for providing Macintosh 'support' and welcome breaks from the torment that is writing.

I would like to thank my 'oppos' from the Royal Marines Reserve Bristol; Rob Cooper, Jim Burcham, Neil Thomas, John Tapper, Tom Scott and Rob Mendham. These gentlemen were an integral part of my Ph.D escapism; without them, I would not be a member of the most cliquey organisation known to man (excluding the Royal family).

Special thanks to Mum, Roger, Dad and Grant for their support and encouragement, especially during the 'final stretch'.

Por ùltimo, pero de ninguna manera menos importante, muchas gracias especiales a 'Dolores', ella es el *'rayo de sol en mi corazon'*. Ella ha sido comprensiva, ha estado a mi lado y ha sido paciente conmigo durante los ùltimos seis meses pasados. Espero hacer lo mismo por ella pronto.

Authors declaration

I declare that the work in this dissertation was carried out in accordance with the Regulations of the University of Bristol. The work is original, except where indicated by special reference in the text, and no part of the dissertation has been submitted for any other academic award. Any views expressed in the dissertation are those of the author.

SIGNED: ..... *DATE:* 17/06/03 .....

List of contents

List of figures

Chapter 6: Investigating the phylogeny of the Neogene *Globorotalia* using cladistics, stratocladistics and stratophenetics

List of tables

List of plates

Chapter 1

Introduction

1.1 Planktonic foraminifera, extinct and extant

The planktonic foraminifera are a group of living organisms with a relatively complete fossil record, which offer unique insights into evolution and multiple aspects of earth history. It is even possible that some deep ocean foraminiferal oozes yet to be discovered may contain an unbroken record of evolution since their initial diversification in the late Mesozoic. The combination of their fossil record, their relatively short species range and distinctive forms make planktonic foraminifera one of the principal biostratigraphical tools for the Cenozoic Era. Furthermore, the isotopic signatures preserved in their tests constitute a geochemical archive of oceanic conditions, which can be used to reconstruct their palaeoecology, past oceanic conditions and past climates. In addition, populations of the extant species are used to model modern plankton ecology and global oceanic circulation. Their preservation potential and well-documented evolutionary lineages also allow direct quantitative and qualitative analysis of macroevolutionary mechanisms that may be otherwise missed in groups with lesser fossil records. Using the planktonic foraminifera, it is possible in principle to study evolution and its effects at the 'species-level' to provide insight into the driving forces behind morphological change (see Chapter 2). Whether the environment plays a key role in influencing evolutionary pathways in the planktonic foraminifera, or whether competition and species interactions have greater influence, one thing is clear; the typological division of planktonic foraminifera into rigidly defined taxa may not accurately represent the true nature of their evolution. So before making conclusions from fossil range data about models of evolution, it is important to critically assess the applicability of range chart data to the fossil group in question. This issue is explored in this thesis.

The planktonic foraminifera are composed of a number of perceptible lineages that evolved comparable shell morphology in temporally separate radiations (Cifelli, 1969; Banner and Lowry, 1985; Norris, 1991). *Globorotalia sensu lato* (which originated in the

Early Miocene) are one such distinctive plexus of planktonic foraminifera. They share general 'globorotaliform' characteristics (low trochospiral coiling attitude, umbilical-peripheral aperture and in some, a distinct keel) with a number of other genera from different time intervals. Historically, this varied globorotaliform test plan appears to be more susceptible to extinction than their more conservative 'globigeriniform' cousins, which have more globose chambers and trochospiral tests (see Wei and Kennett, 1986; Stanley *et al.*, 1988; Norris, 1991). Of the ~50 *Globorotalia* morphospecies (see Figure 2.14 and text for explanation) that have lived throughout the Neogene, only 9 remain in the oceans of today; perhaps the Neogene globorotaliforms are echoing the demise of the Cretaceous and Palaeogene globorotaliforms?

So why study *Globorotalia*? Investigations into globorotaliform diversity, speciation and extinction through time will develop understanding of general evolutionary mechanisms and allow evaluation of evolutionary models, while palaeoecological analysis will aid the quantification of oceanic conditions within which they evolved (see Chapter 4). Furthermore, biostratigraphy is a fundamental constituent of all Phanerozoic sedimentary geology. With the advent and continuation of DSDP/ODP (and the future IODP), the value of pragmatic micropalaeontological dating was realised and timescales were developed (e.g. Blow, 1969; Martini, 1971; Berggren 1973, 1977, 1992; Kennett, 1973; Srinivasan and Kennett, 1981; among others). The widely used timescale of Berggren *et al.* (1995) integrates decades of plankton biostratigraphy, radioisotope geochemistry and palaeomagnetometry to produce the most widely used timescale for dating Cenozoic sediments. This timescale contains calibrated datums from 14 globorotaliid taxa among a total of 34 for the Neogene; thus *Globorotalia* are of prime consequence to Neogene biostratigraphy and geochronology. It is therefore important that the phylogeny of *Globorotalia* is understood (see chapters 5 and 6) in order to produce a stable taxonomy to support this vital component of the Cenozoic timescale and optimise Neogene biostratigraphy.

The focus of this thesis is to study globorotaliid origins, evolution, phylogeny, ecology, and the oceanic conditions in the Miocene epoch during which they lived and diversified.

1.1.1 *Globorotalia* and other modern planktonic foraminifera

The name *Foraminifera (Foraminifère)* was coined by the Haiti-born Frenchman Alcide Dessalines d'Orbigny (1826). It is derived from the Latin *foramen*, meaning 'hole' or 'opening' (which refers to the primary aperture). Upon observing their chamber form and mode of coiling, d'Orbigny originally thought they were tiny nautiloids. Thus, he published his cephalopod-based classification of foraminifera, based on material from beach sands of Cuba and the Canary Islands (d'Orbigny 1839a, 1839b).

Several authors later documented the presence of foraminifera in marine sediments (e.g. Ehrenberg, 1861; Carpenter *et al.*, 1862), but it was not until Owen (1867) that the planktonic life habitat of some foraminifera was reported. This fact was not widely publicised until Brady (1877) published his work from the Challenger expedition. This expedition represents the first purely scientific oceanographic voyage, which commenced in December 1872 with the use of the Royal Naval vessel HMS *Challenger*. Since then, many investigators have worked on foraminifera and published material documenting their use in biostratigraphy, palaeoclimatology, palaeoceanography, palaeobiology, and other scientific disciplines.

Planktonic foraminifera are described as "sexually reproducing heterotrophic marine protists that construct an ornate shell of multiple interconnecting chambers which are typically ~300 μm in diameter" (Pearson, 1998). Planktonic foraminifera are eukaryotic, i.e. organisms that have nucleate cells with vacuoles and organelles and are capable of co-ordinated cell division (Brasier, 1980). They differ from other eukaryotes because they possess granulo-reticulose (net-like) pseudopodia. These are fibrillar extensions used for feeding that emanate from the protoplasm that engulfs the test. The planktonic taxa are also members of the zooplankton, i.e. marine organisms that drift freely in ocean currents and consume algal, bacterial and animal food.

The origins of planktonic foraminifera must lie with the benthic (seafloor dwelling) foraminifera. In fact, the planktonic habitat may have evolved on more than one occasion (see Chapter 4). The earliest recorded planktonic fossils appear in the Late Jurassic (Boudagher-Fadel *et al.*, 1997), so it seems reasonable to assume that foraminifera first developed a benthic habit before diversifying into the planktonic realm. Benthic foraminifera have a fossil record extending back to the Cambrian (Culver, 1991), however, genetic analyses suggest an even earlier origin. Pawlowski *et al.* (1996, 1997) place the

foraminifera with the plasmoidal and cellular slime moulds within the basal eukaryotic phylogenetic tree, and suggest a Precambrian origination before the separation of the major eukaryotic lineages (800-1000 My ago). These conflicting origination estimates were reconciled by Pawlowski *et al.* (1999) with the hypothesis that a 'naked' amoeboid (non-testate) ancestor once existed within the sister group, Class Athalamea. This could help to explain the apparent lack of Pre-Cambrian body fossils. These modern classifications recognise the extensive 'protist' diversity such that foraminifera may actually constitute a Kingdom in their own right (Pawlowski *et al.*, 1996, 1997). Furthermore, Darling *et al.* (1997) propose that planktonic foraminifera did not evolve once from a 'globigierinid-like' ancestor, but polyphyletically from two ancestral benthic lines. Chapter 4 presents data supporting this theory through investigation of depth habitat of early globorotaliids using stable isotopes.

The number of planktonic foraminifera that exist at any one time is generally less than 50 morphospecies (Hemleben *et al.*, 1989). There are approximately 44 morphospecies present in today's oceans. However, the exact number of real 'species' is unknown and may be greatly in excess of this figure, because a number of taxa are reported to comprise multiple genetic variants or cryptic species (Huber *et al.*, 1997; de Vargas *et al.*, 1997, 1999, 2001; Darling *et al.*, 1999, 2000; Kucera and Darling, 2002; de Vargas *et al.*, 2002). From these studies, the extant species *Globigerinella siphonifera*, *Orbulina universa, Globigerinoides ruber/conglobatus, Globigerina bulloides, Neogloboquadrina pachyderma, Turborotalita quinqueloba* and *Globorotalia truncatulinoides* have all been shown to consist of a number of genetic variants, most of which are not distinguishable using morphometry.

The principle Neogene plantkonic lineages, from which the extant taxa evolved, constitute a broad morphological dichotomy, which are generally linked to distinct depth preferences. The shallow-dwelling globigerinids (i.e. pertaining to the genera *Globigerina* and *Globigerinoides*) generally possess globular, inflated chambers and thinner trochospiral tests, e.g., *Globigerinoides ruber* (Figure 1.1A). These omnivorous species are usually covered with a multitude of spines radiating from the primary test, often increasing the size of the organism by orders of magnitude. The spines probably have three primary functions: to act as a symbiont interface together with the cytoplasm, to prevent prey escape, and possibly to aid flotation within the water column (Pearson, 1998). Different spinose species prefer different depths within the surface mixed layer. Globigerinids tend

to have less dense shells due to their thinner, more porous, and reticulate tests. Although all planktonic foraminifera have a primary aperture, some of the shallow-dwellers possess multiple apertures.

In contrast, the globorotaliid forms (of which the *Globorotalia* belong) are more axially-compressed with angular chambers and a single off-centre, narrow aperture. They are discoidal in cross-section and usually possess a keel structure, similar to those seen in ammonites. The pores are generally finer, the shell wall thicker, and more dense. They have a smooth external surface devoid of spines, and are thus *usually* unable to support symbionts, however, *Globorotalia menardii* (Figure 1.1B), is known to seasonally exploit shallow habitats and does support algal symbionts. Because globorotaliids generally exploit habitats below the surface mixed layer, where they feed on algae and sinking phytodetritus, they rarely support algal symbionts, which are light-dependent.

Globorotaliids live at greater depths descending into the thermocline in which the water is denser and colder; sometimes a temperature drop of 15°C over 100-200 m may occur (Segar, 1998). This environment can be radically different to that above the thermocline, i.e. oxygen, illumination, temperature and pH are all lower, while nutrient levels are relatively higher. They usually have a longer ontogenetic life span than the shallow-dwelling forms, but grow more slowly.

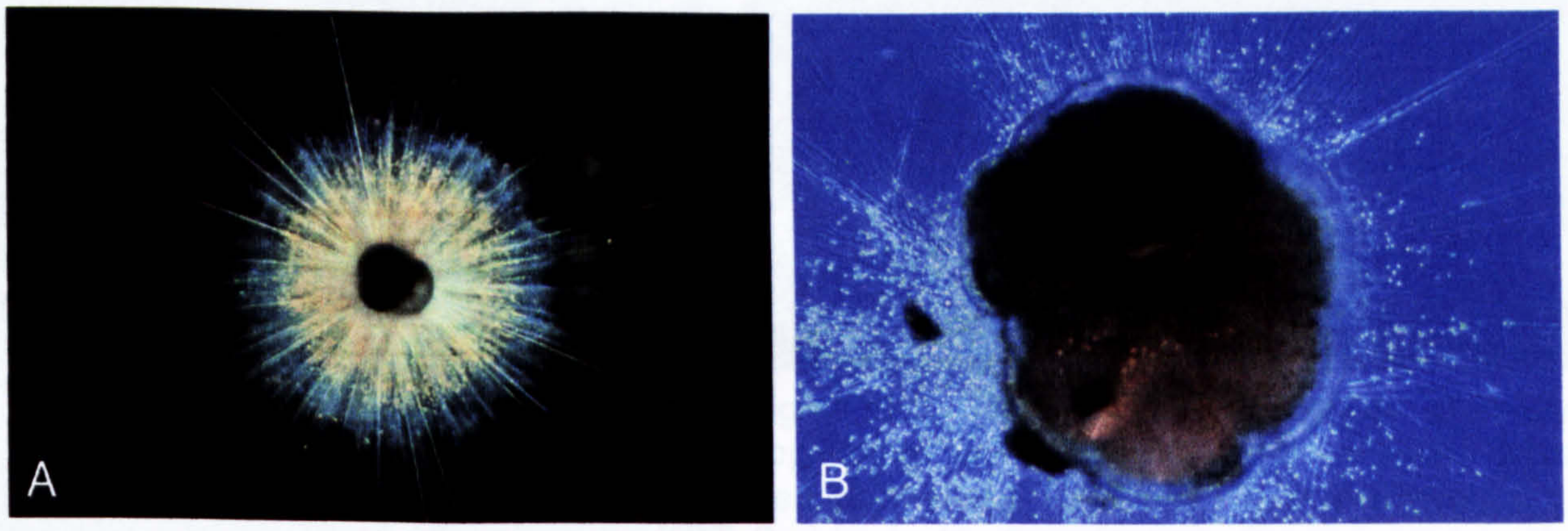

Figure 1.1. Modern planktonic foraminifera from Spero (1998). A – *Globigerinoides ruber* showing radial spines and symbionts (small yellow dots), B – *Globorotalia menardii*; a non-spinose globorotaliid showing radial rhizopodia and symbionts (light blue dots).

Of the extant species, nine belong to the genus *Globorotalia*, although some taxonomies recognise further generic subdivisions. These taxa are *Globorotalia crassaformis*, *Gr. hirsuta*, *Gr. inflata*, *Gr. menardii*, *Gr. scitula*, *Gr. theyeri*, *Gr. truncatulinoides*, *Gr. tumida* and *Gr. ungulata*, all of which are shown in Figure 1.2.

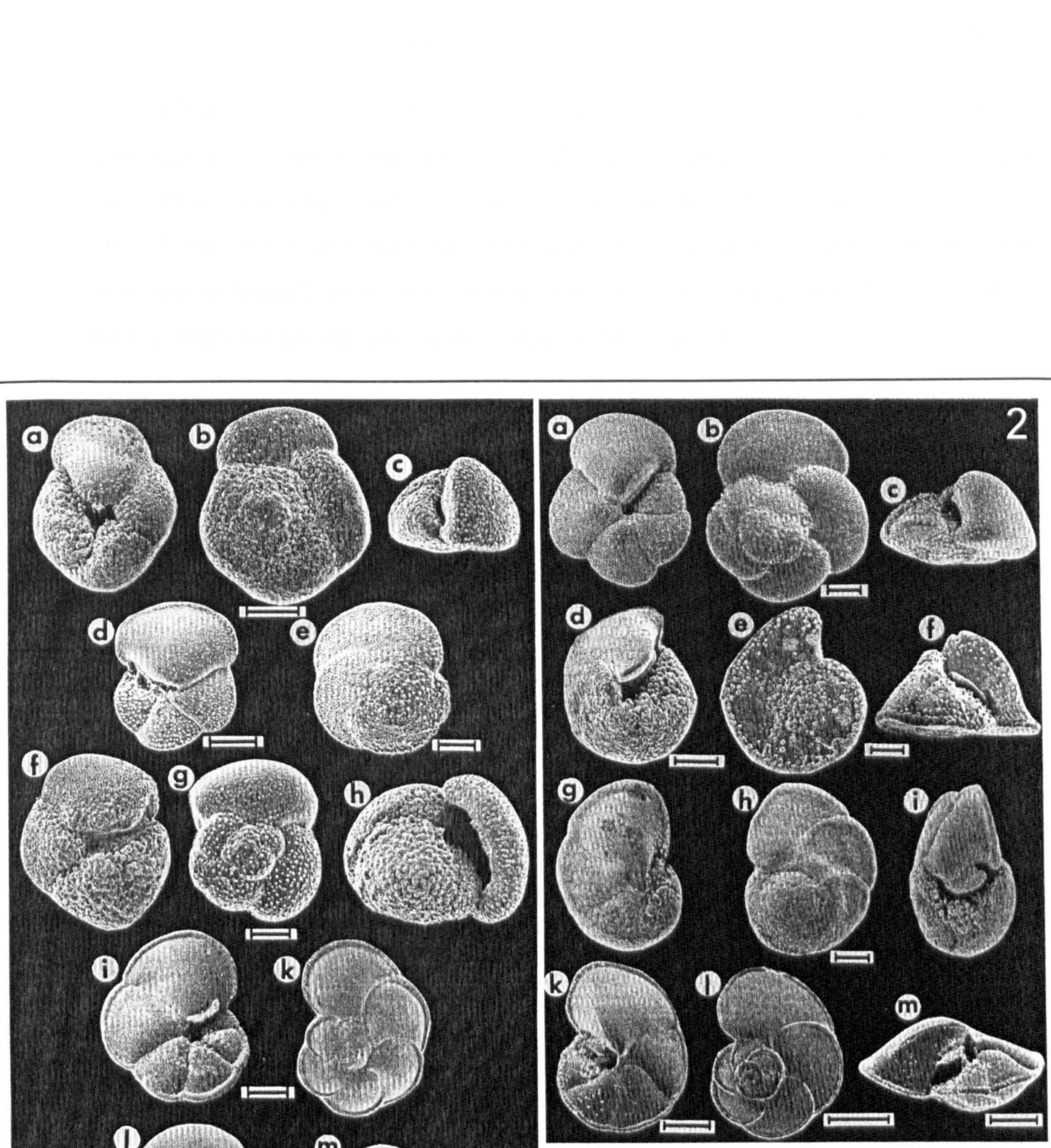

Figure 1.2. The extant globorotaliids currently populating the world's oceans, adapted from Hemleben *et al.* (1989). 1a-c, *Gr. crassaformis*, d-e, *Gr. hirsuta*, f-h, *Gr. inflata*, i-k, *Gr. menardii*, l-m, *Gr. scitula*. 2a-c, *Gr. theyeri*, d-f, *Gr. truncatulinoides*, g-l, *Gr. tumida*, k-m, *Gr. ungulata*.

Hemleben *et al.*'s (1989) list does not include *Gr. cultrata* (because it is commonly thought to be an ecophenotype of *Gr. menardii*), *Gr. cavernula* or *Gr. bermudezi*, shown in Plates 1.9 and 1.10 respectively. *Gr. tumida* is the type species for the genus (Cushman, 1927). In Figure 1.3 these extant taxa are marked by '*', in order to provide an insight into the approximate phylogenetic relationships that link them. The phylogenetic relationships that link these species are investigated further in later chapters.

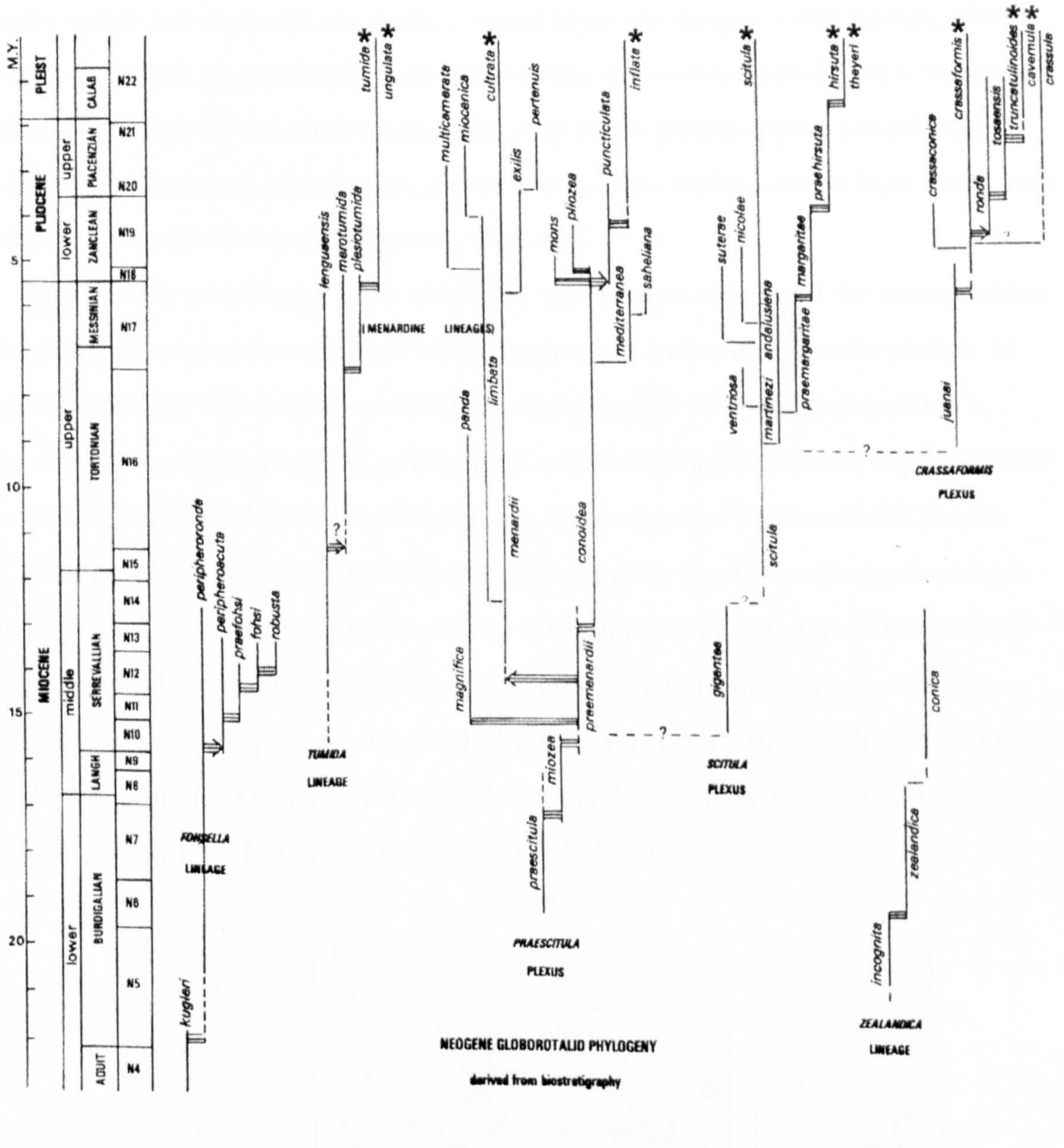

Figure 1.3. The phylogeny of the Neogene globorotaliids showing major groupings, from Cifelli and Scott (1986). Stars indicate discrete extant taxa and how they relate to Cifelli and Scott's separate lineage groupings. *Gr. ungulata, Gr. theyeri* and *Gr. bermudezi* (excluded by Cifelli and Scott) have been added in approximate positions relative to their parent lineages.

1.1.2 Ecology

Physical, chemical and nutritional conditions vary between oceanic layers, which in turn allows separation of potentially competing morphospecies. As adults, the modern globorotaliids tend to reside below the warmer surface layer and commonly either in or below the thermocline (Hemleben *et al.,* 1989) where the water is dense, cold, and nutrient-rich. The thermocline is a sharp, physical temperature discontinuity that can be seasonally stable and separates the surface mixed layer and deeper water masses, which varies in water depth. A permanent deep thermocline (top between 40-80 m) is present all year round, although the seasonal thermocline may reach greater depths periodically. Above this is the seasonal thermocline, above which is the surface mixed layer. Both vary in thickness with seasonality (see Figure 1.4 below).

The surface mixed layer is the relatively warm upper stratum of the oceans where illumination and temperature are high while oxygen, pH and nutrient levels are low. In general this zone has low primary production. Occasionally when the thermocline is shallow (cooler seasons) enhanced mixing may occur creating an increase in productivity at the mixed layer base. Although globorotaliids have a general preference for deeper water, some species have been shown to migrate vertically into the surface-mixed layer seasonally e.g., *Gr. menardii* (Durazzi, 1981). It should also be noted that *Gr. menardii* possesses facultative symbiotic chrysophytes, which may limit migration below the euphotic zone. The non-spinose globorotaliid *Gr. theyeri* occurs principally below the deep chlorophyll maximum (DCM) and commonly descends to depths between 250-375 m, and 500-700 m in their later life cycle (Hemleben *et al.,* 1989).

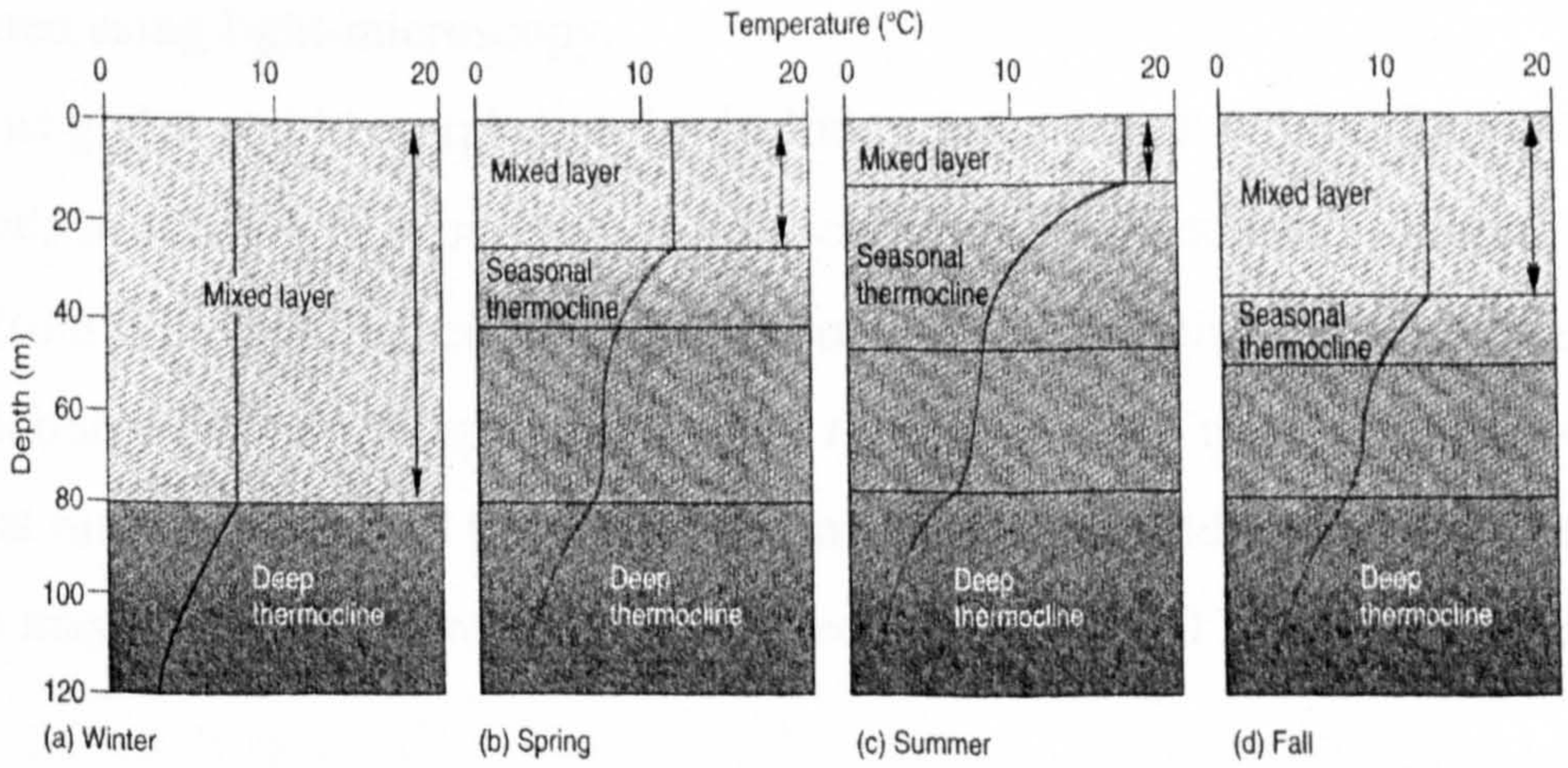

Figure 1.4. Physiology of the subtropical mixed layer and thermocline as affected by seasonality, adapted from Segar (1998).

Modern planktonic foraminifera of all depth habitats have been shown to migrate vertically to shallower depths diurnally and to sink for gametogenesis (Hemleben *et al.*, 1989). Fairbanks *et al.*'s (1982) data supports the notion that all species calcify within the top 100 m of the oceans, however, Deuser *et al.* (1981) showed that some spinose forms as well as the globorotaliids *Gr. hirsuta* and *Gr. truncatulinoides,* continue to grow while sinking to water deeper than 100 m.

Shackleton and Vincent (1978) carried out a number of isotopic analyses of Recent planktonic foraminifera from the Indian Ocean and found that the species belonging to *Globorotalia* (*Gr. menardii, Gr. tumida, Gr. truncatulinoides, Gr. inflata, Gr. crassula, Gr. scitula gigantea*) calcify in deep 'central waters' approaching the oxygen minimum zone. Of these morphospecies, they report the shallowest-dweller to be *Gr. menardii*, which conforms with its symbiotic nature, as discussed above.

1.1.3 Genetic variation

Cryptic species (genotypes) have been shown to exist in numerous modern spinose species e.g., *Globigerinella siphonifera, Orbulina universa, Globigerina bulloides, Globigerinoides ruber* among others (Huber *et al.*, 1997; de Vargas *et al.*, 1997, 1999; Darling *et al.*, 1999), however, little work has been done on the modern globorotaliids. De Vargas *et al.* (2001) conducted the first genetic analysis on the modern globorotaliid *Gr. truncatulinoides*. They concluded that the taxon *Gr. truncatulinoides* actually represents four genetic species, each adapted to particular hydrographic conditions. All four cryptic species show slight morphological variations, but they could not be consistently differentiated using light-microscopy.

Most globorotaliid morphospecies include subspecies or variants for example, *Gr. crassaformis* has four documented morphological forms (see Section 1.2). With the evidence from the cryptic species discussed above, it is reasonable to assume that most modern globorotaliid morphospecies probably represent one or more distinct genetic species that may have adapted to specific oceanic conditions and/or regions. The cryptic genotypes may not be represented by recognised morphological subspecies or variants.

1.1.4 Nutrition

Planktonic foraminifera feed on a variety of organisms captured using their rhizopodia, including larval crustaceans, copepods, diatoms, dinoflagellates, small protozoans and eukaryotic algae and bacteria (Hemleben *et al.*, 1989). Inter-species trophic habits vary from species to species.

Algal prey (e.g. thecate dinoflagellates) have been found partially-digested inside *Gr. truncatulinoides*, *Gr. inflata* and *Gr. menardii* (Lee *et al.*, 1966). Hemleben *et al.* (1989) observed omnivory, but with a strong affinity to herbivory (especially for diatoms) in the trophic habits of *Gr. truncatulinoides, Gr. inflata, Gr. hirsuta* and *Gr. scitula.* They also report fragments of other protists (tintinnids) in the digestive vacuoles of *Gr. menardii.*

In summary, modern globorotaliids are principally omnivorous yet their favoured food is phytoplankton. This contrasts the spinose, shallow forms, which generally prefer zooplankton such as copepods.

1.1.5 Reproduction

Planktonic foraminifera are only known to possess a gamont (sexual) reproduction mode, which contrasts benthic foraminifera that also have an agamont (asexual) stage of their biphasic reproduction cycle (Brasier, 1980; Hemleben *et al.*, 1989). A number of studies (e.g. Spindler and Hemleben, 1982) have documented the release of hundreds of thousands of flagellated cells, which probably constitute gametes, including from the globorotaliid species *Gr. inflata* and *Gr. menardii.* Gamete release in planktonic foraminifera is accompanied by expulsion and digestion of symbionts, spine-resorption, test-encrustation (calcification) and chamber formation (Bé *et al.*, 1983). Despite this detailed knowledge about the timing of some of the reproductive events from freshly-collected marine populations, little is yet known about the life cycles in general of planktonic foraminifera because it has hitherto been impossible to culture a second generation.

Planktonic foraminifera are particularly vulnerable to all hydrodynamic forces because they can only regulate their position vertically in the water column. Therefore, widespread dispersal of individuals over vast areas of the hydrosphere may hinder

successful reproduction in these dioecious organisms (i.e. where gametes from different parent organisms join to form a zygote) because gametes require close proximity for zygote formation. The magnitude of gamete numbers released together with lunar and depth synchronisation may help overcome this factor.

Unfortunately, laboratory culturing methods have yielded no irrefutable evidence for either sexual or asexual reproduction in modern globorotaliid species. The modern species with the best understood reproductive cycle is probably *Hastigerina pelagica*. The reproductive cycle of *H. pelagica* shows good correlation with the lunar cycle (Spindler *et al.*, 1979). A deep habitat may not allow lunar control of globorotaliid reproduction, thus other factors may dictate the globorotaliid cycle.

1.1.6 Predation

Predation on planktonic foraminifera is poorly known because specimens do not survive well in likely predator digestive tracts or faecal material. Likely predators probably belong to the macrozooplankton and other nekton. This may include pteropods, euphausids (herbivorous holoplankton in the same class of crustacea as crabs and lobsters), sergestids and tunicates (Bradbury *et al.*, 1970). Predation by larger crustacea is also probable, but is very difficult to document due to the mechanical and chemical digestive processes associated with likely predators (Berger, 1971). Red shrimp, crabs and salp (widely occurring gelatinous holoplanktonic tunicates) have been observed as predators. Other predators may include holothurians (in Antarctic regions) and terebellid polychaete (benthic suspension feeders) (Segar, 1998).

The ratio of protoplasm to calcite (and thus nutritional value) in planktonic foraminifera is very low, especially in the spinose taxa, therefore impact of predators on planktic populations may be quite large (Hemleben *et al.*, 1989).

1.2 Taxonomy of *Globorotalia* and related taxa

In this section, the taxonomy of the fossil and Recent *Globorotalia* taxa are introduced and discussed. These taxa are subsequently included in the isotopic, morphometric and phylogenetic analysis presented in the later chapters.

The taxonomy of *Globorotalia* is fraught with complications of various suggested classifications. Here the taxa under investigation are placed into four distinct lineages, named by various authors. These are: the *Globorotalia s.s.* lineage (Cushman, 1927), the hirsutellids (Bandy, 1972), the menardellids (Bandy, 1972) and the truncorotaliids (Cushman and Bermudez, 1949). Another such lineage commonly included with Neogene *Globorotalia*, is the fohsellids (a subgenera also named by Bandy, 1972). They are excluded here because it is widely agreed that this distinct lineage has separate ancestry to those concerned here (see figures 1.3, 1.6 and 1.7).

The 'Diagnosis' sections (below) give a brief description of the taxa. This section is not intended to reproduce the type descriptions, for those, the references are given. It is simply the key characteristics that allow pragmatic identification of each taxon (marked in bold). The 'Remarks' section discusses briefly the immediate phylogenetic relationships, common synonyms and the taxonomic controversies. The more fundamental controversies are discussed later in Section 1.3.3 (this chapter). Any known synonyms for each taxon are listed immediately below the current taxonomic nomen. All plates referred to here are located at the end of this chapter.

Specialist descriptive terms are described in Section 6.2.2, Chapter 6. The taxonomy is as follows:

Order FORAMINIFERIDA D'Orbigny 1826

Family GLOBOROTALIIDAE Cushman, 1927

Genus GLOBOROTALIA Cushman, 1927

Type Species – *Pulvinulina menardii* var. *tumida* Brady, 1877

Original description (*Globorotalia*): "Test trochoid; earliest chambers often like *Globigerina*, with a rough cancellated exterior, biconvex, dorsal side more or less flattened, ventral side strongly convex; wall calcareous, perforate, frequently spinose in whole or restricted areas; aperture large, opening into the umbilicus which is either open or partially covered by a lip – Upper Cretaceous to Recent. This genus is directly derived from *Globotruncana* by the suppression of one of the keels. It is largely pelagic, a specialised genus associated with the Globigerinidae" (Cushman, 1927; 1940).

1.2.1 *Globorotalia s.s.* lineage (Cushman, 1927)

This lineage name is employed here to describe those forms closely related to *Gr. tumida* (c.f. Bandy, 1972). This includes the following taxa: *Gr. merotumida, Gr. plesiotumida, Gr. tumida, Gr. ungulata* and *Gr. flexuosa*. Unlike Kennett and Srinivasan (1983), here, *Gr. lenguanensis* and *Gr. paralenguanensis* are not included in this lineage (see Figure 1.7C).

These taxa are generally united by tumid tests (edge view) with more curved spiral sides, ovate equatorial peripheries, coarse apertural lips and strongly curved keels.

Globorotalia flexuosa (Koch)

Plate 1.6, figures 7-9.

Pulvinulina tumida Brady var. *flexuosa* Koch, 1923-24

Diagnosis: The test is large (>500 μm) and thickset, with a heavy keel. The equatorial periphery is oval to elongate and the axial periphery acute. The umbilical lip is prominent and plate-like and the umbilicus is typically surrounded by coarse pustules on the first 2-3 chambers. Test is densely perforate and spiral sutures raised, limbate and obliquely-curved backwards to join keel.

The most distinctive feature is the anterior margin of the final chamber, which is strongly-curved, which usually results in the opening of the aperture.

Remarks: Gr. flexuosa is very similar to *Gr. tumida* other than the heavily deviated anterior part of the final chamber. New observations from Atlantic and Pacific material reveal a range of flexuose forms between the two morphospecies, with true *Gr. flexuosa* constituting those forms with the most twisted final chamber (see Bolli and Saunders, 1985). This morphospecies is probably strictly a variant of *Gr. tumida*, however, it has a definite range and is therefore biostratigraphically useful.

Globorotalia merotumida Blow and Banner

Plate 1.6, figures 19-25.

Globorotalia (Globorotalia) merotumida Blow and Banner, 1965

Diagnosis: Gr. merotumida has a small (100-200 μm), evolute, delicate and finely perforate test with a distinct keel. Axial periphery is acute and the equatorial periphery is nominally lobulate. The chambers are reniform with a regular increase in size from early to later chambers. The apertural lip is thin and the umbilicus restricted, with some pustulation surrounding. Spiral sutures are raised, limbate and oblique to curved.

Remarks: Gr. merotumida is distinguished from *Gr. plesiotumida* in being more compressed (in the keel plane) with a more convex umbilical side. The final chamber constitutes the main differences, e.g. the final chamber in *Gr. merotumida* has less height than in *Gr. plesiotumida*, and it is wider than it is tall in *Gr. merotumida*. The chamber size increase in *Gr. plesiotumida* is not regular because the final chamber is elongate, as in *Gr. tumida*.

Globorotalia plesiotumida Blow and Banner

Plate 1.6, figures 12-18.

Globorotalia (Gr.) tumida (Brady) *plesiotumida* Blow and Banner, 1965

Diagnosis: Gr. plesiotumida shares the majority of its characteristics with *Gr. merotumida*. See above for distinction.

Remarks: Although the Blow and Banner (1965) morphologies can occasionally be isolated, the majority of specimens pertaining to the *plesiotumida* and *merotumida* morphospecies appear to vary between these types. The prime distinction between the two is based on final chamber shape and test convexity, which are generally unreliable to distinguish planktonic foraminifera morphospecies. Their ranges are reported (Kennett and Srinivasan, 1983) to overlap considerably, which may support the presence of an unbroken lineage as opposed to separate species.

Globorotalia tumida (Brady)

Plate 1.6, figures 1-6.

Pulvinulina menardii (d'Orbigny) var. *tumida* Brady, 1877

Diagnosis: See *Gr. flexuosa* for primary characteristics. *Gr. tumida* has swollen chambers except for the radially elongated final chamber. Despite a tumid appearance in edge-view, the keel is usually near-planar.

Remarks: Although many characteristics are shared with *Gr. flexuosa*, the final chamber of *Gr. tumida* is elongate in umbilical view and does not possess the degree of flexing in the final chamber. The tumidity is usually less in the aperture-edge view. This morphospecies also shares a number of common characteristics with *Gr. menardii aff. tumida* (Plate 1.5, figures 20-23), which has lead investigators to infer a phylogenetic link between *Gr. tumida* and *Gr. menardii* (see discussion in Section 1.3).

Gr. tumida (and *Gr. flexuosa*) are thought to have evolved from *Gr. merotumida* and *Gr. plesiotumida* (see discussion in Section 1.3.3.3).

Globorotalia ungulata Bermudez

Plate 1.5, figures 7-13.

Globorotalia ungulata Bermudez, 1960

Diagnosis: Gr. ungulata possesses as small (100-200 μm), smooth, thin, delicately-keeled, finely-perforate test. The umbilical side is generally more vaulted than the spiral-side. The equatorial periphery is ovate and the axial periphery is biconvex. The delicate test sometimes gives this morphospecies a pearlescent sheen.

Remarks: Gr. ungulata shares general test morphology with *Gr. tumida*, the primary difference being the much smaller size and more delicate test. This morphospecies may be an ecophenotype of *Gr. tumida* (Pearson, 1995b).

1.2.2 *Hirsutella* Bandy (1972)

This subgeneric nomen was employed by Bandy (1972) to include sharp-edged to keeled forms with crescentic spiral chamber shapes and densely perforate/pustulate tests, i.e. the *Gr. scitula-Gr. margaritae-Gr. hirsuta* lineage (see Figure 1.7E). The revised phylogeny (presented in Chapter 6) does not agree that *Gr. juanai* and *Gr. challengeri* should be included in this subgenus, however, are included here below for ease.

Bandy's (1972) *Hirsutella* is technically a junior homonym of *Hirsutella* Cooper and Muir-Wood, 1951 (Brachiopoda). Haman *et al.* (1981) proposed that *Obandyella* should replace the erroneously assigned subgeneric nomen. Although technically correct, *Obandyella* is not used here to avoid causing unnecessary confusion.

Globorotalia bermudezi Rögl and Bolli

Plate 1.10, figures 21-23.

Globorotalia bermudezi Rögl and Bolli, 1973.

Diagnosis: Gr. bermudezi possesses a small (100-200 μm), smooth, non-keeled test with 5-6 rounded (umbilically-inflated) chambers in the last whorl, and a subcircular-lobulate equatorial periphery.

Remarks: Gr. bermudezi is probably descended from *Gr. scitula.*

Globorotalia challengeri Srinivasan and Kennett

Plate 1.9, figures 12-14.

Globorotalia challengeri Srinivasan and Kennett, 1981.

Diagnosis: Gr. challengeri is asymmetrically biconvex with a semi-planar spiral side and a strongly convex umbilical side composed of inflated, bulbous chambers. The test is unkeeled, coarsely-perforate and smooth.

Remarks: Gr. challengeri may be derived from *Gr. praescitula* (see Figure 6.10, Chapter 6). Its general form is not easily allied with the remaining taxa in Bandy's *Hirsutella.* Its generally inflated-chamber form is more easily associated with the *Paragloborotalia.*

Globorotalia cibaoensis Bermudez

Plate 1.10, figures 12-14.

Globorotalia cibaoensis Bermudez, 1949.

Diagnosis: Gr. cibaoensis has a totally pustulate, non-keeled, biconvex test with a obtuse axial periphery and 4-5 inflated chambers in the final whorl. The final chamber occasionally becomes finely-keeled.

Remarks: Gr. cibaoensis is probably descended from *Gr. scitula* and may constitute the link between the hirsutellids and the truncorotaliids, as expressed by Kennett and Srinivasan (1983).

Globorotalia hirsuta (d'Orbigny)

Plate 1.9, figures 12-17.

Rotalina hirsuta d'Orbigny, 1839.

Diagnosis: Gr. hirsuta possesses a large (300-400 μm), thick, keeled test with an acute axial periphery, flat umbilical side and a highly convex (high-spired) spiral side. The final whorl contains 4 chambers all of which are covered in small pustules (both sides) and the last of which envelops the width of the previous chambers on the umbilical side.

Results: Gr. hirsuta was derived from *Gr. margaritae* in the Late Pliocene, and with it developed a higher-spired, pustulose test. This species is commonly confused with *Gr. margaritae* partly because d'Orbigny's original type was lost and Blow's (1969) replacement is nearly twice as big and possesses three more chambers!

Gr. hirsuta is a temperate form largely absent from the tropical realm, unlike *Gr. margaritae,* which is a great deal more cosmopolitan (Bolli and Saunders, 1985).

Banner and Blow's (1960) *Gr. canariensis* is probably a junior synonym or variant of *Gr. hirsuta*, unfortunately only the umbilical view of the holotype is figured and the illustration is of low quality.

Globorotalia juanai Bermudez and Bolli

Plate 1.9, figures 1-5.

Globorotalia juanai Bermudez and Bolli, 1969.

Diagnosis: Gr. juanai has a small, keel-less test (200-300 μm) with a rounded axial periphery and inflated chambers on the convex umbilical side, while the spiral side is near flat. The test is densely-perforate and highly pustulose on the umbilical side.

Remarks: According to Kennett and Srinivasan, *Gr. juanai* is derived from *Gr. scitula* and is ancestral to *Gr. margaritae, hirsuta* and *bermudezi*. The phenetic analysis in chapters 5 and 6 support derivation from *Gr. challengeri. Gr. challengeri* has more bulbous chambers and a more coarsely-perforate test.

Globorotalia margaritae Bermudez and Bolli

Plate 1.10, figures 1-5.

Globorotalia margaritae Bermudez and Bolli, 1965.

Diagnosis: Gr. margaritae is axially acute with a strongly convex spiral side and keel, with almost flat umbilical side. The majority of the test is smooth, but distinct pustulation on the umbilical side is apparent. Chamber number in the final whorl is usually five. The aperture is narrow and bordered by a thin lip.

Remarks: Gr. margaritae has variable morphology as exemplified by the intergrading synonyms of *Gr. margaritae evoluta* and *primitiva. Gr. margaritae evoluta* is larger and has a more symmetrical profile, while *Gr. margaritae primitiva* is smaller than *Gr. margaritae* and lacks a complete keel (see Cita, 1973).

Gr. margaritae can be distinguished from its descendent *Gr. hirsuta* because the latter is extremely-spirally convex and pustulate over the entire test. Blow's (1969) *Gr. praehirsuta* is a junior synonym of this taxon.

Globorotalia margaritae evoluta Cita

Plate 1.10, figures 6-8.

Globorotalia margaritae evoluta Cita, 1973.

Diagnosis and remarks: see Gr. margaritae

Globorotalia margaritae primitiva Cita

Plate 1.10, figures 9-11.

Globorotalia margaritae primitiva Cita, 1973.

Diagnosis and remarks: see Gr. margaritae

Globorotalia praemargaritae Catalano and Sprovieri

Plate 1.10, figures 15-17.

Globorotalia praemargaritae Catalano and Sprovieri, 1969.

Diagnosis and remarks: See *Gr. scitula.*

Globorotalia scitula (Brady)

Plate 1.9, figures 6-11.

Pulvinulina scitula Brady, 1882.

Diagnosis: Gr. scitula has a small (200-300 μm) biconvex test with a sub-angular axial periphery with a keel-like rim. Chambers are compressed and number 4-5 in the last whorl. Spiral sutures are raised and non-limbate. Aperture is restricted and bordered by a thin lip.

Remarks: Gr. scitula shares many features with, and is descended from *Gr. praescitula.* The two are distinguished because *Gr. scitula* is larger and does not possess the honeycomb surface texture of *Gr. praescitula. Gr. scitula gigantea* is probably a synonym, and only differs in having a larger test size (500-600 μm).

Gr. scitula and *Gr. praescitula* constitute the prime progenitors for the majority of the Neogene *Globorotalia* (see chapters 5 and 6). *Gr. scitula* was originally erected as a variant of *Gr. canariensis* (*Gr. hirsuta*) and is probably synonymous with *Gr. patagonica* (d'Orbigny). *Gr. praemargaritae* is likely a junior synonym of *Gr. scitula,* as endorsed by Bolli and Saunders, 1985.

Globorotalia scitula gigantea Blow

Plate 1.9, figures 18-20.

Globorotalia scitula gigantea Blow, 1959.

Diagnosis and remarks: See *Gr. scitula.*

Globorotalia theyeri Fleisher

Plate 1.10, figures 18-20.

Globorotalia theyeri Fleisher, 1974.

Diagnosis: Gr. theyeri is a planoconvex form with a lobulate equatorial periphery and an acute axial periphery. The chambers in the final whorl are markedly flared into a thin, discontinuous keel. Spiral sutures are strongly-curved and not raised or limbate.

Remarks: This morphospecies probably arose from *Gr. margaritae* by the acquisition of a flat spiral side and flared chambers. Boltovskoy's *Gr. hirsuta eastropicia* is a junior synonym of *Gr. theyeri.*

1.2.3 *Menardella* Bandy (1972)

Bandy (1972) proposed this subgenus to include the *Gr. praescitula-archeomenardii-praemenardii-menardii* evolutionary lineage (see Figure 1.7 A) united by lenticular, trochospiral tests, prominent keels and smooth, densely perforate tests. This division is endorsed in this thesis.

Many characters are shared between this and the *Globorotalia s.s.* taxa, although some authors do not subscribe to any direct phylogenetic link between the two lineages (discussed later).

Globorotalia archeomenardii Bolli

Plate 1.1, figures 5-9 and 24-26.

Globorotalia archeomenardii Bolli, 1957.

Diagnosis: Gr. archeomenardii has a small test (100-200 μm), acute axial periphery, thin, poorly-developed keel, slightly-lobate equatorial periphery and a strongly-curved spiral side with raised, non-limbate sutures.

Remarks: See *Gr. praescitula* for the differences between the two morphospecies. This is the earliest menardellid morphospecies and is ancestor to *Gr. praemenardii*, which typically exhibits a larger test with a more lobulate equatorial periphery.

Globorotalia cultrata (d'Orbginy)

Plate 1.5, figures 1-6.

Rotalina cultrata d'Orbigny, 1839

Globorotalia cultrata (d'Orbginy), Banner and Blow, 1960 (Neotype)

Diagnosis and Remarks: See discussion under *Gr. menardii.*

Globorotalia exilis Blow

Plate 1.2, figures 1-2 and 5-6.

Globorotalia (Globorotalia) cultrata exilis Blow, 1969.

Diagnosis: Gr. exilis possesses a thin, delicately-keeled, lenticular test (300-400 μm) with lobulate equatorial periphery and acute axial periphery. Chambers in the final whorl commonly number 5-7, while the spiral sutures are limbate, recurved and overlap, merging into keel. Apertural lip is variable from thin to flared.

Remarks: Gr. exilis clearly grades into, and gave rise to, *Gr. pertenuis*. *Gr. exilis* and *Gr. limbata* also intergrade (see Plate 1.2, figures 1-4). This may support the derivation of both *Gr. exilis* and *Gr. pertenuis* from *Gr. limbata* (see results sections in chapters 5 and 6).

Globorotalia fimbriata (Brady)

Plate 1.5, figures 24-25.

Pulvinulina menardii (d'Orbginy) var. *fimbriata* Brady, 1884

Globorotalia cultrata (d'Orbginy) subsp. *fimbriata* (Brady), Banner and Blow, 1960 (lectotype).

Diagnosis and Remarks: Gr. fimbriata resembles *Gr. cultrata* except for the additional feature of small, radially arranged extended pustules ornamenting the peripheral keel. This

morphospecies is only known from the most recent Pleistocene and Holocene and may be an ecophenotype of *Gr. menardii.*

Globorotalia limbata (Fornasini)

Plate 1.2, figures 13-15.

Rotalia limbata Fornasini, 1902.

Diagnosis: Gr. limbata possesses a medium size (300-400 μm), lobulate, biconvex test with an acute axial periphery and pronounced keel. There are 6-8 chambers in the final whorl with raised, limbate and vaulted spiral sutures and sinuous, depressed umbilical sutures. Aperture is open and bordered by a thin lip.

Remarks: Gr. limbata is probably derived from *Gr. menardii* as the two bear close resemblance. *Gr. limbata* was thought synonymous with *Gr. pseudomiocenica*, and although population intergradation appears to occur, the two morphospecies are distinct enough to be consistently isolated. Lamb and Beard's (1972) *Gr. praemiocenica* is most likely a junior synonym of *Gr. limbata* or represents an intermediate between *Gr. limbata* and *Gr. pseudomiocenica.*

Globorotalia menardii (Parker, Jones and Brady)

Plate 1.5, figures 14-19.

Rotalia menardii Parker, Jones and Brady, 1865.

Diagnosis: Gr. menardii s.s. has a large (500-700 μm), compressed, biconvex, axially-acute test with a lobulate periphery. The holotype has a well-developed, thick keel, limbate umbilical sutures, 5-6 chambers and deep umbilicus with a thick plated-lip and pronounced umbilical pustules on the first 2-3 chambers.

Remarks: The controversy surrounding the *Gr. menardii* type specimen is discussed in Section 1.3, this chapter. *Gr. menardii aff. tumida* has the same general form but possesses more inflated chambers and some characters in common with *Gr. tumida* (Plate 1.5, figures 20-23). *Gr. cultrata* and *Gr. fimbriata* also share the same test form with some variations as discussed under the respective taxa. These forms may represent

ecophenotypes that constitute variation within the *Gr. menardii* species concept. Bolli (1970) justifies the splitting of the Middle Miocene *Gr. menardii* variants ('A' and 'B') on the basis that all the Late Miocene and younger forms are included under the nomen *Gr. menardii*. These taxa are discussed below.

Direct intergradation with *Gr. praemenardii* is not observed in material from ODP sites 1195, 926 or 871. *Gr. menardii flexuosa* as reported by Bé and McIntyre (1969) is most probably a Recent ecophenotype currently restricted to the northern Indian Ocean.

***Globorotalia menardii* 'A'** Bolli

Plate 1.4, figures 10-17.

Globorotalia menardii 'A' Bolli, 1970.

Diagnosis and Remarks: Gr. menardii 'A' differs from *Gr. menardii s.s.* in having a smaller test (~300 μm), with a more circular equatorial periphery. Chambers usually still number between 5-6 in the last whorl.

Some isolated specimens from Atlantic and Indo-Pacific material can be assigned to an 'A' or 'B' end-member morphotype, while most lie somewhere in between. The further division of these morphotypes is based on few non-diagnostic characters, and is unnecessary (see chapters 5 and 6).

***Globorotalia menardii* 'B'** Bolli

Plate 1.4, figures 1-9.

Globorotalia menardii 'B' Bolli, 1970.

Diagnosis and Remarks: Gr. menardii 'B' differs from 'A' in possessing 7-7.5 chambers in the final whorl producing a larger diameter (300-400 μm) and a thicker peripheral keel. Bolli (1970) proposed this taxon as the ancestor to *Gr. multicamerata*.

Globorotalia miocenica Palmer

Plate 1.4, figures 24-29.

Globorotalia menardii (d'Orbigny) var. *miocenica* Palmer, 1945.

Diagnosis: Gr. miocenica has a distinctive planoconvex test (300-400 μm) with flat spiral side and strongly-convex umbilical side. It exhibits a pronounced keel around a circular equatorial periphery. Spiral sutures are limbate and merge into the keel, while the aperture is restricted and bordered by a thin lip.

Remarks: Gr. miocenica is probably derived from *Gr. pseudomiocenica,* which displays a similarly circular periphery but lacks the flat spiral side. This species is strongly biconvex around the keel axis.

Globorotalia multicamerata Cushman and Jarvis

Plate 1.3, figures 7-14.

Globorotalia menardii (d'Orbigny) var. *multicamerata* Cushman and Jarvis, 1930.

Diagnosis: Gr. multicamerata is clearly distinguished by its large test size (500-700 μm), acute axial periphery, with 8-10+ chambers in the final whorl and a circular-lobulate equatorial periphery. The keel is often thick, well-developed and the umbilicus is wide, open, and bordered by a multiple-flared apertural lip (Plate 1.3, figure 11).

Remarks: This species may be a variant of *Gr. menardii* (Bolli and Saunders, 1985; Pearson, 1995b) and/or maybe more closely allied to *Gr. pertenuis-exilis*, as seen in transitional morphotypes in Bolli (1970). The lip and multi-chambered characters may result from phenetic association with *Gr. pertenuis-exilis* or could be characters derived independently. See chapters 5 and 6 for phylogenetic analysis.

Globorotalia pertenuis Beard

Plate 1.3, figures 1-6.

Globorotalia pertenuis Beard, 1969.

Diagnosis: Gr. pertenuis is identified by its axially-thin, large diameter (500-700 μm), multi-chambered test (6-8+ in the final whorl) with a circular-lobulate equatorial periphery. The aperture is usually restricted by test compression and a flared, extensive lip.

Remarks: Some specimens of *Gr. pertenuis* show morphological intergradation with *Gr. exilis* and *Gr. multicamerata.* It is distinguished from the former by greater chamber number in the final whorl and more extensive lip architecture, and from the latter by its much thinner, more delicate test with usually fewer chambers.

Gr. pertenuis is probably descended from *Gr. exilis* and indirectly evolved from *Gr. limbata* and *Gr. menardii.*

Globorotalia praemenardii Cushman and Stainforth

Plate 1.1, figures 1-4 and 10-12.

Globorotalia praemenardii Cushman and Stainforth, 1945.

Diagnosis: Gr. praemenardii possesses a medium-sized test (~300 μm), with a moderately-lobulate equatorial periphery and a distinct keel. The axial periphery is acute and the test biconvex and compressed. Spiral sutures are raised and limbate.

Remarks: See *Gr. archeomenardii* for discussion about similarities with this morphospecies. *Gr. praemenardii* is probably ancestral to *Gr. menardii.*

Globorotalia praescitula Blow

Plate 1.1, figures 16-23.

Globorotalia scitula (Brady) *praescitula* Blow, 1959

Diagnosis: Gr. praescitula has a small (100-150 μm), non-keeled, biconvex test with a sub-angular periphery. Some specimens possess a pseudo-honeycombed surface texture reminiscent of that displayed by *Paragloborotalia.*

Remarks: Gr. praescitula and *Gr. archeomenardii* have closely-intergrading morphologies. The type specimens are distinguished by the presence of a keel and a greater spiral-side curvature in *Gr. archeomenardii.* Although some specimens can be separated in this way, many specimens exhibit characteristics from both morphospecies (see Plate 1.1, figures 13-15) and support one continuous evolving morphological lineage rather than two distinct populations.

Gr. praescitula is probably the prime progenitor for the menardellid globorotaliids and possibly for the majority of the Neogene *Globorotalia* (see chapters 5 and 6).

Globorotalia pseudomiocenica Bolli and Bermudez

Plate 1.2, figures 16-23.

Globorotalia pseudomiocenica Bolli and Bermudez, 1965.

Diagnosis: Gr. pseudomiocenica has a strongly-biconvex test (~300 μm) with a sub-circular equatorial periphery and pronounced keel.

Remarks: This species displays considerable morphological variation that sometimes show features in common with *Gr. limbata* and *Gr. menardii*. It is the likely progenitor to *Gr. miocenica*. Bolli (1970) and Bolli and Saunders (1985) suggest derivation from *Gr. menardii* 'A'. Data presented in chapters 5 and 6 suggest *Gr. limbata* as an ancestral taxon.

1.2.4 *Truncorotalia* Cushman and Bermudez (1949)

This subgenus includes the distinctive conicotruncate forms, which in general are keeled, thick-walled and heavily pustulate (see Figure 1.7B). This lineage is likely linked to the hirsutellid bioseries (see Chapter 6).

Globorotalia cavernula Bé

Plate 1.9, figures 24-26.

Globorotalia cavernula Bé, 1967.

Diagnosis: Gr. cavernula has an asymmetrically-biconvex, pustulose test with the umbilical side more convex. The equatorial periphery is ovate to sub-circular. The test is quite delicate and thinly-keeled. The most striking feature is the open coiling structure producing a wide aperture and an imbricate chamber arrangement producing step-like structures at the sutures.

Remarks: Gr. cavernula was probably derived from *Gr. truncatulinoides* in the Quaternary. It is differentiated from its ancestor by the less conical test and the distinctive chamber imbrication.

Globorotalia crassaconica Hornibrook

Plate 1.8, figures 23-25.

Globorotalia crassaconica Hornibrook, 1981.

Diagnosis: Gr. crassaconica has an asymmetrical, ventroconical, keeled, heavily-pustulose test with a flat spiral side and a steep-conical umbilical side. The four chambers in the final whorl are tightly packed and the final chamber is laterally-expanded and drawn out to a rounded point (edge view).

Remarks: Gr. crassaconica is similar to *Gr. crassaformis* and variants. It is distinguished from *Gr. crassaformis* by its broader, steep axial peripheral outline. Cifelli and Scott (1986) endorse phenetic allegiance with *Gr. crassaformis* although state that there is no evidence of transitional populations. *Gr. crassaconica* may descend from *Gr. crassaformis* (see Figure 6.10, Chapter 6).

Globorotalia crassaformis (Galloway and Wissler)

Plate 1.7, figures 18-24.

Globigerina crassaformis Galloway and Wissler, 1927.

Diagnosis: Gr. crasssformis s.s. has a low trochospiral, pustulose-subspinose test with flat spiral side and a conical-convexly rounded umbilical side. Equatorial periphery is slightly lobulate. The aperture is wide, thin and bordered by a narrow lip.

Remarks: This taxon is highly variable and has four well-documented variants, i.e. *Gr. crassaformis hessi, Gr. crassaformis oceanica, Gr. crassaformis ronda* and *Gr. crassaformis viola. Gr. crassaformis hessi* is more quadrangular in equatorial view and the final chamber is usually more reduced. *Gr. crassaformis oceanica* and *ronda* have a more rounded peripheral margin and more inflated umbilical portion, while *ronda* alone has a relatively thickened test. *Gr. crassaformis oceanica* has greater chamber-rounding and a

less conical umbilical side than *ronda. Gr. crassaformis viola* is typically distinguished from *crassaformis s.s.* by the presence of a keel, more angular chambers and a more acute axial periphery. All variants exhibit close affiliation with, and gradation into the senior synonym.

Gr. crassaformis is probably descended from *Gr. crassula*, and ancestral to *Gr. crassaconica* and the *Gr. tosaensis-truncatulinoides* plexus.

Gr. crassacrotonensis Conato & Follador, is a junior synonym of this taxon.

Globorotalia crassaformis hessi Bolli and Premoli-Silva

Plate 1.7, figures 25-26.

Globorotalia crassaformis hessi, Bolli and Premoli-Silva, 1973

Globorotalia crassaformis 'B' Bolli, 1970

Diagnosis and remarks: see *Gr. crassaformis.*

Globorotalia crassaformis oceanica Cushman and Bermudez

Plate 1.7, figures 7-11.

Globorotalia (Turborotalia) crassaformis oceanica Cushman and Bermudez, 1949.

Diagnosis and remarks: see *Gr. crassaformis.*

Globorotalia crassaformis ronda Blow

Plate 1.7, figures 27-29.

Globorotalia (Turborotalia) crassaformis ronda Blow, 1969.

Diagnosis and remarks: see *Gr. crassaformis.*

Globorotalia crassaformis viola Blow

Plate 1.7, figures 12-17.

Globorotalia (Globorotalia) crassula viola Cushman and Bermudez, 1949.

Diagnosis and remarks: see *Gr. crassaformis.*

Globorotalia crassula Cushman and Stewart

Plate 1.7, figures 1-6.

Globorotalia crassula Cushman and Stewart, 1930

Diagnosis: Gr. crassula is biconvex and rounded-conical in axial periphery. It possesses a weak keel, pustules on both sides and a lobulate-subquadrate equatorial periphery.

Remarks: The holotype of *Gr. crassula* is unkeeled, but Blow's (1969) refigured holotype does have a keel. Bolli and Saunders (1985) suggest this feature makes it unlikely to be the ancestor of the non-keeled *Gr. crassaformis*, however, the subspecies *viola* is keeled.

Broad test form shows close similarity with the *Gr. crassaformis spp.* and ancestry of these forms from *Gr. crassula* is supported by the cladistic analyses in Chapter 6. *Gr. crassula* may be descended from and linked to the hirsutellids through *Gr. cibaoensis*.

Gr. aemiliana Colalongo and Sartoni, and *Gr. crotonensis* Conato and Follador, probably represent phenotypic variants of *Gr. crassula* (Kennett and Srinivasan, 1983).

Globorotalia tosaensis (Takayangi and Saito)

Plate 1.8, figures 14-19.

Globorotalia tosaensis Takayangi and Saito, 1962

Diagnosis: Gr. tosaensis is conical with a flat spiral side, circular equatorial periphery and the axial periphery is sub-rounded to sub-acute. The umbilicus is deep and narrow, test is pustulose, and spiral sutures are straight-curved.

Remarks: Gr. tosaensis tenuitheca is primarily distinguished from *Gr. tosaensis s.s.* by the presence of fused pustules together with sharper curvature and lesser incision depth of the spiral sutures. These characters are all within the realms of phenotypic variability.
Gr. tosaensis probably gave rise to *Gr. truncatulinoides*.

Globorotalia tosaensis tenuitheca Blow

Plate 1.8, figures 20-22.

Globorotalia (Turborotalia) tosaensis tenuitheca Blow, 1969.

Diagnosis and remarks: See *Gr. tosaensis.*

Globorotalia truncatulinoides (d'Orbigny)

Plate 1.8, figures 7-10.

Rotalina truncatulinoides d'Orbigny, 1839

Globorotalia (G.) truncatulinoides truncatulinoides (d'Orbigny), Blow. 1969. (Neotype)

Diagnosis: Gr. truncatulinoides has a keeled pustulate test with a circular equatorial periphery and acute axial periphery. The spiral side is flat to slightly concave, while the umbilical side is strongly-conical. Spiral sutures are straight and aperture is narrow and deep.

Remarks: The variant *Gr. truncatulinoides excelsa* has a more acute peripheral keel, a more open umbilicus and fewer pustules covering the surface, compared to *truncatulinoides sensu stricto. Gr. truncatulinoides pachytheca* possesses more rounded chambers and a less conical umbilical side.

All these variations fall within the realms of natural morphological variation.

Globorotalia truncatulinoides **excelsa** Sprovieri, Ruggieri and Unti

Plate 1.8, figures 1-6.

Globorotalia truncatulinoides excelsa Sprovieri, Ruggieri and Unti, 1980.

Diagnosis and remarks: See *Gr. truncatulinoides.*

Globorotalia truncatulinoides pachytheca Blow

Plate 1.8, figures 11-13.

Globorotalia (G.) truncatulinoides pachytheca Blow, 1969.

Diagnosis and remarks: See *Gr. truncatulinoides.*

1.3 Discussion of the taxonomy of *Globorotalia*

1.3.1 Early evolution

The early evolution of the Neogene *Globorotalia* is an issue of great debate, which includes many different hypotheses. Jenkins (1965) defined the origin of *Gr. praescitula* (one of the earliest globorotaliids) as 'cryptic'. Cifelli (1969) later produced a 'general aspect' of evolution of the Neogene planktonic assemblages (Figure 1.5).

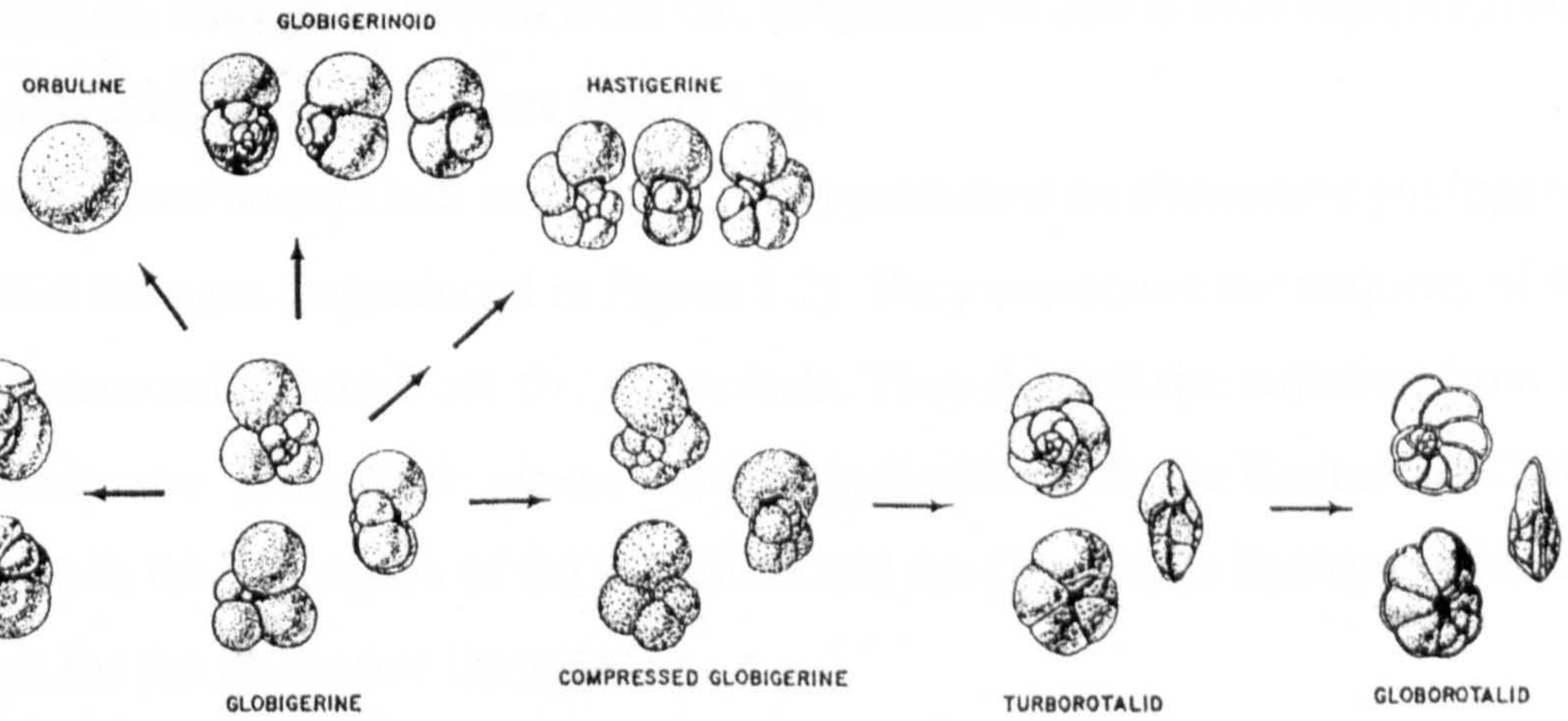

Figure 1.5. 'General aspect of planktonic faunas in the Middle Miocene', adapted from Cifelli (1969).

The terms used by Cifelli refer to general morphological forms and not taxonomic distinctions. The 'turborotalid' forms describe those with compressed angular chambers, while the 'globorotalid' forms denote those possessing the same characters with the addition of a peripheral keel. Cifelli's broad evolutionary aspect formed the basis for later concepts of globorotaliid evolution.

The Neogene keeled forms probably arose from the more conservative globigerines through gradual axial compression and keel construction (as above). The fohsellid globorotaliids are a group that demonstrates Cifelli's transition from compressed globigerines to globorotaliid form well. This group constitutes a single evolving anagenetic lineage consisting of initially unkeeled, to progressively more keeled and compressed morphologies. The menardellids also follow the 'turborotalid' to 'globorotalid' pathway, however, the globoconellids exemplify the reverse of Cifelli's trend, thus this 'aspect' does not always hold true.

In the published phylogeny of Srinivasan and Kennett (1981), *Gr. (F) kugleri* (later assigned to *Paragloborotalia* Cifelli) is ancestral to the fohsellids; *Gr. praescitula* is ancestral to the menardellids; *Gr. paralenguanensis* is ancestral to the *Gr. tumida* lineage; *Gr. crassaformis* is ancestral to the truncorotaliids and *Gr. cibaoensis* is ancestral to the hirsutellids. Srinivasan and Kennett's (1981) 'temperate areas' phylogeny derives the globoconellids from *Gr. nana* through *Gr. praescitula* and *praemenardii*. Their phylogeny is reproduced in Figure 1.6.

Kennett and Srinivasan (1983) later derived *Gr. praescitula* (and therefore everything else descended from it) from *"Gr." nana*. They also proposed that the *Globorotalia s.s.* lineage is derived from *Gr. lenguanensis* and is thus separate from the four (possibly) related lineages (see Figure 1.7).

Three years later Cifelli and Scott (1986) published an alternative phylogeny of the globorotaliid lineages (reproduced in Figure 1.2). They too derive the majority of the Neogene globorotaliid taxa from *Gr. praescitula*. They dubbed the radiation from this morphospecies the '*praescitula* plexus'. Other similarities with the Kennett and Srinivasan scheme include the separation of the fohsellids and the *Gr. tumida* lineages, with the same progenitors for the respective lineages.

Unlike Kennett and Srinivasan (1983), they did not consider the jenkinsellid or tenuitellid taxa. Differences include the separation of the '*zealandica* lineage' and the inclusion of a number of Mediterranean morphospecies, which represent subtle variations on established taxa, e.g. *Gr. mediterranea* is a *Gr. miocenica* variant.

Fordham's (1986) phylogeny included many fewer of the taxa and lineages than in figures 1.2, 1.6 and 1.7, and suggested *G. kugleri* as the primary progenitor to the Neogene globorotaliids and *Subbotina linaperta* as the earliest ancestor to all Neogene planktonic foraminifera. Fordham approached phylogeny from a stratophenetic lineage point of view. In his phylogeny (Figure 1.8) the broad subgeneric groupings of Bandy are still apparent although *Gr. praescitula* is not included.

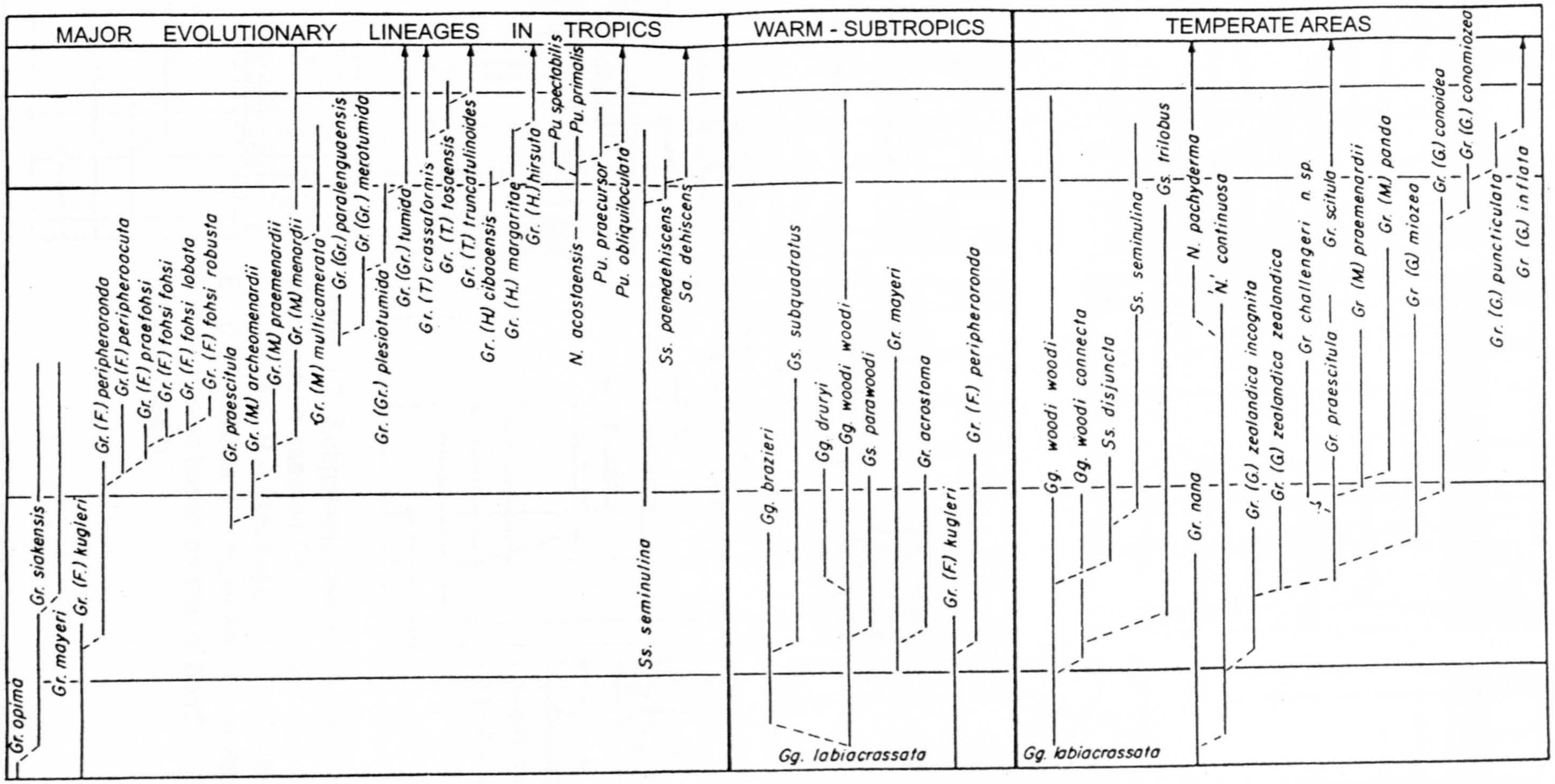

Figure 1.6. Phylogeny of Neogene *Globorotalia* adapted from Srinivasan and Kennett (1981), showing the main globorotaliid lineages.

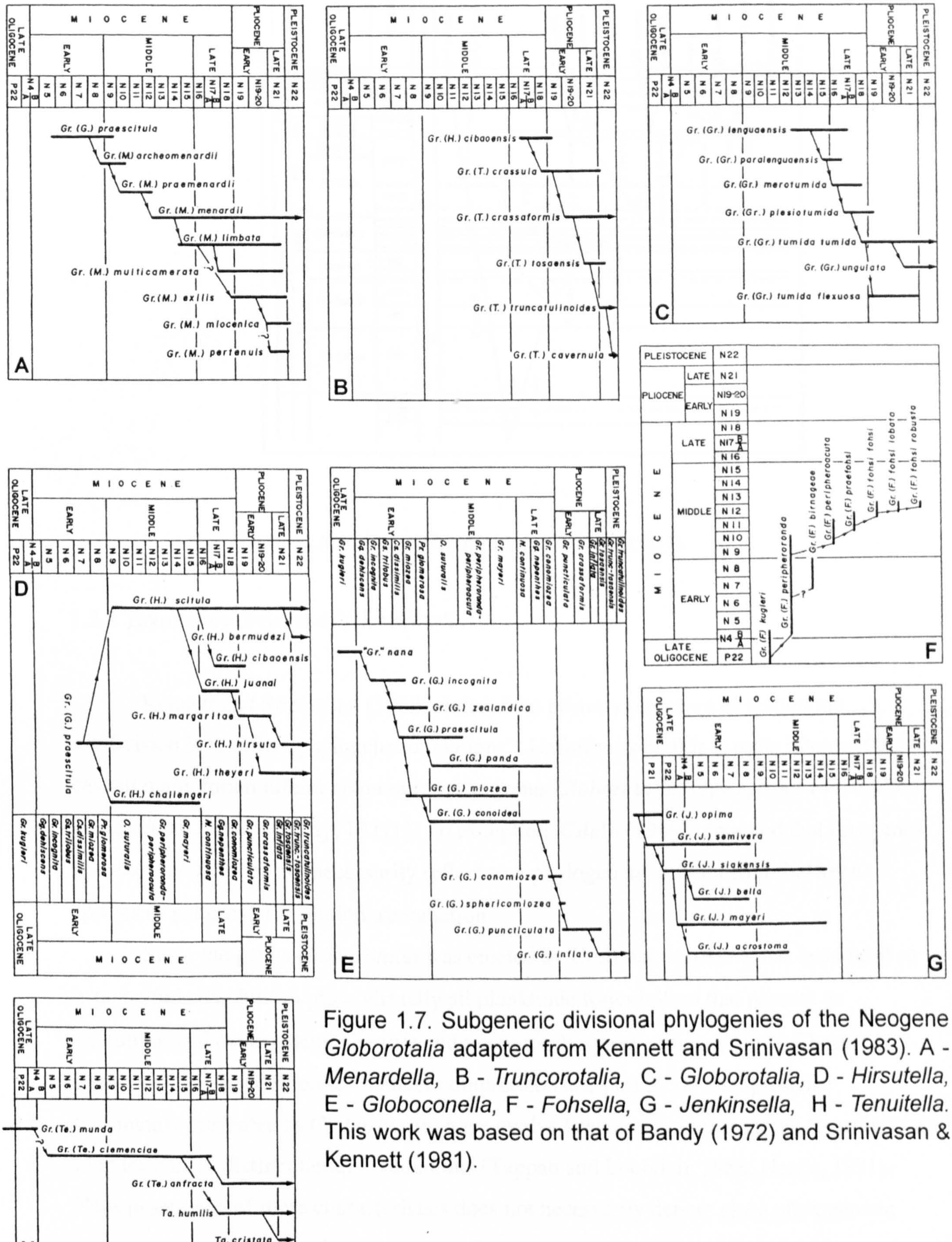

Figure 1.7. Subgeneric divisional phylogenies of the Neogene *Globorotalia* adapted from Kennett and Srinivasan (1983). A - *Menardella*, B - *Truncorotalia*, C - *Globorotalia*, D - *Hirsutella*, E - *Globoconella*, F - *Fohsella*, G - *Jenkinsella*, H - *Tenuitella*. This work was based on that of Bandy (1972) and Srinivasan & Kennett (1981).

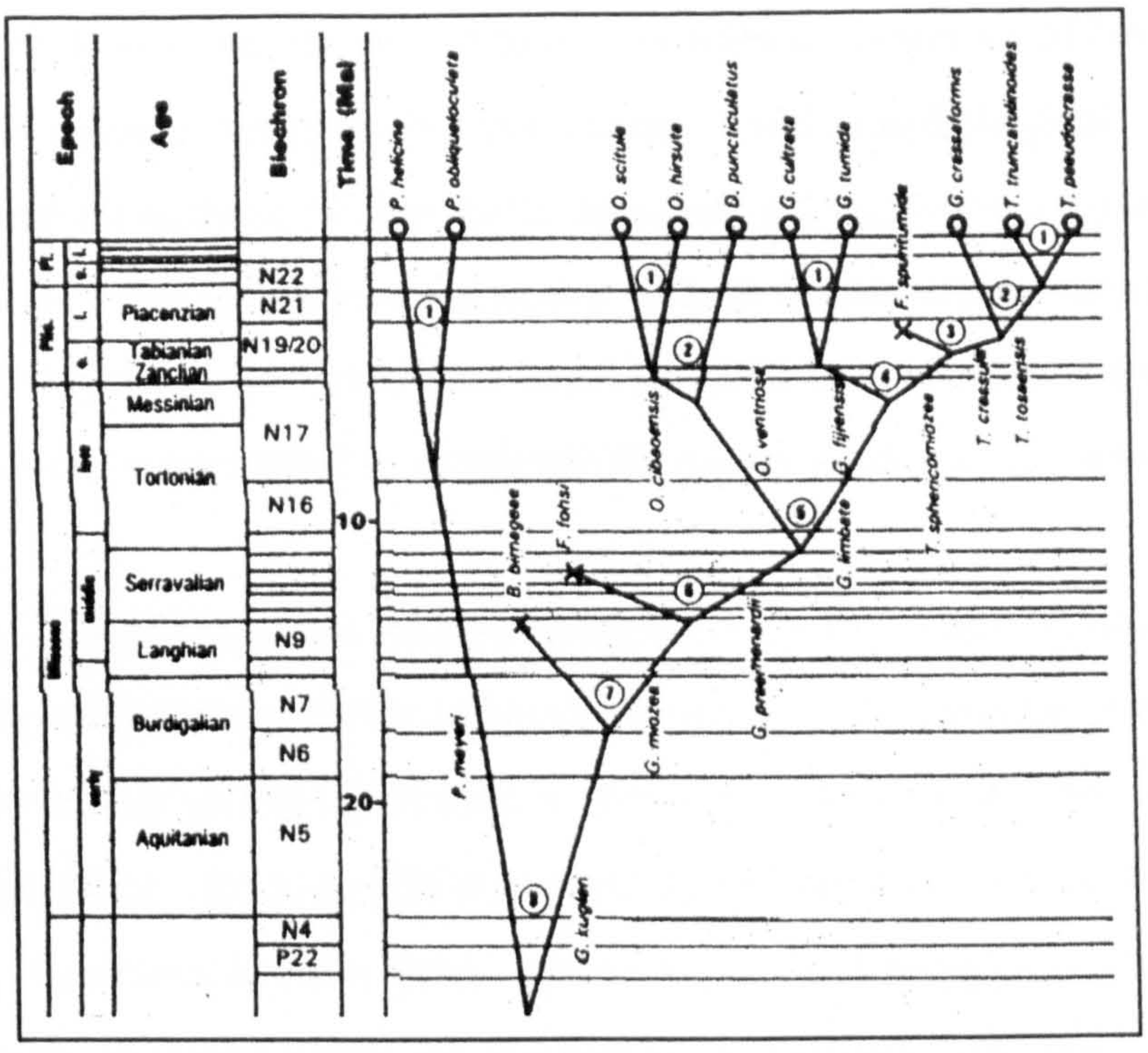

Figure 1.8. Globorotaliid phylogeny of Fordham (1986).

1.3.2 Taxonomic division of *Globorotalia*

Kennett and Srinivasan (1983) stated: "the primary objective of taxonomic subdivision is to reflect phylogenetic relations". Unfortunately, this is quite often not the case in many foraminiferal taxonomies. The genus *Globorotalia* (type species *Pulvinulina menardii* var. *tumida* Brady, 1877) is no exception. Cifelli (1969) remarked that this genus [*Globorotalia*] "does not necessarily reflect true phylogenetic relationships between species or patterns of evolutionary radiation".

Since the genus *Globorotalia* was erected by Cushman in 1927 it has been used as a 'taxonomic dustbin' to place virtually all planktonic foraminifera that possess an extraumbilical to peripheral aperture and a low-trochospiral coiling attitude. These characteristics, in addition to chamber compression and peripheral keel presence (commonly attributed to *Globorotalia*) have evolved separately in planktonic foraminifera in at least three distinct iterative radiations (Tappan and Loeblich, 1988; Norris, 1991). Thus possession of these characteristics does not necessarily denote close phylogenetic relationships. As a result, for many years Cretaceous and Palaeogene taxa with these characteristics were also included in the genus (e.g. species now assigned to *Globotruncana, Globotruncanita, Dicarinella, Morozovella, Turborotalia,* etc).

Globorotalia is now generally agreed to be restricted to a number of Neogene lineages. Regional divergence, intrapopulational variation and morphological intergradation are inherent in these *Globorotalia* lineages, and excessive taxonomic division has resulted in an unsatisfactory taxonomy. This is further complicated by authors working on localised areas and restricted time intervals, who have created taxonomic synonyms. Various authors attempted to subdivide the genus *Globorotalia* with varying degrees of success.

Blow (1969) divided the genus into two subgenera *Globorotalia (Globorotalia)* and *Globorotalia (Turborotalia)* based on the presence or absence of a peripheral keel. This is a purely artificial taxonomic grouping because it split some well-documented continuous morphological lineages (e.g., the fohsellid bioseries) by placing the ancestral *Gr. peripheroacuta* and the descendent *Gr. fohsi robusta* in separate subgenera. Furthermore, the nomen *Turborotalia* was previously erected by Cushman and Bermudez (1949), as a subgenus of *Globorotalia* (type species *Globorotalia centralis* Cushman and Bermudez) to contain the Palaeogene lineage from *T. frontosa* to *T. cunialensis*. This exemplifies the sometimes wantonly non-phylogenetic application of nomenclature that often appears in foraminiferal taxonomy.

With the ongoing work of the DSDP, then the ODP, it became apparent that maybe there were several distinct lineages within the Neogene *Globorotalia* with possibly separate ancestry. To remedy the erroneous taxonomy, Bandy (1972, 1975) and Fleisher (1974) suggested a series of subgenera that would divide *Globorotalia* to give a more accurate reflection of the underlying phylogeny: *Fohsella, Globoconella, Globorotalia, Hirsutella, Menardella, Tenuitella* and *Truncorotalia*. Each subgenus contains taxa with a number of different morphological types that appear to constitute a phylogenetic continuum from ancestor to descendent. Therefore, unlike traditional taxonomies, these groups cannot be defined easily by a small number of specific morphological characteristics that all the taxa possess. This subgeneric construct was intended to be purely phylogenetic and not to have any immediate biostratigraphic utility. A comprehensive review of these groups can be found in Kennett and Srinivasan (1983), in which the authors added a further subgenus, *Jenkinsella* (Figure 1.6). It should be noted that the jenkinsellids are now commonly placed in the genus *Neogloboquadrina* and not associated with *Globorotalia*.

Kennett and Srinivasan (1983) expanded and revised some of the relationships in this paper (Figure 1.7). In their work, the fohsellids, jenkinsellids and the tenuitellids represent isolated evolutionary lineages that were all initially placed in the genus *Globorotalia*. Their respective subgeneric names should be elevated to generic status because the taxa in these groups are now accepted as being unrelated to the remaining *Globorotalia* taxa (Kennett and Srinivasan, 1983). These authors unite the menardellids, truncorotaliids, hirsutellids and globoconellids as derived from *Gr. praescitula* (see Figure 1.7).

If all of these subgenera actually represent phylogenetically-distinct lineages then they are taxonomically valid as separate entities. On the other hand, if any of the lineages could be shown to be linked via a common ancestor to *Gr. tumida*, then Cushman's original genus would stand as the generic nomen of any taxa concerned.

N.B. Bandy's (1972) subgenera will be referred to as separate lineages, preceding the phylogenetic analyses presented in Chapter 6 that address the lineage relationships.

1.3.3 Controversies

1.3.3.1 A Globorotalia praescitula ancestor?

As discussed above, the origin of the Neogene *Globorotalia* is contentious. Some authors suggest that *Globorotalia praescitula* may have early links with a variety of the *Globorotalia zealandica* lineage species (Keller, 1981; Srinivasan and Kennett, 1981; Kennett and Srinivasan, 1983). On the other hand, there has been support for the derivation of the Neogene menardellid *Globorotalia* from the *Paragloborotalia,* a group of compressed, cancellate and sometimes spinose planktonic foraminifera lacking keels (McGowran, 1968; Kennett and Srinivasan, 1983; Cifelli and Scott, 1986; Scott *et al.*, 1990; Spezzaferri, 1994). This issue is also speculative. A possible paragloborotaliid 'honeycomb' surface texture is only relict in *Globorotalia praescitula* (see Plate 1.1, figures 17-19), and sometimes occurs on the earlier chambers of *Gr. scitula*, albeit in a weak form. This texture is termed pseudo-honeycombed for the purpose of the cladistic character definition in Chapter 6. None of the more derived morphospecies from the other globorotaliid lineages has this feature.

The phylogenies reproduced in figures 1.2 and 1.6-1.8 derive the fohsellids from the cancellate-spinose *Paragloborotalia kugleri* (Spezzaferri, 1991 presents

paragloborotaliid wall texture), thus, if *Gr. praescitula* can be shown to descend from this group it is possible that *Fohsella*, *Hirsutella*, *Menardella, Truncorotalia* and *Gr. tumida* lineage are all related. In this case the senior synonym *Globorotalia* would again replace these subgenera. At the present time, insufficient work has been carried out to support this notion, so phylogenetic hypotheses presented in this thesis infer no relationships more basal than *praescitula*. This matter is further complicated by isotopic data presented in Chapter 4, which may favour an ancestor to *Globorotalia praescitula* with benthic affinity.

1.3.3.2 The Globorotalia menardii type-specimen problem

It is generally agreed that the assignation of the *Gr. menardii* type specimen is erroneous (Bolli and Saunders, 1985). D'Orbigny (1826) originally described the species from a Rimini beach sand on the Italian Adriatic coast, which was assumed to be Holocene. No description or illustration was provided other than reference to a model ('no. 10') that was issued to private subscribers only. This original specimen is thought to have been a reworked Miocene contaminant, so Parker *et al.* (1865) applied the name '*Rotalia menardii* D'Orbigny' to select specimens dredged from offshore Isle of Man. Other variations on this nomen have been used. However in 1960, Banner and Blow recognised that Parker (Jones and Brady) were the first to make available the name credited to d'Orbigny. No specimens from Rimini were subsequently found in the collections of d'Orbigny, so Banner and Blow provided a lectotype from Holocene sediments from the Brady collection. Also from this collection came a neotype for *Rotalina cultrata* d'Orbigny (1839), which although originally described from modern sands, syntypes were not preserved. Thus Banner and Blow subjectively regarded *Rotalina cultrata* as the senior synonym of *Rotalina menardii* (Stainforth *et al.*, 1978).

Todd (1961) proposed rejection of this synonymy and retention of the more widely known '*Gr. menardii* (d'Orbigny)' because Banner and Blow did not act in accordance with the International Code for Zoological Nomenclature. Stainforth *et al.* (1978) later proposed a suppression of Brady's Isle of Man material in favour of a neotype from the Late Miocene Senigallia Section, south of Rimini for stratigraphic and geographic reasons.

Banner and Blow (1960) regarded *menardii* and *cultrata* as separate entities, while Stainforth *et al.* (1978) regarded them as synonymous. To further complicate the whole issue Bolli and Saunders isolated distinct Miocene *menardii* morphotypes, *Gr. menardii*

'A' and *Gr. menardii* 'B' for those forms that pre-date the Late Miocene and younger forms covered by *Gr. menardii.*

Despite the shambles surrounding the assignation of the *Gr. menardii* holotype it seems simplest to describe relevant populations with thicker keels and more robust tests as *Gr. menardii* (d'Orbigny), including Bolli's (1970) 'A' and 'B' morphotypes, which can only rarely be distinguished. Furthermore, the more recent taxon *Gr. cultrata* probably represents an ecophenotype and can be used to delineate the more delicately built specimens of *Gr. menardii.*

1.3.3.3 The 'Menardine' lineages

Brady (1877) first described *Pulvinulina menardii* (d'Orbigny) var. *tumida*, i.e. *Gr. tumida*. Later, Banner and Blow (1965) named and described *Globorotalia (G.) merotumida* and *Globorotalia (G.) tumida (Brady) plesiotumida*, and suggested the two taxa were ancestral to *Gr. tumida*. Blow (1969) then employed *Gr. lenguanensis* and *Gr. paralenguanensis* as the earliest taxa in this distinct evolutionary bioseries. These taxa are largely considered a distinct globorotaliid lineage.

In 1972 Bandy divided *Globorotalia* into a number of subgenera (see discussion in Section 1.3.2). One such lineage was *Globorotalia (Menardella)*, erected to unite the *Gr. praescitula-archeomenardii-praemenardii-menardii* bioseries, which is characterised by lenticular trochospiral tests with a prominent keel and a smooth surface texture.

Stainforth *et al.* (1975) later united these two apparently distinct lineages under the heading of 'Menardiform Globorotalias', which were described as "having many features in common, yet differing widely in other aspects". Kennett and Srinivasan (1983) then later described the *Globorotalia s.s.* lineage (*Gr. lenguanensis- Gr. merotumida- Gr. plesiotumida- Gr. tumida- Gr. flexuosa)* as sharing many characteristics in common with *Globorotalia (Menardella)*, but state that the two lineages are 'phylogenetically unrelated'.

Numerous other authors have also considered the unity of *Gr. tumida* and *Gr. menardii* as variants, intermediates or even as conspecific (see Ericson *et al.*, 1961, Bolli, 1970; Brönnimann and Resig, 1971; Stainforth *et al.*, 1975; Thompson, 1982; Kennett and Srinivasan, 1983). However, the phylogenetic separation of the two lineages is well-supported in the literature (Banner and Blow, 1965; Blow, 1969; Kennett and Srinivasan, 1983; Cifelli and Scott, 1986). Although Cifelli and Scott (1986) endorse the latter view,

their phylogeny in Figure 1.2 unites the menardellid and *Globorotalia s.s.* lineages under the heading 'menardine lineages'.

The menardellid and *Globorotalia s.s.* lineage taxa constitute prime zone fossil material for use in biostratigraphy, although as yet, a possible phylogenetic link between the two morphologically innovative lineages is unresolved. Studies presented in later chapters attempt to resolve this issue through morphometrics and various cladistic techniques.

1.3.3.4 The globoconellids

The majority of Bandy's *Globoconella* are regionally-restricted to the temperate realms (Kennett and Srinivasan, 1983) with the exception of *Gr. praescitula, Gr. puncticulata* and *Gr. inflata* (of which, *Gr. triangula* Theyer is probably a variant). Srinivasan and Kennett (1981), Kennett and Srinivasan (1983) and Cifelli and Scott (1986) regard this lineage as derived from *Gr. praescitula* in temperate waters, although there is disagreement about the placement of the species included in Cifelli and Scott's '*zealandica* lineage' and the relationships between the early evolution of the menardellids and the globoconellids. For example, from morphometroc analyses, Scott (1972) concluded that *Gr. praemenardii* and *Gr. miozea* should not be phylogenetically separated. Cifelli and Scott (1986) later placed *Gr. miozea* as the intermediate between *Gr. praescitula* and *Gr. praemenardii.* This publication also suggested *Gr. praemenardii* as the ancestor to the temperate *Gr. conoidea* lineage.

The fieldwork carried out in New Zealand (outlined in Section 1.4.4) sampled deposits intended to yield globoconellid assemblages for phylogenetic analysis; however, the samples showed low diversity and only truncorotaliids were present. Therefore, through absence of material to study, *Globoconella* was not included in the phylogenetic analyses presented in chapters 5 and 6.

1.4 Aims and account of this study

The purpose of this study is to investigate the evolution of the phylogenetically-linked Neogene globorotaliid foraminifera lineages in the context of the changing oceanic realm in which they lived. In it, evolution of the planktonic foraminifera is introduced through the analysis of a database containing recorded first appearance datums (FADs) and last occurrence datums (LODs). From this, absolute diversity, diversification rate,

extinction and speciation trends of the planktonic foraminifera are presented with further depth-habitat division. Miocene globorotaliid evolution is contextualised using quantitative analyses yielding data on Miocene oceanic palaeotemperature and sea level. Isotopic analysis of test calcite of globorotaliids is measured and used to calculate differential depth habitat temperatures throughout the Miocene. Morphometric and phylogenetic analyses are employed to address the intricacies of globorotaliid evolution and aid the optimisation of the taxonomy of the genus *Globorotalia*.

This thesis is divided into seven chapters, which are written as separate studies but which reference each other. A précis of the different projects the author has been involved with throughout the duration of study is given below.

1.4.1 Tanzania – September to October, 2000

The author was involved in the 3rd field season of a project working with the Tanzanian Petroleum Development Corporation (TPDC) in Dar-es-salaam put together by Dr. Paul Pearson, to sample and study the geology of Tanzanian coastal sediments. These Cretaceous to Neogene marine clays have long been known for the exceptional preservation of the foraminifera within them and therefore constituted ideal targets for isotopic analysis and palaeoceanographic/palaeoclimatic study (Blow and Banner, 1962; Blow, 1969). Collaborators on the Tanzanian expeditions were Dr. Paul Pearson, Dr. Peter Ditchfield and Dr. Kate Harcourt-Brown of the University of Bristol; Dr. Joyce Singano and Amina Karega from TPDC and Dr. Chris Nicholas from the University of Cambridge.

The author's research from this fieldwork yielded three exceptionally-preserved Neogene samples, isotopes from which were used to calculate Indian Ocean sea surface temperatures from Early and Middle Miocene timeslices. See Chapter 4 for results. This work is currently awaiting publication.

1.4.2 ODP Leg 194 – January to March, 2001

The author was offered the opportunity to sail as one of two shipboard biostratigraphers on Leg 194. The Leg sailed from Townsville (Australia) to Guam (Micronesia) and was commissioned to core the Marion Plateau on the edge of the Great Barrier Reef National Park, in the Coral Sea. The primary Leg objective was to determine

the magnitude of the Middle Miocene (~12.5–11.4 Ma) eustatic sea level fall to aid the calibration of the Phanerozoic sea level curve (see Shipboard Scientific Party, 2002a for results).

While onboard the JOIDES Resolution, biostratigraphical studies of the Marion Plateau sediments revealed some of the problems surrounding globorotaliid taxonomy and phylogeny. A number of quantitative techniques were then used to test published hypotheses and the validity of the recognised morphospecies using assemblages from Pacific ODP Site 871, and Atlantic Site 926, in addition to Leg 194 material.

The idea for using the morphometric extended eigenshape analysis method came later at the FORAMS 2002 international symposium in Perth (where the author presented some research) from a presentation given by Dr. Norman MacLeod of the British Natural History Museum. The data collection and analysis was carried out at the University of Bristol with the aid of Dr. MacLeod's software and correspondence.

The Post-cruise meeting was held in Granada (Spain) where the author presented the results of the phylogenetic and isotopic analyses presented in this thesis. This also led to future collaboration with Dr. Timothy White of Pennsylvania State University as part of a World University Network-funded project (WUN). The purpose of this project is to investigate a part of the shipboard biostratigraphy using dinoflagellates that was fundamental to the Leg 194 estimate of the Middle Miocene eustatic sea level fall. This will be carried out at Pennsylvania State University in early to mid 2003.

1.4.3 Smithsonian Museum of Natural History – January, 2002

Prior to carrying out fieldwork in New Zealand, the author visited the Cushman Laboratory for Foraminiferal Research to study some of the collections and type specimens (plesiotypes, hypotypes and topotypes) there to aid the author's morphospecies 'concepts'. These observations helped taxon-identification and character coding used to analyse the phylogenies of several Neogene globorotaliid lineages using cladistics, stratocladistics and stratophenetics.

1.4.4 New Zealand – January to February, 2002

The original premise behind this fieldwork season was to provide temperate-water globoconellid specimens to examine and aid the definition of characters for cladistic analysis of the Neogene *Globorotalia*. This trip also presented the opportunity to examine some of Graham Jenkins' original type material (primarily paratypes with the holotype of *Gr. conomiozea* Kennett) held at the Institute for Geological and Nuclear Sciences (IGNS) in Wellington. Perhaps more importantly the author was able to benefit from Dr. George Scott's extensive knowledge of Neogene planktonic foraminifera. Dr. Scott was able to recommended several sites from around New Zealand that would be potentially useful to sample.

Neogene material was sampled from Palliser Bay (North Island), and the South Island locations of Dovedale Stream, Pukeuri, Motornau River and Kapitea Creek. Unfortunately, the samples had low planktonic abundance and diversity, but truncorotaliids were present in the samples and these assemblages were imaged using scanning electron microscopy to aid definition of cladistic characters. Unfortunately, no globoconellids were present in the sampled material.

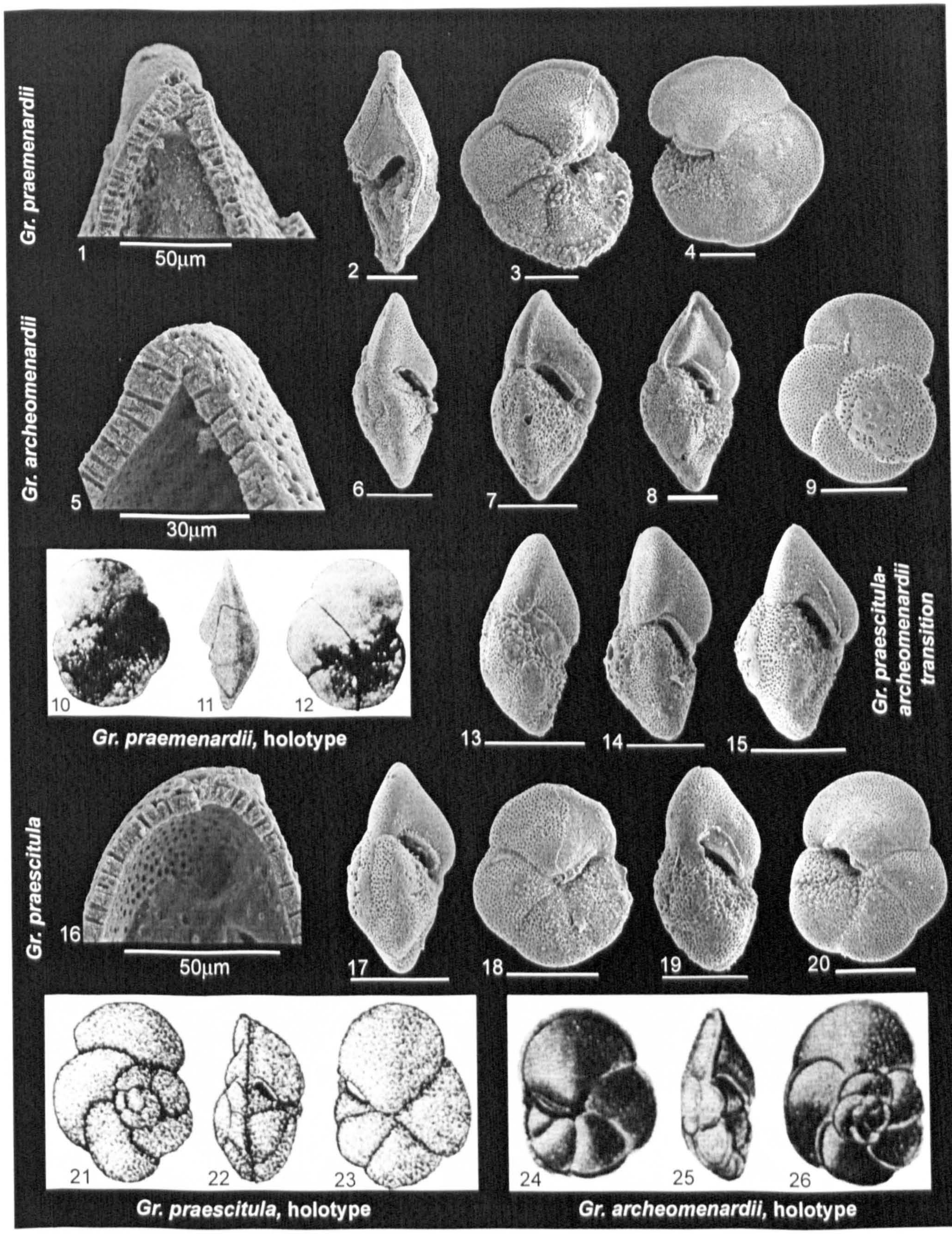

Plate 1.1. **1-4.** *Globorotalia praemenardii*, 871A 4H-1, 126-128 cm (Biozone M9, Middle Miocene). **5-9.** *Globorotalia archeomenardii*, 871A 8H-3, 59-63 cm (Biozone M5, Early Miocene). **10-12.** *Globorotalia praemenardii* Cushman & Stainforth, holotype. **13-15.** *Globorotalia archeomenardii - Globorotalia praesciutla*, 871A 8H-3/8H-4, 59-61 cm/59-63 cm (Biozone M5, Early Miocene). **16-20.** *Globorotalia praescitula*, 871A 8H-3, 59-61 cm (Biozone M5, Early Miocene). **21-23.** *Globorotalia praescitula* (Blow), holotype. **24-26.** *Globorotalia archeomenardii* Bolli, holotype. Images **1**, **5** and **16** show the development of the keel in the menardellid lineage. In edge view the *Gr. archeomenardii - Gr. praesciutla - Gr. praemenardii* lineage is marked by axial comression of the test and development of the keel. *Gr. archeomenardii - Gr. praesciutla* represent end-member morphologies, with a complete range of morphospecies in between (**10-12**). All scale bars are 100 µm unless otherwise stated.

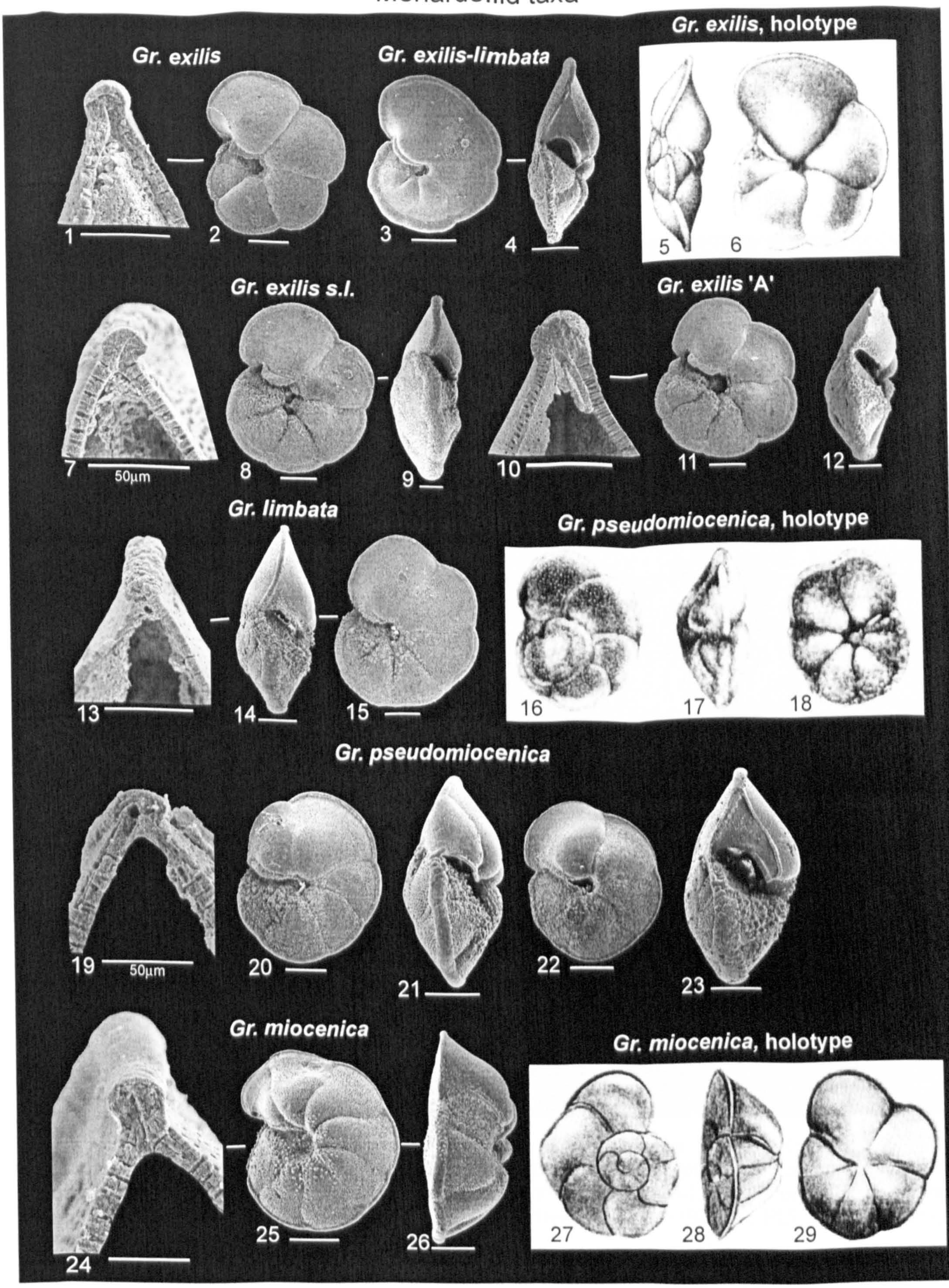

Plate 1.2. **1-2.** *Globorotalia exilis*, 926A 8H-4, 68-70 (Biozone PL4-5, Late Pliocene). **3-4.** *Gr. exilis aff. limbata*, 926A 11H-4, 70-72 cm (Biozone PL2, Early Pliocene). **5-6.** *Gr. exilis* Blow, holotype. **7-9.** *Globorotalia exilis s.l.*, 926A 16H-6, 60-62 cm (Biozone PL1, Early Pliocene). **10-12.** *Globorotalia exilis* 'A', 926A 16H-6, 60-62 cm (Biozone PL1, Early Pliocene). **13-15.** *Globorotalia limbata*, 1195A 6H-6, 10-12 cm (Biozone PL3, Late Pliocene). **16-28.** *Globorotalia pseuodmiocenica* Bolli & Bermudez, holotype. **19-23.** *Globorotalia pseuodmiocenica*, 1195A 5H-5, 10-12 cm (Biozone PL3, Late Pliocene). **24-26.** *Globorotalia miocenica*, 926A 8H-4, 68-70 cm (Biozone PL4-5, Late Pliocene). **27-29.** *Globorotalia miocenica* Palmer, holotype. All scale bars are 100 µm unless otherwise stated.

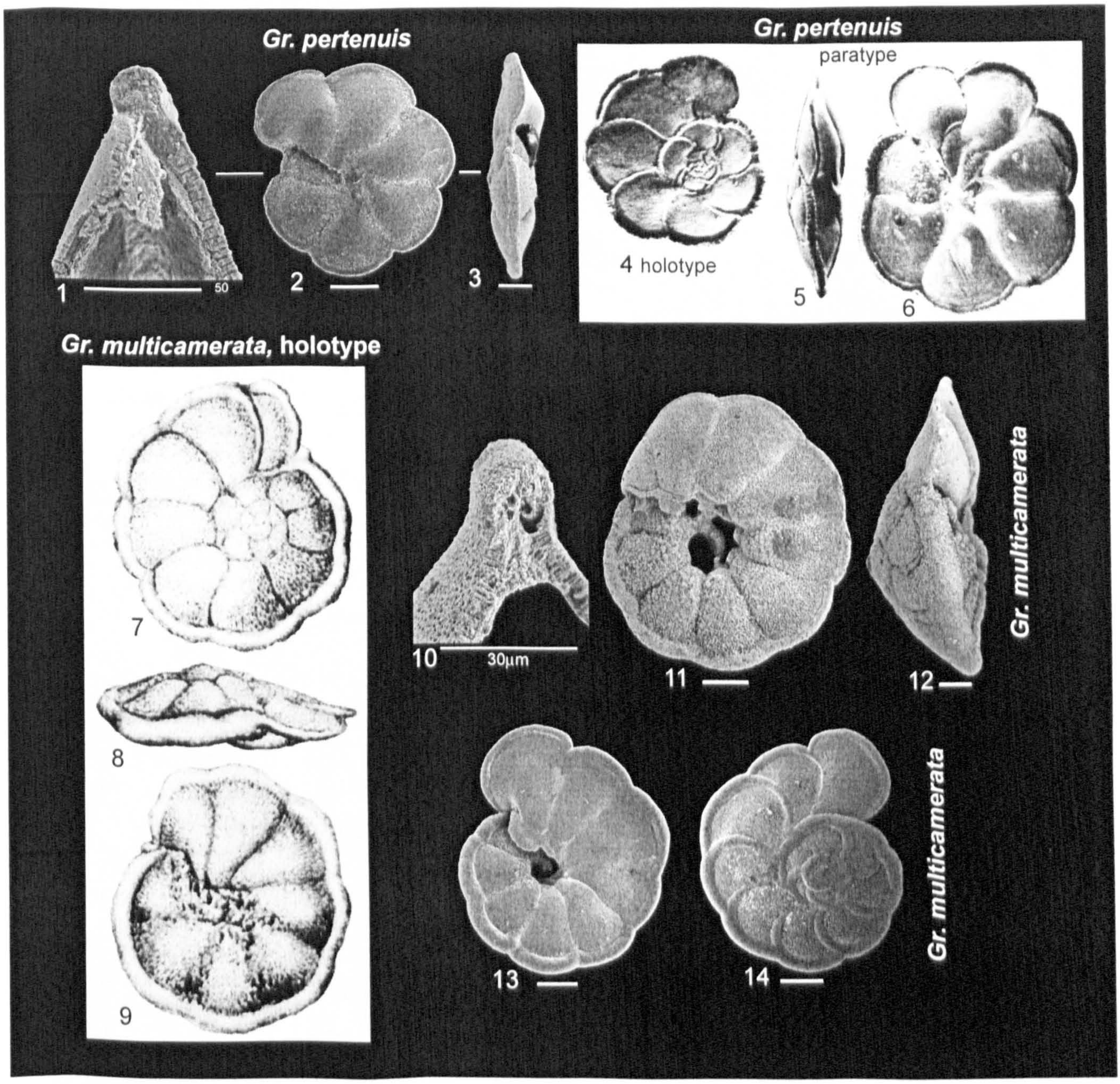

Plate 1.3. **1-3.** *Globorotalia pertenuis,* 926A 9H-6, 75-76 cm (Biozone PL4-5, Late Pliocene). **4-6.** *Globorotalia pertenuis* Beard, holoype (4), and paratype (5-6). **7-9.** *Globorotalia multicamerata* Cushman & Jarvis, holotype. **10-12.** *Globorotalia multicamerata,* 1195A 4H-5, 10-12 cm (Biozone PL5-6, Late Pliocene). **13-14.** *Globorotalia multicamerata s.l.,* 926A 11H-4, 70-72 cm (Biozone PL2, Early Pliocene). All scale bars are 100 µm unless otherwise stated.

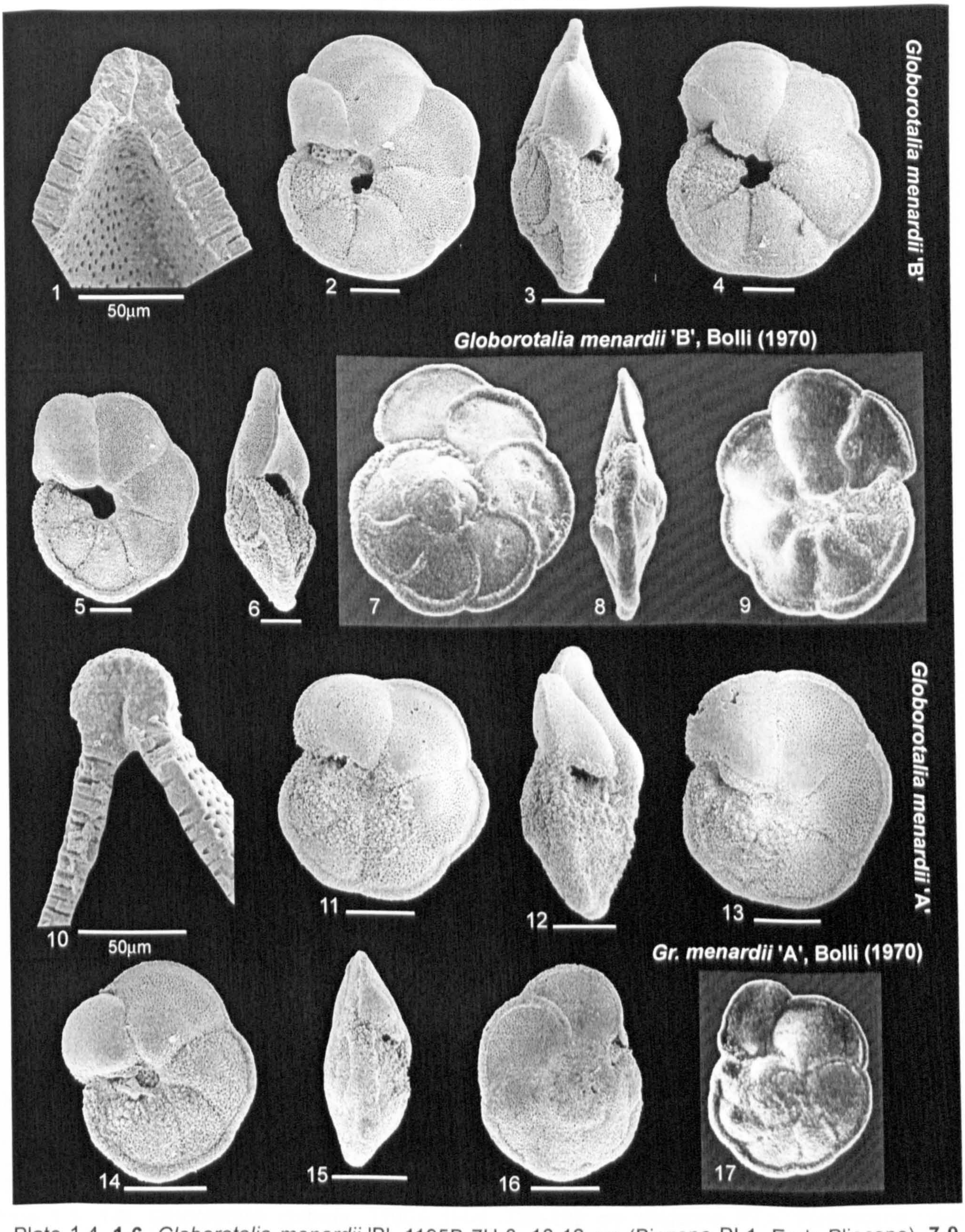

Plate 1.4. **1-6.** *Globorotalia menardii* 'B', 1195B 7H-3, 10-12 cm (Biozone PL1, Early Pliocene). **7-9.** *Globorotalia menardii* 'B', as figured in Bolli (1970). **10-16.** *Globorotalia menardii* 'A', 1195B 15H-1, 10-12 cm (Biozone M13, Late Miocene). **17.** *Globorotalia menardii* 'A', Bolli (1970). The primary morphological differences as stipulated by Bolli (1970) are: *Gr. menardii* 'A' is smaller with 5-6 chambers (against 6-7.5), and it has a more spherical (less lobulate) test and thinner peripheral keel. All scale bars are 100 µm unless otherwise stated.

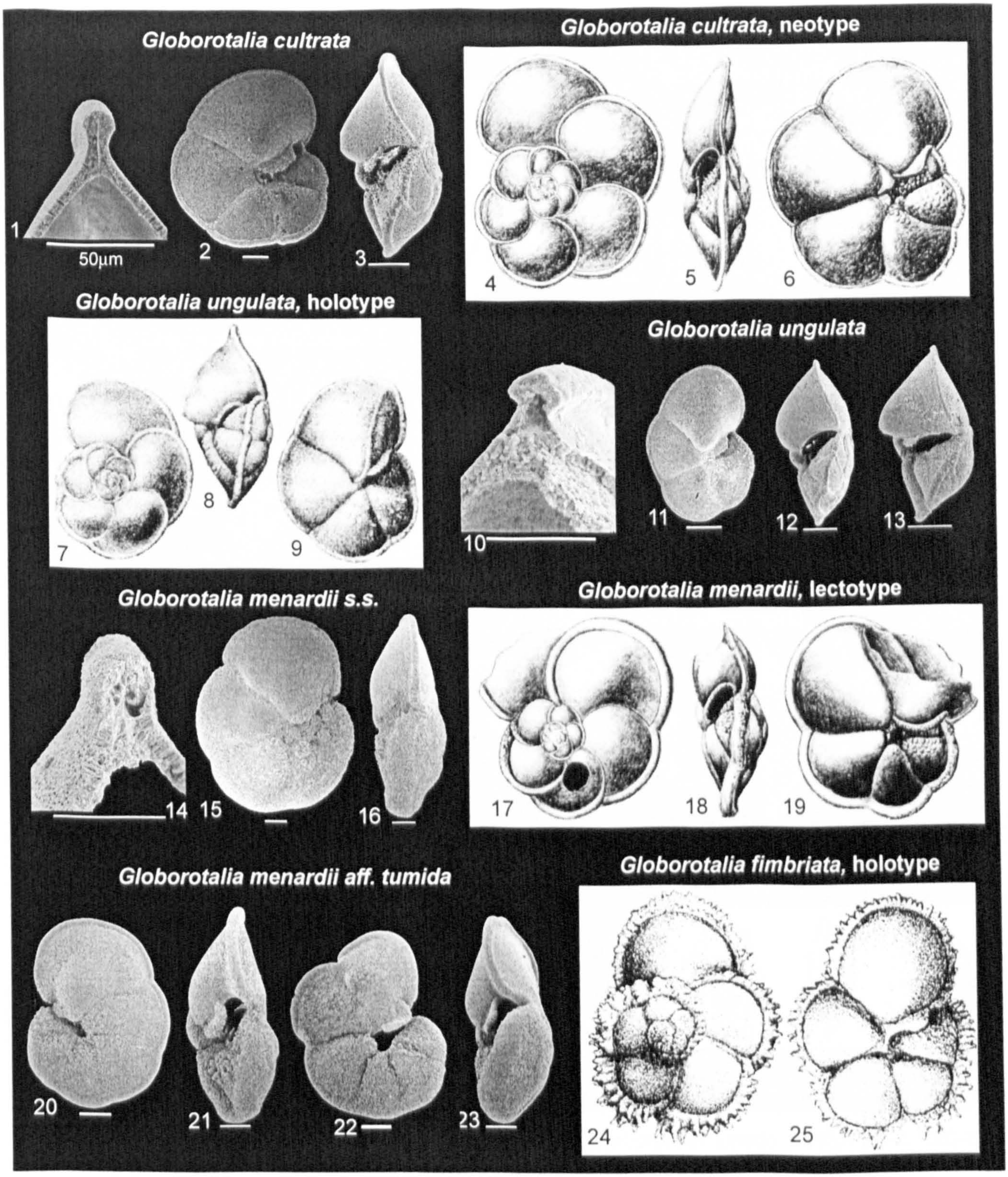

Plate 1.5. **1-3.** *Globorotalia cultrata*, 1195A 1H-1, 120-122 cm (Biozone PT1, Pleistocene). **4-6.** *Globorotalia cultrata* (d'Orbigny), neotype. **7-9.** *Globorotalia ungulata* Bermudez, holotype. **10-13.** *Globorotalia ungulata*, 1195A 2H-2, 120-122 cm (Biozone PT1, Pleistocene). **14-16.** *Globorotalia menardii s.s.*, 1195A 2H-2, 120-122 cm (Biozone PT1, Pleistocene). **17-19.** *Globorotalia menardii* (Parker, Jones & Brady) Banner & Blow, lectotype. **20-23.** *Globorotalia menardii aff. tumida*, 926A 2H-2, 70-72 cm (Biozone PT1, Pleistocene). **24-25.** *Globorotalia fimbriata*, holotype. All scale bars are 100 µm unless otherwise stated.

Globorotalia s.s. lineage taxa

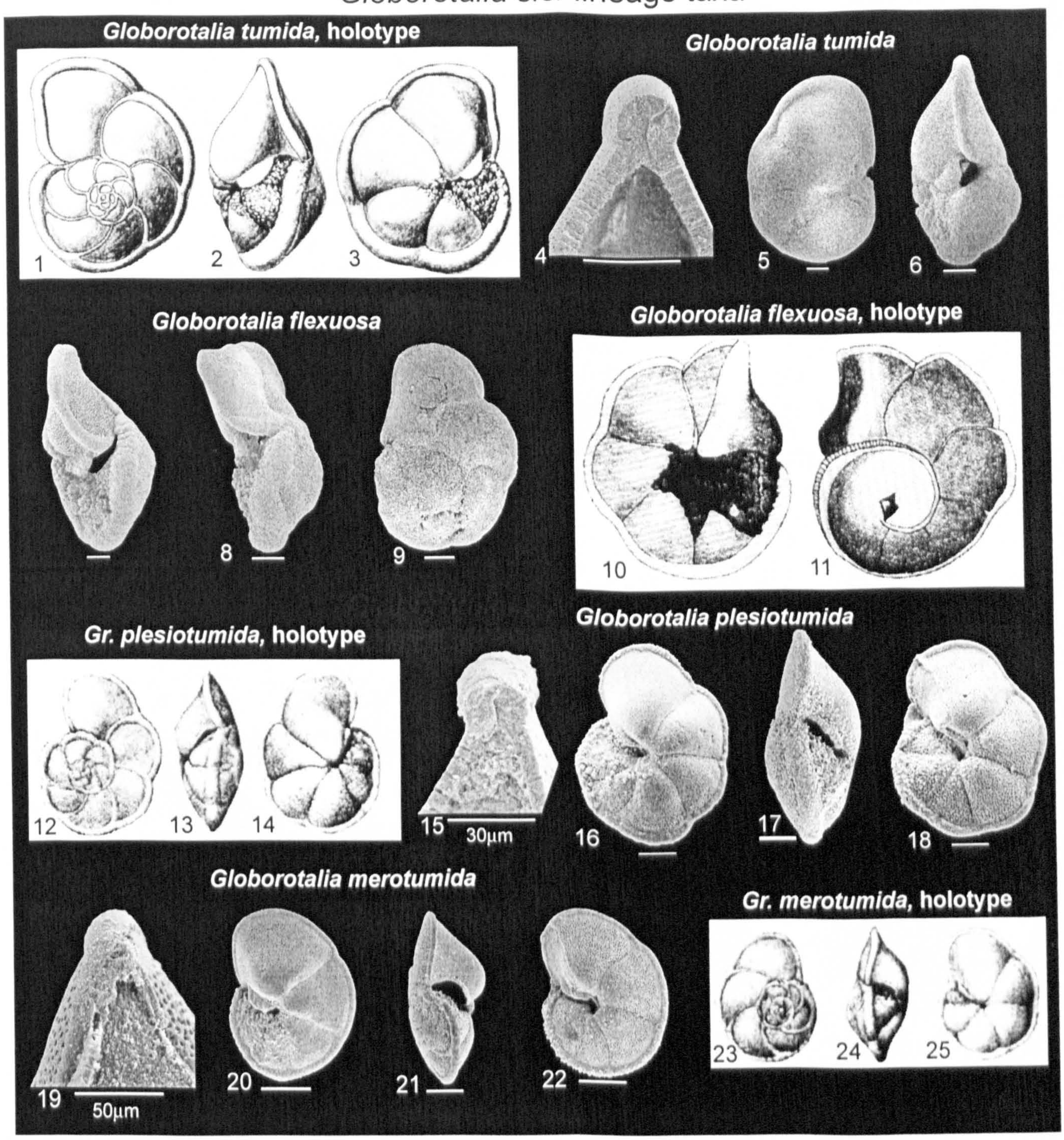

Plate 1.6. **1-3.** *Globorotalia tumida* (Brady), lectotype. **4-6.** *Globorotalia tumida*, 1195A 2H-2, 120-122 (Biozone PT1, Pleistocene). **7-9.** *Globorotalia flexuosa,* 926A 2H-2, 70-72 cm (Biozone PT1, Pleistocene). **10-11.** *Globorotalia flexuosa* (Koch), holotype. **12-14.** *Globorotalia plesiotumida* Banner & Blow, holotype. **15-18.** *Globorotalia plesiotumida,* 926A 16H-6, 60-62 cm (Biozone PL1, Early Pliocene). **19-22.** *Globorotalia merotumida,* 1195A 9H-1, 35-37 cm (Biozone PL1, Early Pliocene). **23-25.** *Globorotalia merotumida* Banner & Blow, holotype. All scale bars are 100 µm unless otherwise stated.

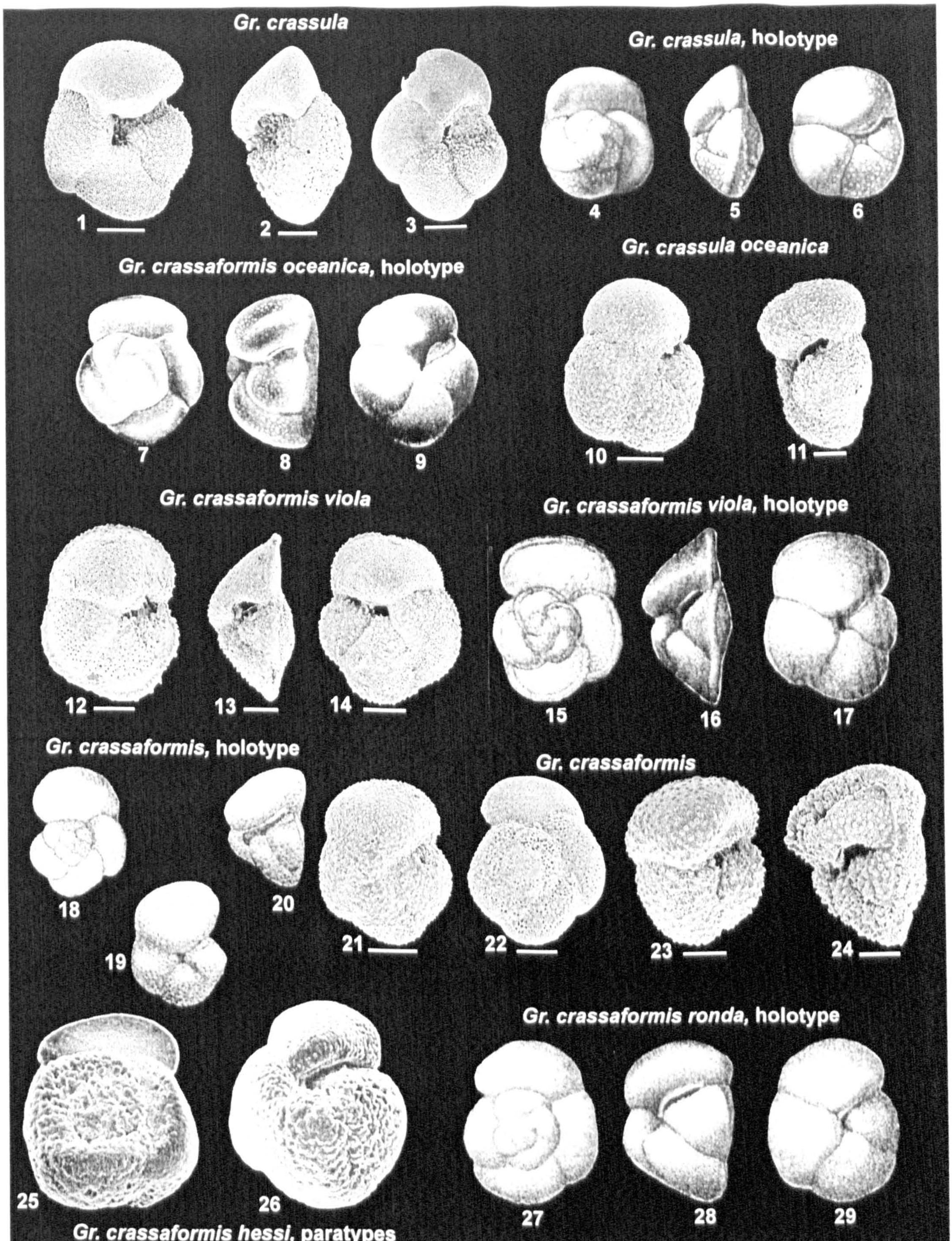

Figure 1.7. **1-3.** *Gr. crassula*, DS02KC04 (Early Pliocene). **4-6.** *Gr. crassula* Cushman & Stewart, holotype. **7-9.** *Gr. crassaformis oceanica* Cushman & Bermudez, holotype. **10-11.** *Gr. crassaformis oceanica*, DS02KC06 (Early Pliocene). **12-14.** *Gr. crassaformis viola*, DS02KC05 (Early Pliocene). **15-17.** *Gr. crassaformis viola* Blow, holotype. **18-20.** *Gr. crassaformis* (Galloway & Wissler), holotype. **21-24.** *Gr. crassaformis*, DS02KC01 (Early Pliocene). **25-26.** *Gr. crassaformis hessi* (Bolli & Premoli Silva), paratypes. **27-29.** *Gr. crassaformis ronda* Blow, holotype. All scale bars represent 100 μm.

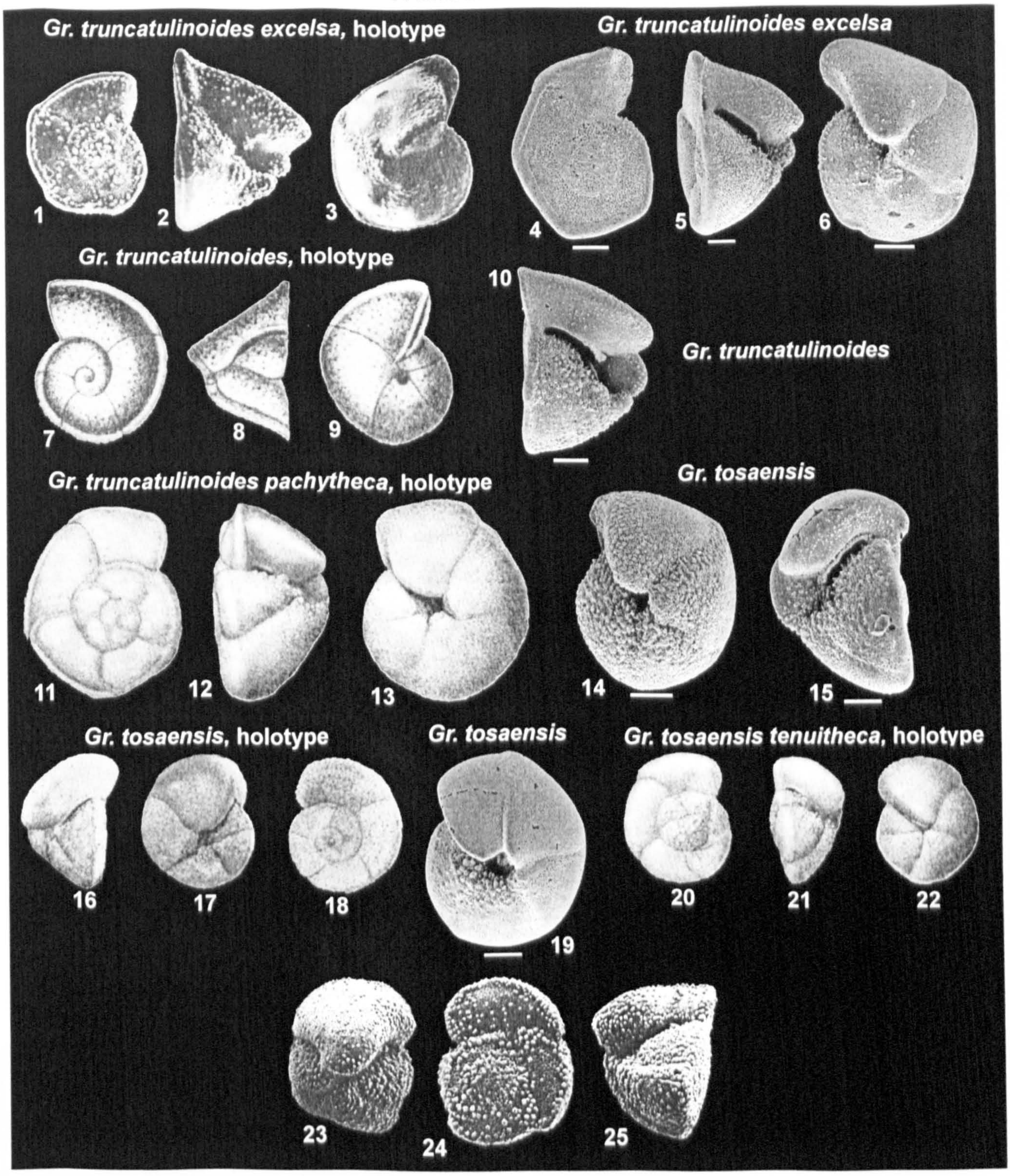

Plate 1.8. **1-3.** *Gr. truncatulinoides excelsa* Sprovieri & Ruggieri, holotype. **4-6.** *Gr. truncatulinoides excelsa*, 1195A 1H-3 45-47 cm (Biozone PT1, Pleistocene). **7-9.** *Gr. truncatulinoides* (d'Orbigny), holotype. **10.** *Gr. truncatulinoides*, 1195A 3H-7 10-12 cm (Biozone PT1, Pleistocene). **11-13.** *Gr. truncatulinoides pachytheca* Blow, holotype. **14-15.** *Gr. tosaensis*, 1195A 4H-1 10-12 cm (Biozone PL4, Late Pliocene). **16-18.** *Gr. tosaensis* Takanyanagi & Saito, holotype. **19.** *Gr. tosaensis*, 1195A 1H-3 45-47 cm (Biozone PT1, Pleistocene). **20-22.** *Gr. tosaensis tenuitheca* Blow, holotype. **23-25.** *Gr. crassaconica* Hornibrook, holotype. Scale bars represent 100 μm.

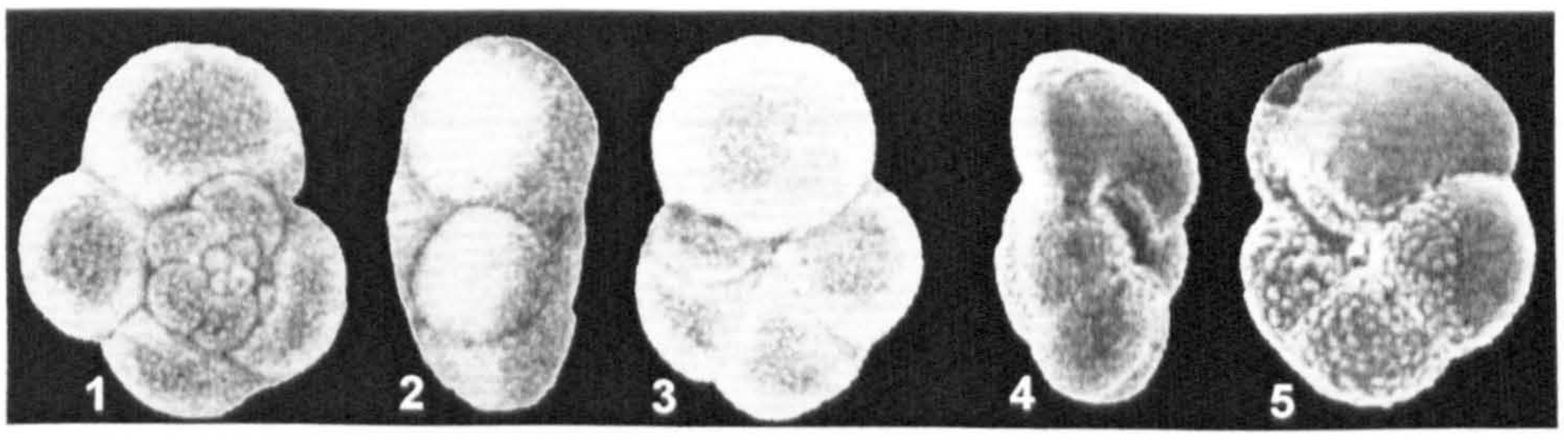

Gr. juanai, holotype

Gr. scitula

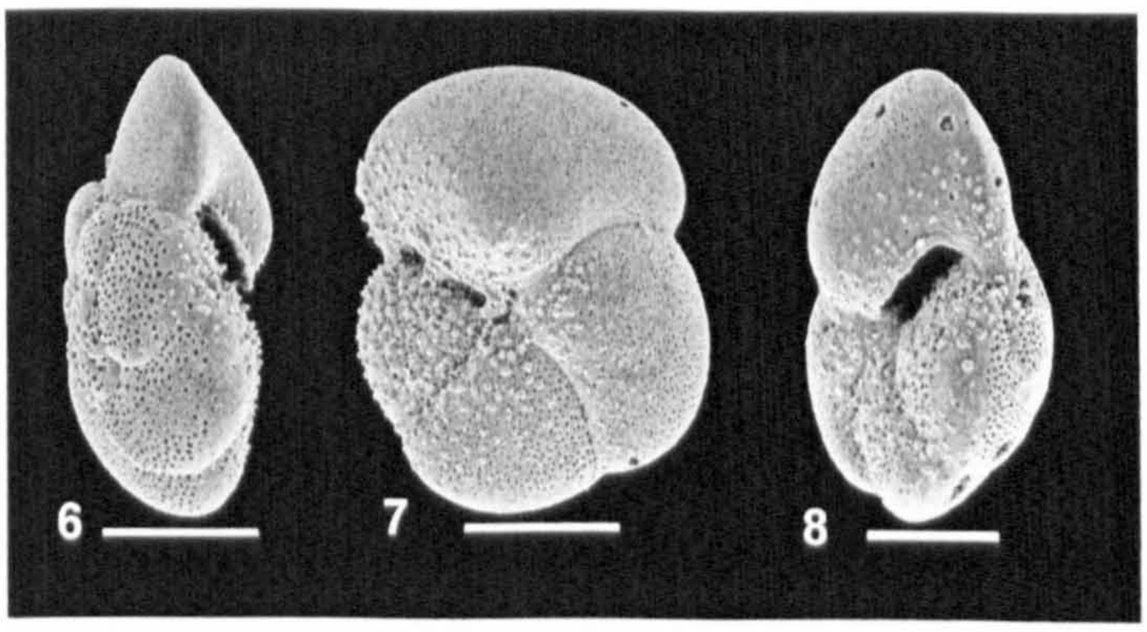

Gr. scitula, holotype

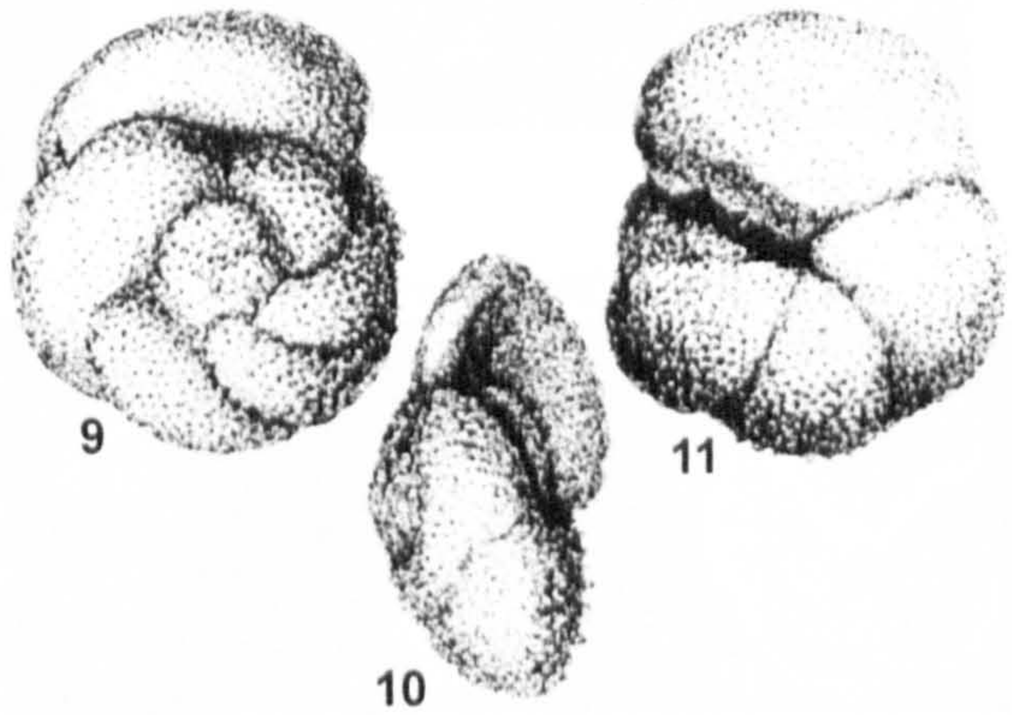

Gr. hirsuta, holotype

Gr. scitula gigantea, holotype

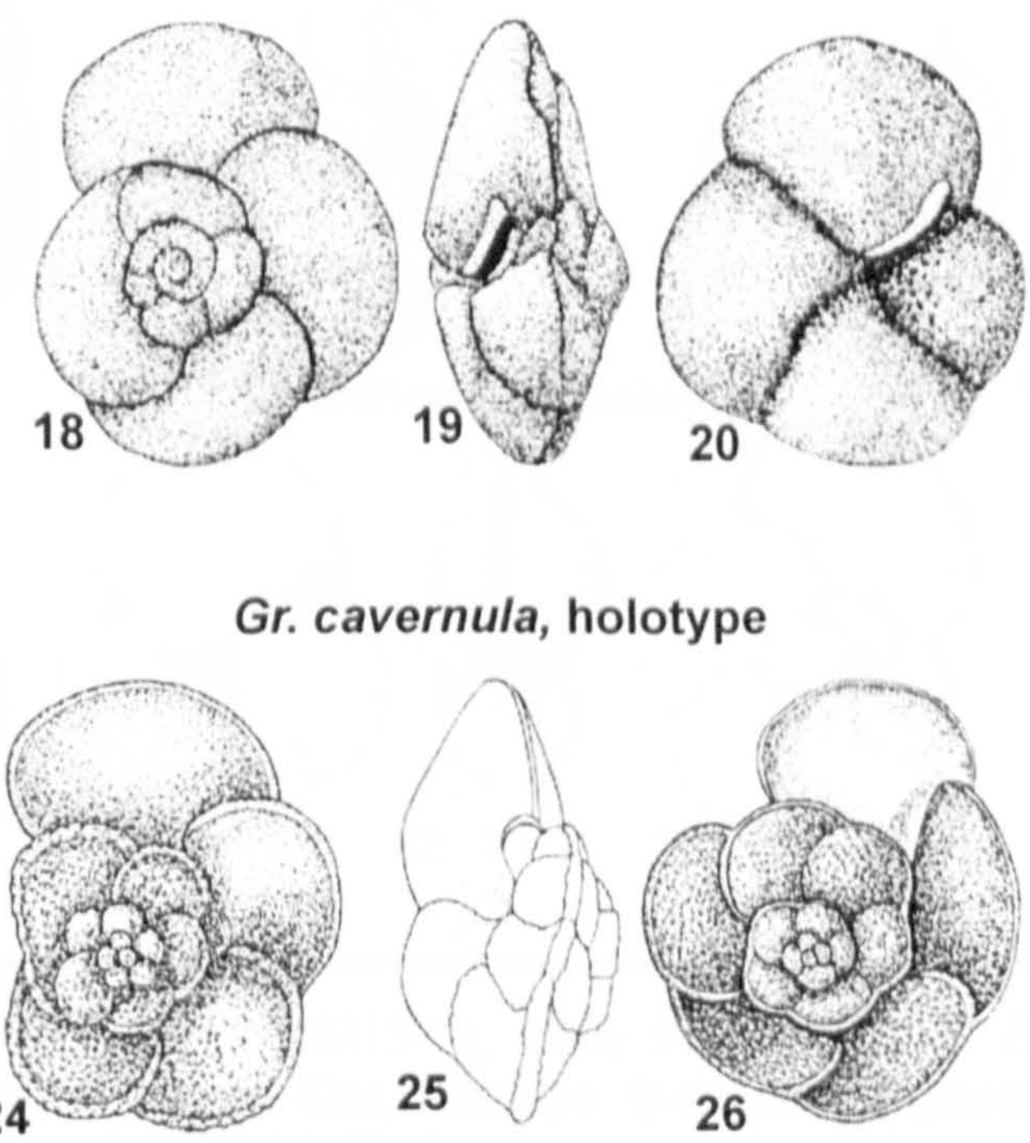

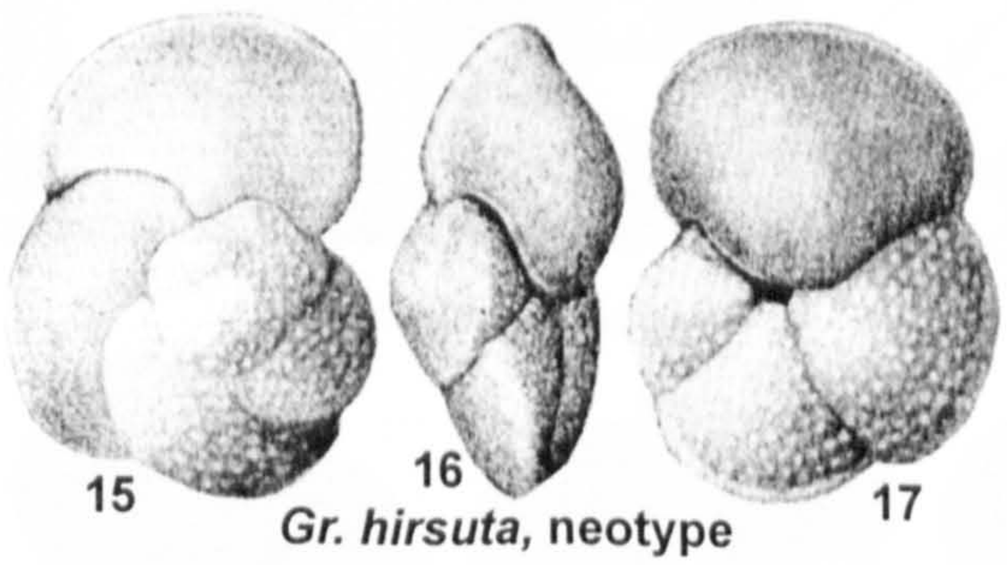

Gr. hirsuta, neotype

Gr. challengeri, holotype

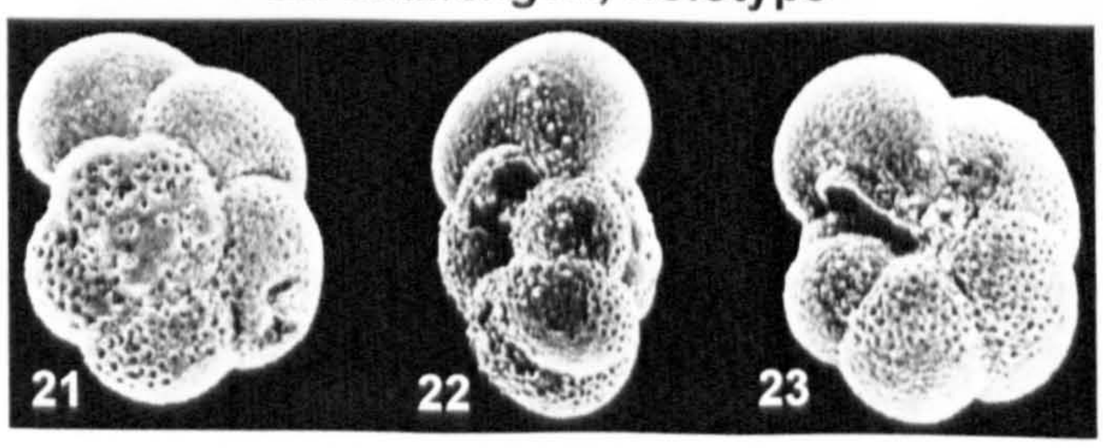

Gr. cavernula, holotype

Plate 1.9. **1-5.** *Gr. juanai* Bermudez & Bolli, holotype. **6-8.** *Gr. scitula,* 1195A 1H-1 120-122 cm, (Biozone PT1, Pleistocene). **9-11.** *Gr. scitula* (Brady), holotype. **12-14.** *Gr. hirsuta* (d'Orbigny), holotype. **15-17.** *Gr. hirsuta hirsuta* (d'Orbigny) Blow, neotype. **18-20.** *Gr. sciutla gigantea* Blow, holotype. **21-23.** *Gr. challengeri* Srinivasan & Kennett, holotype. **24-26.** *Gr. cavernula* Be, holotype. All scale bars represent 100 μm.

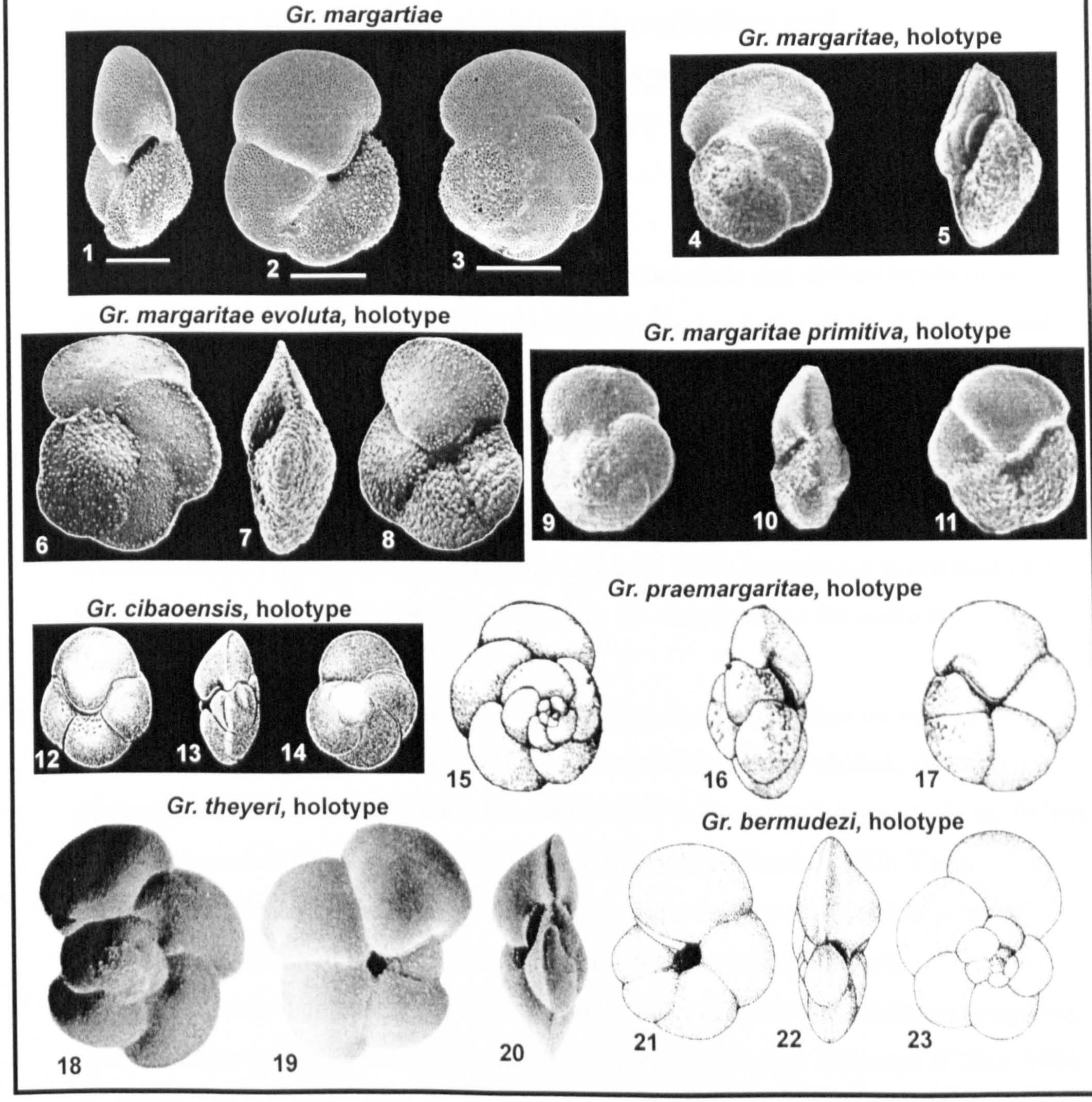

Plate 1.10. **1-3.** *Gr. margaritae*, 1195A 7H-3 10-12 cm, (Biozone M13-14, Early Pliocene). **4-5.** *Gr. margaritae* Bolli & Bermudez, holotype. **6-8.** *Gr. margaritae evoluta* Cita, holotype. **9-11.** *Gr. margaritae primitiva* Cita, holotype. **12-14.** *Gr. cibaoensis* Bermudez, holotype. **15-17.** *Gr. praemargaritae* Catalano & Sprovieri, holotype. **18-20.** *Gr. theyeri* Fleisher, holotype. **21-23.** *Gr. bermudezi* Rogl & Bolli, holotype. All scale bars represent 100 μm.

Chapter 2

Evolutionary history of the planktonic foraminifera and ecological/temporal subdivisions from range data

2.1 Introduction

Micropalaeontologists have long tried to demonstrate that distinct trends in the evolution of marine microfossils were produced by changes in the physical environment, such as climatic changes, changes in sea-level, temperature and oceanic stratification. Such influences have been employed to explain why groups radiate or become extinct at certain times (e.g. Hoffman and Kitchell, 1984; Wei and Kennett, 1986). In contrast, ecologists perceive macroevolutionary mechanisms as scaled up from those that influence microevolution. That is, classical Darwinian intrinsic biotic processes, e.g. predator-prey interactions and competition between organisms are transferred to the realm of macroevolution (e.g., Van Valen, 1973).

These views represent two diametrically opposed philosophies on what drives evolution. In reality both factors probably have some impact on evolution, although it is inherently difficult to quantify the influence of either because finding a control case (where no environmental change has occurred) is highly unlikely (Benton, 1990). These hypotheses still provide the palaeontologist with useful end-member models to try to investigate evolution of fossil groups, such as the planktonic foraminifera.

It is often claimed that the fossil record of the planktonic foraminifera exemplifies cyclic iterative evolution through a number of temporally distinct radiations (Cifelli, 1969; Banner and Lowry, 1985, Norris, 1991). Three of these radiations contain a broad dichotomy of non-keeled and keeled morphotypes, with *Globorotalia* belonging to the latter. Could the physical environment and/or Darwinian natural selection produce such conservative and repetitive evolutionary trends that eventually brought *Globorotalia* into existence?

The fossil and extant *Globorotalia* introduced in Chapter 1 are but a small subset of all planktonic foraminifera. In order to understand evolutionary rates and influences for

Globorotalia, it is necessary to analyse the evolutionary history of all planktonic foraminifera first, then divisions thereof. In this chapter morphospecies-level range data of all planktonic foraminifera (compiled by the author) and the application of modern palaeontological metrics (including survivorship curves) is used to investigate the evolutionary history of the planktonic foraminifera and to assess the limitations of the modern macroevolutionary techniques and datasets employed. The species concepts adopted here are further put into ecological and temporal divisions in order to analyse diversity, speciation and extinction in specific sub-groups.

2.1.1 History of survivorship analysis

In the early 1950s, workers began to examine taxonomic rates of evolution in vertebrate and invertebrate groups using large datasets (Simpson, 1952, 1953; Newell, 1952; Kurten, 1954). More recent parallel datasets have been constructed by Raup and Sepkoski (Raup, 1976a; 1976b; Sepkoski 1993; Raup and Sepkoski, 1986) on marine invertebrates and by Benton (1989, 1995) on terrestrial vertebrates. All such datasets contribute to the core of palaeontological range data, and are of great value in understanding Phanerozoic diversity, speciation and extinction. Palaeontological range data can be used to derive three principal types of information; that is, diversity history, taxonomic evolutionary rates (extinction and speciation) and survivorship patterns.

Simpson (1952, 1953) plotted the first survivorship curves, using an arithmetic ordinate, and found different groups to have different intrinsic survival rates. In 1973, Van Valen pioneered the use of the logarithmic scale for the ordinate in *survivorship analysis* curves. Typically these curves plot taxon duration against number of surviving taxa. A straight 'curve' was thought to imply constant extinction probability with respect to taxon 'age', while any departure from linearity shows that extinction probability changes with taxon age. Van Valen's analyses plotted ~25000 floral and faunal taxa with fossil records, each of which shows the survivorship of taxa (species, genera or families) within a larger taxon (order, class or phylum). Although the curves varied in gradient, he concluded that all were essentially straight, i.e. extinction probability within a subtaxon is constant with respect to longevity, a characteristic that is shared with the other subtaxa. Thus Van Valen proposed the evolutionary law (later dubbed *Van Valen's Law* by Raup, 1975) stating: "within an ecologically homogeneous taxonomic group, extinction occurs at a

stochastically constant rate", i.e. the probability of extinction is uncorrelated with taxonomic 'age'. This discovery seemed to refute some basic assumptions of evolution. As Benton (1990) pointed out: "If evolution is synonymous with adaptive improvement of a species to its environment through time, why are modern mammals no better at survival than their Mesozoic ancestors?".

The Red Queen Hypothesis was formulated to account for linear dynamic survivorship curves. This states "the sum of absolute fitness in a community is constant" (Van Valen, 1976). Van Valen regarded the small, regular fluctuations in the physical environment as a constant factor affecting extinction, while mass extinctions (P-T, K-T *etc.*) differ from background extinction processes. So like Alice and the Red Queen of *Through the Looking Glass* (Carroll, 1865), species must keep running to stay in the same place. His explanation was that the evolutionary *status quo* is maintained by dynamic equilibrium of predator-prey interactions and competition between organisms. It is these interactions that are evolving. To fall behind in the 'evolutionary arms race' is to lose out to extinction.

Even though some workers accepted this model of evolution, opposition stemmed from the counter-intuitive assertion that species do not improve their chances of survival through time (Benton, 1990). In addition, the 'straightness' of Van Valen's curves was estimated visually. This method could yield subjective opinions of what is and is not straight. To remove the subjectivity of visual estimation, Raup (1975) introduced the use of Epstein's (1960a, b) Total Life Method to test statistically the linearity of Van Valen's survivorship curves. This method was then later assumed by a number of studies to test the straightness of Van Valen-type survivorship curves (Wei and Kennett, 1983; Hoffman and Kitchell, 1984; Pearson, 1992, 1995a, 1996). Raup's conclusions using this method were that Van Valen's ammonoid family curve (1973) was not in fact straight, and therefore extinction probability for this group was not constant. Raup also questioned the validity of using dynamic survivorship on palaeontological datasets, because it assumes no systematic increase or decrease in the number of co-existent taxa through time. Raup (1978) then employed cohort analysis, which has the advantage of using geological time and not survivorship time. His curves were concave but all displayed an increase in extinction rates during the Permo-Triassic. Relating extinction probability to longevity is one thing, but relation of extinction probability to the period of time in which a taxon lived is entirely

different. Marked differences in taxonomic longevities between periods using cohort analysis were interpreted by Foote (1988) as an artefact of over-splitting.

McCune (1982) argued that geological time and duration were not the same, and thus "constant extinction rates cannot be deduced from Van Valen's survivorship curves". McCune goes on to suggest that all that can be deduced from a straight survivorship curve is "the probability of extinction of taxa within a group is constant with respect to the duration of those taxa". This is because the abscissa in the plots represents the durations of taxa and not geological time, and the taxonomic durations are amalgamated with no regard for chronological positions. This in itself is an important factor.

Wei and Kennett (1983) used Van Valen's dynamic survivorship method and found linear survivorship relationships in the Neogene planktonic foraminifera (and climatic subsets thereof), but their per-taxon extinction rates in real time were not constant. Conroy and Nichols (1984) later suggested that extinction rates needed to be constant in both duration and geological time to generate linear survivorship curves.

Pearson (1992) pointed out that the shape of a dynamic survivorship curve results from two independent factors: 1) the relative survivorship potentials of coexisting taxa; and 2) the relative spacing of peaks in origination and extinction rates. He stated that if there was variation in real-time probability of extinction, then members within a group were not directly comparable to one another. Pearson (1992, 1995a, 1996) eliminated the effect of non-constant extinction probabilities with the use of the Corrected Survivorship Score (CSS). If a taxon is subjected to a period of high general extinction, it is given a higher score than a taxon that existed during a period of low extinction. This was later refined as the Extinction Survival Score (ESS) (see Section 2.3.4 below and McGowan and Pearson, 1998). Both these methods remove the time-dependency aspect of survivorship analysis, while the pattern of age-dependency remains.

2.1.2 The planktonic foraminifera as a homogeneous group

Before evolutionary and survivorship analysis of range data can be executed, an acceptably homogeneous group must be selected (Van Valen, 1973; Raup, 1975; Pearson, 1992). In simple terms, one must compare 'like with like' in order to extrapolate a meaningful result. The group chosen for analysis in this study is the planktonic

foraminifera, which has been cited as one for the best examples of Van Valen's law at the species level (Van Valen, 1973; Arnold, 1982; but see Pearson, 1992, 1995a, 1996).

The primary dataset of planktonic foraminifera compiled here contains 600 morphospecies and spans the last 173 My of geological time (Appendix 2.1). Broadly speaking, this group is taxonomically and ecologically homogeneous. The planktonic foraminifera all belong to the same taxonomic group and occupy the oceanic realm, although they may not be phylogenetically homogeneous (see discussion in Chapter 4). They are as homogeneous as any group used previously for survivorship analysis. In addition, the analyses using all planktonic foraminifera avoid criticism that might be applied to temporally or spatially-isolated taxonomic subsets. Unlike many of the larger datasets of Phanerozoic life, this dataset is at 'species' (= morphospecies) level and thus avoids bias associated with using higher taxa (see McCune, 1982, for discussion).

Wei and Kennett (1983) presented dynamic survivorship analyses of Neogene planktonic foraminifera divided into latitudinal zones, although they calculate these latitudinal subsets to be statistically similar. Pearson (1992) later suggested further division of foraminiferal datasets into depth habitat, and broad morphological groupings. This chapter presents analyses that do just that.

Survivorship analysis assumes that the 'population' has a temporally stable age distribution. That is, they work on the assumption that the total number co-existing taxa has not increased or decreased systematically over time (Van Valen, 1973; Raup, 1975). This assumption is invalid if systematic changes significantly alter survivorship trends (Raup, 1975), therefore, this chapter also presents results that address the nature of systematic variation in diversity, speciation and extinction throughout the evolutionary history of the planktonic foraminifera.

2.2 Methods

2.2.1 The range database

'Plankrange' (Appendix 2.1) is a database containing all planktonic foraminiferal ranges through geological time, compiled to a temporal resolution of 1My. It is available on the world wide web at: http://palaeo.gly.bris.ac.uk/personnel/stewart/databaseintro.html and in Appendix 2.1. 32 key references reporting stratigraphic ranges of planktonic foraminifera were used to create the database, which contains 600 known morphospecies of planktonic foraminifera from the Jurassic (Bajocian) to the present day. The original species number exceeded 660; however, some of the references used over-split taxonomies, thus a number of synonyms were identified and removed by consulting the literature (listed in Appendix 2.2). Removing synonyms is a tentative process, especially in a group (such as the foraminifera) known for anagenesis (morphologic lineage evolution with no branching) and morphological variation.

Most ranges are defined from one source; however, where different sources present conflicting ranges, the maximum combined range is given, and both sources are referenced. Those dates that are in bold contain inaccuracies resulting from source reference range data not specifying the exact FAD/LOD. In these cases, the midpoint of the biozone/stage is given as the actual datum. All datums/ranges were calibrated to the geochronology of Berggren *et al.* (1995) and Gradstein *et al.* (1994). The diachronous nature of all stratigraphic divisions is acknowledged, which may produce error, however, by converting all datums to absolute time from one integrated geochronology, error is standardised for all taxa.

Table 2.1 reproduces the first line of the database. Column 1 assigns an arbitrary species number, column 2-3 list the generic and specific names; column 4-5 list the earliest recorded name of the species (i.e. valid nomen) and the author who first described it, while columns 6,7 and 8 list the range, first appearance datum (FAD), and the last occurrence datum (LOD), respectively. Column 9 lists the reference from which the range datums were derived, and column 10 contains any 'General Notes' about the taxon and is used mainly for quantifying partial zone ranges and possible generic discrepancies. Column 11 and 12 present depth habitat divisions and supporting references. A proportion of the taxa are included in published isotope-based palaeoecological studies, which correspond to a

reference in the final column (12). Those taxa that do not have any reference, but have a depth habitat assigned were decided by using comparative taxonomic morphologies as a proxy for similar depth habitat. The author acknowledges this may produce some erroneous depth habitat assignations, however, there is no better method available. Depth habitat was only assigned when reasonably confident estimates could be made. Those taxa that could not be assigned a depth estimate without reasonable doubt (which primarily concerns the Jurassic and Early to Middle Cretaceous taxa) were left without a depth classification ('*?*'). The taxa were defined as either surface-dwelling (*S*), intermediate (*I* – sub-surface mixed layer) or deep-dwelling (*D* – thermocline and below). Some modern species are known to migrate vertically through their different life cycle phases (Hemleben *et al.*, 1989). This is impossible to infer accurately for extinct taxa and therefore the depth assignations are no more than an average for any one morphospecies. The author also acknowledges the errors produced by seasonal and/or quasi-permanent changes in global oceanic stratification, which could not be accounted for.

The range source references are numbered 1-33, while the palaeodepth source references are lettered A-U (all database references are given in Appendix 2.2).

No.	Gen name	Sp. name	Orig. Genus Name	Author &Year	Range (My)	FAD (Ma)	LOD (Ma)	Range ref	General notes	DH	DH ref
1	*Abathomphalus*	*intermedius*	*Globotruncana intermedia*	Bolli, 1951	1.8	67.7	65.9	9		D	O

Table 2.1 Example of first line of Plankrange database.

2.2.2 Analysis of the database using ADAPTS

The range data were analysed using the software ADAPTS (Analysis of Diversity, Asymmetry of Phylogenetic Trees and Survivorship) (McGowan and Pearson, 1998). This program imports range data from standard spreadsheet packages to calculate taxonomic rates of evolution and perform taxonomic survivorship analysis, which includes a refinement of the time-averaging Corrected Survivorship Score (CSS) and Extinction Survivorship Score (ESS) (Pearson, 1992, 1995a, 1996, McGowan and Pearson, 1998).

2.2.2.1 Analysis input

McGowan (1998) presents a detailed guide to using this software, available on the world wide web at: http://palaeo-electronica.org/1999_1/adapts/issue1_99.htm. The key protocols are summarised below.

ADAPTS was written using 'MS Qbasic' on a Macintosh Classic with Macintosh Operating System (OS) 7.1. This program is not available for any other platforms and is only compatible with any Macintosh OS version 7. The ADAPTS program and MS Qbasic must be present on the computer hard disk for the program to work. These analyses were executed using a Macintosh SE/30 (Classic). Five data items (in spreadsheet format) are required per taxon analysed. This input format is detailed below in Table 2.2:

Taxon Name	I D Number	FAD	LOD	Range	Ancestor ID
1	2	3	4	5	6

Table 2.2. Input data format for ADAPTS. Columns 2-6 are required.

Taxon name

Used as a reference (not required).

I D Number

All taxa were numbered sequentially, ascending from 1. This number is simply a taxon tag.

FAD

This column represents the First Appearance Datum. In this study, all datums were converted to absolute time to a resolution of 0.1 My using the Berggren *et al.* (1995) timescale.

LOD

Last Occurrence Datum. See above.

Range

The stratigraphic range is FAD minus LOD. This calculation was automated using standard spreadsheet functions.

Ancestor I D

This number represents the parent of the taxon. In this study, no ancestor-descendent analyses were carried out, therefore this field must contain '1'.

2.2.2.2 Running an analysis

For each dataset, columns 2-6 were highlighted and copied onto the clipboard of the computer. ADAPTS automatically lifts the data from the clipboard. Before the analysis can start, the program prompts the user for the dataset parameters i.e., number of taxa, starting point (earliest FAD of all taxa), the temporal resolution and the finishing point (i.e. latest LOD of all taxa). Once completed, the results are copied onto the computer clipboard and can be accessed by 'pasting' into any standard spreadsheet package.

2.2.2.3 Analysis output

For a given dataset of FADs, LODs and ranges, ADAPTS will calculate the following for each temporal increment (although not all were used in this study):

- D – Diversity (using methods of Wei and Kennett, 1986; and Pearson, 1992).
- S – Number of speciation.
- E – Number of extinctions
- r_s – Per-taxon rate of speciation
- r_e – Per-taxon rate of extinction
- r_d – Rate of diversification ($r_s - r_e$)
- r_t – Rate of turnover ($r_s + r_e$)
- ΔD – Rate of change of diversity
- Dynamic survivorship (Van Valen, 1973)
- *CSS* - Corrected Survivorship Score (Pearson, 1992, 1995a)
- *ESS* - Extinction Survival Score (McGowan and Pearson, 1998).

All survivorship curves are automatically tested using Epstein's Test (1960a, b), which evaluates departure from linearity (discussed later).

2.3 Results and discussion

When interpreting any palaeontological range dataset it is important to recognise the limitations of the original data. It is worth considering the influence of key references used to make the database of planktonic foraminifera range data (e.g. Kennett and Srinivasan, 1983; Robaszynski *et al.*, 1984; Bolli and Saunders, 1985; Spezzaferri, 1994; Boudagher-Fadel *et al.*, 1997; Pearson, 1998; Olsson *et al.*, 1999). These references all cover temporally isolated periods of planktonic foraminiferal history. Taxonomists commonly concentrate on certain time-periods only, and if a time interval has been taxonomically over-split (or under-split), then the diversity (speciation and extinction) during and after this time period, may be exaggerated.

Thus increases and decreases in diversity may not accurately represent the magnitude of speciation or extinction events. Furthermore, all datasets of this type are open to a plethora of error sources. These include the accuracy of the recorded FADs and LODs; agreement between workers, the specific geochronology used to quantify the taxonomic range; the disparity between the different geochronologies used, quantifying relative stratigraphic time as absolute, synonymy, species definition, *etc.* Further error could apply to analyses containing an ecological or morphological division to smaller subsets of the original dataset (depth habitat and globorotaliform divisions). Although the stratigraphic record of planktonic microfossils probably constitutes the best-calibrated and most complete datasets available, they are far from complete or totally resolved.

Preservation and monographic biases will no doubt affect the dataset, however, useful inferences can still be derived from the analysis of fossil range data at this resolution assuming the sources primarily document actual ranges.

2.3.1 Diversity

In analysing the fossil record of any group, diversity patterns are of prime importance (Valentine, 1985). Here absolute diversity (i.e. total number of taxa per unit time) and diversification rate are shown. Rate of diversification (r_d) (Sepkoski, 1978) was calculated as follows:

$$r_d = r_s - r_e$$

where r_s is per-taxon rate of speciation, and r_e is per-taxon rate of extinction.

2.3.1.1 All planktonic foraminifera

Figure 2.1 is a plot of diversity of all planktonic foraminifera from the 'Plankrange' dataset through geological time. The planktonic foraminifera originated in the Jurassic (~170 Ma) and are still extant. Diversity shows a gradual increase through time, a common trend already established in larger palaeontological datasets (e.g. Maxwell and Benton, 1990; Sepkoski, 1993). Superimposed on this gradual increase are clear episodes of diversity variation. The greatest decrease (and therefore greatest period of extinction) coincides with the well-known Cretaceous-Tertiary (K-T) mass extinction event. There are also large magnitude extinction events in the upper Eocene and the Middle Miocene. Immediately post-dating large extinction events, diversity generally appears to recover to greater levels than before. The acme of diversity occurs in the Early Miocene, at about the time the globorotaliids and Neogene globigerinids were beginning to radiate. The diversity record (in Figure 2.1) is aligned with the earlier generic diversity of the Globigerinida (Tappan and Loeblich, 1988), and shows broad congruency.

The maximum diversity reached is ~80 morphospecies. This puts some of the diversity falls into perspective e.g., although the Middle to Late Miocene diversity drop only represents a loss of 40 morphospecies, this number is approximately half the species-level diversity at that time. So this fall in diversity is of comparable size to the K-T extinction event in the planktonic foraminifera (~60 morphospecies).

Rate of diversification is shown in Figure 2.2. The highly variable results preceding ~120 Ma are due to the very low numbers of taxa present during this time. This figure shows a number of key phases in which appearance rates exceed disappearance. The most pronounced of these effectively lasts for the entire Palaeocene epoch. This is preceded by a smaller phase of diversification in the early Middle Eocene. Pearson (1990) documented the same phases using morphospecies-level range data of the Palaeogene planktonic foraminifera. The third of these phases precedes a steady decline in diversification rate throughout the later Palaeogene, while the fourth phase occurs in the Late Miocene and precedes a similar drop in the Middle Miocene.

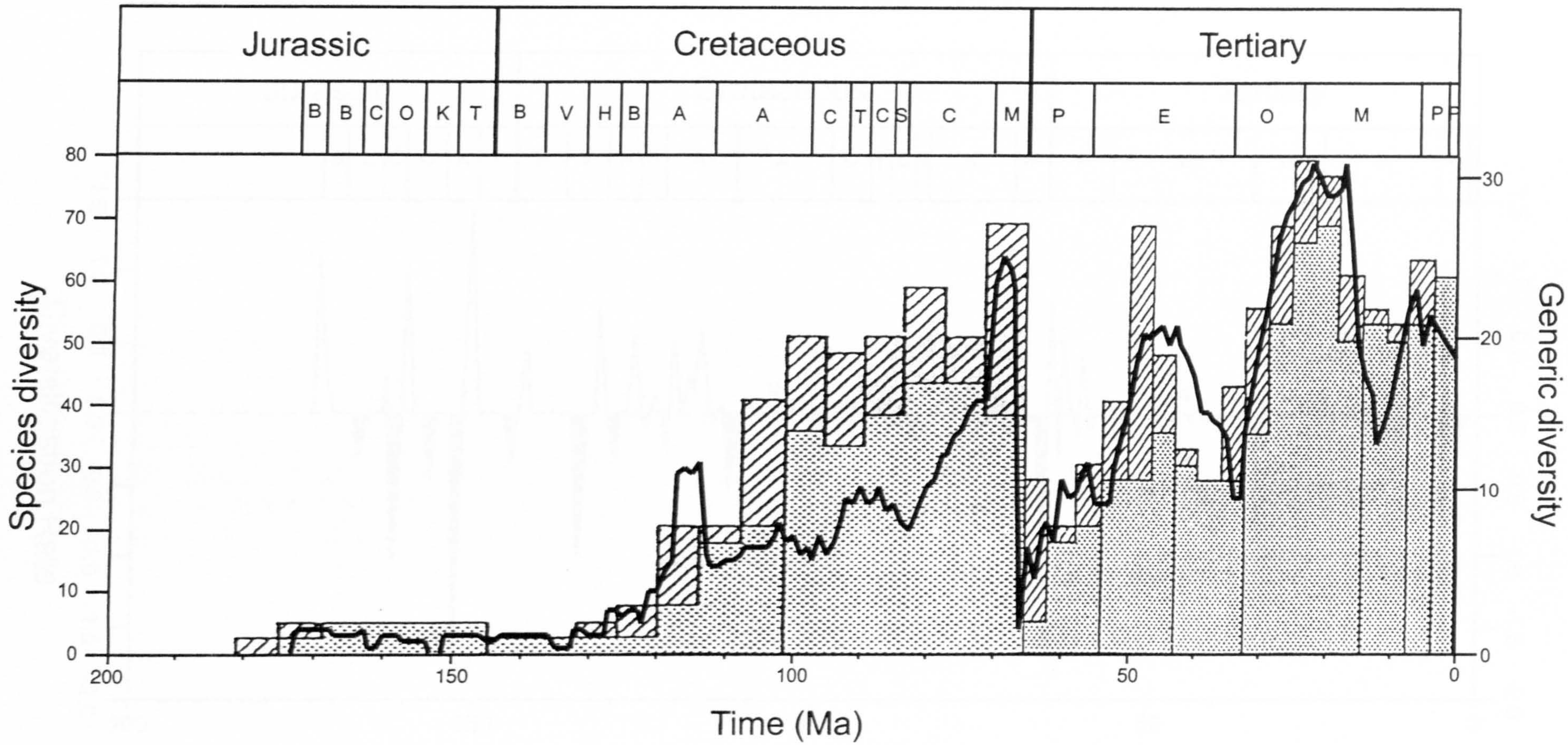

Figure 2.1. Diversity of all planktonic foraminifera through time. The species-level diversity (solid line) from this study is superimposed onto the generic level diversity (histogram) of Tappan and Loeblich (1988), within which the stippled area represents genera persisting from previous stage and the cross-hatched area represents newly evolved genera.

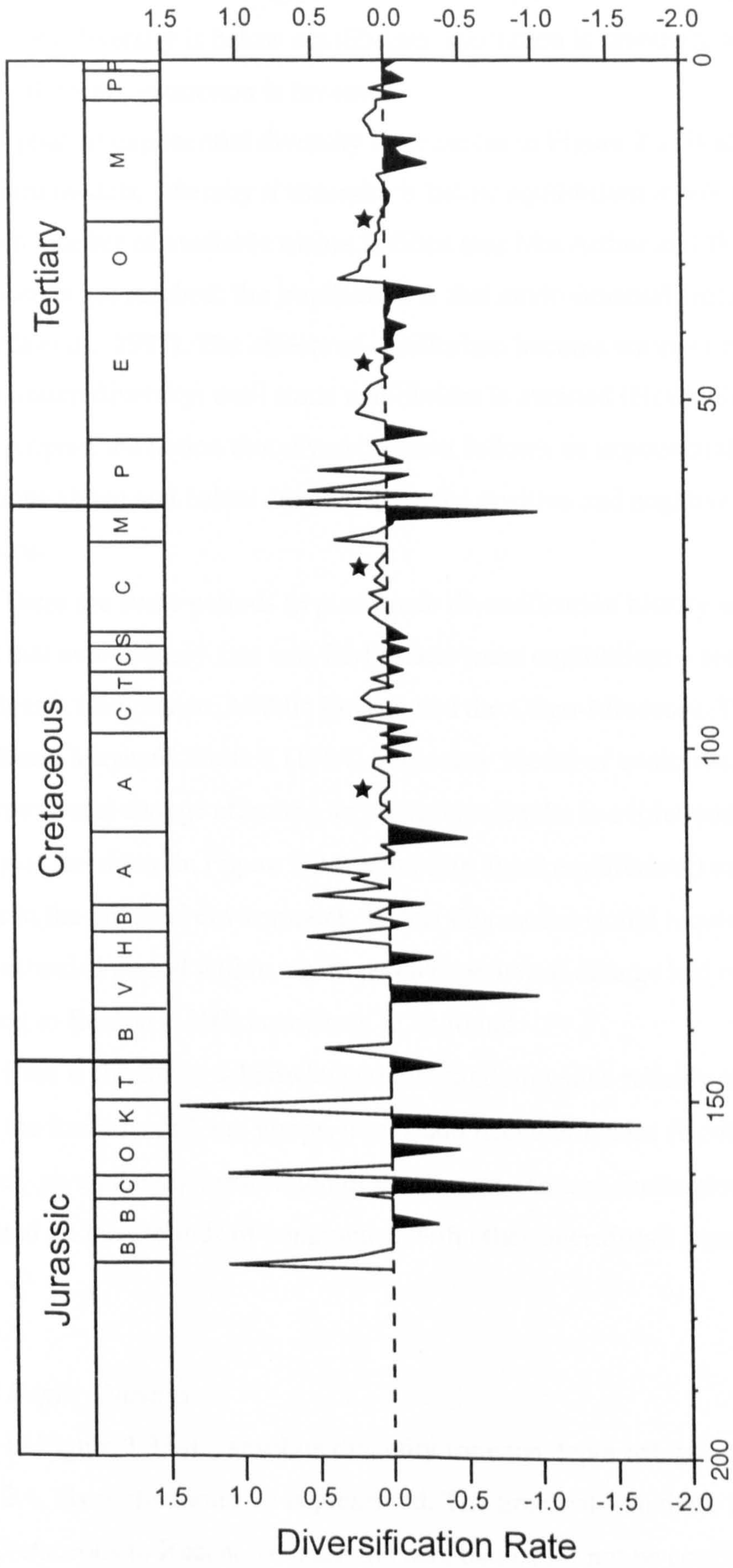

Figure 2.2. Averaged phenetic diversification history. Stars denote points of discussion (see text).

Wei and Kennett (1986) interpreted this type of diversification pattern in Neogene planktonic foraminifera as being produced by an equilibrium diversity model for evolution. That is, when diversity is below equilibrium, speciation is favoured, and when diversity is above equilibrium, extinction is favoured.

Apparent exponential diversity increase (as in Figure 2.1) is also explicable by equilibrium models, whereby if diversity is below equilibrium it will increase until the maximum number of available niches is filled (see MacArthur and Wilson, 1967). If equilibrium is not reached; the implication is that environmental factors can be ignored (Hewzulla *et al.*, 1997). The effects of equilibrium become stronger the closer a population is to maximum diversity; until static equilibrium is attained (Hewzulla *et al.*, 1997). These authors propose the notion that diversification follows an exponential curve, but fluctuations above and below are caused by the positive and negative effects of mass extinctions.

There are some periods in planktonic diversification history which appear to suggest that evolutionary rate was fairly static (near equilibrium – see stars in Figure 2.2 e.g., Albian?, Campanian, Middle Eocene and the Oligo-Miocene). This could support Stenseth and Maynard Smith's (1984) Stationary Model of evolution, in which the absence of environmental change affecting an ecosystem results in evolutionary halting. If so, the majority of the signal in Figure 2.2 (fluctuating about equilibrium) may be dominated by changes in the physical environment. To test this model would require a case study which had an extended period within which no environmental change had occurred, which according to Benton (1990) is unlikely to be found.

Here it should be acknowledged that random walks reliably simulate the features seen in the fossil record, i.e. jumps, trends and irregular cycles (Bookstein, 1987). However, given the high resolution of the dataset, random fluctuation can certainly be eliminated on the grounds of congruence with other microfossil groups and geological data.

2.3.1.2 Depth divisions

In Figure 2.3A-C, absolute diversity for each depth habitat is plotted, while in Figure 2.4, diversification rate is presented. The timescales in these figures only cover the Early Cretaceous to Recent, because the taxa that could not be confidently assigned to a

specific depth habitat (71 morphospecies) were largely confined to the period preceding 125 Ma.

The surface-dwelling record (Figure 2.3A) contains the largest number of morphospecies (262) of the three divisions, and follows the general trend of the whole dataset (Figure 2.1). Simultaneous peaks and falls in diversity can be seen in the Eocene and the Miocene; however, the K-T event could not produce comparably large absolute drops in diversity because diversity was already (relatively) low at the time. The K-T event removed nearly all surface-dwellers from existence, furthermore, surface-dwellers did not increase rapidly in diversity until after the K-T event. Prior to this, diversity remained at a fairly constant level. Rate of diversification (Figure 2.4A) shows a relatively stable signal for the surface-dwellers, with three main diversification phases: the Early Cretaceous (?), the K-T boundary, and the Early Oligocene.

The intermediate-dwelling (Figure 2.3B) planktonic foraminifera (123 species) appear to have a more discontinuous diversity record, with peaks in diversity in the Late Cretaceous and Neogene, but two episodes in which diversity was zero (Middle Cretaceous and Palaeocene). The K-T event appears to have eradicated all intermediate-dwelling taxa and a period of >10 My was required for the return of the newly evolved taxa in this ecospace. Both the surface and intermediate-dwellers show similar peaks and depressions during the Cenozoic, i.e. separate peaks in the Eocene and Miocene with drops in diversity at the end Eocene and Middle-Late Miocene. Rate of diversification (Figure 2.4B) shows a very erratic pattern for the intermediates, with several long periods of zero diversification rate, but this may be more an artefact of the assignation of depth habitats and general lack of published isotopic data.

The deep-dwelling (Figure 2.3C) planktonic foraminifera (144 morphospecies) reach maximum diversity in the Eocene-Oligocene, at a time when diversity in the other habitats is low. Large diversity falls can be seen at the K-T boundary, the end Eocene and the Middle-Late Miocene; however, all are generally less pronounced than for the shallower depth habitats. This may indicate a greater isolation of deep environments from most habitat perturbations. There are also diversity peaks in the Turonian and Maastrichtian common to the surface-dwellers.

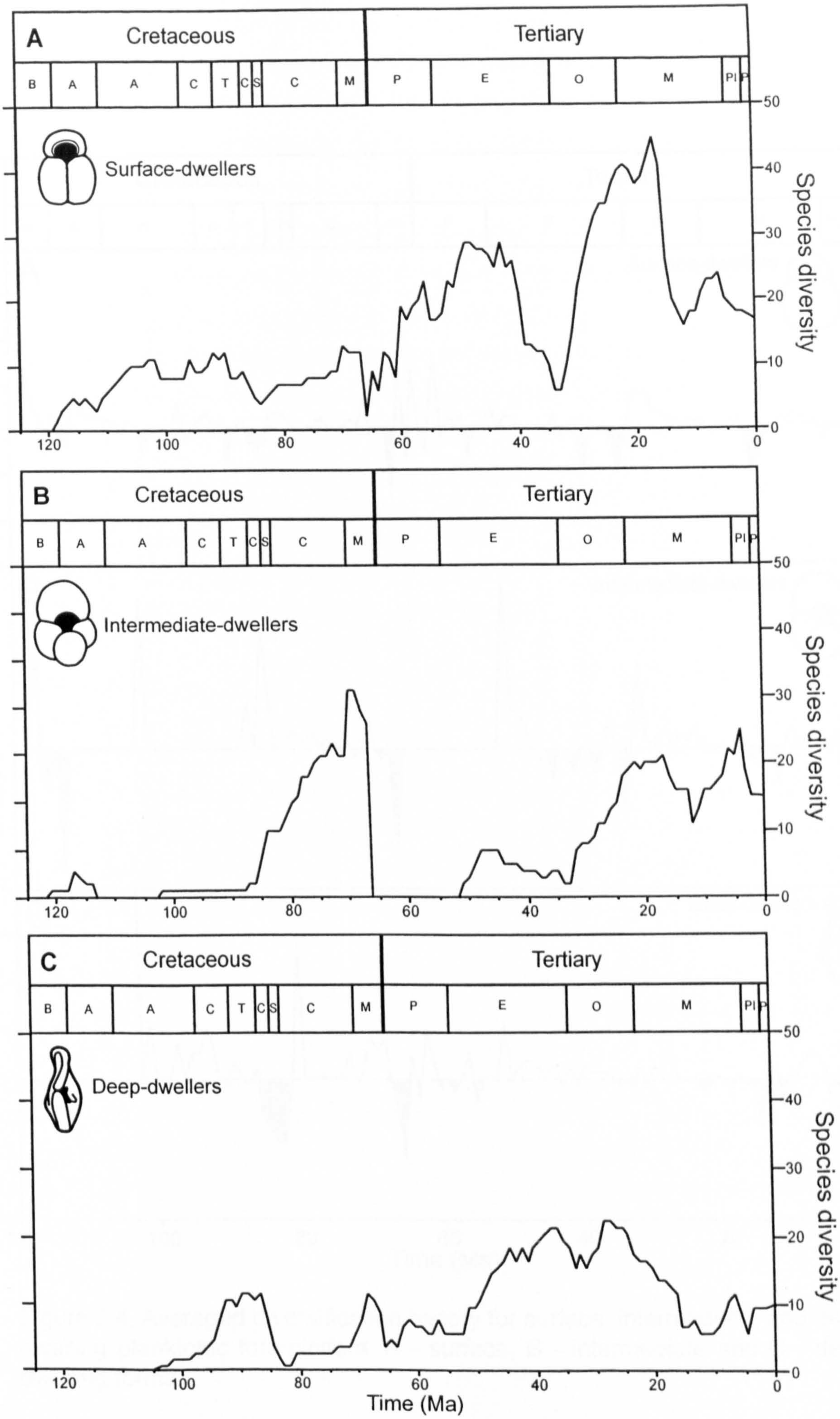

Figure 2.3. Diversity of planktonic foraminifera from a surface (A), intermediate (B) and deep (C) depth habitats through time.

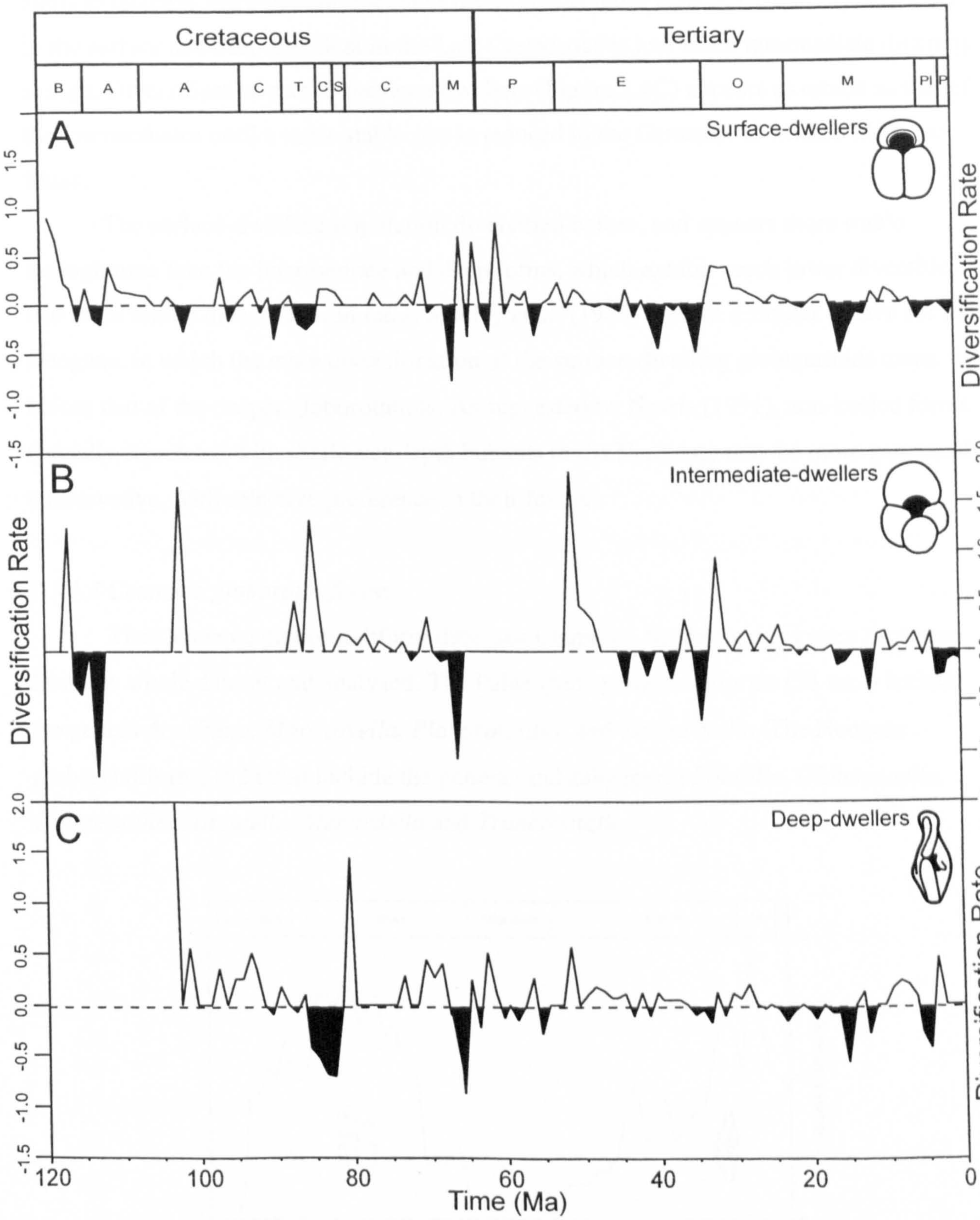

Figure 2.4. Averaged diversification history for surface, intermediate, and deep-dwelling planktonic foraminifera. A - surface, B - intermediate and C - deep-dwelling forms.

The deep-dwellers show a relatively small decline at the E-O extinction and show a broad diversity peak from the Middle Eocene to Early Miocene. Deep-dwelling diversity starts to increase when the intermediates are extinct (Figure 2.3B, C). Similarly, diversity in the surface and deep-dwellers in the Late Cretaceous is low when intermediate diversity is high. Diversification rate in the deep-dwellers (Figure 2.4C) appears as erratic as that of the intermediates until a more stable rate is reduced in the Cenozoic to Middle Miocene times.

The surface-dwelling population diversified before, and appears more stable through time than the intermediate and deep forms, which exhibit much lower diversities and more erratic diversification rates. Stanley *et al.* (1988) present a similar pattern for the Neogene, in which the main diversification of the surface-dwelling globigerinids came before that of the deeper globorotaliids. As suggested by Norris (1991), non-keeled forms (broadly correlated with shallower depth habitats in the Neogene) may be more genetically conservative, with selective preference in their favour.

2.3.1.3 Cenozoic globorotaliforms

The Cenozoic globorotaliform data (see Chapter 1 for discussion) were separated from the whole dataset and analysed. The Palaeogene globorotaliforms (58 taxa) include the genera *Acarinina, Morozovella, Planorotalites,* and *Turborotalia*. The Neogene globorotaliforms (52 taxa) include the genera (and subgenera) *Fohsella, Globoconella, Globorotalia, Hirsutella, Menardella* and *Truncorotalia*.

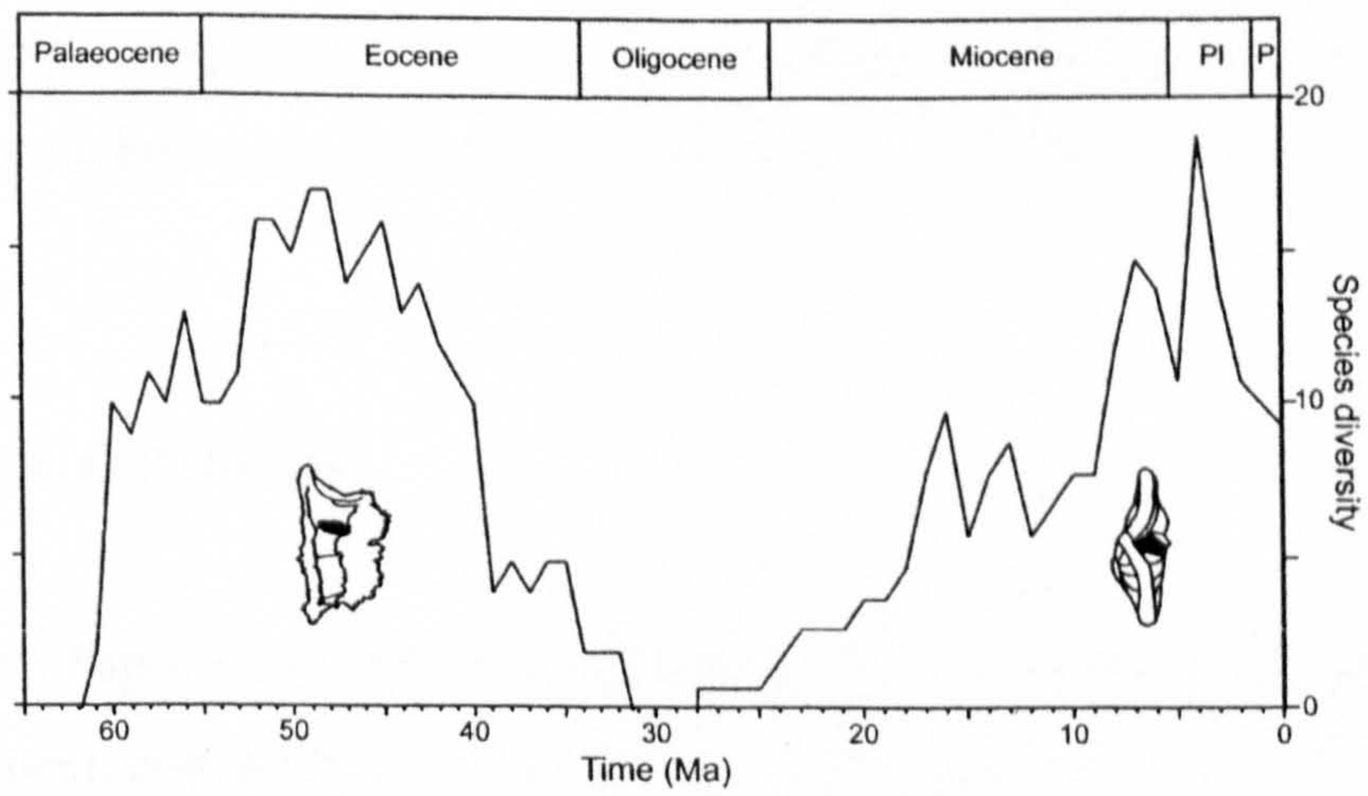

Figure 2.5. Diversity of Palaeogene (left) and Neogene (right) globorotaliforms.

In Figure 2.5, diversity of the two discrete globorotaliform groups in plotted. The Palaeogene globorotaliforms (left) originated in the Early Palaeocene and became extinct at the end of the Eocene over a period of ~3-4 My. Diversity increased steadily towards the acme during the Eocene, with a small decline at the Palaeocene-Eocene boundary. The Neogene globorotaliforms initiated 2 My after the extinction of the Palaeogene globorotaliforms, and diversity developed towards its peak in the Middle Pliocene. After this, diversity declined to present-day levels. Small drops in diversity occurred in the late Middle Miocene and at the Mio-Pliocene boundary.

The Palaeogene globorotaliform data display a much steeper diversity curve indicating a more rapid radiation and demise. Their radiation post-dates a large mass extinction, and thus the geometry may reflect an opportunistic filling of vacant niche space, in line with equilibrium models of diversity. Climatic stability and warming through the Palaeocene (Zachos *et al.*, 2001) could also create favourable conditions for plankton evolution (e.g. Stenseth and Maynard-Smith's Stationary Model). The Neogene globorotaliforms show a more gradual increase in diversity and a more skewed distribution through time, although the trend is truncated by the present day. The K-T extinction is linked to bolide impact (Alvarez *et al.*, 1980) while the E-O is generally not (Keller *et al.*, 1992). The difference between the two is that the K-T extinction affected all planktonic foraminifera considerably, whereas the E-O extinction did not affect the conservative globigeriniforms (see Spezzaferri, 1994). This is where the morphotype-ecological association is inconsistent, because some of these conservative Oligocene forms were probably deep-dwelling, despite having globigeriniform morphology, e.g., *Catapsydrax (Globorotaloides) Dentoglobigerina*, *Globoquadrina etc.* (see Figure 2.3). The absence of unoccupied deep niches could have slowed the radiation of Neogene globorotaliforms, as seen here.

2.3.2 Speciation and extinction

Analysis of speciation and extinction rates could provide some insight into the effect of Red Queen competition and dynamic equilibrium processes on the evolutionary history of the planktonic foraminifera. Rates of extinction and speciation are also of prime importance to survivorship analysis, however, it is not sufficient to plot the absolute numbers of these variables against time. This is because extinction and speciation rates are

ultimately linked to diversity, i.e. greater numbers of taxa will potentially yield more speciation and extinction events; therefore comparisons between groups with different diversities are not valid unless a normalisation is used. To address this problem Sepkoski (1978) developed the per-taxon method for analysing rates of speciation and extinction calculated from palaeontological datasets. The per-taxon rates represent the average probabilities of individual taxa branching or becoming extinct per unit time, by normalising the absolute rates to diversity:

$$R_e = 1/D \cdot E/t$$

where E is the number of absolute extinctions in a time interval t, and D is the average diversity through the interval. This method was later employed to compare extinction and speciation rates in planktonic foraminiferal populations (Wei and Kennett, 1983; Pearson, 1992, 1995a).

2.3.2.1 All planktonic foraminifera

The per-taxon speciation and extinction rates for the Cretaceous and Tertiary planktonic foraminifera are plotted in Figure 2.6. The extinction and speciation data prior to ~125 Ma (the majority of which are from Boudagher-Fadel *et al.*, 1997) are likely to contain a great degree of noise from taxonomic over-splitting. Furthermore, preservation and stratigraphic resolution are generally poor for Jurassic assemblages, so this interval was ignored. The post-Cenomanian signal is probably more reliable than the pre-Cenomanian, due to the extensive range of research that has been carried out on planktonic foraminifera to refine planktonic foraminiferal biostratigraphy of the Late Cretaceous and Cenozoic.

Speciation and extinction peaks generally coincide (usually with an offset) and have similar amplitudes. Large extinction events are present at the Aptian-Albian, the K-T boundary, the Eocene-Oligocene boundary, and the Middle Miocene. Speciation levels are often high directly following large extinctions, e.g. in the Palaeogene and Oligocene. It is reasonable to assume that vacated evolutionary space allows recovery-speciation during these intervals.

2.3.2.2 Depth divisions

The planktonic foraminifera taxa from the Plankrange dataset were next divided into the three depth habitat divisions, for which per-taxon speciation and extinction rates were calculated (Figure 2.7A-C).

The surface-dwellers (Figure 2.7A) exhibit the less variable signal. Large extinction peaks appear for the K-T, E-O boundaries and the Middle Miocene. Interestingly, a number of extinction events of similar magnitude postdate the K-T event, all of which are associated with equal or greater speciation events. As in Figure 2.6, the E-O boundary and Middle Miocene are marked by large extinction events. The former is followed by a large speciation spike that probably represents the radiation of the principal Neogene genera..

Much fewer data are available for the intermediate-dwelling taxa (Figure 2.7B). Isolated K-T, E-O and Miocene extinction spikes are still evident although less pronounced. Large isolated speciation peaks in the Aptian, Coniacian and Eocene account for the two main evolutionary diversifications for this depth habitat (see Figure 2.3).

The deep-dwelling taxa (Figure 2.7C) appear to have a similar record of speciation and extinction levels to that seen in the surface-dwelling group; however, several peaks have greater magnitudes than those in either of the other depth habitats.
The E-O event appears to have passed over the deep-dwelling taxa here. The possible reasons for this are discussed below.

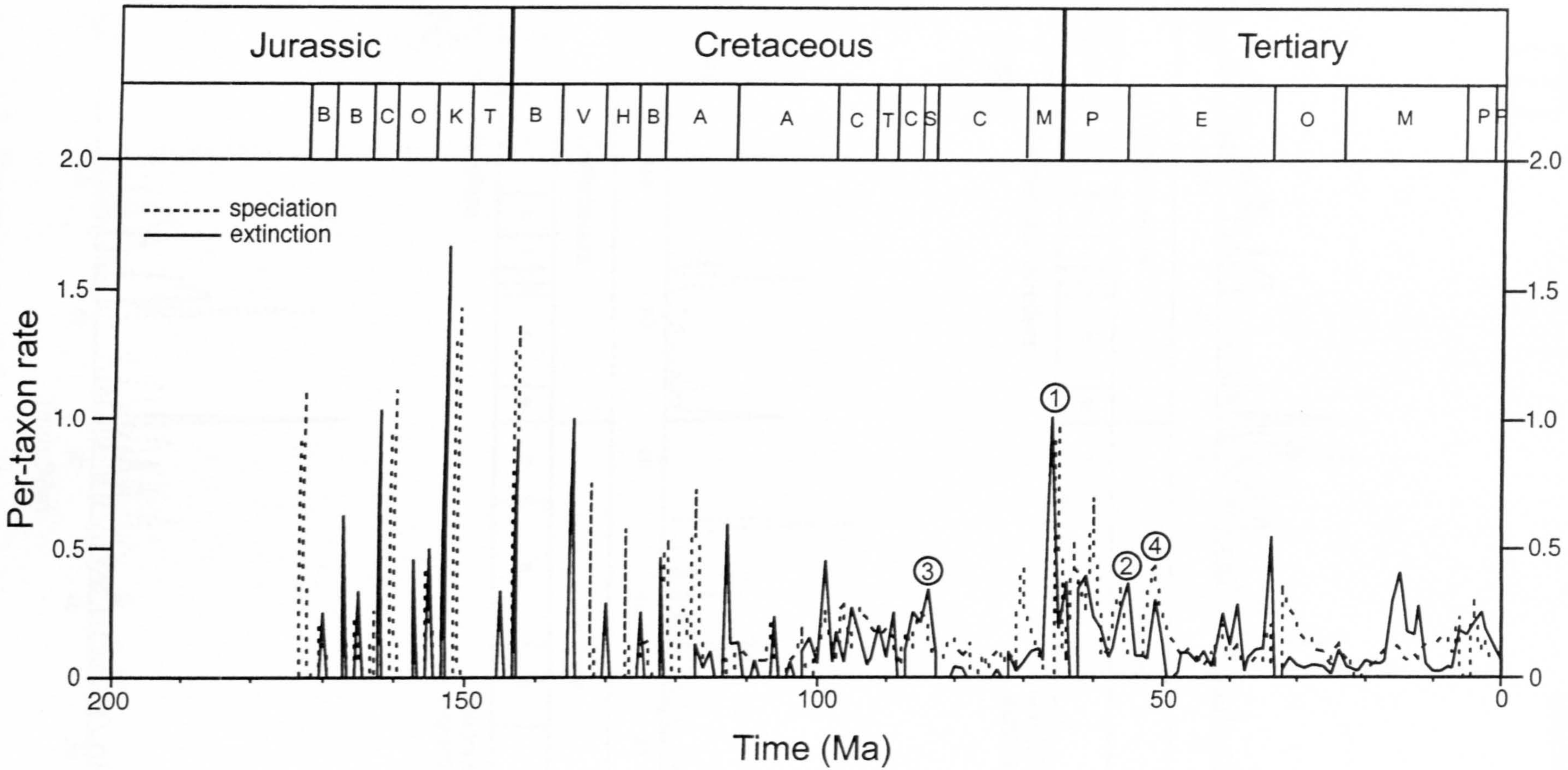

Figure 2.6. Per-taxon extinction and speciation rates of all (600 species) planktonic foraminifera from Jurassic to Recent. Circled numbers denote points of interest and are discussed in the text. Circled numbers indicate points of discussion referred to in the text.

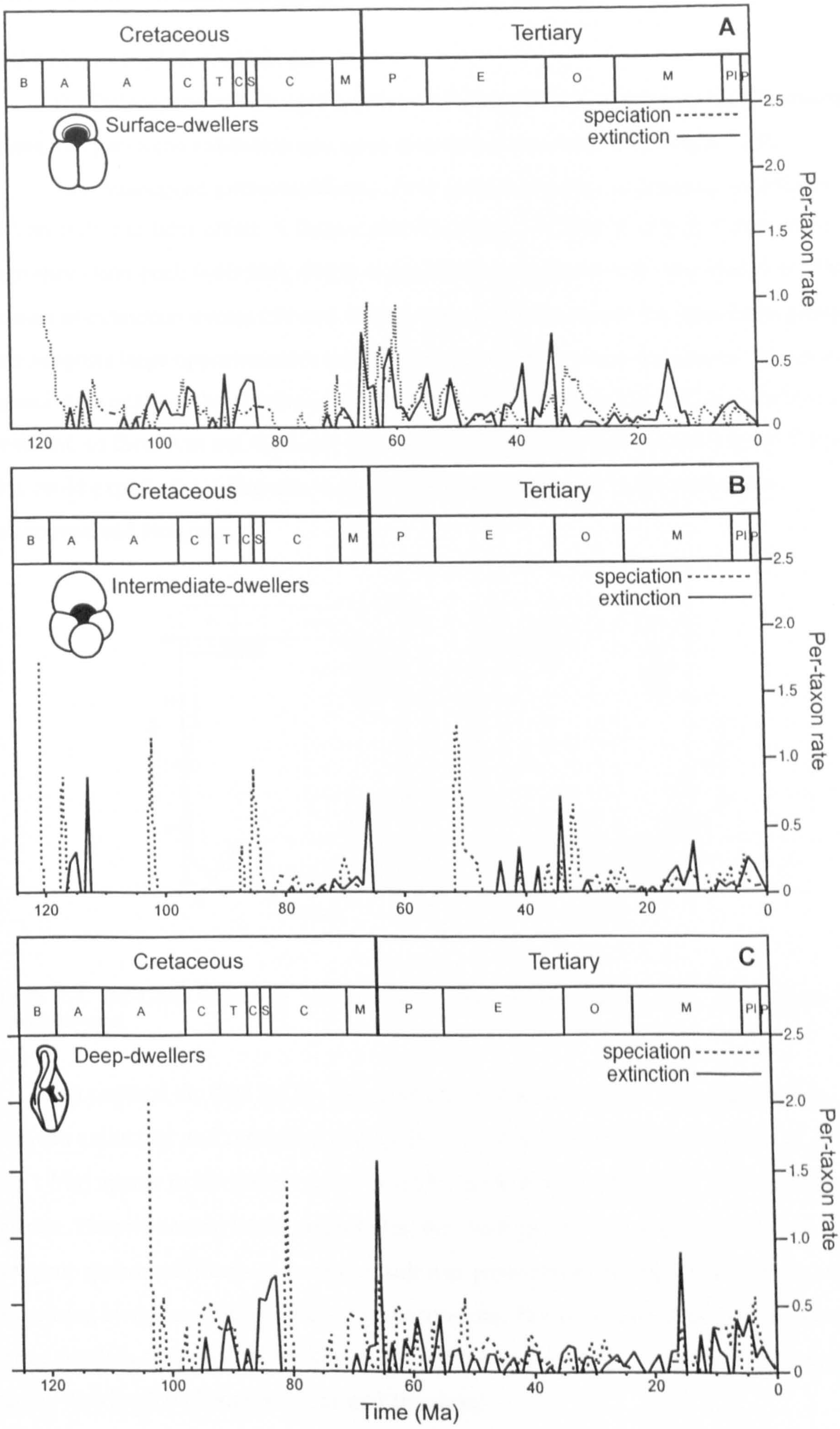

Figure 2.7. Per-taxon speciation and extinction rates of surface (A), intermediate (B) and deep-dwelling (C) planktonic foraminiferal populations.

2.3.2.3 Cenozoic globorotaliforms

The Palaeogene and Neogene globorotaliforms were isolated from the Plankrange dataset and per-taxon extinction and speciation rates were calculated (Figure 2.8).

The Palaeogene globorotaliforms show consistent peak congruence, sometimes with an earlier or later offset. A large extinction event (~62 Ma) is closely followed by a large speciation peak (~60 Ma), which is greater than any seen in the Neogene taxa. Two prominent extinction events (34 and 31 Ma) appear to have sealed the fate of this group. This supports large opportunistic replacement after the K-T event because its effects were pervasive throughout the planktonic foraminifera. The effects of the E-O event were not as prevalent, so there was not the same quantity of ecospace available as after the K-T event. This could explain the difference in speciation peak magnitude at the start of the Palaeogene and Neogene.

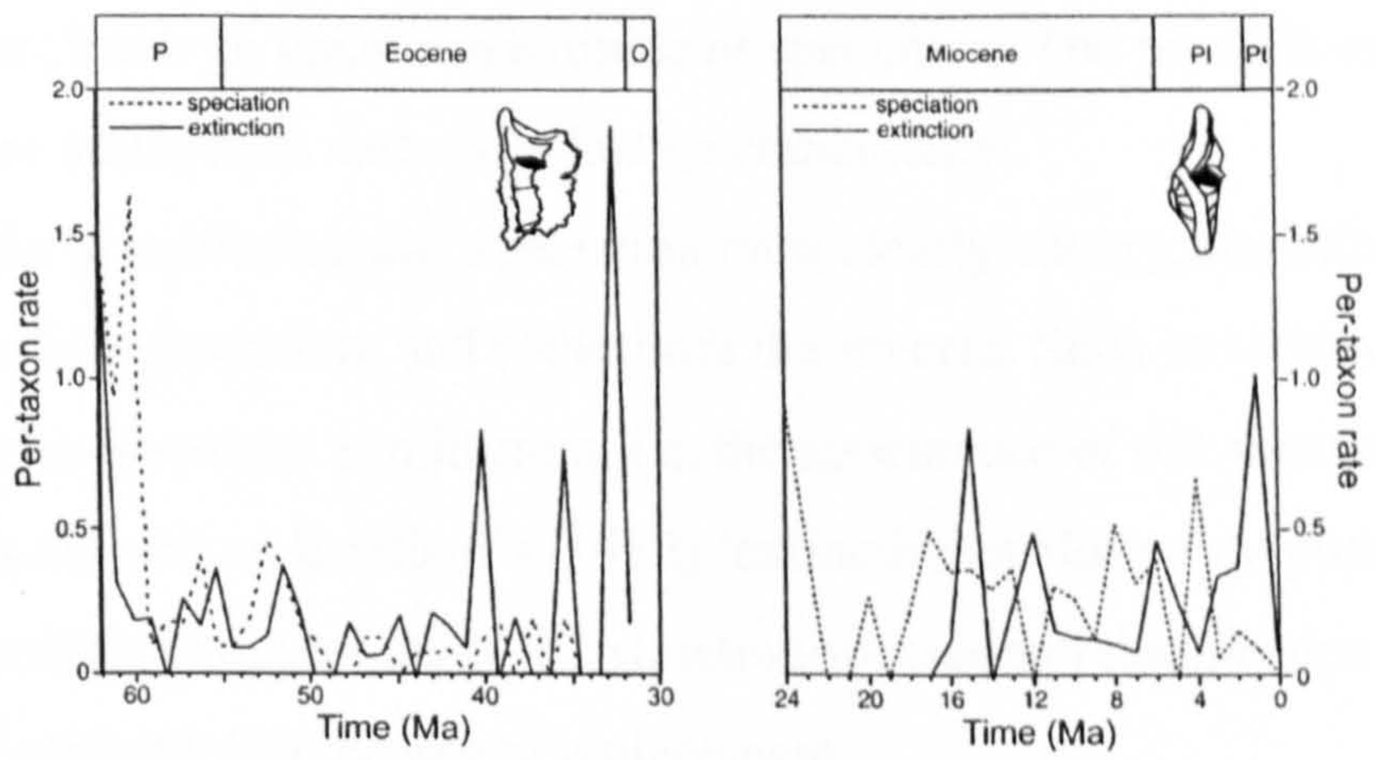

Figure 2.8. Per-taxon extinction and speciation rates of Palaeogene (left) and Neogene (right) globorotaliforms.

In contrast the data for the Neogene globorotaliforms show little relationship between extinction and speciation events. Four prominent extinction events (at 15, 12, 6 and 1 Ma) appear to have suppressed diversity throughout the Neogene in a step-wise fashion. Despite having lower magnitudes, the 'background' rates appear higher in the Neogene globorotaliforms. A similar result was presented by Stanley *et al.* (1988), when comparing Neogene globigerinids to globorotaliids. The latter exhibited higher rates for lower absolute diversity, which was explained by smaller population sizes with more patchy distribution (Foraminiferida and Bivalvia).

2.3.2.4 Inferences

The whole dataset and subsets thereof show highly variable extinction rates since the Jurassic. This result parallels those reported by Wei and Kennett (1983), Stanley *et al.* (1988), Pearson (1992) and Prokoph *et al.* (2000) for other datasets of Cenozoic planktonic foraminifera.

The planktonic foraminifera were clearly subjected to several large extinction events from the late Mesozoic to present day, although the assemblages from different depth habitats were not affected equally. Various points of interest are marked by the circled numbers 1-4 (Figure 2.6). Point 1 marks the K-T boundary with a prominent extinction spike. There is a speciation peak of the same magnitude almost congruent with it, but lagging slightly (~1 My). Point 2 marks extinction and speciation peaks of similar magnitude, but with speciation preceding extinction. Point 3 marks congruent speciation and extinction peaks, with a greater magnitude of extinction, while point 4 denotes the same congruence, but with greater magnitude of speciation. The possible causes of these patterns are more ambiguous and could just be coincidental.

The peaks in extinction and speciation rates clearly covary, sometimes with extinction preceding speciation, and sometimes the reverse. Such covariation could be explained in terms of species equilibrium, i.e. the appearance of one biospecies may drive another towards extinction. Emiliani's (1982) 'extinctive evolution' hypothesis could certainly be invoked to support the K-T extinction/speciation relationships (figures 2.6-2.8), by way of opportunistic ecospace replacement.

Collins (1989) also observed the covariation of speciation and extinction rates in the data of Blow (1979), and proposed evolutionary equilibrium as an explanation. Wei and Kennett (1986) invoke the diversity equilibrium concept and suggest that equilibrium diversity is maintained by the maximum availability of resources or ecospace in a given environment. When the diversity increases above the equilibrium, evolution is more likely to favour extinction, and when diversity is below equilibrium, speciation is favoured.

A possible alternative explanation for this apparent covariation in extinction and speciation rates is that environmental fluctuations promote the probability of both processes simultaneously (Stenseth and Maynard Smith's Stationary Model). The correlation may result from the pseudospeciation and pseudoextinction of phena in evolving lineages. This is discussed more in Section 2.3.5 below.

2.3.3 Periodicity in the planktonic record?

Mechanisms of long-term evolution from interpretation of the fossil record fall into two greatly contended schools of thought. Non-linear models endorse more intrinsic instabilities within ecosystems opening habitats to persistent taxa (e.g. Bak *et al.*, 1988; Plotnick and McKinney, 1993), while at the other end of the spectrum, catastrophic models suggest evolution and mass extinction are driven by extrinsic events with a periodicity of between 26-35 My. Examples of the latter philosophy include bolide impact (e.g. Raup and Sepkoski, 1984; Rampino and Stothers, 1986), sea-level change (Hallam, 1989), volcanism (Stothers, 1986), and magnetic reversal (Stothers, 1993). Figure 2.9 below is a reproduction of Raup and Sepkoski's (1984) periodicity figure that generated considerable interest and controversy in the 1980s. This figure illustrated the 26 My extinction periodicity proposed by these authors from a familial-level data set of fossil marine vertebrates, invertebrates and protozoans for the last 250 My.

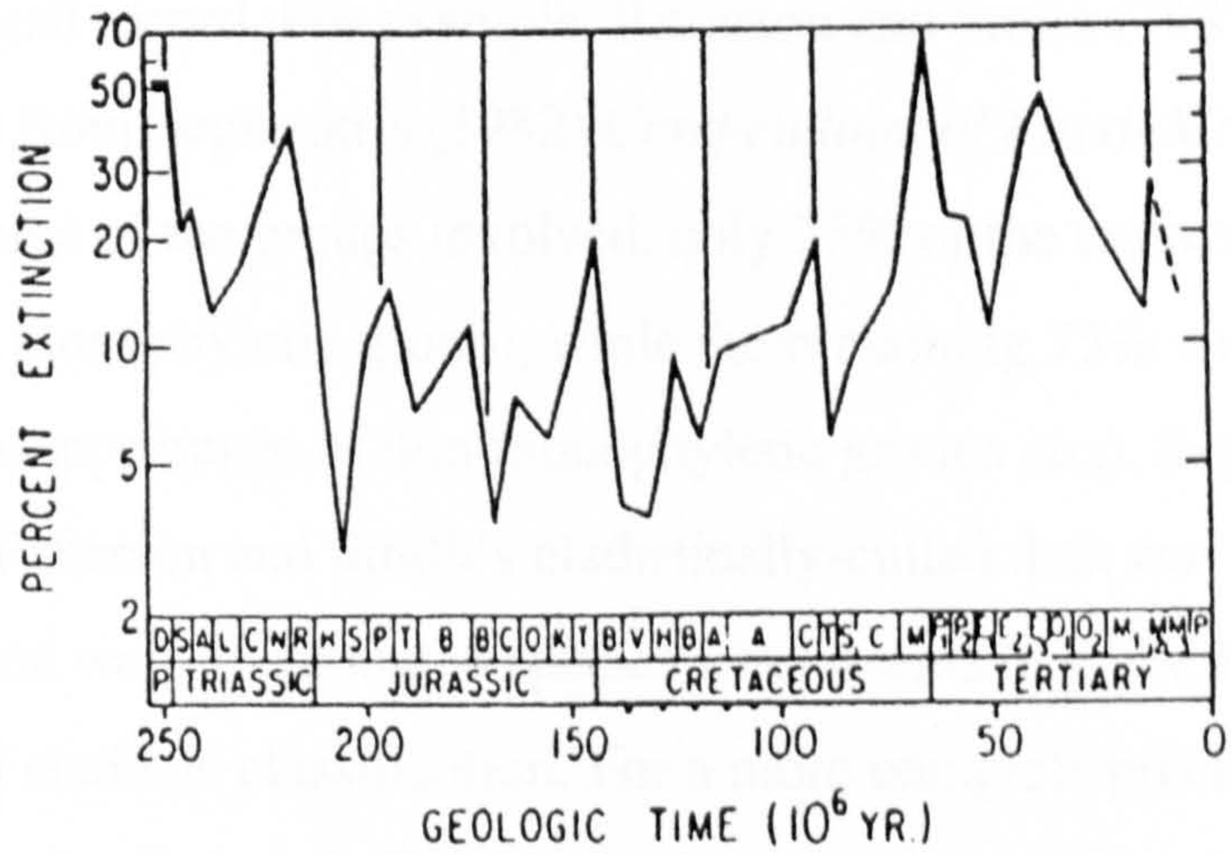

Figure 2.9. Original extinction record of fossil families of marine vertebrates, invertebrates and protozoans for the past 250 Ma of Raup and Sepkoski (1984). Letter codes identify stratigraphic stages. The 26 My best-fit for the Cretaceous and Tertiary is shown by the lines.

Raup and Sepkoski's time-series results were seemingly supported by Fourier analysis of their data, from which a pronounced harmonic peak was derived that corresponded to ~30 My. They admitted later that this could be an artefact of the temporal spacing between extinction peaks allowing random data to appear periodic to Fourier analysis (Raup and Sepkoski, 1986). However, their other statistical analyses (nonparametric and autocorrelational) also seem to support cycles close to 26 My.

If this periodicity is actually a signal and not an artefact of the data or statistical tests used, then is the periodicity an intrinsic (biotic) or extrinsic (environmental) phenomenon? If the physical environment is responsible, then is it terrestrial or extraterrestrial?

Results of this nature breed fanciful hypotheses, the most famous of which is probably that of Nemesis, so named by Davis *et al.*, (1984). Nemesis is the Sun's hypothetical companion star which has a trajectory that brings it close to the Sun every 26 million years, at which point it passes through the comet-filled Oort Cloud and dislodges extraterrestrial bodies in the general direction of Earth (see also Raup, 1986). Unfortunately nobody has been able to prove the existence of the star. At least two of the extinctions (K-T and Late Eocene) are associated with some evidence of coincidental bolide impact (see Alvarez *et al.*, 1980; Alvarez *et al.*, 1982), although it has been impossible to establish a definite correlation between extinction and impact in the Late Eocene (in contrast, see Keller *et al.*, 1992).

Various authors have criticised the datasets and methodology used to imply periodicity in the fossil record. For example, Patterson and Smith (1987) re-evaluated the family-level dataset from Sepkoski's (1982) *Compendium of Fossil Marine Families* and concluded that in some of the groups involved, only 25% of the extinctions were real (disappearance of a monophyletic group), while the remaining 75% were chiefly noise (mistaken dating, disappearance of non-monophyletic groups *etc.*). Sepkoski's reply (1987) argued that Patterson and Smith's cladistically-culled data was invalid because it failed to show several well-documented species level events (e.g. the K-T event), and that this is an artefact of cladistic classification. For a more complete précis of arguments and counter-arguments regarding periodicity in the fossil record, see the discussion in Sepkoski (1990).

A fundamental problem with the datasets used as evidence for periodicity in extinction rates is that they contain organisms that are often poorly represented (e.g. terrestrial taxa, marine vertebrates) in the fossil record, and thus range data may be artificially truncated by missing the true last occurrence datum (Signor-Lipps effect, Signor and Lipps, 1982). The record of extinction in the pelagic realm is particularly useful because it is commonplace to have sediments that consist almost entirely of fossils. Perhaps in order to test the periodicity hypothesis, more datasets of planktonic marine microfossils should be targeted. However, further complications are added when trying to

identify true extinction and speciation in such groups as the planktonic foraminifera (see discussion in Section 2.3.5.2).

Prokoph *et al.* (2000) tested a similar morphospecies-level planktonic foraminiferal dataset to that used here, containing 622 morphospecies (22 more than the Plankrange dataset*), through the last 127 million years. Fourier analysis of the per-taxon extinction and speciation rate time series data revealed a ~31 My periodicity (see Figure 2.10 below), above the red and white noise levels of Mann and Lees (1996), even with the K-T boundary extinction set to zero.

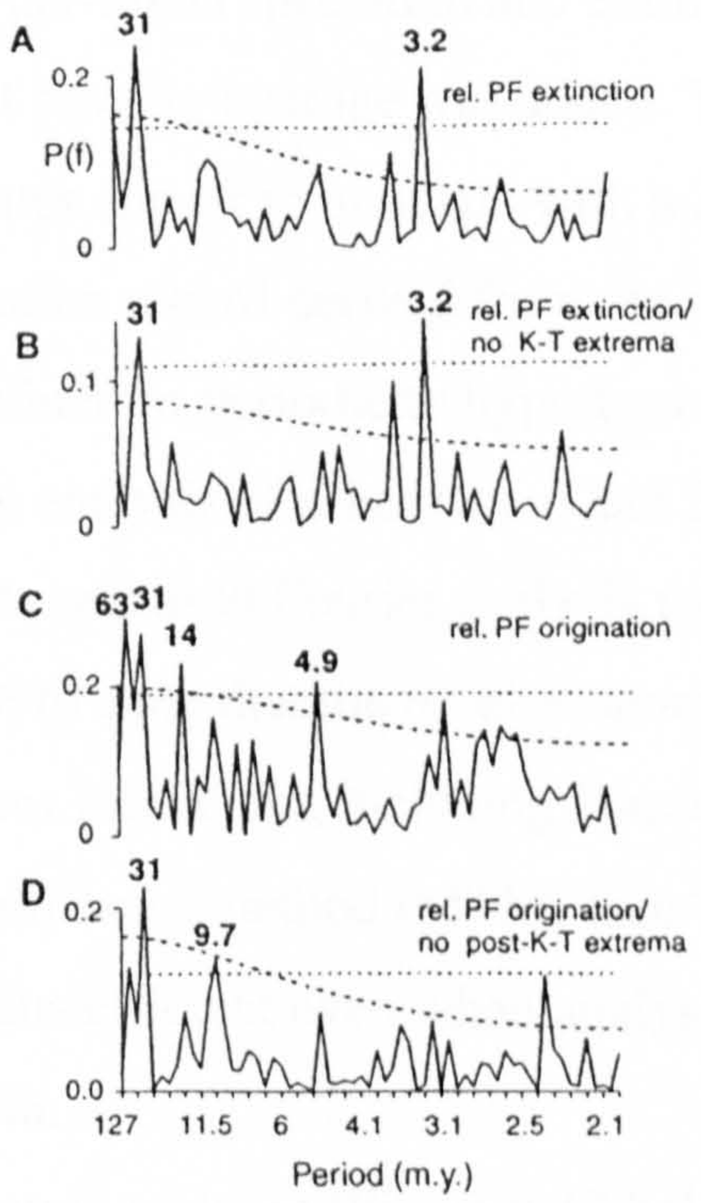

Figure 2.10. Spectral analysis of (A) relative planktonic foraminifera (PF) extinction; (B) relative PF extinction with data at Cretaceous-Tertiary (K-T) boundary set to zero; (C) relative PF speciation; and (D) relative PF speciation with data at K-T boundary set to zero. Dotted horizontal lines mark 95% confidence level for non-randomness of spectral estimation; dashed lines mark red noise level (Mann and Lees, 1996). Figure adapted from Prokoph *et al.*, 2000.

The data were then randomly shuffled and analysed using spectral analysis, which revealed none of the same periodicities and a strong increase of dimensionality consistent with random behaviour (Prokoph *et al.*, 2000). Because spectral analysis cannot detect whether the apparent cyclicity in the planktonic record is random or deterministic (Prokoph and Barthelmes, 1996), these authors tested their record against four synthesised models supposed to replicate random data, with added white noise (a combination of

---

* The dataset of used in Prokoph *et al.* (2000) was constructed using a fraction of the range references used in the Plankrange dataset, and it appears over-split taxa were more willingly included.

multiple frequencies). The results of this correlation function analysis were interpreted to suggest that the planktonic foraminiferal record was influenced by deterministic and not stochastic processes.

Any cyclicity signal within this kind of dataset could be obscured by a number of potential error sources: imperfection and diachroneity in the fossil record, timescale imprecision, normalisation of biostratigraphic datums to a single timescale, use of different timescales, taxonomic over-splitting and synonymy; to name but a few. Perhaps more importantly, the inability of range data to deal with anagenetic lineages could provide the most important source of error (this is discussed further in Section 2.3.5).

In Figure 2.11A-B, the per-taxon speciation and extinction curves (from Figure 2.6) were separated and a five-point moving average was added. The smoothed curves in both the extinction and speciation rates appear to undulate with a 25-35 My cyclicity. At face value, the extinction and speciation record derived from the morphospecies-level dataset used here might support the extinction-periodicity hypothesis.

As discussed above, the analysis of other (Raup and Sepkoski, 1984, 1986; Prokoph *et al.*, 2000) fossil data sets used Fourier analysis to imply a periodic signal in extinction data. Yiou *et al.* (1996) state that the relative shortness of natural time series renders most analysis techniques inefficient, including Fourier analysis. The use of more robust methods such as the multi-taper method (MTM) (see Thomson, 1982) is recommended because it remains efficient even when analysing a series, which is non-continuous and/or sparse in data.

Preliminary power spectral analyses (Figure 2.12 below), conducted in collaboration with Heiko Pälike, using the MTM revealed statistically-significant (above the 95% threshold for estimated red noise) frequencies in per-taxon extinction and speciation rates in the Plankrange series, equivalent to 36 My, ~4.9 My and ~2.4 My. This non-parametric method employs a small set of tapers (= eigenvectors/windows) to reduce the variance of spectral estimates. In principle, the MTM allows spectra generation with higher frequency than other methods (e.g. Blackman-Tukey and maximum entropy) and is useful for analysing time series believed to exhibit continuous and singular components (Percival and Walden, 1993). Statistically significant periodic frequencies in the data (presented here) are broadly consistent with those of Prokoph *et al.* (2000): 31 My, 14 My, 4.9 My and 3.2 My.

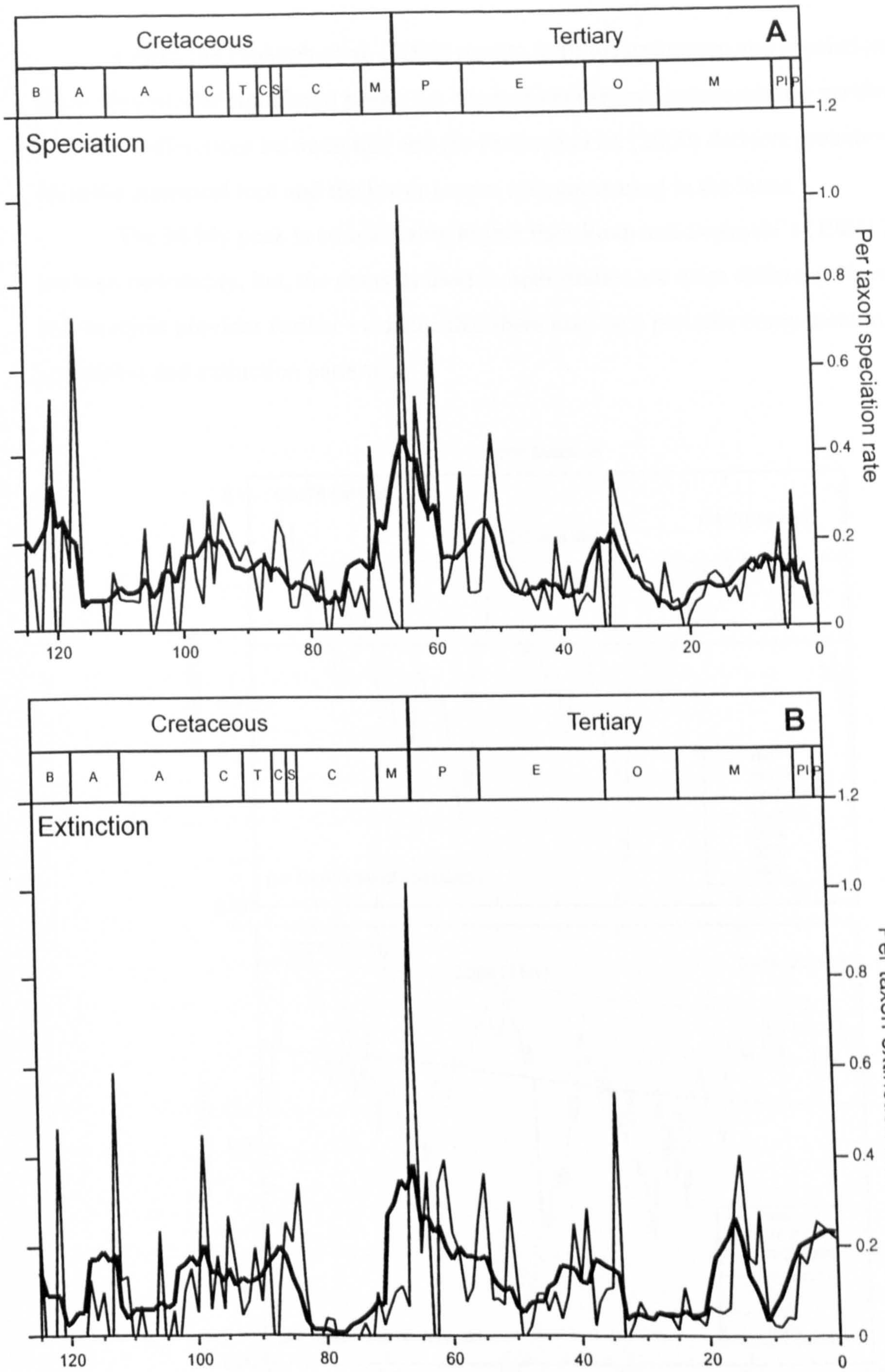

Figure 2.11. Per taxon speciation (top) and extinction (bottom) rates for all planktonic foraminifera (600 species) from Cretaceous to Recent (thin line), with smoothed five-point moving averages (thick line).

Unlike the Prokoph *et al.* (2000) results, both the extinction and speciation results show very similar significant peaks, i.e. the periodicities are independently verified by both datasets. Differences between this and the Prokoph *et al.* (2000) datasets probably arise from the statistical tool and the fewer source references used in the latter.

The 36 My peak is considerably higher than Raup and Sepkoski's (1984) 26 My average periodicity, but, the datasets used in both studies are quite different. Nevertheless, this analysis provides further evidence that there may be a periodic component to speciation and extinction patterns.

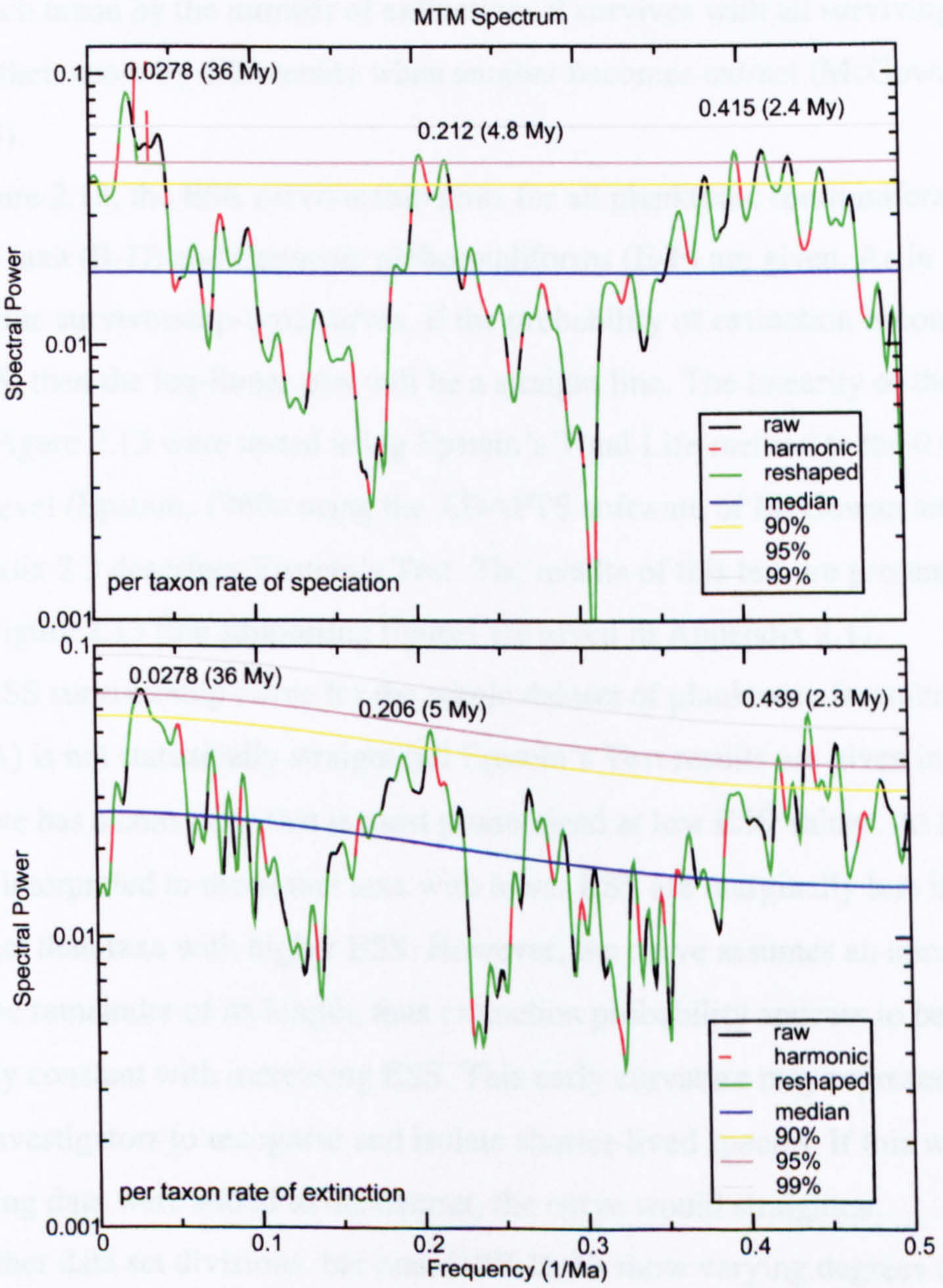

Figure 2.12. MTM power spectral analysis of the Plankrange data showing significant periodicities and estimated noise levels. Red peaks (top left of speciation signal) are components of the spectrum associated with a periodic signal. The red spectral trace indicates where the estimated harmonic or periodic component of the spectrum should be displayed, as a function of frequency; while the reshaped spectral trace (in green) indicates where noise has been removed, and the signal recalculated.

Future work will involve computing per-taxon extinction and speciation data at a higher temporal resolution (i.e. 0.7 My) to avoid error associated with a periodicity arising from multiplication of the temporal resolution (1 My).

2.3.4 Survivorship of the planktonic foraminifera

Survivorship analysis was conducted on the Plankrange database with the use of the Extinction Survival Score (ESS) (see McGowan and Pearson, 1998 for discussion). This correction was used to eliminate the effect of non-constant extinction probability. The ESS scores each taxon by the number of extinctions it survives with all surviving taxa incrementing their score by 1/Diversity when another becomes extinct (McGowan and Pearson, 1998).

In Figure 2.13, the ESS survivorship plots for all planktonic foraminifera (A), depth-divided taxa (B-D) and Cenozoic globorotaliforms (E-F) are given. As in Van Valen's dynamic survivorship-type curves, if the probability of extinction is constant with respect to ESS, then the log-linear plot will be a straight line. The linearity of the curves presented in Figure 2.13 were tested using Epstein's Total Life method to the 0.05 significance level (Epstein, 1960a using the ADAPTS software of McGowan and Pearson, 1998). Appendix 2.3 describes Epstein's Test. The results of this test are presented with each plot in Figure 2.13 (the supporting figures are given in Appendix 2.1).

The ESS survivorship curve for the whole dataset of planktonic foraminifera (Figure 2.13A) is not statistically straight (all Epstein's Test results are given in Appendix 2.4). The curve has a convexity that is most pronounced at low ESS values. At face value, this could be interpreted to mean that taxa with lower ESS are marginally less likely to become extinct than taxa with higher ESS. However, the curve assumes an almost linear attitude for the remainder of its length, thus extinction probability appears to become approximately constant with increasing ESS. This early curvature may represent the inability of investigators to recognise and isolate shorter-lived species. If this was the case and the missing data were added to the dataset, the curve would straighten.

All other data set divisions, bar one, (12B-D, F) show varying degrees of convexity, and all fail Epstein's Test. The Neogene globorotaliforms (12E) are the only taxonomic subset analysed that have a statistically straight survivorship curve according to Epstein's Test, although this subset only narrowly passes (Appendix 2.4).

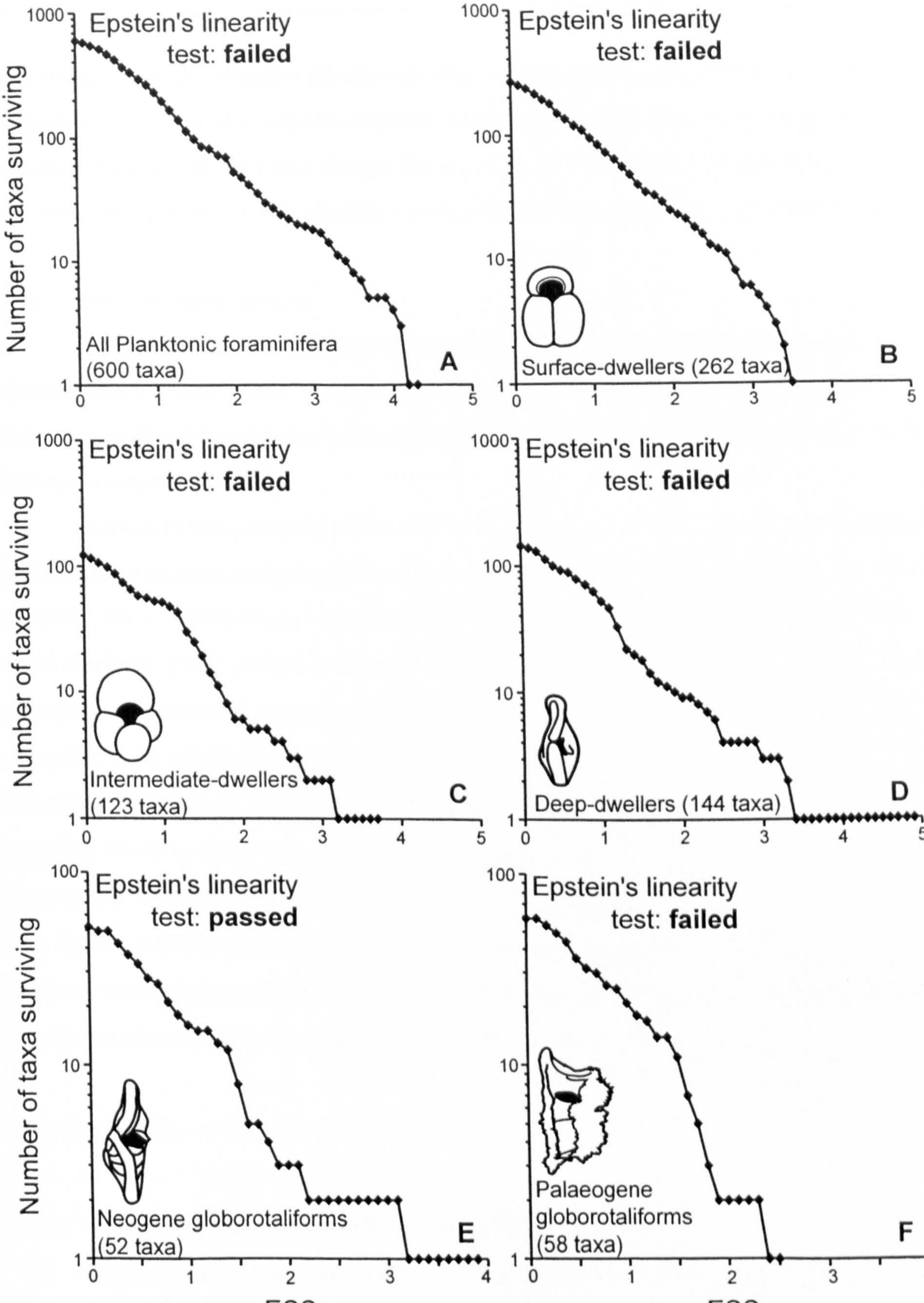

Figure 2.13. ESS survivorship plots for all planktonic foraminifera (A) and the various subsets thereof (B-F). Each curve is tested for linearity using Epstein's test (1960a,b). Only the Neogene globorotaliforms (E) have a statistically straight survivorship curve. Epstein's Test values are given in Appendix 2.3.N.B. The *x* axis denotes the ESS class. The class intervals used for generating ESS life tables are not specifically age-related, and so intervals start at 0 and increase by increments of 0.1. ESS and longevity are not strictly synonymous.

This implies that the Neogene globorotaliforms have a constant probability of extinction, independent of extinctions survived and diversity, although, this plot appears no more 'straight' than any of the other plots in Figure 2.13. As highlighted in Appendix 2.3, Hoffman and Kitchell (1984) pointed out that Epstein's method is not completely reliable.

2.3.4.1 Survivorship summary

The general tendency for the datasets analysed is that of low convexity which becomes more linear. These observations *may* support (ESS) longevity-dependent extinction probabilities for the 'young' taxa (those with low ESS), which then appears to become constant later.

Pearson (1992) used the Corrected Survivorship Score (CSS) to test the extinction probability of various datasets of Palaeogene planktonic foraminifera (those of Saunders *et al.*, 1973; Blow, 1979; Premoli Silva and Boersma, 1983; Tourmarkine and Luterbacher, 1985; Corfield, 1987). Pearson found that all datasets gave convex curves and were used to support a hypothesis of increasing extinction probability with taxonomic age, although the group had been originally used to exemplify the law of constant extinction without this correction. It should be noted that Raup (1978) stipulated that in order to avoid serious sampling errors in the survivorship approach, large datasets are necessary. With smaller datasets it is more difficult to fail Epstein's Test and therefore reject the null hypothesis (e.g. figures 2.13E and 2.13F). The fact that five of six datasets failed Epstein's Test implies a strong inherent pattern. In only the Neogene globorotaliforms, was the null hypothesis of constant extinction probability not rejected.

2.3.5 Discussion

2.3.5.1 A 'driving force' for planktonic foraminiferal evolution?

If species within an ecosystem are well-adapted, finely tuned by competitive pressures and natural selection and the physical environment has only minor effects, then the Red Queen mode of evolution holds (Benton, 1990). On the other hand, in Stenseth and Maynard Smith's (1984) Stationary Model of evolution, abiotic factors (environmental change) drive evolution and environmental stability breeds evolutionary quiescence.

In the history of the planktonic foraminifera (Figure 2.2), there are only certain periods when diversification rate is near zero. Isolated periods of near-community-stasis do

exist, which may imply to the Red Queen model, but, the majority of the diversification history fluctuates considerably, implying evidence for the Red Queen is only weak. Wei and Kennett (1986) employ the Stationary Model as the driving force for evolution in the Neogene planktonic foraminifera. Could environmental factors (fundamental to the Stationary Model) be driving evolution in all planktonic foraminifera?

It is likely that palaeoceanographic changes influence marine biotic evolution. Turnover in Cenozoic microfossils (radiolaria, calcareous nannofossils and planktonic foraminifera) show similar trends (see Hoffman and Kitchell, 1984). In addition, timing of diversification of marine molluscs in the Neogene is similar to that of the planktonic foraminifera (Hansen, 1988). Cifelli and Scott (1986) remarked that Neogene globorotaliids were diversifying at a time of changing water masses. Wei and Kennett (1986) correlated turnover peaks in the Neogene globorotaliids with oceanographic events in the Middle Miocene (16-14 Ma), and latest Miocene (6-5 Ma), albeit tentatively. Palaeogene groups also show some correlation: evolutionary rates are slow in the Middle Eocene and Oligocene in the planktonic foraminifera, radiolaria and calcareous nannofossils (data in Perch-Neilsen, 1985; Sanfillipo, *et al.*, 1985). If synchronous marine plankton turnover is evidence of oceanic transition affecting marine ecosystems, then periods of evolutionary quiescence may imply environmental stability (Pearson, 1990).

A number of studies have attempted to link various oceanographic causal factors to plankton evolution: global temperature indicated by isotopic studies (Jenkins, 1973; Jenkins and Shackleton, 1979; Brasier, 1988; Keller *et al.*, 1992), latitudinally-controlled temperature gradients (Lipps, 1970; Stehli *et al.*, 1972), vertical thermal gradients (Boersma and Premoli Sliva, 1986), water mass subdivision (Ottens and Nederbragt, 1992), horizontal and vertical productivity gradients (Boersma and Premoli Sliva, 1986; Hallock, 1987; Hallock *et al.*, 1991), geographic range (Wei and Kennett, 1983, 1986; Stanley *et al.*, 1988), sea level and plate tectonic events (Pearson, 1990). Furthermore, some studies of phyletic evolution in foraminifera conclude that increased evolutionary rates are related to oceanographic changes (e.g. Malmgren and Berggren, 1987). Palaeoceanographic factors probably play some part in influencing planktonic evolution and diversity, but proving direct correlation or degree of influence to plankton evolution is inherently difficult.

The fossil record of the planktonic foraminifera is not dominated by continuing morphological innovation, as suggested by the Red Queen. A major characteristic of their

history is heterochronous homeomorphy, i.e. convergent evolution of similar body plans reciprocated in three radiations (Cretaceous, Palaeogene and Neogene) (e.g. Cifelli, 1969; Norris, 1991). It seems highly unlikely that the directional convergence observed in the planktonic foraminifera was caused by similar palaeoceanographic changes occurring in three separate epochs that steer evolutionary trends (see Norris, 1991 for discussion). "To adhere strictly to the Stationary Model [and thus only abiotic factors driving evolution] would be to deny the very essence of evolution as an innovative process" (Pearson, 1990). Equally, the simplistic view of the Red Queen model as continuous unidirectional evolution (Benton, 1990) could not alone produce iteration on this scale.

A number of other parameters influence the evolutionary history of the planktonic foraminifera, i.e. population dynamics, mass extinction and genetic conservatism. Stanley *et al.*'s (1988) study of macroevolution in the two major Neogene clades (globigerinids and globorotaliids), found that mean longevities of globorotaliids were about half those of globigerinids (6.3 My vs. 10.5 My), while survivorship rates were lower too (although no correction was used). A similar result for longevity, was later presented by Norris (1991) when investigating the apparent directional evolutionary trend from non-keeled to keeled forms, for the Cretaceous, Palaeogene and Neogene. Norris found that mean morphospecies durations for keeled forms were also approximately half that of non-keeled forms (5-6 My vs. 8-10 My), and demonstrated that each of the three planktonic foraminiferal radiations were initiated by small-sized, un-keeled taxa. Further, Stanley *et al.* found that per-taxon rates of speciation and extinction were high in Neogene globorotaliids, even when there was no change in diversity; this was not the case for the Neogene globigerinids. They concluded that evolutionary turnover was more rapid in the Neogene globorotaliids than globigerinids. In this case, is evolution selectively discriminating keeled forms throughout geological history, and if so, why?

The study presented in this chapter (Figure 2.3) shows much lower diversities and less stability in the intermediate and deep-dwelling populations, than for the surface-dwelling populations. Diversification rates in the intermediate and deep-dwelling populations (in Figure 2.4) are also generally more erratic than in the surface-dwellers; and certainly for the deep-dwellers, per-taxon speciation and extinction rates (Figure 2.8) are equal to, or slightly higher than those of surface-dwellers for about half the absolute diversity (Figure 2.3). Stanley *et al.*'s hypothesis that Neogene globorotaliids have smaller and less stable populations may also hold true for deep and intermediate-dwelling

populations of all planktonic foraminifera. Interestingly, this pattern is mirrored by that of Neogene marine Bivalvia, in which small, patchy, unstable populations also show high rates of extinction and speciation (Raffi *et al.*, 1985; Stanley, 1986).

When comparing Palaeogene and Neogene globorotaliforms (Figures 2.5 and 2.8), although absolute diversity magnitudes are approximately equal, speciation and extinction rates in the Neogene taxa are generally higher (excluding outliers at ~ 60 Ma and ~ 32 Ma in the Palaeogene taxa). So it seems that the non-keeled species may be more resistant to extinction than keeled species, perhaps through being more genetically conservative. Norris (1991) suggested that mass extinctions at the K-T and E-O boundaries helped drive evolutionary trends by selectively eliminating certain morphotypes and permitting the survivors to found the next radiation. If the pioneering taxa in each radiation are non-keeled, then it follows that they have the potential for longer durations.

Alternatively, higher evolutionary rates could be attributed to taxonomic artefact owing to the fact that the compressed globorotaliid form makes for more taxonomic characters and so an easier (more split?) taxonomy.

2.3.5.2 The range data problem

The conclusions drawn in this chapter all rely on the adequacy of the original range data to represent fossil 'species' through time. If evolution in a group were misinterpreted, inaccurate ranges could be recorded.

Simpson (1953) separated structural evolutionary rates in single lineages (i.e. anagenesis) from taxonomic evolutionary rates, i.e. the rates of cladogenesis (lineage branching) and extinction in a clade or higher taxon. Ideally evolutionary investigations must include both. Where cladogenesis occurs, distinct taxa with distinct FADs/LODs can potentially be delineated. However, the Linnaean taxonomic method of phenetic assignation does not deal with anagenesis well. Division of anagenetic lineages to fit range data presents a problem. How does one isolate a 'species' in such a lineage, and where do those 'species' originate and expire in time? Artificial division of anagenetic lineages could lead to misleading results and spurious conclusions.

There are many different species concepts, each subject to its own limitations and implications (see Smith, 1994 for review). None of these species concepts adequately reflects the fluidity of foraminiferal evolution. For example, Mayr's (1969) biological species concept (advocated by a large number of biologists) relies on the potential for the

recognition of interbreeding in morphologically-distinct populations (biospecies). Although Brasier (1980) reports an asexual breeding phase for benthic foraminifera, Hemleben *et al.* (1989) suggest probable sexual reproduction in modern planktonic foraminifera with no evidence of an asexual phase. Mayr's biological species concept is not directly applicable to fossil planktonic foraminifera because population interbreeding cannot be tested. The term (bio)species should probably be restricted to extant taxa only, in which interbreeding can potentially be observed.

In contrast, Simpson's evolutionary species concept is based on the assumption of correlation between reproductive isolation and degree of lineal morphological divergence, and is therefore reduced to the subjectivity of morphological definition (Smith, 1994). Yet there is still the need to refer to planktonic foraminiferal species and the subtle morphological species distinctions, because of their extensive utility in biostratigraphy and palaeoecology. Quilty (1969: p. 42) criticised planktonic foraminiferal taxonomy because it is based on "...specifically non-diagnostic characters... [which]...have no taxonomic significance, even though they have some empirical stratigraphical significance." Quilty's comment is manifestly flawed. If a character has a genuine stratigraphic significance, it *must* have evolutionary basis. The fact that planktonic foraminiferal species taxonomy is tested extensively by biostratigraphers makes it far more robust than a taxonomy created by evolutionary theorists for obscure fossil groups, even if higher level groupings may be willfully artificial. Moreover, it remains that stratigraphic utility is the driving force behind micropalaeontological taxonomy (Pearson, 1992).

Planktonic microfossil populations tend to be well-mixed and population lineages sometimes evolve gradually with morphologies that completely intergrade (Kellogg, 1975, 1983; Malmgren and Kennett, 1981; Arnold, 1983; Corfield and Granlund, 1988; Norris *et al.*, 1996). It is possible to recognise discrete morphological groups in such populations, which may or may not represent distinct biological species. Typically, species are defined by an arbitrary point in morphospace (a type specimen), which may only represent a small part of the genetic (and consequent morphological) variation that occurs naturally in species within interbreeding populations. Fordham (1986) proposed the term phena (singular phenon) for typologically defined taxa, and refers to the 'minimum morphological units in the fossil record that are consistently diagnosable on the basis of meaningful characters'. Pearson (1993) avoided use of this term because of its links with

numerical taxonomy. Instead he introduced the concept of morphospecies to avoid confusion between biological and morphological species ideas (Figure 2.14).

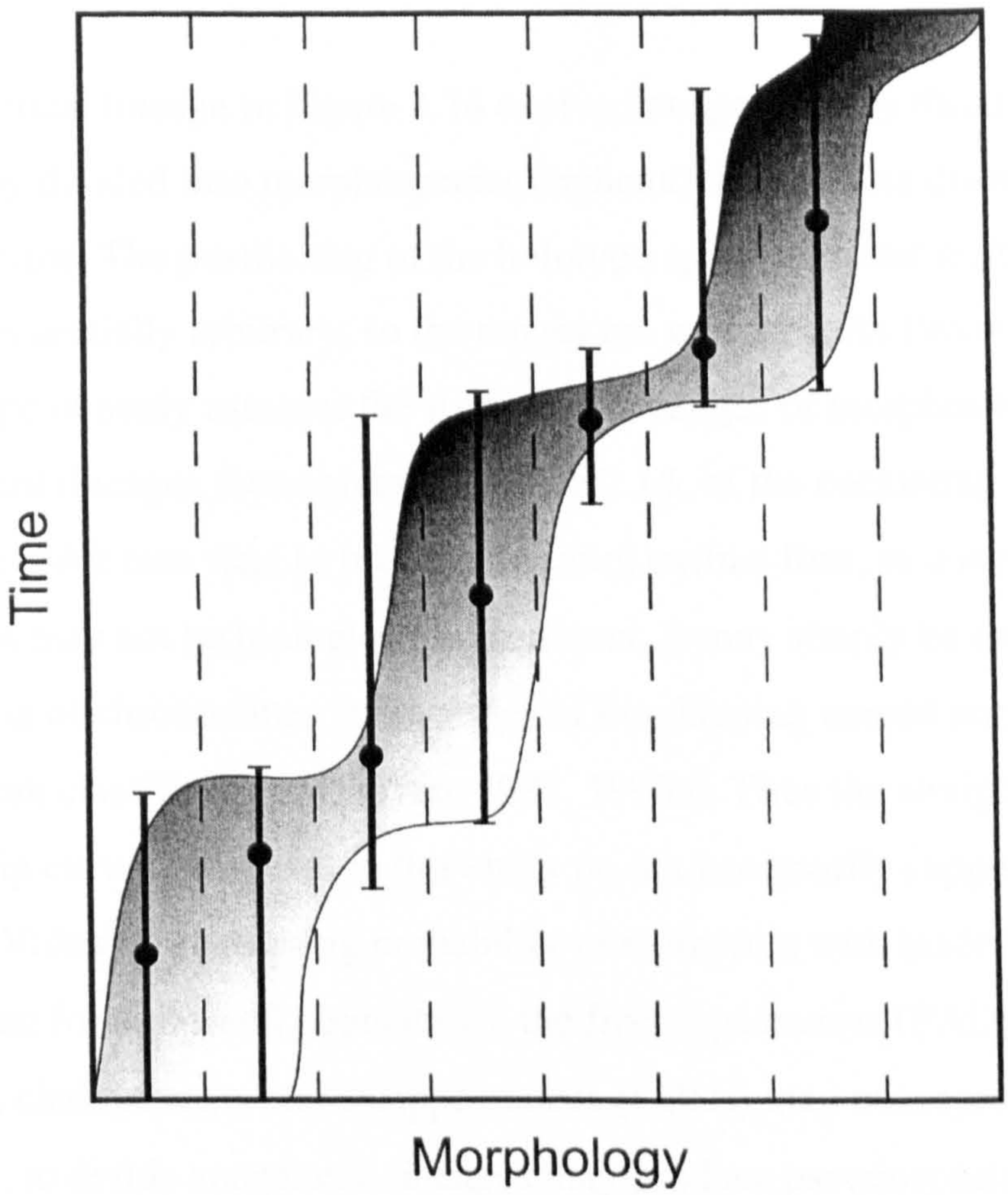

Figure 2.14. The arbitrary subdivision of an evolving lineage, adapted from Pearson (1993). This lineage is subdivided into its morphospecies (black bars) within the evolutionary morphospace (grey-shading). Type-specimens (black circles) are chosen to define the taxa. The taxonomic grid delineates the taxonomic concepts artificially imposed on the lineage.

This debate is further complicated by the recognition of distinct genotypes (cryptic species) within morphospecies of modern planktonic foraminifera (Huber *et al.*, 1997; de Vargas *et al.*, 1997, 1999, 2001; Darling *et al.*, 1999; Stewart *et al.*, 2001; Kucera and Kennett, 2002), where a single morphospecies may contain multiple genotypes. Moreover, some extant planktonic foraminiferal biospecies exhibit a number of generic-level forms through ontogeny (see Hemleben *et al.*, 1989). The exclusion of cryptic species, although necessary because fossil forms are generally not extant, could produce great underestimation in measured evolutionary metrics. If all cryptic species were to be included, absolute diversities, diversification, extinction and speciation rates would all be higher.

All reference to planktonic foraminiferal species in this thesis, as identified by their Linnaean binomen (e.g. *Globorotalia tumida*), relate to the specific published holotype concept, which in reality are morphospecies and do not necessarily represent biological species.

The hypothetical lineage in Figure 2.14 evolved anagenetically through time. This lineage is artificially divided into morphospecies (=phena) that possess distinct and different ranges in time. The positioning of the holotype specimens and the taxonomic grid (on the *x* axis) are essentially arbitrary, so the ranges are arbitrary. As Pearson (1992) pointed out, this type of study assesses the stratigraphic ranges of morphospecies as opposed to the parent lineages themselves. In Figure 2.14, of the coexisting morphospecies, the older taxa tend to become (pseudo) extinct first, so convexity of survivorship curves may not be biologically significant. It may simply be an artificial result of the division of chronoclines into a series of overlapping named segments by adhering to Linnaean classification (Pearson, 1992, 1995a). Thus the straight to slightly convex survivorship curves presented in this study do not necessarily support age-independent (Van Valen) or increasing probability of extinction with taxonomic longevity.

In planktonic foraminiferal populations, the first appearances (FADs) may not always result from cladogenesis, and disappearances (LODs) may not represent true extinctions; that is, to divide anagenetic lineages may produce pseudospeciation and pseudoextinction. In such a case, it follows that fossil stratigraphic ranges are artificial constructs. Whether anagenesis is more prevalent in marine protists than in other groups, all palaeontologists attempting to analyse evolution in this way need to consider the potential effects of this phenomenon on their results. In any given monophyletic group, a proportion of the originations will have been cladogenetic and a proportion of the extinctions will have been true extinctions. The effects of pseudospeciation and pseudoextinction could render any conclusion about diversity, speciation and extinction uncertain. So is this a significant problem for interpretations using range data of this kind?

It could be argued that anagenesis only accounts for a minor component of evolution in the history of planktonic foraminifera. For a dataset containing 600 taxa, quantifying anagenesis is probably a fruitless and inherently subjective task.

From my own experience of the Neogene record, anagenetic lineages are often restricted to few (2-3) morphospecies (see Chapter 6), before the lineage is 'broken' by true extinction or cladogenesis. However, there are examples where such lineages contain

more morphospecies, e.g. the fohsellids. This example perfectly exemplifies the importance of cryptic speciation to anagenetic concepts. Traditionally, this lineage is viewed as an unbroken anagenetic lineage from *F. peripheroronda* to *F. robusta*. An alternative could be a multi-species plexus with a directional trend.

Ultimately, taxonomic ranges represent periods of time in which morphospace is occupied. I would argue that morphospecies-level datasets of this kind *are* useful in studying evolution, but workers must be aware of the limitations applied through the methodology.

Some authors (Stanley *et al.*, 1988; Pearson, 1996) reported to have eliminated pseudoextinction/pseudospeciation from their analysis of Cenozoic planktonic foraminifera by analysing total lineage durations, and not species-level ranges. This procedure could eliminate the uncertainty associated with pseudospeciation and pseudoextinction from the geological record of the group in question, leaving only genuine cladogenesis and terminal extinction.

Pearson's (1996) lineage phylogenetic survivorship analysis (normalised using the CSS) produced survivorship curves that were acceptably straight using Epstein's Test, which apparently supported Van Valen's hypothesis of longevity-independent extinction probability. This directly contrasts with the convex curves produced using the earlier morphospecies longevity analysis (Pearson, 1992), which appeared to support increasing extinction probability with taxonomic age. The conclusion was that survivorship analysis of morphospecies-level datasets could yield results that are *wholly* taxonomic artefact.

In Stanley *et al.*'s study, pseudoextinction was eliminated by "identifying phyletic transitions between chronospecies", using the subjective taxonomy of Kennett and Srinivasan (1983). Regardless of whether a worker agrees with their selections and omissions, this process is probably as subjective as the artificial division of anagenetic lineages.

Quantifying anagenesis and removing the effects of pseudoextinction on the range data presented in this chapter would probably be a thankless and effectively impossible task. To attempt this for the much larger datasets of higher taxa (e.g. of the Raup, Sepkoski and Benton type), would be an even more so! We should take comfort from the words of Simpson (1944, p. xviii):

"For almost every topic discussed in the following pages the data are insufficient. The student who attempts interpretations under these circumstances does so in the face of certainty that some of his conclusions will be rejected. It is, however, pusillanimous to avoid making our best efforts today because they may appear inadequate tomorrow. Indeed, there would be no tomorrow for science if this common attitude were universal. Facts are useless to science unless they are understood".

2.4 Conclusions

The evolutionary history of the planktonic foraminifera is shown here to have been dominated by considerable fluctuations in turnover, with intermittent periods of near-static evolution. Attribution of this pattern to Stationary models (dominated by physical environment), or equilibrium models (dominated by Red Queen biotic interactions) is still uncertain. In reality, both factors have probably played significant roles in shaping the evolution of planktonic foraminifera and other extinct groups.

Evidence is presented here that intermediate and deep-dwelling populations may have higher rates of turnover for lower diversity than their shallow-dwelling cousins. This could be explained by relative structural instability in these ecological groups as suggested by some authors (Stanley *et al.*, 1988; Norris, 1991). In addition, the evolutionary history of the Neogene globorotaliforms (which contain *Globorotalia*) appear to show greater turnover for a more slowly developing diversity than the Palaeogene forms, which could be consistent with pressure from globigeriniforms already occupying the deeper niches. This kind of pressure did not apply to the Palaeogene globorotaliforms because the K-T mass extinction left very few (~4) taxa alive.

What is clear is that substantial extinction 'events' have had significant influence on the evolution of the planktonic foraminifera. Such events, coupled with the population characteristics of the deeper-dwellers, may have contributed to the heterochronous homeomorphic pattern (the repetitive development of a similar morphological dichotomy in distinct radiations through time) that is so well known in planktonic foraminiferal history.

Preliminary results presented in this chapter could provide further evidence that evolution is influenced by one or more biological and/or physical periodic events, as supported by various authors over the last 20 years. The results presented here employ the

spectral analysis multi-taper method, which has been shown to be more reliable when analysing time series of the type presented here (non-continuous and derived from nature). Statistically significant periodic frequencies equivalent to 36 My, 4.9 My and 2.4 My are supported in both per-taxon speciation and extinction data to a 1My resolution, for the past 125 My of planktonic foraminiferal history.

Range data were also used to study survivorship patterns in the planktonic foraminifera (and ecological depth divisions thereof). By applying the ESS to these groups the resultant survivorship curves (figures 2.13A-D) revealed slightly convex curves in all but one of the data sets. One might argue that extinction probability increases with extinctions survived, or if the initial convexity were an artefact of missing data from unidentified short ranging taxa, then the planktonic foraminifera do actually support the law of constant extinction (as suggested by Van Valen, 1973; Arnold, 1982).

Finally, all conclusions presented here depend on the ability of the original data to represent the ranges of the taxa under consideration accurately. Anagenetic lineages, of the type known to occur in the planktonic foraminifera, may present a problem in the morphospecies-level dataset. Some workers have used lineage phylogenies to eliminate the effects of pseudospeciation and pseudoextinction; however this approach is still affected by the subjectivity of the stratophenetic phylogenetic method (see Chapter 6) that is inherent in the taxonomic sources used to compile palaeontological range data. It is argued here that morphospecies-level range data are still useful and potentially informative, provided that the limitations and potential sources of error are understood.

Integrated approaches to planktonic foraminiferal phylogeny (of the type presented in chapters 5-6) will provide better understanding of anagenesis, and its effect on range chart databases. Although much can be done with this kind of dataset, the basic diversity analyses (e.g. figures 2.1, 2.3, and 2.5) probably constitute the most informative and interesting results. Further insight into palaeoceanographic and evolutionary processes could be gained by direct comparison with similar data derived from other marine microfossil groups.

Chapter 3

Materials

In this chapter, the source fossil material and the methodologies used in the remaining studies (Chapters 4-6) presented in this thesis are discussed. A more detailed account of study-specific methodology is given in some individual chapters. This chapter describes the purpose, background and methodology of field excursions to Tanzania and New Zealand, fossil material from which was used in this thesis. In addition, the majority of the planktonic assemblages used to conduct the investigations presented in this thesis came from shipboard sampling during Ocean Drilling Program Leg 194. This chapter also summarises the scientific basis behind Leg 194, the methods used to recover the material, and the importance of planktonic foraminifera in creating accurate age models upon which the Leg science is based.

3.1 Tanzania: 9th September – 7th October, 2000

3.1.1 Introduction and scientific justification

The importance of preservation quality in foraminifera used to calculate ocean palaeotemperatures is now being appreciated (Norris and Wilson, 1998; Wilson and Norris, 2001; Pearson *et al.*, 2001; Wilson *et al.*, 2002). Many of the samples previously used for sea surface temperature (SST) estimation are from pelagic chalks and oozes in which foraminiferal shells typically become recrystallised on a micrometer-scale. This recrystallisation can potentially introduce a substantial component of neomorphic calcite which may bias the isotopic analyses toward "cool" values (Schrag *et al*, 1995; Schrag, 1999).

Typically, an investigator will assume foraminiferal assemblages to be 'well-preserved' if there is no visible test recrystallisation. However, the tests of planktonic foraminifera may be susceptible to micrometer-scale diagenesis because they are constructed of asymmetrical microgranules with a large surface area, and thus have a high

microporosity (Hemleben *et al.*, 1989). This type of small-scale alteration may not necessarily affect the larger-scale features (e.g. lamellar wall structure, surface texture, pores and spines) but could cause significant deviations from 'true' isotopic values (Pearson *et al.*, 2001).

According to some, only exceptionally preserved planktonic foraminiferal shells can be expected to yield oxygen isotopes that give reliable palaeotemperature estimates. Such material can occasionally be extracted from soft, impermeable marine mudstones that have experienced only moderate burial depths (Norris and Wilson, 1998; Wilson and Norris, 2001; Pearson *et al.*, 2001). Other authors, such as Zachos *et al.* (2002) refute the claim (see Pearson *et al.*, 2001) that planktonic foraminiferal assemblages can be overprinted by as much as 50%, although they do not support this counter-argument with evidence.

The mudstones of southern coastal Tanzania have long been known to yield exceptionally well-preserved foraminifera (Ramsay, 1962; Blow and Banner, 1962; Blow, 1979), which is attributed to the very low porosity, permeability and burial depth of these sediments. These mudstones are soft, pliable and rich in detrital carbonate, often including well-preserved molluscan aragonite fragments in addition to calcareous microfauna. After deposition, calcareous microfossils probably equilibrate quickly with the local pore fluids. Further diagenetic alteration was likely to have been prevented by the lack of subsequent fluid flow through strata from which these samples were taken.

Thus the objective of the Tanzanian field project was to sample these well-preserved assemblages and conduct new isotopic analyses to calculate marine temperatures in the Indian Ocean during the Neogene.

3.1.2 Field methodology

The samples were collected using a manual auger from coastal exposures on the north side of the Lindi Bay area of southern Tanzania, approximately 3 km north of Lindi (Figure 3.1). Each sample was located using the Global Positioning System (the sample coordinates are listed below).

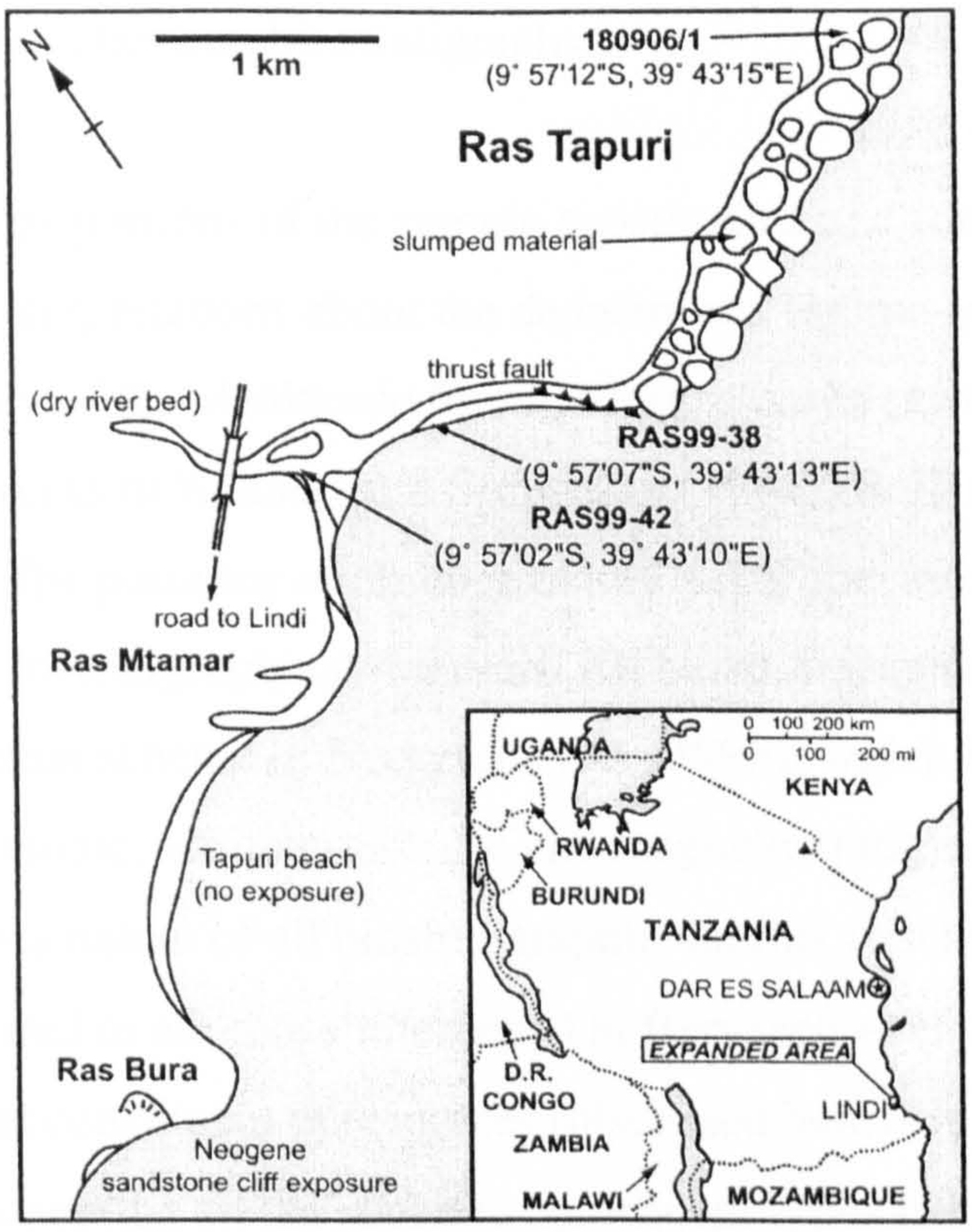

Figure 3.1. Location map for samples yielding exceptionally-preserved planktonic foraminifera. Adapted from C.J. Nicholas, unpublished.

3.1.3 Laboratory methodology

Sediment samples were soaked in de-ionised water and 10% hydrogen peroxide solution for a period of 24 hours. The foraminifera were extracted and separated using a constant flow of water over 63 μm and 150 μm paired sieves. 10-20 adult specimens of all identifiable species were picked for isotopic analysis to remove specimen error. Particulate adhesions to the shells were cleaned by ultrasonic treatment in de-ionised water. Samples were analysed for $\delta^{18}O$ and $\delta^{13}C$ isotopes in a VG Prism mass spectrometer at the Godwin Laboratory, University of Cambridge (all isotopic results are subject to a ±0.08‰ oxygen and a ±0.06‰ carbon isotopic analytical precision).

3.1.4 Sample characteristics and biostratigraphy

The relative proportions of the sample constituents and foraminiferal assemblages were used to make interpretations about the depositional regime and palaeodepth.

The taxonomy of the planktonic foraminifera is based primarily on holotype references and the works of Kennett and Srinivasan (1983), Bolli and Saunders (1985), and Spezzaferri (1994). The presence or absence of key zonal species allows the samples to be assigned to certain biostratigraphical intervals. All biostratigraphical assignments refer to the tropical biozonation scheme of Berggren *et al.* (1995), which is calibrated against independent radioisotopic, astrochronologic and magnetostratigraphic reference section data. The diachronous nature of all biostratigraphic datums is acknowledged, therefore 'absolute' ages referred to are those referenced in Berggren *et al.* (1995).

The sediment constituent percentages (discussed below in sample descriptions) were calculated by counting all the separate constituent types from one 10×10 mm square on a standard picking tray from the >63 μm dry residue of each sample. The constituent figures were then converted into percentages.

3.1.4.1 Sample RAS99-42 (9°57'02"S, 39°43'10"E)

Sample RAS99-42 was collected from a small exposure on the south side of a dry streambed, south of the Ras Tapuri headland. This sample was taken from a grey/blue laminated clay underlying an orange-coloured fossiliferous sandstone in the cliff exposure, 1-2 m above sea level.

This sample primarily consists of rounded to sub-angular quartz grains (43%) of <500 μm size. Planktonic foraminifera (1%) in the sample are small and exceptionally well-preserved, with the majority <200 μm in size. The benthic foraminifera (1%) are primarily well-preserved, <500 μm in size, and belong to the following genera: *Cibicides*, *Cibicidoides*, *Triloculina* and *Uvigerina*. The other major constituents present are calcareous and lithic fragments (28%) and detrital mica (21%). Organic material, echinoid fragments, red volcanic glass and rare ostracode fragments constitute trace components. The planktonic/benthic ratio (P/B) for this sample (as described in Gibson, 1989), is 44:56.

Globigerina ciperoensis and *Globigerina angulisuturalis* are common in this sample, with ranges between biozones P19-M2, and P21-M1b respectively (Spezzaferi, 1994). *Globoquadrina tapuriensis* is also present, which has a LOD at the top of biozone

P22 (Spezzaferri, 1994). The sample contains rare *Globigerinoides trilobus sensu lato*. The FAD of this species is placed within biozone M1b (Kennett and Srinivasan, 1983). There may be diachroneity in the FAD and LODs of *Gq. tapuriensis* and *Gds. trilobus s.l.*, however the FAD of the *trilobus* plexus (*Gds. trilobus, Gds. immaturus, Gds. quadrilobatus* and *Gds. sacculifer*) is more widely documented, therefore this datum is considered more reliable. Sample RAS99-42 is placed within the Early Miocene equivalent M1b biozone, based on the combined LOD of *G. angulisuturalis* and FAD of *Gds. trilobus sensu lato*. Figure 3.2 summarises the biostratigraphy of RAS99-42.

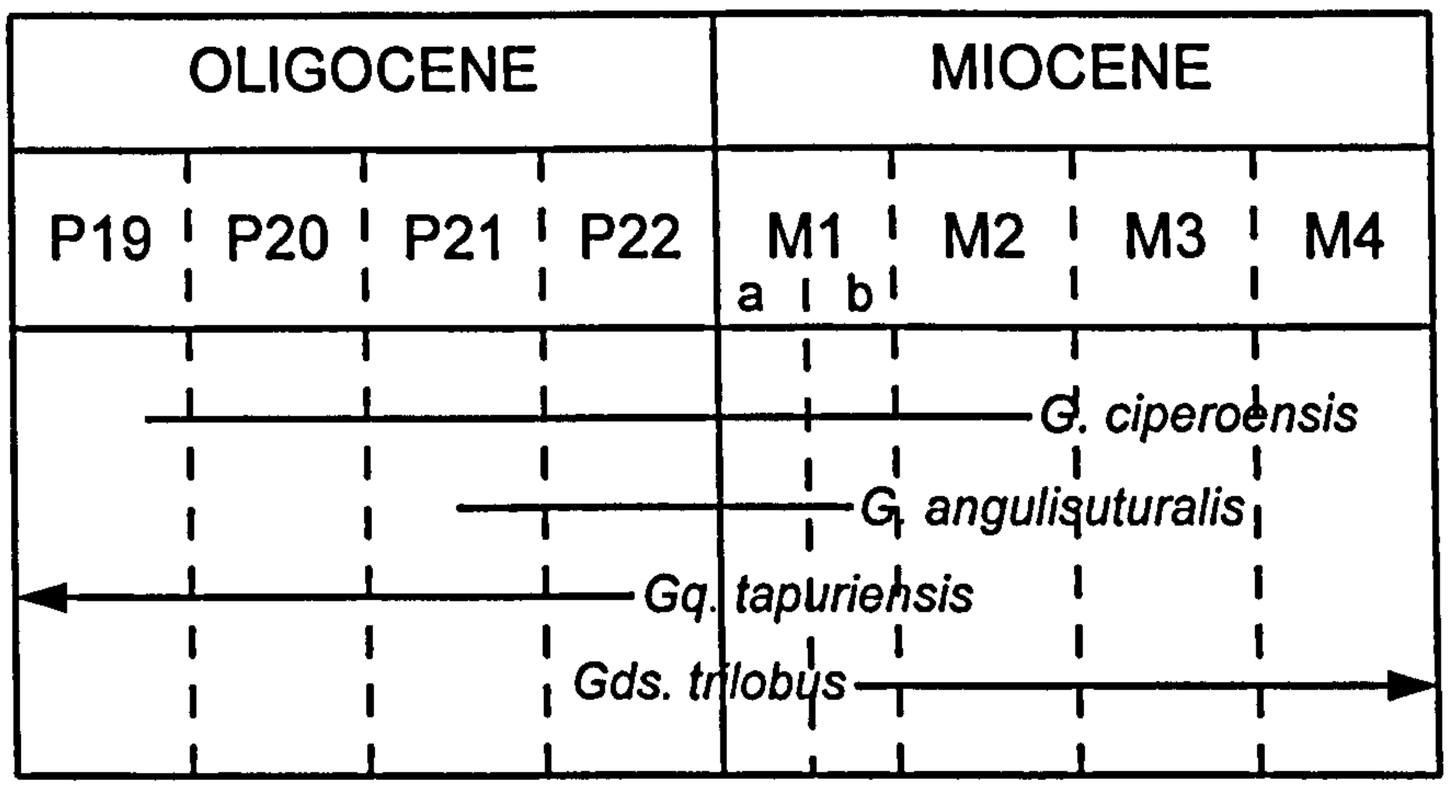

Figure 3.2. Summary of RAS99-42 biostratigraphy.

3.1.4.2 Sample RAS99-38 (9°57'07"S, 39°43'13"E)

Sample RAS99-38 was collected from a small clay exposure in the wave cut platform (exposed above sand level) to the south of the Ras Tapuri headland at the north end of Ras Tapuri beach. The sample was collected 1 m above sea level.

Both planktonic and benthic foraminifera total 10% each. *Bolivina, Cibicides, Cibicidoides, Dentalina* and *Uvigerina*, are the most common benthic genera. The preservation is variable, ranging from pristine to moderate (test surface recrystallisation visible to the naked eye on some foraminiferal specimens). Some of the less well-preserved specimens are filled with iron-oxide cement. The matrix is dominated by spherical to sub-rounded detrital quartz (48%), (not exceeding 1 mm in diameter and averaging ~100 μm), and oxidised framboidal pyrite nodules (29%). Other constituents in the matrix are chlorite mica (2%) and rare ostracode carapaces (<1%). The P/B ratio for this sample is 52:48.

This sample contains *Fohsella lobata*, which defines Middle Miocene zone M9 (Berggren *et al.*, 1995).

3.1.4.3 Sample 180906/1 (9°57'12"S, 39°43'15"E)

Sample 180906/1 was collected from a discrete exposure of olive-green clay protruding above the beach sand surface, 2 m shoreward of the cliff section and approximately 1 m above sea level, from the central area of the Ras Tapuri headland.

The sample consists of 5% planktonic foraminifera with excellent to moderate preservation, averaging 100-200 μm in size. Benthic foraminifera (principally *Bulimina, Cibicides, Cibicidoides, Dentalina, Nodogenerina, Spaeroidina and Uvigerina*) also compose about 5% and are generally <500 μm in size. Framboidal pyrite nodules dominate the matrix (40%), while the remaining matrix consists of chlorite mica and calcareous fragments (30%), and spherical, sub-rounded quartz grains (19%). The P/B ratio was calculated as 55:45.

The presence of *Globoturborotalita nepenthes* in the finer fraction confines the lower age limit of this sample to biozone M11 (Middle Miocene). The common occurrence of *P. mayeri* and *P. siakensis* in the sample, confines the upper limit to the top of biozone M12 (Middle to Late Miocene). The M11-M12 boundary is marked by the FAD of *Neogloboquadrina acostaensis*, which is absent from this sample, thus the sample is placed between biozone M11-M12.

3.2 Magnitude of the Middle Miocene (biozone M9-M11) sea level fall:ODP Leg 194, Marion Plateau, Australia – January to March, 2001

3.2.1 Estimating sea-level change

Measuring the amplitude and timing of eustatic sea level variations is important for the contribution of data to the global Phanerozoic curve, for the accurate interpretation of continental margin and interior basin sedimentary sequences, and has important implications for oceanic productivity. Yet this remains one of the most challenging scientific problems. Since Suess (1906), researchers have documented the apparent synchronicity between sea level events and tectonic episodes from different parts of the world. Moreover, with more recent developments in seismic sequence stratigraphy and the

initiation and progression of the DSDP and ODP in the 1960s and 1970s, important progress has been made in the determination of global sea level curves using passive margin sequence stratigraphy (Sloss, 1963; Vail *et al.*, 1977; Vail and Hardenbol, 1979; Haq *et al.*, 1987). In contrast, other researchers have utilised modelling of depositional regimes (Watts and Thorne, 1984), calibration of oxygen isotope curves (Major and Matthews, 1983) and analysis of depositional regimes in carbonate atolls (Lincoln and Schlanger, 1987) to tackle the same problem. There are often significant differences between the results produced by these independent datasets and there are a number of factors that could potentially introduce error. One of the primary criticisms of constructing global sea level curves is the lack of adequate corrections for local and regional subsidence, which may add potential error (Haq *et al.*, 1987). Other criticisms include questionable timing (and therefore global correlation) of synchronous events and their relationships to events in the deep sea, the requirement to update sea level curves in light of more recent refinements, and the occasional non-publication of supporting evidence.

3.2.2 Introduction to Leg 194

Global sea level is primarily controlled by, and fluctuates with, tectonic activity (i.e. mid-ocean ridge) and changes in climate. The latter is intimately linked to extent of glaciation. Assessing Middle Miocene sea-level fall represents an important proxy for quantifying Antarctic glaciation in this interval, and develops understanding of climatic change during the Neogene. Thus, Ocean Drilling Program Leg 194 (Townsville, Australia to Guam) was commissioned to core sediments from the Marion Plateau (in the Coral Sea) between January and March 2001. The primary objective of this was to determine the magnitude of the Middle Miocene (~12.5–11.4 Ma) eustatic sea level fall to aid the calibration of the Phanerozoic sea level curve (see Isern *et al.*, 2002 for results).

All drill sites for Leg 194 penetrated the Marion Plateau, a carbonate platform located between 18°S and 23°S, on the seaward side of the south-central Great Barrier Reef, on the northeastern Australian continental margin (Figure 3.3). Leg 194 sampled eight sites through 500-700m of Oligocene to Holocene mixed carbonate-siliciclastic sediments, five of which penetrated to acoustic basement (largely mafic volcanics).

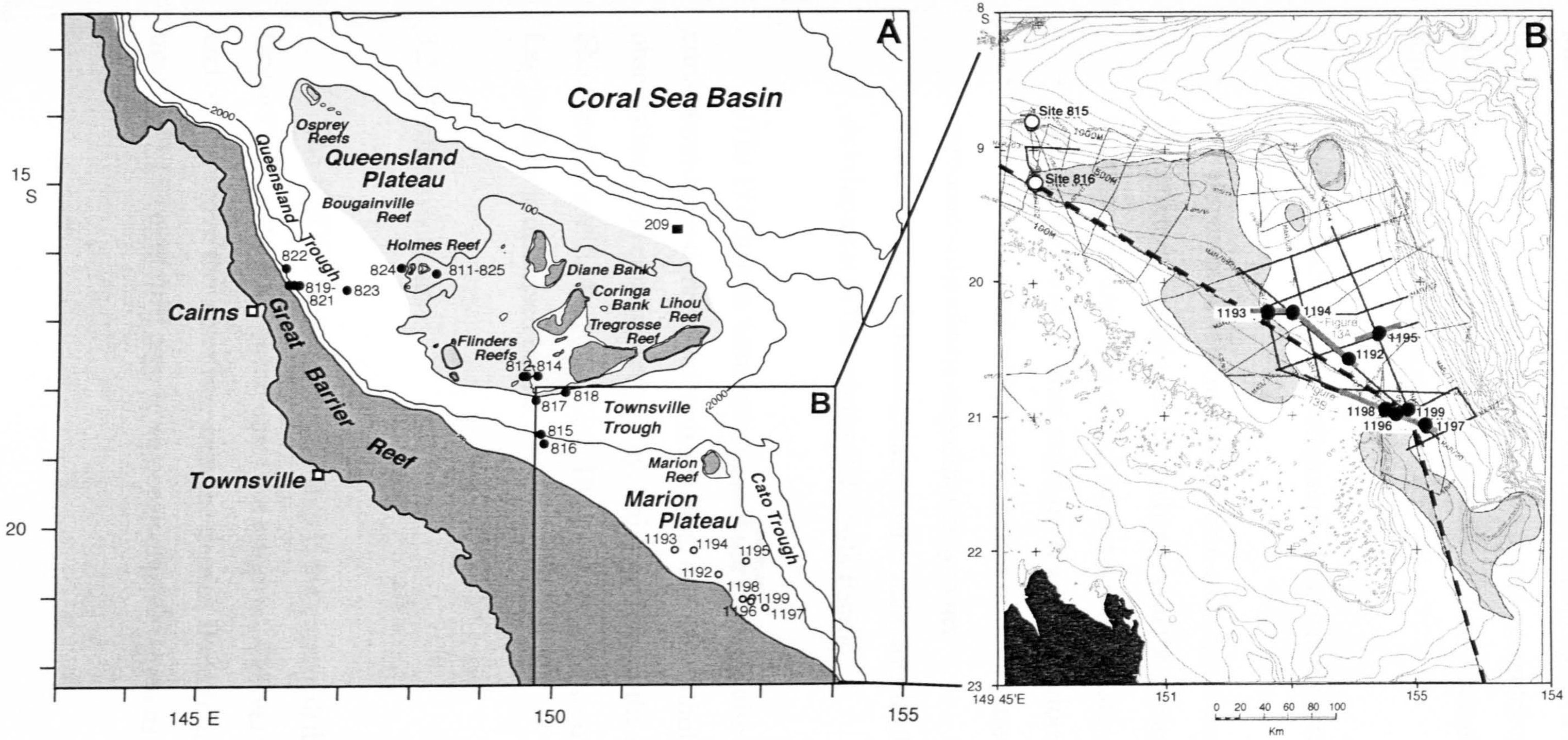

Figure 3.3. Map illustrating location of Leg 194 drill sites. Other sites are marked - DSDP Site 209 (solid square), ODP Leg 133 (solid circles) and ODP Leg 194 (open circles). The box in the lower right corner gives the position of B (inset). B is a closeup map showing locations of ODP Leg 133 (open circles) and Leg 194 (solid circles). Thin solid lines represent the location of multichannel seismic lines from AGSO Survey 75. Heavy lines denote the locations of multichannel seismic lines from Leg 194 survey (MAR data). Orange shaded areas are estimated extent of the Northern Marion Platform (NMP) and the SMP. Dashed boundary marks the Great Barrier Reef Marine Park. Figure adapted from Shipboard Scientific Party, 2002a.

The cores recovered record the sea level fluctuations of two primary carbonate platform depositional systems, the Northern Marion Platform (NMP) and the Southern Marion Platform (SMP), and how the depositional facies were affected by sea level variations. Integrated analysis of the growth and geometry of these two carbonate platforms allowed the primary Leg objective to be addressed together with the supplementary objectives (listed below):

- Characterisation and development of carbonate platforms in a current-dominated environment.
- Development of subtropical and cool-subtropical carbonate platforms.
- The effect of eustatic sea level changes on the evolution of the sequence stratigraphic units in a mixed carbonate-siliciclastic sediment system.
- Oligocene-Pliocene third order sea level fluctuations.
- Sources and mechanisms of fluid flow through pure carbonate and mixed carbonate-siliciclastic depositional systems.
- The influence of palaeoceanographic and climatic changes on carbonate platform development in the subtropical South Pacific.

The 194 themes were investigated during the cruise through the correlation of pre-cruise semi-three-dimensional seismic data, drill core lithological and biofacies observations, and chronostratigraphy. Full Leg 194 results and conclusions are presented in Shipboard Scientific Party (2002a). The biostratigraphic contributions (of the author) to the Leg findings is discussed below.

3.2.3 Drilling methods

The JOIDES Resolution drill ship is the current drilling platform through which the Ocean Drilling Program ocean cores are retrieved. The vessel is 143 m long, 21 m wide and 61.5 m above the water line with the derrick fitted (Figure 3.4). The rig can suspend as much as 9,150 m of drill pipe to an ocean depth as great as 8,235 m.

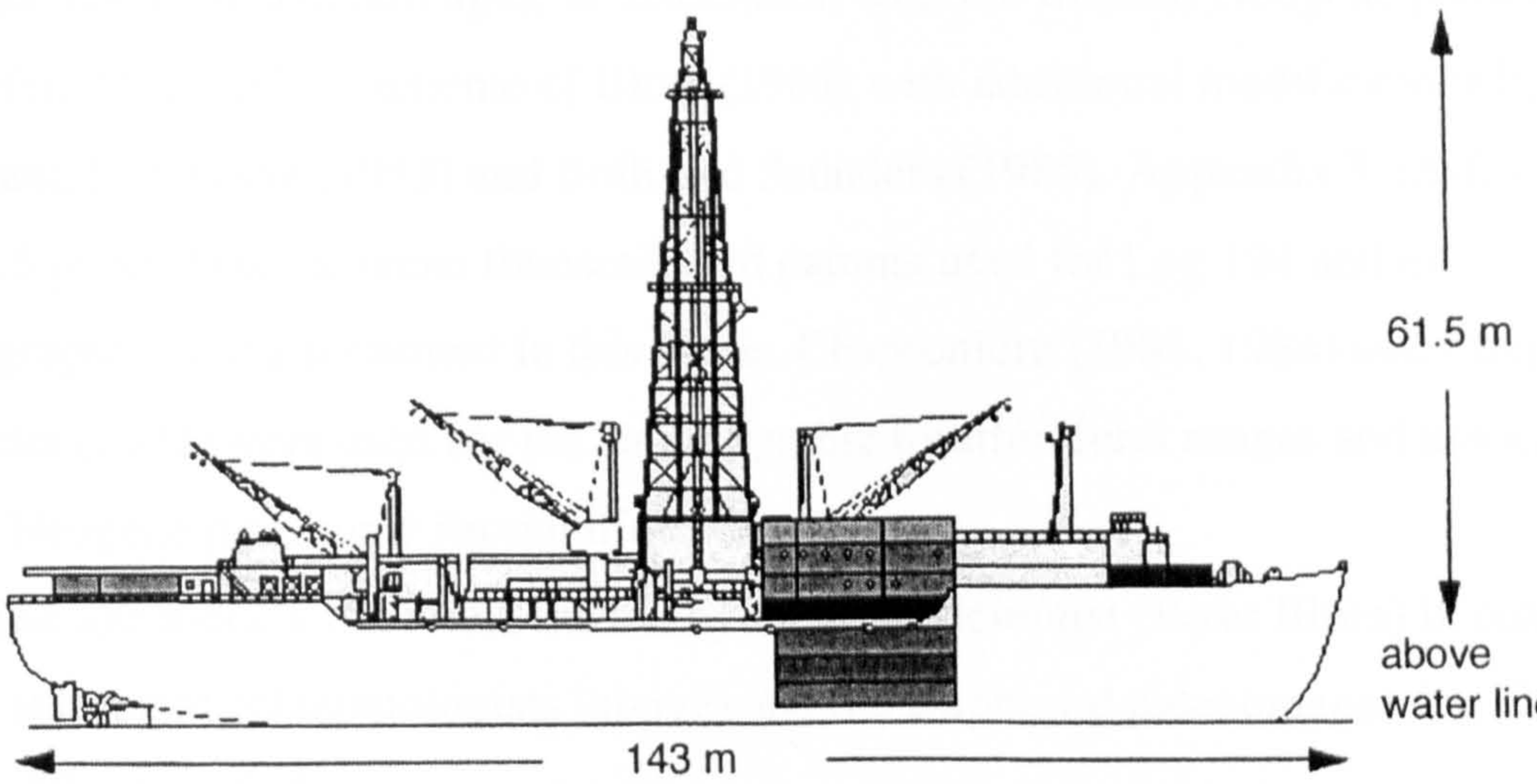

Figure 3.4. Schematic of the JOIDES Resolution, adapted from www-odp.tamu.edu.

During Leg 194 drilling, the vessel was kept in position over the site by use of 12 thrusters, synchronised by a central computer. Three standard coring systems were utilised, i.e. the Advanced Piston Corer (APC), Extended Core Barrel (XCB) and the Rotary Core Barrel (RCB). In addition, the Advanced Diamond Core Barrel (ADCB) was deployed to tackle the harder rock intervals, although not altogether successfully. Each coring system was applied to specific lithologic intervals to maximise core recovery. The total Leg recovery was 41.4 % of the cored interval, that is 2054.9 m of a possible 4965.1 m.

For each core (9.5 m), the shipboard biostratigraphers collected material from the core catcher, positioned at the base of each core, to carry out the shipboard biostratigraphy.

3.2.4 Leg biostratigraphy

The preliminary shipboard biostratigraphy was determined using planktonic foraminifera (Duncan Stewart and Mike Howell) and calcareous nannofossils (Wuchang Wei) from the core-catcher samples. Additional samples were analysed where further refinement was necessary. Larger and smaller benthic foraminifera (Pamela Hallock) were primarily utilised for palaeoenvironmental/palaeobathymetrical analysis, but in certain cases where planktonic assemblages were absent or the sedimentary facies did not contain suitable assemblages, benthic foraminifera were used for broad biostratigraphic purposes. The timescale of Berggren *et al.* (1995) was used for the planktonic foraminifera and

calcareous nannofossil datum ages, in association with the tropical Neogene planktonic foraminifera 'N-zonation' scheme of Blow (1969) with additional modifications by Kennett and Srinivasan (1983) and Bolli and Saunders (1985). Appendix 3.1A-C and Figure 3.5 present the Neogene timescale and datums used for Leg 194 and all biostratigraphic dating presented in this thesis. Chaproniere (1981, 1984) and Chaproniere and Betzler (1993) were used for the larger benthic foraminiferal ranges and associations with the Neogene planktonic foraminiferal zones.

The age models were constructed by the Staff Scientist (Peter Blum) in conjunction with the shipboard palaeontologists (above) and the shipboard palaeomagnetists (Mike Fuller and Tesfaye Birke).

3.2.4.1 Sample preparation

Sample preparation methods varied according to the degree of lithification. Samples from hemipelagic muds were ultrasonically agitated in a 10% hydrogen peroxide solution and were then washed over a <63-μm sieve. Semi-lithified samples were manually disaggregated into smaller pieces, sonicated, and sometimes heated in a 10% hydrogen peroxide solution. All samples were oven-dried at approximately 60°C and then sieved into <1-mm; <250-μm; <150-μm and >150-μm fractions. The <250-μm and <150-μm fractions were used for the examination of planktonic foraminifers. Planktonic foraminiferal abundances and preservation were quantitatively estimated to aid palaeoenvironmental interpretation. The complete shipboard planktonic foraminifera biostratigraphy is given in Appendix 3.2.

Abundant, well-preserved planktonic assemblages were present in most hemipelagic sequences drilled during Leg 194. Substantial thicknesses of this facies type were encountered primarily at sites 1192, 1195 and 1198. In general, good preservation was limited to sediments of Late Miocene and younger age. Below this, preservation deteriorated and planktonic abundances declined. Similar observations were made in sedimentary sequences immediately adjacent to the carbonate platforms (1194, 1197) or in any cores that penetrated platform derived material (1198). Sites 1193, 1196 and 1199 penetrated the carbonate platforms for either all or most of their cored interval.

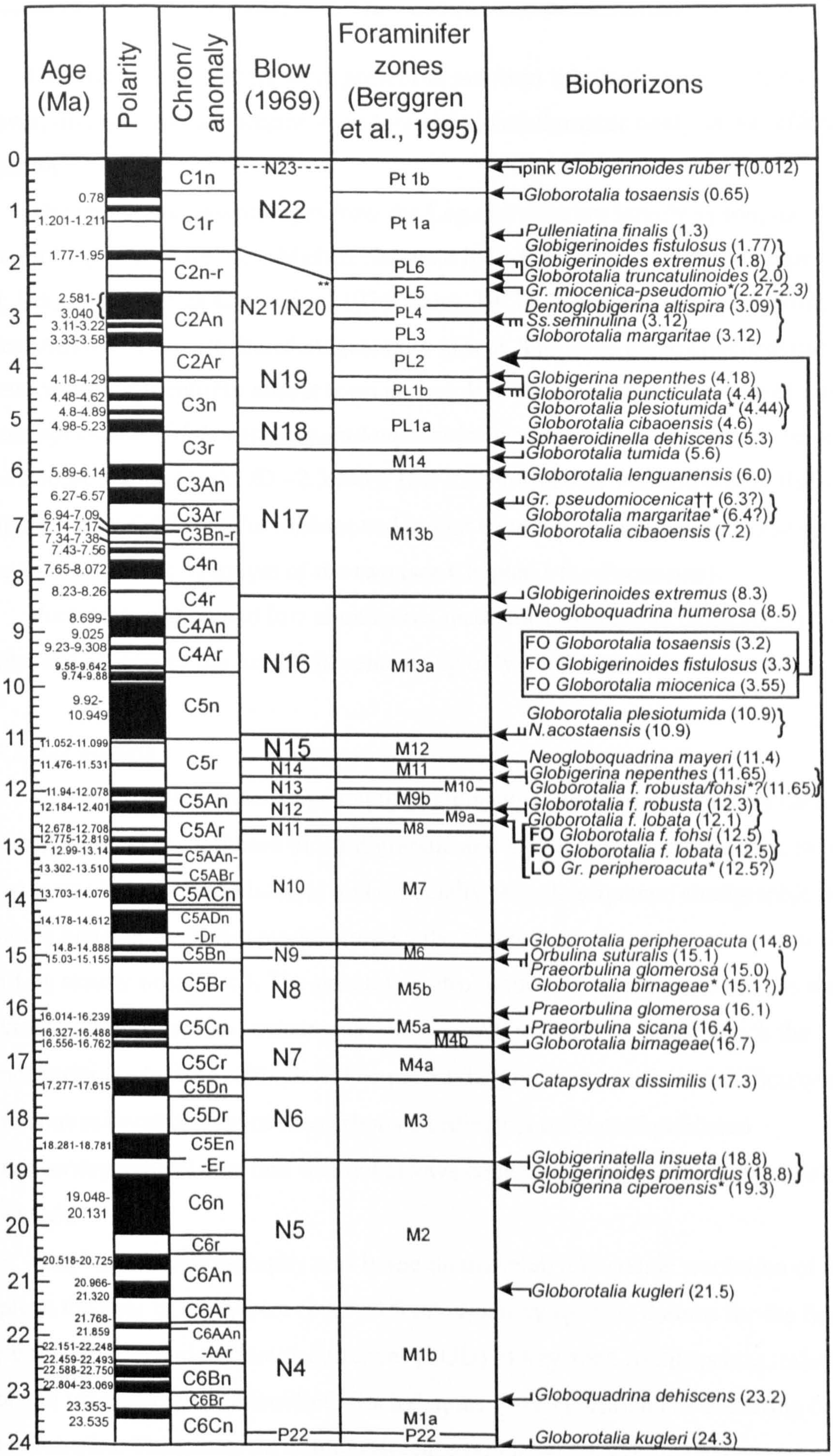

Figure 3.5. Planktonic foraminifer datums employed on Leg 194. The majority of the datums are from Berggren *et al.* (1995). Symbols denote the use of other references: Bolli & Saunders, 1980 (††); Berggren, Kent & Van Couvering, 1985b (†); Kennett & Srinivasan, 1983 (*) and isochronous boundary from Spencer-Cervato, 1997 and Chaisson, 1997 (**).

Planktonic foraminifera were present in platform lithologic cross-sections, however, diversity and abundance were low and biostratigraphic analysis was effectively impossible.

The planktonic assemblages from the Leg 194 sites are largely synonymous with the assemblages from well-established Neogene Indo-Pacific tropical chronologies (Blow, 1969; Berggren and Van Couvering, 1974; Saito, 1977). A number of taxa endemic to the tropical Atlantic realm are therefore generally absent. The zone fossil *Globorotalia miocenica* is almost entirely absent form all Leg 194 sites, with the exception of a few isolated specimens. *Globorotalia pseudomiocenica* was used quite extensively to delineate Late Pliocene sediments (LOD ~2.3 Ma). This morphospecies was sometimes difficult to distinguish from *Globorotalia limbata* and in fact Kennett and Srinivasan (1983) believe the latter is the senior synonym of the two (see Chapter 1 for discussion).

Poor preservation and low abundances made for problematic biostratigraphy of the Middle, and especially the Early Miocene, using only planktonic foraminifera.

3.2.4.2 Age Models

Age models (continuous age-depth relationships) were constructed for each of the eight drill sites using shipboard biostratigraphic and magnetostratigraphic data, to provide age estimates for any depth interval and especially seismic sequence stratigraphic and lithologic boundaries. These models formed the chronological framework upon which all other Leg results were based. The primary control points used in the age models were the planktonic foraminifera and calcareous nannoplankton datums, against which the magnetostratigraphy was calibrated. The patchy Leg recovery, technical difficulty and the low ferrous mineral content of the carbonate sediments recovered produced magnetostratigraphical data that was not always congruent with the biostratigraphic framework.

Shipboard biostratigraphy was based on the relatively coarse resolution of one sample at the base of every core (every 9.5 m), whereby specific datums for the first appearance (FAD) and the last occurrences (LOD) of key zone fossil species, relative to a calibrated timescale, were identified. Such datums were interpreted as occurring *between* certain samples. Therefore, the datum reference points on the age models are usually associated with (depth interval) error bars to account for the interpreted depth of a specific datum. The planktonic foraminifera/calcareous nannofossil datum points are positioned at

the midpoint for the interval, but in reality this actual datum could occur at any point within that error margin. At some intervals near the top or base of a cored sequence, the FAD or LOD of a particular species could not be identified, in which case other species within the assemblage were used to give an age range for a specific depth interval. In cases where the age uncertainty exceeds the time interval represented, an age-depth box is used to signify the age and depth uncertainty intervals. This is particularly useful for the 194 sites that penetrate lithified carbonate platform, e.g. 1193, 1196 and 1199.

The Marion Plateau sedimentation rates were calculated as 10 – 100 m/My (Shipboard Scientific Party, 2002d), while the time represented by core-catcher sample spacing (9.5 m) is equivalent to 0.1 – 1 My. The core catcher sample resolution is therefore significantly larger than the errors associated with typical Cenozoic biostratigraphic datums (0.1–0.2 My), and depth error bars are required. Some of the platform sequences could only be dated using benthic foraminifera, which have larger age range errors (>1 My). The result is that some of the age models contain poorly resolved age-depth boxes, however they usually provide useful age constraints.

Depth error range also includes the uncertainty associated with sample position within the drilled core interval. If the amount of recovered material is less than the cored interval, the recovered interval may come from any position within the cored interval. In this case the BCI correction is used ('bottom of cored interval'), which increases the depth interval of uncertainty to a more realistic interval, but which may be <100% larger than the recovery if the recovery is limited to the core-catcher (Shipboard Scientific Party, 2002d). Therefore, within-core recovery must also be considered when constructing site age models.

Construction of the age models simply involved fitting straight line segments through as many control point error bars as possible, so that slope changes were kept to a minimum. This procedure removes the artificial kinks (sedimentation rate changes) that might not exist if sampling resolution were increased. Horizontal slope segments represent depositional hiatuses (e.g. hardground formation), the duration of which is marked by its length. Sedimentation rates for specific time intervals can be calculated from the age-depth plots from the slopes of the straight line segments, although they are only average rates that may vary over smaller time intervals.

All the Leg 194 Site age-depth relationships are presented in Figure 3.6. The discussion for which is given in the figure caption.

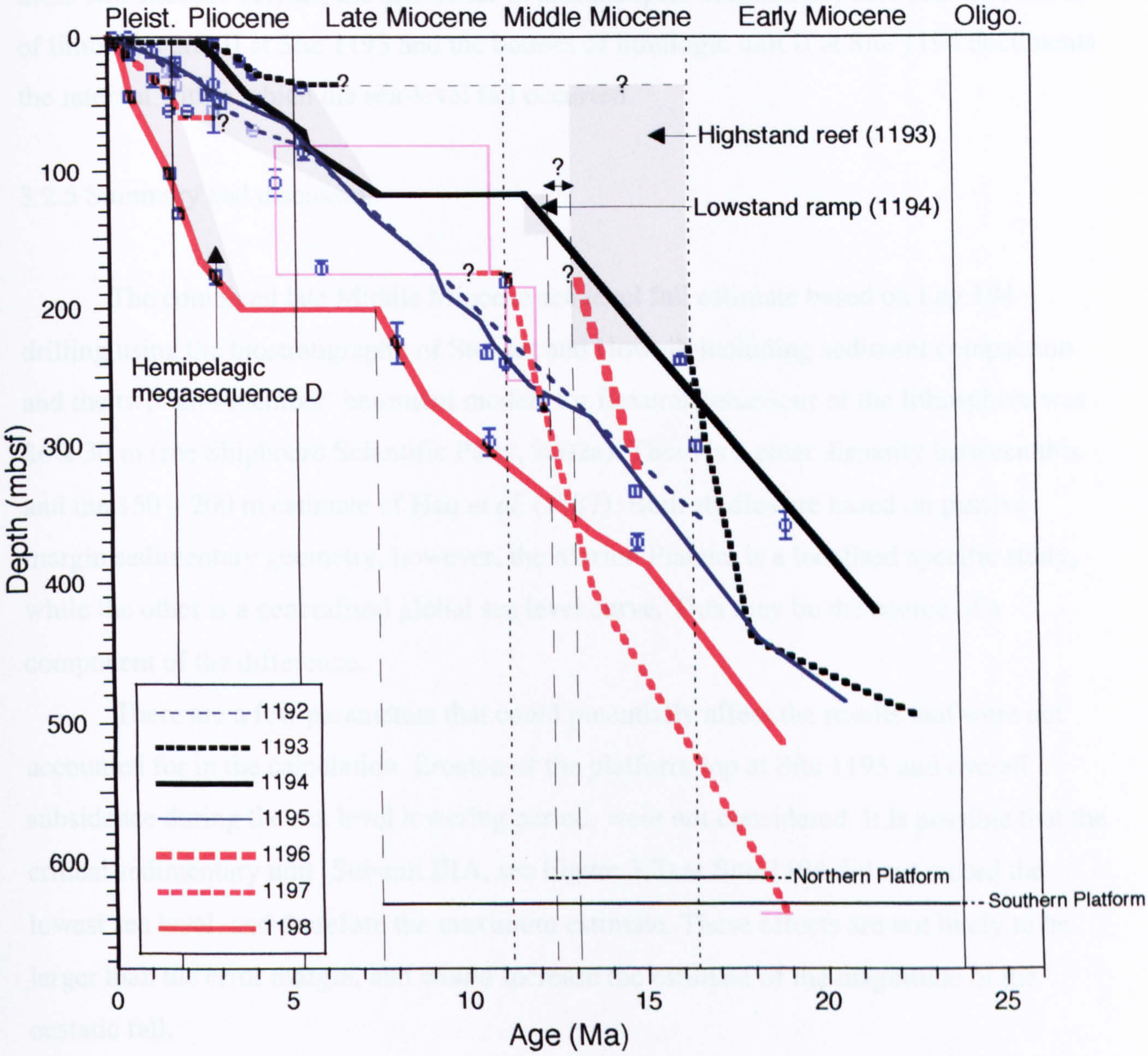

Figure 3.6. Continuous age-depth relationships (age models) for Leg 194 sites, adapted from Shipboard Scientific Party, 2002a. Site 1192 and 1195 trends represent distal, drift-dominated hemipelagic deposition. Hiatuses are marked by breaks in section and '?'. The shaded area filling the top left corner of the figure represents the hemipelagic Megasequence D, which infills the topography created by the Miocene carbonate buildup. Shaded boxes represent age constraints for key horizons with sedimentation that did not allow accurate biostratigraphical dating. The blue data points represent the planktonic foraminifera datums. The pink squares represent 1197 biostratigraphical uncertainty.

The age models for sites 1193 and 1194 demonstrate the key horizons used to calculate the Middle Miocene sea-level fall, i.e. between the 'highstand reef' and the 'lowstand ramp'. These structures are illustrated in Figure 3.7 at sites 1193 ('highstand reef') and 1194 ('lowstand ramp') in the Northern Marion Platform. If the age models for these two sites are correct, the difference in altitude (plus subsidence) between the bottom of lithologic unit II at Site 1193 and the bottom of lithologic unit II at Site 1194 documents the interval within which the sea-level fall occurred.

3.2.5 Summary and discussion

The combined late Middle Miocene sea level fall estimate based on Leg 194 drilling using the biostratigraphy of Stewart and Howell, including sediment compaction and the two 'end-member' basement models for flexural behaviour of the lithosphere was 86 ± 30 m (see Shipboard Scientific Party, 2002a). There is a clear disparity between this and the 150 – 200 m estimate of Haq *et al.* (1987). Both studies are based on passive margin sedimentary geometry, however, the Marion Plateau is a localised specific study, while the other is a generalised global sea level curve. This may be the source of a component of the difference.

There are a few parameters that could potentially affect the results that were not accounted for in the calculation. Erosion of the platform top at Site 1193 and overall subsidence during the sea level lowering period, were not considered. It is possible that the critical sedimentary unit (Subunit IIIA, see Figure 3.7) at Site 1194 did not record the lowest sea level, and therefore the maximum estimate. These effects are not likely to be larger than the error margin, and would increase the estimate of the magnitude of the eustatic fall.

It must also be considered that there could be a substantial error margin in the palaeo-water depth estimates (<40 m). These estimates are made using the presence/absence and abundance of fossil assemblages and certain constituent mineral grains.

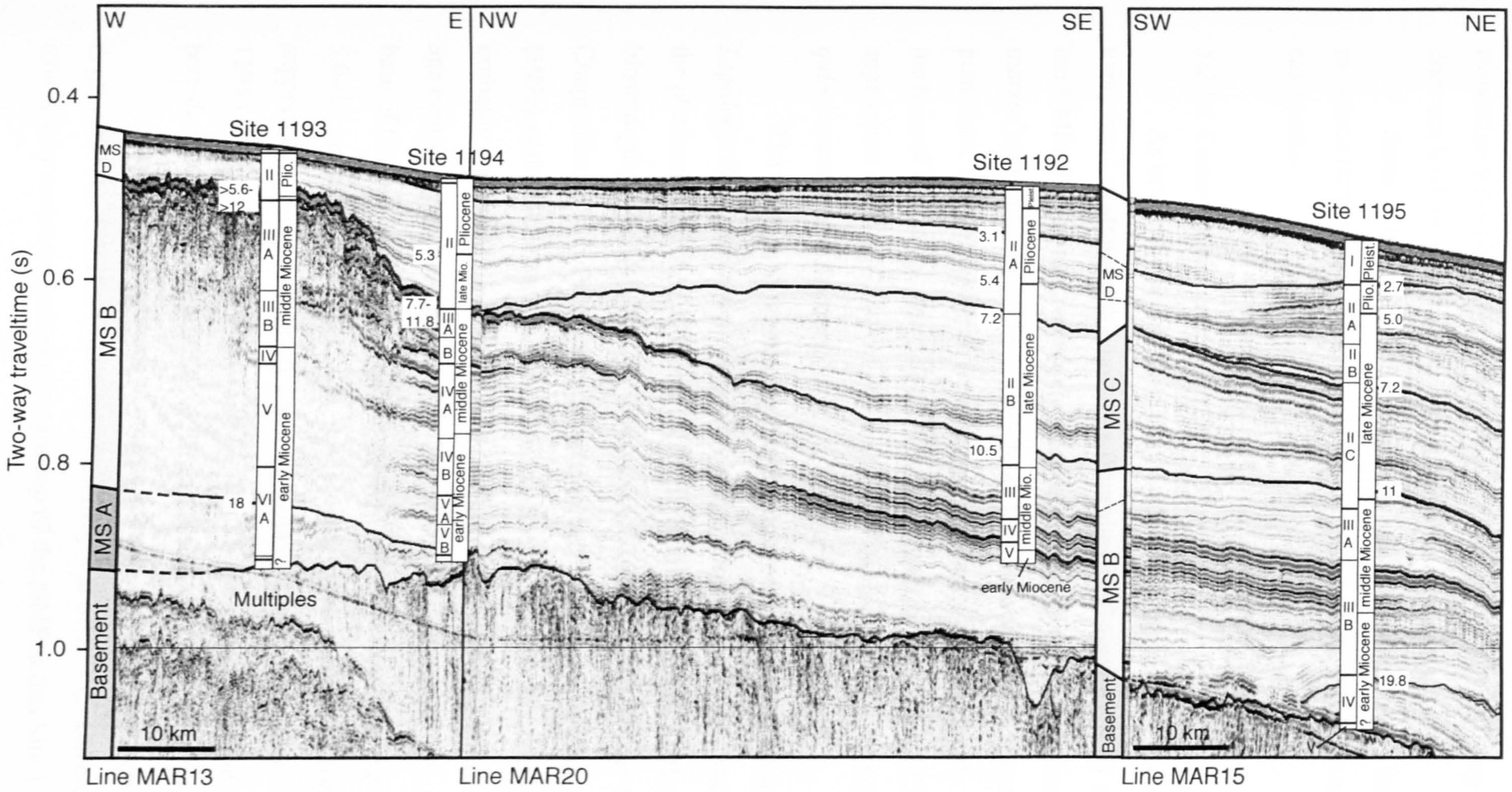

Figure 3.7. Northern seismic transect along lines MAR13, MAR20 and MAR15, showing positions of sites 1192, 1193, 1194 and 1195. The four sedimentary megasequences (A-D) and the basement are marked by prominent black lined boundaries. Sites 1193 and 1194 penetrate the Northern Marion Plateau (NMP). The schematic site cores detail the shipboard chronostratigraphic data (epoch boundaries and absolute ages of the megasequence boundaries, defined by shipboard age models and time-depth conversion) together with megasequence subdivisions (Roman numerals). These lithologic boundary units do not correlate across sites because they are based on sedimentologic description of the drilled cores. MS = megasequence. Figure adapted from Shipboard Scientific Party (2002a).

At sites 1193 and 1194, the presence of certain benthic foraminifera and bryozoans were used to infer depositional setting and palaeowater depths of 10 – 50 m and 30 – 50m, respectively (Shipboard Scientific Party, 2002b, 2002c). By its very nature, this technique does not lend itself well to the calculation of exact figures.

Some of the crucial biostratigraphy was limited to benthic foraminifera, which may introduce further error to the exact ages of the key stratigraphic horizons used for the calculation.

3.2.5.1 Cause for concern

As briefly outlined above, the Middle Miocene eustatic sea level fall was calculated using two key stratigraphic horizons from sites 1193 (in the NMP) and 1194 (adjacent to the NMP). The former represents (earlier) relative sea level high-stand, while the latter marks (later) relative sea level low-stand. Drilling at Site 1193 revealed ~35 m of planktonic foraminifera-rich hemipelagic sediments unconformably overlying the NMP, the base of which was dated as 5.6 Ma (1193A 4H-6, 80cm to 4H-CC), using the first appearance (FA) of *Globorotalia tumida* and the last occurrence (LO) of *Discoaster quinqueramus* (see Appendix 3.3).

The benthic foraminiferal associations containing *Amphistegina* spp., *Lepidocyclina (Nephrolepidina) howchini*, *Cycloclypeus* sp. and *Miogypisina* spp., from the platform sequence (>35 mbsf) restricted the accumulation platform to between benthic biostratigraphy zones LF5-LF7 (equivalent to biozones M3-M6, or 18.8-14.8 Ma) based on Chaproniere (1981, 1984). Similar assemblages are reported in Chaproniere and Betzler (1993) as dated between 24-12 Ma (Early to early Middle Miocene). This age-span probably represents the whole of the platform build-up and is consistent with the gap in the age control points in Appendix 3.3. Thus the hiatus between the top of the platform and the base of the overlying sediments (Megasequence B/C boundary, Figure 3.7) is at least 5.6~12 Ma, and possibly ~15 Ma. In this case, previous age hypotheses for the NMP are supported. A similar approach was used to date the Megasequence B/C boundary at Site 1194 (~117 mbsf) as between 11.9-7.5 Ma. Thus it appears that the Megasequence B/C boundary offers the opportunity to measure sea level fall in the Middle Miocene.

However, this estimate is heavily reliant on the accurate age and palaeo-water depth estimates from foraminiferal assemblages at Site 1193. Unfortunately, the extensively cemented sediments at the top of the NMP at this Site 1193 were not suitable

for age-analysis using planktonic foraminifera and/or calcareous nannofossils, which constitute the more accurately calibrated biotic age indicators. Instead this horizon is tentatively dated using a benthic foraminiferal assemblage, the range of which was initially thought to terminate in the Middle Miocene (~12 Ma), thus supporting the validity of the sea level fall model estimate. However, there is disagreement in the literature about the ranges of some of the key benthic biostratigraphic zone fossil ranges used to date the lithified platform material encountered at Site 1193 (e.g. Betzler, 1997). In this publication, Betzler reviews the range of *Lepidocyclina* on the Queensland Plateau and suggests this genus might continue into the Pliocene. If this is the case, then it is possible that the Leg 194 estimate was calculated using sedimentary packages of the wrong age. The Leg 194 sea level estimate relies heavily on the accurate dating of these key horizons, and the benthic assemblages used may be unreliable.

3.2.5.2 Future work

It is possible that use of a different, non-calcitic age-diagnostic microfossil group could constitute a more dependable age proxy. A proposal has been submitted for World University Network funding (2003) to sample further material from the NMP of Site 1193 (35-225 mbsf) for biostratigraphical analysis using dinoflagellates (microscopic organic phytoplankton). Unlike calcareous microfossils (foraminifera, calcareous nannofossils), organic assemblages can be easily removed from lithified carbonate material and used for further biostratigraphy of this critical site.

This project will ideally validate the temporal assumptions made from the Leg 194 results in order to produce an accurate magnitude of sea level fall. However, if the analyses indicate that this part of the NMP was deposited in the Late Miocene and not the Middle Miocene as is believed, then the shipboard scientific party sea level fall estimate will be incorrect.

3.3 New Zealand fieldwork:19th January – 2nd February, 2002

The purpose of the fieldwork was to sample key localities previously documented as containing temperate-water, Neogene globorotaliids for morphological and isotopic study (see Jenkins, 1971). Early Miocene age horizons were targeted to yield early menardellid specimens (e.g., *G. archeomenardii* and *G. praemenardii*) while upper Middle

Miocene lithologies were targeted to yield truncorotaliid and globoconellid assemblages. Morphological analysis of these samples could help to establish a close phylogenetic link between *Globoconella* and the 'core' Neogene *Globorotalia* plexus, already hypothesised to contain the *Menardella, Truncorotalia, Hirsutella* and the *Globorotalia s.s.* lineage. The sampling locations were chosen after consultation with George Scott (Institute of Geological and Nuclear Sciences, Wellington) and are shown in Figure 3.8 below.

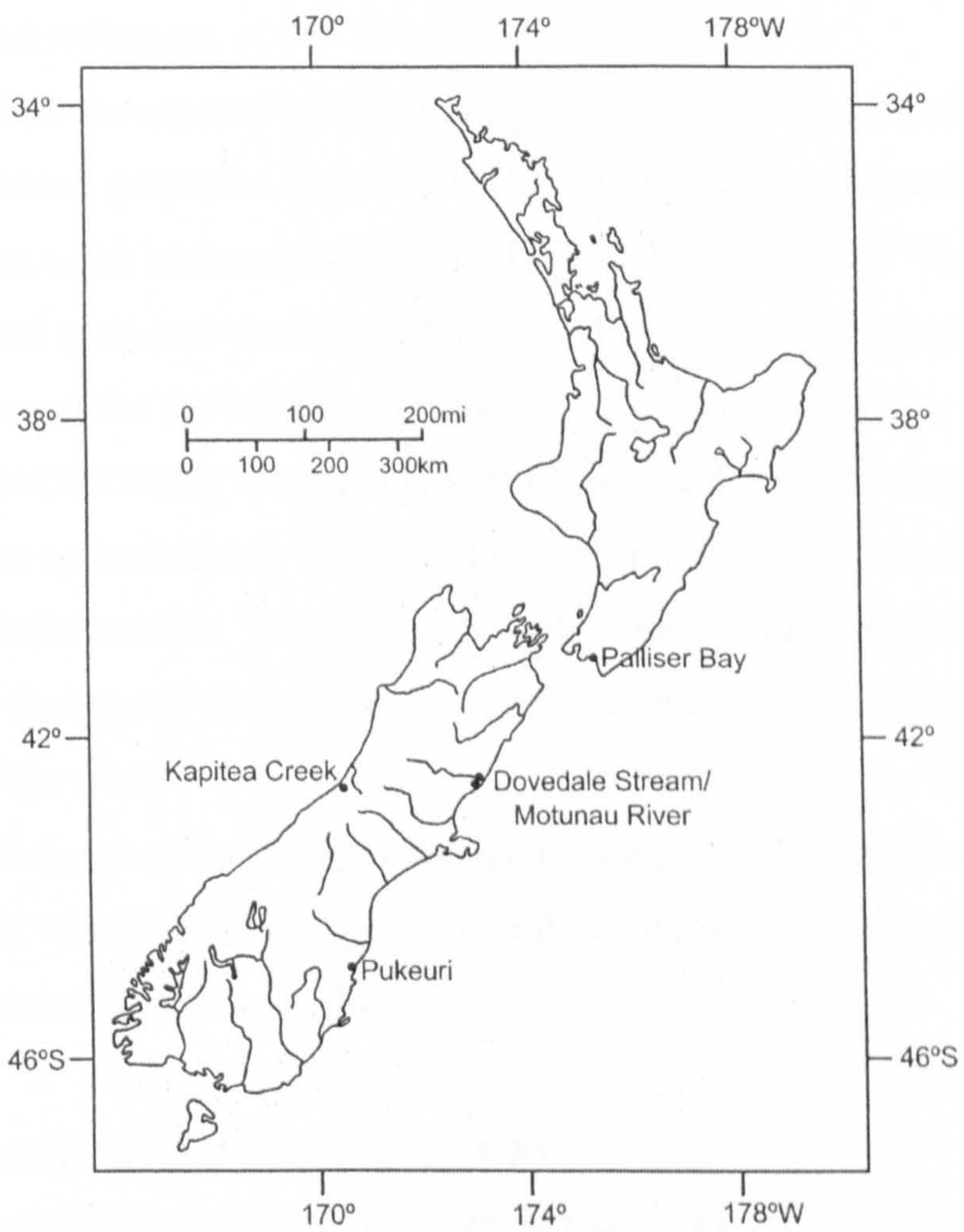

Figure 3.8. Locations of New Zealand sample localities. Adapted from Jenkins (1971).

The expedition also allowed the perusal of type-collections from the Cushman collection at the Smithsonian NMNH (Washington DC) and the Jenkins reference collection of foraminifera held at the Institute of Geological and Nuclear Sciences (Wellington, New Zealand).

3.3.1 Localities

3.3.1.1 Lake Ferry - Palliser Bay, North Island.

This locality is situated in Palliser Bay on the southern tip of the North Island, southwest of Wellington. It is approximately 2 km east along the bay from the 'Lake Ferry Hotel', in the NE corner of Palliser Bay. It was further located on the cliff exposure on the west side of a small river 'gorge' approximately 20 m wide. These are Upper Miocene (Tongaporutuan) sediments.

The sediments exposed in the 40 m cliff section consisted primarily of a horizontally bedded, grey/blue silt-mud. This is overlain unconformably by 2 m of orange-coloured, fluvial sands and conglomerates, also with negligible dip. The unconformable contact displayed erosional-channel and fissure-fill structures. This contact appeared to be laterally continuous for the length of the Bay.

Samples DS02PB01 through DS02PB04 were collected from the west side of the stream exposure approximately 10 m apart in stratigraphic thickness starting 1m below the marine mud-fluvial contact. The same sediments appeared to extend to Cape Palliser at the eastern end of the bay. At the Lake Ferry Hotel end of Palliser Bay there is a gentle dip of 1-4 degrees to the west.

The blue/grey mud sediment contained isolated gastropod, bivalve and scaphopods fossils, some of which were dispersed randomly while others were concentrated in laterally discontinuous bands (death assemblages).

3.3.1.2 Pukeuri (45° 01.891'S, 171° 01.625'E)

This sampling locality (see NZMS260, Sheet J41, Oamaru 1:50000 map) was positioned 200 m northwest of the Pukeuri-Highway 1 junction (8 km north of Oamaru, South Island), up highway 83, which curves towards the northwest. The sampled exposure is on the north side of the road, approximately 2 m high, of unknown formation of Altonian (Lower-Middle Miocene). The lithology is a yellow marly silty-mudstone and contains common bivalve and gastropod faunas, indicating a marine origin. The exposure is bisected by many carbonate veins.

Sample DS02P01 was collected from the more silty sediment from the middle of the exposure. Most of the invertebrate shells are tough and articulated, and therefore most

are probably autochthonous. Bedding is weak-horizontal, if present at all, and carbonate concretions (<30 cm) appear to be roughly aligned along the bedding.

3.3.1.3 Motunau River

The samples from Motunau River were taken approximately 3 km northwest of the Motunau Beach where the mouth of the river meets the sea, on the east coast of the South Island, north of Christchurch. All samples can be located on NZMS260, Sheet N34, 1:50000 Motunau map. The samples were targeted using George Scott's (IGNS) original stratigraphic column of the section (unpublished). The samples were collected from the Miocene Motunau Group.

Sample DS02MR01 was positioned by GPS at: 43° 02.326'S, 173° 03.497'E. It was taken from the west side of the Motunau River on a prominent meander. The material sampled was a blue/grey silty-marl. The exposure here has prominent (possibly cyclic) banded strata 4-5 cm apart, dipping 4-5 degrees to the south. Some more lithified concretions (<10 cm) appear intermittently aligned with the bedding.

Sample DS02MR02 was positioned by GPS at: 43° 02.236'S, 173° 03.391'E. This sample was taken from the same banded siltstone lithological unit on the next west-turning meander of the river approximately 200-300 m upstream of DS02MR01, on the west bank on the river. Here, the exposure consists of finer dark and light-coloured alternating laminations. Iron oxide-rich nodules (<5 cm), occur intermittently along bedding, which dips 5-10 degrees to the southwest.

Sample DS02MR03 was positioned by GPS at: 43° 02.270'S, 173° 03.473'E. This sample was acquired from between samples DS02MR01 and 02, in the same lithological sequence, on the south side of the river meander.

Sample DS02MR04 was positioned by GPS at: 43° 02.425'S, 173° 03.688'E. This sample was taken from a blue/grey glauconitic (?) silt-fine sandstone. The fine laminated sand beds (~10 cm thick) alternate with thicker silty horizons (~20 cm thick). The sample was taken from the bottom of the east bank river exposure (~30 m high). At the base of the exposure there is a contact with a well-cemented, mega-brecciated limestone. At the top of the section there is a graded contact into a creamy sandstone unit 10-15 m thick. The approximate dip/strike measured was 30°/230.

Sample DS02MR05 was positioned by GPS at: 43° 02.480'S, 173° 03.748'E. This sample was taken approximately 1 km downstream from DS02MR04, from a very fine

sandstone, also grey-blue in colour. This unit was probably stratigraphically-higher than the creamy sandstone described above. The sample is from the east river bank from an exposure 2 m above the river level. The sediment was homogeneous, massive and poorly-bedded.

3.3.1.4 Dovedale Stream

Dovedale Stream is located near Motunau; the mouth of which meets the southern Pacific Ocean on the east coast of the South Island. The sample localities can be reached along 'Mt. Cass Road' at its junction with Highway 1. The localities are in the river exposures in Dovedale Stream, 500 m north of the hamlet 'Glenafric'. The samples are located on NZMS 260, Sheet N34, 1:50000 map. Samples were taken from blue siltstones of Lower to Middle Miocene age (Scott, pers. comm.).

Sample DS02DS01 was located by GPS at: 43° 05.201'S, 172° 52.930'E. This sample was taken along a track running towards the stream northeast from Mt. Cass Road, where a tributary of the stream runs across the track. The exposure here consists of homogeneous blue siltstone containing small bivalves and enigmatic coralline biogenic structures. The exposure exhibits prominent bedding 10-20 °/090. The beds vary in thickness from 10-50 cm. The blue siltstone unit is approximately 15 m thick, above which red, conglomeratic alluvium unconformably rests (see Palliser Bay).

Sample DS02DS02 (43° 05.089'S, 172° 52.060'E) was taken from a small exposure of the same unit approximately 1km upstream on the southern bank of the Dovedale Stream. There is no bedding or lamination present and the sample was collected 5 m below the same unconformity described above.

3.3.1.5 Kapitea Creek

All samples collected from this section can be located on NZMS 260, Sheet J32, Hokitika 1:50000 map. Kapitea Creek is positioned 4 km south of Kumara Junction, on the west coast of the South Island. All samples were also located with reference to Scott (1982). All samples were collected from the Upper Miocene (Kapitean) Eight Mile Formation (see Scott, 1982).

Sample DS02KC01 (42° 37.369'S, 171° 07.683'E) was taken from a 5 m high exposure on the north bank, 0.4 km upstream from the track bridge. The sampled sediment

was a blue homogenous mudstone, 3 m thick, unconformably overlain by alluvium. The sample was taken 2 m above the base of the exposure and 1 m below the alluvial contact.

DS02KC02 (42° 37.482'S, 171° 07.665'E) was sampled from the same unit approximately 0.6 km upstream of the bridge, from the west bank of the creek. There was no discernable bedding and small shelly bivalves were present in the exposure.

DS02KC03 (42° 37.650'S, 171° 07.899'E) was sampled from a 1 m high exposure, on the south bank, 1 km upstream of the bridge.

DS02KC04 (42° 37.283'S, 171° 07.352'E) was sampled 50 m downstream from the creek bridge, from the same unit in an exposure 5 m high. There was no lithologic structure present in the exposure.

DS02KC05 (43° 05.089'S, 172° 52.060'E) was sampled from the same unit, 500 m downstream of the bridge, on a detached meander on the south bank of the river. No structure was present.

DS02KC06 (42° 36.726'S, 171° 06.176'E) was sampled from the same blue mudstone unit 500 m upstream of the railway bridge east of highway 6. The exposure was 1 m high on the south bank of the creek. This locality is 1.9 km west of the bridge.

3.3.2 Material

The planktonic assemblages were prepared using the same methods outlined in Section 3.1.3, this chapter. Unfortunately the sampled sediments did not yield any specimens from the *Globoconella* lineage, but they did yield truncorotaliid assemblages, which were cladistically coded and included in phylogenetic analysis presented in Chapter 6 (SEM images are presented in Plate 1.7, Chapter 1).

Chapter 4

Globorotaliid palaeoecology and Miocene oceanic temperature reconstruction

4.1 Introduction

The Miocene epoch (23.8 – 5.3 Ma, see Berggren *et al.*, 1995) was a time of significant Cenozoic climatic and palaeoceanographic transition, during which major southern hemispheric ice sheets became a permanent feature on the earth (Zachos *et al.*, 2001). These principal palaeoclimatic changes undoubtedly influenced marine biotic evolution during this time period.

The base of the Miocene marks the initiation of extensive oceanic microfossil radiations (Kennett, 1985), especially in the planktonic foraminifera, which produced the distinctive Neogene lineages of which the globorotaliids represent a major component. From the Early to Middle Miocene, the compressed, smooth-walled globorotaliid architecture developed, and was fully established by the Middle Miocene (Cifelli and Scott, 1986). The termination of the Miocene is associated with a number of global palaeoenvironmental changes (Kennett, 1985) that produce the relative 'icehouse' climate we live in today. By end Miocene times, the globorotaliid lineages had much lower diversity having experienced a number of extinctions following the Middle Miocene 'climatic optimum'. The highly transitional climatic trends of the Miocene that may have shaped the globorotaliid evolution were, in part, influenced by conditions before this, in the latest Palaeogene.

4.1.1 Late Palaeogene to Neogene climate and planktonic foraminiferal evolution

A significant reduction in planktonic foraminiferal diversity occurred at the end of the Eocene, which included a severe reduction in the low trochospiral-keeled forms (Cifelli and Scott, 1986 see Chapter 1). The extinctions occurring at this time may have provided the vacant evolutionary space into which, the globorotaliid radiation could propagate.

The Eocene-Oligocene transition was accompanied by a sharp drop in $\delta^{18}O$ of benthic foraminiferal test calcite (a proxy for oceanic cooling) and the expansion of the Antarctic polar ice sheets (the *Oi-1 Glaciation*), levels of which continue to fluctuate throughout the Oligocene (Shackleton, 1984; Shackleton *et al.*, 1986; Miller *et al.*, 1987; Zachos *et al.*, 1994; Lear *et al.*, 2000; Zachos *et al.*, 2001). At this time, major southern hemisphere ice sheets became a permanent feature on the Earth. The glaciation of Antarctica at the Eocene/Oligocene transition has previously been thought to result from opening of Southern Ocean gateways, which produced the 'Antarctic Circum-polar Current' and thus thermal isolation (Kennett, 1977). Recent climatic modelling by DeConto and Pollard (2003) suggests this factor is secondary to a decline in atmospheric CO_2 that first allowed the formation of small dynamic ice caps on high Antarctic plateaux.

The Oligocene epoch marks a low point of planktonic foraminiferal diversity, principally occupied by the simple, generalised forms, exemplified by the genera *Globigerina, Dentoglobigerina, Zeaglobigerina* and *Paragloborotalia* (Spezzaferri, 1994). During the Oligocene epoch a number of tectonic changes resulted in significant oceanic modifications that may have influenced marine evolution. The most significant of these was the expansion and intensification of the circum-Antarctic current, resulting from the opening of the Drake Passage (between modern day southern Argentina and Antarctica) from the Middle to Late Oligocene onward. This intensified cooling at high latitudes and warming at low latitudes (Livermore *et al.*, 2001). Increased glaciation and high latitude cooling produced a trend towards steepening of the surface water thermal gradients, strengthening of the gyral circulation and the Equatorial Countercurrent system; and the development of tropical and subtropical faunal provinces (Wright and Thunell, 1988).

Following the Oligocene glacial condition, foraminiferal isotope trends reflect a sharp rise in oceanic temperatures towards the end of the Oligocene, accompanied by the development of partial or ephemeral ice sheets (Lear *et al.*, 2000). Global ice volume then remained low throughout the early part of the Miocene (Lear *et al.*, 2000), a time when the primitive globorotaliids were evolving from paragloborotaliid or benthic (see section 4.2.3 below) stocks. If a paragloborotaliid was the ancestor, this evolutionary pathway was associated with development of the smooth test wall from the honeycomb paragloborotaliid wall texture, and was never reversed (Cifelli and Scott, 1986). Globorotaliid diversity then increased through the Early to Middle Miocene (see Chapter 2) in phase with gradual climatic warming, which culminated in the Middle Miocene

'climatic optimum', circa 15 Ma. Major expansion of the Antarctic ice sheet occurred episodically during the Middle Miocene and was in phase with further cooling of deep ocean waters (Savin *et al.*, 1985; Miller *et al.*, 1987; Hudson and Anderson, 1989). At this time the Australian landmass drifted northwards, closing the Indonesian seaway and in turn developing the Equatorial Undercurrent system in the Pacific Ocean (Kennett, 1985). This system has recently been found to exert a significant influence on tropical Pacific productivity (Loubere, 2000).

The Middle Miocene 'climatic optimum' then yielded to gradual oceanic and climatic cooling linked to the onset of small scale glaciation in the northern hemisphere and the re-establishment of the Antarctic ice-sheets. Wei and Kennett (1986) attributed near-equilibrium diversity in the planktonic foraminifera to the climatic stability during the Middle to Late Miocene. The end Miocene was then accompanied by further global cooling and a number of other palaeoceanographic events such as the Mediterranean salinity crisis (Kennett, 1985; Lear *et al.*, 2000; Zachos *et al.*, 2001). At this time planktonic foraminiferal diversity declined, with significant extinctions of the fohsellids and the globoconellid globorotaliids (Kennett and Srinivasan, 1983).

By Pleistocene times large polar ice caps were well developed at both the north and south poles and the Panamanian seaway closed, effectively separating the Atlantic and Pacific oceanic circulation and planktonic populations (Coates and Obando, 1996). The Large-scale palaeoceanographic fluctuations and high-frequency climatic oscillations throughout the Plio-Pleistocene (Wei and Kennett, 1986) may have been responsible for reduced globorotaliid diversity and the development of endemic populations, which paved the way to the small number of globorotaliid morphospecies that currently reside in today's oceans.

Without stable isotopic data from benthic and planktonic foraminifera, such discussion of palaeoclimate would be an order of magnitude more speculative. Analysis of stable isotopes from foraminiferal tests constitutes the 'backbone' of Cenozoic palaeoclimatic studies.

4.1.2 Aims

Chapter 1 introduced modern globorotaliids and discussed preferred depth-ecology, while in Chapter 2 potential factors driving foraminiferal evolution were discussed. Of

these, the physical environment has been previously suggested by some authors as driving evolution, although no individual study demonstrates an unequivocal link between evolution and the changing oceanic parameters.

This chapter presents isotopic data used to define the ecological preferences of fossil globorotaliid morphospecies from the menardellid and *Globorotalia s.s.* lineages (some of which have not been previously analysed isotopically) and the temperatures of the Miocene oceans in which they resided. That is, two different applications of planktonic foraminifera as instruments to measure past oceanic conditions.

4.2 Palaeoecology and foraminiferal evolution

4.2.1 Introduction

Modern planktonic foraminifera have been shown to occupy a range of hydrographic and latitudinal realms and to exhibit diverse morphologies thought to reflect the environmental conditions to which they are exposed (Hemleben *et al.*, 1989). Unfortunately, there are no consistent morphological characteristics that consistently delineate function or ecology in extinct lineages. However, the extent of iterative homoeomorphy in the planktonic foraminifera (Cifelli, 1969) supplies the palaeontologist with a broad benchmark from which to infer the palaeobiology of extinct lineages through comparison with extant forms. This kind of comparison between extinct and extant taxa is commonly used with the benthic foraminifera e.g., for estimating palaeo-depths (see Chapter 3).

Studies of modern oceans (e.g. Bé *et al.*, 1985) have shown that planktonic foraminifera occupy different ecological domains (e.g., surface mixed layer, thermocline) that roughly correspond to morphological and taxonomic groupings. Principally, the Neogene *Globorotalia* are non-spinose, low-trochospirally coiled, keeled taxa which usually occupy the sub-surface mixed layer depth realms, but may occur abundantly in temperate waters in the surface mixed layer during the winter (Durazzi, 1981; Hemleben, 1985). Shackleton and Vincent (1978) published one of the first studies inferring depth habitats using isotopic signals of Recent and Holocene planktonic foraminifera. Their analyses were used to infer a range from ' intermediate water' to 'deeper central water' ecological preference for several globorotaliid species. The exception to this general

intermediate depth habitat is modern *Gr. menardii*, which occurs in deeper warmer waters, and near-surface in colder sites (Hemleben *et al.*, 1989).

For fossil assemblages, isotopic analysis of foraminiferal shells offers a proxy for the same kind of ecological information that can be recorded empirically in modern species. Limited stable isotopic analyses of fossil globorotaliids have been published (e.g., Keller *et al.*, 1985; Norris *et al.*, 1993; Pearson and Shackleton, 1995), but relatively few taxa were involved, which were sometimes generically-grouped without isolation of individual morphospecies or variants.

The purpose of this section is to explore the preferred depth habitats of some Miocene globorotaliid morphospecies using stable isotopic analyses of planktonic assemblages from two ODP sites. This includes isotopic data from some of the more primitive globorotaliids from Site 871 (Limalok Guyot, Pacific, previously studied by Pearson and Shackleton, 1995), and later morphospecies in assemblages from Site 1195 (Coral Sea, Indo-Pacific).

4.2.2 Foraminiferal palaeoecology using stable isotopes

Stable oxygen and carbon isotope analysis of test calcite is a well-established technique for investigating palaeoecology in foraminifera (see Spero, 1998; Pearson, 1998 for review). Measured oxygen isotope ratios of test calcite can be used to yield estimates for palaeotemperatures of the seawater and since temperature varies with water depth, $\delta^{18}O$ data (proportion of ^{16}O to ^{18}O relative to a standard) from species in the same sample are believed to reflect depth-related or seasonal temperature differences (Mulitza *et al.*, 1997; Pearson, 1998). Those planktonic foraminifera residing in the surface (warmer) mixed layer tend to yield lighter (more negative) $\delta^{18}O$ values than those living within or below the thermocline, where waters are typically cooler. The $\delta^{13}C$ (proportion of ^{13}C to ^{12}C) isotopic signal provides further information about palaeodepth independent of the oxygen isotopic method. Algal photosynthesisers in the water column preferentially remove ^{12}C during photosynthesis from the shallow mixed layer of the oceans. Organic particles then eventually sink to greater depths and become oxidised, which releases the isolated ^{12}C back into the water. The result is a measurable depth gradient of $\delta^{13}C$, with respect to the total dissolved inorganic carbon ($\sum CO_2$) (Kroopnick, 1974).

These stable isotope methods have been applied extensively to fossil assemblages to infer palaeoecological and evolutionary patterns (e.g. Douglas and Savin, 1978; Keller *et al.*, 1985; Norris *et al.*, 1993; Pearson *et al.*, 1993, 1997a,b; Huber *et al.*, 1999; Coxall *et al.*, 2000). However, there are a number of extrinsic and species-specific effects that can alter the isotope signals (see discussion in Section 4.3.4), e.g. temperature, alkalinity, diagenesis, vital effects. Of these, diagenetic replacement has the greatest potential to alter the isotopic ratios. The susceptibility of fossil planktonic foraminiferal tests to diagenesis must be acknowledged when interpreting any foraminiferal test isotopic data. When conducting isotopic analysis using planktonic foraminifera assemblages, with obvious test recrystallisation should always be avoided because calcite alteration will undoubtedly affect isotopic ratios in the shell. It should be noted that there is an important distinction between the potential diagenetic effect of using foraminiferal calcite isotopic ratios to infer depth ecology and temperature. Diagenetic effect is less important when making interpretations about depth habitat, because they rely on relative species differentials and not absolute figures. However, when using foraminiferal test isotopic ratios to produce palaeotemperature estimates, because absolute values are required, diagenesis can have a significant effect on the results. This point is discussed further in Section 4.3.1.

4.2.3 Ecological evolution of some early globorotaliids

Ocean Drilling Program Site 871 Early Miocene planktonic assemblages are known for their good preservation (Pearson, 1995b). Pearson and Shackleton (1995) conducted multi-species palaeoecological isotopic analyses including limited data from the early menardellid globorotaliids (*Gr. praescitula*, *Gr. archeomenardii* and *Gr. praemenardii*). To expand on these results, isotopic analyses of these three morphospecies were carried out to infer depth habitat preferences. Analysis of *Gr. praescitula* has great significance because it is the possible progenitor to the Neogene globorotaliids (see Chapter 1 for discussion). The isotopic data is presented in Appendix 4.1.

Figure 4.1 presents the isotopic results for *Gr. praescitula*, *Gr. archeomenardii* and *Gr. praemenardii*. In this figure, the globorotaliid species data is compared to that of *Globigerinoides ruber* (surface-dweller) and *"Globoquadrina" venezuelana* (thermocline-dweller) and includes two isolated outlier sample points (greyed out) from Pearson and Shackleton (1995b).

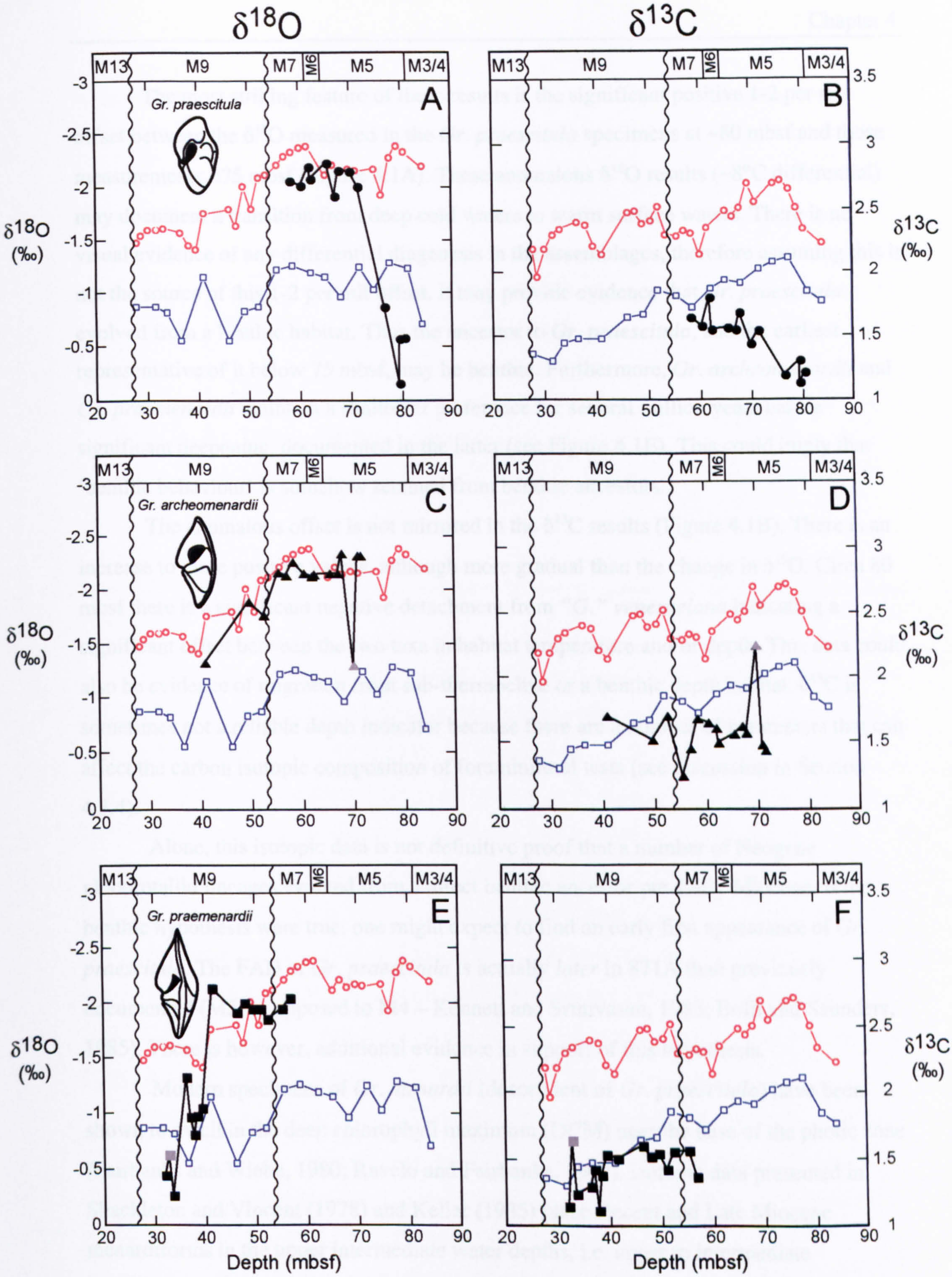

Figure 4.1. Oxygen and carbon isotope results for three early globorotaliids from ODP Hole 871A. Red open circles - isotope records of *Globigerinoides ruber; blue open squares - "Globoquadrina" venezuelana* and isolated grey points are all from Pearson and Shackleton (1995). All isotopic results are subject to a ±0.08‰ oxygen and a ±0.06‰ carbon isotopic analytical precision. The biozonation represents Early (M1-4) to Middle Miocene (M5-M12) times. Wavy lines signify unconformities in the cored 871A sedimentary sequence.

The most striking feature of these results is the significant positive 1-2 per mil offset between the $\delta^{18}O$ measured in the *Gr. praescitula* specimens at ~80 mbsf and those measurements <75 mbsf (Figure 4.1A). These anomalous $\delta^{18}O$ results (~8°C differential) may document a transition from deep cold waters to warm surface waters. There is no visual evidence of any differential diagenesis in the assemblages, therefore assuming this is not the source of this 1-2 per mil offset, it may provide evidence that *Gr. praescitula* evolved from a benthic habitat. Thus the ancestor to *Gr. praescitula*, and the earliest representative of it below 75 mbsf, may be benthic. Furthermore, *Gr. archeomenardii* and *Gr. praemenardii* maintain a shallower preference for several million years before significant deepening, documented in the latter (see Figure 4.1E). This could imply that 'benthic behaviour' is somehow retained from benthic ancestors.

The anomalous offset is not mirrored in the $\delta^{13}C$ results (Figure 4.1B). There is an increase to more positive values, although more gradual than the change in $\delta^{18}O$. Circa 80 mbsf there is a significant negative detachment from *"G." venezuelana* indicating a significant offset between the two taxa in habitat temperature and/or depth. This data could also be evidence of migration from sub-thermocline or a benthic depth habitat. $\delta^{13}C$ is sometimes not a reliable depth indicator because there are a number of parameters that can affect the carbon isotopic composition of foraminiferal tests (see discussion in Section 4.3.4).

Alone, this isotopic data is not definitive proof that a number of Neogene globorotaliid lineages evolved from a direct benthic ancestor pre-Early Miocene. If the benthic hypothesis were true, one might expect to find an early first appearance of *Gr. praescitula*. The FAD of *Gr. praescitula* is actually *later* in 871A than previously documented (M5, as opposed to M4 – Kennett and Srinivasan, 1983; Bolli and Saunders, 1985). There is however, additional evidence in support of this hypothesis.

Modern specimens of *Gr. menardii* (descendent of *Gr. praescitula*) have been shown to dwell in the deep chlorophyll maximum (DCM) near the base of the photic zone (Fairbanks and Wiebe, 1980; Ravelo and Fairbanks, 1992). Isotopic data presented in Shackleton and Vincent (1978) and Keller (1985) place Recent and Late Miocene menardiforms in the upper intermediate water depths, i.e. upper to intermediate thermocline. Hilbrecht and Thierstein (1996) later documented crawling and burrowing behaviour in live *Gr. menardii* cultures (Figure 4.2) and interpreted this benthic mode as an adaptation of species living in the DCM or neritic environments to exploit floating

organic aggregates as a 'pseudobenthic' habitat and a source of food. This could help to explain the long range and apparent success of this taxon. If benthic strategies are observed in a modern globorotaliid species, perhaps this is a characteristic retained from an ancestor (*Gr. praescitula* or an older benthic progenitor)?

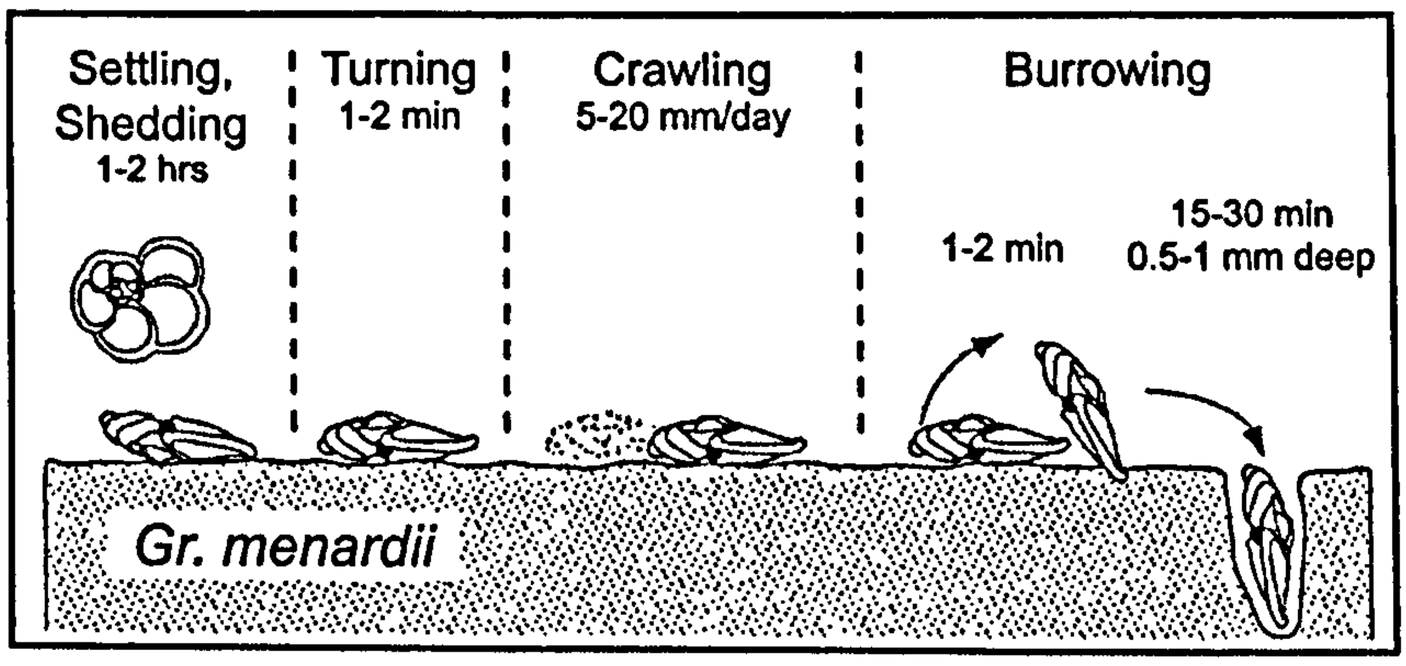

Figure 4.2. 'Benthic' behaviour observed in modern *Globorotalia menardii* specimens, adapted from Hilbrecht & Thierstein (1996).

The origin of *Globorotalia* has long been contentious (see Chapter 1). As discussed in Chapter 1, it is certain that the foraminifera developed a planktonic mode from a benthic ancestor (Pawlowski *et al.*, 1996, 1997, 1999), but could this have happened more than once? It is generally thought that *Gr. praescitula* is derived from a contemporary within the Globigerinacea (e.g., Kennett and Srinivasan, 1983; Fordham, 1986), although no obvious globigerinacean relative of *Gr. praescitula* has been found in the Early Miocene. This has been challenged by phylogenetic analysis of partial sequences of small subunit (SSU) ribosomal rRNA and DNA (Darling *et al.*, 1997; de Vargas *et al.*, 1997). Both studies suggest that isolated modern planktonic foraminifera are sister to at least two distinct benthic plexi e.g., taxa from the genera *Ammonia*, *Trochammina* and *Astorhiza*. In Figure 4.3 below, the phylogeny of de Vargas *et al.* (1997) is reproduced.

Furthermore, observations of *Gr. praescitula* from material from Pacific ODP Site 871A and assemblages collected in New Zealand reveal it to be quite morphologically distinct from any taxon suggested as its ancestor. *Gr. praescitula* cannot be easily allied with any other taxon in the globigerinacea.

Alone, none of these separate lines of evidence constitute definitive proof that several Neogene globorotaliid lineages were derived from a benthic ancestor; collectively these data constitute reasonable evidence in support of the polyphyletic development of the planktonic habitat. If this is the case, it is a very interesting result.

The *Gr. archeomenardii* oxygen isotope signal (1C) gradually declines through the Early to Middle Miocene approximately following the *Gds. ruber* signal. As suggested by Pearson and Shackleton (1995) this does not necessarily support depth habitat descent, because this shift seen in *Gds. ruber* may be the result of surface-water cooling and weakening of the thermocline during Middle Miocene times. *Gr. archeomenardii* appears to share a similar depth preference with *Gds. ruber*, i.e. near surface.

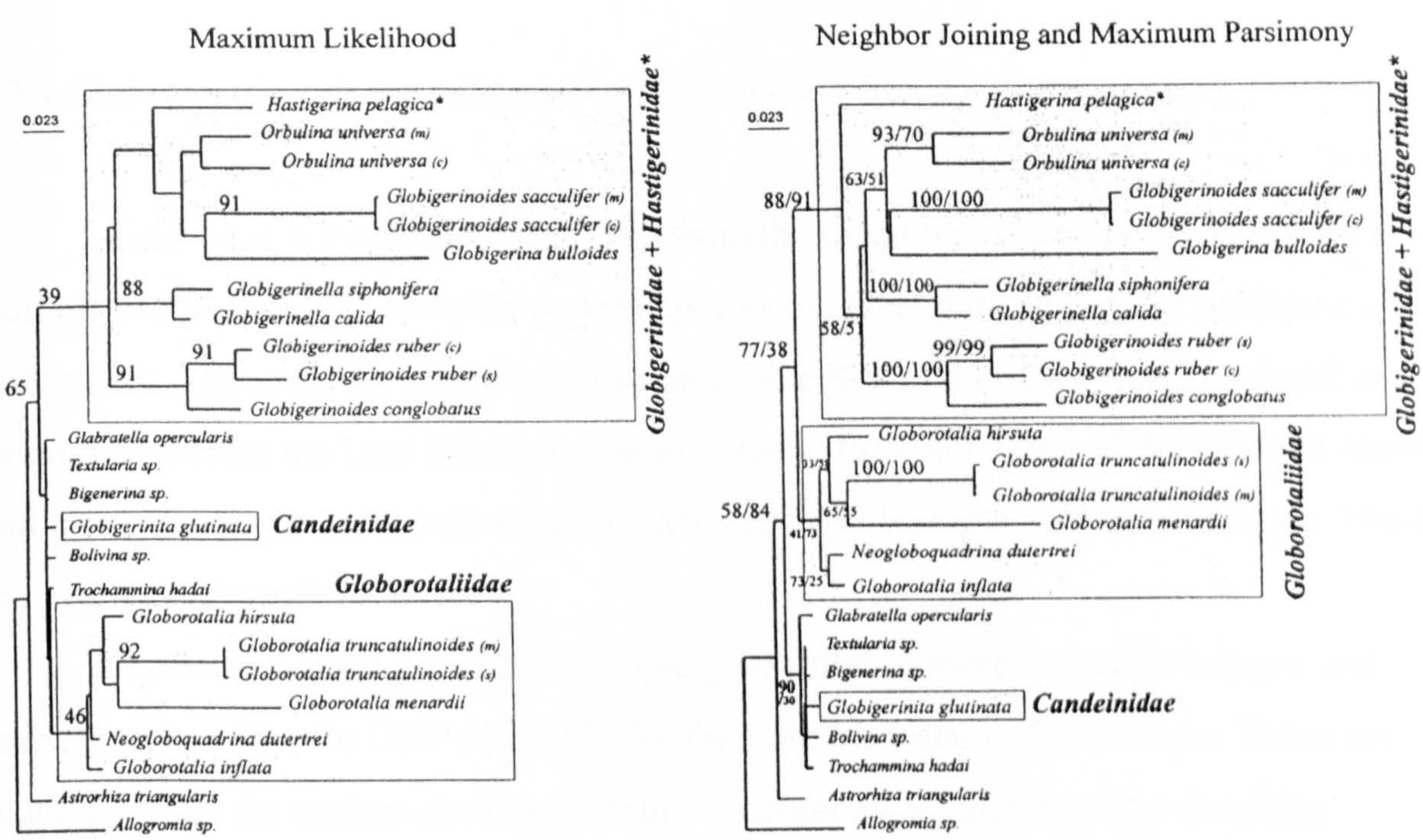

Figure 4.3. Phylogeny of 14 planktonic foraminifera (rectangles) and 7 benthic foraminifera from genetic data. Taken from de Vargas *et al.* (1997). The ML and NJ-MP trees were obtained using 521 unambiguously aligned sites. Bootstrap proportions greater than 50% are given for each internal branch.

Hodell and Vayavananda (1993) proposed that the early menardellid lineage evolved to an intermediate level from a deep-water habitat, which in turn induced the *Fohsella* ("*Globorotalia* [*Fohsella*]") extinction at the top of biozone M9. The data presented here supports Pearson and Shackleton's (1995) inference that *Gr. archeomenardii* already occupied a similar depth habitat to *Fohsella* (surface to intermediate) some time before the extinction.

The majority of the *Gr. archeomenardii* carbon isotope values (Figure 4.1D) are more negative than the corresponding *"G." venezuelana* data. This contradicts the oxygen isotope values (Figure 4.1C), which suggest a shallower habitat and may result from a species-specific vital effect (see Section 4.3.4).

The isotopic data for *Gr. praemenardii* (Figure 4.1E) is the reverse of the trend seen in *Gr. praescitula* (Figure 4.1A). The oxygen isotope data record an overall decline of 1.5-2 per mil between 40-30 mbsf (middle M9 biozone). This again could indicate a sudden migration to cooler (and deeper?) waters. The $\delta^{13}C$ (Figure 4.1F) also shows a fall, albeit of smaller magnitude and more gradual nature, with deviation from the data trends of both *Gds. ruber* and *"G." venezuelana*. Once again the carbon isotope values fall consistently below those of *"G." venezuelana*.

4.2.4 Globorotaliid palaeoecology inferred from ODP Site 1195 assemblages

Assemblages from ODP Site 1195 from the Coral Sea were chosen to conduct isotopic analyses of globorotaliid morphospecies to investigate ecological preferences and differences. The analyses complement those of Site 871 in that they were restricted to assemblages from the Late Miocene onwards due to the limitations of the material cored and the mediocre preservation of Middle Miocene and younger core assemblages. The data are given in Appendix 4.1.

Figures 4.4 and 4.5 present multiple globorotaliid morphospecies oxygen and carbon isotope data for ODP Site 1195 for the Late Miocene to Pleistocene. These are plotted against the surface-dwelling *Globigerinoides ruber* and the deep-dwelling *Globorotalia scitula* and *Globorotalia crassaformis* (as investigated in Shackleton and Vincent, 1978). *Gr. scitula* was not present in the samples for all intervals, therefore *Gr. crassaformis* was also used as a deep-dwelling control taxon.

The oxygen (Figure 4.4A-D) results show similar values for all the species, with an overall decline in $\delta^{18}O$ from the Late Miocene through the Pleistocene.

This general decline in oxygen values is indicative of cooling of the ambient waters linked to the Late Miocene climatic cooling trend and not the result of depth migration *en masse*, since *Gds. Rubber* still occupies a surficial habitat.

The oxygen values of all the investigated globorotaliid species plot below the surface-dwelling *Globigerinoides ruber* and most consistently plot above the deep-dwellers. Thus the majority of the morphospecies analysed probably preferred a thermocline or subthermocline depth habitat.

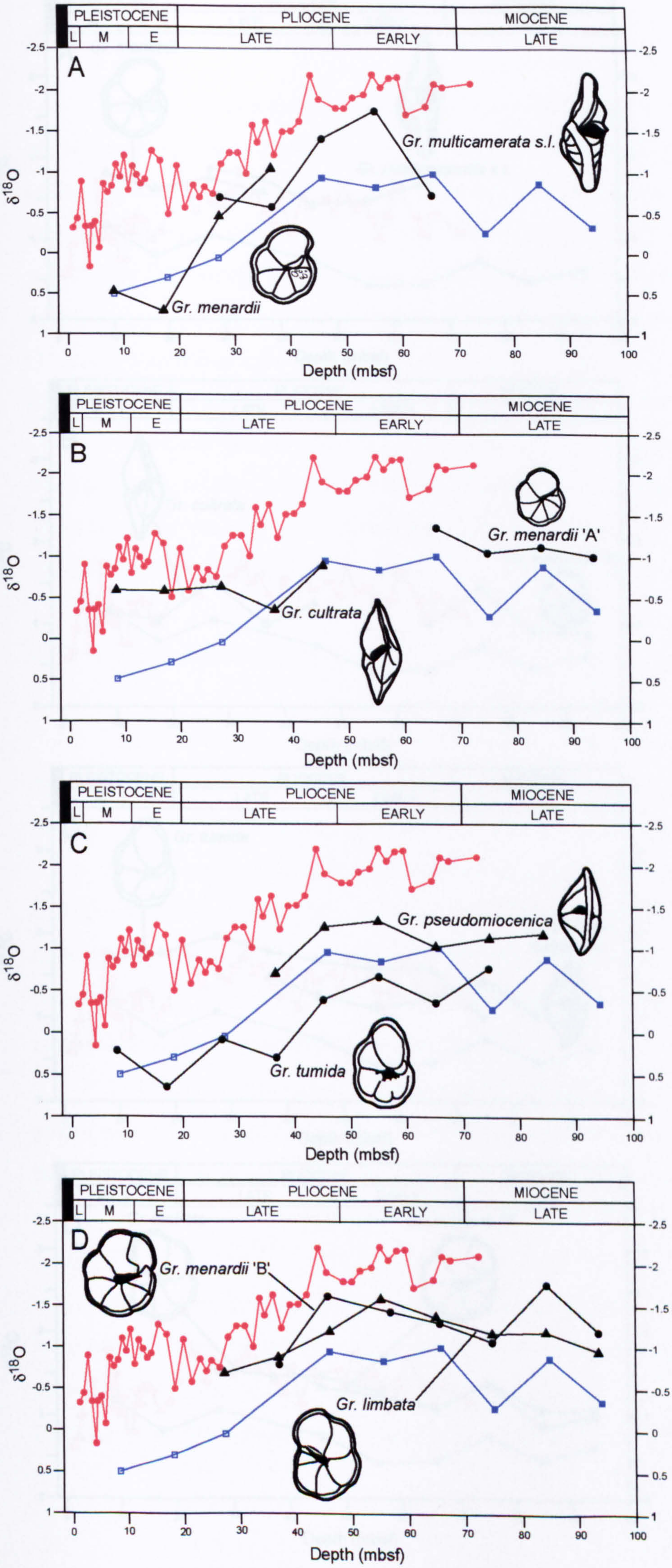

$\delta^{18}O$

Figure 4.4. Oxygen isotopes from Late Miocene to Pleistocene globorotaliid morphospecies (black circles and triangles) plotted against the surface-dwelling species *Gds. ruber* (red filled circles), and the deeper-dwelling species *Gr. crassaformis* (blue open squares) and *Gr. scitula* (blue closed squares), from ODP Site 1195. All isotopic results are subject to a ±0.08‰ oxygen and a ±0.06‰ carbon isotopic analytical precision.

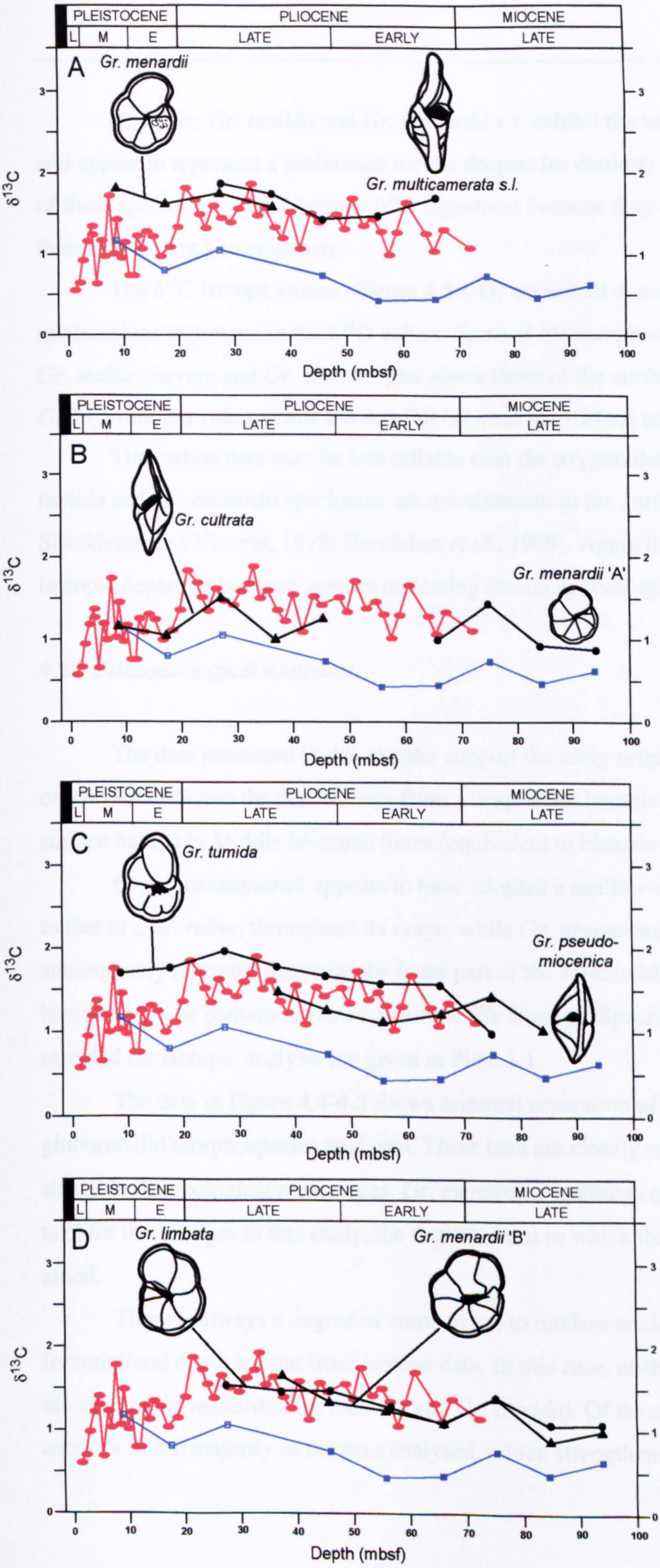

$\delta^{13}C$

Figure 4.5. Carbon isotopes from Late Miocene to Pleistocene globorotaliid morphospecies (black circles and triangles) plotted against the surface-dwelling species *Gds. ruber* (red circles), and the deeper-dwelling species *Gr. crassaformis* (blue open squares) and *Gr. scitula* (blue closed squares), from ODP Site 1195. All isotopic results are subject to a ±0.08‰ oxygen and a ±0.06‰ carbon isotopic analytical precision.

However, *Gr. tumida* and *Gr. menardii s.s.* exhibit the heaviest oxygen signatures and appear to represent a preference for the deepest (or coolest) habitats. Extant specimens of these species may yield heavier $\delta^{18}O$ signatures because they deposit more calcite on their tests during gametogensis.

The $\delta^{13}C$ isotope values (Figure 4.5A-D) are not all consistent with the relationships expressed in the $\delta^{18}O$ values. Some of the morphospecies data (*Gr. menardii*, *Gr. multicamerata* and *Gr. tumida*) plot above those of the surface-dwelling *Globigerinoides ruber*, while the rest fall between the surface and deep-dwelling taxa.

The carbon data may be less reliable than the oxygen data because modern *Gr. tumida* and *Gr. menardii* specimens are not abundant in the surface mixed layer (see Shackleton and Vincent, 1978; Hemleben *et al.*, 1989). Again there is no significant isotopic departure between species indicating similar species-specific habitat preferences.

4.2.5 Palaeoecological summary

The data presented in this chapter support the early origin of *Gr. praescitula-archeomenardii* and the descendents from a deep-water benthic habitat before adopting a surface habitat in Middle Miocene times (equivalent to biozone M5) similar to *Gds. ruber.*

Gr. archeomenardii appears to have adopted a shallow-dwelling attitude equivalent to that of *Gds. ruber*, throughout its range, while *Gr. praemenardii* appears to have subsequently migrated deeper in the latter part of the Middle Miocene (equivalent to biozone M9), or perhaps regained a benthic life strategy. Specimens from the horizons sampled for isotopic analysis are given in Plate 1.1.

The data in Figure 4.4-4.5 shows minimal separation of all the Late Miocene globorotaliid morphospecies analysed. These taxa are closely related phylogenetically and share similar ecological preferences. *Gr. menardii* constitutes one of the primary ancestral taxa for the lineages in this study, the depth habitat to which the other taxa are probably allied.

There is always a degree of comparison to modern analogues when extrapolating foraminiferal depth habitat from isotope data. In this case, of the taxa under analysis, three are extant (*Gr. menardii, Gr. cultrata* and *Gr. tumida*). Of these, *Gr. menardii* is a likely ancestor of the majority of the taxa analysed, which strengthens palaeoecological

comparisons between the extant and extinct taxa (unless *Gr. menardii* has developed a number of apomorphic characteristics more recently).

4.3 Miocene sea surface temperatures from exceptionally preserved Tanzanian assemblages

Three samples were collected from hemipelagic muds from coastal exposures in Tanzania, which contained exceptionally well-preserved planktonic and benthic Miocene foraminiferal assemblages (see Chapter 3). These assemblages were analysed for stable oxygen and carbon isotopes and were used to calculate sea surface and bottom water temperatures in the Indian Ocean during the Early and Middle Miocene. The results quantify a small section of the marine conditions that existed during the early radiation and development of the globorotaliids. In addition, this data provides further constraints for modelling past oceanic models and reinforces the importance of targeting well-preserved material for accurate palaeotemperature calculations.

4.3.1 Miocene oceanic palaeotemperatures

The last major synthesis of Miocene sea-surface temperatures and palaeoceanographic change followed the initial phase of deep-sea drilling (Kennett, 1985, and references cited therein). At that time it was argued from $\delta^{18}O$ evidence that tropical SSTs were typically around 20°C and meridional temperature gradients were generally much lower than today (Savin *et al.*, 1985; Keller, 1985). Since Savin *et al.* (1985), it has become increasingly apparent that $\delta^{18}O$ analysis of planktonic foraminiferal shells may be affected greatly by diagenesis during early burial in the cold sea-floor environment (Killingley, 1983; Schrag *et al.*, 1995; Wilson and Opdyke, 1996; Norris and Wilson, 1998; Schrag, 1999; Crowley and Zachos, 2000; Wilson and Norris, 2001; Pearson *et al.*, 2001; Wilson *et al.*, 2002). In 1995, Van Eijden and Ganssen estimated similar Oligo-Miocene boundary SSTs from Indian Ocean foraminiferal isotopes to those of Savin *et al.* (18-20°C). However, they deemed these estimates to be 'unrealistically low'.

The material from pelagic oozes and chalks used to calculate these temperatures in Kennett *et al.* (1985) were re-inspected by the author using scanning electron microscopy.

Despite being described as (or appearing) 'well/excellently-preserved', micron-scale recrystallisation had clearly affected the fossil foraminiferal tests. Plate 4.1 presents high magnification SEM images detailing the preservation of the Tanzanian material. Images 4.1B, 4.1D, 4.1F, and 4.1H show many of the key features associated with excellent preservation, including the preservation of test wall crystallites, hexagonal porepits, original spines and the remnants of organic pore lining. These images directly contrast images 4.1A, 4.1C, 4.1E and 4.1G, which illustrate the preservation of planktonic foraminiferal assemblages from selected DSDP/ODP sites that have been used extensively in previous $\delta^{18}O$ studies.

This small-scale recrystallisation is distinct from the more obvious surface recrystallisation that is well documented in planktonic foraminifera fossils. The type of preservation encountered in planktonic assemblages from Tanzania maintains the original 'glassy', translucent nature of the foraminiferal test and the original crystallites can still be seen using high-level scanning electron microscopy. This kind of wall texture is present in modern planktonic foraminiferal and fossil assemblages that have not been subjected to pervasive microscopic diagenesis. *This* level of preservation should be referred to as 'excellent' and the corresponding material 'well-preserved'. Other authors have also described material of similar preservation-level from clay-rich sediments, to which these characteristics can be attributed (see Norris and Wilson, 1998; Wilson and Norris, 2001; Pearson *et al.*, 2001; Wilson *et al.*, 2002).

Three samples collected in Tanzania yielded assemblages with such preservation and were used to calculate new surface and bottom palaeotemperatures in the Indian Ocean for the Early and Middle Miocene.

4.3.2 Depositional setting

The samples contain diverse mixed-layer and thermocline to sub-thermocline dwelling planktonic foraminifera (globoquadrinids, dentoglobigerinids), however, globorotaliids are generally rare in the Middle Miocene samples, so a deep water, fully open-ocean environment cannot be inferred. The planktonic assemblages identified support a middle to outer-shelf depositional environment. This is corroborated by the benthic foraminiferal assemblages and P/B ratios, which support a bathyal (>100 m) slope-depth depositional environment (van Morkhoven *et al.*, 1986; Gibson, 1989; Hallock, pers. comm., 2002).

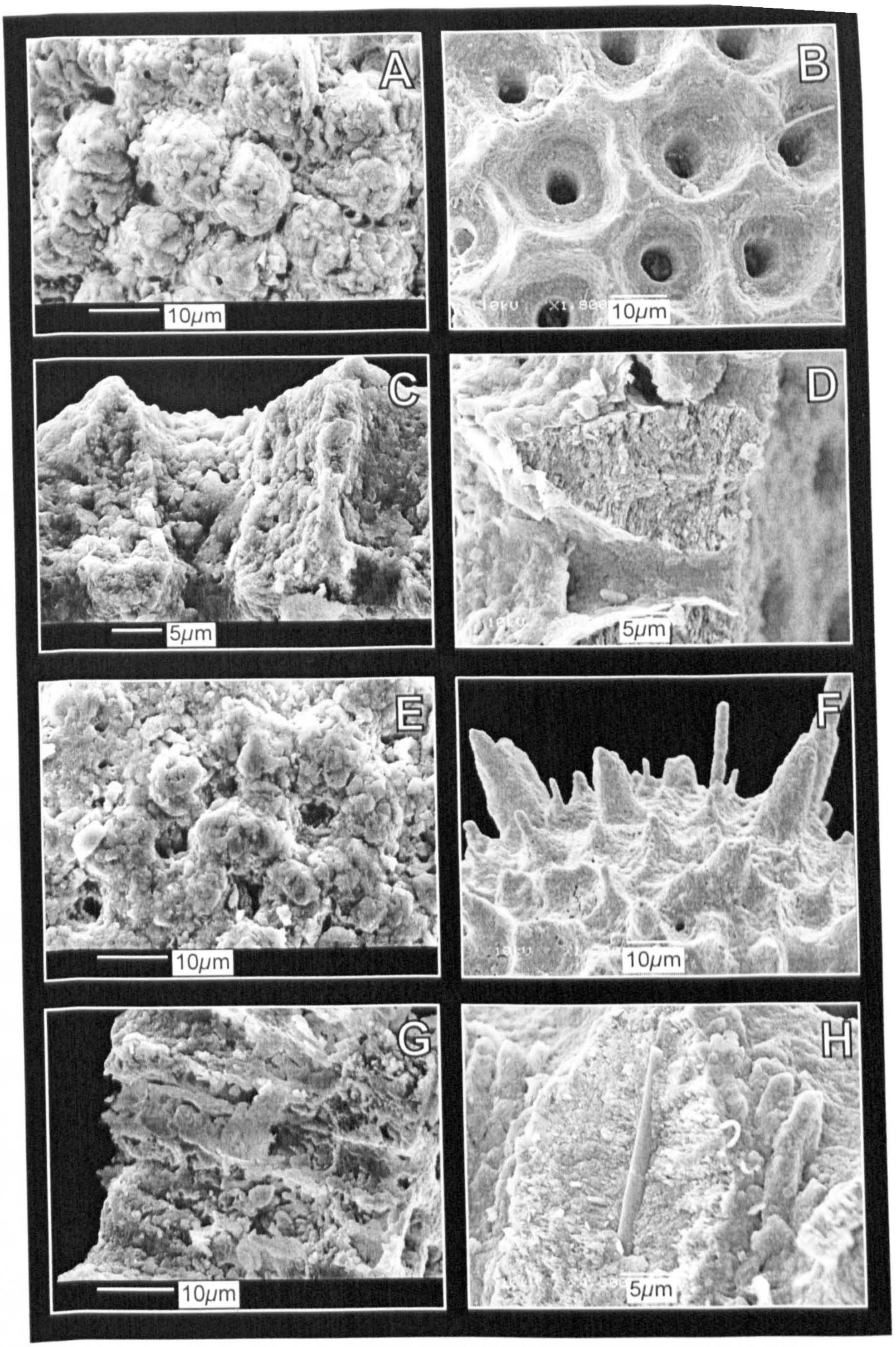

Plate 4.1 High-magnification scanning electron micrographs of planktonic foraminifera contrasting the preservation of the previously analysed DSDP/ODP (left) and Tanzanian (right) material. **A.** Close-up, recrystallised suface texture of *G. praebulloides*, exhibiting remnant pores and spine holes, Early Miocene, DSDP 59, 448 6R-1, 52-53cm, Palau-Kyushu Ridge. **B.** Surface detail of *Gds. quadrilobatus* showing smooth, unaltered, surface texture with hexagonal pore-pits, Middle Miocene, 180906/1, Ras Tapuri, Tanzania. **C.** Test wall section of *Globoturborotalita sp.*, showing pervasive recrystallisation throughout the test and lack of crystallites (like those seen in 1.4), lowermost Miocene, ODP 154, 926B 50X-4, 54-56cm., Ceara Rise **D.** *Globigerina sp.*, cross-section of test wall exhibiting original microgranular texture, Early Miocene, RAS99-42, Lindi, Tanzania. **E.** Recrystallised wall of *"G." venezuelana*, Late Oligocene, ODP 121, 758A 22X-3, 99-100cm, Ninetyeast Ridge. **F.** Multiple spine morphologies of test surface of *Globoturborotalita. sp.*, Early Miocene, RAS99-42, Lindi, Tanzania. **G.** Recrystallised test section of *P. mayeri*, Middle Miocene, DSDP 22 216A 4R-1, 64-65cm, Ninetyeast Ridge. **H.** Detail of subsurface spine and crystallites preserved in *Gds. quadrilobatus*, Middle Miocene, 180906/1, Ras Tapuri, Tanzania.

Further evidence of shelf proximity comes from the relatively high proportions of worked quartz. The presence of framboidal pyrite nodules suggests a relatively oxygen-rich depositional setting, and therefore the environment is probably not abyssal.

4.3.3 Palaeotemperature calculation

Carbon and oxygen isotopic ratios for the samples analysed are given in Appendix 4.2. The oxygen isotope values reported here are expressed with reference to the PDB (Pee Dee Belemnite) standard using the 'delta notation' (Shackleton, 1984).

The palaeotemperature equation employed in this study was that of Erez and Luz (1983), which is calibrated using the planktonic foraminifer *Globigerinoides sacculifer*:

$$T = 17.0 - 4.52(\delta_c{}^{18}\mathrm{O} - \delta_w{}^{18}\mathrm{O}) + 0.03(\delta_c{}^{18}\mathrm{O} - \delta_w{}^{18}\mathrm{O})^2$$

where T, $\delta_c{}^{18}O$ and $\delta_w{}^{18}O$ are the palaeotemperature, isotopic composition of the test calcite (relative to PDB) and seawater (relative to SMOW) respectively.

The most negative $\delta^{18}O$ value is taken to represent the seasonal maximum SST (Emiliani, 1954). The outer shelf environments of deposition for these assemblages may be affected by boundary currents and may not be representative of open-ocean salinities of the same latitude, therefore a latitude correction for seawater $\delta^{18}O$ (e.g. Zachos, 1994) has not been applied to the calculation.

4.3.4 Foraminiferal stable isotope analyses

Isotopic ratios of oxygen and carbon from the shells of foraminifera are one of the most important available resources for understanding past climate change and oceanographic conditions. It is widely agreed that the isotopic ratios of these elements can be utilised to generate information about the diverse set of foraminiferal niches, depth habitats, seawater palaeotemperature and water mass distribution (see Spero, 1998 for review).

Urey (1947) discovered that the isotopic fractionation between seawater and calcite is temperature-dependent with respect to oxygen, i.e. the precipitation of the ^{18}O isotope in thermodynamic equilibrium is inversely proportional to the temperature of the water in

which the calcite is precipitated. The studies of Emiliani (1954, 1955) demonstrated that measured oxygen isotope ratios ($\delta^{18}O$) of test calcite can be used to yield estimates for palaeotemperatures of the seawater within which foraminifera originally constructed their tests. Temperature varies with water depth, so this data can also be used as an imprecise estimate for depth habitat (Emiliani, 1954). This method has been applied successfully to modern species with known depth stratification (Shackleton and Vincent, 1978; Fairbanks *et al.*, 1982), and extensively to extinct species (Berger *et al.*, 1978; Douglas and Savin, 1978). The $\delta^{13}C$ isotopic signal is primarily used to derive information about palaeodepth as discussed above.

There are multiple potential sources of error that an investigator must take into account before accurate estimates can be made using these stable isotope methods (Savin, 1977; Berger and Vincent, 1986; Miller *et al.*, 1987; Spero, 1998). These potential factors are discussed below.

4.3.4.1 Vital effect

The vital or metabolic effect describes variations in shell isotopic composition from the thermodynamic equilibrium due to physiological factors (Hemleben *et al.*, 1989). Erez and Honjo (1981) and Spero (1997) suggest that this effect is species-specific and does not influence all modern species equally. In an attempt to measure the vital effect, modern planktonic species have been employed to calibrate the numerous palaeotemperature equations in existence (Epstein *et al.*, 1953; modified in Craig, 1965; O'Neil *et al.*, 1969; Shackleton, 1974; Erez and Luz, 1983) with ambiguous results (Spero, 1998). For example, calculations using Epstein *et al.'s* (1953) equation with planktonic foraminifera from Bermuda consistently produced temperatures 1-2°C higher (negative $\delta^{18}O$ deviation) than the measured SSTs. In this case, it is not clear whether it is the foraminifera themselves or the equation parameters that are causing the offset

Respiration results in $\delta^{18}O$ depletion in the test (Lane and Doyle, 1956) and therefore may constitute a large part of the species-specific vital effect. Incorporation of the depleted respiratory products during calcification could result in depleted foraminifer test $\delta^{18}O$ values, however, it is contentious as to whether these depleted products would be used in calcification (Belanger *et al.*, 1981). It is possible that some species and not others incorporate significant respiratory oxygen into their tests (Norris *et al.*, 1993).

The degree of vital effect is also closely linked to fractionation parameters such as photosynthetic algal symbiont activity, calcification rate and modifications in growth rate (Spero, 1992; Spero *et al.*, 1997). These various factors are all concatenated and there is often a degree of overlap between regulating processes.

4.3.4.2 Ontogenetic and ecotypic effects

It has been suggested that juvenile species calcify at shallower depths than their adult equivalents and therefore may experience different isotopic compositions (Berger, 1978; Bijma *et al.* 1990; Erez *et al.* 1991). In addition, Spero and Lea (1996) measured a <0.8 ‰ progressive increase in $\delta^{18}O$ from the first to the last chambers of the planktonic foraminifer *Globigerina bulloides*. A similar and more pronounced trend was noted in carbon isotopes. They surmised that incorporation of respired CO_2 during test calcification was the cause, with higher metabolic rates in juveniles yielding the greatest depletion in $\delta^{18}O$, while subsequent maturation produces a trend towards equilibrium. This observation was corroborated by Kroon and Darling (1995), although the real-ocean trends reported here were half the size.

It follows that specimens picked for isotope analysis should be mature in order to minimise the effect of growth rate modifications and sampling bias, unless an investigator is specifically targeting isotopic differences through ontogeny.

4.3.4.3 Symbionts

Spero and Lea (1993) reported that the presence of photosynthetic symbionts had a negligible fractionation effect on the test $\delta^{18}O$ values for the species *Globigerinoides sacculifer* (350-850 μm size range). However, this study also reported an average chamber $\delta^{18}O$ decrease with increased irradiance levels, which was backed up by a similar result with the symbiotic species, *Orbulina universa* (Spero, 1992; Spero and Lea, 1993; Spero *et al.*, 1997). This phenomenon may be the result of a kinetic effect, in which higher light intensity causes greater skeletogenesis, which in turn favours stronger fractionation effects and thus greater $\delta^{18}O$ depletion (Rohling and Cooke, 1999). Increased irradiance levels have also been associated with increased growth rates in photosynthetic symbiont-bearing corals (Chalker, 1975) and larger foraminifera (Ter Kuile and Erez, 1984).

Algal symbionts are thought to generate carbon isotopic disequilibrium by preferentially removing ^{12}C during photosynthesis from the water immediately surrounding

the foraminifer, thus locally enriching the seawater total inorganic carbon ($\sum CO_2$) with respect to ^{13}C and masking the true ambient $\delta^{13}C$ (Spero and Williams, 1988, 1989). See Figure 4.6 below:

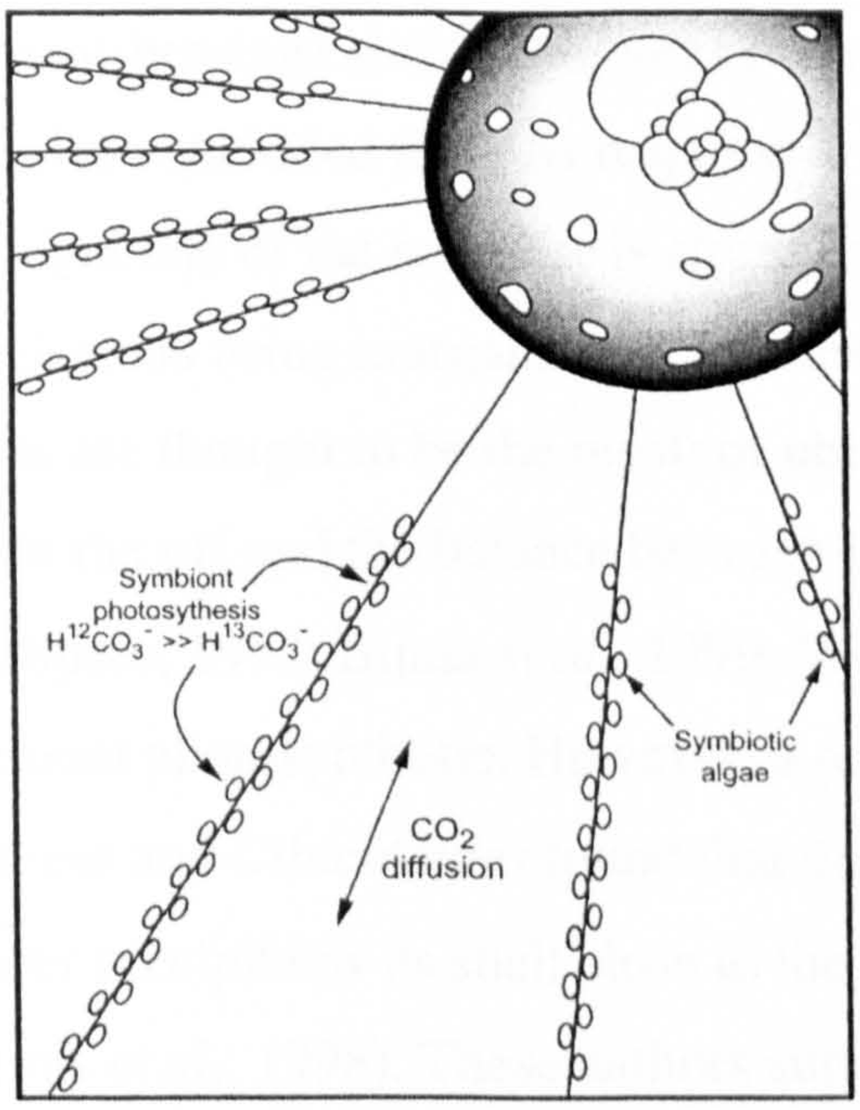

Figure 4.6. Illustration of *O. universa* foraminifera:symbiont relationship (adapted from Spero, 1998) depicting the microenvironment enrichment in $^{13}CO_2$ by symbiont uptake of ^{12}C-rich CO_2.

4.3.4.4 Gametogenesis

A number of modern planktonic foraminifer species deposit a layer of strongly ^{18}O-enriched calcite that can compose up to 30% of the test mass immediately prior to gametogenesis (Bé, 1980; Duplessy, 1981). These gametogenic calcite layers are usually strongly $\delta^{18}O$-enriched relative to earlier chambers, so can be expected to influence isotopic measurements. This may be partly because some foraminifera sink to greater (cooler) depths for reproduction, as suggested for *G. sacculifer* (Duplessey *et al.*, 1981), *O. universa*, *N. dutertrei,* and *Gr. menardii* (Bouvier-Soumagnac and Duplessey, 1985). As an individual migrates, physiological and chemical conditions vary down through the water column, indicators of which may be incorporated into the test calcite in the oxygen and carbon isotopic ratios. Spero and Lea (1993) suggested that another mechanism may be responsible because they stipulated the majority of living foraminifera would not support calcification at such great depths, but the depth-calcification hypothesis was then later *supported* by Spero and Lea (Bemis *et al.*, 1998).

4.3.4.5 Kinetic effect and alkalinity

Variable carbonate chemistry adds extra uncertainty to most of the potential error sources discussed. Carbonate concentration [CO_3^{2-}] of water was found to be inversely proportional to the $\delta^{18}O$ (and $\delta^{13}C$) of calcite incorporated into the foraminifer test in *Orbulina universa* (symbiont-bearing) and *G. bulloides* (non symbiont-bearing) (Spero *et al.*, 1997). These authors also concluded that this response was not related to symbiont photosynthesis and the magnitude of the response is strongly species-specific. McCrea (1950) made similar conclusions using inorganic precipitates.

These observations are thought to be the result of ubiquitous, abiological, kinetic fractionation dependent on the pH and the balance between CO_2 hydration and hydroxylation reactions (Spero, 1997; Bijma *et al.*, 1999; Wolf-Gladrow *et al.*, 1999) and may be unrelated to symbiont photosynthesis. However, a re-evaluation of existing data for the benthic genera *Uvigerina* and *Cibicidoides* found that the former exhibits mild $\delta^{18}O$ enrichment, while the latter precipitates its shell close to the oxygen isotopic equilibrium of ambient seawater (Bemis *et al.*, 1998). These authors suggest that the more infaunal habitat (lower pore-water pH and decreased [CO_3^{2-}]) of *Uvigerina* causes the offset. More work on different taxa may test this theory.

Alkalinity has a complex relationship with the concentration of [CO_3^{2-}] ions and pH of the seawater. The ocean is a well-buffered system and the modern surface ocean varies in [CO_3^{2-}] ion content from 100 - 300 μmol kg^{-1} (Crowley and Zachos, 2000). It is possible that [CO_3^{2-}] ion content was higher in the past during times of inflated pCO_2. If a [CO_3^{2-}] ion concentration of 500-600 μmol kg^{-1} was reached, the kinetic disequilibrium would be <0.4‰, which is equivalent to a change of 1.5-2.0°C in marine palaeotemperature estimates (Crowley and Zachos, 2000).

4.3.4.6 Salinity and seawater $\delta^{18}O$ variations

Marine salinity is fundamentally connected to changes in precipitation and evaporation (P-E) and mixing of water masses (Rohling and Cooke, 1999). The 'salinity effect' describes variations in $\delta^{18}O$ due to evaporation and freshwater input. Rohling and Bigg (1998) suggest the replacement term 'freshwater budget effect' because both isotopic composition and seawater salinity are affected by the same hydrological processes. Net P-E variations in the ambient water mass and $\delta_w{}^{18}O$ (the isotopic composition of seawater)

affect $\delta^{18}O$ gradients, and therefore isotopic temperature estimates (Zachos, 1994; D'Hondt and Arthur, 1996).

The glacial effect also influences the isotopic ratios and salinity of seawater. This effect describes the long-term isotopic enrichment of the oceans through glacial periods, during which, the lighter ^{16}O isotope is preferentially fixed into ice sheets, which relatively enriches the oceans in ^{18}O. Throughout interglacial periods the 'freshwater' is locked up in the ice sheets until climatic warming reintroduces it into the oceans, reducing oceanic salinity. This is essentially the freshwater budget effect acting over longer periods of time. The volumetric extent of glaciation is especially important when calculating accurate palaeotemperatures for periods of extensive glaciation e.g., the Late Oligocene to Middle Miocene (Lear *et al.*, 2000). Figure 4.7 illustrates how fractionation processes in the hydrological cycle affect oxygen isotope ratios.

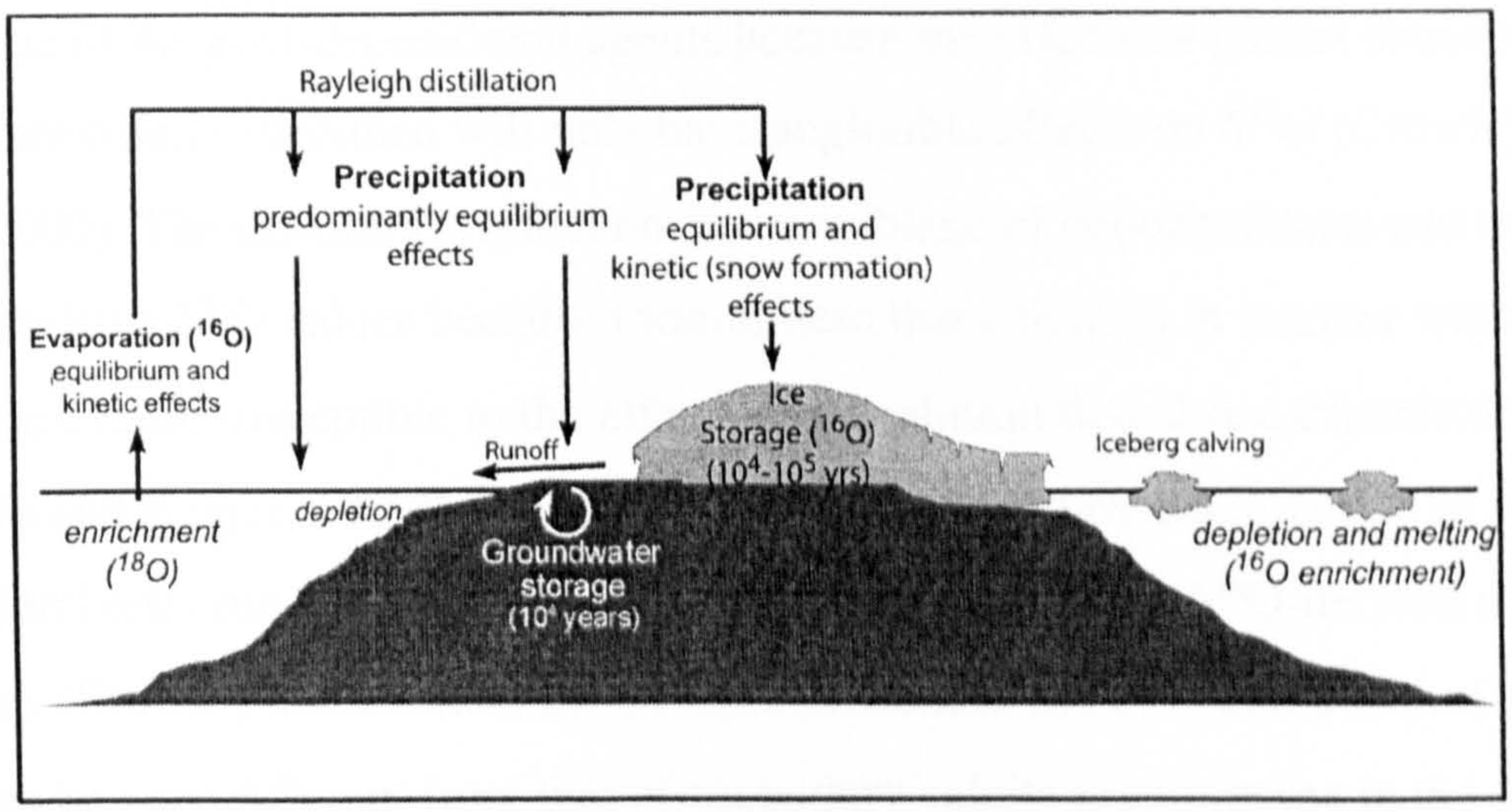

Figure 4.7. The influences of the hydrological cycle on oxygen isotopic ratios, modified from Rohling and Cooke (1999). The storage effects 'fix' ^{16}O and subsequently ^{18}O enrichment in the oceans. Italics describe the process effects on seawater isotopic compositions.

The result is that palaeosalinity (used to infer sea-level fluctuations) and palaeotemperature studies using fossil carbonate usually require a correction for the glacial/freshwater budget effect.

4.3.4.7 Depth habitat and seasonal calcification

Depth habitat and seasonal calcification may cause positive deviations from the surface water $\delta^{18}O$ equilibrium. More positive $\delta^{18}O$ values could be the result of calcification in deeper or seasonally cooler waters (Bouvier-Soumagnac and Duplessy,

1985; Deuser, 1987). Seasonal upwelling can also be responsible for a bias towards colder values because this process concentrates deep, cool $\delta^{18}O$ signatures at shallower depths (Sautter and Thunell, 1991; Kroon and Darling, 1995). Crowley and Zachos (2000) estimated the error associated with depth of calcification uncertainties as <0.4‰ (<2.0°C) $\delta^{18}O$.

4.3.5 Factors affecting isotopic composition of foraminiferal calcite specific to this study

In this study, the primary concern is the extent of post-depositional diagenetic alteration. This includes dissolution, secondary calcification and recrystallisation. Foraminiferal tests are often subject to mineral alteration mediated by mobile pore fluids. This alteration can affect the isotopic ratios that were initially incorporated in the test at the time of formation (Schrag *et al.*, 1995; Schrag, 1999). Dissolution is probably the least problematic of the post-depositional agents because the effects of partial dissolution on a single foraminiferal specimen will only have negligible effects on $\delta^{18}O$ (Crowley and Zachos, 2000). The dissolution effect on an assemblage of deposited tests can create a shift towards positive $\delta^{18}O$ values because foraminifera that calcified in warmer water (more Mg-rich) are more susceptible to the effects of dissolution than those deposited in cooler water (Wu and Berger, 1989). Recrystallisation and secondary calcification of foraminiferal tests may be a more substantial source of error for $\delta^{18}O$-derived tropical SST techniques (Crowley and Zachos, 2000). This is because the $\delta^{18}O$ composition of primary calcite can be very different from that of secondary calcite precipitating in the sediment (Killingley, 1983; Schrag *et al.*, 1995).

New research has recently raised doubts about the validity of planktonic foraminiferal stable isotope measurements in Cretaceous and Palaeogene samples (Norris and Wilson, 1998; Pearson *et al.*, 2001). The micrometer-scale alteration, discussed earlier in apparently 'well-preserved' assemblages, may create larger palaeotemperature errors than previously thought. Unfortunately, it is not yet possible to quantify the amount or timing of the diagenetic calcite added, or the degree of recrystallisation (Crowley and Zachos, 2000).

Seawater $\delta^{18}O$ variation is another possible source of error for this study. The mean $\delta_c^{18}O$ values (isotopic composition of foraminiferal test calcite) of the surface-dwelling planktonic foraminifera are not only dependent on the temperature, rate of calcification and

volumetric extent of glaciation, but principally on the $\delta_w{}^{18}O$ values (isotopic composition of seawater) (Zachos *et al.*, 1994; D'Hondt and Arthur, 1996). Glacial extent is especially relevant for the palaeotemperature calculations for the Middle Miocene samples, which were deposited at a time of more extensive glaciation than today (Savin *et al.*, 1985; Miller *et al.*, 1987; Hudson and Anderson, 1989). To compensate for the volume of ice sheets inferred to exist in the time intervals, a correction of –0.4 ‰ $\delta_w{}^{18}O$ was used for the sample data as a mean value for the Early and Middle Miocene (Lear *et al.*, 2000).

It could be argued that the depositional environment may be subject to freshwater input from coastal rivers distorting the isotopic signal towards lighter (warmer) values. There are a number of reasons why this is probably insignificant. Large rivers are absent from the current geographic setting. Kent *et al.*'s (1971) paleogeographic reconstruction suggests this was also the case for the Oligo-Miocene and estimate the palaeo-shoreline to be ~30 km further inland than at present. Modern planktonic foraminifera are open-ocean organisms, intolerant of low salinities, and are not found in abundance in shallow-shelf or coastal environments where a freshwater component is often present (Hemleben *et al.*, 1989). Tropical freshwater runoff has $\delta^{18}O$ values more similar to seawater than those from high latitudes, implying a larger freshwater input would be needed to substantially affect the marine $\delta^{18}O$ in the tropics than at high latitudes (Rohling and Cooke, 1999). If the salinity at the time of crystallisation was affected by a large freshwater component, one would not expect to find the fully diverse planktonic assemblages that have been described from the samples. Bush and Philander (1997) suggest normal marine salinity conditions off the east African coast are maintained by the Somali current transporting equatorial Indian Ocean water onto the shelf and are thought to have existed since the Cretaceous. Finally, hemipelagic clays are indicative of a relatively deep-water (>100 m) environment and are usually deposited in fully marine oceanic conditions.

4.3.6 Stable oxygen and carbon isotope results

The isotope results were used to calculate marine temperatures using the method outlined above. Appendix 4.2 lists all the taxa, isotopic values and calculated palaeotemperatures from the three Tanzanian samples in this study. The species with the most negative values are in bold and these are used to estimate the warmest SSTs. For biozone M1b (Early Miocene) isotopic values of *Globigerina gnaucki* were used to

calculate a SST of 30°C; for biozone M9 (Middle Miocene) *Globigerinoides ruber-subquadratus*, a SST of 27°C and for biozones M11-M12 (Middle Miocene) *Globigerina nepenthes*, a SST of 29°C. The benthic data allow the warmest bottom water temperatures to be calculated. For biozone M1b isotopic data from *Uvigerina* spp. were used to calculate a bottom water temperature of 21.3°C; for biozone M9 *Cibicidoides* spp., a bottom water temperature of 15°C and for biozones M11-M12 *Cibicidoides* spp., a bottom water temperature of 14.3°C.

It is well established that oxygen and carbon isotopic ratios are related to the temperature and depth of calcification (Urey, 1947; Emiliani, 1954). Figure 4.8A-C rank the different planktonic foraminifera species according to their carbon and oxygen ratios. Generally, those species that calcified in the surface waters tend to yield lighter (more negative) $\delta^{18}O$, and heavier (more positive) $\delta^{13}C$. The reverse is true for those species that calcified below the surface mixed layer. Therefore, the surface indicator morphospecies usually cluster in the top right corner of carbon vs. oxygen graphical plots. In this study, some of the morphospecies indicating the highest temperatures have relatively more negative $\delta^{13}C$ values, and cluster at the bottom. This is discussed further below.

Figure 4.9A-C illustrate the oxygen isotope data plotted as a function of latitude, of the Tanzanian samples, against a number of other (primarily DSDP/ODP) sites from the Atlantic, Pacific and Indian oceans for the equivalent time slices. Appendix 4.3 lists all the sites, species and oxygen isotope data used for this figure. The inferred meridional surface and thermocline temperature gradients have been calculated using all other data (excluding the Tanzanian data) by means of a 2nd order polynomial model. The other data in Figure 4.9A yield a maximum SST of 18°C. It is clear from the plot that the $\delta^{18}O$ values from Sample RAS99-42 are significantly more negative. Even the thermocline species from this sample have more negative $\delta^{18}O$ values (warmer) than the most negative surface dwelling morphospecies of any of the other sites. In fact, the bottom-water temperatures are warmer than a significant number of the deep-water planktonic temperatures from other sites presented in this figure. It should be noted that to obtain significant comparative data, the earliest timeslice has been extended to include the Early Miocene biozone M1a. The data from the youngest timeslice (Figure 4.9C) are insufficient to calculate temperature gradients.

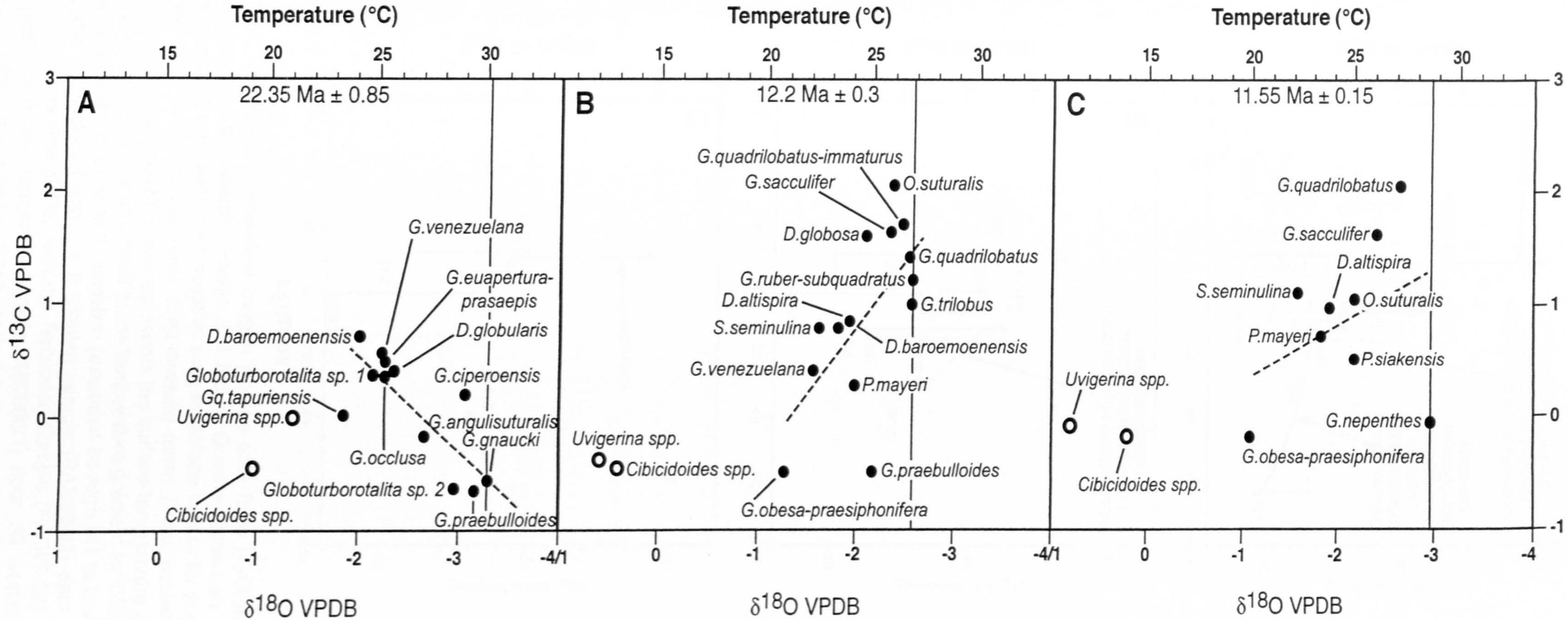

Figure 4.8A-C. Multi-species stable isotope array from the Tanzanian samples: A) Early Miocene (M1b) Sample RAS99-42, B) Middle Miocene (M9) Sample RAS99-38 and C) Middle Miocene (M11) Sample 180906/1. Solid black circles indicate planktonic foraminifera, while open circles indicate benthic foraminifera. The dashed black line is the best linear fit for the data spread, and the solid black line marks the maximum estimated palaeotemperature. All isotopic results are subject to a ±0.08‰ oxygen and a ±0.06‰ carbon isotopic analytical precision.

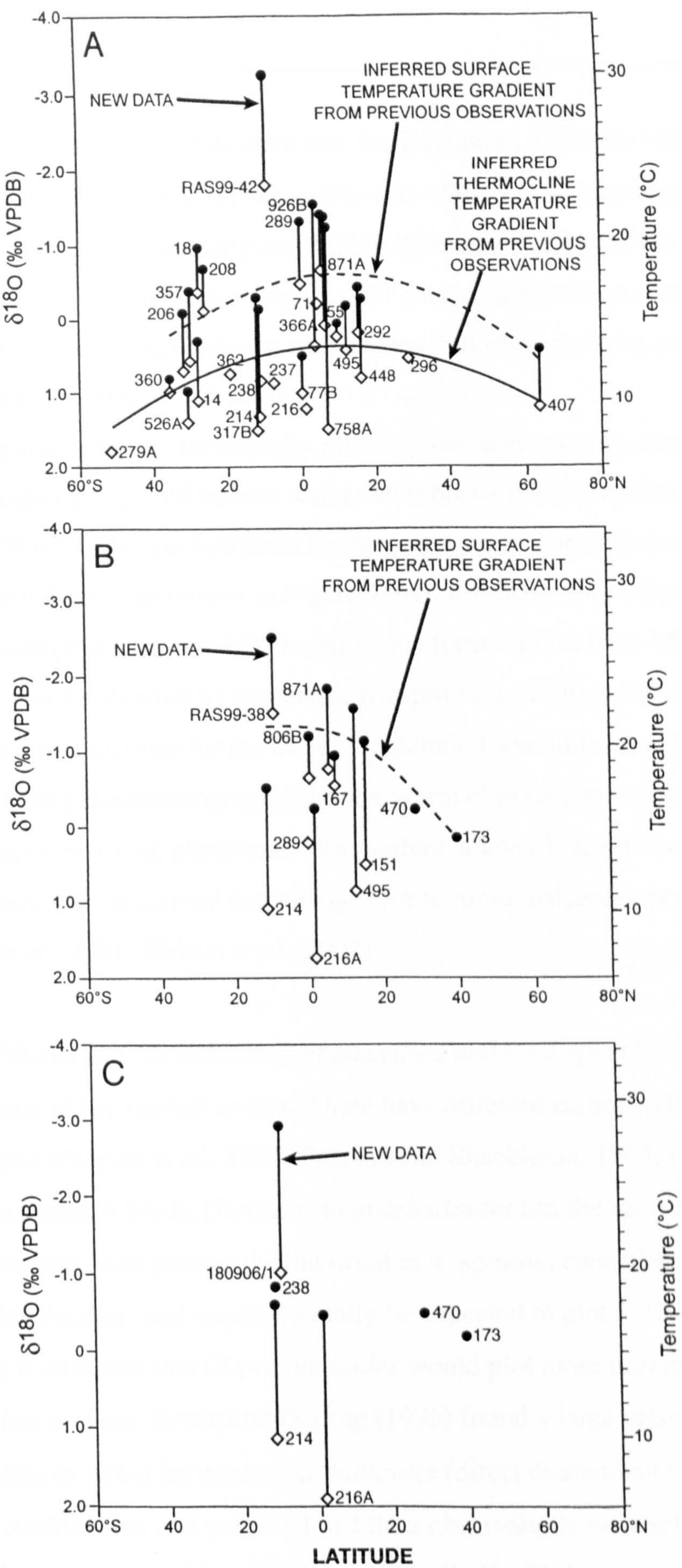

Figure 4.9A-C. Planktonic foraminifera oxygen isotope data from DSDP/ODP sites for three timeslices from the Atlantic, Pacific and Indian Oceans plotted as a function of latitude. Black circles represent most negative oxygen isotope values for surface-dwelling forms, while open diamonds represent deep-dwelling forms (most positive values). In Figure 8A, the upper polynomial curve represents the surface temperature gradient while the lower curve represents the sub-thermocline temperature gradient for DSDP/ODP data. A) Isotope data for the biozone M1b timeslice (extended through M1 to increase amount of comparable data) plotted with the Tanzanian sample (RAS99-42) data of equivalent time slice. B) M9 timeslice plotted with the Tanzanian Sample (RAS99-38) data. C) M11 timeslice plotted with the Tanzanian Sample (180906/1) data. All isotopic results are subject to a ±0.08‰ oxygen and a ±0.06‰ carbon isotopic analytical precision.

From Figure 4.9, it is evident that the Tanzanian $\delta^{18}O$ data values for the surface mixed layer (predominantly between –2‰ and –3‰) are substantially more negative than previously reported for the Early and Middle Miocene (Keller, 1985) and therefore suggest warmer SSTs (~10°C) for these intervals. Of course, some of the comparative data are collected from sites from cooler oceanic realms, but of all the data, none are comparable to the new data presented in this study.

The source of this incongruity probably lies with varying components of diagenetic calcite precipitated by cold bottom waters after burial that overprints the original isotopic signature (Plate 4.1 below compares the preservation of Tanzanian material with that used to calculate palaeotemperatures in Figure 4.9A). It follows that a significant proportion of the stable isotope data derived from planktonic foraminifera from Miocene carbonate-rich sediments may be affected by diagenetic overprinting. If this is the case, then it has considerable implications for the use of planktonic foraminiferal stable isotopes for the study of global palaeoceanography and long-term climate prediction. In fact, some investigators employing planktonic foraminifera acknowledge the importance of 'glassy', exceptionally well-preserved assemblages for accurate palaeotemperature reconstructions (Pearson *et al.*, 2001; Wilson *et al.*, 2002).

4.3.6.1 $\delta^{18}O$ and $\delta^{13}C$ as indicators of upwelling and vital effect?

Some of the species analysed here have different carbon values to those reported in other studies (Pearson *et al.*, 1993; Pearson and Shackleton, 1995; Pearson *et al.*, 1997a, 1997b). In Figure 4.8A-B, *Globigerina praebulloides* has the most negative $\delta^{13}C$ value. This species has been previously classified as a 'spinose, cancellate, intermediate-thermocline dweller' and would normally be expected to plot 1-2‰ lighter (Pearson, 1997b). It is expected that *G. praebulloides* would plot more proximally to its subspecies *Globigerina occlusa*. Kroon and Darling (1995) found a large offset towards lower $\delta^{13}C$ values (–2‰ to –3‰) for modern *G. bulloides* (direct descendant of *G. praebulloides*) from the Arabian Sea and proposed that their observations were related to upwelling zones (rich in ^{12}C) and ontogenetic growth rates. Similarly, *Globigerinella obesa-praesiphonifera* values (Figure 4.8A-B) are more negative than expected for species calcifying in an intermediate depth habitat. Although limited, the data in this study coupled with previously published data, may point towards a significant vital effect in *G. praebulloides* and *G. obesa-praesiphonifera*.

Figure 4.8A includes data for the taxonomically unassigned *Globoturborotalita* 'sp. 1' and 'sp. 2'. Interestingly, their oxygen and carbon isotope signatures are quite different. *Globoturborotalita sp.* 1 ($\delta^{18}O$ -2.13‰, $\delta^{13}C$ 0.38‰) is positioned close to the deeper taxa, while *Globoturborotalita* sp. 2 has lighter oxygen values ($\delta^{18}O$ -2.96‰, $\delta^{13}C$ -0.63‰) implying one of the warmest SSTs.

In the carbon versus oxygen plots (Figure 4.8A-C) a marked change in slope from the Early to Middle Miocene is evident. It is possible that this change in gradient (together with the species-specific isotopic discrepancies) may result from an anomalous oceanic structuring e.g., a change in upwelling. However, up-welled waters are usually much cooler than tropical surface waters (Kroon and Darling, 1995) and if this was a significant factor, one would expect to see more positive deviation in $\delta^{18}O$ values between the three timeslices.

4.3.6.2 Supporting evidence for palaeotemperature reconstructions

Oligocene to basal Miocene (biozone P19-M1) tropical SSTs have previously been determined from the Indian Ocean Site 758A, from which assemblages (preservation level defined as 'good to excellent') were used to reconstruct SSTs between 18-20°C (Van Eijden and Ganssen, 1995). Even assuming extensive icecaps in the Antarctic, the authors deemed these estimates to be unrealistically low. Furthermore, Kobashi *et al.* (2001) calculated SSTs from tropical shallow marine mollusc oxygen isotopes from the Mississippi Embayment (30°N), which gave mean annual temperatures of 23-24°C and summer temperatures of 29-31°C for the Early and Middle Miocene, both of which are significantly higher than previously published studies from this area. Despite difference in latitude, the temperatures are comparable.

The benthic isotope analyses presented in this chapter support the high SSTs measured in the planktonic foraminifera (Figure 4.8A-C). The benthic generic isotopes measured in this study reconstruct bottom temperatures of ~20°C for the Early Miocene and ~12-14°C for the Middle Miocene timeslices. Vincent *et al.* (1985) measured benthic oxygen isotopes from Miocene equatorial Indian Ocean DSDP sites 214, 216, 237 and 238. They used the benthic species *Oridorsalis umbonatus*, which yields $\delta^{18}O$ values close to the genus *Uvigerina*, as used in this study (Vincent *et al.*, 1985; Savin *et al.*, 1981). On average, for the four sites, this benthic $\delta^{18}O$ data is 3-3.5 ‰ heavier (more positive) than the Tanzanian values for the Early Miocene timeslice, and 2-2.5 ‰ heavier for the Middle

Miocene. This is equivalent to the offset in the planktonic isotope values. However, a smaller difference should be expected, due to the more dissolution-resistant benthic foraminiferal tests. These DSDP sites were positioned such that they would not be affected by warm shelf currents, of the type that may apply to the Tanzanian assemblages.

So how do these temperatures compare to the modern day? Modern Indian Ocean summer SSTs in the equatorial region (latitude: 20°N to 20°S) are between 26-30°C (Levitus and Boyer, 1994). It has also been proposed that modern tropical SSTs cannot exceed 30-32°C, i.e. those found today in the West Pacific Warm Pool (WPWP), due to the negative feedback processes of cloud shielding, oceanic circulation patterns and tropical seawater evaporation (Ramanathan and Collins, 1991). Although the palaeotemperatures calculated from the geographically isolated dataset presented in this chapter do not exceed these suggested temperature limits, it is unlikely that they record the highest SSTs in the Indian Ocean for the Early and Middle Miocene. This data does not invalidate the 'Thermostat hypothesis', although it is now more likely that it could be disproven.

4.3.7 Summary

Previous Oligo-Miocene SST estimates in the tropical southern Pacific and Indian oceans are ~20°C (Savin *et al.*, 1985; Van Eijden and Gannsen, 1995). Despite the errors associated with this palaeotemperature technique, the anomalously negative $\delta^{18}O$ data presented here were used to calculate comparable tropical Indian Ocean SST estimates ~10°C higher than documented before, i.e. equivalent to, or warmer than modern SSTs for the Early Miocene (~30°C) and Middle Miocene (~27-29°C). These results are consistent with modern measurements and estimates derived from analysis of mollusc shells. It is very unlikely that the three isolated samples represent the warmest Indian Ocean SSTs.

It is possible that fine-scale foraminiferal shell recrystallisation of the type that occurs in open ocean pelagic oozes and chalks at shallow burial depths has more influence on the stable isotopic values of foraminiferal shells than has previously been acknowledged. This data suggests that this diagenetic effect is equally applicable to the Neogene, as has been shown for the Cretaceous and Palaeogene foraminiferal isotope estimates (Norris and Wilson, 1998; Pearson *et al.*, 2001). The hemipelagic muds, from which these assemblages were derived, should be targeted for future stable isotopic

analysis of foraminifera in order to sample assemblages that have not been microscopically recrystallised. This should be accompanied by high magnification scanning electron microscopy to assess the degree of microscopic alteration.

4.4 Conclusions

This study presents isotopic analysis of the more primitive menardellid taxa (e.g. *Gr. praescitula*, *Gr. archeomenardii* and *Gr. praemenardii*). These taxa have been generally overlooked with respect to isotope ecological analysis (although some data are presented in Pearson and Shackleton, 1995). This may be partly due to *Gr. praescitula* and *Gr. archeomenardii* being small and particularly difficult to distinguish, with most specimens possessing a combination of the characters used to define the holotype specimens (see Plate 1.1, Chapter 1). The oxygen isotope data of *Gr. praescitula* together with results from genetic analyses and live culture observations support the development of the planktonic depth preference from benthic ancestors, therefore, the polyphyletic development of the planktonic mode. The Neogene *Globorotalia* are one example of this phenomenon; there may be others as yet not identified.

The oxygen isotope data support the idea that from a benthic habitat, *Gr. praescitula* developed a surface affinity (by biozone M5) synonymous with that of *Globigerinoides ruber*. This depth preference was then retained by its 'descendants', *Gr. archeomenardii,* and throughout the early history of *Gr. praemenardii*. The later part of the oxygen isotope trend of *Gr. praemenardii* (in biozone M9) with a positive shift of 1.5 per mil, may be associated with a return to a deep habitat. The Site 871 material is certainly well preserved and no obvious differential diagenesis marked the specimens through the Early to Middle Miocene interval analysed. Thus it is reasonable to discard heterogeneous alteration as a possible cause for the large shifts. On the other hand, the changes in $\delta^{18}O$ could be documenting different genetic species, however, no obvious morphological distinction could be made. It is not possible to rule this out as a cause for this phenomenon, although it is impossible to test.

Despite earlier fluctuations, by the Late Miocene the globorotaliid taxa analysed here appear to have stabilised into an intermediate to deep-water preference. The general intermediate to deep-water habitat of the Recent (Shackleton and Vincent, 1978) and the fossil globorotaliids (Keller *et al.*, 1985; Norris *et al.*, 1993; Pearson and Shackleton, 1995)

is supported by the data presented in this study. Some of the individual morphospecies belonging to the menardellid lineage (*Gr. menardii* 'A' and 'B', *Gr. cultrata, Gr. multicamerata, Gr. limbata,* and *Gr. pseudomiocenica*) have either been overlooked or rarely included in previously isolated for isotopic analysis, therefore this study presents new isotopic data that aid the comprehension of the ecology of extinct planktonic foraminifera. From these Late Miocene taxa, *Gr. tumida* and *Gr. menardii* probably represent the deepest dwellers, although it is reasonable to assume that like the observations of modern *Gr. menardii* (see Hemleben *et al.*, 1989), some of these morphospecies may migrate to shallower photic depths seasonally.

In addition, this chapter presents a case study that evaluates Miocene ocean temperatures that the Neogene globorotaliids were subjected to, using the planktonic foraminiferal assemblages themselves. Here, isotopic analyses of well-preserved foraminiferal shells are used to calculate sea-surface and bottom temperatures of the Indian Ocean in the Early and Middle Miocene. The temperatures calculated from these well preserved assemblages are ~10°C higher than any other published estimates from other assemblages of Early and Middle Miocene age. It is reasonable to assume that these estimates are the result of the exceptional shell preservation associated with impermeable hemipelagic clays. This has significant implications for all palaeothermometry using planktonic foraminifera, i.e. future studies should target this kind of lithology and assemblage preservation to yield accurate estimates.

The distribution and development of planktonic foraminifera is undoubtedly dictated by a complex set of variables, one of which is oceanic temperature. Utilising modern analytical techniques this chapter has shown how it is possible to use planktonic foraminifera themselves to obtain detailed information about the past oceans in which they resided.

Chapter 5

Eigenshape morphometric analysis of multiple Neogene *Globorotalia* lineages from the tropical Indo-Pacific, Pacific and Atlantic oceanic realms.

5.1 Introduction to morphometrics and eigenshape analysis

Darwin was among the first to formally describe the processes of evolution, whereby one biological species can give rise to, or evolve into, another over long periods of geological time (Darwin, 1859). From this work came the original assumption that morphology can yield information about phylogeny, a tenet that phenetics, systematics and morphometrics were founded upon.

The field of morphometrics attempts to quantitatively measure morphological homology to test phylogenetic connection hypotheses. Bookstein (1991) states "the objects of morphometric study are not the forms themselves, but rather the associations, causes and effects". It is not the intricacies of form that are important, but what they tell us about shape similarity between a number of independent objects. Not only are morphometrics and phylogenetics intimately connected, but according to MacLeod and Forey (2002) without some form of description and quantification of morphological change between individuals, populations, species and higher taxa, phylogenetic analysis is *impossible*. This statement is indefensible because the vast majority of phylogenetic analyses were at some point based on qualitative data. Nevertheless, adding quantitative objectivity to phylogenetic analysis is highly valuable.

Phylogeny has long been a fiercely debated subject within the disciplines of palaeontology, biology and zoology, so when using one or more morphometric techniques it is necessary to carefully define what questions we are attempting to answer. Arguably, the most widely used and informative tool for assessing phylogenetic association is the eye-brain system. Micropalaeontologists have long used this system to assess morphological similarity and difference, to deduce phylogeny in planktonic foraminifera. However, it is all very well suggesting phylogenetic hypotheses through use of this

inherently qualitative and subjective method, but it is something else to support these hypotheses with quantitative morphometric data. One thing is certain, with the advent of affordable computing hardware and imaging software the potential of quantitative analysis of taxonomic morphologies has advanced by several orders of magnitude since the days of hand-held calipers and scales. However, has this capability increased our ability to determine phylogeny? With a plethora of different statistical techniques to use, do we have a clearer, or even a *different* idea of phylogeny in the taxa we study?

All morphometric methodologies involve aspects of point-to-point matching (landmark-based analyses), and curve-to-curve matching (outline-based analyses). Some are more useful than others for specific problems, which is dependent on the nature of the objects and hypotheses under analysis. This basic division alone has created a polarisation within the morphometrics community (Rohlf and Bookstein, 1990; Marcus *et al.*, 1993, 1996 and references therein). Historically, this community has been divided into two distinct schools of thought: those who advocate only landmark-based methods (Blackith and Reyment, 1971; Pimentel, 1979; Neff and Marcus, 1980; Reyment *et al.*, 1984; Reyment, 1991) and those who favour outline-based methods (Clark, 1981; Ferson *et al.*, 1985). When both methods are discussed, there is usually some rhetorical promotion for one of the 'rival' factions, often in reference to a preferred analytical method (e.g., Bookstein *et al.*, 1982; Ehrlich *et al.*, 1983; Read and Lestrel, 1986; Zelditch *et al.*, 1995; Lestrel, 1997). This can cause confusion for readers and research may be channelled along set analytical paths, sometimes at the expense of the work itself (MacLeod and Rose, 1993; MacLeod, 1999). Some of the techniques are discussed here, and one specific technique is used to collect morphometric data because it is most suited to the task in question, however, the author does not intend to discredit the utility of any of the other techniques.

As in many areas of science, combining techniques and developing composite methods often constitute the strongest and most comprehensive analytical tools. Extended eigenshape analysis (MacLeod and Rose, 1993; MacLeod, 1999) bridges the gap between the two factions by combining the information content of outlines (standard eigenshape analysis) with that of landmarks, to compare the covariances of form. Both eigenshape methods have been employed previously to measure shape variation in planktonic foraminifera (Lohmann, 1983; Lohmann and Malmgren, 1983; Malmgren *et al.*, 1983; Lohmann and Scweitzer, 1990; Kucera and Malmgren, 1996; Norris *et al.*, 1996).

There have been no previous morphometric analyses including both the menardellid and *Globorotalia s.s.* lineages, so the intention here is to contribute to alternative hypotheses of phylogeny with a quantitative basis. In addition, this study could help in identifying synonyms (see Chapter 1 for discussion of the taxonomic controversies). Of course, a morphometric study only captures a subset of the real morphological variability among taxa, and for example, if eigenshape analysis fails to distinguish two taxa, it does not necessarily follow that they are identical.

5.1.1 Objectives

Extended eigenshape analysis produces results that suggest relative phenetic distances, i.e. how similar shapes are and therefore how closely related the taxa that possess those shapes may be. It cannot directly address questions of ancestry. Any questions related to ancestry of the globorotaliid lineages will be addressed in Chapter 6 using other quantitative phenetic methods. Here extended eigenshape analysis is employed to answer the following:

1) Are *Gr. praescitula* and *Gr. archeomenardii* distinct morphospecies?
1) Are *Gr. limbata* and *Gr. pseudomiocenica* synonyms describing the same form?
1) Is *Gr. pseudomiocenica* morphologically similar to *Gr. miocenica*?
1) Is *Gr. multicamerata* more morphologically similar to *Gr. menardii* or *Gr. limbata*?
1) Is *Gr. multicamerata* morphologically similar to *Gr. pertenuis-exilis*?
1) Are *Gr. pertenuis* and *Gr. exilis* distinct morphospecies?
1) Are *Gr. menardii* 'A', 'B', *cultrata* and *fimbriata* distinct morphospecies?
1) Are *Gr. merotumida* and *Gr. plesiotumida* distinct morphospecies and are they closely allied in shape to *Gr. tumida*?

5.2 Why eigenshape analysis?

There are a number of different morphometric analysis methods available to the investigator, the majority of which work on the same principle, i.e. the representation of a large number of empirical variables, by the smallest number of derived variables. There are

some subtle differences between the methods, as discussed below; the role of which is to explain why eigenshape analysis is the most suitable technique to answer the questions outlined above.

5.2.1 Principal component analysis (PCA), factor analysis and canonical variate analysis (CVA)

PCA and CVA analysis methods are based on the singular value decomposition (SVD) of an appropriate matrix, and attempt to reduce the dimensionality of the data from the original p variables, to a smaller number (k) of derived variables that represent the original data sufficiently (NAG Ltd, 2001). For example, if we have a dataset with p variables ($x_1, x_2, \ldots x_p$) defining n objects (=individuals), these variable-directed multivariate methods examine the relationship among p variables in order to reduce the dimensionality of the problem. The primary distinction among these methods is that PCA and factor analysis concentrate on the relationships among all the variables, while CVA examines the between-group structure, if the individuals are grouped.

CVA can be regarded as a generalisation of component analysis because it treats >2 samples simultaneously. It is also "a generalisation of the construction of generalised distance charts, in which the underlying axes of variation are first constructed, then used to plot the positions of the various groups" (Blackith and Reyment, 1971). In CVA we have k samples, each drawn from a universe (in which the dispersion matrices must be homologous). Each of the universes constructs a cluster of points in a p-variate Cartesian space, which are elliptical if the variables are multivariate normally distributed (Blackith and Reyment, 1971.) In CVA, the individuals (n) can be organised into (g) groups, then total variation can be regarded as the combination of between-group and within-group variation. To maximise the between-group variation to the within-group variation, suitable discrimination between groups must be allowed. CVA determines the linear combinations of the p (canonical variates) variables, which maximise this ratio (NAG Ltd, 2001). CVA extracts from the covariance matrix linear combinations of measured variables that optimise between-group relative to within-group variation, while in PCA, the variance of the scores is optimised (Zelditch *et al.*, 1995).

PCA discovers new variables, which are linear combinations of the p empirical variables so that they have maximum variation and are orthogonal (uncorrelated), in CVA

the variables are not orthogonal. The first principal component is the linear combination of the variables that display the greatest amount of variance (as in eigenshape analysis) (NAG Ltd, 2001). A feature PCA shares with some of the other methods is that the original variables are usually represented by $k<p$ principal components, i.e. k principal components reflects a high proportion of the variance of the original p variables (NAG Ltd, 2001).

5.2.2 Geometric shape (factor) analysis

The role of factor analysis is to represent the covariances in the p variables (e.g. dimensional measurements of size, angularity, coiling and chamber number) in terms of $k<p$ hypothetical factors (variables), $f_1, f_2, \ldots f_k$, and the variances are accounted for by unique components in addition to the factors (Blackith and Reyment, 1971). These factors are assumed to have unit variance and to be independent. Lohmann (1983) regards these factors or 'descriptors of shape', to be as complex as the shapes they describe, and implies that some of the variables are always redundant, because they reflect different aspects of changes in the same morphological feature. These can be removed by multivariate data reduction techniques, but the investigator must choose which variables to measure at the beginning.

5.2.3 Fourier shape analysis

This is an outline-based method that concentrates on the object silhouette, by use of the amplitude terms in a Fourier transform of the boundary coordinates that define its outline as shape descriptors (e.g. Yonker and Ehrlich, 1977; Anstey and Pachut, 1980; Cranfield and Anstey, 1981, Crampton and Maxwell, 2000). For reasons discussed below, this method is better suited to sand-grain morphology and similar problems, than the complexity of foraminiferal outlines (Lohmann, 1983).

5.2.4 Thin-plate spline analysis (TPS)

Zelditch *et al.* (1995) describe this method as "a way to obtain shape variables that have location on the form and to ensure that the homology of anatomical parts provides the common basis for comparisons". In this method shape change is first decomposed into

uniform and non-uniform components, the latter is then further decomposed into geometrically independent components (becoming progressively more localised) which each describe shape change on a smaller spatial scale (Zelditch *et al.*, 1995). These non-uniform components are known as principal warps. Using TPS analysis, an investigator is interpreting the eigenvectors of the bending-energy matrix as a collection of potential descriptors of deformation, i.e. a function of the spacing and the location of landmarks of a form (Bookstein, 1991; Zelditch *et al.*, 1995). The principal warps depend only on the 'mean' form (starting form) and all other forms within a data set are then compared to this mean form (Bookstein, 1991). Partial warps are then calculated by multiplying the principal warps (eigenvectors) of an individual's data (final form landmark positions). Where principal warp vectors give the geometric terms within which shape differences can be described, partial warps describe realised changes in those geometric terms (Fink and Zelditch, 1995; Zelditch *et al.*, 1995). The decomposition of the partial warps are then used to locate characters that can be exposed to the tests of homology that are applied to all other characters e.g., conjunction, similarity and congruence.

MacLeod (2002) tested partial warp analyses and concluded that they do not perform well in either simulated or actual phylogenetic systematic analyses because they have "an inherent instability and lack of adequate spatial localisation".

5.2.5 Landmarks and homology

In reality any biological or palaeontological object has no true corners, edges or vertices. No objects are truly two-dimensional and all objects are rounded on a particular scale. However, it is convenient for us to model observed outlines by reconstruction with seams or apices (Bookstein, 1978). Corners or vertices of a modelled object outline represent points that are associated perceptually or naturally with a biological form; these 'special points' are known as landmarks.

Landmarks are assumed to be homologous, i.e. "fully comparable in their histological and topological characteristics, from specimen to specimen" (Bookstein, 1978; Bookstein, 1991). Bookstein further subdivided landmarks as anatomical or extremal. Anatomical landmarks are defined by some biological differentia e.g., cranial sutures, incisor cusps, etc. Extremal landmarks are inferred from the geometry as opposed to the biology of the situation, i.e. points corresponding to high curvature, near-corners or

structure tips that can be described without use of a Cartesian coordinate system, or characterisations involving distance from previously well-defined landmarks. An example of a landmark that is both anatomical and extremal was used to start the outline sequencing in the globorotaliid study (see Figure 5.6). The sequencing commenced from the proloculus (anatomical landmark), which is equivalent to the point of highest curvature on the spiral side of the test (extremal landmark). Bookstein (1978, 1991) considered landmarks most informative when they correspond to corners or points of high curvature (i.e. extremal). Landmarks are limited by the inability to define the form of any surface or edge; they simply supply fixed reference points upon it. To define form we require an adequate sample of regular points upon a surface where we reconstruct the continuum in between, i.e. a digitised coordinated outline (Bookstein, 1978).

The relation between outlines, landmarks and biological homology is a complex one, fraught with misunderstanding and misrepresentation. Some confusion stems from the term homology having contrasting semantics, depending on the disciplinary context within which it is used. Smith (1994) describes homology as a theory that "marks the recognition that a character in one taxon represents 'the same' feature as a similar, but often not-identical, structure in another taxon". That is, characters are considered 'similar' because they are inherited from a common ancestor.

In a morphometric context, homology refers to the selection of landmarks defined from a number of objects, that are thought to be biologically/morphologically comparable. Smith (1994) considers landmark-based techniques and methods that quantitatively describe form, as only applicable to easily homologised structures. Zelditch *et al.* (1995) suggested that in morphometrics, the term homologous should be replaced by 'corresponding' or 'comparable', when referring to landmarks.

Zelditch *et al.* (1995) also used this concept of homology to discount outline-based morphometric methods. They declared that "[currently available] outline-based methods do not ensure that corresponding points on the outlines are properly matched", i.e. such methods fail to include information about biological homology, and as a result fail to distinguish among fundamentally different object classes (Figure 5.1A). These authors deem fourier and eigenshape analysis unsuited to phylogenetic systematics on principle, and suggest the use of the landmark-based morphometrics method, thin-plate spline (TPS). Further, Zelditch *et al.* (1995) suggest that some methods for analysing landmark data fail to restrict comparisons to phylogenetically comparable parts of an organism.

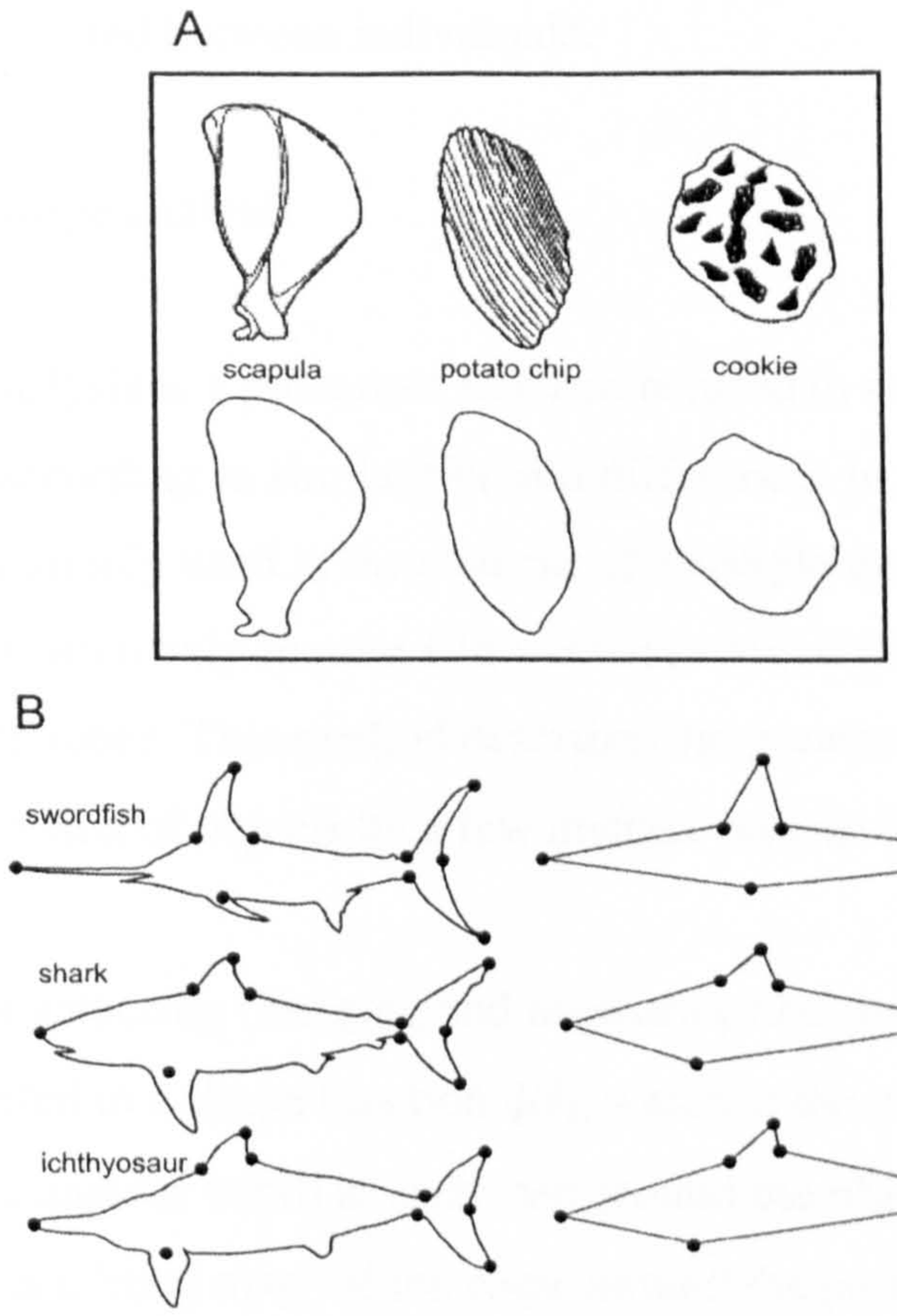

Figure 5.1. The relationship between outlines, landmarks and biological homology, adapted from (A) Zelditch *et al.* (1995), and (B) Riedel and Jeffries, 1978. In A, Zelditch *et al.* used the shapes of a scapula, potato chip and a cookie to discount outline-based morphometrics by stating that such methods do not include information about biological homology, and therefore fail to distinguish among fundamentally different object classes. MacLeod (1999) argues that this reasoning is not valid if outline sequencing commences at a biologically corresponding point (i.e. a landmark). An example of how landmark-based morphological sampling protocols do not automatically give consistent object-class distinctions, is shown in B. The landmark constellations are valid representations of the swordfish, shark and ichthyosaur body forms, but the landmarks are not biologically homologous.

MacLeod (1999) argued that if outline sequencing commences at a biologically corresponding point (i.e. a landmark, as in eigenshape analysis), object class difference is obvious. Figure 5.1B is an example of how landmark-based morphological sampling protocols do not automatically give consistent object-class distinctions. The landmark constellations in this figure are valid representations of the swordfish, shark and ichthyosaur body forms that could be used in many biological contexts (e.g. functional morphology) for which a morphometric approach would be useful. However, the landmarks are not biologically homologous. If landmark-based morphometric methods can be used to test biological hypotheses, when homology data is unavailable, then outline-based methods should not be dismissed (MacLeod, 1999). Furthermore, the landmarks

used in this study to describe foraminifera (i.e. proloculus, keel, chamber apices, *etc.*) are easily identified and located between individuals.

5.2.6 Standard eigenshape analysis

Eigenshape analysis is a procedure that can be used to arrange objects such as microfossil outlines according to similarities and differences in shape (Lohmann, 1983). This procedure is commonly used in the analysis of multiple dimensions of an object, although microfossils often only require a few independent dimensions to account for the majority of shape difference. This method describes the greatest amount of morphological variation from a collection of objects by a few distinct principal morphologies (Malmgren *et al.*, 1983).

Once the data gathering (imaging and measuring) has been achieved the shapes in the matrix are converted to a shape function $\phi(l)$, which is the net angular change in direction (cumulative angular bend) at each step around the object's edge (see Figure 5.2). It can be thought of as a 'road map' of the route around the perimeter (Lohmann, 1983). The $\phi(l)$ function is then converted to the $\phi*(l)$ function, this is the "normalised net angular change in the direction ϕ at each step around the perimeter (l) of the foraminifera shell" (Zahn and Roskies, 1972). This shape function $\phi*(l)$ equates to the closed outline of the microfossil in question. $\phi(l)$ (Figure 5.2b) is normalised to $\phi*(l)$ (Figure 5.2c) by removing a circle of suitable size from the 'road map'. $\phi*(l)$ is a representation of how a shape differs from a circle excluding size with the same start and ending points (Zahn and Roskies, 1972). It contains all the necessary information to reconstruct the shape of a microfossil exactly. Bookstein's (1978) tangent angle function is a similar to Zahn and Roskies' (1972) function, both of which form identical shape reproductions of an objects periphery at close sampling intervals.

In contrast, radial fourier analysis uses the polar coordinate shape function $r(\theta)$ to represent an outline, where r is the length of a radius vector from the shape centre to the edge and θ is the rotation angle of the radius vector. Zahn and Roskies (1972) argued that the function $\phi(l)$ is preferable over the polar coordinate shape function, because it is always a single-valued continuous function unaffected by outline complexity, and its derivation does not need choosing or any manual centroid determination. The latter characteristic

applies itself well to microfossils, which rarely have centres located at the centroid (Zahn and Roskies, 1972; Lohmann and Schweitzer, 1990a; Lohmann, 1983).

A whole suite of shapes could actually be represented by a standardised shape function such as $\phi*(l)$; each individual only differing in amplitude of its $\phi*(l)$. Subsequently, the amplitude of $\phi*(l)$ is standardised to a unit variance as the result of calculating correlations between shapes (Lohmann, 1983). If required, all amplitude and size information needs to be accounted for separately from the analysis itself, as explained in the Section 5.3.

In order to compare the different shapes in the data matrix certain points on one shape must be matched with the equivalent (morphologically comparable) points on the other shapes. These *landmarks* (Bookstein, 1978) are used to homologise the matrix. In standard eigenshape analysis the digitisation of an objects outline is initiated at a common landmark point (somewhere on the periphery) and this is used to align the outlines in the matrix (Lohmann, 1983; Lohmann and Schweitzer 1990b). The shapes are homologised by mutually rotating the $\phi*(l)$ (phi) functions until maximum correlation is achieved. This requires the selection of one reference shape as representative of the matrix, while the other shapes are rotated with respect to it. All outlines must be defined by the same number of equal-length segments before calculating the phi functions, in order to avoid erroneous results.

Using standard eigenshape analysis, after the transformation of the outlines into the phi functions, the singular value decomposition (Lohmann, 1983; Jöreskog *et al.*, 1976) is used to derive linear combinations of the functions that account the majority of the variance, from the matrix of correlations of all the variables (functions or shape functions). The correlation (or covariance) of each of the eigenfunctions compared to each of the original functions is then calculated. The greatest amount of empirical morphological variation is represented by the fewest independent axes (correlation to eigenshapes). With a foraminiferal matrix, the shapes in question typically show varying but strong degrees of similarity, so most of the observed morphological shape variation can be summarised by linear combinations of a small number of uncorrelated shape functions (Lohmann, 1983).

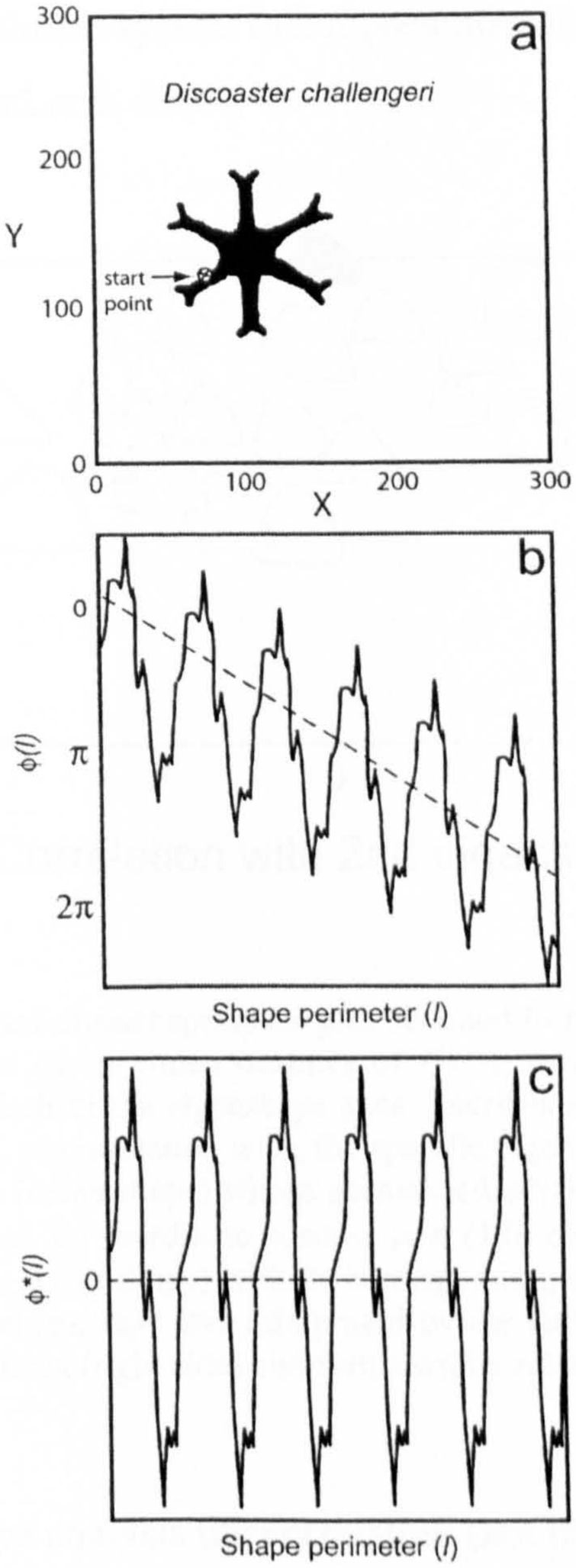

Figure 5.2. Description of the nannofossil species *Discoaster challengeri* using Zahn and Roskies' $\phi(l)$ and $\phi^*(l)$ shape functions. 3a, from the start point the fossil was defined by coordinates in a clockwise manner back round to the start point. 3b, the function $\phi(l)$ is the net angular change in direction (cumulative angular bend) at each defined point around the periphery. 3c is the function $\phi^*(l)$ derived from $\phi(l)$ by removing a circle of appropriate size (the dashed 2π ramp in Figure 5.2b). Both functions are single-valued and continuous even for objects with embayments and re-entrants. Adapted from Lohmann (1983).

The analysis produces (1) a suite of eigenvalues for each principal component of shape variation ('vector lengths that are proportional to the amount of observed interspecimen variance represented by each axis'); (2) equations for the eigenshape axes ('hierarchically ordered latent shape trends that account for the principal modes of shape variation within sample'); and (3) eigenscores (correlations or covariances between the observed shapes and the eigenshape functions) (MacLeod, 1999). The scores are used to place each specimen outline relative to the others in the analysis, in "shape space", i.e. "a

new, variance-optimised coordinate system that represents a linear decomposition of the sample" (e.g. Figure 5.3) (MacLeod, 1999).

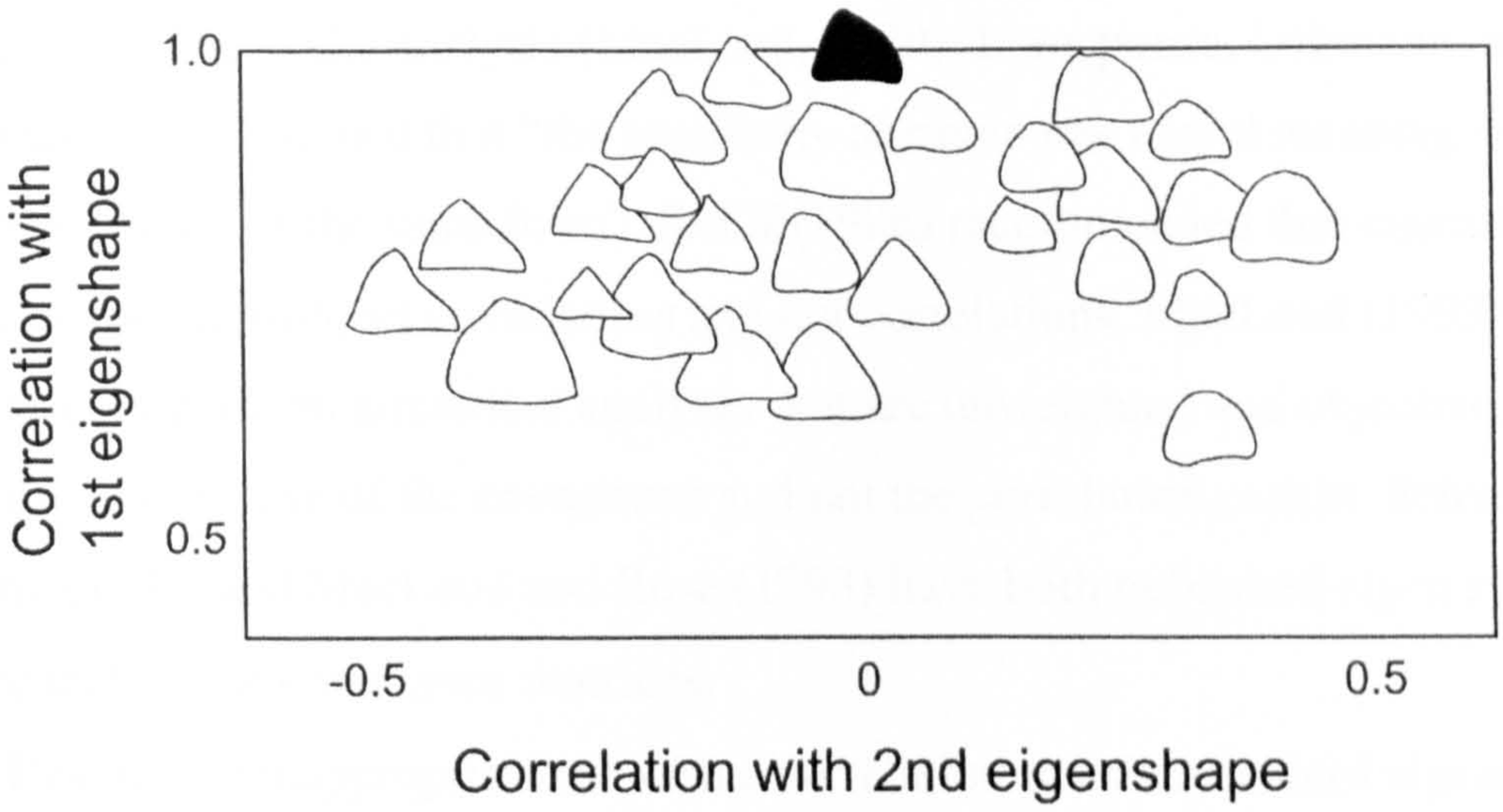

Figure 5.3. An example of a standard eigenshape space plot obtained from a singular value decomposition of the inter-object correlation matrix of specimen outlines of *Gr. truncatulinoides* from the same sample (adapted from Lohmann, 1983). Each of the eigenshape axes describes a continuous range of morphologies each differing by the amplitude of, or correlation with, the specific eigenfunction. The black specimen at the top represents the first eigenshape (mean shape) whose normalised $\phi^*(l)$ shape function is the series of first R-mode principal component scores. Its coordinate position is at (1,0) on an ES-1 vs. ES-2 plot because any along-axis eigenshape model (e.g., mean shape) with its corresponding eigenfunction (ES-1) will always be 1.0. In this example, the second eigenshape was interpreted by the authors as attributable to the variation between forms with an open umbilicus (right side) and forms with a relatively more closed umbilicus (on the left).

In standard eigenshape analysis the correlation (not the covariance) matrix is used as a basis for the singular value decomposition (Lohmann, 1983). The correlation matrix operates between –1 and +1 on both the *x* and the *y* axes, therefore a correlation value of +1 on the *x* axis, correlates exactly with the *x* axis variable (e.g., correlation with eigenfunction 1) while a correlation of –1 on the *y* axis negatively correlates with the *y* axis variable (e.g., correlation with eigenfunction 2). For example, in Figure 5.3 the black shape represents the morphology of the first eigenshape, i.e. the shape that describes the most variation in the sample (the mean shape). Thus the correlation of any along-axis eigenshape model with its specific eigenshape must be 1.0. MacLeod (1999) argued that a more 'intuitively satisfying' way of reflecting the mean shape within eigenshape space is to calculate "the mean of all corresponding terms within the set of shape functions comprising the sample", i.e. the mean ES-1 score.

The use of the correlation matrix has been criticised by Rohlf (1986) because standardising the $\phi*$ shape functions removes an element of the empirical shape variability

for each object, which equates to normalising the object annularity (Lohmann, 1983; Lohmann and Schweitzer, 1990a). This apparent normalisation can result in morphologically distinct shapes appearing as similar. Use of the correlation matrix attaches artificial weighting to the analysis (MacLeod, 1999). In response, Lohmann and Schweitzer (1990a) argued that "the angularity attribute has useful meaning only when comparing objects of the same form". Rohlf (1986) recommended that eigenshape analysis be done on the inter-object covariances and not correlations. MacLeod (1999) stated that it is important to perform numerical analyses that are unweighted and objective, as exemplified by the use of the covariance and not the correlation matrix. Schweitzer and Lohmann (1990) and MacLeod and Rose (1993) have both published eigen studies using software that utilise covariance matrices.

Despite the inappropriate use of the correlation matrix, standard eigenshape analysis is a powerful tool that can be used to determine a series of shape trends from empirical observation and specify latent shape spaces from which inter-object relationships can be shown. It can also be used to create idealised shape models easily displayed in graphical form and communicated in an intuitively comprehensive manner (MacLeod, 1999).

The mathematics behind standard eigenshape analysis is very similar to that of *R*-mode principal component analysis (Lohmann, 1983). Z is the matrix of homologised $\phi*(l)$ shape functions,

$$Z=US^{1/2}V'$$

where V' is the transposed matrix of unit eigenvectors associated with the eigenvalues of $Z'Z$. S is the diagonal matrix of eigenvalues of $Z'Z$ and U is the matrix of eigenvectors of ZZ' (Golub and Reinsch, 1970). U and V must both contain the same number of eigenvectors because $Z'Z$ and ZZ' have the same number of identical positive eigenvalues (Pielou, 1969).

If the shape functions in the data matrix Z are all normalised to unit variance and zero mean, then $Z'Z$ gives the matrix of correlations between the original shapes. The eigenvalues and eigenvectors of the correlations between the distinct $\phi*(l)$ shape functions define the minimum number of orthogonal shape functions needed to describe the empirical shapes (Lohmann, 1983). The eigenshape functions in U are these empirical

orthogonal shape functions and can be calculated directly from ZZ' or as R-mode principal component scores (Cooley and Lohnes, 1971):

$$U=ZVS^{-1/2}$$

These R-mode principal component scores are the *"standardised amplitudes* (standardised to unit variance) of the eigenvectors at each point around a otherwise shapeless form, i.e., a circle" (Lohmann, 1983). They represent an eigenshape in exactly the same way standardised $\phi*(l)$ functions describe observed shapes. The elements in V are the correlations between the observed shapes and the eigenshapes, when scaled by their specific eigenvalues to R-mode principal component loadings (Lohmann, 1983):

$$Z'U = VS^{1/2}$$

5.2.6 Extended eigenshape (landmark registered) analysis

The problem inherent within standard eigenshape analysis is that of interobject correspondence. This method uses only a single landmark point (the starting position) and assumes a geometric correspondence between points in the shape function sequence. The overall effect of this shortfall is to 'smear' the shape variation over a greater region of the object outline than if the relative points were more stringently tied to the biological implications of specific structures (MacLeod, 1999).

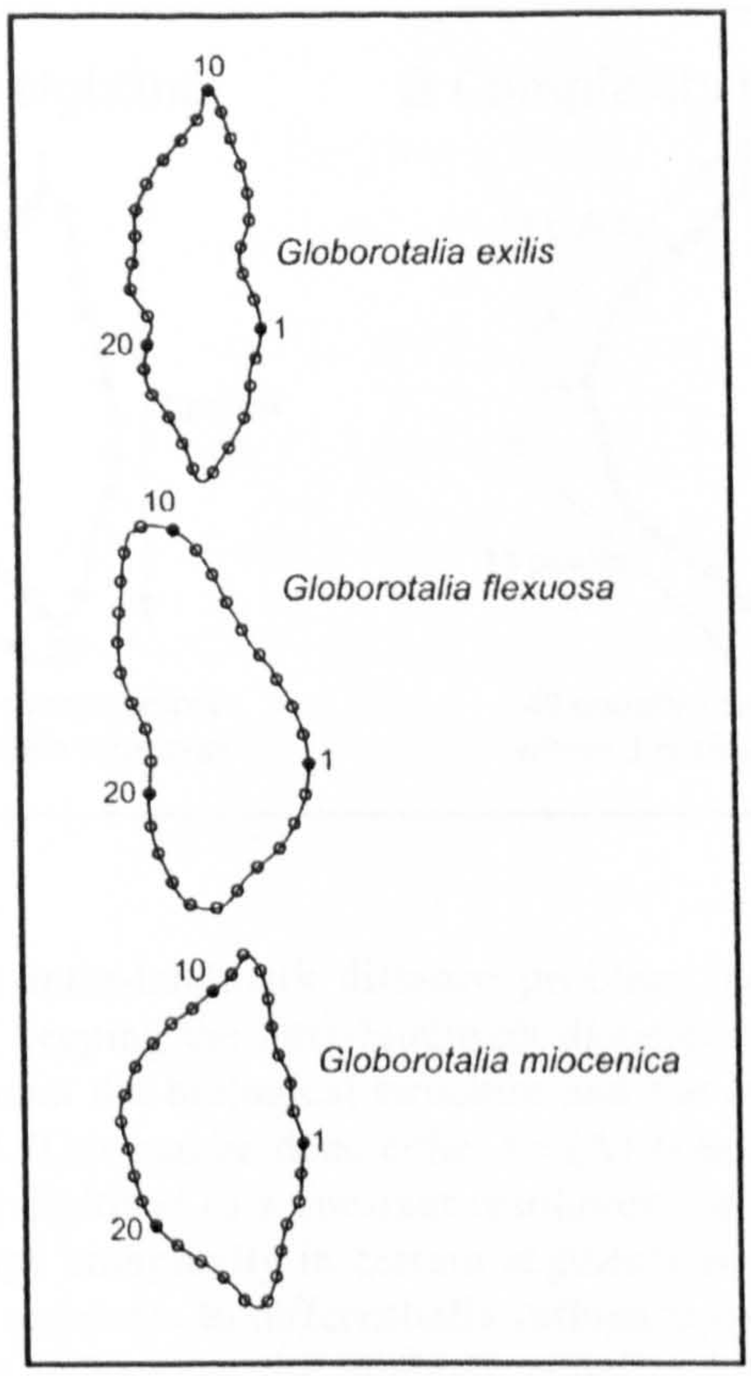

Figure 5.4. The problem with the standard eigenshape morphometric method. Because this method uses only a single outline landmark point (the starting point) to define the periphery of an object, objects that are strongly divergent in morphology can be represented by different points within the boundary outline sequence. This example of Neogene globorotaliids shows the 30 points used to define the outlines fall in quite different locations with respect to the foraminiferal tests. The standard eigenshape algorithm was designed to assume a geometric correspondence between points in the shape function sequence, wherein lies the problem. This correspondence is not reflected in the outline point distribution relative to the underlying biological structure. The outline points need to be more closely tied to the underlying biological implications of structures between objects to avoid 'smearing' the shape variation within a group of objects.

Manually located landmark points are used with extended eigenshape analysis to 'force' the object peripheral coordinates into alignment, and therefore the degree of extrinsic shape variation produced by mismatch can be reduced. Additional landmarks are positioned on the periphery to constrain the sequencing of the outline coordinate points.

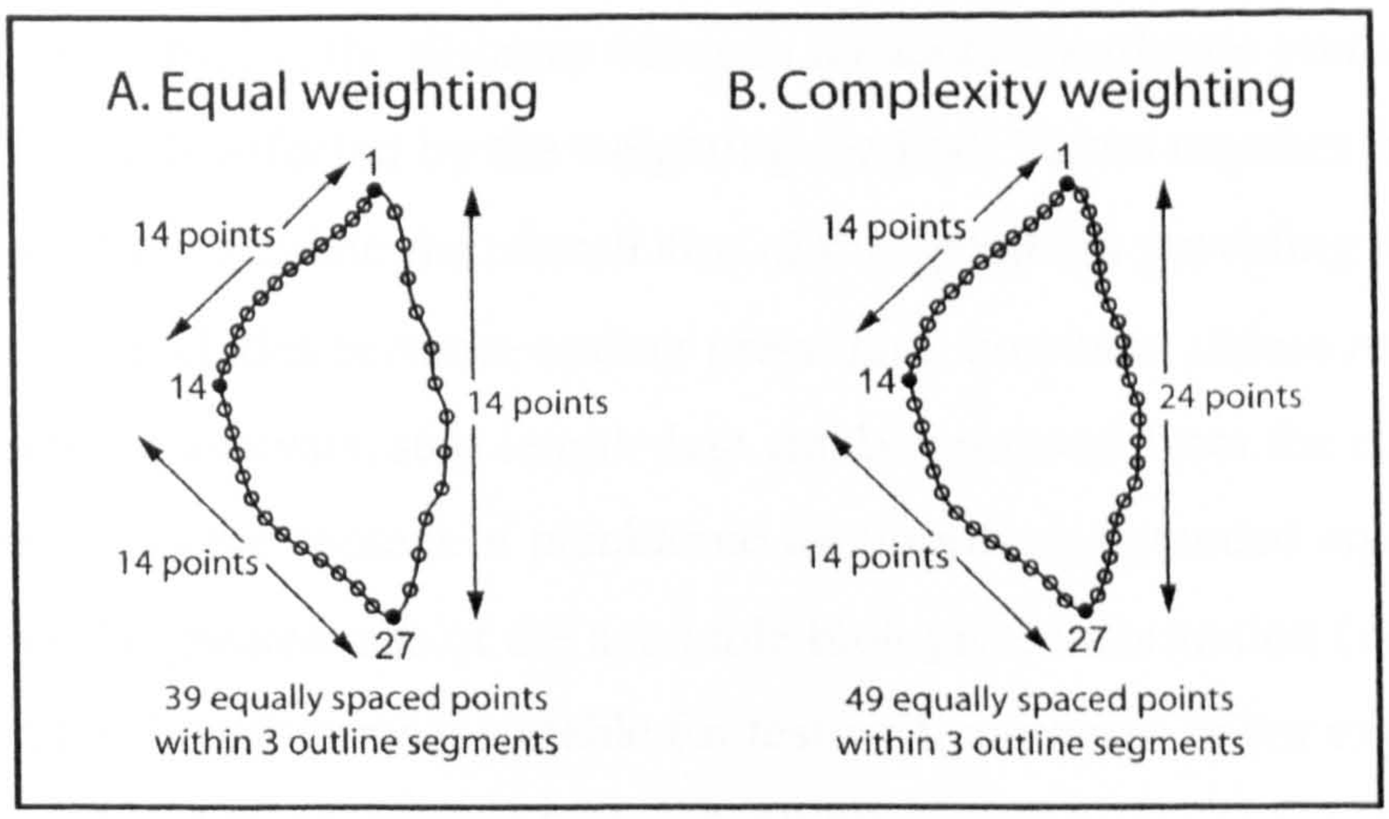

Figure 5.5. Two solutions to the inter-landmark distance problem (adapted from MacLeod, 1999). The standard eigenshape constraint of keeping the inter-landmark distance constant must be relaxed in order to improve the correspondence between the biological structure and the outline sequence. The two weighting methods are described in A and B. This can be done either by (A) breaking the segments down into a series of landmark points (black points) digitised to a constant resolution, or (B) a variable resolution. The latter method is preferable because shape complexity in certain segments is variable. The complexity-weighting method allows the more complex segments to differentially influence the multivariate analysis. In the equal-weighting method each segment influences the analysis equally, however, both schemes increase the correspondence between the geometric and biological assumptions of any eigenshape analysis (MacLeod, 1999).

In Figure 5.5 the two digitisation protocols that can be used to secure greater correspondence between an object's outline sequence and the biological structure it describes, are presented. Once the landmarks are located, the individual segments of outline can either be divided into the same number of coordinate points (A - equally weighted), or each segment can be divided into different numbers of coordinate points, based on the complexity of the segment (B - complexly weighted). Segment III (B) will require relatively more coordinates to constrain it to a constant precision. The second method uses the tolerance criterion to arbitrate the number of peripheral coordinates required to reach a consistent minimum accuracy throughout all segments for all objects in the sample (MacLeod, 1999). This differential weighting must be justified by the specifics of the dataset under analysis, moreover, it will reduce the ability of the regions showing little shape variation affecting the inter-specimen similarity estimates. Despite this, landmark registration significantly increases the amount of shape variation extracted by the digitisation methods (MacLeod and Rose, 1993; MacLeod, 1999). These authors found that >15% of empirical shape variation distribution across the higher eigenshape axes (2-n) was the result of mismatches or 'smearing' across expanded regions of the form.

The step-lengths, i.e. the distance between adjacent coordinate points on the boundary are obviously affected by the weighting method. Taken together, these step-lengths can be used to calculate the overall size of the specimen providing the imaging and digitisation process includes accurate scaling procedure, however, unless required for further morphometric analysis, step-length data can be removed from the eigenanalysis.

In summary, in the context of planktonic foraminifera, extended eigenshape analysis involves the greatest use of the available biological information (i.e. landmarks and outlines) and is therefore most suitable for testing hypotheses or for exploratory analysis (MacLeod and Rose, 1993; MacLeod, 1999).

5.3 Materials and methods

A total of 21 morphospecies from the genus *Globorotalia* from Middle Miocene (biozone M5) to Pleistocene epochs (biozone PT1) were analysed. This period of time covers the ranges of all species from the menardellid and *Globorotalia s.s.* lineages. Specimens were sampled from ODP holes 1195A and 1195B (from the Marion Plateau, northeast Australia), 926A (Ceara Rise, western equatorial Atlantic) and 871A (Limalok Guyot, Western Pacific). For taxonomic identification the type illustrations for each taxon were used for 'species concepts', in addition to the discussion in the taxonomic reviews featured in Kennett and Srinivasan (1983), Bolli (1970), Bolli and Saunders (1985).

5.3.1 Sampling strategy

The 21 morphospecies analysed in this study were sampled from six different intervals across three sites, as described above. These intervals were spaced according to the stratigraphic ranges of the taxa concerned together with the known preservational limitations of the sites in question. The intervals were then cross-correlated between the holes using the shipboard biostratigraphies (Shipboard Scientific Party, 1995; Pearson, 1995b; Shipboard Scientific Party, 2002a).

The majority of the Neogene globorotaliid radiation in the tropics occurred from the Late Miocene onwards (Kennett and Srinivasan, 1983; Bolli and Saunders, 1985), so the Late Miocene to Pleistocene-equivalent biozones (of sites 1195 and 926) were divided into four horizons to sample the speciation events and cover the majority of the taxa: lower

PL1a, middle PL2, middle PL5 and lower Pt1b (based on stratigraphy of Berggren *et al.*, 1995, see Appendix 3.1A-C). The purpose of sampling Site 871 was to include the more ancestral menardellid taxa, therefore this Site was divided into two sample horizons from the (Middle Miocene) lower M9b and upper M5b biozones. The sampling strategy is detailed in the table below:

Epoch	Biozone	Age (Ma)	Site	Sample(s)	Site	Sample(s)
Pleistocene	lower Pt1b	~0.6	1195A	2H-1, 120-122cm	926A	2H-2, 70-72cm
Late Pliocene	middle PL5	~2.6	1195A	5H-5, 10-12cm	926A	8H-4, 68-70cm
Early Pliocene	middle PL2	~3.8	1195A	7H-6, 10-12cm	926A	11H-4, 70-72cm
Late Miocene	lower PL1a	~5.4	1195B	9H-1/10H-1, 10-12cm	926A	16H-6, 60-62cm
Middle Miocene	lower M9b	~12.2	871A	4H-1, 126-128cm & 4H-2, 59-61cm		
Middle Miocene	upper M5b	~15.5	871A	8H2,3,4,5, 59-61cm		

Table 5.1. Source timeslice samples used to pick assemblages for eigenshape analysis.

5.3.2 Specimen preparation

Thirty specimens were picked randomly from the >150 μm size fraction of each pre-designated sample (the minimum as suggested by Malmgren *et al.*, 1983) to account for within population morphological variation. Species were assigned using the key characters as discussed in the taxonomy (Chapter 1). The eigenshape analysis software used in this study limits the number of objects in any one analysis to 500. This in turn limits the number of objects (specimens) one can use for each morphospecies if the analysis involves many. It is therefore not possible to use 75 specimens (as used by Malmgren *et al.*, 1983) to account for within-species variation if analysis of more than six taxa is desired.

All specimens were orientated on a slide using a water-soluble adhesive with edge-apertural view uppermost. It should be noted that orientation about the *x,y* plane is arbitrary and will not affect the outline shape of the specimen. The landmarking of points on the edge of the object facilitates alignment within the extended eigenshape covariance algorithms. More importantly, rotation in the *z* direction *can* significantly affect an object's outline and thus the analysis. It is crucial that sufficient time is spent ensuring rotation about the *z* axis is minimised (Lohmann, 1983). This is by far the most time consuming and delicate part of the data gathering procedure.

All specimens were then digitised using a Leica MZ 6 with a Leica IC A camera attachment and Image-Pro® Plus 4.1 for Windows™. The images were all taken using the highest magnification available on this microscope model (x40). Any rotation in the *z* direction at the adhesion stage was also counteracted using a custom made slide holder that rotated about the *x*, *y* and *z* axes (universal stage).

5.3.3 Acquisition of the specimens outline data

Acquisition of the individual shape outline data as Cartesian *x*, *y* coordinates was executed using the software *tpsDIG32* 1.31 (available from the world wide web at: http://life.bio.sunysb.edu/morph/) for Windows™ 3.1 and later operating systems.

It is important that the method of digitisation is the same for all specimens in the data set. The outlines were defined to a standardised equally spaced 200 loci around the specimen perimeter and therefore an effectively continuous representation of the outline.

Each specimen was manually defined by four landmarks. The two keel landmarks (landmarks 1 and 4) were located at the apex of each keel or equivalent point. Landmark 2 was located at the final chamber apex and landmark 3 was located at the concave test enclave where the base of the final chamber meets the umbilicus (see Figure 5.6). This landmark on some specimens corresponded to the umbilicus.

All the specimen images were outlined using either a sinistral specimen or a dextral specimen that had been digitally reversed about the *y* axis, so that all the specimens were orientated with the spiral side on the right in edge view (i.e. as if all sinistrally-coiled). The digitisation start point was always the apex of the spire (the point of highest curvature on the spiral side of the test), i.e. the point on the periphery of the test that is furthest to the right, assuming alignment of the specimen is *y* axis-keel parallel. This is usually a prominent feature in the Neogene globorotaliid lineages. If using the software *tpsDIG32* the outline will always advance in an anticlockwise sequence. If using other software it is important that the direction of loci sequencing is always the same. Any landmarks defined on the periphery should always be in the same inter-specimen relative position and in the same order.

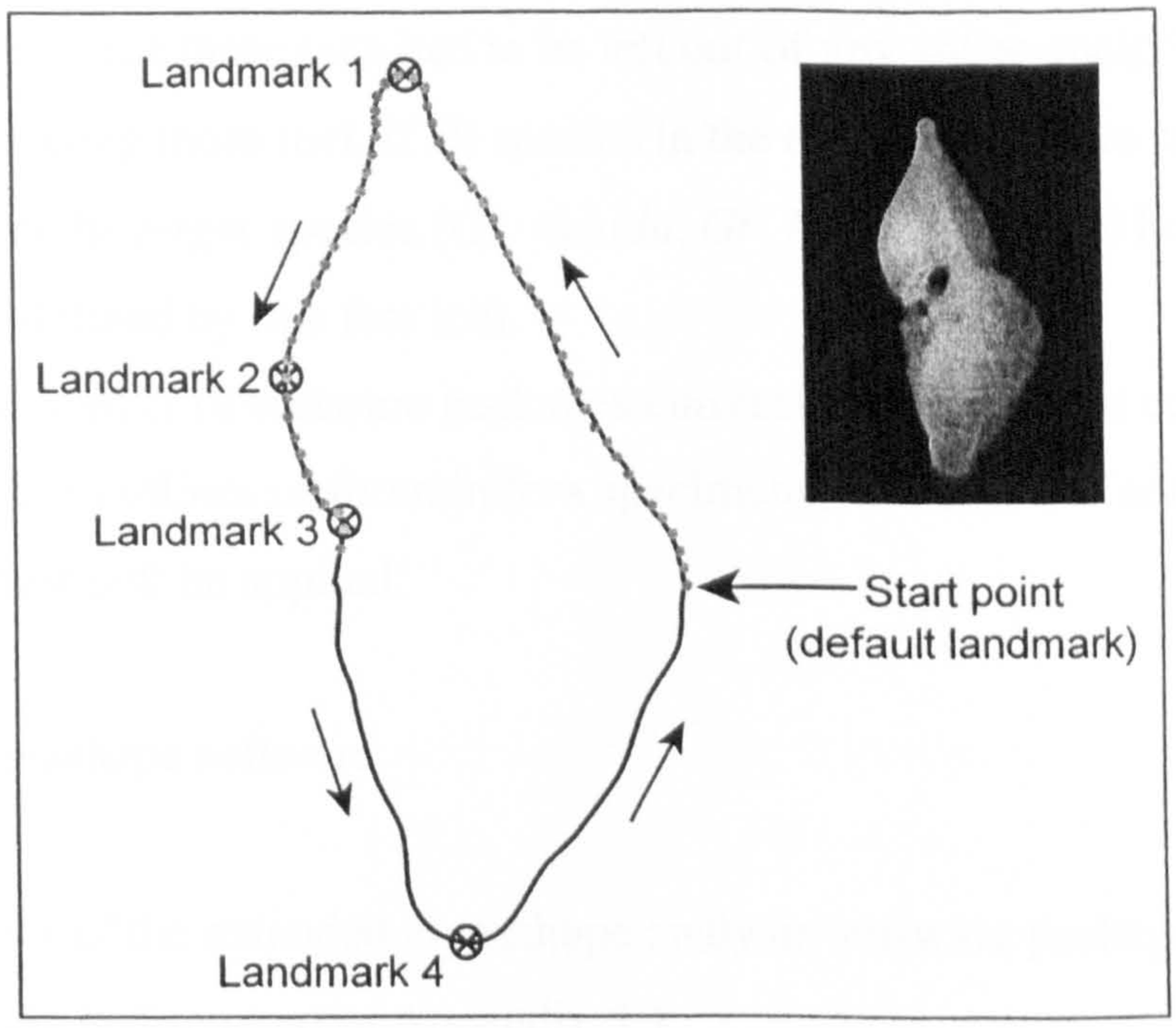

Figure 5.6. Silhouette of *Gr. menardii s.s.* and standardised digitisation method. All specimen images are orientated with the spiral side to the right (sinistral coiling). Those images that have a dextral habit are reversed before outline digitisation. The start point for the outline digitisation is always the proloculus, and the loci defining the perimeter were always sequenced in an anticlockwise direction. The landmarks were manually located at homologous points to those above. Inset is the original light-microscope image.

Lohmann (1983) and Lohmann and Schweitzer (1990a) used several hundred loci to define the outlines of the foraminifera specimens, although in practice between 100-200 points for each outline is adequate for eigenshape analysis (see also Lohmann and Malmgren, 1983; Malmgren *et al.*, 1983; MacLeod and Rose, 1993; Norris *et al.*, 1996). The maximum number of loci and landmarks is also limited by the eigenshape software used in the data analysis. To compare outline data, all objects in the data matrix must be defined by the same number of loci. The *tpsDIG32* software suggests a maximum number of loci to define the outline based on the resolution of the image, which can be altered to suit requirements. Furthermore, it is important that the number of loci used to define the outlines of all the objects in the data matrix is tailored to suit the variation of object sizes within the matrix e.g., the matrix used in this study contained relatively large foraminifera species such as *Gr. tumida* (<1000 μm) and relatively small species such as *Gr. archeomenardii* (150-250 μm). Assuming a constant image magnification and a finite image resolution, the number of loci must be small enough to adequately represent the smallest object in the data set, and large enough to adequately represent the larger objects. The images of the some of the *Gr. archeomenardii* and *Gr. praescitula* specimens were small enough so that the image resolution would only allow <150 loci points to define the

periphery. This meant that these taxa had to be left out of any shape analysis that contained individuals defined using more loci. If all species in the data matrix were simply defined by 150 loci, some of the larger species (*Gr. tumida*, *Gr. flexuosa*) would lose significant shape resolution if defined by this few loci.

There are a number of software packages currently available that could be used to image and digitise the outlines of foraminifera specimens; to which the considerations discussed above must still be applied.

5.3.4 Extended eigenshape software

The specifics of the extended eigenshape analysis software package used for data analysis in this study is discussed in Appendix 5.1.

5.3.5 Calculating the shape functions

The data files in the form described are inputted into the *X, Y → Ext. Phi* program to convert the outline and landmark coordinates into their equivalent extended $\phi*(l)$ (phi) shape functions. This function is a description of a specific shape, independent of size (Lohmann, 1983). The data file must be in the same folder as the program in order for the program to locate the data file.

The program requires the name of the input file, the output file, the title for the top of the function file, the number of objects within the file, the number of coordinate pairs, the number of landmarks and the degree of accuracy for the phi function data. If any of the above has been entered incorrectly or is in the wrong format there will be an error message and the process must be started again.

5.3.6 Extended eigenshape analysis

The output phi function file from the previous program is the input for the *Ext. Eigenshape* program which uses the shape functions to calculate the eigenshapes, mean shapes, eigenvalues and covariances (scores).

First the program requires the input of the phi function file name. It will then ask if the user wants the step-lengths calculated, which are used to calculate the areas (in closed

outline shapes) and the lengths (in open outlined shapes) of the objects. All size information is removed from the analysis phase of the procedure, and all size calculations are done outside the eigenshape analysis. Size calculations can only be made if there is an accurate scaling step in the imaging and outline processes, which depends on the software used to carry out these procedures. It is not necessary to include any scaling or size data for the extended eigenshape analysis, however, if the size data is required at a later date for another reason then an accurate scaling procedure must be inserted into the imaging and outlining process.

The program then asks which of the eigenshapes, eigenvalues, mean shapes and scores the user wants saved to file. The program also asks the user if they want the size estimates. If this is requested, the data will be the first column in the 'scores' file. The sizes are not to be confused with the actual eigenshape scores. There should be a significant difference in the size of the numbers by some orders of magnitude.

The scores file lists the covariances of the individual phi shape functions with the individual eigenshape functions. This output file will list the covariance scores for the number of eigenshapes requested (up to the number of phi functions entered). Typically, the covariances with respect to the first eigenshape, account for ~95% of the total morphological variation within a microfossil dataset of this kind. Significant graphical plots of the objects within eigenshape space can commonly be summarised using covariances of the first three eigenshapes, i.e. first *vs.* the second, the second *vs.* the third and the first *vs.* the third, on an *x-y* scatter graph. This is done by reading the score data into any graphical package e.g., Kaleidagraph. Figure 5.7 is an example of a two-dimensional plot of the covariance scores from extended eigenshape analysis of a hypothetical object dataset.

Typically, a group of related objects (e.g., fossil outlines) will yield scores that cluster into distinct groups if the shapes of those objects are quantifiably different to one another. This of course depends on the use of an appropriate taxonomy and accurate identification. The degree of overlap between groups suggests a certain degree of similarity in shape between the respective groups that coincide e.g., in Figure 5.7 species B and D share considerable eigenspace area and therefore possess morphologies more comparable with each other than either does with species A or E. Clusters A, C, D and E could all be said to represent distinct morphotypes, while B shares varying degrees of similarity with A, C and D.

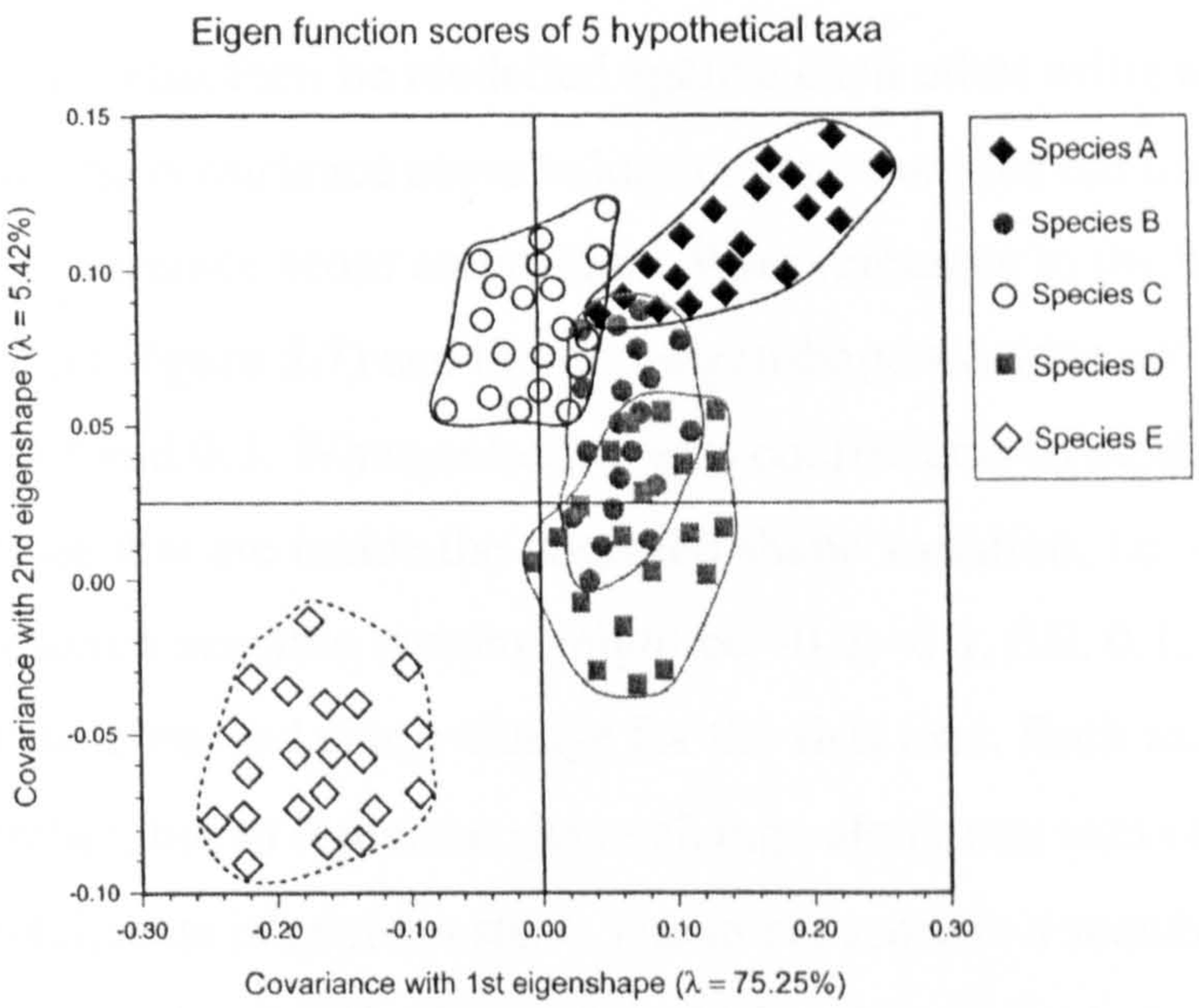

Figure 5.7. Hypothetical extended eigenshape space plot of 20 specimens from 5 taxa. In this example the first and second eigenshapes account for 80.67% of the total shape variation in the sample. Species A, B, and C all show distinct clusters with small degrees of overlap from which it is deduced that these species represent separate morphotypes, some of which may be related to one another. Species B and D have a greater degree of overlap and could be interpreted as having similar morphologies. Species E forms a completely separate cluster and appears not to share morphological affinity with the other taxa in the dataset. The 'λ' value is the percentage of shape variation that the particular eigenshape (or principal component) represents.

It could be that B is ancestral to these three taxa, however, this interpretation would also have to include stratigraphic and phenetic evidence. If a group falls inside another, the two groups can be interpreted as essentially indistinguishable, i.e. the range of morphological variation in one species falls within the range or natural variation within the other.

5.3.7 Modelling the eigenshape axes

The eigenshapes file (output from the *Ext. Eigenshape* software) is the input for the Ext. Eshape Models program (see Appendix 5.1). This program first requests which eigenshapes the investigator requires modelling from the *eigenshapes* file. This file will contain as many eigenshapes as the Ext Eigenshape program was instructed to compute. Conventionally, the first three eigenshape axes are modelled because typically they account for a large proportion of the morphological variation in a dataset. Next, the program requests if the investigator wants the outline step-lengths to constrain the model.

The answer is "no", unless correct scaling protocol has been incorporated into the image outline procedure.

The desired axes must then be modelled against each other using modelling coefficients. These are the covariance score values that account for the total data cluster area exhibited in the covariance score output files. With reference to the hypothetical covariance score plot (in Figure 5.7) and the first eigenshape axis, the score clusters are all contained between –0.3 and 0.3. When selecting axis coefficients to model an axis it is important to pick values that are inside the observed shape variation, i.e. within the cluster space. To model this axis a sensible spacing might be –0.2, -0.1, 0.0, 0.1, and 0.2. This will yield five models of the observed shape change for the first axis. Each axis must be modelled against another, but to represent shape change along one axis only, the comparative axis coefficients is kept constant. The mean score is a sensible secondary modelling axis coefficient, i.e. 0.025 (Figure 5.7). Using this method, the program asks for all the individual coefficients of the axis an investigator wants to plot against a secondary axis, which is essentially arbitrary providing the secondary axis coefficient is the mean for data clusters, and is constant while the primary axis is being modelled.

Through trial and error the following is the easiest way of modelling the first three axes: ES-1 (primary axis) is modelled against ES-2 (secondary axis), then ES-1 remains the primary axis but is kept constant (e.g. mean value of 0.00, Figure 5.7) and ES-2 (secondary axis) is modelled, then ES-1 remains the primary axis and is kept constant, while ES-3 (secondary axis) is modelled.

Once the modelling is finished answering *no* to all the following steps will allow the user to exit the program. The program will output the modelling *history* file, which simply describes the modelling process, and a *phi* file, which contains the phi functions for the models. This *phi* file can then be read into *Phi→x,y*, which converts the phi functions into the *x-y* representations of the models. These can then be read into a graphing package and plotted.

The shape models can be superimposed on top of each other or aligned along theoretical axes to show what kind of morphological changes along axis variables represent. This is shown later in Figure 5.8.

5.4 Results

In this study 1410 specimens (30 specimens for each of the 47 timeslice-species) were orientated on slides and digitally imaged, then described in terms of outline and landmark coordinates, upon which extended eigenshape analyses was performed. For the time-independent analysis (shaded grey taxa in Table 5.2) the software limited the total objects in one analysis to <500, so only 25 specimens for each species could be used. For all other analyses, 30 specimens were used. Biostratigraphic zones are from the work of Berggren *et al.* (1995). The table below shows which morphospecies had specimens described for analysis:

	Gr. archeomenardii	Gr. cultrata	Gr. exilis 'A'	Gr. exilis s.l.	Gr. exilis s.s.	Gr. flexuosa	Gr. limbata	Gr. menardii 'A'	Gr. menardii 'B'	Gr. menardii s.l.	Gr. menardii s.s.	Gr. merotumida	Gr. miocenica	Gr. multicamerata	Gr. pertenuis	Gr. plesiotumida	Gr. praemenardii	Gr. praescitula	Gr. pseudomiocenica	Gr. tumida	Gr. ungulata
1195A Pt1b		X									**X**									**X**	
1195A PL5		**X**					X		**X**		X			X					X	X	**X**
1195A PL2							**X**		X		X			**X**					**X**	X	
1195B M14							X	**X**	X			**X**		X		**X**			X	X	
871A M9										X							**X**				
871A M5b	X																	X			
926A Pt1b		X				**X**				**X**										X	X
926A LP PL5					X								**X**		**X**						
926A EP PL2					**X**									X*		X			X		
926A LM M14			**X**	**X**			X	X	X										X		

Table 5.2. Summary of taxa and site/biozone sampled. The x's mark the presence of the corresponding taxa in a particular site/timeslice, for which 30 specimens were described by outline and landmark coordinates. The * indicates where the species was '*sensu lato*'. The 19 taxa shaded represent those used in the time-independent (see figures 5.9-5.12) analyses (total 475 specimens), while those unshaded were utilised in the time-dependent analyses (figures 5.13-5.17). Biozones are from Berggren *et al.* (1995).

5.4.1 Eigenshape axis modelling

The axis modelling of the primary (time-independent) analysis (figures 5.9-12) followed the procedure outlined in Section 5.3.7. Figure 5.8 defines qualitatively what the eigenshapes (and covariance axes) actually represent in terms of the *Globorotalia* dataset. In this figure the 1st, 2nd and 3rd eigenshape along-axis shape change are modelled using the

covariance values inside the foraminifera outlines against the mean of one of the other axes.

In this study the first eigenshape corresponds to the average of all the shapes in the sample. The second eigenshape represents the primary dimension of shape variation about the average (first eigenshape), and the third eigenshape represents the next dimension, *etc.* (Lohmann, 1983). The central outline in this figure represents the average shape, i.e. the first eigenshape.

The first eigenshape axis models show that this axis delineates test variation in terms of flattening of the spiral side and decreasing the test tumidosity, i.e. from *menardii s.s.* to the *Gr. exilis* morphospecies. The models describing the 2.03 and 2.10 first eigen axis values (Figure 5.8) display shape eccentricities that do not necessarily occur in the dataset, because the models fall outside the boundaries of observed shape space and/or within the regions of sparsely-populated areas of empirical shape space. The second eigenshape axis delineates test compression from subspherical and biconvex (*Gr. miocenica*-type forms with a high spire) to thin test forms with a more compressed umbilicus and pronounced final chamber geometry. The third eigenshape axis describes change from broad test forms with distended final chambers and distinct keels (e.g. *Gr. cultrata*) to forms that are more 'pear-shaped' with thick, less pronounced keels and a symmetrical umbilical side (e.g. *Gr. tumida*).

5.4.2 Discussion of time-independent primary analysis – figures 5.9 to 5.10

Figures 5.9-5.12 present the eigenscores from the primary time-independent analysis of 19 of the 21 taxa (25 specimens per species). The 19 taxa were taken from a number of timeslice-assemblages from sites 1195 and 926, as shown in Table 5.2. Figure 5.9 presents the covariances with the first and second eigenshapes; Figure 5.10 is a close-up of some of the key relationships expressed in Figure 5.9; Figure 5.11, the first and third eigenshapes, and Figure 5.12, the second and third eigenshapes.

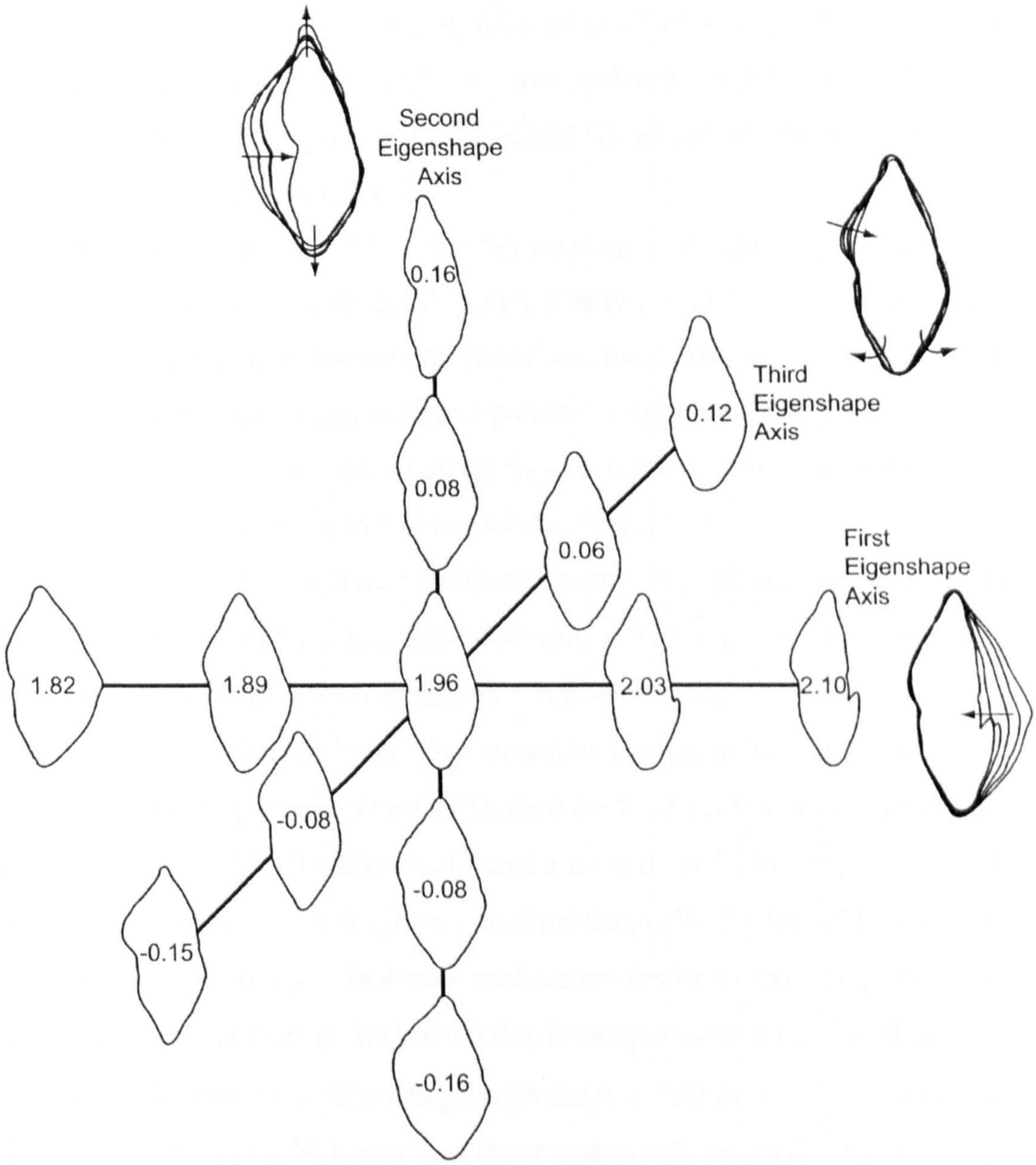

Figure 5.8. A set of along-axis shape models constructed for the globorotaliid time-independent primary dataset used in Table 5.2 and figures 5.9-12. The models express the shape variation captured by the first three eigenshape axes and are centred in the regions of empirical shape space around the mean shape (1.96, 0, 0). These models are powerful heuristic devices to explain the eigenshape analysis results graphically. Superimpositions (down-axis plots) are shown for the three axes in the figure. The arrows describe the direction of the along-axis test variation. A shape model can be created for any coordinate/or along any trajectory through eigenshape space. Those models that exhibit geometrically eccentric shapes are those that fall beyond boundaries of observed shape space and/or within the sparsely populated regions of observed space (e.g. outlines that fail to close or cross themselves). These represent geometric extrapolation beyond the bounds imposed by the sample's intrinsic shape variability.

Appendix 5.2 presents the eigenvalues that accompany this analysis. For this analysis of 475 specimens (25 specimens x 19 species), 100% of the variation can be described by covariances with 235 eigenshapes (latent shape functions). However, the first three eigenshapes account for 98.4% of the total variation, so it is only necessary to display the eigen score plots for these three eigenshapes. In fact, the first eigenshape accounts for

97.963% of the total variation alone. These high values for the first eigenshape are typical of covariance-based analysis of objects that are fairly similar to each other (MacLeod, *pers. comm.*). Similar figures are given in Corfield and Granlund (1988) for eigenshape analysis of the Palaeocene *Morozovella*.

In figures 5.9A, 5.10A and 5.12A all data points are plotted against the first 3 eigenshape covariances. Figures 5.9B, 5.11B and 5.12B have the data points removed and only the subjectively-drawn morphospace 'bubbles' encapsulating the space occupied by those points are remaining. This gives a clearer picture of the relationship between the clusters of each species. For each cluster outline there is a corresponding species-edge view although this bares no relation to any modelled eigenshape.

Malmgren *et al.* (1983) employed a different method for presenting their analysis data. Between-sample shape differences were determined by a separate eigenshape analysis of all the within-sample first eigenshapes, while between-sample shape change was displayed by the second eigenshape. This would be equivalent to using the first eigenshape for each taxon specimen group (25), then analysing all the first eigenshapes of each species together. Graphically, this would create a single point that represents each taxon in eigenspace. Although simpler, this is methodologically dubious. There are some critical assumptions in this analysis that may produce misleading results (discussed below).

Malmgren *et al.*'s (1983) analysis used the decomposition of the correlation matrix (as discussed above) in which standardising the $\phi*$ shape functions removes an element of the empirical shape variability. Not only this, these authors also regarded the un-scaled ES-1 (eigenshape 1) of their analysis as the mean shape. This un-scaled ES-1 can be transformed into a representation of the mean shape, but the two are not synonymous unless it is scaled appropriately (MacLeod, pers. comm.).

It should be noted that the algorithm within the software used in the analysis reported in this chapter *does* calculate an appropriately scaled estimate of the mean shape. Furthermore, the use of the mean shape to represent a sample is valid only if the sample is unimodal and the mean falls reasonably close to the mode. It is unlikely that Malmgren *et al.*'s (1983) samples were unimodal. Foraminiferal populations are renowned for variance (about a mean shape), therefore if inferences are going to be made about differences between samples it is not appropriate to ignore the between-sample variance. Strictly speaking, the second eigenshape does not always represent between-sample shape change, although this is usually the case.

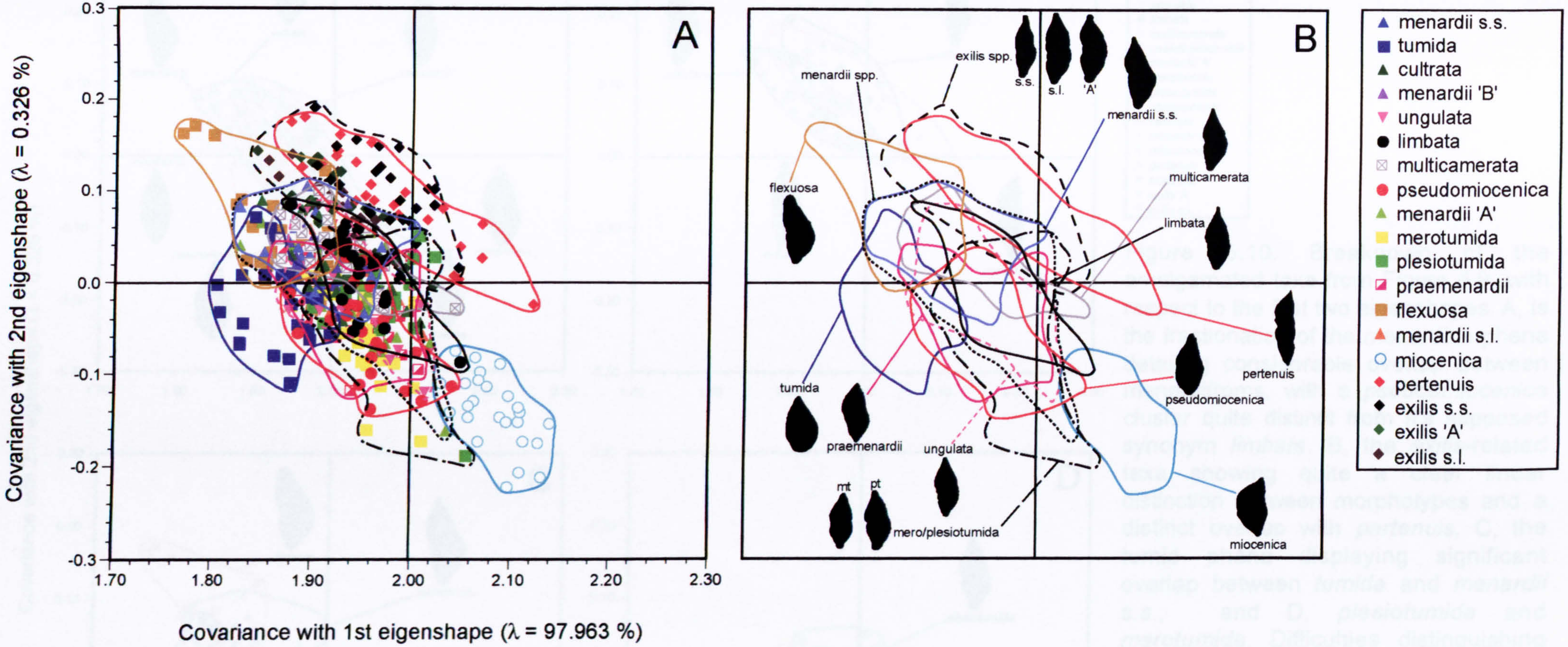

Figure 5.9. Extended eigenshape space plot for 25 specimens each of the 19 taxa from the Late Miocene to Pleistocene of ODP sites 926 and 1195. This representation of shape variability was obtained by calculating the covariances between shape functions of each object outline and the first two latent shape functions (eigenshapes), from a Singular Value Decomposition (SVD) of the interobject shape function covariance matrix (Macleod, 1999). The first two eigenshapes account for 98.289% of the total shape variation in the sample. All object data points are plotted in eigehshape space in A. In B, the points have been removed to give a clearer representation of the eigenspace occupied by each individual phenon. Some morphospecies show clear separation and overlaps with others, indicating morphological similarity or dissimilarity. *N.B.* each taxon is representative of specimens from one site and one timeslice. The 'λ' value is the percentage of shape variation that the particular eigenshape (or principal component) represents. The edge-view foraminifera shapes are purely for reference and are not linked to any eigenshape analysis.

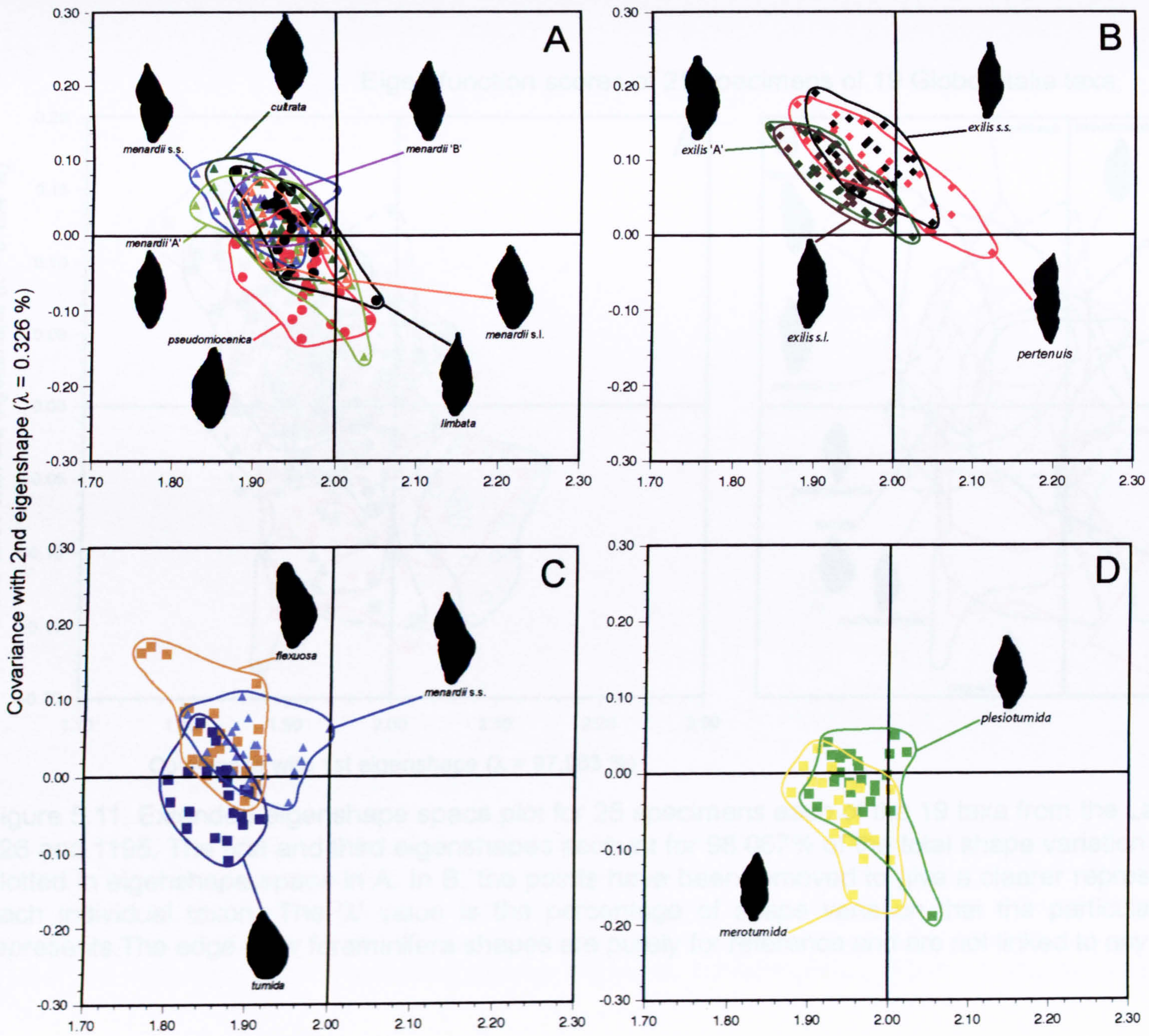

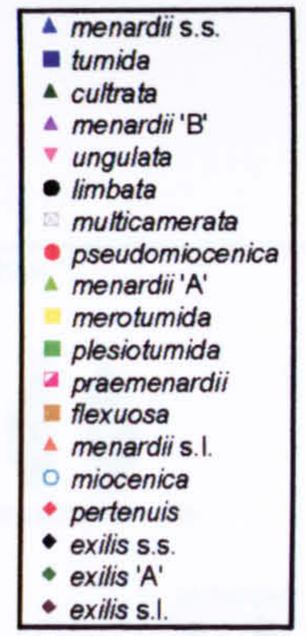

Figure 5.10. Breakdown of the amalgamated taxa from Figure 5.9, with respect to the first two eigenshapes. A, is the fractionation of the menardine phena detailing considerable overlap between menardifroms, with a *pseudomiocenica* cluster quite distinct from it's supposed synonym *limbata*, B, the *exilis*-related taxa showing quite a clear linear distinction between morphotypes and a distinct overlap with *pertenuis,* C, the tumid phena displaying significant overlap between *tumida* and *menardii s.s.*, and D, *plesiotumida* and *merotumida.* Difficulties distinguishing the morphotypes is supported by indistinct clusters. The 'λ' value is the percentage of shape variation that the particular eigenshape (or principal component) represents. The edge-view foraminifera shapes are purely for reference and are not linked to any eigenshape analysis.

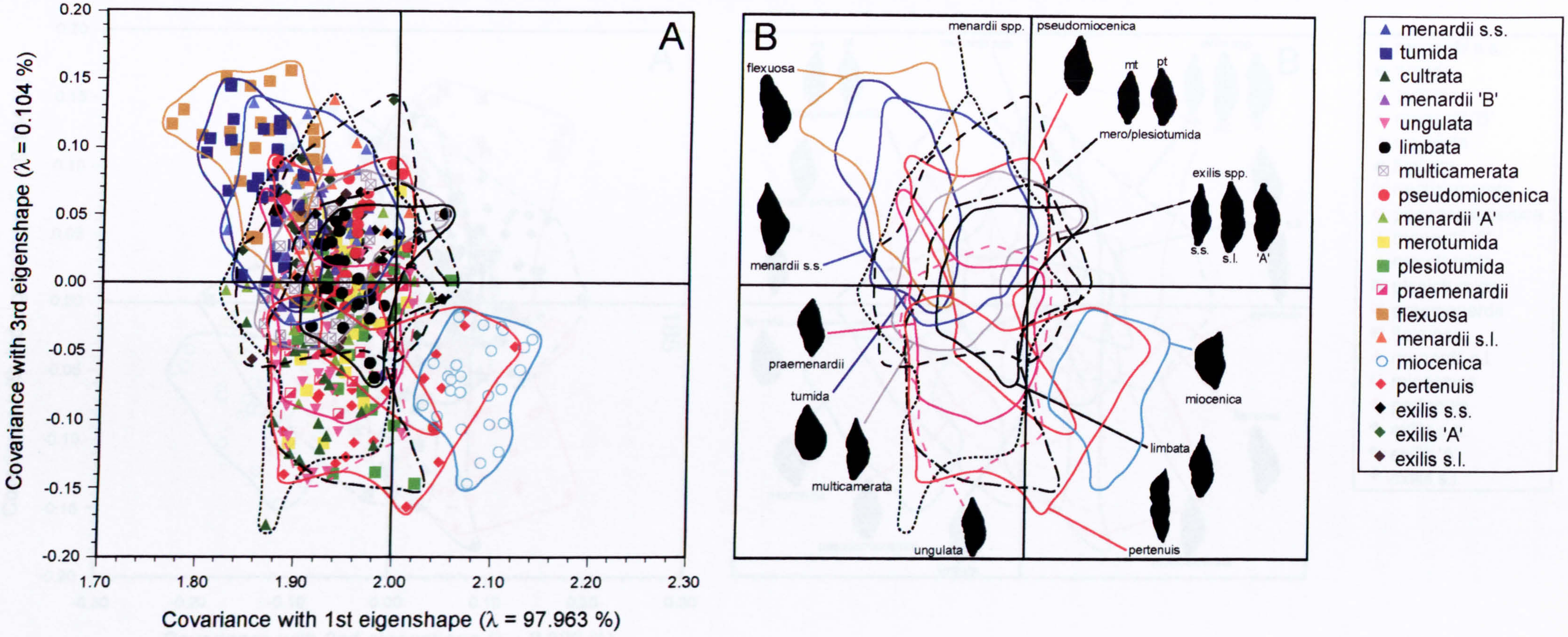

Figure 5.11. Extended eigenshape space plot for 25 specimens each of the 19 taxa from the Late Miocene to Pleistocene of ODP sites 926 and 1195. The first and third eigenshapes account for 98.067% of the total shape variation in the sample. All object data points are plotted in eigehshape space in A. In B, the points have been removed to give a clearer representation of the eigenspace occupied by each individual taxon. The 'λ' value is the percentage of shape variation that the particular eigenshape (or principal component) represents.The edge-view foraminifera shapes are purely for reference and are not linked to any eigenshape analysis.

Eigen function scores of 25 specimens of 19 Globorotalia taxa

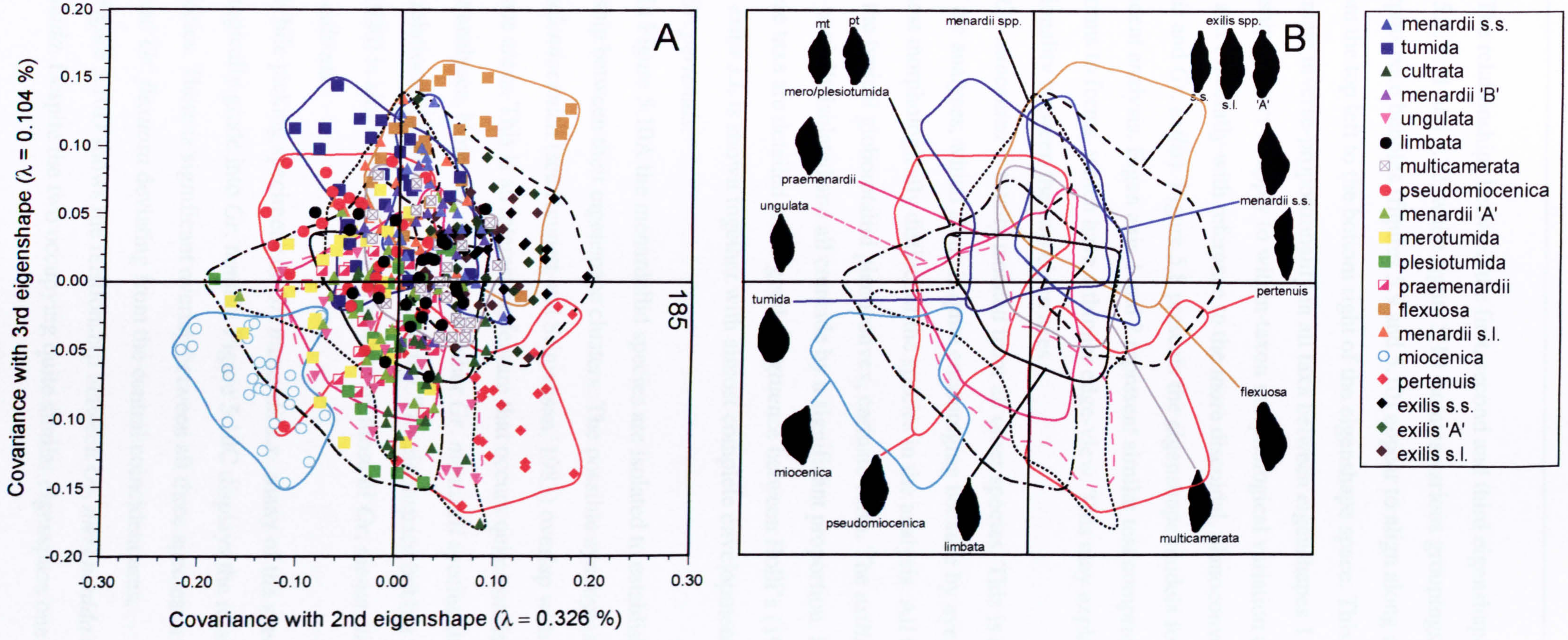

Figure 5.12. Extended eigenshape space plot for 25 specimens each of the 19 taxa from the Late Miocene to Pleistocene of ODP sites 926 and 1195. The second and third eigenshapes account for 0.43% of the total shape variation in the sample. All object data points are plotted in eigehshape space in A. In B, the points have been removed to give a clearer representation of the eigenspace occupied by each individual phenon. The 'λ' value is the percentage of shape variation that the particular eigenshape (or principal component) represents. The edge-view foraminifera shapes are purely for reference and are not linked to any eigenshape analysis.

The relationships between the first, second and third eigenshapes are shown in figures 5.9, 5.11 and 5.12, while figure 5.10 isolates various groupings from Figure 5.9. All morphospace bubbles (figures 5.9 and 5.10) appear to align along a morphocline that runs from the top left to the bottom right of the eigenshape space. This implies an approximate inverse-proportionality in all taxa between eigenshapes 1 and 2. This relationship appears to apply to within-taxon morphological variation and not between-species and especially with reference to the more discoidal, planoconvex species (e.g. *Gr. pertenuis* and *Gr. exilis*). Figure 5.8 presents the eigenshape models for the time-independent analysis. Eigen axis 1 and 2 represent similar test compression from more tumid forms to forms, which have a thinner edge-view. This may explain the apparent proportionality between the two eigen axes.

Gr. miocenica is totally isolated from all other species. This is a feature common to most of the analyses, which alone is quite encouraging because by eye, this morphospecies is the most morphologically distinct of the species in the analysis. All the other taxa assume the typical globorotaliid planoconvex, carinate form. The *exilis-pertenuis* clusters are also partially isolated and all coincide by a significant proportion. In Figure 5.10B, only these taxa are detailed and a good congruence between Bolli's (1970) *Gr. exilis* 'A' and *Gr. exilis s.l.* is shown together with almost complete envelopment of *Gr. exilis s.s.* within *Gr. pertenuis*.

In Figure 5.10A the menardellid species are isolated to establish a clearer relationship between their eigenspace clusters. The possible synonyms of *Gr. limbata* and *Gr. pseudomiocenica* (see Kennett and Srinivasan, 1983) overlap with half of their eigenspace areas. This is an interesting feature that occurs quite consistently within the different analyses. However, none of the other *Gr. menardii* species show any particularly notable relationships other than some overlap. The eigenspace bubble for *Gr. menardii* 'B' (Bolli, 1970) is almost completely subsumed by those of *Gr. menardii* 'A' (Bolli, 1970) and *Gr. cultrata*.

While picking specimens of *Gr. menardii s.s.*, many of the specimens appeared to morphologically grade into *Gr. tumida*. Figure 5.10C displays the relationships among these species. There is significant overlap between all three species in this figure with *Gr. tumida* and *Gr. flexuosa* deviating from the central coincident area.

Figure 5.10D shows the relationship between *Gr. merotumida* and *Gr. plesiotumida*. Despite the two occupying quite similar eigenspace one could argue that

there are distinct clusters, with *Gr. plesiotumida* towards the top of the plot and *Gr. merotumida* towards the bottom, but with a morphological overlap in the middle. Note in Figure 5.9 these two taxa share little eigenspace with their suggested (see Banner and Blow, 1965) descendent *Gr. tumida*, indicating a substantial morphological discontinuity, which directly contradicts the gradual morphological transition suggested by Malmgren *et al.* (1983).

Also from Figure 5.9 *Gr. praemenardii* lies in a centralised position relative to the larger mass of data; a theme which occurs in the temporally-dependent analyses. This could reflect a 'generalised' ancestral morphology that developed into the more derived morphologies.

Gr. multicamerata and *Gr. limbata* share little eigenspace with the *Gr. exilis* and *Gr. pertenuis* species. This could imply no direct ancestry and homoplastic derivation of the >8 chamber characteristic. *Gr. multicamerata* also shares a significant area with both *Gr. menardii* 'A' and 'B'.

5.4.3 Discussion of primary analysis – figures 5.11-5.12

These figures appear to have less cluster definition and phenetic distinction than the eigenshape 1 versus eigenshape 2 plot (Figure 5.9). There is also much less of a developed morphocline in Figure 5.11 with more overlap between many of the phenetic clusters.

In both figures 5.11 and 5.12 *Gr. limbata* and *Gr. pseudomiocenica* coincide by up to half their areas. *Gr. limbata* is also totally contained within the *'menardii spp.'* eigenspace. As before, *Gr. miocenica* maintains a relatively separate cluster, although with some overlap with a few taxa.

The *'exilis spp.'* group in the two figures lies within the *Gr. pertenuis* eigenspace, both of which no longer exhibit the separation from the other species as seen previously (Figure 5.9). The distinct relationship seen in this figure is not apparent in the ES-1 *vs.* ES-3 and the ES-2 *vs.* ES-3 plots. Both plots present significant overlap between the *exilis* group and with *Gr. limbata* and Gr. *multicamerata.*

The eigenspace range of the multiple *menardii* species has expanded relative to Figure 5.9, and *Gr. menardii s.s.* still exhibits a strong correspondence with the *Gr. tumida-flexuosa* couplet. Again, *Gr. praemenardii* and *Gr. ungulata* share a large proportion of this central eigenspace. The possible inaccuracies of these plots are

illustrated here in the apparent correspondence of the morphologically dissimilar *Gr. exilis spp.* and the *Gr. tumida-flexuosa* morphospecies. The *Gr. merotumida-plesiotumida* couplet display little correspondence with *Gr. tumida-flexuosa* in Figure 5.11, however, considerably more in Figure 5.12.

5.4.4 Time slice eigen analyses

With the large number of taxa in the above analyses it is clear that there is a great deal of overlap, which may obscure the eigenspace relationships. To gain a clearer view of phenetic relationships a number of time-dependant studies were executed. Figures 5.13-5.17A-C present eigen analysis data of the first three eigenshapes, for multiple taxa from four timeslices from Middle Miocene to Pleistocene. The fewer taxa involved in these some of these analyses succeed in presenting greater phenetic separation.

5.4.3.1 Middle Miocene (equivalent biozone M5b)

Gr. archeomenardii was differentiated from *Gr. praescitula* by the presence of a visibly definable primitive keel and an even spiral-side curvature. Although, it should be noted that some specimens completely lacking a keel (*Gr. praescitula*) do possess prominently convex spiral sides.

The eigenspace clusters (Figure 5.13A-C) show no obvious patterns or distinctions between *Gr. praescitula* and *Gr. archeomenardii*. Both occupy approximately similar areas. This may be the result of a number of factors. The taxon in question may possess intergrading morphologies, which are difficult to separate using a light transmitting microscope; test size is small (<150μm) and therefore image definition and resolution are reduced; the extended eigen analysis method is simply not as efficient at recognising edge-view shape differences in this case; or there is no consistent shape difference between the two morphospecies.

Middle Miocene M5b

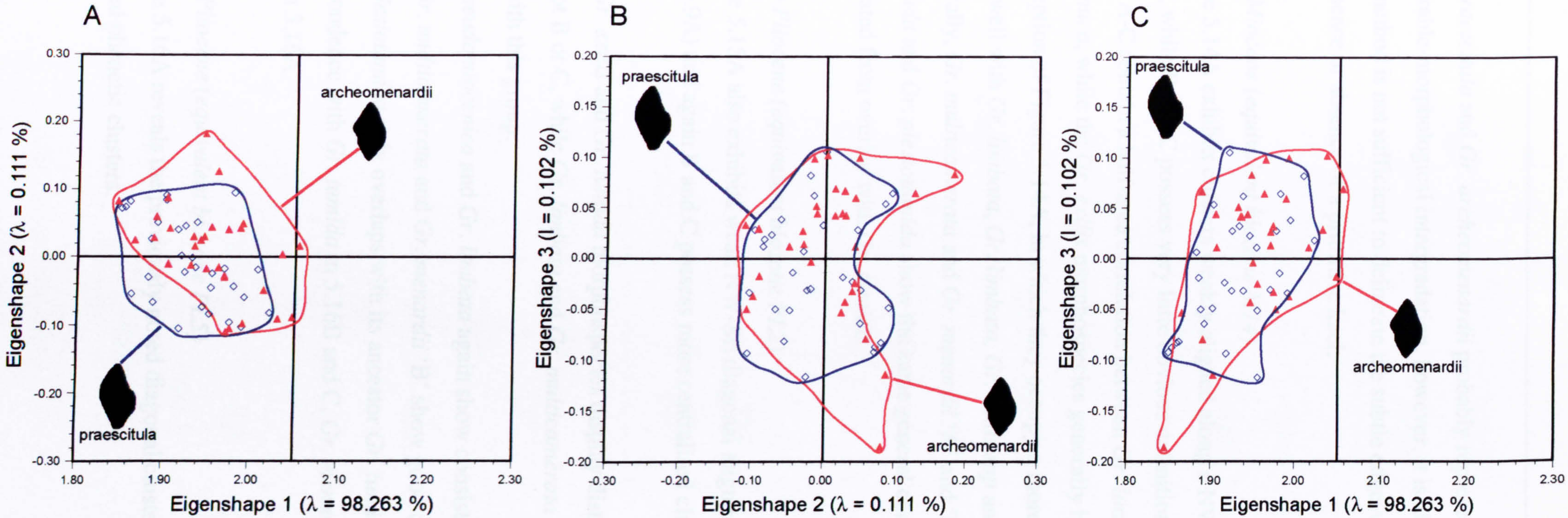

Figure 5.13. Two-dimensional shape distributions of extended eigenshape analysis of two taxa from the Middl Miocene biozone M5b of ODP holes 871A (Northwest pacific). 30 specimens of each taxon were plotted using th covariance with the 1st 3 eigenshapes, in the same 'eigen space', (A) ES1 versus ES2, (B) ES2 versus ES3 and (C ES1 versus ES3. Each taxon therefore occupies a cluster of eigenshape space. Increasing overlap between cluster indicates a greater degree of shape similarity of the umbilical view edge morphology. The 'λ' value is the percentag of shape variation that the particular eigenshape (or principal component) represents.

Gr. praescitula and *Gr. archeomenardii* probably represent two morphospecies with considerable-morphological intergradation, however, it is also likely that the eigenshape method is not sufficient to delineate the subtle edge-view differences that result from the presence or absence of a primitive keel.

5.4.3.2 Late Miocene (equivalent biozone M14)

Figure 5.14A exhibits clusters weakly aligned along a NW-SE diagonal morphocline, while B and C possess very little obvious definition.

Plots A-C contain a half-area correlation between *Gr. limbata* and *Gr. pseudomiocenica*, while the *Gr. exilis* morphospecies generally have a centralised cluster with the exception of Figure 5.14A, in which they occupy a more restricted eigenspace that corresponds well with *Gr. limbata*, *Gr. limbata*, *Gr. exilis spp* and *Gr. multicamerata.*

Typically, *Gr. multicamerata* and *Gr. menardii* 'A' and 'B' show good congruence. *Gr. merotumida* and *Gr. plesiotumida* show the same general correspondence and are largely separated from overlap with *Gr. tumida.*

5.4.3.3 Early Pliocene (equivalent biozone PL2)

Figure 5.15A also exhibits weak NW-SE diagonal alignment of the morphocline (see Figure 5.9A) and again B and C possess more centralised clustering and less definition.

The *Gr. exilis* and *Gr. tumida* morphospecies display distinct separated clusters in 5.16A, but not B or C, while *Gr. limbata* and *Gr. multicamerata* share varying amounts of eigenspace with this group.

Gr. pseudomiocenica and *Gr. limbata* again show consistent half-overlap of cluster area, while *Gr. multicamerata* and *Gr. menardii* 'B' show good correspondence.

Gr. plesiotumida only overlaps with its ancestor *Gr. tumida* in 5.16B, and despite good correspondence with *Gr. tumida* in 5.16B and C, *Gr. menardii s.s.* does not correspond in 5.16A.

5.4.3.3 Late Pliocene (equivalent biozone PL5)

Figure 5.16A reveals the previously noted diagonal cluster alignment and the most clearly defined phenetic clusters.

Late Miocene M14

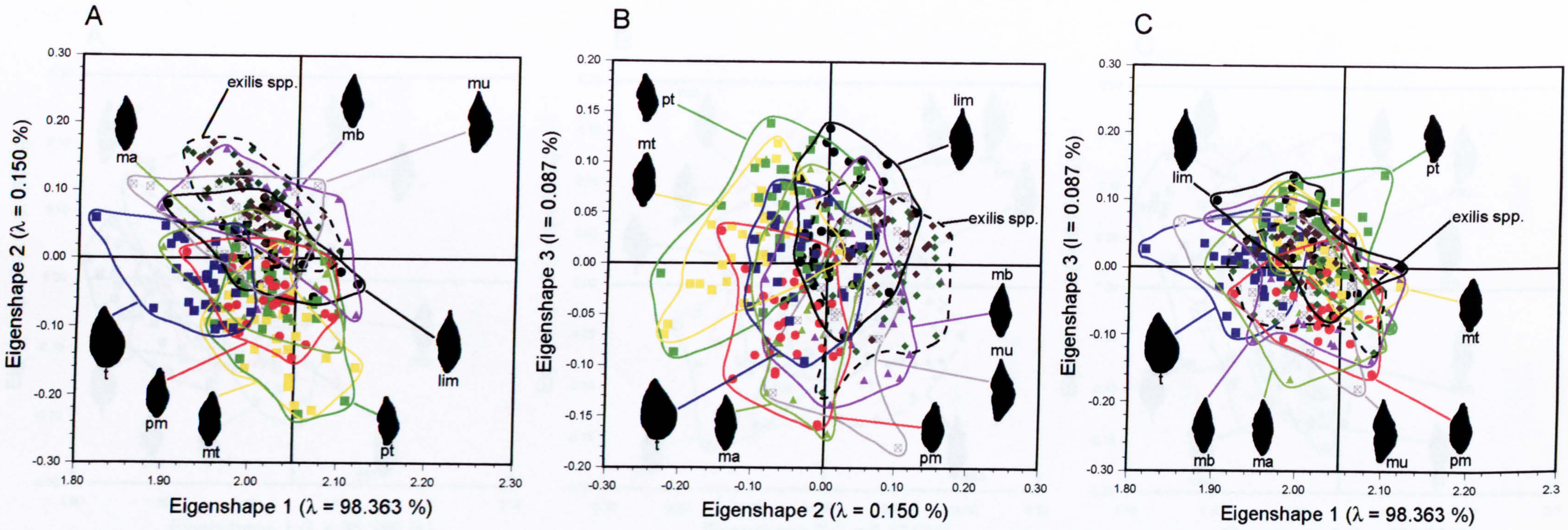

- limbata1195A
- menardii 'A' 1195A
- menardii 'B' 1195A
- merotumida 1195A
- multicamerata 1195A
- plesiotumida 1195A
- pseuodmiocenica 1195A
- tumida 1195A
- exilis 'A' 926A
- exilis s.l. 926A

Figure 5.14. Two-dimensional shape distributions of extended eigenshape analysis of seven taxa from the Late Miocene of ODP holes 1195A (Indo-pacific) and 926A (north Atlantic). 30 specimens of each taxon were plotted using the covariance with the 1st 3 eigenshapes, in the same 'eigen space', (A) ES1 versus ES2, (B) ES2 versus ES3 and (C) ES1 versus ES3. Each taxon therefore occupies a cluster of eigenshape space. The more overlap between clusters, the more similar the umbilical view edge morphology. The 'λ' value is the percentage of shape variation that the particular eigenshape (or principal component) represents.

Early Pliocene PL2

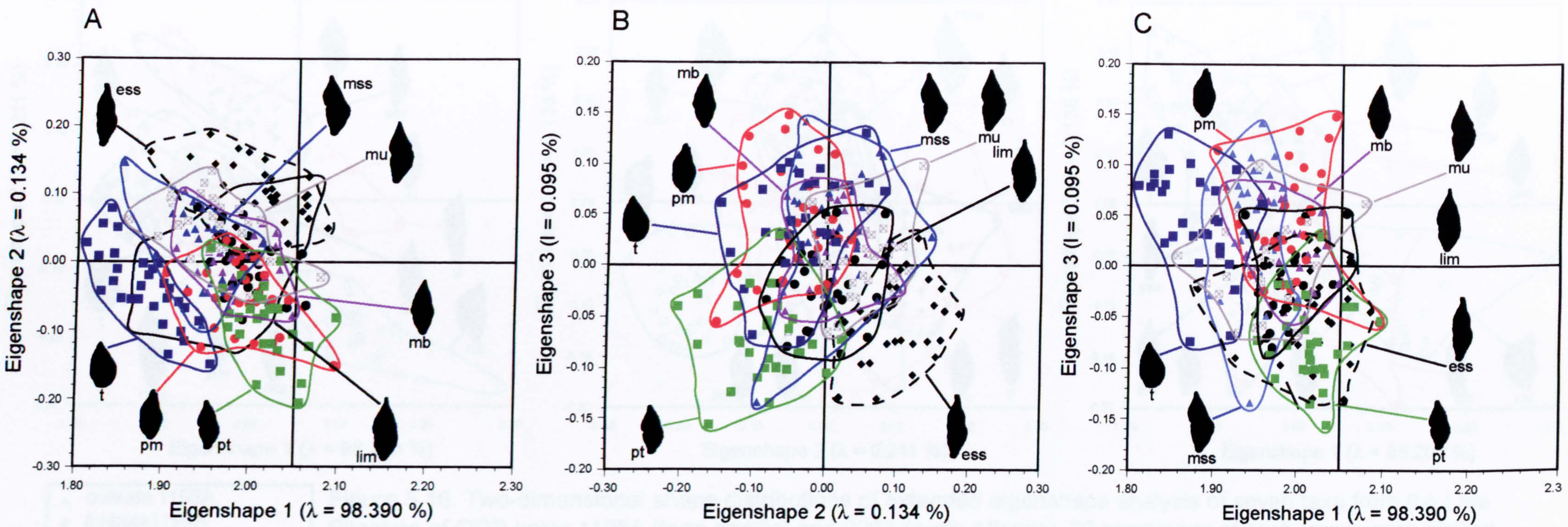

- limbata1195A
- menardii 'B' 1195A
- menardii s.s. 1195A
- multicamerata 1195A
- pseuodmiocenica 1195A
- tumida 1195A
- exilis s.s. 926A
- plesiotumida 926A

Figure 5.15. Two-dimensional shape distributions of extended eigenshape analysis of seven taxa from the Early Pliocene of ODP holes 1195A (Indo-pacific) and 926A (north Atlantic). 30 specimens of each taxon were plotted using the covariance with the 1st 3 eigenshapes, in the same 'eigen space', (A) ES1 versus ES2, (B) ES2 versus ES3 and (C) ES1 versus ES3. Each taxon therefore occupies a cluster of eigenshape space. The more overlap between clusters, the more similar the umbilical view edge morphology. The 'λ' value is the percentage of shape variation that the particular eigenshape (or principal component) represents.

Late Pliocene PL5

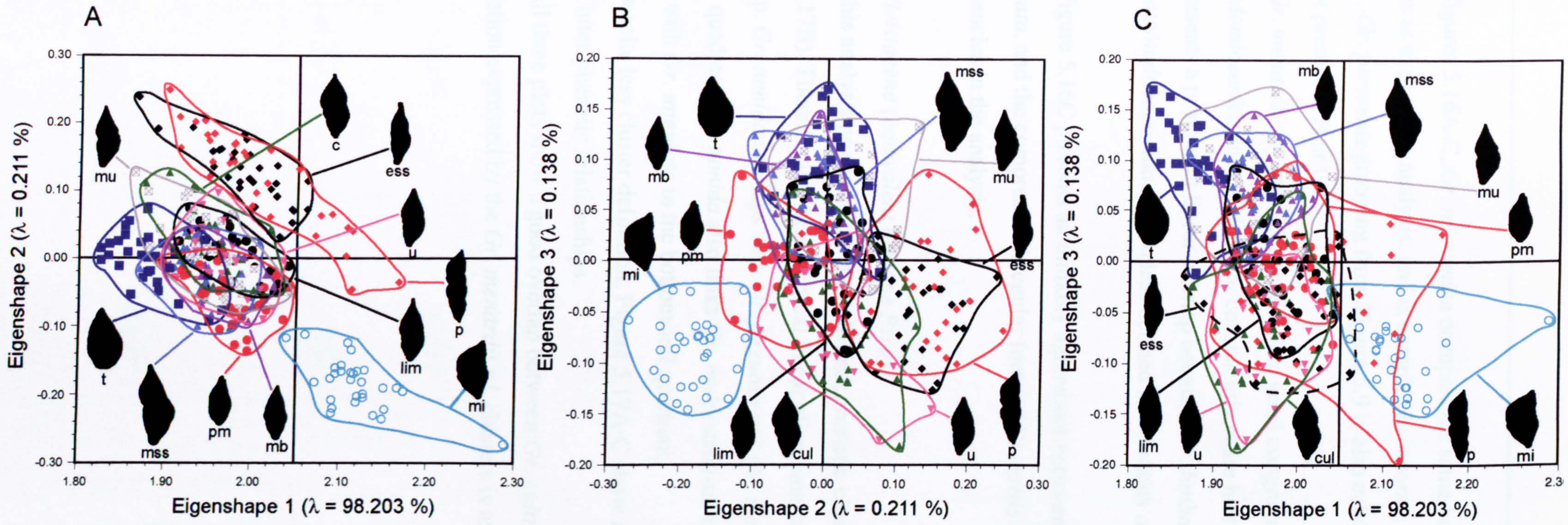

- cultrata 1195A
- limbata1195A
- menardii 'B' 1195A
- menardii s.s. 1195A
- multicamerata 1195A
- pseudmiocenica 1195A
- tumida 1195A
- ungulata 1195A
- exilis s.s. 926A
- miocenica 926A
- pertenuis 926A

Figure 5.16. Two-dimensional shape distributions of extended eigenshape analysis of seven taxa from the Late Pliocene of ODP holes 1195A (Indo-pacific) and 926A (north Atlantic). 30 specimens of each taxon were plotted using the covariance with the 1st 3 eigenshapes, in the same 'eigen space', (A) ES1 versus ES2, (B) ES2 versus ES3 and (C) ES1 versus ES3. Each taxon therefore occupies a cluster of eigenshape space. The more overlap between clusters, the more similar the umbilical view edge morphology. The 'λ' value is the percentage of shape variation that the particular eigenshape (or principal component) represents.

Also in figures 5.16A-C, *Gr. miocenica* occupies the same bottom-left and bottom right quadrants as in previous analysis, and is completely separate from all other forms. The *Gr. exilis s.s.-Gr. pertenuis* grouping from Figure 5.9 is also echoed in this analysis in 5.17A, but is not present in B or C.

Gr. menardii s.s. and *Gr. tumida* share good congruence in figures 5.16A-C, while *Gr. pseudomiocenica* and *Gr. limbata* consistently share half their eigenspace. Figure 5.16B presents a prominent linear overlap between *Gr. limbata/menardii s.l./menardii* 'B'*/limbata/multicamerata*, with a less defined but obvious offset of the *exilis-pertenuis* species.

Figure 5.16C presents an unlikely agreement between the inflated menardellid form *Gr. cultrata*, and the compressed irregular form of *Gr. exilis*. This may be evidence of inconsistencies in the analysis.

5.4.3.4 Pleistocene (equivalent biozone Pt1b)

This analysis produced the most distinct phenetic clusters of the whole suite (see Figure 5.17B). There is clear near-vertical linear alignment with an approximate gradation in overlap. *Gr. tumida* overlaps with *Gr. flexuosa* and *Gr. menardii s.s./menardii s.l.* in the top-right quadrant. *Gr. tumida* also links *Gr. multicamerata* to *Gr. cultrata,* which in turn, overlaps with *Gr. ungulata* in the bottom-left quadrant.

Despite less cluster definition, Figure 5.17A-C show a similar order of overlap, and the same inter-phenetic relationships.

All three plots show a good overlap between *Gr. cultrata* and *Gr. ungulata* and the total variation expressed by the *Gr. menardii s.l.* clusters is assimilated by *Gr. menardii s.s.*

Pleistocene Pt1b

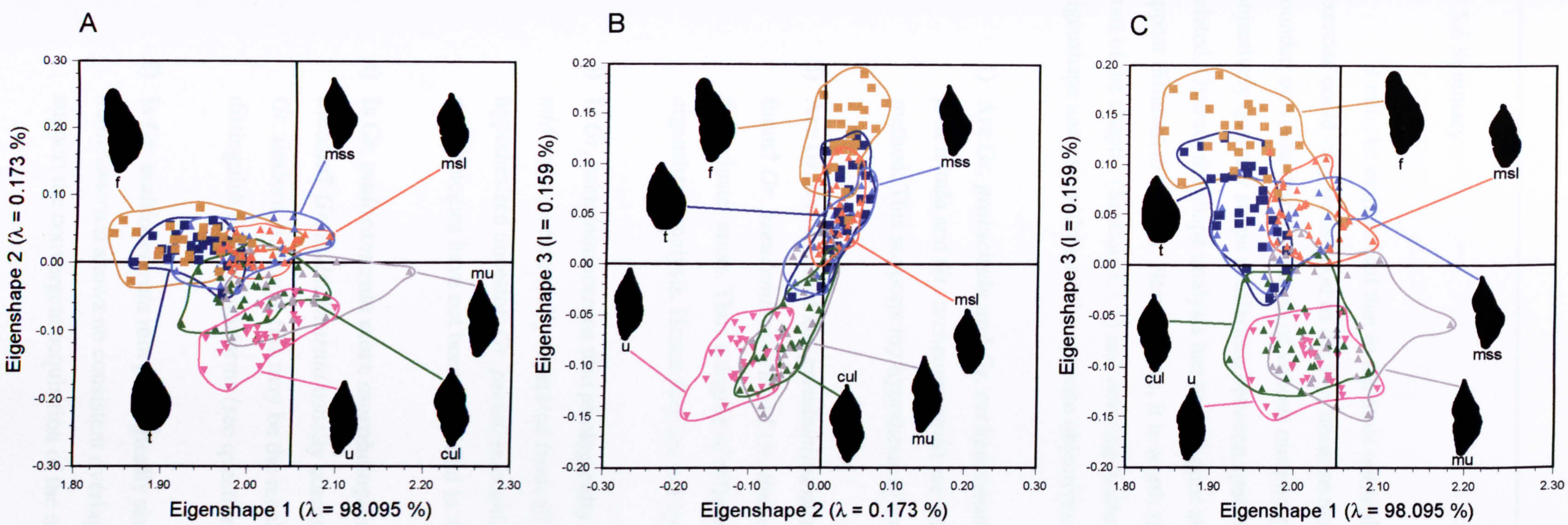

- cultrata 1195A
- menardii s.s.1195A
- tumida 1195A
- cultrata 926A
- flexuosa 926A
- menardii s.l. 926A
- ungulata 926A

Figure 5.17. Two-dimensional shape distributions of extended eigenshape analysis of seven taxa from the Pleistocene of ODP holes 1195A (Indo-pacific) and 926A (north Atlantic). 30 specimens of each taxon were plotted using the covariance with the 1st 3 eigenshapes, in the same 'eigen space', (A) ES1 versus ES2, (B) ES2 versus ES3 and (C) ES1 versus ES3. Each taxon therefore occupies a cluster of eigenshape space. The more overlap between clusters, the more similar the umbilical view edge morphology. The 'λ' value is the percentage of shape variation that the particular eigenshape (or principal component) represents.

5.5.6 Summary

It must be emphasised that in the most optimal circumstances this morphometric exercise could only be as good as the eye, because the starting point of the study is founded on visual discrimination of various morphospecies. The object of the study was to objectively quantify shape similarities between species thought to be phylogenetically-related. Overall, the shape analysis has proved poor at distinguishing morphotypes that appear different to the eye. Nevertheless, it is worth revisiting the hypotheses set out at the start of the chapter (Section 5.1.1) and drawing limited conclusions. The extent to which eigenshape analysis addressed the exercise objectives is discussed below:

1) **Are *Gr. praescitula* and *Gr. archeomenardii* distinct morphospecies?** *Gr. praescitula* and *Gr. archeomenardii* are largely indistinguishable using this method. This supports my hypothesis of extreme morphological intergradation.

2) **Are *Gr. limbata* and *Gr. pseudomiocenica* synonyms describing the same form?** *Gr. pseudomiocenica* and *Gr. limbata* consistently share only half of their cluster areas. Thus a degree of difference is consistently identified by the eigenshape analysis. Hence they are not synonymous.

3) **Is *Gr. pseudomiocenica* morphologically similar to *Gr. miocenica*?** *Gr. miocenica* is essentially separated from all other species, including its hypothesised ancestor, *Gr. pseudomiocenica*. It may be related, but intermediate morphologies have not been identified in this study.

4) **Is *Gr. multicamerata* more morphologically similar to *Gr. menardii* or *Gr. limbata*?** *Gr. multicamerata* usually correspond well with *Gr. menardii* 'B' and *Gr. limbata*, although this may be the result of the method's inability to distinguish the menardiforms (see question 9).

5) **Is *Gr. multicamerata* morphologically similar to *Gr. pertenuis-exilis*?** *Gr. multicamerata* shows no consistent overlap with either species. This may support the convergent acquisition of the numerous-chamber character as a

further example of homoplasy in foraminifera, or this may result from the inability of this method to distinguish the edge forms close to *Gr. menardii.*

6) **Are *Gr. pertenuis* and *Gr. exilis* distinct morphospecies?** The *exilis* species commonly share overlap with the *Gr. pertenuis* eigenspace, and together are sometimes significantly isolated from the remaining cluster distributions. These taxa are probably closely related and exhibit a degree of intergradation of forms.

7) **Are *Gr. menardii* 'A', 'B', *cultrata* and *fimbriata* distinct morphospecies?** Extended eigenshape analysis routinely cannot adequately distinguish menardiforms in edge view (*Gr. menardii* 'A', *Gr. menardii* 'B', *Gr. menardii s.s.- Gr. menardii s.l.- Gr. cultrata-Gr. limbata-Gr. praemenardii-Gr. multicamerata).* Extended eigenshape analysis also cannot sufficiently distinguish *Gr. menardii* 'A' from 'B'. This suggests that these taxa have similar edge forms, although is not conclusive as to whether they are distinct species.

8) **Are *Gr. merotumida* and *Gr. plesiotumida* distinct morphospecies and are they closely allied in shape to *Gr. tumida*?** *Gr. merotumida* and *Gr. plesiotumida* commonly occupy the same eigenspace and both species rarely overlap with *Gr. tumida.* This may support a single anagenetic lineage for these two taxa, but their link to *Gr. tumida* may be supported by cladistic analysis.

5.5 Discussion and conclusions

There are some features of the eigenspace cluster distributions, which reoccur in a number of the analyses, and provide quantitative evidence for consistent relationships between morphologies. These results addressed some of the questions outlined in the introduction. However, a number of the analyses in this study show few distinct or obvious eigenspace relationships between the species involved in them. From this, it would be easy to assume that extended eigenshape analysis is not as efficient at recognising and distinguishing the complex morphological shapes that micropalaeontologists have been doing for decades. It is not as simple as this.

Foraminiferal intra-morphospecies morphology is inherently variable while inter-morphospecies variation for a group such as the Neogene *Globorotalia* may not be sufficiently variable for eigenshape morphometrics to easily make sense of. However, extended eigenshape analysis does not analyse simple individual characters, as might be pre-determined by the investigator to establish phylogenetic links, but a complex combination of highly-variable outlines and landmarks that equate to numerous of cladistic characters. How much of the data that the investigator's eye and brain analyses to distinguish morphospecies is contained in the edge view of discoid foraminifera? Visual taxonomy relies on many features not visible in this orientation, such as suture shape, aperture morphology, etc. Hence failure of the shape analysis to discriminate morphologies does not mean that two morphospecies actually intergrade. The shapes represented by the Neogene *Globorotalia* edge-views are probably the single most phylogenetically informative views of the tests, but do they vary sufficiently and consistently enough to be able to distinguish inter-morphospecies differences? Corfield and Granlund (1988) suggest that the edge view of Palaeocene morozovellids is not a good measure of real species differences; although, their analysis is complicated by the muricae structures on the test and the problems associated with the standard eigenshape method discussed above.

The results in this chapter show that extended eigenshape analysis *can* distinguish some test forms consistently. Although, analysing too many divergent morphologies at once may force them to overlap in the 1st, 2nd and 3rd eigenshape space. In the majority of the analyses, the first eigenshape (i.e. average shape for the morphological dataset) accounts for ~97% of the variation. The relative inability of the technique to distinguish all morphospecies forms may lie in the fact that they are all very similar (in edge-view) to

start with. Perhaps the eye-brain system used by the skilled micropalaeontologist is doing far more than two-dimensional eigenshape analysis can achieve? The micropalaeontologist certainly does not simply consider one view when assessing shape similarity. There maybe far more unconscious processes influencing the micropalaeontologist than they themselves are probably aware. Two-dimensional representations may fail to capture phylogenetic distinctions between all taxonomic groups adequately, using only one view of a foraminifera test. MacLeod (1999) does report a three-dimensional eigenshape technique, however, currently it is not applicable to complex three-dimensional objects posed by foraminiferal tests, and is limited by imaging technology. Development of more sophisticated three-dimensional scanning technologies may enable modelling of complex three-dimensional objects to infer phenetic relationships.

Conventional two-dimensional eigenshape analysis has been used to analyse small parts of biological shapes to code and quantify phylogenetic characters that are not obvious to the naked eye (MacLeod, 2002). In this study MacLeod showed how eigenshape analysis of published trilobite pygidium characters revealed further characters that the original authors did not identify. Perhaps with reference to foraminifera, this is where additional utility may be found. Isolating small parts of the test e.g., keel cross-section or final chamber shape may produce more conclusive results in trying to identify character states that can then used as part of a cladistic analysis.

Finally, it is important to recognise that this technique is one of many objective tools that can be used to suggest phylogenetic relationships between members of a group of individual taxa. No one phylogenetic tool is perfect for any specific job and we cannot expect the results from a single statistical tool to give us a full and *absolute* answer. The results presented here provide a basis, to which analyses of character and stratigraphic data were added (see Chapter 6), to help create a new phylogeny for the Neogene *Globorotalia*.

Chapter 6

Investigating the phylogeny of the Neogene *Globorotalia* using cladistics, stratocladistics and stratophenetics

6.1 Introduction

In Chapter 5 morphometrics was used as a proxy for phenetic distance. For the study presented in this chapter, cladistics was employed to infer history of evolutionary branching in the Neogene *Globorotalia* using a matrix of observed characters constructed by the author.

The cladistic procedure constructs phylogenetic hypotheses based on the possession of synapomorphies, which are shared-derived (morphological, physiological, molecular, etc) characters (Hennig, 1966; Farris, 1988; Swofford, 1993, 2000; Smith, 1994). These objectively defined morphological character states unite clades at any taxonomic level, i.e. species, genus, family, etc. Any taxon can be coded, whether phylogenetic affinity is known or unknown, which facilitates addition of extra taxa (or characters) to a pre-existing analysis with great ease. After coding and computational analysis, all taxa within a clade are represented as 'sister-taxa' without directly defining ancestry. Thus, cladistics is a useful tool for creating hypotheses of phylogenetic relationships and has enabled the palaeontologist to significantly increase the rigour and objectivity of phylogenetic hypotheses. However, it is not without its disadvantages, some of which apply to cladistic studies using foraminifera.

Cladistic analysis relies on the selection of independent, unambiguous, and phylogenetically informative characters. To isolate these characters is more demanding for foraminifera than other groups, because 'morphospecies'-level discriminations are based on shape criteria and discrimination of populations using morphometry (Pearson, 2001). To code actual 'species' can only be done properly if each taxon is coded using the holotype specimen, otherwise an investigator is coding their own or another investigator's species concept. In this study, holotypes were used to code the taxa involved. Although, as discussed in Chapter 2, holotypes are arbitrarily assigned specimens defined by a

taxonomic binomen that represent a potential area of 'morphospace', and may not adequately represent within-taxon morphological variation. Fossil morphospecies are completely un-testable as biospecies. When coding planktonic foraminiferal holotypes for cladistic analysis, an investigator is essentially researching the phylogeny of a series of arbitrary forms, because the typological Linnaean system does not cope well with evolutional fluidity, of the type documented in this group. Nevertheless, cladistics can potentially supply useful information about broad phenetic associations.

Most cladistic analyses operate on the principal of parsimony. This procedure assumes minimal amounts of character change and reversal as the most likely evolutionary pathway for a developing taxonomic lineage (Smith, 1994). Unfortunately, planktonic foraminiferal phylogenies are widely thought to contain heterochronous convergent evolution (Cifelli, 1969; Banner and Lowry, 1985; Norris, 1991) and thus homoplasy, whereby certain features are developed independently more than once e.g., the multiple independent acquisition and loss of the keel. Therefore, foraminiferal phylogenies usually possess a number of homoplastic characters and may not be particularly well-suited to cladistic methodologies.

One of the principal complications with the cladistic method is that analyses cannot represent ancestor-descendant relationships (of the type that are important for establishing accurate phylogenies of extinct taxa) and does not consider stratigraphy a phylogenetically-informative character. Cladists believe that ancestor-descendent relationships cannot be determined and are therefore irrelevant. For example, Gee (2001) argues that there is no way of objectively demonstrating ancestry in the fossil record. He also argues that to use stratigraphy as a character to imply phylogeny, and then use phylogeny to support hypotheses about stratigraphy is to form a circular argument. Similarly, Siddall (1998) believes that the search for ancestor-descendent relationships is flawed because it places a "premium on negative evidence", i.e. only a lack of autapomorphies (negative evidence) can define an ancestor. However, if all taxa are portrayed as sisters, even when ancestry and anagenesis must have occurred, then branching will be greatly overestimated and rates of evolution and phylogenetic hypotheses misleading (see Chapter 2). Ancestry is an integral part of phylogeny; without the former, how do we effectively understand the latter?

The fossil record of the planktonic foraminifera is unlike that of most fossil groups. Instead of there being two or three incomplete body fossils per taxon, planktonic

foraminifera are highly abundant, well-preserved, widespread in marine sediment samples and sometimes preserved in unbroken stratigraphy for several million years (e.g. ODP Site 1195, Marion Plateau – see Chapter 3). Many planktonic foraminiferal lineages have been extensively and independently examined against a multitude of stratigraphic sequences, calibrated by radioisotopic dating and tested with independent biochronological datasets (Berggren, *et al.*, 1995). Although true ancestry can never be 'known', it is reasonable to formulate hypotheses of phylogeny and ancestry using knowledge of the fossil record, then test those hypotheses using the techniques available. Comparing one closely spaced sample with the next can reveal morphologically isolated and continuous lineages, which it is reasonable to infer represent lines of genetic descent (Kellogg, 1983; Malmgren and Berggren, 1987; Hodell and Vayavananda, 1993; Wei, 1994). Specimens with intermediate morphologies representing morphological links between one species and another (intergrading morphotypes) can be shown to exist (see Section 6.4 below).

The relatively complete planktonic foraminiferal fossil record lends itself well to the stratophenetic method, which has traditionally been the tool of choice for the micropalaeontologist. This method, as employed by Gingerich (1979, 1990), Kennett and Srinivasan (1983), Bolli and Saunders (1985), Cifelli and Scott (1986), Fordham (1986) and Pearson (1993, 1998) among others, is used to establish close phylogenetic relationships between morphologically similar taxa from compatible stratigraphic ranges. However, since the advent of cladistics, many phenetic taxonomies have been shown to be inadequate (Smith, 1994), so cladistic testing of pre-existing planktonic foraminifera phylogenies could still provide useful data to help reconcile taxonomic controversies and refine current taxonomies. Unlike cladistics, stratophenetic solutions *do* report information about ancestor-descendant relationships. This technique is often criticised because results are subject to an investigators own understanding of a specific taxonomy.

The Holy Grail of phylogenetic methods would be to successfully combine the objectivity and repeatability of cladistics with the value of stratigraphic information, especially that of relatively (stratigraphically) complete groups e.g., marine plankton. Stratocladistics was developed to do this, however as shown later, is limited by user manipulation and non-exhaustive solution-searching of the type used in cladistics (see Fisher, 1988, 1994; Fox *et al.*, 1999 for review). Using this method, stratigraphic range data can be coded as a phylogenetically informative character and included in a cladistic analysis. In this study, cladistic and stratocladistic solutions were matched with known

stratigraphic ranges. In some cases, large potential *ghost ranges* were isolated (e.g. <10 My), i.e. "an entire branch of an evolutionary tree for which there is no fossil record, but which needs to be hypothesised after combining cladistic and biostratigraphic data" (Norell and Novacek, 1992). The relatively high stratigraphic resolution in planktonic foraminifera acts as a 'quality control' for cladistic solutions. It is 'unacceptable' to sustain 10 My ghost ranges. In a group with high fossil resolution, it is highly unlikely that this amount of range could be overlooked!

Likelihood (probability) methods have also been developed to test the range of hypotheses consistent with the data. Using this method, probabilities are assigned to each topology for each data type, then for each topology the likelihoods for each type of data are combined and the greatest score is selected as the best topology. This method is at the moment limited to combining DNA data and stratigraphy (Huelsenbeck and Crandall, 1997), and has not been applied to morphologic data.

Arguably, the community needs an objective method that combines character and range data, and can be tailored to suit the level of record 'completeness' versus the reliability of the range data. In such a method an investigator would form a compromise between the range and character data. In the case of planktonic foraminifera, range data would hold higher rank over character data and the acceptable ghost range threshold would be low, i.e. when reconciling most parsimonious cladistic solutions against known stratigraphic ranges. Unfortunately, a fully objective method for reconciling cladistics with range data was not achieved here. The strength of this study is derived from the combination of phylogenetic approaches to evaluate previously published ideas about the evolution of several Neogene *Globorotalia* lineages from a common ancestor, and to suggest alternative hypotheses for the taxonomic relationships between the taxa concerned. Cladistics constitutes the objective basis, the taxonomic relationships from which are tested using published stratigraphies, stratocladistics and detailed knowledge of the Neogene fossil record. The result is a better understood phylogeny, which qualifies anagenesis and could be used to construct more accurate taxonomy and therefore range data charts (of the type used in Chapter 2) to study evolutionary rates.

The subgenera included are Bandy's (1972) *Menardella*, *Hirsutella*, and *Truncorotalia* with the *Globorotalia s.s.* lineage. See Chapter 1 for discussion.

6.1.2 Cladistic questions to be answered

In Chapter 5 (Section 1.1) a number of questions were posed that morphometrics attempted to address (1-8 below). The phylogenetic techniques used in this chapter will attempt to support the answers to some of those questions and further extend the line of questioning with reference to the Neogene *Globorotalia* lineages. The answers to the following additional questions (9-15 below) are sought through use of cladistics, stratocladistics and stratophenetics. Of questions 1-8, those with an asterisk can potentially be further addressed using the methods in this chapter. Questions two, six and seven can only be partially assessed with cladistics, using taxonomic proximity. Questions 3-5 were slightly altered to suit the nature of the analysis technique (see brackets), based on the assumption that morphologic and phylogenetic proximity are synonymous.

1) Are *Gr. praescitula* and *Gr. archeomenardii* distinct morphospecies?

2) *Are *Gr. limbata* and *Gr. pseudomiocenica* synonyms describing the same form?

3) *Is *Gr. pseudomiocenica* morphologically similar (related) to *Gr. miocenica*?

4) *Is *Gr. multicamerata* more morphologically similar (related) to *Gr. menardii* or *Gr. limbata*?

5) *Is *Gr. multicamerata* morphologically similar (related) to *Gr. pertenuis-exilis*?

6) *Are *Gr. pertenuis* and *Gr. exilis* distinct morphospecies?

7) *Are *Gr. menardii* 'A', 'B', *cultrata* and *fimbriata* distinct morphospecies?

8) *Are *Gr. merotumida* and *Gr. plesiotumida* distinct morphospecies and are they closely allied in shape to *Gr. tumida*?

---

9) Are the menardellid and *Globorotalia s.s.* lineages sufficiently similar to support phylogenetic linkage?

10) Through which species are the menardellid and *Globorotalia s.s.* lineages linked?

11) Is *Gr. praescitula* a likely ancestor to the *Menardella, Hirsutella, Truncorotalia* and the *Globorotalia s.s.* stocks?

12) Is *Gr. scitula* a likely 'core' progenitor to some of the lineages?

13) Do the above stocks form distinct clades using cladistic analysis?

14) What are the interspecific phylogenetic relationships within the hirsutellids?

15) Are *Gr. juanai* and *Gr. challengeri* part of a larger hirsutellid clade?

16) Through which taxon are the truncorotaliids linked to the other *Globorotalia*?

17) Are the truncorotaliid morphospecies easily distinguished using cladistics?

6.2 Phylogeny of multiple *Globorotalia* lineages

6.2.1 The *Globorotalia* taxa under analysis

Cifelli and Scott (1986) hint that *Globorotalia praescitula* may be the common ancestral species to a monophyletic group of Neogene planktonic foraminifera, which includes the *Globorotalia s.s.* lineage, Bandy's (1972) subgenera *Menardella* and *Hirsutella* and Cushman and Bermudez' (1949) subgenus *Truncorotalia*. Figure 1.7 and the discussion in Chapter 1 presents this proposed phylogeny and a review of the literature. To test this hypothesis, an analysis including all 44 taxa from these groups was executed. Well-documented synonyms of the taxa from these groups are also included in the analyses. The taxa are listed below.

Most of the taxa included in the taxonomic groups listed above are included in the analysis, however there are a few that are excluded. Originally Blow (1969), and later Kennett and Srinivasan (1983) endorsed the hypothesis of the *Globorotalia s.s.* lineage descendancy from the non-keeled *Gr. lenguanensis-paralenguanensis* couplet. These taxa were not included because they share general morphology and wall texture with the fohsellids and are unlikely ancestral to the *Globorotalia s.s.* lineage. These authors also considered *Gr. pseudomiocenica* as a junior synonym of *Gr. limbata* (Blow, 1969; Kennett and Srinivasan, 1983), however new observations and analyses (Plate 1.1, Chapter 1; Chapter 5) reveal that the two morphospecies can be consistently separated, thus these species were coded separately and included in the final cladistic phylogeny.

Bolli's (1970) *Gr. menardii* morphospecies, *'A'* and *'B'*, *Gr. cultrata* and *Gr. fimbriata*, were coded for the cladistic analysis to test their affinity to *Gr. menardii s.s.*

Finally, *Gr. miozea* has previously been proposed as the descendent of *Gr. praescitula* and the ancestor of *Gr. praemenardii* (Scott, 1972), however, was not included in the analysis because it is a member of the globoconellids. See Chapter 1 (Section 1.3.3.4) for taxonomic discussion.

Included taxa are as follows:

Globorotalia s.s. lineage

1. *Globorotalia fimbriata* (Brady)
2. *Globorotalia flexuosa* (Koch)
3. *Globorotalia merotumida* Blow and Banner
4. *Globorotalia plesiotumida* Blow and Banner
5. *Globorotalia praescitula* Blow (outgroup to the cladistic analysis)
6. *Globorotalia tumida* (Brady)
7. *Globorotalia ungulata* Bermudez

Menardellids

8. *Globorotalia archeomenardii* Bolli
9. *Globorotalia cultrata* (d'Orbginy)
10. *Globorotalia exilis* Blow
11. *Globorotalia limbata* (Fornasini)
12. *Globorotalia menardii s.s.* (Parker, Jones and Brady)
13. *Globorotalia menardii* 'A' Bolli
14. *Globorotalia menardii* 'B' Bolli
15. *Globorotalia miocenica* Palmer
16. *Globorotalia multicamerata* Cushman and Jarvis
17. *Globorotalia pertenuis* Beard
18. *Globorotalia praemenardii* Cushman and Stainforth
19. *Globorotalia pseudomiocenica* Bolli and Bermudez

Hirsutellids

20. *Globorotalia bermudezi* Rögl and Bolli
21. *Globorotalia cibaoensis* Bermudez
22. *Globorotalia challengeri* Srinivasan and Kennett
23. *Globorotalia hirsuta* (d'Orbigny)

24. *Globorotalia juanai* Bermudez and Bolli
25. *Globorotalia margaritae* Bermudez and Bolli
26. *Globorotalia margaritae evoluta* Cita
27. *Globorotalia margaritae primitiva* Cita
28. *Globorotalia praemargaritae* Catalano and Sprovieri
29. *Globorotalia scitula* (Brady)
30. *Globorotalia scitula gigantea* Blow
31. *Globorotalia theyeri* Fleisher

Truncorotaliids

32. *Globorotalia cavernula* Bé
33. *Globorotalia crassaconica* Hornibrook
34. *Globorotalia crassaformis* (Galloway and Wissler)
35. *Globorotalia crassaformis hessi* Bolli and Premoli-Silva
36. *Globorotalia crassaformis oceanica* Cushman and Bermudez
37. *Globorotalia crassaformis ronda* Blow
38. *Globorotalia crassaformis viola* Blow
39. *Globorotalia crassula* Cushman and Stewart
40. *Globorotalia tosaensis* (Takayangi and Saito)
41. *Globorotalia tosaensis tenuitheca* Blow
42. *Globorotalia truncatulinoides* (d'Orbigny)
43. *Globorotalia truncatulinoides* excelsa *Sprovieri and Ruggieri*
44. *Globorotalia truncatulinoides pachytheca* Blow

6.2.2 Phylogenetic coding

The characters used in the analysis were coded in a phylogenetically conservative manner, i.e. mostly unordered and multistate, none of which were weighted. Characters were coded as ordered (1 character) only when a well-documented evolutionary trend could be shown. The coding of multistate characters prevents default weighting towards the groups that do not possess the character, as in binary coding. Inapplicable characters were used when certain multistate characters were absent or reduced in certain taxa and

coded as not applicable ('*?*') e.g., keel type: delicate (*0*), medium (*1*), thick and robust (2), no keel (*?*). This is considered a conservative coding method and further prevents weighting towards those taxa without a certain character, as a monophyletic group (Strong and Lipscomb, 1999).

All morphospecies were originally coded from holotype descriptions and images. Where the original literature was not available the holotype reproductions in Bolli and Saunders (1985) were used, and in some cases type material (see Chapter 1). To support morphospecies characteristics further descriptions and images from Kennett and Srinivasan (1983) were utilised together with new SEM photomicrographs of assemblages from ODP sites 1195, 926 and 871. The character data matrix for all cladistic analyses in this chapter is given in Appendix 6.1.

6.2.2.1 Test decoration

Although used extensively in the construction of Palaeocene planktonic foraminifera phylogenies (Hemleben *et al.*, 1999), wall texture characteristics do not show great variation in the small number of *Globorotalia* morphospecies considered here. Pustulation and encrustation occur in some morphospecies and typically vary with size. Although individual test pores covary with specimen size, species-specific variations in perforation density are noticeable. Most planktonic foraminifera add a component of gametogenic calcite to the test during this phase of their life cycles (Hemleben *et al.*, 1989). Gametogenic calcite extent is species-specific, i.e. some morphospecies consistently add greater components to their tests than others (e.g. *Gr. tumida*, *Gr. flexuosa*). This is evident through the presence of thicker umbilical pustules and more swollen tests. Thus differential gametogenesis is summarised by certain character states in a number of characters, because it is easier to separate the differing effects of gametogenesis on the test rather than gametogenesis as a whole.

Character 1: Surface texture

State 0: pseudo-honeycomb

State 1: smooth.

There is some support for the derivation of the Neogene menardellid *Globorotalia* from the *Paragloborotalia,* a group of compressed, reticulate planktonic foraminifera

lacking keels (Cifelli and Scott, 1986; Scott *et al.*, 1990). As already discussed, there is growing evidence that *Globorotalia* is derived from benthic foraminifera. Despite the origins, the paragloborotaliid 'honeycomb' surface texture is only relict in *Globorotalia praescitula* and sometimes occurs on the earlier chambers (Plate 1.1, Chapter 1), albeit in a weak form. Here this texture is termed *pseudo-honeycombed* for the purpose of this character definition. None of the more derived morphospecies from the menardellid and *Globorotalia s.s.* lineages retain this primitive feature. This character was coded as ordered for this is a clearly documented evolutionary trend.

The analyses were also performed with this character coded as unweighted, in which *Gr. praescitula* occupied the same basal position as proposed in figures 6.5 and 6.6.

Character 2: Depression around pores

State 0 – present

State 1 – absent

This character refers to forms that commonly possess a test surface which possesses pronounced depressions around the pores creating a less smooth finish to the test. This character was only coded from chambers preceding the final chamber because the final chamber is not always fully developed at death.

Character 3: Umbilical pustules

State 0 – consistently present

State 1 – absent

Pustules decorating the early chambers and the umbilical periphery are common in all morphospecies. Morphology is commonly conical and size generally decreases towards the periphery. Pustules have been observed to act as anchor points for rhizopodia (thin fibrilar bodies projecting from the test) (Hemleben *et al.*, 1989), thus the larger and more mature specimens tend to have larger pustules presumably to support longer rhizopodia. The degree of pustulation may therefore be related to species-specific food gathering strategy. More encrusted pustules are likely formed during gametogenic calcification and may reflect a degree of specimen maturity, however, similar pustule morphology is

encountered in the same morphospecies and is primarily species-specific. Those taxa defined as *absent* although occasionally exhibit umbilical pustules, generally do not.

Character 4: Umbilical pustule morphology

State 0 – fine

State 1 – medium

State 2 – coarse

State ? – not applicable

Character 5: Bulk umbilical pustule position

State 0 – 1st 2.5 chambers

State 1 – 1st 4 chambers

State 2 – whole umbilical side

Character 6: All shoulders pustulate

State 0 – present

State 1 – absent

This character refers to the common occurrence of a well-developed, dense pustule-concentration projecting from all chamber *shoulders* around the umbilicus. All shoulders pustulate is only common in the *Globorotalia s.s.* lineage.

Character 7: Pustule fusing

State 0 – present

State 1 – absent

This character unites taxa that attain a level of pustulation whereby the pustules start to fuse together to form a more encrusted test. This feature is common in the *Truncorotalia.*

Character 8: Spiral side pustulation

State 0 – present

State 1 – absent

Character 9: Pustulate keel

State 0 – present

State 1 – absent

State ? – lacking a keel

Character 10: Test perforation density

State 0 – sparsely perforate

State 1 – densely perforate

All the globorotaliid species included in the analysis typically have a test surface with pores 2-7 μm in diameter. Test perforation density varies between species, with the more delicately built species generally exhibiting lower pore density. This character was tested using high magnification microscopy of the penultimate chamber. Those taxa that displayed >2 pore widths between pores were coded as sparsely perforate, while those with ≤2 pore widths (on average) between pores were coded as densely perforate.

In general, the taxa with more delicate tests tend to be sparsely-perforate, e.g. *Gr. merotumida* and *Gr. ungulata*, however, there appears to be no link between previously established subgeneric groupings and pore density. Some authors have suggested pore size is related to temperature in some modern taxa (see Hemleben *et al.*, 1989, for review), although not all.

6.2.2.2 Keel morphology

The presence and development of a keel around the test periphery is an important phylogenetic characteristic in planktonic foraminifera (Caron, 1985). Most globorotaliids concerned have been described as possessing a keel of one form or another, except, for example, *Gr. praescitula* which was described (Blow, 1959) as exhibiting a *"sub-acute periphery although not keeled"*. Specimens of this morphospecies commonly exhibit an imperforate band, although morphological intergradation with *Gr. archeomenardii* is observed in ODP Hole 871A material (Plate 1.1, Chapter 1). *Gr. praescitula* marks the problems of early holotype descriptions and the hand sketches used to depict the type specimens. Although the description alludes to the absence of a keel, the illustration seems to suggest the presence of one. In this case, additional published work and new

observations needed to be employed. A hypotype viewed at the Smithsonian NMNH did not have a keel. Unfortunately, the holotype was not viewed on this occasion.

Keel development in the menardellid lineage is accompanied by axial compression of chambers. Edge morphology progresses from a broad, sweeping arched chamber-edge (*Gr. praescitula*), to a definite imperforate fold in the test (*Gr. menardii*) (Plates 1.1-1.2, Chapter 1). In contrast, the other lineages show a less directed keel development pattern. A number of characters relating to the keel structure and morphology are discussed below:

Character 11: Imperforate band

State 0 – present

State 1 – absent

Although keels are imperforate, the term *imperforate band* refers to a thickness of test (where the keel would be) that is partially or wholly imperforate, but distinctly less perforated than the rest of the chambers in the specimen. For example, *Gr. praescitula* was coded as not possessing a keel, instead this taxon displays an imperforate band around the periphery. The *Gr. archeomenardii* holotype possesses a keel, however, some of the specimens from ODP Hole 871A possess an imperforate band or a hybrid of the two features. This example represents one of the problems of coding characters for species that exhibit great intrapopulational mixing.

Character 12: Keel

State 0 – present

State 1 – partial keel

State 2 – absent

This refers to any clear imperforate axial projection that can be delineated from the rest of the test. *Gr. archeomenardii* possesses a primitive keel, which is often not developed into the true keel fold that many of the other taxa possess, although some morphotypes do possess a definite keel structure. Other morphospecies such as *Gr. crassaformis ronda* and *Gr. challengeri* are non-keeled.

Character 13: Edge morphology

State 0 – low, sweeping arched edge (e.g. *Gr. praescitula* Plate 1.1, Chapter 1)

State 1 – clear angular development of the edge structure (e.g. primitive *Gr. archeomenardii* keel – Plate 1.1, Chapter 1)

State 2 – distinct lip lacking folded test (e.g. *Gr. praemenardii* Plate 1.1, Chapter 1)

State 3 – True keel with developed fold (e.g. *Gr. menardii* Plate 1.2, Chapter 1)

State 4 – Distinct asymmetric edge/keel as seen in *Gr. truncatulinoides.*

State 5 – bulbous non-keeled edge as exemplified by *Gr. challengeri.*

A true keel is represented by a definite lip-like extensional fold of the test periphery in the axis of coiling (plates 1.1-1.10, Chapter 1; i.e. states 2-4 below).

Figure 6.1. Edge morphologies coded for cladistic analysis. Numbers in brackets denote the character state.

Character 14: Keel thickness

State 0 – delicate and thin

State 1 – medium keel

State 2 – robust, thick keel

This character is scaled semi-quantitatively relative to the taxa under analysis. *Gr. cultrata* represents state 0 (maximum test thickness in edge view is ≥10 thicknesses of basal keel), while *Gr. tumida* represents state 2 (maximum test thickness is ≤4 thicknesses of basal keel). All the other taxa fall somewhere in between these limits. Keel thickness cannot be defined by absolute widths because it is a function of test size.

Character 15: Keel curvature

State 0 – linear

State 1 – slightly curved

State 2 – curved

State 3 – strongly curved

State ? – not applicable

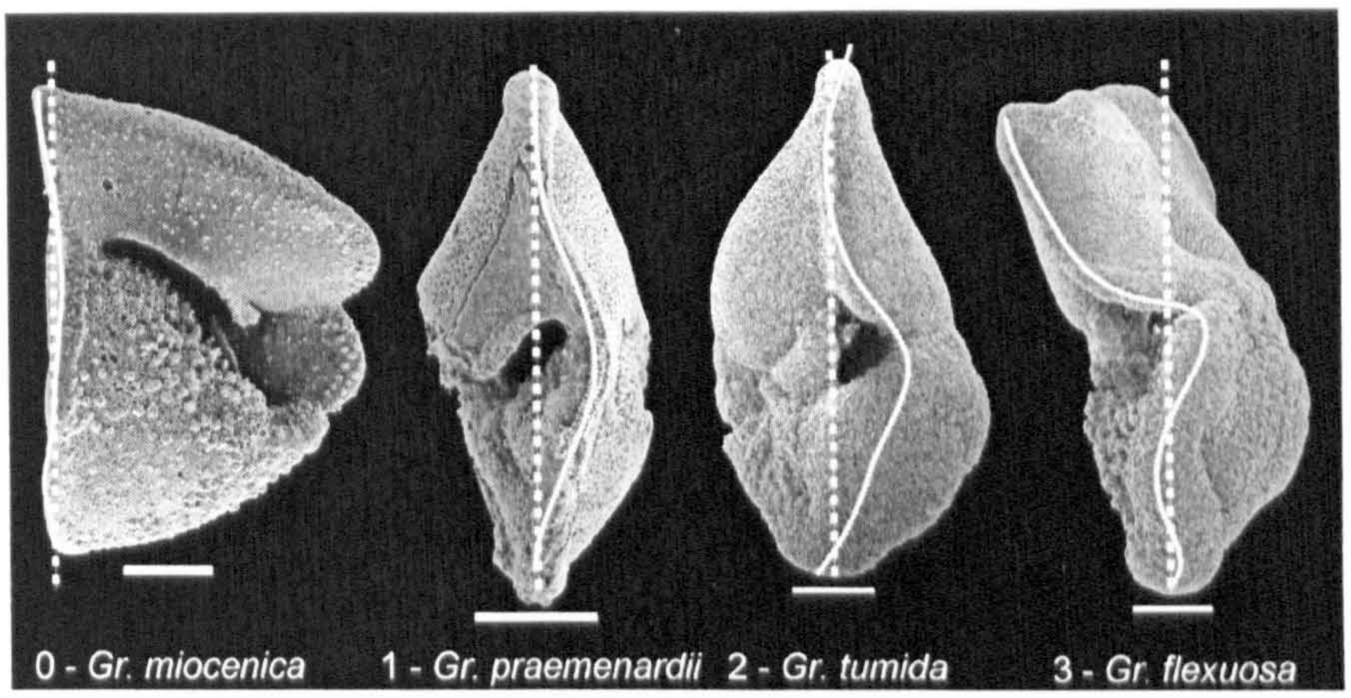

Figure 6.2. Keel curvature. How much the keel deviates from a plane when observing a specimen in edge-view.

Keel curvature (Figure 6.2) refers to how much the keel deviates from a hypothetical straight coiling plane. Increasing keel curvature in these lineages becomes apparent in the more extreme morphologies e.g., the development of *Gr. flexuosa* and *Gr. pertenuis*. The morphospecies with the larger chamber numbers often display greater degrees of curvature.

Character 16: Radially flared keel pustules

State 0 – present

State 1 – absent

These structures commonly occur only in the morphospecies *Gr. fimbriata* and probably represent ecophenotypic variation of the *Gr. menardii* or *Gr. cultrata* morphospecies. *Gr. cultrata* sometimes exhibits an irregular keel edge, but not to the same degree as *Gr. fimbriata*.

6.2.2.3 Chamber configuration

This group of characters describes the arrangement of the chambers relative to one another. Some of these characters are partially dictated by ontogeny, yet they are all species-specific, providing the specimens coded are fully mature.

Character 17: Test coiling

State 0 – low trochospire

State 1 – very low trochospire

State 2 – lenticular trochospire

State 3 – medium trochospire

State 4 – high trochospire

The Neogene globorotaliids usually display trochospiral (conical-helical) coiling of differing degrees. Most taxa have a low trochospirally-coiled test. Certain taxa have tests with flat spiral sides (e.g. *Gr. miocenica* and *Gr. truncatulinoides*) and thus a very low trochospirally-coiled test. Those taxa whose tests are almost planispiral and lens-shaped in edge-view (e.g. *Gr. exilis*) were coded as state 2.

Character 18: Coiling direction

State 0 – >75% sinistral

State 1 – >75% dextral

State 2 – neither

State ? – unknown

Coiling attitude was measured directly from the site 1195, 926 and 871 assemblages. 150 specimens were picked for each morphospecies from each timeslice they were present in (see Appendix 6.2). Most of the morphospecies were sampled from multiple sites and timeslices, so the coiling percentages were averaged e.g., if one morphospecies was sampled from three timeslices, the percentages were combined, then a percentage of the total calculated. Taxa with over 75% coiling in either direction were coded with either 0 or 1, while those with <75%, were coded as 2. State ? was applied to *Gr. fimbriata*, which was not present in any of the assemblages.

Character 19: Test whorl number

State 0 – 2

State 1 – 2.5

State 2 – 3

For this character it was necessary to identify adult specimens only from material because this characteristic varies with ontogeny.

Character 20: Number of chambers in final whorl

State 0 – 5 or less

State 1 – 6

State 2 – 6-8

State 2 – >8

Character 21: Chamber size increase continuity

State 0 – uniform

State 1 – non-uniform

Chamber size continuity describes the regular/uniform or irregular/non-uniform size increase as the chambers develop.

Character 22: Tumidity (degree of swelling)

State 0 – none/low

State 1 – medium

State 2 – high

In edge view, tumidity qualitatively assesses the degree of swelling/inflation of the whole test (affinity to the shape of a pear) and does not refer to individual chamber shape. Increasing tumidity probably results from greater gametogenic calcite addition.

6.2.2.4 Aperture characteristics

The umbilical side of the test contains most of the morphological information that is used in morphospecies identification, to which the aperture-umbilical arrangement are of vital utility. The aperture shape is commonly dictated by the axial-compression of the test and the level of apertural-lip development. Unlike the Cretaceous globotruncanids, aperture-umbilical morphology in the Neogene globorotaliids is relatively conservative. All the taxa considered in this analysis have an interiomarginal (umbilical-extraumbilical) aperture, therefore aperture positioning cannot be used as an informative character.

Character 23: Edge view aperture linearity

State 0 – linear and flat

State 1 – arched

The aperture tends to be long, thin and linear in attitude when the test is more discoidal and compressed, thus the more oblate the test the more arched the aperture (in edge view). For example, the more menardiform morphospecies tend to appropriate aperture morphology of state 0.

Character 24: Edge view truncated apertural arch

State 0 – present

State 1 – absent

Many of the taxa under analysis have apertures that are curved into, and terminated before reaching the keel. However, the type specimens of *Gr. miocenica* and *Gr. pseudomiocenica, Gr. multicamerata* and *Gr. ungulata* possess an aperture that appears truncated by the edge of the keel. These were coded as 0.

Character 25: Edge view aperture semicircularity

State 0 – present

State 1 – absent

Character 26: Apertural lip shape

State 0 – thin and linear

State 1 – plated

State 2 – flared

State 3 – thick linear

Of the apertural characters, lip morphology is probably one of the most phylogenetically useful. Character state 1 describes the taxa with lips that resemble half a dinner plate, while state 2 describes taxa with flared, broad lips. The former delineates the menardellid taxa, while the latter unites *Gr. pertenuis* and *Gr. multicamerata* (see Bolli,

1970; Bolli and Saunders, 1985). The type specimen of *Gr. exilis* (Blow, 1969) does appear to have a plate-like lip, but this specimen has also been shown to display multi-lobed flared morphology (Bolli, 1970; Kennett and Srinivasan, 1983; Cifelli and Scott, 1986; Pearson, 1995b). Observations from ODP sites 1195 and 926 corroborate this finding, thus *Gr. exilis* is coded as states '1 & 2'.

Character 27: Lip symmetry

State 0 – symmetrical

State 1 – asymmetrical

Lip symmetry further defines the taxa with symmetrical plated and linear lips.

Character 28: Umbilicus

State 0 – small, narrow, shallow

State 1 – small, narrow, deep

State 2 – wide and shallow

State 3 – closed

State 4 – wide and deep

6.2.2.5 General Geometry

Character 29: Test biconvexity

State 0 – asymmetrically biconvex

State 1 – equally biconvex

Test biconvexity refers to the degree of convexity about the central keel-parallel axis. Typically, the Neogene *Globorotalia* are asymmetrically biconvex about the central axis (in edge view), excluding some of the more discoidal, compressed forms.

Character 30: Spiral side geometry

State 0 – flat

State 1 – weakly convex

State 2 – convex

State 3 – strongly convex

State 4 – flat concave

Character 31: Equatorial peripheral shape

State 0 – quasi-circular/circular

State 1 – weakly lobulate

State 2 – lobulate

State 3 – ovate

State 4 – sub-angular

State 5 – subquadrate

The equatorial peripheral shape delineates the shape of the specimen in the plane of coiling, perpendicular to the coiling axis. This varies from circular in *Gr. miocenica* to ovate (egg-shaped) in *Gr. tumida* and sub-angular in *Gr. praescitula*. *Lobulate* defines those lobed shapes between circular and ovate forms.

Character 32: Axial periphery

State 0 – acute

State 1 – medium obtuse

State 2 – wide obtuse

State 3 – planoconvex

Axial periphery describes the angle to the edges of the final chamber from the axial plane (vertical). *Acute* approximates to an angle of <20°, *medium obtuse* – 20-30°, *wide obtuse* – 30-45°, and *planoconvex* refers to the flat spiral-sided (*Gr. miocenica*) forms.

Character 33: Conical test form

State 0 – present

State 1 – absent

This character describes how close the edge view test-shape is to a cone. This feature is common to the truncorotaliids, although not all. Although conical test forms are highly trochospiral, not all trochospiral test forms are conical.

Character 34: Edge view final chamber point tapering

State 0 – present

State 1 – absent

This character describes the presence of tapering in the final chamber in edge view e.g., the final chamber of *Gr. truncatulinoides* tapers to a fine point as do some of the taxa closely-related to it.

6.2.2.6 Spiral Suture morphology

Character 35: Spiral sutures

State 0 – raised and non-limbate

State 1 – raised and limbate

State 2 – flush-slightly depressed

The spiral sutures are *raised* when each chamber is lifted above the level of the later chamber. *Limbate* sutures are those that are bordered by a lip (raised edge), which equates to the old keel trace.

Character 36: Spiral suture curvature

State 0 – obliquely curved

State 1 – strongly curved

State 2 – recurved

State 3 – quasi-straight to straight

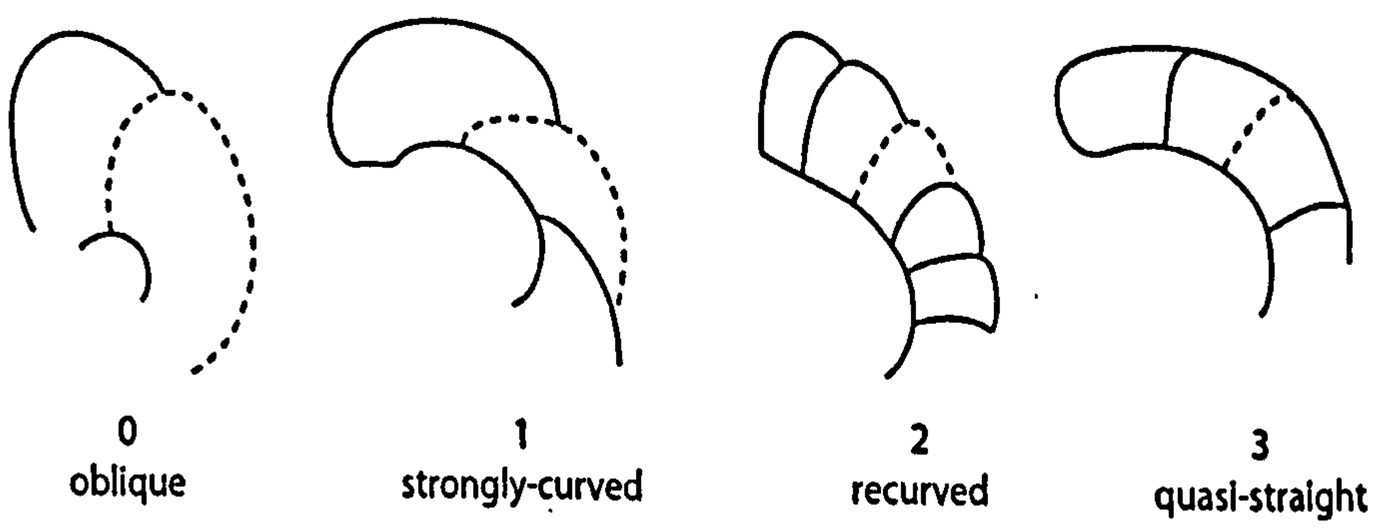

Figure 6.3. Spiral suture curvature types. The dashed line indicates to which suture each state refers.

Obliquely curved spiral sutures are those that curve obliquely backwards so that the sutural trace resembles a hemisphere (e.g. *Gr. tumida*). *Strongly curved* applies to those with spiral sutures in one continuous sweeping curve radiating from the central spire (e.g. *Gr. menardii*), while *recurved* applies to those sutures that curve most at the periphery (*Gr. exilis*), i.e. there are two portions of the suture with distinct angles of curvature. See Figure 6.3 above.

Character 37: Spiral suture-peripheral continuity

State 0 – undulose

State 1 – partially joining periphery

State 2 – fully joining periphery

This character describes how the chamber sutures meet the test periphery. Those that form clear undulose chamber traces on the peripheral edge were coded as state 0 (e.g. *Gr. exilis*), while those that merge into a continuous, unbroken edge/keel were coded as state 2 (e.g. *Gr. truncatulinoides*).

Character 38: Down-stepping spiral suture overlap

State 0 – present

State 1 – absent

This describes the significant drop from one chamber to another along the chamber edge as you travel through the whorl away from the spire centre. This is a feature apparent in some hirsutellid and truncorotaliid taxa.

Character 39: Spiral sutural overlap

State 0 – present

State 1 – absent

This character describes a feature where later chambers compress into and obscure the spiral sutures.

Character 40: Umbilical sutures

Obliquely curved spiral sutures are those that curve obliquely backwards so that the sutural trace resembles a hemisphere (e.g. *Gr. tumida*). *Strongly curved* applies to those with spiral sutures in one continuous sweeping curve radiating from the central spire (e.g. *Gr. menardii*), while *recurved* applies to those sutures that curve most at the periphery (*Gr. exilis*), i.e. there are two portions of the suture with distinct angles of curvature. See Figure 6.3 above.

Character 37: Spiral suture-peripheral continuity

State 0 – undulose

State 1 – partially joining periphery

State 2 – fully joining periphery

This character describes how the chamber sutures meet the test periphery. Those that form clear undulose chamber traces on the peripheral edge were coded as state 0 (e.g. *Gr. exilis*), while those that merge into a continuous, unbroken edge/keel were coded as state 2 (e.g. *Gr. truncatulinoides*).

Character 38: Down-stepping spiral suture overlap

State 0 – present

State 1 – absent

This describes the significant drop from one chamber to another along the chamber edge as you travel through the whorl away from the spire centre. This is a feature apparent in some hirsutellid and truncorotaliid taxa.

Character 39: Spiral sutural overlap

State 0 – present

State 1 – absent

This character describes a feature where later chambers compress into and obscure the spiral sutures.

Character 40: Umbilical sutures

State 0 – depressed and radial

State 1 – depressed and slightly curved

State 2 – depressed and sinuous

Character 41: Umbilical sutural overlap

State 0 – present

State 1 – absent

6.2.2.7 General chamber characteristics

All characters concerning the final chamber shape were coded using either the type specimen or actual specimens considered to be mature and without anomalous final chamber forms.

Character 42: Final (umbilical) chamber elongation

State 0 – not elongate

State 1 – elongate

State 2 – elongate and flexuose

Final chamber elongation refers to the umbilical view of the final chamber. This is apparent only in some of the *Globorotalia s.s.* lineage taxa.

Character 43: Final spiral chamber shape

State 0 – B1

State 1 – B2

State 2 – B3

State 3 – C

State 4 – D

The final spiral-side chamber shape types were defined by Bizon and Glaçon (1978) and adapted by Cifelli and Scott (1986). The classification is based on the angular position of the leading margin and the location of the trailing margin. The types specific to this study are shown in Figure 6.4.

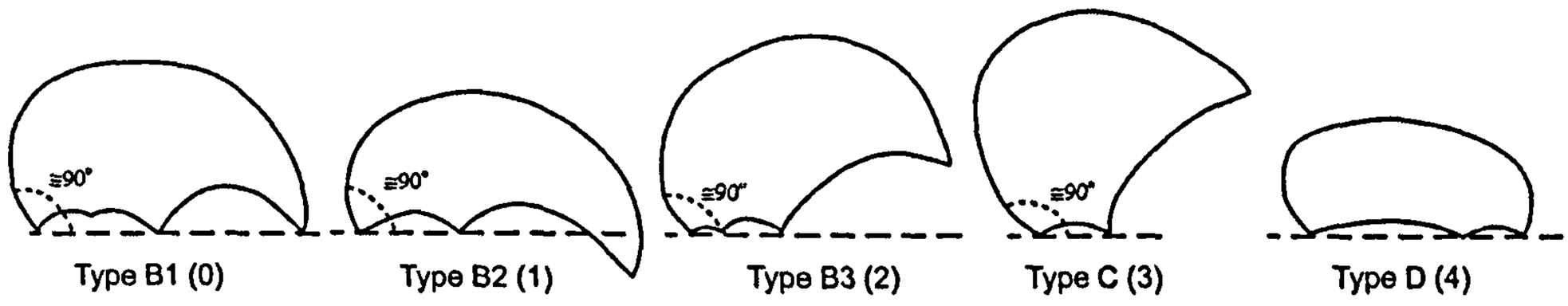

Figure 6.4. Classification of the spiral shapes of chambers, adapted from Bizon and Glaçon (1978). Numbers in brackets indicate the cladistic coding state.

Character 44: Final umbilical chamber shape

State 0 – wedge

State 1 – angular-rhomboid

State 2 – triangular

Character 45: Chamber globosity

State 0 – globose

State 1 – partially globose

State 2 – not globose

Character 46: Chamber flaring

State 0 – markedly flared

State 1 – completely absent

Flaring denotes the protrusion of chambers radially from the spire centroid.

Character 47: Larger penultimate than ultimate chamber in majority of specimens

State 0 – present

State 1 – absent

Character 48 - Edge view final chamber wider than previous

State 0 – present

State 1 – absent

State ? – n/a

This character refers to the breadth of the final chamber if looking at the apertural view. When the final chamber is wider (i.e. terminates furthest from the spiral side), it was coded as state 0. Where previous chambers are wider, the state 1 is applicable. This is only relevant to the more planoconvex forms.

Character 49: Edge view final chamber embracement

State 0 – totally embracing

State 1 – partially embracing

State ? – non-embracing

This character describes the umbilical view of the test where the final chamber stretches across the width and 'embraces' the previous chambers and the whole test. This is exemplified in the holotype of *Gr. hirsuta.*

6.2.2.8 Stratigraphic coding

Cladistic trees were not originally designed to include stratigraphic information. This is (allegedly and controversially) one of the primary disadvantages of using cladistics against stratophenetics. When cladistics is used for a group with an excellent fossil record the analysis results can suggest sister-group relationships between taxa that may have seemingly impossibly reconcilable ranges in time. Fisher proposed that stratigraphy could add important information to the cladistic analysis of palaeontological data and developed the stratocladistic methodology (Fisher, 1988; 1994). This method uses parsimony to reduce homoplastic and missing range hypotheses (Fox *et al.*, 1999). Fisher (1994) and Fox *et al.* (1999) describe this method in detail, while the latter also concluded that stratocladistics is more accurate than cladistics at reconstructing phylogeny, even with an incomplete fossil record. These authors suggest that disregarding stratigraphic data excludes valuable evidence from cladistic analysis. They calculated, that with a fossil record greater than 60% incomplete, stratocladistics will provide a better match to a known 'true' tree. The fossil record of Cenozoic planktonic foraminifera is well refined for use in biostratigraphy and is likely to be sufficiently complete for appropriate use of the stratocladistic method. Stratigraphy was coded as follows:

Character 50: Stratigraphy

State 0 – M2-M3

State 1 – M4-M5

State 2 – M6-M7

State 3 – M8-M9

State 4 – M10-M11

State 5 – M12-M13a

State 6 – M13b-PL1a

State 7 – PL1b-PL2

State 8 – PL3-PL6

State 9 – PT1a-PT1b

The stratigraphic states were coded with two Berggren *et al.* (1995) biozones per character state for the full range of the taxa under analysis (exceptions occur in short zones). A taxon was coded with all the character states, which cover its full range, i.e. if a species range covered biozones M2-M7, the taxon was be coded as '*0&1&2*'. The stratocladistic method of Fisher (1994) and Fox *et al.* (1999) to enable use of stratigraphic information is described below.

6.2.3 Cladistic and stratocladistic methodology

All characters were coded for the 44 taxa listed in Section 6.2. Character 1 was coded as ordered, while all other characters were coded as unordered with the exception of character 50, which was coded as 'stratigraphic'. The stratigraphic character was not included in the original cladistic analysis using PAUP because this character type is not recognised by this software. *Gr. praescitula* was chosen as the outgroup/root for the succession because this taxon has been suggested as common ancestor to the Neogene globorotaliid lineages under analysis (as discussed in chapters 1 and 4).

The Program PAUP 4.04 (PPC) (Swofford, 2000) was used to execute parsimony analysis on the data matrix. The analysis was configured to a heuristic search of 100 replicates, using stepwise addition and tree bisection-reconnection (TBR) branch swapping. The number of replicates used maximises the chance of locating the most parsimonius tree (MPT) solution.

The stratocladistic method described in Fox *et al.* (1999) was used to activate the stratigraphic data. The multistate stratigraphic character can be read and further defined as *stratigraphic*, using MacClade version 3.07 (Maddison and Maddison, 1997). MacClade was used to order by length, the MPTs consistent with the stratigraphic character. Branches were then swapped manually until the tree with the shortest length was found, which is thought to be the closest to the stratocladistic tree (Harcourt-Brown, 2001).

6.3 Results and discussion

The cladistic analysis produced 283 equally most parsimonious solutions. The strict-consensus tree (Figure 6.5) contains only those relationships found in all of the 283 solutions, while the majority-rule consensus tree (Figure 6.6) contains those relationships that occur in >50% of the 283 solutions. In both figures, the remaining relationships are defined as polytomies (node at the base of 3> branches). The numbers at specific nodes in Figure 6.6 denote the percentage of MPTs that included that specific relationship. Those nodes with no associated figures occur in <50% of the MPTs.

The stratocladistic tree (Figure 6.7) was constructed using the procedure outlined in Section 6.2. With the activation of the stratigraphic character, the cladistic tree length (number of character state changes) was increased from 303 to 377. This was then reduced to 344 by manually swapping branches in MacClade.

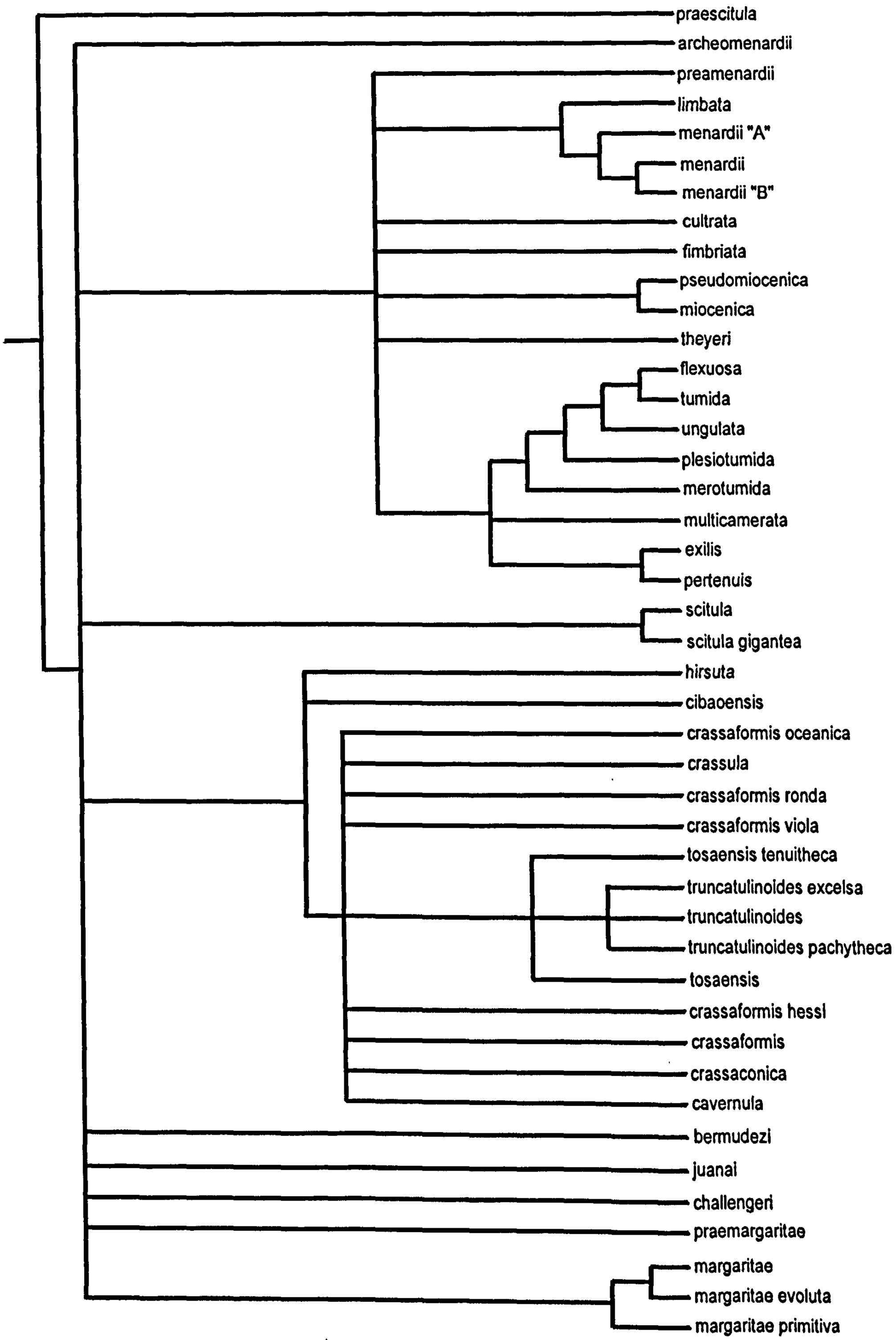

Figure 6.5. Strict consensus cladistic phylogeny of 283 most parsimonious tree solutions of the selected 44 Neogene *Globorotalia* taxa. Tree length - 354, C.I. - 0.33, R.I. - 0.6.

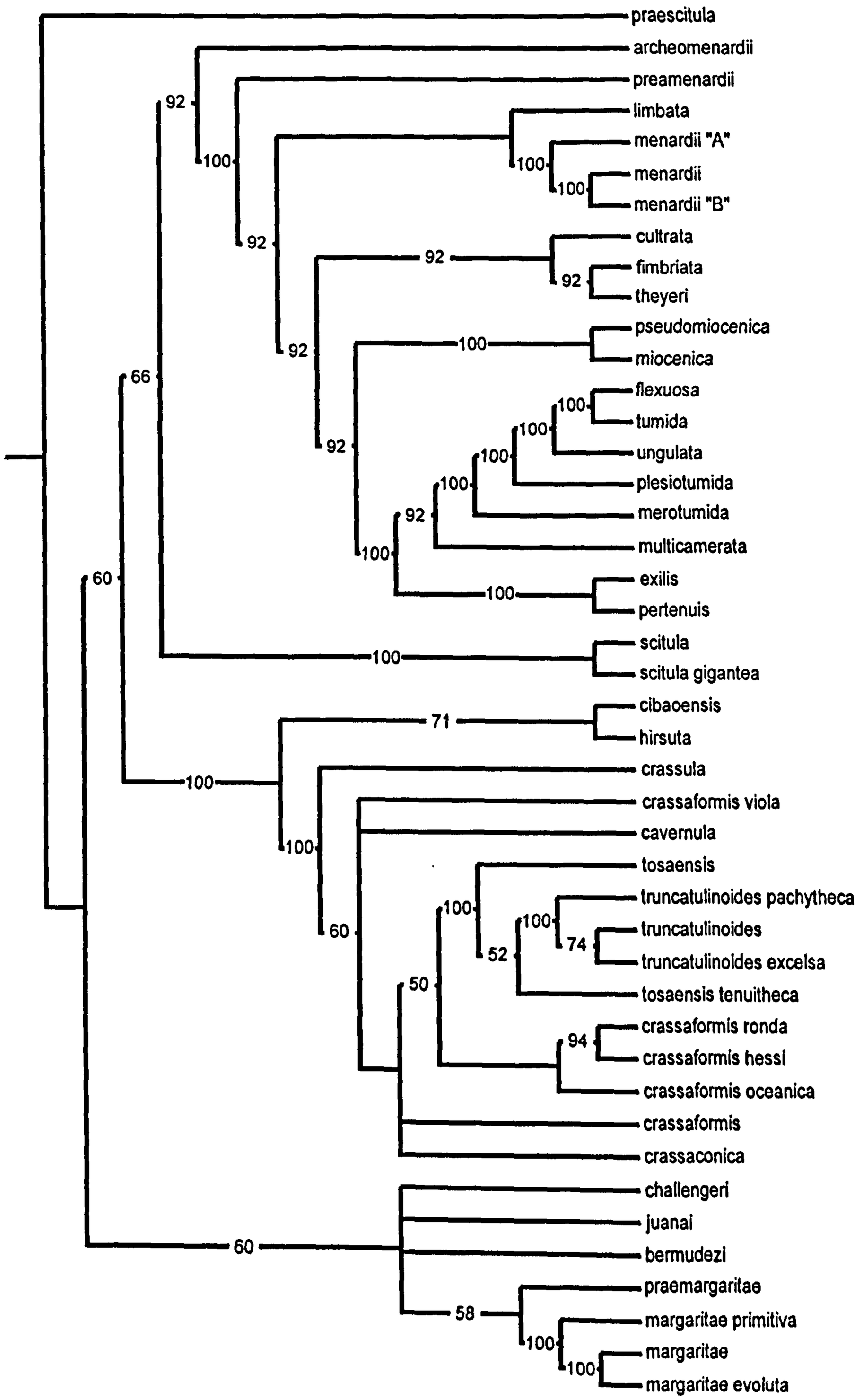

Figure 6.6. Majority rule consensus cladistic phylogeny of 283 most parsimonious tree solutions for 44 Neogene *Globorotalia* taxa. Number at nodes represent bootstrap support for that node. Nodes with no numbers had a bootstrap support of <50%. Tree length - 303, C.I. - 0.39, R.I. - 0.68.

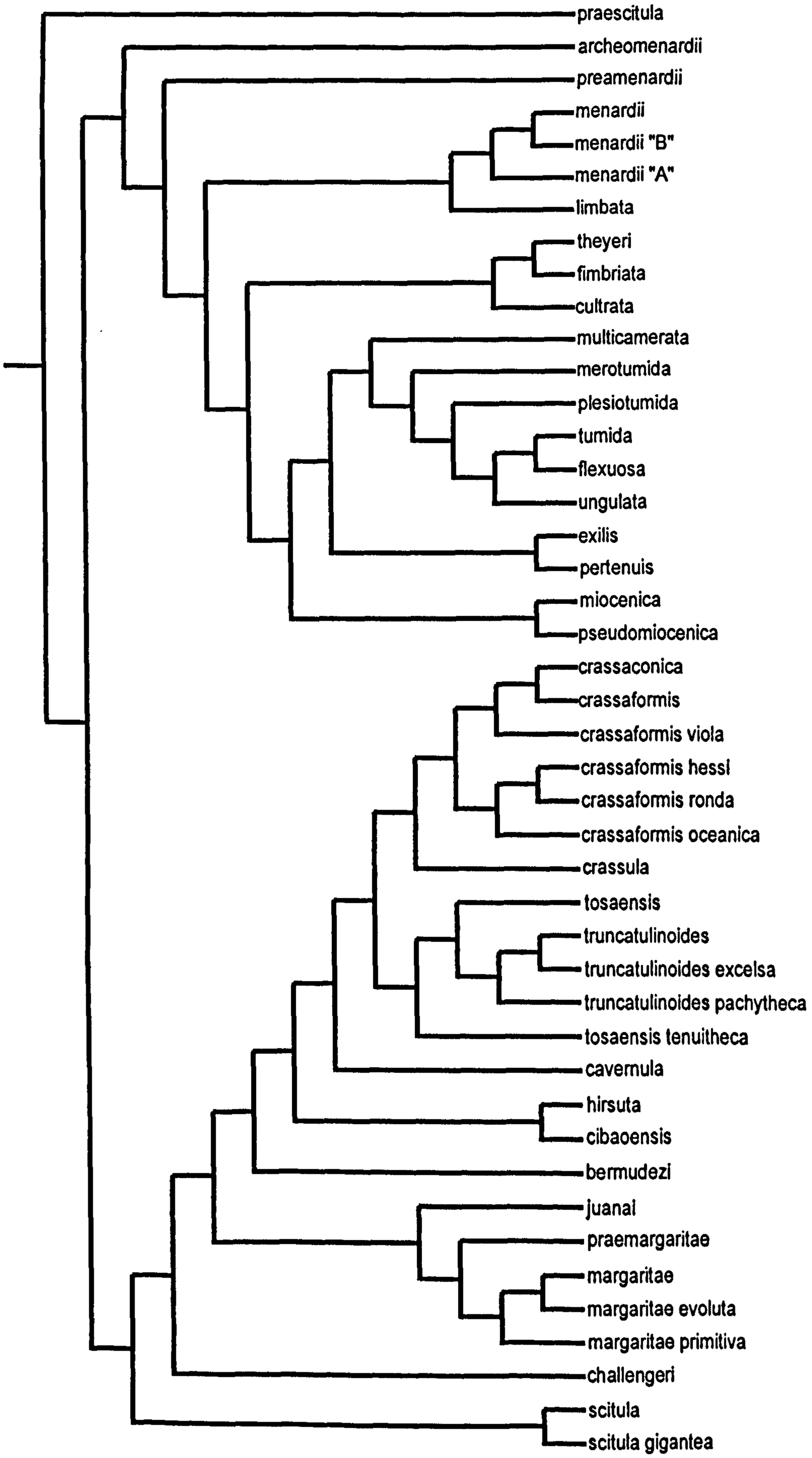

Figure 6.7. Stratocladistic phylogeny of the 44 selected Neogene *Globorotalia* taxa. Tree length - 344, C.I. - 0.39, R.I., 0.68.

Three metrics were used to measure each tree (see captions in figures 6.5-7). These are tree length, Consistency Index (CI) and Retention Index (RI). CI is calculated from the number of homoplasies that must be assumed in the most parsimonious solution (Smith, 1994). Lower CI (scale of 0-1) is thought to result from high levels of homoplasy. A CI of near 0.5, with reference to a specific character, suggests that in the MPT the specific character has changed twice, either by way of secondary loss of the derived state within the clade or convergent evolution in a second clade. The RI measures the proportion of terminal taxa that preserve the character identified as a synapomorphy (shared derived character) for that group (Smith, 1994). RI is also an indicator of homoplasy. High values supports low amounts of homoplastic change. The cladistic (figures 6.5 and 6.6) and stratocladistic (Figure 6.7) trees have similar values for CI that may be consistent with high levels of homoplasy in the dataset.

6.3.1 Summary of relationships

From the cladistic and stratocladistc analyses a number of key relationships can be extracted. (1) The *Globorotalia s.s.* clade is consistently expressed in all the trees, as is the *Gr. menardii* morphospecies clade (with *Gr. limbata*) and the juxtaposition of *Gr. miocenica-Gr. pseudomiocenica*, which have all been previously suggested in the literature. (2) All results support the basal association of *Gr. praescitula-Gr. archeomenardii-Gr. praemenardii*. (3) The analysis results also commonly juxtapose *Gr. exilis* with *Gr. pertenuis*. (4) In the majority-rule (Figure 6.6) and stratocladistic trees (Figure 6.7) *Gr. scitula* appears to serve as the link between the menardine-*Globorotalia s.s.* clade and the hirsutellid-truncorotaliid clade. (5) The truncorotaliids are grouped in the cladistic and stratocladistic trees, within which the *Gr. truncatulinoides* and *Gr. tosaensis* morphospecies are united. (6) While the *Gr. margaritae* morphospecies are also commonly united, the remaining hirsutellids (*Gr. bermudezi, Gr. challengeri, Gr. juanai, Gr. theyeri, Gr. cibaoensis* and *Gr. hirsuta*) do not consistently occupy specific positions.

The reason the hirsutellid taxa are not resolved into one clade (as might be suggested by their taxonomic subgeneric level) may be because *Hirsutella* simply groups taxa descended from *Gr. scitula,* which form discrete and possibly unrelated sublineages as implied by Kennett and Srinivasan (1983).

These relationships discussed here formed the basis for the phylogeny of the *Globorotalia* presented below.

6.3.1.1 Combining phylogeny and stratigraphy

How can the two different types of data be weighted against one another? There can be no fully objective solution, because the data are of entirely different categories. So as a procedural step to investigate the problem further, the published range data from a number of sources were superimposed on the phylogenetic trees. The range data used in this chapter came from the 'Plankrange' dataset presented in Chapter 2 (see Appendix 2.1) and ultimately the published sources used to construct this dataset. In figures 6.8 and 6.9, the majority-rule consensus tree and the stratocladistic tree are combined with the range data, respectively.

If a hypothetical phylogeny (i.e. including ghost ranges) has a total survival time (total ranges) greater than that of a 'true' phylogeny (i.e. all known ranges added together), then one can assume there is some inaccuracy in the phylogeny or the stratigraphy. In this study the stratigraphy is assumed to be fully 'reliable'. Compared to the majority of palaeontological datasets, that of the planktonic foraminifera is fairly well resolved.

Here, minimum survival time (total aggregate of known stratigraphical range) for the 44 *Globorotalia* taxa in this study is 153.2 My. The total survival time, including the grey extended-range portions forced by the trees, is 219 My (cladistic tree) and 201.8 My (stratocladistic tree); implying an 'age debt' of 65.8 and 48.6 million years of cryptic phylogeny. 'Range' only refers to published range (black lines) or ghost range forced by the tree, that extends from the published range (grey). This clear discrepancy of ~50-70 My between the solutions (presented here) and the *true* phylogeny can not be reasonably sustained given the number of globally-correlated stratigraphies that document the ranges of the taxa concerned.

The stratocladistic phylogeny did succeed in reducing the total range time by reducing some of the ghost lineages. This may indicate a utility in this method, however, a very large discrepancy still exists. A number of taxa exhibit considerable ghost range in either or both the cladistic and stratocladistic trees presented in figures 6.8 and 6.9: *Gr. menardii, Gr. fimbriata, Gr. miocenica, Gr. ungulata, Gr. multicamerata, Gr. pertenuis, Gr. hirsuta, Gr. cavernula, Gr. crassaformis viola, Gr. crassaformis hessi, Gr. juanai* and *Gr. bermudezi.*

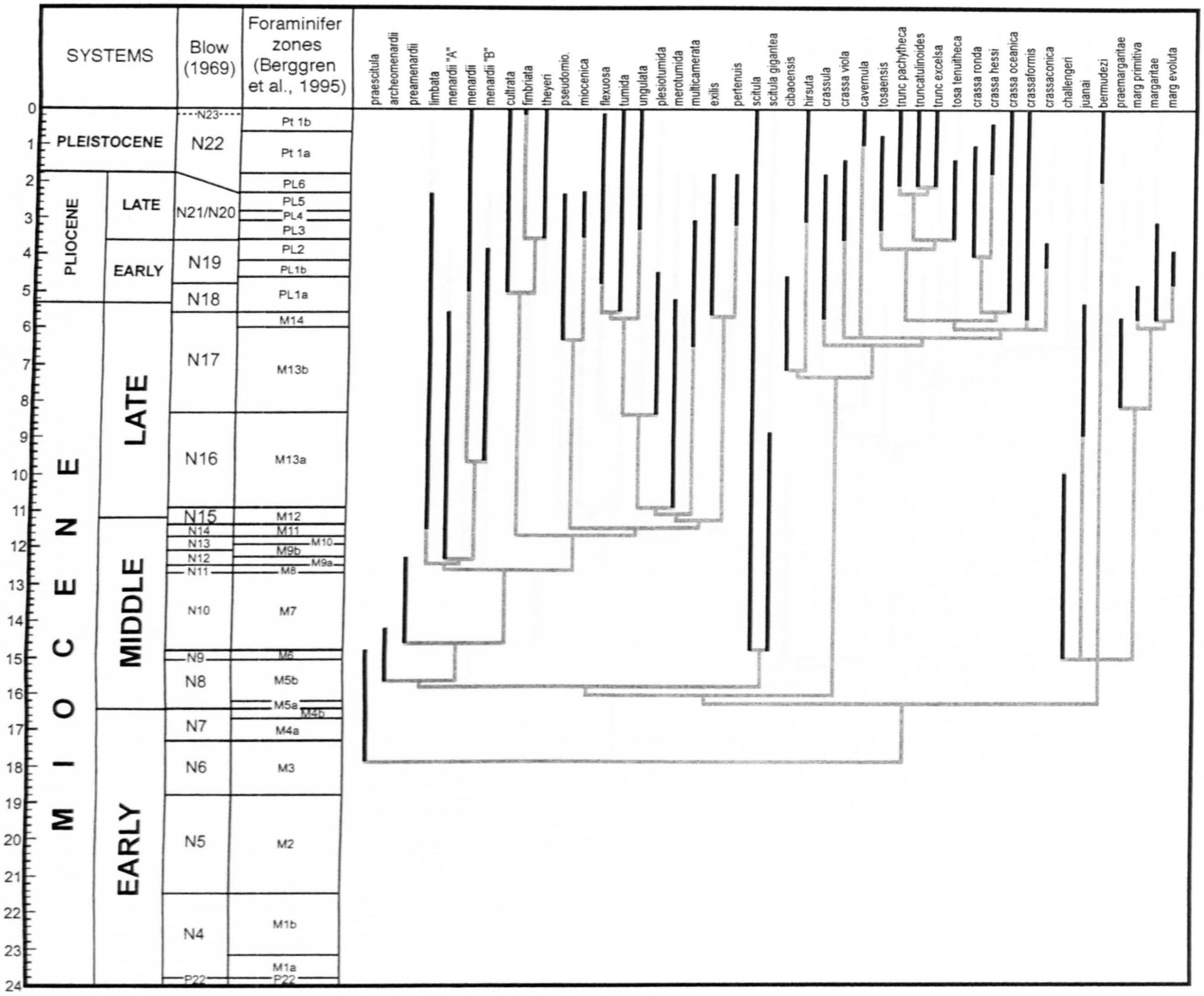

Figure 6.8. Consensus cladistic phylogeny (from Figure 6.6) of four Neogene *Globorotalia* lineages (*Menardella, Hirsutella, Truncorotalia* and the *Gr. tumida* lineage) superimposed underneath the established stratigraphic ranges of the taxa involved. The ranges represent the maximum reported ranges from Kennett and Srinivasan (1983) and Bolli and Saunders (1985). Ghost ranges in grey.

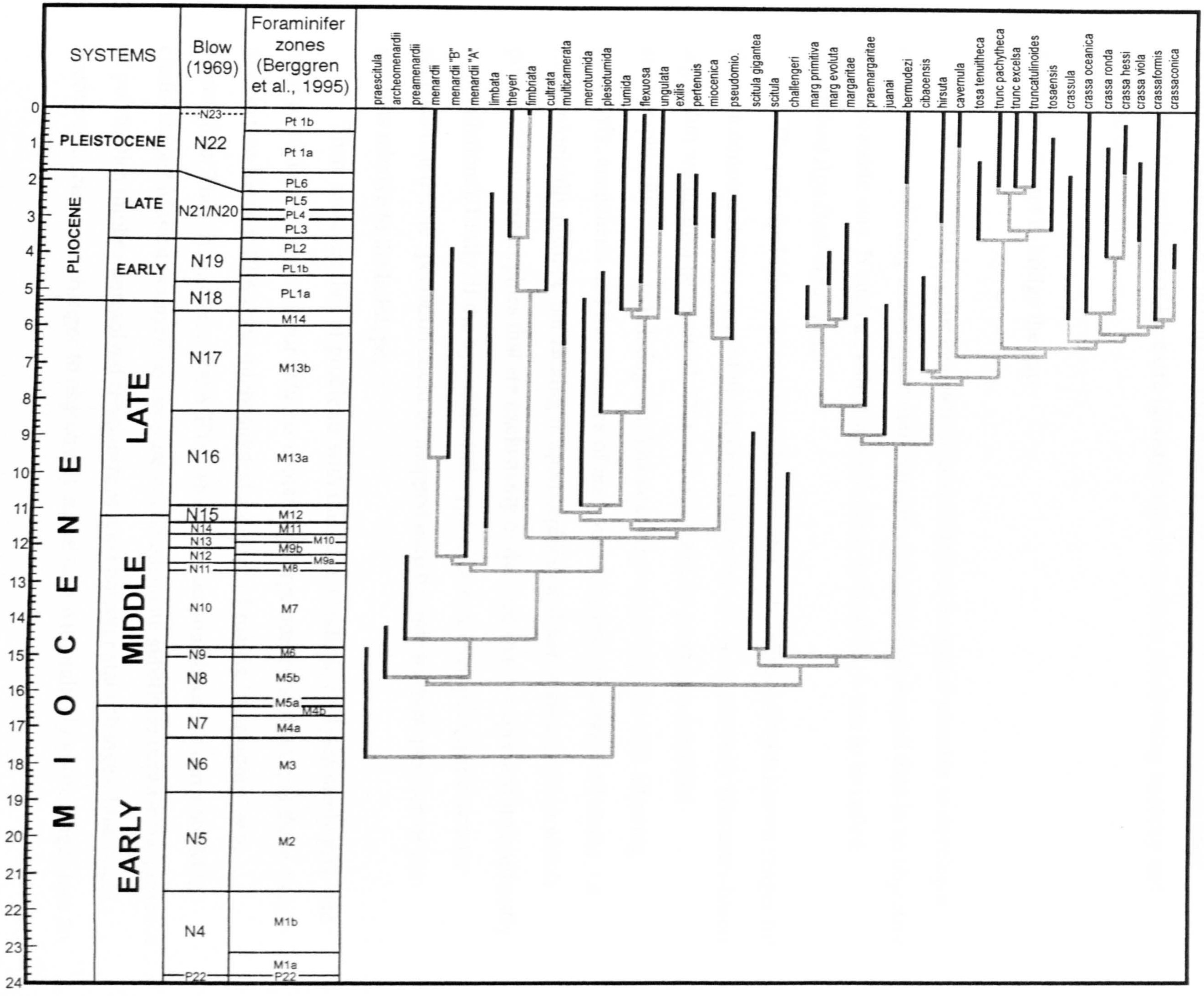

Figure 6.9. Stratocladistic phylogeny (from Figure 6.7) of selected Neogene *Globorotalia* lineages (*Menardella, Hirsutella, Truncorotalia* and the *Gr. tumida* lineage) superimposed underneath the established stratigraphic ranges of the taxa involved. The ranges represent the maximum reported ranges from Kennett and Srinivasan (1983) and Bolli and Saunders (1985). Ghost ranges in grey.

These ghost ranges are partly produced by the position of the taxa within in the phylogeny, however, without 'massaging' (and removing the objectivity) of the data matrix it would be difficult to account for these obvious deficiencies using only cladistics. More importantly, the cladistic procedure does not allow for anagenesis, paraphyly (which probably applies to most taxonomic groups); does not accept that ancestry can be isolated in the fossil record and does not handle multiple descendance from a single ancestor well. Multiple descendance can only be expressed by the presence of an unresolved node. Arguably, the majority of the extra (ghost) range result from disallowing ancestry and multiple descendancy.

6.3.2 An attempt to bridge the gap

While conducting the analyses discussed above, it *seemed* possible to develop a method for combining stratigraphic and character-based morphological data in an objective and repeatable way. If such a method were to come to fruition, it was to be called *Minimised Age Debt cladistics!*

The principal idea was to take a cladistic tree and combine it with known ranges for the taxa concerned. The removal of all ghost ranges by use of a systematic character-based algorithm would then be required. This could potentially produce a modified stratigraphically-calibrated cladogram. The next step would then involve allowing paraphyly, anagenesis and the presence of *metataxa* (any taxa of unresolved status, i.e. morphologically distinct, but lacking in apomorphies) and *parametataxa* (taxa which possess >1 autapomorphies that are exclusively of the type that is expressed intermittently in populations). Lastly, if the age of the holotype is known, then principal character changes that define speciation could be mapped onto the tree to show position of the changes relative to the holotype.

There are a number of problems with this idea. Cladistic analyses rarely give one most parsimonious solution for datasets containing large numbers of taxa; in those cases that do (see Sereno, 1999) one might suggest a degree of matrix 'massaging' was responsible. Thus, if you have 500 MPTs, which tree do you choose to carry out MAD cladistics on? Majority-consensus trees are not an adequate substitute because the presence of polytomies implies unresolved relationships and character state changes. One might choose character state changes to objectively move taxa with unlikely ghost ranges into an

'acceptable' position, i.e. find a position with congruent stratigraphy requiring fewest character state changes. However, if this was the *modus operandi*, then by moving one taxon, a new tree is created with different character state changes, tree length, CI, RI, *etc.* Cladistics will not allow this procedure for removing implausible ghost ranges by translocating taxa. Although less of a problem, defining anagenesis in a lineage is dependent on an investigators own experience of the taxa concerned, and is still partially subjective. Furthermore, an attempt was made to temporally position the holotype specimens of several taxa on a specific portion of the relevant taxon range, which unfortunately succumbed to the inaccuracies and ambiguities of the holotype literature!

The search for a method to successfully combine morphologic and stratigraphic data goes on. In the mean time, must micropalaeontologists just accept the solutions produced by cladistics and stratocladistics (figures 6.8 and 6.9)? It would be difficult to find a working biostratigrapher who would endorse these phylogenies. All would agree, however, that they are in part useful in discerning 'true' phylogeny.

6.4 Reconciling the phylogenies

The results presented above do show a number of differing relationships that may be the result of convergence and reversals in foraminiferal evolution and incorrect or imprecisely defined stratigraphic ranges. The differences may also result from the way characters are defined and weighted. Some characters may be more indicative of phylogeny, than others. An analysis of the RI of characters approximates how well the characters 'fit' the resultant MPTs. This revealed that characters related to test shape showed most tendency to convergence, while those related to wall texture and edge morphology were usually less convergent and therefore more indicative of phylogeny. No characters were extrinsically weighted in these analyses, however, breaking down a linked character complex can produce a similar effect. This is generally unavoidable if character coding is to remain objective. The taxa under analysis here do not vary significantly, thus isolating characters was made more difficult and splitting characters was partially unavoidable.

The stratocladistic method suffers from the same kind of subtle weighting problems, however in this case, stratigraphy is coded and given the same character weight as all other characters. In order to keep the analyses as subjective as possible stratigraphy

was not weighted, although when analysing a group that possesses relatively complete stratigraphy; it intuitively holds a great deal more importance in terms of taxonomic relationships than other characters. To infer anything but the smallest of ghost range is probably erroneous in this case.

Stratophenetics does utilise stratigraphy and morphology to produce phylogenetic hypotheses, *but* it is inherently subjective. However, using the common relationships expressed in the cladistic and stratocladistic analyses to create a phylogeny, may remove a large proportion of the subjectivity. To these relationships (described in Section 6.3.1), selected cases of anagenesis and multiple ancestry can then be added where observed in the fossil record. The taxa that exhibit unlikely ghost ranges were then repositioned using the stratophenetic method.

Figure 6.10 is a composite phylogeny of Neogene *Globorotalia* taxa (outlined in Chapters 1 and 6), which reconciles the information presented in both the cladistic and stratocladistic trees with published phylogenetic theories and the morphometric results presented in Chapter 5. The shaded areas reflect observed and hypothesised intrapopulational intergradation of morphologies. Despite consistent viable relationships being expressed in the cladistic and stratocladistic trees, several inconsistencies still had to be resolved to construct Figure 6.10 (discussed below). *Gr. praescitula* and its descendent *Gr. scitula* constitute likely progenitors to all the taxa in Figure 6.10, with some possible distinct lineages, i.e. the menardellids (discussed in Section 6.2.5), the truncorotaliid taxa and the *Gr. margaritae* group with some isolated smaller clades. A feature common to the trees is a distinct truncorotaliid clade at the base of which are the hirsutellids, *Gr. cibaoensis* and *Gr. hirsuta*. Kennett and Srinivasan (1983) also suggested *Gr. cibaoensis* as the link between the hirsutellids and the truncorotaliids.

The *Gr. margaritae* group resolve well in both trees, from which the similar overall morphologies of *Gr. hirsuta* and *Gr. theyeri* can be linked using stratophenetics to form a discrete ancestry from *Gr. scitula*. *Gr. theyeri* is consistently expressed within the *Gr. cultrata-fimbriata* clade. This highlights the inability of the cladistic method to effectively delineate some forms. Plates 1.9-1.10 (Chapter 1) show clearly the similarity between *Gr. hirsuta* and *Gr. theyeri*, with *Gr. margaritae*. They all share highly compressed, thin tests with a lobulate equatorial periphery and crescentic (to flared) spiral chamber shape. *Gr. hirsuta* then developed greater spiral curvature and heavy pustulation, while *Gr. theyeri* became smooth, more planoconvex with enhanced chamber flaring.

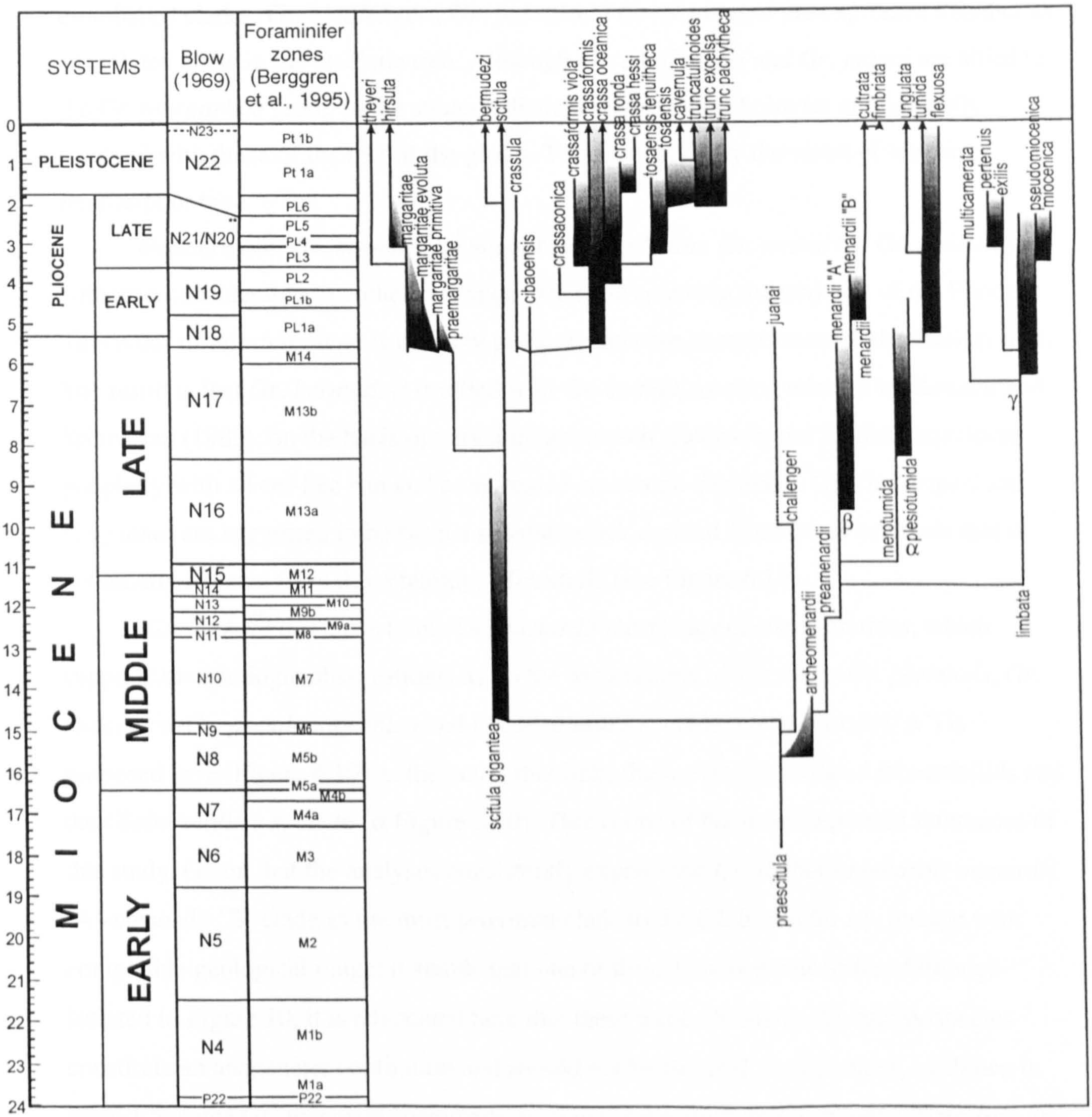

Figure 6.10. Composite phylogeny of selected Neogene *Globorotalia* lineages created through the reconciliation of cladistic, stratocladistic and stratophenetic data. Ranges plotted here are total published range time, some of which are derived from multiple sources. Dotted lines indicate hypothesised extra range to validate the taxonomic associations. Shading indicates between-taxon intrapopulation morphological variation (either observed or hypothesised). The symbols α, β and γ are referred to in the text.

Gr. theyeri only superficially resembles the *Gr. cultrata-fimbriata* morphotypes and likewise for *Gr. hirsuta* to *Gr. cibaoensis*.

The remainder of Bandy's *Hirsutella* do not resolve so well with any of the established clades. *Gr. challengeri*, *Gr. juanai* and *Gr. bermudezi* are expressed together as an isolated clade in the cladistic tree. Although *Gr. challengeri* and *Gr. juanai* are allied to the *Gr. margaritae* group in the stratocladistic tree, their morphologies are not easily resolved with those of the rest of the group. This is most likely the result of lumping feature-poor taxa.

Furthermore, *Gr. bermudezi* cannot be derived from *Gr. juanai* (or *Gr. challengeri*) without a considerable hypothetical range extension spanning the majority of the Pliocene. This order of inferred range is unlikely given the relative completeness of the fossil record. The result is that *Gr. bermudezi* is allied with *Gr. scitula*, as also endorsed by Kennett and Srinivasan (1983), on the basis of very similar smooth, biconvex and lobulate equatorial periphery with a keel-like rim and compressed crescentic chambers. *Gr. challengeri* and *Gr. juanai* are suggested to be from a separate stock derived from *Gr. praescitula* that is potentially isolated from the remaining *Hirsutella* (see Figure 6.10).

Gr. limbata lies close to the *Gr. menardii* morphospecies in both trees, which supports morphologic observations; as do the associations of *Gr. exilis-Gr. pertenuis*, *Gr. miocenica-Gr. pseudomiocenica* and *Globorotalia s.s.* clade. *Gr. menardii* ('A') is proposed here (Figure 6.10) as the taxon that links the previously isolated menardellids and the *Globorotalia s.s.* clade (α Figure 6.10). This is one of the most important inferences of this study. Given that the analyses consistently express the *Gr. limbata-menardii-menardii* 'A'-*menardii* 'B' clade as the most proximal clade to the *Globorotalia s.s.* lineage with compatible geological range; it stands that one of these taxa is the ancestor. Although isolated in Figure 10, it is advocated here that these three *Gr. menardii* morphospecies constitute an anagenetic continuum and should not be isolated. Furthermore, as shown in Plate 1.5, some *Gr. menardii* specimens display great affinity to *Gr. tumida*. Therefore, in Figure 6.10 the *Gr. menardii* bioseries provides a link between the menardellid and *Globorotalia s.s.* lineages.

Gr. limbata connects the menardellid sublineages (β and γ - see Figure 6.10). This unity implies that the menardellids and *Globorotalia s.s.* should not be taxonomically isolated and perhaps the subgeneric nomen *Menardella* should be discarded in favour of the senior synonym *Globorotalia*. In total, 13 characters (numbers 10, 14, 15, 18, 21, 22,

26, 30, 31, 36, 37, 42 and 43) define the *Globorotalia s.s.* clade within the menardellid clade. These characters principally involve keel morphology, chamber shape, lip shape, tumidity and spiral suture morphology. Thus a substantial weight of the character matrix supports this clade within the menardellids. As discussed in Section 1.3.3.3 (Chapter 1), some authors acknowledge some similarity between these lineages, but do not describe why they are kept apart in phylogenies. Ultimately, this is the greatest problem with stratophenetics; an individual decides if two taxa/lineages/genera are unrelated, and often no justification is given.

In summary, the phylogeny presented in Figure 6.10 represents a culmination of the morphometric analysis presented in Chapter 5; the cladistic, stratocladistic and stratophenetic analysis presented in this chapter and new observations of material collected during ODP Leg 194 (and others). Given the tools available, this is an attempt to optimise the phylogeny of the four globorotaliid lineages introduced in Chapter 1.

6.4.1 Creating a lineage phylogeny

As outlined in Chapter 2, morphospecies-level range data may contain a component of error as a result of the typological taxonomic system not being able to identify anagenesis in the fossil record. Using the composite phylogeny presented here (Figure 6.10) it is possible to follow Fordham's (1986) lineage approach and quantify cladogenesis versus anagenesis in the globorotaliid record.

In Figure 6.11 the composite phylogeny (of Figure 6.10) is given (A) and anagenesis is isolated (B). Actual times of cladogenesis and extinction (as opposed to pseudospeciation and pseudoextinction) are also proposed (C). This method used here was modified from Pearson (1993).

Figure 6.11 demonstrates the separate 'clades' (shaded bubbles) in the taxa analysed in this chapter. *1* isolates the majority of the hirsutellids, *2* isolates the truncorotaliids and *3* isolates the menardellids and *Globorotalia s.s.* lineage. This leaves *Gr. challengeri* and *Gr. juanai* in a separate lineage derived from *Gr. praescitula*. The same groupings are shown in figures 6.8-6.10, although not as clearly. This result supports the inclusion of the menardellid taxa and the *Globorotalia s.s.* taxa as a single monophyletic unit under one generic nomen, i.e. *Globorotalia*.

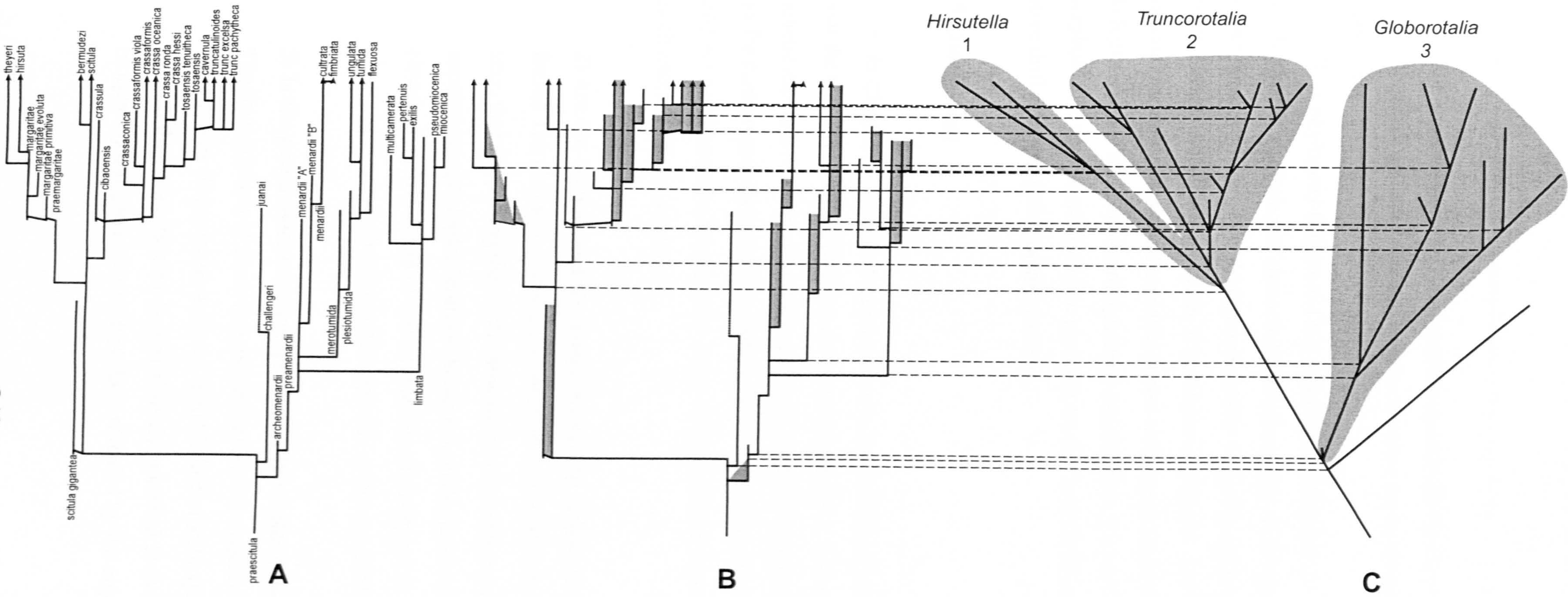

Figure 6.11. Suggested lineage phylogeny of the *Globorotalia* based on multiple phylogenetic analyses. (A) Dendrogram records the stratigraphical ranges of morphospecies linked to show hypothesised evolutionary relationships. (B) Population observation reveals that some morphospecies are linked by intermediates (grey shading). (C) A lineage phylogeny documents actual cladogenesis (as opposed to pseudospeciation or pseudoextinction). The lineage phylogeny reveals three primary branching events (1-3), the majority of the hirsutellids (1), the truncorotaliids (2) and the menardellids+*Globorotalia s.s.* (3). Approach modified from Pearson (1993).

The separation of the *Truncorotalia* and the *Hirsutella* is also supported here. These subgenera could be elevated to generic status for taxonomic and biostratigraphic simplicity.

This phylogeny (Figure 6.11C) is fully acknowledged as a subjective composite of morphometric, cladistic and stratocladistic information. It is highly unlikely to find favour among those who deny any phylogenetic utility in stratigraphic information, and insist on a purely objective cladistic approach. It is, however, testable. The branching points in the diagram, for example, should correlate better with genetic information than either the cladogram or the traditional stratophenetic phylogenies. It can also be modified by further morphometric and biostratigraphic research on the Neogene *Globorotalia* from existing or future drill sites and stratigraphic sections.

6.5 Conclusions

In Chapter 5 a series of questions were defined to address phylogenetic questions about the taxa involved through the use of morphometrics, followed by cladistic and phenetic methods. The morphometric analyses produced a series of results that paved the way for further analysis using the methods discussed in this chapter. Those questions that could not be addressed adequately by using morphometrics alone (outlined in Section 6.1, this chapter) are discussed below:

2) Are *Gr. limbata* and *Gr. pseudomiocenica* synonyms describing the same form? The character-based analyses in this chapter do not closely juxtapose these taxa, thus supporting the implication of the eigenshape analysis that they are separate morphological entities. Some morphological intergradation has been observed in Atlantic and Pacific material, although not to the same degree as that observed between *Gr. praescitula* and *Gr. archeomenardii.*

3) Is *Gr. pseudomiocenica* morphologically similar (related) to *Gr. miocenica*? The juxtaposition of these two morphospecies as closest sister-taxa is one of the more robust clades in the analyses. Established morphospecies ranges further support the notion that the former is likely ancestral to the latter. The clear morphological gap between these taxa revealed by the eigenshape analysis suggests

that the origin of *miocenica* might be one of the more punctuated events in the record.

4) Is *Gr. multicamerata* more morphologically similar (related) to *Gr. menardii* or *Gr. limbata*? The cladistic analyses support a close relationship between *Gr. multicamerata* and the *Gr. limbata-exilis-pertenuis-miocenica-pseudomiocenica* clade. I propose that *Gr. multicamerata* is derived from *Gr. limbata* (Figure 6.10) as is supported by morphometrics and cladistics. To place it here reconciles the cladistic result and any links with *Gr. pertenuis* as reported in Bolli (1970).

5) Is *Gr. multicamerata* morphologically similar (related) to *Gr. pertenuis-exilis*? See question 4.

6) Are *Gr. pertenuis* and *Gr. exilis* distinct morphospecies? *Gr. exilis* and *Gr. pertenuis* are closely allied in all analyses. This is reiterated in the intermediate morphological forms between the two morphospecies that occur in Site 926 material. Although distinct end-member morphotypes can be routinely isolated, there is probably significant inter-populational variation.

7) Are *Gr. menardii* 'A', 'B', *cultrata* and *fimbriata* distinct morphospecies? These taxa are closely allied in all analyses. Coupled with the lack of distinction in the eigenshape analysis and new observations, it is reasonable to suppose that these taxa represent isolated forms in one anagenetic lineage (see Figure 6.4). I suggest that *Gr. cultrata* and *Gr. fimbriata* are most likely geographically and/or temporally-localised ecophenotypes, while Bolli's 'A' and 'B' species probably represent natural within-population variation of *Gr. menardii*. I support the use of the senior synonym *Gr. menardii* for Miocene and younger forms (Stainforth *et al.*, 1975, Kennett and Srinivasan, 1983). Furthermore, with reference to planktonic foraminifera, the denomination of every existing morphological variant serves only to extend taxonomic and biostratigraphic confusion. All new species should be accompanied by a series of lectotypes which represent natural morphological variation, and if possible a defined biostratigraphic utility.

8) Are *Gr. merotumida* and *Gr. plesiotumida* distinct morphospecies and are they closely allied in shape to *Gr. tumida*? In the analyses presented here *Gr. merotumida* and *Gr. plesiotumida* are closely allied. These morphospecies were originally differentiated by Banner and Blow (1965) by small and unreliable characteristics (see Chapter 1 for discussion). It is routinely difficult to attribute individual species to either concept, notwithstanding the range of subtle forms in between. It is likely that they represent the ancestral taxa or taxon to the *Globorotalia s.s.* stock.

9) Are the menardellid and *Globorotalia s.s.* lineages sufficiently similar to support phylogenetic linkage? The analyses results support the notion that these lineages are closely linked phylogenetically.

10) Through which species are the menardellid and *Globorotalia s.s.* lineages linked? Eigenshape analysis, cladistics and new observations support a link between the *Globorotalia s.s.* stock and the *menardii* species. A direct link places the speciation from the *Gr. menardii* 'A' part of the range. If the *menardii* morphospecies were treated as a single anagenetic lineage then this constitutes an ancestor with sufficient morphological variability to derive the *Globorotalia s.s.* lineage.

11) Is *Gr. praescitula* a likely ancestor to the *Menardella, Hirsutella, Truncorotalia* and the *Globorotalia s.s.* stocks? There is little doubt that *Gr. praescitula* intergrades with *Gr. archeomenardii*, from which it is reasonable to assume that the remaining menardellid and *Globorotalia s.s.* taxa were derived. *Gr. scitula* is supported as the direct descendent of *Gr. praescitula*, and through cladistics, is linked to both the hirsutellids and truncorotaliids. A single lineage ancestry for all four subgenera from this one morphospecies is endorsed here.

12) Is *Gr. scitula* a likely 'core' progenitor to some of the lineages? See question 11.

13) Do the separate subgenera form distinct clades using cladistic analysis? The menardellids and *Globorotalia s.s.* taxa form a distinct clade, as do the truncorotaliids and to a degree the hirsutellids (see Figure 6.5-6.7).

14) What are the intraspecific relationships within the hirsutellids? There appears to be a dichotomy within the hirsutellids. The majority resolve well into the *Gr. margaritae* clade derived from *Gr. scitula*, while *Gr. challengeri* and *Gr. juanai* have closer links with *Gr. praescitula* and may constitute a distinct lineage (Figure 6.10). It is unlikely that *Gr. bermudezi* is descended from this discrete lineage due to the considerable ghost range that would have to be inferred. The hirsutellids maybe derived from the same ancestor but include distinct lineages.

15) Through which taxon are the truncorotaliids linked to the other *Globorotalia*? Kennett and Srinivasan (1983) propose *Gr. cibaoensis* while Cifelli and Scott (1986) advocate *Gr.* juanai as the ancestor. The stratophenetic and cladistic analyses here support the former hypothesis.

16) Are the truncorotaliid morphospecies easily distinguished using cladistics? The three *Gr. truncatulinoides* subspecies are essentially indistinguishable. *Gr. truncatulinoides* and *Gr. crassaformis* morphotypes in ocean core material, which regularly exhibit complete inter-specific variability. Although the 'end-member' types can be isolated, the population majority falls between them. One can only hope to constrain the actual inter-specific relationships regarding this group using the cladistic, stratocladistic and stratophenetic methods.

Thus morphometrics, cladistics and stratocladistics have been used to provide the raw evolutionary associations which were refined using detailed knowledge of the fossil population morphologies and published stratigraphic data. It is clear that there is some disparity between the results of the stratophenetic and cladistic methods in this case. One could argue that the stratocladistic method yielded something very similar to the cladistic results, however, this may result from the inconsistencies in the manual nature of branch-swapping associated with the stratocladistic method. Although useful, this method does rely on the inconsistencies of manually rearranging trees.

There are several factors that may explain the differences between the solutions of the methods. Firstly, even for a relatively large number of taxa, planktonic foraminifera are not particularly morphologically diverse and consist of a small calcitic test, which is relatively character-poor, compared to many higher taxonomic groups. The relative lack of distinguishing morphological characters forces the use of characters that may have little bearing on phylogeny, for example, surface texture characters have been shown to be more phylogenetically informative than those that defined overall test shape.

Secondly, foraminifera have been shown to develop similar characters convergently, resulting in phylogenies that are rife with homoplasy and notoriously difficult to deal with using parsimony-based analyses (Harcourt-Brown, 2001). One advantage is that any cladistic solutions can be directly tested against the relatively reliable fossil record attributed to planktonic foraminifera. This is certainly not the case with the majority of extinct groups which rarely have one specimen preserved for a particular timeslice, let alone several billion in existing collections. Using these known ranges we can deduce accurately where the cladistic analysis is yielding misleading results. This is especially apparent when one considers the extensive ghost ranges, which sometimes have to be inferred when reconciling cladistic and range data.

Thirdly, cladistic phylogenetic solutions indicate no information about ancestor-descendent relationships and assume that ancestral taxa are very rare in the incomplete fossil record common to most extant taxonomic groups (see Smith, 1994 for discussion). With planktonic foraminifera it is likely that an investigator *will* sample ancestral taxa. Not only this, but as suggested in Figure 6.10, some species apparently engender multiple descendent lineages, which cannot be resolved by parsimony analysis. These factors must account for the difference in survival time between the cladistic (Figure 6.8) and composite (Figure 6.10) phylogenies.

Combining the three techniques produces a more robust solution to answer the initial questions about phylogeny of Neogene *Globorotalia*. Figure 6.10 constitutes a composite phylogeny that implies ancestry of four taxonomically separate groups from a single ancestor. What is more, unlike most cladistically-derived phylogenies, it is tested and reconciled against well-established taxonomic ranges in geological time.

In conclusion, Figures 6.10 and 6.11 represent steps towards a more accurate phylogeny and taxonomy of an important portion of the planktonic foraminifera, which is essential if accurate range data are to be constructed, from which meaningful evolutionary

rates can be measured. Here, questions were asked about the nature of the evolutionary relationships between 44 taxa belonging to the genus *Globorotalia*. Essentially, those phylogenies outlined in Chapter 1 were tested using cladistics, stratocladistics and stratophenetics.

New observations support the notion that certain anagenetic lineages contain forms that should not be isolated as separate taxa using the traditional Linnaean classification; in particular the division of the *Gr. menardii* (*Gr. menardii s.s.*, 'A', 'B', *Gr. cultrata* and *Gr. fimbriata*) and *Gr. merotumida-Gr. plesiotumida* anagenetic lineages is discouraged here. The results presented here also support the validity of both the *Gr. pseudomiocenica* and *Gr. limbata* morphospecies concepts. More importantly, these results do not advocate the validity of the nomen *Menardella*. Instead, the senior synonym *Globorotalia* should be invoked to refer to the menardellid morphospecies. Furthermore, the *Hirsutella* and *Truncorotalia* divisions should be promoted to generic status to assist taxonomic and biostratigraphic simplicity. This serves to inform the investigator that taxa included in these groups are closely related.

Chapter 7

Conclusions

As outlined in the introduction, the objective of this project was to investigate the origin, evolution, phylogeny, ecology and diversity of *Globorotalia*, an important group of non-spinose planktonic foraminifera, and to gain insight into the oceanic conditions in the Neogene period during which they evolved. The relative 'icehouse' conditions of the Neogene include significant oceanic and climatic transition, in which marine temperatures and sea level fluctuations were synchronised to polar glacial events (Zachos *et al.*, 1994; Lear *et al.*, 2000). This project presents new data that quantifies environmental parameters to provide an environmental context to the group under study. The work thus has practical application, as well as providing the clearest view yet of the evolutionary and ecological radiation of one of the most important and best-recorded groups in the fossil record, which could help simplify Neogene marine biostratigraphy.

The origin of *Globorotalia* has long been debated, although authors generally agree that *Gr. praescitula* was the first species. Some authors (e.g. Kennett and Srinivasan, 1983; Fordham, 1986) derived the globorotaliids from pre-existing planktonic foraminifera within the *Globigerinacea*. This has been challenged by genetic evidence. Studies by Darling *et al.* (1997) and de Vargas *et al.* (1997) of SSU rDNA and RNA suggest a close relationship between modern globorotaliids and taxa from the genera *Ammonia*, *Trochammina* and *Astorhiza*. In addition, no obvious Globigerinacean relatives of *Gr. praescitula* have been found in the Early Miocene in this or any other study. Here, the $\delta^{18}O$ and $\delta^{13}C$ results support a deep, possibly benthic habitat preference for *Gr. praescitula* in the Early Miocene. Although this issue is not resolved here, the combined stratigraphic, isotopic, behavioural and genetic evidence supports the evolution of the majority of the Neogene globorotaliids from a benthic ancestor, and therefore the polyphyletic development of the planktonic mode in the Foraminiferida. Isotope data of its descendant, *Gr. archeomenardii,* are interpreted as near-surface, while data from *Gr. praemenardii* tests reveal a steep $\delta^{18}O$ decrease in the late Middle Miocene that could even imply a return to deep, cold waters and/or a benthic mode.

New isotopic analysis of multiple Late Miocene globorotaliid morphospecies reveals a preference for the intermediate to deep water habitats, which is consistent with that observed in their descendants living the oceans of today. This depth preference is commonly associated with a distinct globorotaliform morphotype, which describes a low-trochospiral, sometimes keeled test form, which was independently developed in unrelated lineages from different times (Cifelli, 1969; Banner and Lowry, 1985; Norris, 1991). The Neogene *Globorotalia* belong to this morphological group. Historically, globorotaliform populations have sustained greater taxonomic losses through extinction than their globigeriniform contemporaries.

Various authors have applied different models of evolution to explain the fossil record of the planktonic foraminifera e.g., those dominated by the physical environment (Stenseth and Maynard Smith, 1984), and those driven by inter-biotic competitive pressures (Van Valen, 1973), although neither reach a satisfactory conclusion. Preliminary analysis of range-chart data reveal the possibility that an extrinsic force with a cyclic nature may be influencing extinction and speciation in the marine realm. This result is very important in understanding macroevolution. It could constitute further evidence in support of Raup and Sepkoski's (1984, 1986) controversial extinction periodicity theory. Previous fossil data sets used in support of this theory (Raup and Sepkoski, 1984, 1986; Prokoph *et al.*, 2000) have used Fourier analysis to imply a periodic signal in extinction data. According to Yiou *et al.* (1996), the relative shortness of natural time series renders most analysis techniques inefficient, including Fourier analysis. They recommend the use of more robust methods such as the multi-taper method (see Thomson, 1982) as used here, which is still efficient when a series is non-continuous and 'sparse' in data. Statistically significant periodic frequencies in the data presented here; equivalent to 36 My, 4.9 My and 2.4 My are broadly consistent with those of Prokoph *et al.* (2000) who present periodic frequencies equivalent to 31 My, 14 My, 4.9 My and 3.2 My. In the Plankrange dataset (presented here) the significant frequencies are independently verified by both the extinction and speciation data, while in the Prokoph *et al.* dataset, they are not. Differences between the Plankrange and the Prokoph *et al.* datasets probably arise from the different choice of statistical tool and the fewer source references used to construct the latter.

A good understanding of the phylogeny of planktonic foraminiferal lineages is critical to enable construction of accurate range data to give insight into evolution, and to facilitate the construction of simple and pragmatic taxonomies for use in biostratigraphy.

Because the *Globorotalia* are of prime importance to the accurate biostratigraphical dating of Neogene marine sediments, it is imperative that their phylogeny is understood.

Phylogenetic investigations of planktonic foraminifera have traditionally used subjective methodology and therefore attracted great criticism from cladists (Siddall, 1998; Gee, 2001). Quantitative data derived from morphology-based analysis techniques can generate much needed objectivity in investigating phenetic relationships. Here, extended eigenshape morphometric analysis of two-dimensional globorotaliid outlines provided valuable data regarding taxonomic associations. Using this method, the most distinct (although not all) forms could be consistently differentiated. The inability to distinguish all forms could be for a number of reasons. Firstly, a two-dimensional outline clearly cannot contain as much data as a three-dimensional object (assessed by eye). Secondly, a continuous outline represents a complex arrangement of morphological characters. Perhaps the analysis of outline portions could yield more consistent results? Thirdly, even when analysing numerous specimens per taxon, the morphological variation in planktonic foraminifera may simply be too great. The future application of this technique could lie in complex three-dimensional morphological mapping, yet, we must wait for the appropriate technology to become available. Nevertheless, this exercise provided some basis for the analysis of character and stratigraphic data using cladistics, stratocladistics and stratophenetics.

In my opinion, none of these three methods alone satisfactorily rises to the challenge of creating a comprehensive phylogeny or combining morphological and stratigraphical data. The strength of this study lies in the combination of the three, in lieu of a single truly objective, repeatable technique. Cladistic and stratocladistic analysis of morphological characters were used to propose a number of phylogenetic affiliations, which formed the objective basis of a revised phylogeny of four distinct globorotaliid lineages. The relatively well-constrained stratigraphic record of the planktonic foraminifera was then applied as a 'quality control' to enable stratophenetic repositioning of taxa with extensive ghost ranges, produced by alignment of a phylogenetic tree with published stratigraphic ranges. The majority of the ghost ranges must arise from the inability of the cladistic procedure to allow for ancestry (single or multiple), anagenesis and paraphyly.

Cladists argue that ancestors cannot be defined in the fossil record (Gee, 2001) and that all taxa included in a cladistic analysis must be monophyletic (Smith, 1994). As far as

cladistics is concerned, they are right. Nevertheless, Linnaean taxonomies are rarely monophyletic, and ancestors obviously *did* exist. It is reasonable to propose that by detailed examination of a multitude of specimens from closely spaced samples; some morphotypes predate, and yet appear similar to others, and so may be ancestors. As for anagenesis, new observations support the notion that anagenesis did occur in the evolutionary history of the planktonic foraminifera e.g., between *Gr. praescitula* and *Gr. archeomenardii* and between the *Gr. menardii* morphotypes.

The results from these phylogenetic analyses strongly support the unity of the *Globorotalia s.s.* lineage with the menardellids under one generic nomen (*Globorotalia*) for phylogenetic accuracy and taxonomic simplicity. Furthermore, the subgenus *Truncorotalia* is found to refer to a distinct clade and the preferred solution is to elevate it to generic status for taxonomic continuity and simplicity. The majority of the *Hirsutella* likewise belong to a distinct clade, and therefore this nomen should also be elevated to generic status. The exceptions are *Gr. juanai* and *Gr. challengeri*; these taxa should be included under the genus *Globorotalia* because they are not derived from *Gr. scitula* like the rest of the hirsutellids (see Figure 6.11). A balanced approach to phylogenetic reconstruction should be adopted when testing phylogenetic hypotheses. Assessing the level of cladogenesis (as in Figure 6.11) assists in producing lineage phylogenies which can then be used to construct range chart data that might more accurately reflect the fossil record of the group under analysis.

In conclusion, this project highlights the importance, and explores the utility of the globorotaliid planktonic foraminifera as sensitive fossil tracers of evolutionary and palaeoenvironmental information, and develops some of the analytical methods that are used in their study. By combining the results of geochemical, stratigraphical, morphometrical and morphological investigations; reassessment of globorotaliid phylogeny and taxonomy has been developed that reports a new understanding of the evolutionary relationships within the Neogene globorotaliids and the Miocene oceans.

References

Alvarez, W., Alvarez, L.W., Asaro, F., Michel, H.V., 1980. Extraterrestrial cause for the Cretaceous-Tertiary extinction. *Science*, 208:1095-1108.

Alvarez, W., Asaro, F., Michel, H.V., Alvarez, L.W., 1982. Iridium anomaly approximately synchronous with the terminal Eocene extinctions. *Science*, 216 (4548):886-888.

Anstey, R.L., Pachut, J.F., 1980. Fourier packing ordinate: a univariate size-independent measurement of polygonal packing variation in Paleozoic bryozoans. *Journal of Mathematical Geology*, 12:139-156.

Arnold, A.J., 1982. Species survivorship in the Cenozoic Globigerinida. *Third North American Paleontological Convention Proceedings*, 1:9-12.

Arnold, A.J., 1983. Phyletic evolution in the *Globorotalia crassaformis* (Galloway and Wisler) lineage: a preliminary report. *Paleobiology*, 9:390-397.

Bak, P., Tang, C., Wiesenfeld, K., 1988. Self-organised criticality. *Physical Review*, ser. A, 38:364-374.

Bandy, O.L., 1972. Origin and development of the *Globorotalia* (*Turborotalia*) *pachyderma* (Ehrenberg). *Micropaleontology*, 18(3):294-318.

Bandy, O.L., 1975. Messinian evaporite deposition and the Miocene/Pliocene boundary, Pasquasia-Capodarso Sections, Sicily. *In*, Saito, T., and Burckle L.H., (eds.), *Late Neogene Epoch Boundaries*, New York, American Museum Natural History Micropaleontology Press, p. 49-63.

Banner, F.T., Blow, W.H., 1960: Some primary types of species belonging to the superfamily Globigerinaceae. *Contributions to the Cushman Foundation for Foraminiferal Research*, 11.

Banner, F.T., Blow, W.H., 1965. Two new taxa of the *Globorotalia* (Globigerinacea, Foraminifera) assisting determination of the Late Miocene/Middle Miocene boundary. *Nature*. 207:1351-1354.

Banner, F.T., Lowry, F.M.D., 1985. The stratigraphical record of planktonic foraminifera and its evolutionary implications. *Special Papers in Palaeontology*, 33:117-130.

Bé, A.W.H., 1980. Gametogenic calcification in a spinose planktonic foraminifer, *Globigerinoides sacculifer* (Brady). *Marine Micropaleontology*, 5:283-310.

Bé, A.W.H., Anderson, O.R., Faber, W.W., Jnr., 1983. Sequence of morphological and cytoplasmic changes during gametogenesis in the planktonic foraminifera *Globigerinoides sacculifer* (Brady). *Micropaleontology*, 29:310-325.

Bé, A.W.H., Bishop, J.K.B., Sverdlove, M.S., Gardner, W.D., 1985. Standing stock, vertical distribution and flux of planktonic foraminifera in the Panama Basin. *Marine Micropaleontology*, 9:307-333.

Bé, A.W.H., McIntyre, A., 1969. *Globorotalia menardii flexuosa* (Koch): An 'extinct' foraminiferal subspecies living in the northern Indian Ocean. *Deep-Sea Research*, 17:595-601.

Belanger, P.E., Curry, W.B., Matthews, R.K., 1981. Core-top evaluation of benthic foraminiferal isotopic ratios for paleoceanographic interpretations. *Palaeogeography, Palaeoclimatology, Palaeoecology*, 33:221-231.

Bemis, B.E., Spero, H., Bijma, J., Lea, D.W., 1998. Re-evaluation of the oxygen isotopic composition of the planktonic foraminifera: experimental results and revised paleotemperature equations. *Paleoceanography*, 13:221-231.

Benton, M.J., 1989. Mass extinctions among the tetrapods and the quality of the fossil record. *Philsophical Transactions of the Royal Society of London*, B. 325:369-386.

Benton, M.J., 1990. The Red Queen Hypothesis. Pp. 119-124. *In*, Briggs, D.E.G., Crowther, P.R., (eds.), *Palaeobiology: a synthesis*. Blackwell Scientific Publications, Oxford.

Benton, M.J., 1995. Diversification and extinction in the history of life. *Science*, 268:52-58.

Berger, W.H., 1971. Planktonic foraminifera: sediment production in an oceanic front. *Journal of Foraminiferal Research*, 1:95-118.

Berger, W.H., and Vincent, E., 1986. Deep-sea carbonates: Reading the carbon-isotope signal: *Geologische Rundschau*, 75(1):249-269.

Berger, W.H., Killingley, J.S., Vincent, E., 1978. Stable isotopes in deep-sea carbonates: Box Core ERDC-92, West Equatorial Pacific. *Oceanologica Acta*, 1:203-216.

Berggren, W.A., 1973. The Pliocene time scale: calibration of planktonic foraminifera and calcareous nannoplankton zones. *Nature*, 243:391-397.

Berggren, W.A., 1977. Late Neogene planktonic foraminiferal biostratigraphy of the Rio Grande Rise (South Atlantic). *Marine Micropaleontology*, 2:265-313.

Berggren, W.A., 1992. Neogene planktonic foraminifer magnetobiostratigraphy of the southern Kerguelen Plateau (Sites 747, 748 and 751). College Station, *Proceedings of the Ocean Drilling Program Scientific Results*, 120:631-647. College Station, TX (Ocean Drilling Program).

Berggren, W.A., Van Couvering, J.A., 1974. The Late Neogene: biostratigraphy, geochronology and paleoclimatology of the last 15 million years in marine and continental sequences. *Palaeogeography, Palaeoclimatology, Palaeoecology*, 16(1-2):1-126.

Berggren, W.A., Kent, D.V., Swisher, C.C., Aubry, M.-P., 1995. A revised Cenozoic geochronology and chronostratigraphy. *In*, Berggren, W.A., Kent, D.V., Aubry, M.-P., and Hardenbol, J. (eds.), *Geochronology, Time Scales and stratigraphic correlation*. SEPM special publication 54:129-212.

Betzler, C., 1997. Ecological control on geometries of carbonate platforms: Miocene/Pliocene shallow-water microfaunas and carbonate biofacies from the Queensland Plateau (NE Australia). *Facies*, 37:147-166.

Beztler, C., Kroon, D., Gartner, S., Wei, W., 1993. Eocene to Miocene chronostratigraphy of the Queensland Plateau: control of Climate and sea level on platform evolution. *In*, McKenzie, J.A., Davies, P.J., Palmer-Julson, A., *et al.*. *Proceedings of the Ocean Drilling Program Scientific Results*, 133.

Bijma, J., Faber, W.W., Hemleben, C., 1990. Temperature and salinity limits for growth and survival of some planktonic foraminifers in laboratory cultures. *Journal of Foraminiferal Research*, 20(2):95-116.

Bijma J., Spero, H.J., and Lea, D.W., 1999. Reassessing foraminiferal stable isotope geochemistry: Impact of the oceanic carbonate system (experimental results). *In*, Fischer G., Wefer, G. (eds.), 1999, *Uses of proxies in paleoceanography: Examples from the South Atlantic*. Springer-Verlag, Berlin Heidelberg, p. 489-512.

Bizon, G., Glaçon, G., 1978. Morphological investigations on the genus *Globorotalia* form Site 372. *In*, *Initial Reports of the Deep Sea Drilling Project*, 42(1):687-707. Washington D.C., National Science Foundation.

Blackith, R.E., Reyment, R.A., 1971. *Multivariate morphometrics*. Academic Press, London.

Blow, 1959. Age, correlation, and biostratigraphy of the Upper Tocuyo (San Lorenzo) and Pozon formations, eastern Falcon, Venezuela. *Bulletin of American Paleontology*, Ithaca, N.Y., 39(178):67-251.

Blow, W.H., 1969. Late Middle Eocene to Recent planktonic foraminiferal biostratigraphy. *In*, Bronnimann, P. and Renz, H.H. (eds.), *Proceedings of the First International Conference on Planktonic Microfossils*, Geneva, 1:199-421.

Blow, W.H., 1979. *The Cainozoic Globigerinida: A study of the Morphology, Taxonomy and Evolutionary relationships and the Stratigraphical Distribution of some Globigerinida (mainly Globigerinacea).* Brill E.J., (ed.), Leiden. 3 vols., pp. 1413.

Blow, W.H., Banner, F.T., 1962. The Mid-Tertiary (Upper Eocene to Aquitanian) Globigerinaceae. *In*, Eames, F.E. *et al.* (eds.), *Fundamentals of Mid-Tertiary Stratigraphical Correlation.* Cambridge University Press, Cambridge, p. 61-163.

Boersma, A., Premoli Silva, I., 1986. Terminal Eocene events: planktonic foraminifera and isotopic evidence. *In*, C. Pomerol and I. Premoli Silva, (eds.), *Terminal Eocene Events*. Amsterdam, Elsevier, p. 213-223.

Bolli, H.M., 1970. The foraminifera of sites 23-31, Leg 4, Chapter 25. *In*, Bader, R.G., *Initial Reports of the Deep Sea Drilling Project*, 4:577-643. Washington D.C., National Science Foundation.

Bolli, H.M., Saunders, J.B., and Perch-Nielsen, K., (eds.), 1985. *Plankton Stratigraphy*. Cambridge Earth Science Series, Cambridge.

Bookstein, F.L., 1978. The measurement of biological shape and shape change: Springer-Verlag, Berlin.

Bookstein, F.L., 1987. Random walk and the existence of evolutionary rates. *Paleobiology*, 13(4):446-464.

Bookstein, F.L., 1991. *Morphometric tools for landmark data: geometry and biology.* Cambridge University Press, Cambridge.

Bookstein, F.L., Strauss, R.E., Humphries, J.M., Chernoff, B., Elder, R.L., Smith, G.R., 1982. A comment on the uses of Fourier methods in systematics. *Systematic Zoology*, 31:85-92.

Boudagher-Fadel, M.K., Banner, F.T., Whittaker, J.E., 1997. *The Early Evolutionary History of Planktonic Foraminifera.* British Micropalaeontological Society publication. Chapman and Hall, London.

Bouvier-Soumagnac, Y., Duplessy, J.C., 1985. Carbon and Oxygen isotopic composition of planktonic foraminifera from laboratory culture, plankton tows and recent sediment: implications for the reconstruction of paleoclimatic conditions and of the global carbon cycle. *Journal of Foraminiferal Research*, 15:302-320.

Bradbury, M.G., *et al.*, 1970. Studies in the fauna associated with the deep scattering layers in the equatorial Indian Ocean, conducted on R/V Te Vega during October and November 1964. *In*, Farquhar, G.B. (ed.), Proceedings of the International Symposium on Biological Sound Scattering in the Ocean, p. 409-452.

Brady, H.B., 1877. Supplementary note on the foraminifera of the chalk (?) of the New Britain Group. *Geology Magazine*, 2(4):534-546.

Brasier, M. D., 1980. *Microfossils*. George Allen & Unwin Ltd., London.

Brasier, M.D., 1988. Foraminiferid extinction and ecological collapse during global biological event. Pp. 37-64. *In*, Larwood, G.P., (ed.), *Extinction and Survival in the Fossil Record*. Oxford: Clarendon Press.

Brönnimann, P., Resig, J., 1971. A Neogene Globigerinacea Biochronological Time-Scale of the Southwestern Pacific. *In*: Initial Reports of the Deep Sea Drilling Project, 7:1235-1469. Washington D.C., National Science Foundation.

Bush, A.B.G., Philander, S.G.H., 1997. The Late Cretaceous: Simulation with a coupled atmospheric-ocean general circulation model. *Paleoceanography* , 12:495-516.

Caron, M. 1985. Cretaceous planktic foraminifera. *In*, Bolli, H.M., Saunders, J.B., and Perch-Nielsen, K., [eds.], 1985. Plankton Stratigraphy. Cambridge University Press.

Carpenter, W.B., Parker, W.K., Jones, T.R., 1862. *Introduction to the study of the foraminifera.* Royal Society Publishing, London.

Carroll, L., 1872. *Through the looking-Glass and what Alice found there.* Macmillan & Co., UK.

Chalker, B.E., Taylor, D.L., 1975. Light-enhanced calcification of the coral *Acropora cervicornis.* *Proceedings of the Royal Society of London*, 190:323-331.

Chaproniere, G.C.H., 1981. Australian mid-Tertiary larger foraminiferal associations and their bearing on the East Indian Letter Classification. *BMR Journal of Australian Geol and Geophysics*, 6:145-151.

Chaproniere, G.C.H., 1984. The Neogene larger foraminiferal sequence in the Australian and New Zealand regions, and it's relevance to the East Indian Letter Classification. *Palaeogeography, Palaeoclimatology, Palaeoecology*, 46:25-35.

Chaproniere, G.C.H., Betzler, C., 1993. Larger foraminiferal biostratigraphy of Sites 815, 816, and 826, Leg 133, northeastern Australia . *In*, McKenzie, J.A., Davies, P.J., Palmer-Julson, A., *et al.*, *Proceedings of the Ocean Drilling Program Scientific Results*, 133: College Station, TX (Ocean Drilling Program), 39-49.

Cifelli, R, Scott, G.H., 1986. Stratigraphic record of the Neogene Globorotalid Radiation (Planktonic Foraminiferida). Smithsonian Contributions to Paleobiology, 58. Smithsonian Institution Press, Washington D.C.

Cifelli, R. 1969. Radiation of Cenozoic planktonic foraminifera. *Systematic Zoology*, 18:154-168.

Cita, M.B., 1973. Pliocene biostratigraphy and chronostratigraphy. *Initial Reports of the Deep Sea Drilling Project*, 13:1343-79. Washington D.C., National Science Foundation.

Clark, M.W., 1981. Quantitative shape analysis: a review. *Mathematical Geology*, 13:303-320.

Coates, A.G. and Obando, J.A., 1996. Pp. 21-56. The geologic evolution of the Central American Isthmus. *In*, Jackson, J.B.C, Budd, A.F. and Coates, A.G. (eds.), *Evolution and Environment in Tropical America.* Chicago, University of Chicago Press.

Collins, L.S., 1989. Evolutionary rates of rapid radiation: the Paleogene planktonic foraminifera. *Palaios*, 4:251-263.

Conroy, M.J., Nichols, J.D., 1984. Testing for variation in taxonomic extinction probabilities: a suggested methodology and some results. *Paleobiology*, 10(3):328-337.

Cooley, W.S., Lohnes, P.R., 1971. *Multivariate data analysis.* Wiley and Sons, New York.

Corfield, R.M., 1987. The environmental control of evolution in the Palaeocene and Early Eocene planktonic Foraminifera. Unpublished Ph.D thesis. University of Cambridge, England.

Corfield, R.M., Granlund, A.H., 1988. Speciation and structural evolution in the Palaeocene *Morozovella* lineage (planktonic Foraminiferida). *Journal of Micropalaeontology*, 7(1):59-72.

Coxall, H. K, Pearson, P.N., Shackleton, N.J., Hall, M. A., 2000. Hantkeninid depth adaptation: An evolving life strategy in a changing ocean. *Geology*, 28(1):87-90.

Craig, H., 1965. The measurement of oxygen isotope palaeotemperatures. Pp.161-182. *In*, Tongiori, E. (ed.), *Stable Isotopes in Oceanographic Studies and Paleotemperatures*. Spoleto, 1965: Con. Naz. Ric. Lab. Geol. Nucl., Pisa.

Cramtpon, J.S., Maxwell, P.A., 2000. Size: all it's shaped up to be? Evolution of shape through the lifespan of the Cenozoic bivalve *Spissatella* (*Crassatellidae*). Pp. 399-423. *In*, Harper, E.M., Taylor, J.D., and Crame, J.A., (eds.) *The Evolutionary Biology of the Bivalvia.* Geological Society, London, Special Publications, 177.

Cranfield, D.J., Anstey, R.L., 1981. Harmonic analysis of cephalopod suture patterns. *Journal of Mathematical Geology*, 13:23-35.

Crowley, T.J and Zachos, J.C., 2000. Comparison of zonal temperature profiles for the past warm time periods. Pp. 50-76. *In*: Huber, B.T., MacLeod, K.S. & Wing, S.C. (eds.), *Warm Climates in Earth History.* Cambridge University Press, Cambridge.

Culver, S.J., 1991. Early Cambrian foraminifera from West Africa, *Science*, 254:689-691.

Cushman, J.A., 1927. Some characteristic Mexican foraminifera. *Journal of Paleontology*, 1(2):147-172.

Cushman, J.A., 1940. Foraminifera. Their classification and economic use. Harvard University Press, Cambridge, Massachusetts.

Cushman, J.A., Bermudez, P.J., 1949. Some Cuban species of *Globorotalia. Contributions from the Cushman laboratory for Foraminiferal Research*, 25:26-44.

Darling, F.K., Wade, C.M., Kroon, D., Leigh Brown, A.J., 1997. Planktic foraminiferal molecular evolution and their polyphyletic origins from benthic taxa. *Marine Micropaleontology*, 30:251-266.

Darling, F.K., Wade, M.C., Kroon, D, Leigh-Brown, J.A., 1999. The diversity and distribution of modern planktonic foraminiferal small subunit ribosomal RNA genotypes and their potential as tracers of present and past ocean circulations. *Paleoceanography*, 14:3-12.

Darling, K.F., Wade, C.M., Stewart, I.A., Kroon, D., Dingle, R., Leigh Brown, A.J., 2000. Molecular evidence for genetic mixing of Arctic and Antarctic subpolar populations of planktonic foraminifers. *Nature*, 405:43-47.

Darwin, C. 1859. *The Origin of Species.* 1996 Edition, Oxford University Press.

Davis, M., Hut, P., Muller, R.A., 1984. Extinction of species by periodic comet showers. *Nature*, 308(5961):715-717.

DeConto, R.M., Pollard, D., 2003. Rapid Cenozoic glaciation of Antarctica induced by declining atmospheric CO_2. *Nature*, 421(6920):245-249.

de Vargas, C., Zaninetti, L., Hilbrecht, H., Pawlowski, J., 1997. Phylogeny and rates of molecular evolution of planktonic foraminifera: SSU rDNA sequences compared to the fossil record. *Journal of Molecular Evolution*, 45(3):285-294.

de Vargas, C., Norris, R., Zaninetti, L., *et al.*, 1999. Molecular evidence of cryptic speciation in planktonic foraminifers and their relation to oceanic provinces. *Proceedings of the National Academy of Science*, USA 96(6):2864-2868.

de Vargas, C., Renaud, S., Hilbrecht, H., et al., 2001. Pleistocene adaptive radiation in *Globorotalia truncatulinoides*: genetic, morphologic, and environmental evidence. *Paleobiology*, 27(1):104-125.

de Vargas, C., Bonzon, M., Rees, N.W., Pawlowski, J., Zaninetti, L., 2002. A molecular approach to biodiversity and biogeography in the planktonic foraminifer *Globigerinella siphonifera* (d'Orbigny). *Marine Micropaleontology*, 45:101-116.

Deuser, W.G., 1987. Seasonal variations in isotopic composition and deep-water fluxes of the test of perennially abundant planktonic foraminifera of the Sargasso Sea: results from the sediment-trap collections and their paleoceanographic significance. *Journal of Foraminifeal Research*, 26A:495-505.

Deuser, W.G., Ross, E.H., Hemleben, Ch., Spindler, M., 1981. Seasonal changes in species composition, mass, size, and isotopic composition of planktonic foraminifera settling into the deep Sargasso Sea. *Palaeogeography, Palaeoclimatology, Palaeoecology*, 33:103-127.

D'Hondt, S. & Arthur, M.A., 1996. Late Cretaceous oceans and the cool tropic paradox. *Science*, 271:1838-1841.

D'Orbigny, A. D., 1826. Tableau methodique de la classè des cephalopods. *Ann. Sci. Nat.*, Paris, 7:243-314.

D'Orbigny, A. D., 1839a. Foraminifères; *In*, de la Sagra, R. (ed.), *Histoire physique, politique et naturelle de l'Ile de Cuba*, 8:1-224.

D'Orbigny, A. D., 1839b. Foraminifères des Iles Canaries; *In*, Barker-Webb, P., and Berthelot, S., (eds.): *Histoire naturelle de Iles Canaries* 2, pt.2, Zool., Paris, p. 119-146.

Douglas, R.G., Savin, S.M., 1978. Oxygen isotope evidence for the depth stratification of the Tertiary and Cretaceous planktonic foraminifera. *Marine Micropaleontology*, 3:175-196.

Duplessy, J.C., Blanc, P.L., and Bé, A.W.H., 1981. Oxygen-18 enrichment of planktonic foraminifera due to gametogenic calcification below the euphotic zone, *Science*, 213:1247-1249.

Durazzi, J.I., 1981. Stable-isotope studies of planktonic foraminifera in North Atlantic core tops. *Palaeogeography, Palaeoclimatology, Palaeoecology*, 33:157-172.

Ehrenberg, C.G., 1861. Über die Tiefgrund-Verhältnisse des Ozeans am Eingange der Davisstrasse und bei Island, *K.Preuss. Akad. Wiss.* Berlin, Monatsber., p. 275-315.

Ehrlich, R., Pharr Jr., R.B., Healy Williams, N., 1983. Comments on the validity of Fourier descriptors in systematics: a reply to Bookstein *et al.*, *Systematic Zoology*, 31:85-92.

Emiliani, C., 1954. Depth habitats of some species of pelagic foraminifera as indicated by oxygen isotope ratios. *American Journal of Science*, 252:149-158.

Emiliani, C., 1955. Mineralogical and chemical composition of the tests of certain pelagic foraminifera. *Micropaleontology*, 1:377-380.

Emiliani, C., 1969. A new paleontology. *Micropaleontology*, 15(3):265-300.

Emiliani, C., 1982. Extinctive evolution: extinction and competitive evolution combine into a unified model of evolution. *Journal of Theoretical Biology*, 97:13-33.

Epstein, B., 1960a. Tests for the validity of the assumption that the underlying distribution of life is eponential. Part I. *Tectonometrics*, 2:83-101.

Epstein, B., 1960b. Tests for the validity of the assumption that the underlying distribution of life is eponential. Part II. *Tectonometrics*, 2:167-183.

Epstein, S., Buchsbaum, R., Lowenstam, H.A., Urey, H.C., 1953. Revised carbonate-water isotopic temperature scale. *Geological Society of America Bulletin*, 64:1315-1325.

Erez, J., Honjo, S., 1981. Comparison of isotopic composition of planktonic foraminifera in plankton tows, sediment traps and sediments. *Palaeogeography, Palaeoclimatology, Palaeoecology*, 33(1981):129-156.

Erez, B. & Luz, J., 1983. Experimental paleotemperature equation for planktonic foraminifera. *Geochim. Cosmochim. Acta* 47:1025-1031.

Erez, J., Almogi-Labin, A., Avraham, S., 1991. On the life history of planktonic foraminifera: lunar reproduction cycle in *Globigerinoides sacculifer* (Brady). *Paleoceanography*, 6(3):295-306.

Ericson, D.B., Ewing, M., Wollin, G., Heezen, B.C., 1961. Atlantic Deep-Sea sediment Cores. *Geological Society of America Bulletin*, 72(2):193-285.

Fairbanks, R.G., Wiebe, P.H., 1980. Foraminifera and chlorophyll maximum: Vertical distribution, seasonal succession, and paleoceanographic significance. *Science*, 209:61-63.

Fairbanks, R.G., Sverdlove, M.S., Free, R., Wiebe, P.H., Be, A.W.H., 1982. Vertical distribution and isotopic fractionation of living planktonic foraminifera form the Panama Basin. *Nature*, 298:841-844.

Farris, J.S., 1988. HENNIG86, Version 1.5. Port Jefferson Station, New York. (Computer Program).

Ferson, S., Rohlf, F.J., Koehn, R.K., 1985. Measuring shape variation in two dimensional outlines. *Systematic Zoology*, 34:56-68.

Fink, W.L., Zelditch, M.L., 1995. Phylogenetic analysis of ontogenetic shape transformations: A reassessment of the piranha genus *Pygocentrus* (*Teleostei*). *Systematic Biology*, 44(3):343-360.

Fisher, D.C., 1988. Stratocladistics: Integrating stratigraphic and morphologic data in phylogenetic inference. *Geological Society of America*, (abstracts) 20:A186.

Fisher, D.C., 1994. Stratocladistcs: morphological and temporal patterns and their relation to phylogenetic process. *In*, Grande, L., Rieppel, O. (eds.). *Interpreting the hierarchy of nature*. Academic Press, San Diego.

Fleisher, R.L., 1974. Cenozoic planktonic foraminifera and biostratigraphy, Arabian Sea; DSDP, Leg 23A, in R.B. Whitmarsh, *et al.*, *Initial Reports of the Deep Sea Drilling Project*, 23:1001-1072. Washington D.C., National Science Foundation.

Foote, M., 1988. Survivorship analysis of Cambrian and Ordovician trilobites. *Paleobiology*, 14:258-271.

Fordham, B.G., 1986. Miocene-Pleistocene planktic foraminifers from D.S.D.P. sites 208 and 77, and phylogeny and classification of Cenozoic species. *Evolutionary Monographs*, 6. Geological Survey of Queensland, Australia.

Fox, D.L., Fisher, D.C., Leighton, L.R., 1999. Reconstructing phylogeny with and without temporal data. *Science*, 584:1816-1819.

Gaina, C., Müller, R.D., Royer, J.-Y., Symonds, P., 1999. The evolution of the Louisiade Triple Junction. *Journal of Geophysical Research*, 104:12927-12940.

Gee, H., 2001. Published discussion regarding book review. *The Palaeontological Association Newsletter*, 47:33-42.

Gibson, T.G. 1989. Planktonic-benthonic foraminiferal ratios: modern patterns and Tertiary applications. *Marine Micropalaeontology*, 15:29-52.

Gingerich, P.D., 1979. The stratigraphic approach to phylogeny reconstruction in vertebrate paleontology. Pp. 41-77. *In*, J. Cracraft and N. Eldrige (eds.), *Phylogenetic analysis and Paleontology*. Columbia University Press, New York.

Gingerich, P.D., 1990. Stratophenetics. Pp. 437-442. *In*, Briggs, D.E.G. & Crowther, P.R. (eds.), *Paleobiology: a synthesis*. Blackwell Scientific, Oxford.

Golub, G.H., Reinsch, C., 1970. Singular value decomposition and least squares solutions. *Numerical Mathematics*, 14:403-420.

Gradstein, F.M., Agterberg, F.P., Ogg, J.G., Hardenbol, P., Van Veen, J., Thierry, J., Huang, Z., 1994. A Mesozoic timescale. *Journal of Geophysical Research*, 99(24):051-24, 074.

Hallam, A., 1989. The case for sea-level change as a dominant causal factor in mass extinction of marine invertebrates. *Royal Society of London Philosophical Transactions*, ser. B, 325:437-455.

Hallock, P., 1987. Fluctuations in the trophic resource continuum: a factor in global diversity cycles? *Paleoceanography*, 2:457-471.

Hallock, P., Premoli Silva, I., Boersma, A., 1991. Similarities between planktonic and larger benthic foraminiferal evolutionary trends through Palaeogene paleoceanographic change. *Palaeogeography, Palaeoclimatology, Palaeoecology*, 83:49-64.

Haman, D., Huddleston, R.W., Donahue, J.P., 1981. *Obandyella*, a new name for *Hirsutella* Bandy, 1972 (Foraminiferida), non Cooper and Muir-Wood, 1951 (*Brachiopoda*). *Proceedings of the Biological Society of Washington*, 93(4):1264-1265.

Hansen, T.A., 1988. Early Tertiary radiation of marine molluscs and the long-term effects of the Cretaceous-Tertiary extinctions. *Paleobiology*, 14(1):37-51.

Haq, B.U., Hardenbol, J., Vail, P.R., 1987. Chronology of fluctuating sea levels since the Triassic. *Science*, 235:1156-1167.

Harcourt-Brown, K. G., 2001. Phylogenetic tree shape with special reference to the phylogeny of the Cretaceous globotruncanid foraminifera. Ph.D thesis, University of Bristol, U.K.

Hemleben, C., Spindler, M. & Anderson, O.R., 1989. *Modern Planktonic Foraminifera*. Springer-Verlag, New York.

Hemleben, C., Spindler, M., Breitinger, I., Deuser, W. G., 1985. Field and laboratory studies of on the ontogeny and ecology of some globorotaliid species from the Sargasso Sea off Bermuda. *Journal of Foraminiferal Research*, 15:254-272.

Hemleben, C.H, Olsson, R.K., Berggren, W.A., Norris, R.D., 1999. Wall texture, classification and phylogeny. *In*, Olsson, R.K., Hemleben, C.H., Berggren, W.A., Huber. B.T. (eds.), *Atlas of Palaeocene Planktonic Foraminifera*. Smithsonian Contributions to Paleobiology 85.

Hennig, W. 1966. *Phylogenetic Systematics*. University of Illinois Press, Urbana, 1966.

Huelsenbeck, J.P., Crandall, K.A., 1997. Phylogeny estimation and hypothesis testing using maximum likelihood. *Ann. Rev. Ecol. Syst.*, 28:437-466.

Hewzulla, D., Boulter, M.C., Benton, M.J., Halley, J.M., 1997. Evolutionary patterns from mass originations and mass extinctions. *Philosophical Transactions of the Royal Society of London*, B. 354:463-469.

Hilbrecht, H. Thierstein, H.R., 1996. Benthic behaviour of planktonic foraminifera. *Geology*, 24(3):200-202.

Hodell, D.A., Vayavananda, A., 1993. Middle Miocene paleoceanography of the western equatorial Pacific (DSDP Site 289) and the evolution of *Globorotalia* (*Fohsella*). *Marine Micropaleontology.*, 22:279-310.

Hoffman, A., Kitchell, J.A., 1984. Evolution of the pelagic planktic system: a paleobiologic test of models of multispecies evolution. *Paleobiology*, 10:9-33.

Huber, B.T., Bijma, J., Darling, K. 1997. Cryptic speciation in the living planktonic foraminifera *Globigerinella siphonifera* (d'Orbigny). *Paleobiology*, 23(1):33-62.

Huber, B.T., Leckie, R.M., Norris, R.D., Bralower, T.J., CoBabe, E., 1999. Foraminiferal assemblage and stable isotopic change across the Cenomanian-Turonian boundary in the subtropical North Atlantic. *Journal of Foraminiferal Research*, 29(4):392-417.

Hudson, J.D., Anderson, T.F., 1989. Ocean temperatures and isotopic compositions through time. *Transactions of the Royal Society of Edinburgh: Earth Sciences*, 80:183-192.

Isern A.R., Anselmetti, F.S., Blum, P., *et al.*, *Proceedings of the Ocean Drilling Program Initial Reports*, 194, 1-105 [CD-ROM]. Available from Ocean Drilling Program, Texas A&M University, College Station TX.

Jenkins, D.G., 1965. Planktonic Foraminifera and Tertiary Intercontinental Correlations. *Micropaleontology*, 11(3):265-277.

Jenkins, D.G., 1971. New Zealand Cenozoic Planktonic Foraminifera. *New Zealand Geological Survey Paleontological Bulletin*, 42:1-275.

Jenkins, D.G, 1973. Diversity changes in the New Zealand Cenozoic planktonic foraminifera. *Journal of Foraminiferal Research*, 3:78-88

Jenkins, D.G., Shackleton, N.J., 1979. Parallel changes in species diversity and paleotemperature in the lower Miocene. *Nature*, 278:5051.

Jöreskog, K.G., Klovan, J.E., Reyment, R.A., 1976. *Geological factor analysis*. Elsevier, Amsterdam.

Keller, G., 1981. The Genus *Globorotalia* in the Early Miocene of the Equatorial and Northwestern Pacific. *Journal of Foraminiferal Research*, 11(2):118-132.

Keller, G., 1985. Depth stratification of planktonic foraminifers in the Miocene Ocean. *In*, Kennett, J.P. (ed.), *The Miocene Ocean: Paleoceanography and Biogeography*, GSA Memoir 163. The Geological Society of America, Boulder, Colorado, U.S.

Keller, G., MacLeod, N., Barrera, E., 1992. Eocene-Oligocene faunal turnover in planktonic foraminifera, and Antarctic glaciation. Pp. 218-244. *In*, Prothero, D.R. and Berggren, W.A., (eds.), *Eocene and Oligocene Biotic Evolution*. Princeton University Press, Princeton.

Kellogg, D.E., 1975. The role of phyletic change in the evolution of *Pseudocubus vema* (*Radiolaria*). *Paleobiology*, 1:359-370.

Kellogg, D.E., 1983. Phenology of morphometric change in radiolarian lineages from deep sea cores: implications for macroevolution. *Paleobiology*, 9:355-362.

Kennett, J.P., 1973. Middle and Late Cenozoic planktonic foraminiferal biostratigraphy of the southwest Pacific - DSDP Leg 21. Washington, D.C., *Initial Reports of the Deep Sea Drilling Project*, 21:575-640. Washington D.C.: National Science Foundation.

Kennett, J.P., 1977. Cenozoic evolution of Antarctic glaciation, the circum-Antarctic Ocean, and their impact on global paleoceanography. *Journal of Geophysical Research*, 82(27):3843-3860.

Kennett, J.P., 1985. *The Miocene Ocean: Paleoceanography and Biogeography*. GSA Memoir 163.

Kennett, J.P., Srinivasan, M.S., 1983. *Neogene Planktonic Foraminifera. A Phylogenetic Atlas*, Hutchinson Ross Publishing Company, U.S.

Kent, P.E., Hunt, M.A. & Johnstone, M.A., 1971. The Geology and Geophysics of Coastal Tanzania. *Natural Environment Research Council Geophysical Paper* no. 6, Her Majesty's Stationery Office, London.

Killingley, J.S., 1983. Effects of diagenetic recrystallisation on $^{16}O/^{18}O$ values of deep-sea sediments. *Nature*, 301:594-597.

Kobashi, T., Grossman, E.L., Yancey, T.E., Dockery, D.T., 2001. Re-evaluation of conflicting Eocene tropical temperature estimates: Molluskan oxygen-isotope evidence for warm low-latitudes. *Geology*, 29(11):983-986.

Kroon, D, Darling, K., 1995. Size and upwelling control of the stable isotope composition of *Neogloboquadrina dutertrei* (d'Orbigny), *Globigerinoides ruber* (d'Orbigny) and *Globigerina bulloides* d'Orbigny: Examples from the Panama Basin and Arabian Sea. *Journal of Foraminiferal Research*, 25(1):39-52.

Kroopnick, P.M., 1974. Correlations between ^{13}C and CO_2 in surface waters and atmospheric CO_2. *Earth and Planetary Science Letters*, 22:397-403.

Kucera, M., Malmgren, B.A., 1996. Latitudinal variation in the planktic foraminifera *Contusotruncana contusa* in the terminal Cretaceous ocean. *Marine Micropaleontology*, 28:31-52.

Kucera, M., Darling, K.F., 2002. Cryptic species of planktonic foraminifera: their effect on palaeoceanographic reconstructions. *Philosophical Transactions of the Royal Society*, A 360(1793): 695-718.

Kucera, M., Kennett, J.P., 2002. Causes and consequences of a middle Pleistocene origin of the modern planktonic foraminifer *Neogloboquadrina pachyderma* sinistral. *Geology*, 30(6):539-542.

Kurten, B., 1954. Population dynamics: a new method in palaeontology. *Journal of Paleontology*, 28:286-292.

Lamb, J.L., Beard, J.H., 1972. Late Neogene Planktonic Foraminifers in the Caribbean, Gulf of Mexico, and Italian stratotypes. *University of Kansas Paleontological Contributions*, 57:1-67.

Lane, G.A., Doyle, M., 1956. Fractionation of oxygen isotopes during respiration. *Science*, 123:574.

Lear, C.H., Elderfield, H., Wilson, P.A., 2000. Cenozoic deep-sea temperatures and the global ice volumes from Mg/Ca in benthic foraminiferal calcite. *Science*, 287:269-272.

Lee, J.J., McEnery, M.E., Pierce, S., Freudenthal, H.D., Muller, W.A., 1966. tracer experiments in feeding littoral foraminifera. *Journal of Protozoology*., 13:659-670.

Lestrel, P.E., 1997. Introduction. Pp. 3-21. *In*, Lestrel, P.E, (ed.), Fourier descriptors and their applications in biology. Cambridge University Press, Cambridge.

Levitus, S., and Boyer, T., 1994. World Ocean Atlas 1994 Volume 4: Temperature. NOAA Atlas NESDIS 4, U.S. Department of Commerce, Washington, D.C.

Lincoln, J.M., Schlanger, S.O., 1987. Miocene sea level falls related to the geological history of the Midway Atoll. *Geology*, 15:454-457.

Lipps, T.H., 1970. Plankton evolution. *Evolution*, 24:1-22.

Livermore, R. A., Eagles, G., and Fairhead, J. D., 2001. The ocean gateway at Drake Passage. Geological Evolution of the Earth Systems: Mesozoic-Cenozoic. June 2001 abstract.

Lohmann, G.P., 1983. Eigenshape analysis of microfossils: A general morphometric procedure for describing changes in shape: *Mathematical Geology*, 15:659-672.

Lohmann, G.P., Malmgren, B.A., 1983. Equatorward migration of *Globorotalia truncatulinoides* ecophenotypes through the Late Pleistocene: gradual evolution or ocean change? *Paleobiology*, 9:414-421.

Lohmann, G.P., Schweitzer, P.N., 1990a. On eigenshape analysis. Pp. 147-166. *In*, Rohlf, F.J., and Bookstein, F.L., (eds.), Proceedings of the Michigan Morphometrics Workshop, Special publication 2: Ann Arbor, Michigan, The University of Michigan Museum of Zoology.

Lohmann, G.P., Schweitzer, P.N., 1990b. *Globorotalia truncatulinoides*' growth and chemistry as probes of the past thermocline: 1:shell size. *Paleoceanography*, 5:55-75.

Loubere, P., 2000. Marine control of biological production in the eastern equatorial Pacific Ocean. *Nature*, 406:497-500.

MacArthur, R.H., Wilson, E.O., 1967. *The theory of island biogeography*. Princeton University Press.

MacLeod, N., 1999. Generalising and extending the eigenshape method of shape visualisation and analysis. *Paleobiology*, 25(1):107-138.

MacLeod, N., 2002. Phylogenetic signals in morphometric data. *In*, MacLeod, N and Forey, P.L (eds.), *Morphology, Shape and Phylogeny*. Systematics Association Special Volume Series. Taylor and Francis, London and New York.

MacLeod, N, Forey, P.L., 2002. Introduction in 'Morphology, Shape and Phylogeny'. *In*, MacLeod, N and Forey, P.L (eds.), Systematics Association Special Volume Series. Taylor and Francis, London and New York.

MacLeod, N., and Rose, K.D., 1993. Inferring locomotor behaviour in Paleogene mammals via eigenshape analysis. *American Journal of Science*, 293(A):300-355.

Maddison, W.P, Maddison, D.R., 1997. *MacClade*. Sinauer Associates Inc. Publishers, Sunderland, Massachusetts.

Major, R.P., Matthews, R.K., 1983. Isotopic composition of bank margin carbonates on Midway Atoll: amplitude constraint on post-early Miocene eustacy. *Geology*, 11:335-338.

Malmgren, B.A., Berggren, W.A., and Lohmann, G.P., 1983. Evidence for punctuated gradualism in the Late Neogene *Globorotalia tumida* lineage of planktonic foraminifera. *Paleobiology*, 9(4):377-389.

Malmgren, B.A., Berggren, W.A., 1987. Evolutionary change in some late Neogene planktonic foraminiferal lineages and their relationships to paleoceanographic change. *Paleoceanography*, 2(5):445-456.

Malmgren, B.A., Kennett, J.P., 1981. Phyletic gradualism in a Late Cenozoic planktonic foraminiferal lineage, D.S.D.P. Site 284, Southwest Pacific. *Paleobiology*, 7:230-240.

Mann, M.S., Lees, J.M., 1996. Robust estimation of background noise and signal detection in climatic time-series. *Climate Change*, 33:409-445.

Marcus, L.F., Bello, E, Garcia-Valdecasas, A., 1993. *Contributions to morphometrics*. Museo Nacional de Ciencias Naturales 8, Madrid.

Marcus, L.F., Corti, M, Loy, A., Naylor, G.J.P., Slice, D.E., 1996. *Advances in morphometrics*. Pelnum, New York.

Martini, E., 1971. Standard Tertiary and Quaternary calcareous nannoplankton zonation. Pp. 739-785. *In*, Farinacci, A. (ed.), Proceedings of the Second Planktonic Conference, Roma 1970. Roma, Tecnoscienza.

Maxwell, W.D., Benton, M.J., 1990. Historical tests of the absolute completeness of the fossil record of tetrapods. *Paleobiology*, 16:332-335.

Mayr, E., 1969. *Principles of Systematic Zoology*. McGraw-Hill, New York.

McCrea, J.M., 1950. On the isotope chemistry of carbonates and a paleotemperature scale. *Journal of Chemical Physics*, 18:849-857.

McCune, A.R., 1982. On the fallacy of constant extinction rates. *Evolution*, 36(3):610-614.

McGowan, A.J., Pearson, P.N., 1998. A.D.A.P.T.S (Analysis of diversity, asymmetry of phylogenetic trees and survivorship): A new software tool. MSc. Thesis, University of Bristol. Available at: http://palaeo-electronica.org/1999_1/adapts/issue1_99.htm.

McGowran, B., 1968. Reclassification of Early Tertiary *Globorotalia*. *Micropaleontology*, 14(2):179-198.

Miller, K.G., Fairbanks, R.G., Mountain, G.S., 1987. Tertiary oxygen isotope synthesis, sea level history, and continental margin erosion. *Paleoceanography*, 2:1-19.

Mulitza, S., Dürkroop, A., Hale, W., Wefer, G., 1997. Planktonic foraminifera as recorders of past surface water stratification. *Geology*, 25:335-338.

NAG Ltd. (2001) The NAG Fortran Library Manual, Mark 20. The Numerical Algorithms Group, Oxford.http://www.nag.co.uk/.

Neff, N.A., Marcus, L.F., 1980. *A survey of multivariate methods for systematists*. Privately published, New York.

Newell, N.D., 1952. Periodicity in invertebrate evolution. *Journal of Paleontology*, 26:371-385.

Norell, M. A., Novacek, M. J., 1992. The fossil record and evolution - comparing cladistic and paleontological evidence for vertebrate history. *Science*, 255(5052):1690-1693.

Norris, R.D., 1991. Biased extinction and evolutionary trends. *Paleobiology*, 17(4):388-399.

Norris, R.D., Corfield, R.M., Cartlidge, J.E., 1993. Evolution of depth ecology in the planktic foraminifera lineage *Globorotalia* (*Fohsella*). *Geology*, 21:975-978.

Norris, R.D., Corfield, R.M., Cartlidge, J.E., 1996. What is gradualism? Cryptic speciation in globorotaliid foraminifera. *Paleobiology*, 22(3):386-405.

Norris, R.D., Wilson, P.A., 1998. Low-latitude sea-surface temperatures for the mid-Cretaceous and the evolution of planktic foraminifera. *Geology*, 26:823-826.

Olsson, R.K., Hemleben, C., Berggren, W.A. & Huber, B.T., 1999. *Atlas of Palaeocene Planktonic Foraminifera*. Smithsonian Contributions To Palaeobiology, 85.

O'Neil, J.R., Clayton, R.N., Mayeda, T.K., 1969. Oxygen isotope fractionation on divalent metal carbonates. *Journal of Chemical Physics*, 51:5547-5558.

Ottens, J.J., Nederbragt, A.J., 1992. Planktonic foraminiferal diversity as indicator of ocean environments. *Marine Micropaleontology*, 19:1328.

Owen, S.R.J., 1867. On the surface-fauna of mid-ocean. *Zoological Journal of the Linnaean Society of London.*, 9:147.

Parker, W.K., Jones, T.R., Brady, H.B., 1865. On the nomenclature of the foraminifera. Pt. XII (misprinted as part X continued). The species enumerated by d'Orbigny in the Annales des sciences naturelles, vol. 7, 1826. *Ann. Mag. Nat. Hist.*, London, ser. 3, vol. 16, p.20.

Patterson, C., Smith, A.B., 1987. Is the periodicity of extinctions a taxonomic artefact. *Nature*, 330:248-251.

Pawlowski, J., Bolivar, I., Fahrni, J.F., Cavalier-Smith, T., Guoy, M., 1996. Early evolution of foraminifera suggested by SSU rRNA Gene Sequences. *Molecular Biology and Evolution*, 13(3):445-450.

Pawlowski, J., Bolivar, I., Fahrni, J., De Vargas, C., Bowser, S. S., 1999. Naked foraminiferans revealed. *Nature*, 399: (6731).

Pawlowski, J., Bolivar, I., Guiard-Maffia, J., Gouy, M., 1997. Phylogenetic position of foraminifera from LSU rRNA gene sequences. *Molecular Biology and Evolution*, 11(6):929-938.

Pearson, P.N., 1990. Evolution and Phylogeny of the Palaeogene Planktonic Foraminifera. Ph.D Thesis, The University of Cambridge, U.K.

Pearson, P.N., 1992. Survivorship analysis of fossil taxa when real-time extinction rates vary: the Palaeogene planktonic foraminifera. *Paleobiology*, 18:115-131.

Pearson, P.N., 1993. A lineage phylogeny for the Paleocene planktonic foraminifera. *Micropaleontology*, 39(3):193-232.

Pearson, P.N., 1995a. Investigating age-dependency of species extinction rates using dynamic survivorship analysis. *Historical Biology*, 10:119-136.

Pearson, P.N., 1995b. Planktonic foraminifer biostratigraphy and the development of the pelagic caps on guyots in the Marshall island group. Pp. 21-59. *In*, Haggerty, J.A., Premoli-Silva, I., Rack, F., and McNutt, M.K., (eds.), 1995. *Proceedings of the Ocean Drilling Program Scientific Results*, 144.

Pearson, P.N., 1996. Cladogenetic, extinction and survivorship patterns from a lineage phylogeny: the Palaeogene planktonic foraminifera. *Micropalaeontology*, 42:179-188.

Pearson, P.N., 1998. Stable isotopes and the study of evolution in planktonic foraminifera. Reprinted from Norris, R.D. & Corfield, R.M. 1998. Isotope paleobiology and paleoecology. *The Paleontological Society Papers*, 4:138-178.

Pearson, P.N., 2001. Published discussion regarding book review. *The Palaeontological Association Newsletter*, 47:33-42.

Pearson, P.N., Ditchfield, P.W., Singano, J., Harcourt-Brown, K.G., Nicholas, C.J., Shackleton, N.J., Hall, M.A., 2001. Warm Late Cretaceous and Eocene tropical sea-surface temperatures. *Nature*, 413:481-487.

Pearson, P.N., Shackleton, N.J., 1995. Neogene multispecies planktonic foraminifer stable isotope record, Site 871, Limalok Guyot. *Proceedings of the Ocean Drilling Program, Scientific Results*, 144:401-410. Ocean Drilling Program, Texas A&M University, College Station TX.

Pearson, P.N., Shackleton, N.J. & Hall, M.A., 1993. Stable isotope palaeoecology of middle Eocene planktonic foraminifera and multi-species isotope stratigraphy, DSDP Site 523, South Atlantic. *Journal of Foraminiferal Research*, 23:123-140.

Pearson, P.N., Shackleton, N.J., Hall, M.A., 1997a. Stable isotopic evidence for the sympatric divergence of *Globigerinoides trilobus* and *Orbulina universa* (planktonic foraminifer). *Journal of the Geological Society of London*, 154:295-302.

Pearson, P.N., Shackleton, N.J., Weedon, G.P., Hall, M.A., 1997b. Multispecies planktonic foraminifer stable isotope stratigraphy through Oligo/Miocene boundary climatic cycles, Site 926. *Proceedings of the Ocean Drilling Program, Scientific Results*, 154:441-449. Ocean Drilling Program, Texas A&M University, College Station TX.

Perch-Nielsen, K., 1985. Cenozoic calcareous nannofossils. Pp. 87-154. *In*, Bolli, H.M., Saunders J.B., Perch-Nielsen, K. (eds.), *Plankton Stratigraphy*. Cambridge University Press, Cambridge.

Percival, D.B., Walden, A.T., 1993. *Spectral analysis for physical applications-Multitaper and conventional univariate techniques*. Cambridge University Press, Cambridge.

Pielou, E.C, 1969. *An introduction to mathematical ecology*. John Wiley and Sons, New York.

Pimentel, R.A., 1979. *Morphometrics: the multivariate analysis of biological data*. Kendall/Hunt, Dubuque, Iowa.

Plotnick, R., McKinney, M., 1993. Ecosystem organization and extinction dynamics. *Palaios*, 8:215-212.

Premoli Silva, I., Boersma, A., 1983. Paleocene planktonic foraminiferal biogeography and the paleoceanography of Atlantic Ocean. *Micropaleontology*, 29(4):355-381.

Prokoph, A., Barthelmes, F., 1996. Detection of nonstationarities in geological time series: Wavelet transform of chaotic and cyclic sequences. *Computer and Geosciences*, 22:1097-1108.

Prokoph, A., Fowler, A.D., Timothy Patterson, R., 2000. Evidence for periodicity and nonlinearity in a high-resolution fossil record of long-term evolution. *Geology*, 28(10):867-870.

Quilty, P.G., 1969. Upper Eocene planktonic Foraminiferida from Albany, Western Australia. Journal of the Royal Society of Western Australia, 52:41-58.

Raffi, S., Stanley, S.M., Marasti, R., 1985. Biogeographic patterns and Plio-Pleistocene extinction of Bivalvia in the Mediterranean and southern North Sea. *Paleobiology*, 11:368-389.

Ramanathan, V., Collins, W., 1991. Thermodynamic regulation of ocean warming by cirrus clouds deduced from satellite observations of the 1987, El Nino. *Nature*, 351:27-32.

Rampino, M.R., Stothers, R.B., 1986. Geologic periodicities and the galaxy. Pp. 241-259. *In*, Smoluchowski, R., *et al.* (eds.), *The galaxy and the solar system.* Tucson, University of Arizona Press.

Ramsay, W.R., 1962. Hantkenininae in the Tertiary rocks of Tanganyika. *Contributions from the Cushman Foundation for Foraminiferal Research*, 12:79-89.

Raup, D.M., 1975. Taxonomic survivorship curves and Van Valen's Law. *Paleobiology*, 1:82-96.

Raup, D.M., 1976a. Species diversity and the Phanerozoic: a tabulation. *Paleobiology*, 2:279-288.

Raup, D.M., 1976b. Species diversity and the Phanerozoic: a interpretation. *Paleobiology*, 2:289-297.

Raup, D.M., 1978. Cohort analysis of generic survivorship. *Paleobiology*, 4:1-15.

Raup, D.M., 1986. *The Nemesis Affair*. Penguin Books Canada Ltd., Ontario, Canada.

Raup, D.M., Sepkoski, J.J., 1984. Periodicity of extinctions in the geologic past. *Proceedings of the National Academy of Science, USA*, 81:801-805.

Raup, D.M., Sepkoski, J.J., 1986. Periodic extinctions of families and genera. *Science*, 231:833-836.

Ravelo, A.C., Fairbanks, R.G., 1992. Oxygen isotopic composition of multiple species of planktonic foraminifera: Recorders of a modern photic zone temperature gradient. *Paleoceanography*, 7:195-213.

Read, D.W., Lestrel, P.E., 1986. Comment on the uses of homologous point measures in systematics: a reply to Bookstein *et al. Systematic Zoology*, 35:241-253.

Reyment, R.A., 1991. *Multidimensional Paleobiology*. Pergamon, Oxford.

Reyment, R.A., Blackith, R.E., Campbell, N.A., 1984. *Multivariate morphometrics*, 2nd edition. Academic Press, London.

Riedel, R., Jeffries, R. P. S., 1978. *Order in living organisms: a systems analysis of evolution.* Wiley, Chichester, England.

Robaszynski, F., Caron, M., Gonzalez Donoso, J.M., Wonders, A.A.H., 1984. E.W.G.P.F. Atlas of Late Cretaceous Globotruncanids. *Revue de Micropaleontologie*, 26(3-4):145-305.

Rohlf, F.J., 1986. Relationships among eigenshape analysis, fourier analysis, and analysis of coordinates. *Mathematical Geology*, 18:845-857.

Rohlf, F.J., Bookstein, F.L., 1990. Proceedings of the Michigan Morphometrics Workshop, Special publication 2. Ann Arbor, Michigan, The University of Michigan Museum of Zoology.

Rohling, E.J., and Bigg, G.R., 1998. Paleosalinity and ^{18}O: A critical assessment. *Journal of Geophysical Research*, 103, (C1):1307-1318.

Rohling, E.J., Cooke, S., 1999. Stable oxygen and carbon isotope ratios in foraminiferal carbonate. Pp. 239-258. *In*, B.K. Sen Gupta (ed.) *Modern Foraminifera*, Kluwer Academic, Dordrecht, The Netherlands.

Saito, T., 1977. Late Cenozoic planktonic foraminiferal datum levels: the present state of the knowledge towards accomplishing pan-Pacific correlation. Pp. 61-80. 1st International Congress of Pacific Neogene Stratigraphy, Tokyo 1976, Proceedings.

Sanfillipio, A., Westburg-Smith, M.J., Riedel, W.R., 1985. Cenozoic radiolaria. Pp. 631-712. *In.*, Bolli, H.M., Saunders J.B., Perch-Nielsen, K., (eds.), *Plankton Stratigraphy*. Cambridge University Press, Cambridge.

Saunders, J.B., Beaudry, H.M., Bolli, H.M., Hay, W.W., Permoli Silva, I., Riedel, W.R., Rogl, F, Sanfillipo, A., 1973. Paleocene to Recent microfossil distribution in the marine and land areas of the Caribbean. *Initial Reports of the Deep Sea Drilling Project*, 15:769-773. Washington D.C., National Science Foundation.

Sautter, L.R., Thunell, R.C., 1991. Seasonal variability in the ^{18}O and ^{13}C of planktonic foraminifer from an upwelling environment: sediment trap results from the San Pedro Basin: Southern California. *Paleoceanography*, 6:307-355.

Savin, S.M., 1977. The History of the Earth's surface temperature during the past 100 million years. *Annual Reviews of the Earth and Planetary Sciences*, 5:319-355.

Savin, S.M., Abel, L., Barrera, E., Hodell, D., Keller, G., Kennett, J.P., Killingley, J., Murphy, M., Vincent, E., 1985. The evolution of Miocene surface and near-surface marine temperatures: Oxygen isotopic evidence. *In*, Kennett, J.P. (ed.), *The Miocene Ocean: Paleoceanography and Biogeography*. GSA Memoir 163. The Geological Society of America, Boulder, Colorado, U.S.

Savin, S.M., Douglas, R.G., Keller, G., Killingley, J.S., Shaughnessy, L., Sommer, M.A., Vincent, E., Woodruff, F. 1981. Miocene benthic foraminiferal isotope records: a synthesis. *Marine Micropaleontology*, 6:423-450.

Schrag, D.P., 1999. Effects of diagenesis on the isotopic record of Late Paleogene tropical sea surface temperatures. *Chemical Geology*, 161:215-244.

Schrag, D.P., DePaolo, D.J. & Richter, F.M., 1995. Reconstructing past sea surface temperatures: Correcting for diagenesis of bulk marine carbonate. *Geochimica Cosmochimica Acta*, 59:2265-2278.

Schweitzer, P.N., Lohmann, G.P., 1990. Life-history and the evolution of ontogeny in the ostracode genus Cyprideis. Paleobiology 16:107-125.

Scott, G.H., 1972. The relationship between the Miocene Foraminiferida *Globorotalia miozea miozea* and *G. praemenardii*. *Micropaleontology*, 18(1):81-93.

Scott, G. H., 1982. Review of Kapitean stratotype and boundary with Opoitian Stage (upper Neogene, New Zealand). *New Zealand Journal of Geology and Geophysics*, 23:475-485.

Scott, G.H., Bishop, S., Burt, B.J., 1990. Guide to some Neogene Globorotalids (Foraminiferida) from New Zealand. *NZGS Paleontology Bulletin 61*.

Segar, D. A., 1998. *Introduction to Ocean Sciences*. Wadsworth publishing company, 497p.

Sepkoski, J.J., 1978. A kinetic model of Phanerozoic taxonomic diversity. 1. Analysis of marine orders. *Paleobiology* 4:233-251.

Sepkoski, J.J., 1982. A compendium of fossil marine families. Milwaukee Public Museum Contributions to Biology and *Geology*, 51:1-125.

Sepkoski, J.J., 1987. Reply to article of Patterson and Smith (1987). *Nature*, 330:251-252.

Sepkoski, J.J., 1990. Periodicity. Pp. 171-178. *In*, Briggs, D.E.G., Crowther, P.R., (eds.), *Palaeobiology: a synthesis*. Blackwell Scientific Publications; Oxford.

Sepkoski, J.J., 1993. Ten years in the library: how changes in taxonomic databases affect perception of macroevolutionary pattern. *Paleobiology*, 19:43-51.

Sereno, P.C., 1999. The evolution of dinosaurs. *Science*, 284(5423):2137-2147.

Shackleton, N.J., 1974. Attainment of isotopic equilibrium between ocean water and the benthonic foraminifera genus *Uvigerina*: isotopic changes in the ocean during the last glacial. *CNRS, Colloques Internationals*, 219:203-209.

Shackleton, N.J., 1984. Pp. 27-34. *In*, Brenchley, P. (ed.), *Fossils and Climate*. John Wiley, Chichester, U.K.

Shackleton, N.J., 1986. Palaeogene stable isotope events. *Palaeogeography, Palaeoclimatology, Palaeoecology*, 57:91-102.

Shackleton, N.J., Vincent, E., 1978. Oxygen and carbon isotope studies in Recent foraminifera from the southwest Indian Ocean. *Marine Micropaleontology*, 3:1-13.

Shaw, R.D., 1978. Seafloor spreading in the Tasman Sea: A Lord Howe Rise-eastern Australian reconstruction. *Australian Society for Explorational Geophysics Bulletin*, 9:75-81.

Shipboard Scientific Party, 1995. Site 926. *In*, Curry, W.B., Shackleton, N.J., Richter, C., *et al.*, *Proceedings of the Ocean Drilling Program Initial Reports*, 154. Ocean Drilling Program, Texas A&M University, College Station TX.

Shipboard Scientific Party, 2002a. Leg 194 summary. *In*, Isern A.R., Anselmetti, F.S., Blum, P., *et al.*, *Proceedings of the Ocean Drilling Program Initial Reports*, 194:1-88. Ocean Drilling Program, Texas A&M University, College Station TX.

Shipboard Scientific Party, 2002b. Site 1193. *In*, Isern A.R., Anselmetti, F.S., Blum, P., *et al.*, *Proceedings of the Ocean Drilling Program Initial Reports*, 194:1-105 [CD-ROM]. Ocean Drilling Program, Texas A&M University, College Station TX.

Shipboard Scientific Party, 2002c. Site 1194. *In*, Isern A.R., Anselmetti, F.S., Blum, P., *et al.*, *Proceedings of the Ocean Drilling Program Initial Reports*, 194:1-116 [CD-ROM]. Ocean Drilling Program, Texas A&M University, College Station TX.

Shipboard Scientific Party, 2002d. Chapter 2. *In*, Isern A.R., Anselmetti, F.S., Blum, P., *et al.*, *Proceedings of the Ocean Drilling Program Initial Reports*, 194:1-58 [CD-ROM]. Ocean Drilling Program, Texas A&M University, College Station TX.

Shipboard Scientific Party, 2002e. Sites 1198. *In*, Isern A.R., Anselmetti, F.S., Blum, P., *et al.*, *Proceedings of the Ocean Drilling Program Initial Reports*, 194:1-149 [CD-ROM]. Ocean Drilling Program, Texas A&M University, College Station TX.

Siddall, M., 1998. Online *Nature* debate - http://www.nature.com/nature/debates/fossil/fossil_frameset.html.

Signor, P.W., III, Lipps, J.H., 1982. Sampling bias, gradual extinction patterns and catastrophes in the fossil record. *Geological Society of America Special Paper*, 190.

Simpson, G.G., 1944. *Tempo and mode of evolution.* Columbia University Press, New York.

Simpson, G.G., 1952. Periodicity in vertebrate evolution. *Journal of Paleontology*, 26:359-370.

Simpson, G.G., 1953. *The Major Features of Evolution.* Columbia University Press, New York.

Sloss, L.L., 1963. Sequences in the cratonic interior of North America. *Geological Society of America Bulletin*, 74:93-114.

Smith, A.B, 1994. *Systematics in the fossil record.* Blackwell scientific publications, Oxford.

Spero, H.J., 1992. Do planktonic foraminifera accurately record shifts in the carbon isotopic composition of seawater CO_2? *Marine Micropaleontology*, 19:275-285.

Spero, H.J., 1998. Life history and stable isotope geochemistry of planktonic foraminifera. In Manger, W.L., Meeks, L.K., (eds.). Isotope paleobiology and palaeoecology. *Paleontological Society Papers*, 4:7-36.

Spero, H.J., Bijma, J., Lea, J.W. & Bemis, B.E., 1997. Effect of seawater carbonate chemistry on planktonic foraminiferal carbon and oxygen isotope values. *Nature*, 390:497-500.

Spero, H.J., Lea, D.W., 1993. Intraspecific stable isotope variability in the planktic foraminifera *Gloibgerinoides sacculifer*: results from laboratory experiments. *Marine Micropaleontology*, 22:221-234.

Spero, H.J., Lea, D.W., 1996. Experimental determination of stable isotope variability in *Globigerina bulloides*: implications for paleoceanographic reconstructions. *Marine Micropaleontology*, 28:231-246.

Spero, H.J, Williams, D.F., 1988. Extracting environmental information from planktonic foraminiferal ^{13}C data. *Nature*, 335:717-719.

Spero, H.J., Williams, D.F., 1989. Opening the carbon isotope vital effect black box. Seasonal temperatures in the euphotic zone, *Paleoceanography*, 4(6):593-601.

Spezzaferri, S., 1991. Evolution and taxonomy of the *Paragloborotalia kugleri* (Bolli) lineage. *Journal of Foraminiferal Research*, 41(4):313-318.

Spezzaferri, S. P., 1994. Planktonic foraminiferal biostratigraphy and taxonomy of the Oligocene and lower Miocene in the oceanic record. An overview. *Palaeontographica Italica, Pubblicata a cura della societa toscana di scienze naturali*, Vol. LXXXI.

Spindler, M., Hemleben, Ch., 1982. Formation and possible function of annulate lamellae in planktonic foraminifera in a planktonic foraminifer. *Journal of Ultrastructural Research*, 81:341-350.

Spindler, M., Hemleben, Ch., Bayer, U., Bé, A.W.H., Anderson, O.R., 1979. Lunar periodicity of reproduction in the planktonic foraminifer *Hastigerina pelagica* (Foraminifera). *Mar. Ecol. Prog.*, 1(1):61-64.

Srinivasan, M.S., Kennett, J.P., 1981. Neogene Planktonic Foraminiferal Biostratigraphy and Evolution: Equatorial to Subantarctic, South Pacific. *Marine Micropaleontology*, 6(5/6):499-533.

Stainforth, R.M., Lamb, J.L., Jeffors, R.M., 1978. *Rotalia menardii* Parker, Jones and Brady, 1865 (Foraminiferida): Proposed suppression of lectotype and designation of neotype Z.N. (S) 2145. *Bulletin of Zoological Nomenclature London*, 34(4):252-260.

Stainforth, R.M., Lamb, J.L., Luterbacher, H., Beard, J.H., Jeffords, R.M., 1975. Cenozoic planktonic foraminiferal zonation and characteristics of index forms. *University of Kansas Paleontological Contributions Atricle*, 62:1-425.

Stanley, S.M., 1986. Anatomy of a regional mass extinction: Plio-Pleistocene decimation of the Western Atlantic bivalve fauna. *Palaios*, 1:17-36.

Stanley, S.M., Wetmore, K.L., Kennett, J.P., 1988. Macroevolutionary differences between the two major clades of Neogene planktonic foraminifera. *Paleobiology*, 14(3):235-249.

Stehli, F.G, Douglas, R.G., Kafescioglu, I.A., 1972. Models for the evolution of planktonic foraminifera. Pp. 160-191. *In*, Schopf, T.J.M., (ed.), *Models in Paleobiology*. Freeman Cooper, San Francisco.

Stenseth, N.C., Maynard Smith, J., 1984. Coevolution in ecosystems: Red Queen evolution or stasis? *Evolution*, 38:870-880.

Stewart, I.A., Darling, K.F., Kroon, D., *et al.*, 2001. Genotypic variability in subarctic Atlantic planktic foraminifera. *Marine Micropaleontology*, 43(1-2):143-153.

Stothers, R.B., 1986. Periodicity of the Earth's magnetic reversals. *Nature*, 322:444-446.

Stothers, R.B., 1993. Flood basalts and extinction events. Geophysical Research Letters, 20:1399-1402.

Strong, E.E., Lipscomb, D., 1999. Character coding and inapplicable data. *Cladistics*, 15:363-371.

Suess, E., 1906. *The Face of the Earth*. Clarendon, Oxford, vol. 2, p.535.

Swofford, D.L., 1993. PAUP, Phylogenetic Analysis Using Parsimony, Version 3.1. (Computer program)

Swofford, D.L., 2000. PAUP: Phylogenetic Analysis Using Parsimony, version 4.04. (Computer program). Illinois Natural History Survey, Chicago, Illinois.

Tappan, H., Loeblich, A.R., 1988. Foraminiferal evolution, diversification and extinction. *Journal of Palaeontology*, 62: 695-741.

Ter Kuile, B., Erez, J., 1984. In situ growth rate experiments on the symbiont-bearing foraminifera *Amphistegina lobifera* and *Amphisorus hemprichii*. *Journal of the Chemical Society*, 1:562-581.

Thomson, D.J., 1982. Spectrum estimation and harmonic analysis. *IEEE Proceedings*, 70(9):1055-1096.

Thompson, P.R., 1982. Foraminifers of the middle America Trench. *In*: *Initial Reports of the Deep Sea Drilling Project*, 67:351-381. Washington D.C., National Science Foundation.

Todd, R. 1961. On selection of lectotypes and neotypes. *Contributions to the Cushman Foundation for Foraminiferal Research.*, 12:121-122.

Toumarkine, M., Luterbacher, H., 1985. Paleocene and Eocene planktonic foraminifera. Pp. 87-154. *In*, Bolli, H.M., Saunders, J.B., Perch-Neilsen, K., (eds.). *Plankton Stratigraphy*. Cambridge University Press, Cambridge.

Urey, H.C., 1947. The thermodynamic properties of isotopic substances. *Journal of the Chemical Society London*, 562-581.

Vail, P.R., Hardenbol, J., 1979. Sea-level changes during the Tertiary. *Oceanus*, 22:71-79.

Vail, P.R., Mitchum, R.M., Jnr., Todd, R.G., Widemier, J.M., Thompson, S., III, Sangree, J.B., Bubb, J.N., Hatelid, W.G., 1977. Seismic stratigraphy and global changes in sea level. *In*, Payton, C.E. (ed.), *Seismic Stratigraphy: Applications to Hydrocarbon Exploration*. AAPG Mem., 26:49-212.

Valentine, J.W., 1985. Diversity as data. Pp. 3-8. *In*, J.W. Valentine (ed.) *Phanerozoic Diversity Patterns*. Princeton University Press, Princeton, New Jersey.

Van Eijden, A.J.M., Ganssen, G.M., 1995. An Oligocene multi-species foraminiferal oxygen and carbon isotope record from ODP Hole 758A (Indian Ocean): paleoceanographic and paleo-ecologic implications. *Marine Micropaleontology*, 25:47-65.

Van Morkhoven, F.P.C.M., Berggren, W.A., Edwards, A.S., et al., 1986. Cenozoic cosmopolitan deep-water benthic foraminifera. *Mem. Cent. Rech. Explor. Prod. Elf Aquitaine*, 11, Cambridge University Press, 329-426.

Van Valen, L., 1973. A new evolutionary law. *Evolutionary Theory*, 1:1-30.

Van Valen, L., 1976. The Red Queen lives. *Nature*, 260:575.

Vincent, E., Killingley, J.S., Berger, W.H., 1985. Miocene oxygen and carbon isotope stratigraphy of the tropical Indian Ocean. *In*: Kennett, J.P. (ed.), The *Miocene Ocean: Paleoceanography and Biogeography*. GSA Memoir 163.

Watts, A.B., Thorne, J.A., 1984. Tectonics, global changes in sea-level and their relationship to stratigraphic sequences at the U.S. Atlantic continental margin. *Marine and Petroleum Geology*, 1(4):319- 339.

Wei, K-Y., 1994. Allometric heterochrony in the Pliocene-Pleistocene planktic foraminiferal clade *Globoconella*. *Paleobiology* , 14:345-363.

Wei, Kuo-Yen, Kennett, J.P., 1983. Nonconstant extinction rates of Neogene planktonic foraminifera. *Nature*, 305:218-220.

Wei, Kuo-Yen, Kennett, J.P., 1986. Taxonomic evolution of Neogene planktonic foraminifera and paleoceanographic relations. *Paleoceanography*, 1:67-84.

Wilson, P.A., Norris, R.D., 2001. Warm tropical ocean surface and global anoxia during the mid-Cretaceous period. *Nature*, 412:425-429.

Wilson, P.A., Norris, R.D., Cooper, M.J., 2002. Testing the Cretaceous greenhouse hypothesis using glassy foraminiferal calcite from the core of the Turonian tropics on Demerara Rise. *Geology*, 30(7):607-610.

Wilson, P.A., Opdyke, B.N., 1996. Equatorial sea-surface temperatures of the Maastrichtian revealed through remarkable preservation of metastable carbonate. *Geology*, 24(6):555-558.

Wolf-Gladrow, D.A., Bijma, J., Zeebe, R.E., 1999. Model simulation of the carbonate chemistry in the microenvironment of symbiont bearing foraminifera. *Marine Chemistry*, 64:181-198.

Wright, J.D., Thunell, R.C., 1988. Neogene planktonic foraminiferal biogeography and paleoceanography of the Indian Ocean. *Micropaleontology*, 34(3):193-216, 1988.

Wu, G., Berger, W. H., 1989. Planktonic foraminifera: differential dissolution and the Quaternary stable isotope record in the west-equatorial Pacific. *Paleoceanography*, 4:181-198.

Yiou, P., Baert, E., Loutre, M.F., 1996. Spectral analysis of climatic data. *Surveys in Geophysics*, 17:619-663.

Younker, J.L., Ehrlich, R., 1977. Fourier biometrics: harmonic amplitudes as multivariate shape descriptors. *Systematic Zoology*, 26:336-342.

Zachos, J.C., Arthur, M.A., Bralower, T.J., Spero, H.J., 2002. Tropical temperatures in greenhouse episodes. *Nature*, 419(6910):897-898.

Zachos, J.C., Pagani, M., Sloan, L., Thomas, E., Billups, K., 2001. Trends, rhythms, and aberrations in global climate 65 Ma to present. *Science*, 292:686-69.

Zachos, J.C., Stott, L.D. & Lohmann, K.C., 1994. Evolution of early Cenozoic marine temperatures. *Paleoceanography*, 9:353-387.

Zahn, C.T., Roskies, R.Z., 1972. Fourier descriptors for the plane closed curves: *IEEE Computers Transactions*, C-21:269-281.

Zelditch, M.L., Fink, W.L., Swiderski, D.L., 1995. Morphometrics, homology, and phylogenetics: quantified characters as synapomorphies. *Systematic Biology*, 44:179-189.

Appendix 2.1. Morphospecies level range database of all planktonic foraminifera.

No.	Genus Name	Species Name	Original Genus Name	Author & Year	Range (My)	F A D (Ma)	L O D (Ma)	Range Source Reference	General Notes	Depth Habitat	DH Reference
1	Abathomphalus	intermedius	Globotruncana intermedia	Bolli, 1951	1.8	67.7	65.9	9		D	O
2		mayaroensis	Globotruncana mayaroensis	Bolli, 1951	1.7	66.7	65	9		D	O
3	Acarinina	acarinata	Acarinina acarinata	Subbotina, 1953	3.7	59.2	**55.5**	14	P4-early P6	S	
4		angulosa	Globigerina soldadoensis angulosa	Bolli, 1957	10.5	51.8	41.3	2		S	
5		aquiensis	Acarinina aquiensis (Loeblich & Tappan)	Loeblich & Tappan, 1957	6.9	59.2	**52.3**	14	P4-early P7	S	
6		bullbrooki	Globorotalia bullbrooki	Bolli, 1957	11.9	50.4	38.5	2		S	K,O
7		coalingensis	Globigerina coalingensis	Cushman & Hanna, 1927	10.3	56.8	46.5	2		S	K,O
8		collactea	Globorotalia collactea	Finlay, 1939	11.1	49.6	38.5	2		S	K,O
9		cuneicamerata	Acarinina cuneicamerata (Blow)	Blow, 1979	4	**49**	**45**	11	Late P9-MidP11	S	
10		esnaensis	Acarinina esnaensis (Le Roy)	Le Roy, 1953	5.5	55.9	50.4	14		S	
11		matthewsae	Acarinina matthewsae	Blow, 1979	5.4	49	43.6	Pearson pers. comm.	Late P9-Early P12	S	
12		mckannai	Globigerina mckannai	White, 1928	1.9	58.7	56.8	2		S	
13		nitida	Globigerina nitida	Martin, 1943	2.8	59.2	56.4	2		S	
14		pentacamerata	Globorotalia pentacamerata	Subbotina, 1947	8.7	52.3	43.6	2		S	
15		primitiva	Globoquadrina primitiva	Finlay, 1947	11.2	50.6	39.4	2		S	
16		pseudotopilensis	Acarinina pseudotopilensis	Subbotina, 1953	10.5	51.8	41.3	2		S	
17		quetra	Globorotalia quetra	Bolli, 1957	2.5	52.1	49.6	2		S	
18		rohri	Truncorotaloides rohri	Bronnimann & Bermudez, 1953	11.1	49.6	38.5	2		S	
19		soldadoensis	Globigerina soldadoensis	Bronnimann, 1952	7.6	56.9	49.3	2		S	K,O
20		spinuloflata	Globigerina spinuloflata	Bandy, 1949	11.9	50.4	38.5	7		S	
21		strabocella	Globorotalia strabocella	Loeblich & Tappan, 1957	1.3	60.5	59.2	2		S	
22		subsphaerica	Globigerina subsphaerica	Subbotina, 1947	17.6	59.2	41.6	2		S	
23		topilensis	Globigerina topilensis	Cushman, 1925	5.4	45.6	40.2	2		S	K,O
24		triplex	Acarinina triplex	Subbotina, 1953	8.7	53.5	44.8	2		S	
25		wilcoxensis	Globorotalia wilcoxensis	Cushman & Ponton, 1932	3.8	54.2	50.4	2		S	
26	Alanlordella	aptiensis	Globigerinelloides aptiense	Longoria, 1974	2.9	115.1	112.2	1		?	
27	Archaeoglobigerina	australis	Archaeoglobigerina australis	Huber, 1990	8.9	73.9	65	24		?	
28		blowi	Archeaoglobigerina blowi	Pessagno, 1967	22.4	87.4	65	9		?	
29		bosquensis	Archeaoglobigerina bosquensis	Pessagno, 1967	3.5	87	83.5	7		?	
30		cretacea	Globigerina cretacea	d'Orbigny, 1840	19.1	89	69.9	9		?	
31		mateola	Archeaoglobigerina mateola	Huber, 1990	12.3	77.3	65	24		?	
32	Ascoliella	nitida	Favusella nitida	Michael, 1973	17.7	116.6	98.9	1		?	
33		quadrata	Favusella quadrata	Michael, 1973	6.7	105.6	98.9	1		?	
34		scitula	Favusella scitula	Michael, 1973	13.3	112.2	98.9	1		?	
35		voloshinae	Favusella voloshinae	Longoria & Gamper, 1977	6.7	105.6	98.9	1		?	
36	Beella	digitata	Globigerina digitata	Brady, 1879	2	2	0	5		?	
37		praedigitata	Globigerina praedigitata	Parker, 1967	6.2	8.2	2	5		?	
38	Biglobigerinella	barri	Biglobigerinella barri	Bolli, Loeblich & Tappan, 1957	4.4	116.6	112.2	1		?	
39	Biticinella	breggiensis	Anomalina breggiensis	Gandolfi, 1942	8.7	108.7	100	7		S	I
40	Blefuscuiana	aptiana s.s.	Hedbergella aptiana	Bartenstein, 1965	21.4	127	105.6	1		?	
41		convexa	Loeblichella convexa	Longoria, 1974	2.6	116.6	114	1		?	
42		excelsa s.s.	Hedbergella excelsa	Longoria, 1974	4.4	121	116.6	1		?	
43		hispaniae	Hedbergella hispaniae	Longoria, 1974	2.6	114.8	112.2	1		?	
44		infracretacea s.s.	Globigerina infracretacea	Glaessner, 1937	13.4	119	105.6	1		?	
45		kuznetsovae	Blefuscuiana kuznetsovae	Banner & Desai, 1988	4.4	116.6	112.2	1		?	
46		laculata s.s.	Blefuscuiana laculata	Banner, Copestake & White, 1993	3	127	124	1		?	
47		occulta s.s.	Hedbergella occulta	Longoria, 1974	8.8	121	112.2	1		?	
48		praetrocoidea	Hedbergella praetrocoidea	Kretchmar & Gorbachik, 1986	4.4	121	116.6	1		?	
49		speetonensis s.s.	Blefuscuiana speetonensis	Banner & Desai, 1988	4.1	114.1	110	1		?	
50	Blowiella	maridalensis	Planomalina maridalensis	Bolli, 1959	4.4	116.6	112.2	1		?	
51		solida	Blowiella solida	Kretchmar & Gorbachik, 1986	4.4	116.6	112.2	1		?	
52	Candeina	nitida	Candeina nitida	d'Orbigny, 1839	7.1	7.1	0	5		S	
53	Cassigerinella	chipolensis	Cassidulina chipolensis	Cushman & Ponton, 1932	27.5	39.4	11.9	5+6		S	
54		boudecensis	Cassigerinella boudecensis	Pokorny, 1955	10.7	26	15.3	7		S	
55		globulosa	Cassidulina globulosa	Egger, 1957	11.4	28.7	17.3	6		S	
56		martinezpicoi	Riveroinella martinezpicoi	Bermudez & Seiglie, 1967	13.3	28.4	15.1	5+6		S	
57	Cassigerinelloita	amekiensis	Cassigerinelloita amekiensis (Stolk)	Stolk, 1965	4.2	49.5	45.3	28		S	
58	Catapsydrax	africanus	Globigerinita africana	Blow & Banner, 1962	3.9	25.9	22	13		D	F
59	/Globorotaloides	carcoselleensis	Globorotaloides carcoselleensis	Toumarkine & Bolli, 1975/0	10.6	45.8	35.2	7		D	F
60		dissimilis	Globigerina dissimilis	Cushman & Bermudez, 1937	22.9	40.2	17.3	2+5		D	F
61		globiformis	Globigerinita globiformis	Blow & Banner, 1962	19.9	38.7	18.8	6		D	F

62		hexagona	Globigerina hexagona	Natland, 1938	12.6	27.7	15.1	5+6		D	F
63		howei	Catapsydrax howei	Blow & Banner, 1962	4.8	40	35.2	13		D	F
64		martini	Globigerinita martini	Blow & Banner, 1962	22.9	40.1	**17.2**	6		S	O
65		parvulus	Catapsydrax parvulus	Bolli, Loeblich & Tappan, 1957	6.7	17	10.3	5		D	F
66		pera	Catapsydrax pera (Todd)	Todd, 1957	4.7	**38.4**	**33.7**	13	Late P14-P18	D	F
67		permicrus	Globorotalia (Turborotalia) permicra	Blow & Banner, 1962	13.4	28.5	15.1	6		D	F
68		stainforthi	Catapsydrax stainforthi	Bolli, Loeblich & Tappan, 1957	11.8	26.9	15.1	5		D	F
69		suteri	Globorotaloides suteri	Bolli, 1957	29	44.8	15.8	6+7		D	F
70		taroubaensis	Globigerinita taroubaensis	Bronnimann, 1952	10.6	50.7	40.1	14		D	F
71		testarugosa	Globorotalia testarugosa	Jenkins, 1960	4.9	28	23.1	6		D	F
72		turgida	Globigerina linaperta Finlay var. turgida	Finlay, 1939	12.1	**56.2**	44.1	26		D	F
73		unicavus	Catapsydrax unicavus	Bolli, Loeblich & Tappan, 1957	12.9	30.3	17.4	5+6		D	O
74		variabilis	Globorotaloides variabilis	Bolli, 1957	26.8	**32**	5.2	5+6		D	F
75	Chiloguembelina	crinita	Gumbelina crinita	Glaessner, 1937	4	59.2	55.2	2		D	A
76		cubensis	Guembelina cubensis	Palmer, 1934	21	49.2	28.2	2		D	A
77		midwayensis	Gumbelina midwayensis	Cushman, 1940	9.6	64.9	55.3	2		D	A
78		morsei	Gumbelina morsei	Kline, 1943	1.9	64.9	63	2		D	A
79		multicellaris	Chiloguembelina multicellaris	Hussen, 1949	5.1	45.8	40.7	20		D	A
80		subtriangularis	Chiloguembelina subtriangularis	Beckman, 1957	2.1	61.7	59.6	2		D	A
81		trinitatensis	Gumbelina trinitatensis	Cushman & Renz, 1942	1.1	55.9	**54.8**	20		D	A
82		victoriana	Chiloguembelina victoriana	Beckmann, 1957	13.5	40.6	27.1	20		D	A
83		wilcoxensis	Gumbelina wilcoxensis	Cushman & Ponton, 1932	9.6	58.7	49.1	20		D	A
84	Clavatorella	bermudezi	Hastigerinella bermudezi	Bolli, 1957	4.3	15.9	11.6	5		D	N
85		nicobaroensis	Clavatorella nicobarensis	Srinivasan & Kennett, 1974	5	8.9	3.9	5		D	N
86	Claviblowiella	saundersai	Planomalina saundersi	Bolli, 1959	5.7	117	111.3	1		?	
87		sigali	Globigerinelloides sigali	Longoria, 1974	4.4	116.6	112.2	1		?	
88	Clavigerinella	akersi	Clavigerinella akersi	Bolli, Loeblich & Tappan, 1957	5.3	48.9	43.6	7		I	B,K
89		columbiana	Hastigerinella colombiana	Petters, 1954	6.7	47.6	40.9	2		I	B,K
90		eocanica	Hastigerinella eocanica	Nuttall, 1928	15.5	49.2	33.7	2		I	B,K
91		jarvisi	Hastigerinella eocanica	Cushman, 1930	5.4	49	43.6	7		I	B,K
92	Clavihedbergella	moremani	Hastigerinella moremani	Cushman, 1931	5	**93**	**88**	21		?	
93	Compactogerina	stellapolaris	Globuligerina stellapolaris	Grigelis, 1977	6.7	150.7	144	1		?	
94	Conoglobigerina	avarica	Globigerina (Conoglobigerina) avarica	Morozova, 1961	5	171.8	166.8	1		?	
95		avariformis	Conoglobigerina avariformis	Kasimova, 1984	3.7	172.9	169.2	1		?	
96		balakhmatovae	Globigerina (Eoglobigerina) balakhmatovae	Morozova, 1961	6.1	172.9	166.8	1		?	
97		caucasia	Globuligerina caucasica	Gorbachik & Prorshina, 1979	7.7	142.2	134.5	1		?	
98		conica	Globigerina conica	Ioveceva & Trifonova, 1961	8.5	150.7	142.2	1		?	
99		dagestanica	Globigerina (Conoglobigerina) dagestanica	Morozova, 1961	8.5	172.9	164.4	1		?	
100		gulekhensis	Globuligerina gulekhensis	Gorbachik & Poroshina, 1979	7.7	142.2	134.5	1		?	
101		jurassica	Globigerina jurassica	Hofman, 1958	7.3	169.2	161.9	1		?	
102		meganomica	Globuligerina meganomica	Kuznetsova, 1980	1.7	162.9	161.2	1		?	
103		terquemi	Globigerina terquemi	Ioveceva & Trifonova, 1961	8.5	150.7	142.2	1		?	
104	Contusotruncana	contusa	Pulvinulina arca Cushman var. contusa	Cushman, 1926	3.2	68.2	65	9		S?	G
105		fornicata	Globotruncana fornicata	Plummer, 1931	18.2	85.6	67.4	9		D	
106		patelliformis	Globotruncana (Globotruncana) patelliformis	Gandolfi, 1955	13	79.7	66.7	9		D	
107		plicata	Globotruncana conica White var. plicata	White, 1928	3.9	69.3	65.4	9		D	
108		plummerae	Globotruncana (Globotruncana) fornicata Plummer subsp. plummerae	Gandolfi, 1955	10.8	79.7	68.9	9		D	
109		walfischensis	Globotruncana walfischensis	Todd, 1970	4.8	69.8	65	9		D	
110	Cribrohantkenina	inflata	Hantkenina inflata	Howe, 1928	1.2	35.1	33.9	7		I	B
111	Dentoglobigerina	altispira	Globigerina altispira	Cushman & Jarvis, 1936	18.3	21.5	3.2	5		S	L
112		baroemoenensis	Globigerina baroemoenensis	LeRoy, 1939	27.3	**32**	4.7	6		S	
113		galavisi	Globigerina galavisi	Bermudez, 1961	6.2	29.4	23.2	6		S	S
114		globosa	Globoquadrina altispira globosa	Bolli, 1957	25.9	30.3	4.4	5+6		S	
115		globularis	Globoquadrina globularis	Bermudez, 1961	13.2	**32**	**18.8**	6		S	
116		langhiana	Dentoglobigerina langhiana (Cita & Gelati)	Cita & Gelati, 1960	14.9	28.4	13.5	6		S	
117		larmeui	Globoquadrina larmeui	Akers, 1955	15.8	30.9	15.1	6		S	
118		yeguaensis	Globigerina yeguaensis	Weinzierl & Applin, 1929	14.3	43.9	29.6	13		D	
119	Dicarinella	algeriana	Praeglobotruncana algeriana	Caron, 1966	3.6	93.9	90.3	8		D	
120		asymetrica	Globotruncana asymetrica	Sigal, 1952	1.5	85	83.5	9		D	
121		concavata	Rotalia concavata	Brotzen, 1934	3.1	87	83.9	9		D	
122		hagni	Praeglobotruncana hagni	Scheibnerova, 1962	3.7	92.7	89	9		D	
123		imbricata	Globotruncana (Globotruncana) imbricata	Mornod, 1949-1950	6.2	92.8	86.6	9		D	
124		primitiva	Globotruncana (Globotr.) ventricosa White subsp. primitiva	Dalbiez, 1955	3.6	89	85.4	9		D	
125	Eoglobigerina	edita	Globigerina edita	Subbotina, 1953	3.6	64.9	61.3	2		S	
126		eobulloides	Globigerina (Eoglobigerina) eobulloides	Morozova, 1959	2	65	63	2		S	
127		spiralis	Globigerina spiralis	Bolli, 1957	1.2	62.1	60.9	2		S	

128	Falsotruncana	maslakovae	Faslotruncana maslakovae	Caron, 1981	0.6	89.2	88.6	7		D	
129	Favusella	hiltermani	Hedbergella hiltermani	Loeblich & Tappan, 1961	2.7	98.9	96.2	1		?	
130		stiftia	Favusella stiftia	Rosler, Lutze & Pflaumann, 1979	11	132	121	1		?	
131		washitensis	Globigerina washitensis	Carsey, 1926	20.4	116.6	96.2	1		?	
132	Fohsella	birnageae	Globorotalia birnageae	Blow, 1969	12	27.1	15.1	5		I	E,F
133		fohsi	Globorotalia fohsi	Cushman & Ellisor, 1939	1.6	13.5	11.9	5		I	E,F
134		lobata	Globorotalia fohsi lobata	Bermudez, 1949	1	12.9	11.9	5		I	E,F,H
135		peripheroacuta	Globorotalia (Turborotalia) peripherocuta	Blow & Banner, 1966	1	15.1	14.1	5		I	E,F
136		peripheroronda	Globorotalia (Turborotalia) peripheroronda	Blow & Banner, 1966	8.8	23.1	14.3	5		I	E,F
137		praefohsi	Globorotalia (Turborotalia) praefoshi	Blow & Banner, 1966	1.9	14.8	12.9	5		I	E,F,H
138		robusta	Globorotalia fohsi robusta	Bolli, 1950/ Cushman & Ellisor, 1939	0.6	12.5	11.9	5		I	E,F
139	Gansserina	gansseri	Globotruncana gansseri	Bolli, 1951	2.3	68.2	65.9	9		D	
140		wiedenmayeri	Globotruncana (Globotruncana) wiedenmayeri	Gandolfi, 1955	4	69	65	9		D	
141	Globanomalina	archeocompressa	Globorotalia (Turborotalia) archeocompressa	Blow, 1979	1.7	65	63.3	2		S	
142		australiformis	Globorotalia australiformis	Jenkins, 1965	5.8	55.9	50.1	2		S	
143		chapmani	Globorotalia chapmani	Parr, 1938	8.5	59.2	50.7	2		S	
144		compressa	Globigerina compressa	Plummer, 1926	1.5	62.2	60.7	2		S	
145		ehrenbergi	Globorotalia ehrenbergi	Bolli, 1957	1.9	61.1	59.2	2		S	
146		imitata	Globorotalia imitata	Subbotina, 1953	5.8	61.7	55.9	2		S	
147		ovalis	Globanomalina ovalis	Haque, 1956	6	56.8	50.8	2		S	
148		planocompressa	Globorotalia planocompressa planocompressa	Shutskaya, 1965	3.4	64.9	61.5	2		S	
149		planoconica	Globorotalia planoconica	Subbotina, 1953	9.4	56.6	47.2	2		S	
150		pseudomenardii	Globorotalia pseudomenardii	Bolli, 1957	3.3	59.2	55.9	2		S	
151	Globigerina	angulofficinalis	Globigerina angulofficinalis	Blow, 1959	2.8	30.5	27.7	2		S	
152		angulisuturalis	Globigerina ciperoensis angulisutralis	Bolli, 1957	5.9	28.9	23	2+5		S	
153		bulloides	Globigerina bulloides	d'Orbigny, 1826	15	15	0	5		I	F
154		cariacoensis	Globigerina cariacoensis	Rogl & Bolli, 1973	1.7	1.7	0	7		S	
155		ciperoensis	Globigerina ciperoensis ciperoensis	Bolli, 1957	11.2	30.5	19.3	2+5		S	
156		corpulenta	Globigerina corpulenta	Subbotina, 1953	6.9	40.6	**33.7**	7		S	
157		crytomphala	Globigerina bulloides d'Orbigny var. cryptomphala	Glaessner, 1937	16	49.7	**33.7**	7		S	
158		eamesi	Globigerina eamesi	Blow, 1959	24.3	26.3	2	5		S	
159		falconensis	Globigerina falconensis	Blow, 1959	16.9	16.9	0	5		S	
160		fariasi	"Globigerina" ciperoensis fariasi	Bermudez, 1961	13.4	28.5	15.1	6		S	
161		gnaucki	Globigerina ouachitensis gnaucki	Blow & Banner, 1962	3	25.2	22.2	6		S	
162		medizzai	Globigerina medizzai	Toumarkine & Bolli, 1975	7.7	42.9	35.2	7		S	
163		occlusa	Globigerina praebulloides occlusa	Blow & Banner, 1962	7	28	21	6		S	
164		officinalis	Globigerina officinalis	Subbotina, 1953	21.5	40.3	18.8	2		S	
165		ottnangiensis	"Globigerina" ciperoensis ottangiensis	Rogl, 1969	13.5	29.4	15.9	6		S	
166		ouachitaensis	Globigerina ouachitensis	Howe & Wallace, 1932	7.7	29.2	21.5	6		S	
167		praebulloides	Globigerina praebulloides	Blow, 1959	28.2	33.8	5.6	2		S	N
168		quinqueloba	Globigerina quinqueloba	Natland, 1938	21.5	21.5	0	5		S	
169		umbilicata	Globigerina umbilicata	Orr & Zaitzeff, 1971	1.9	2.5	0.6	5		S	
170		venezuelana s.l.	Globigerina venezuelana	Hedberg, 1937	40.2	44.4	4.2	6+7		D	L
171	"Globigerina"	euapertura	"Globigerina" euapertura	Jenkins, 1960	15.6	**30.3**	**14.7**	6	Dentoglobigerina?	D	N
172		prasaepis	"Globigerina" prasaepis	Blow, 1969	15.6	**32**	**16.4**	6		D	
173	Globigerinatella	insueta	Globigerinatella insueta	Cushman & Stainforth, 1945	4	18.8	14.8	6		S	L
174	Globigerinatheka	barri	Globigerinatheka barri	Bronnimann, 1952	9.1	45.8	36.7	2		S	
175		curryi	Globigerapsis subconglobata curryi	Proto Decima & Bolli, 1957	2.3	42.9	40.6	2		S	
176		euganea	Globigerinatheka subconglobata euganea	Proto Decima & Bolli, 1970	2	42.3	40.3	2		S	
177		index	Globigerinoides index	Finlay, 1939	11.5	45.8	34.3	2		S	K,O
178		kugleri	Globigerapsis kugleri	Bolli, Loeblich & Tappan, 1957	2.9	42.6	39.7	2		S	O
179		luterbacheri	Globigerinatheka luterbacheri	Bolli, 1972	5.3	40.1	34.8	2		S	
180		mexicana	Globigerina mexicana	Cushman, 1925	9.8	46.5	36.7	2		S	
181		micra	Globigerinoides subconglobatus Chalilov var. micra	Shutskaya, 1958	5.2	49.8	44.6	2		S	
182		rubriformis	Globigerinoides	Subbotina, 1953	9.4	43.3	33.9	2		S	
183		semiinvoluta	Globigerinoides semiinvolutus	Keijzer, 1945	3.9	38.1	34.2	2		S	O
184		senni	Muricoglobigerina senni (Beckmann)	Beckmann, 1954	13.2	50.6	37.4	2		I	K
185		subconglobata	Globigerinoides subconglobatus	Shutskaya, 1958	9.8	49	39.2	2		S	
186		tropicalis	Globigerapsis tropicalis	Blow & Banner, 1962	2.5	36.7	34.2	2		S	
187	Globigerinella	adamsi	Globigerinella adamsi	Banner & Blow, 1959	0.01	0.01	0	7		I	
188		aequilateralis	Globigerina aequilateralis	Brady, 1879	12.7	12.7	0	5	siphonifera-syn.	I	Q
189		calida	Globigerina calida	Parker, 1962	3.6	3.6	0	5		I	
190		obesa	Globorotalia obesa	Bolli, 1957	32	32	0	2+5		I	
191		praesiphonifera	Hastigerina siphonifera praesiphonifera	Blow, 1969	9.9	21.8	11.9	5		I	
192		pseudobesa	Turborotalia pseudobesa	Salvatorini, 1966	7.5	11.3	3.8	5		I	
193	Globigerinelloides	algerianus	Globigerinelloides algeriana	Cushman & ten Dam, 1948	1.5	116.2	114.7	1		I	C
194		blowi	Globigerinelloides blowi (Bolli)	Bolli, 1959	4.5	120.4	115.9	1		I	C

195		duboisi	Globigerinella duboisi	Chevalier, 1961	4.4	116.6	112.2	1		I	C
196		ferreolensis	Bitcinella ferreolensis	Moullade, 1961	4.4	116.6	112.2	1		I	C
197		prairiehillensis	Globigerinelloides prairiehillensis	Pessagno, 1967	12	79	67	1		I	C
198		subcarinata	Globigerinella messinae subcarinata	Bronnimann, 1952	6.1	71.1	65	1		I	C
199		ultramicra	Globigerinella ultramicra	Subbotina, 1949	31.2	101.6	70.4	1		I	C
200	Globigerinita	glutinata	Globigerinita glutinata/ Globigerina glutinata	Parker, 1962/ Egger, 1893	29.5	29.5	0	5		S	Q
201		incrusta	Globigerinita incrusta	Akers, 1955	13.2	28	**14.8**	6		S	
202		parkerae	Globigerinoides parkerae	Bermudez, 1961	13.5	13.5	0	5		S	
203		uvula	Pylodexia uvula	Ehrenberg, 1861	27.3	27.3	0	5		S	
204	Globigerinoides	bisphericus	Globigerinoides bisphericus	Todd, 1957	1.5	16.4	14.9	13		S	F,K
205		bollii	Globigerinoides bollii	Blow, 1959	7.1	23.1	16	5		S	F
206		immaturus	Globigerinoides sacculiferus (Brady) var. immaturus	LeRoy, 1939	12	24.5	12.5	5		S	F
207		inusitatus	Globigerinoides inusitatus	Jenkins, 1966	2.5	27	24.5	6		S	F
208		obliquus	Globigerinoides obliqua	Bolli, 1957	12.1	26.9	14.8	5		S	F
209		parawoodi	Globigerinoides parawoodi	Keller, 1981	7.2	23	15.8	5		S	F
210		primordius	Globigerinoides quadrilobatus (d'Orbigny) subsp. primordius	Blow & Banner, 1962	9.9	29.2	19.3	2+5		S	F
211		quadrilobatus	Globigerina quadrilobata	d'Orbigny 1846	8.9	23.8	**14.9**	5		S	F
212		subquadratus	Globigerinoides subquadratus	Bronnimann, 1954	9	23.8	**14.8**	5		S	F
213		subsacculifer	Globigerinoides sacculifer subsacculifer	Cita, Premoli Silva & Rossi, 1965	7.8	23.1	**15.3**	6		S	F
214		trilobus	Globigerina triloba	Reuss, 1850	7.4	22.2	**14.8**	5		S	F,K
215	"Globigerinoides"	altiapertura	Globigerinoides triloba altiapertura	Bolli, 1957	6.2	22.5	16.3	5		S	F
216		bulloideus	Globigerinoides bulloideus	Crescenti, 1966	2.8	6.3	3.5	5		S	F
217		conglobatus	Globigerina conglobata	Brady, 1879	5.9	5.9	0	5		S	F,Q
218		diminutus	Globigerinoides diminita	Bolli, 1957	2.5	17.3	14.8	5		S	F
219		extremus	Globigerinoides obliquus extremus	Bolli & Bermudez, 1965	6.5	8.5	2	5		S	F
220		fistulosus	Globigerina fistulosus	Schubert, 1910	0.8	2.8	2	5		S	F
221		kennetti	Globigerinoides kennetti	Keller & Poore, 1980	2.7	8.4	5.7	5		S	F
222		mitra	Globigerinoides mitra	Todd, 1957	5.9	17.8	11.9	5		S	F
223		primordius	Globigerinoides primordius	Blow & Banner, 1962	7.8	27.1	19.3	5		S	F,N
224		ruber	Globigerina rubra	d'Orbigny, 1839	10.4	10.4	0	5+6		S	F,Q
225		sacculifer	Globigerina sacculifer	Brady, 1877	17.4	17.4	0	5		S	F,Q
226		seigliei	Globigerinoides rubra (d'Orbigny) seigliei	Bermudez & Bolli, 1969	2.7	8.4	5.7	5		S	F
227		sicanus	Globigerinoides sicanus	De Stefani, 1950	1.6	16.4	14.8	5		S	F
228	Globoconella	conoidea	Globorotalia miozea conoidea	Walters, 1965	9.3	16.4	7.1	5		I	F,P
229		conomiozea	Globorotalia conomiozea	Kennett, 1966	2.1	7.3	5.2	5		I	P
230		incognita	Globorotalia zealandica incognita	Walters, 1965	4.9	19.8	14.9	5		I	P
231		inflata	Globoconella inflata (d'Orbigny)	d'Orbigny, 1839	3.1	3.1	0	5		I	P,Q
232		miozea	Globorotalia miozea	Finlay, 1939	1.6	**16.4**	**14.8**	5		I	F,P
233		panda	Globorotalia menardii (d'Orbigny) sub sp. panda	Jenkins, 1960	10.2	16.4	6.2	5		I	P
234		pliozea	Globorotalia pliozea	Hornibrook, 1982	3.9	3.9	0	15		I	P
235		puncticulata	Globigerina puncticulata	Deshayes, 1832	4.6	7.3	2.7	5		I	P
236		sphericomiozea	Globorotalia miozea sphericomiozea	Walters, 1965	0.3	5.3	5	5		I	P
237		triangula	Globigerina triangula	d'Orbigny, 1839	2.1	3.1	1	30	syn of inflata?	I	P
238		zealandica	Globorotalia zealandica	Hornibrook, 1958/9	7.4	22.2	**14.8**	5		I	P
239	Globoconusa	daubjergensis	Globigerina daubjergensis	Bronnimann, 1953	3.2	64.9	61.7	2		S	
240	Globoquadrina	binaiensis	Globigerina binaiensis	Koch, 1935	5.8	26	20.2	2		I	F
241		conglomerata	Globigerina conglomerata	Schwager, 1866	3.6	3.6	0	16		I	
242		dehiscens	Globorotalia dehiscens	Chapman, Parr & Collins, 1934	20.3	25.1	4.8	5		I	
243		praedehiscens	Globoquadrina dehiscens praedehiscens	Blow & Banner, 1962	16	31.1	15.1	2		I	F
244		rohri	Globigerina rohri	Bolli, 1957	19.5	32	12.5	6		I	
245		sellii	Globoquadrina sellii	Borsetti, 1959	12.4	31.2	18.8	2		I	S
246		tapuriensis	Globigerina tripartita tapuriensis	Blow & Banner, 1962	8.1	33.8	25.7	2		I	
247		tripartita	Globigerina bulloides d'Orbiny var. tripartita	Koch, 1926	13.9	38.9	25	2		D	F
248	Globorotalia	flexuosa	Pulvinulina tumida Brady var. flexuosa	Koch, 1923	3.7	5.7	2	5		D	R
249		lenguanensis	Globorotalia lenguaensis	Bolli, 1957	4.1	13.5	9.4	5		D	
250		mediterranea	Globorotalia mediterranea	Catalano & Sprovieri	1.6	7.2	5.6	Cifelli & Scott, 1986		D	
251		merotumida	Globorotalia (Globorotalia) merotumida	Blow & Banner, 1965	4.2	10	5.8	5		D	
252		nicolae	Globorotalia nicolae	Catalano & Sprovieri	1.6	6.3	4.7	Cifelli & Scott, 1986		D	
253		paralenguanensis	Globorotalia (Globorotalia) paralenguaensis	Blow, 1969	2.2	10.2	8	5		D	
254		pleisotumida	Globorotalia (Globorotalia) plesiotumida	Blow & Banner, 1965	3.5	8	4.5	5		D	
255		praescitula	Globorotalia scitula (Brady) praescitula	Blow, 1959	3	17.8	14.8	5&7		S	R
256		saheliana	Globorotalia saheliana	Catalano & Sprovieri	0.6	6.1	5.5	Cifelli & Scott, 1986		D	
257		suterae	Globorotalia suterae	Catalano & Sprovieri	2.6	8.4	5.8	7		D	
258		tumida	Pulvinulina menardii (d'Orbigny) var. tumida	Brady, 1877	5.8	5.8	0	5		D	Q,R
259		ungulata	Globorotalia ungulata	Bermudez, 1960	3.2	3.2	0	5		D	
260	Globotruncana	aegyptiaca	Globotruncana aegyptiaca	Nakkady, 1951	4.8	69.8	65	9		I	C
261		arca	Pulvinulina arca	Cushman, 1926	18.3	84.3	66	9		I	C

262		bulloides	Globotruncana linnei (d'Orbigny) subsp. bulloides	Volger, 1941	16.7	84.1	67.4	9		I	C
263		dupeublei	Globotruncana dupeublei	Caron et. al., 1984	2.5	67.5	65	9		I	C
264		esnehensis	Globotruncana arca (Cushman) var. esnehensis	Nakkady, 1950	5	70	65	9		I	C
265		falsostuarti	Globotruncana falsostuarti	Sigal, 1952	7.2	72.2	65	9		I	C
266		insignis	Globotruncana rosetta insignis	Gandolfi, 1955	9.9	75.8	65.9	9		I	C
267		lapparenti	Globotruncana lapparenti	Brotzen, 1936	15	84.1	69.1	7		I	C
268		linneiana	Rosalina linneiana	d'Orbigny, 1839	15.8	83.9	68.1	9		I	C
269		mariei	Globotruncana mariei	Banner & Blow, 1960	15.8	83.7	67.9	9		I	C
270		nothi	Rugotruncana nothi nov.sp.	Bronnimann & Brown,1955	3.1	68.1	65	32		I	C
271		orientalis	Globotruncana orientalis	El Naggar, 1966	13.4	81	67.6	9		I	C
272		pseudoconica	Globotruncana pseudoconica nov.sp.	Solakius, 1982	5	70	65	33		I	C
273		rosetta	Globigerina rosetta	Carsey, 1926	12.5	77.5	65	9		I	C
274		rugosa	Rosalinella rugosa	Marie, 1941	7.3	78.8	71.5	9		I	C
275		ventricosa	Globotruncana canaliculata var. ventricosa	White, 1928	11	79.4	68.4	9		I	C
276	Globotruncanella	citae	Globotruncana citae	Bolli, 1951	3.2	68.2	65	7		D	C
277		havanensis	Globotruncana havanensis	Voorwijk, 1937	8.1	73.1	65	9		D	C
278		minuta	Globotruncanella minuta	Caron et. al., 1984	3.1	68.1	65	9		D	C
279		petaloidea	Globotruncana (Rugoglobigerina) petaloidea subsp. petaloidea	Gandolfi, 1955	4.8	69.8	65	9		D	C
280		pschadae	Globorotalia pschadae	Keller, 1946	4.3	69.3	65	9		D	C
281	Globotruncanita	atlantica	Globotruncana atlantica	Caron, 1972	6.2	77.5	71.3	9		I	C
282		calcarata	Globotruncana calcerata	Cushman, 1927	4.1	75.4	71.3	9		I	C
283		conica	Globotruncana conica	White, 1928	3.1	68.1	65	9		I	C
284		elevata	Globorotalia elevata	Brotzen, 1934	10.1	83.7	73.6	9		I	C
285		fareedi	Globotruncana fareedi	El-Naggar, 1966	6.3	72.2	65.9	23		I	C
286		pettersi	Globotruncanita pettersi (Gandolfi)	Gandolfi, 1955	4.1	69.1	65	9		I	C
287		stuarti	Rosalina stuarti	de Lapparent, 1918	8.1	73.1	65	9		I	C
288		stuartiformis	Globotruncana (Globotruncana) elevata stuartiformis	Dalbiez, 1955	17.5	83.7	66.2	9		I	C
289		subspinosa	Globotruncana (Globotruncana) subspinosa	Pessagno, 1960	9.9	77.6	67.7	9		I	C
290	Globuligerina	bathoniana	Globigerina bathoniana	Pazdrowa, 1969	14.4	166.8	152.4	1		?	
291		calloviensis	Globuligerina calloviensis	Kuznetsova, 1980	3.4	164.4	161	1		?	
292		hoterivica	Globigerina hoterivica	Subbotina, 1953	25.6	142.2	116.6	7		?	
293		oxfordiana	Globigerina oxfordiana	Gregelis, 1958	2.6	159.4	156.8	1		?	
294	Gorbachikella	kugleri	Globigerina kugleri	Bolli, 1959	19.8	132	112.2	1		?	
295	Gublerina	acuta	Gublerina acuta	De Klasz, 1953	6.3	71.3	65	21	subsp.robusta	?	
296		glaessneri	Gublerina glaessneri	Bronnimann & Brown, 1953	2.3	67.3	65	21		?	
297	Guembelitria	cenomana	Guembelina cenomana	Keller, 1935	7.5	100	92.5	7		?	
298		cretacea	Guembelitria cretacea	Cushman, 1933	5.5	68.6	63.1	2		?	
299	Guembelitrioides	higginsi	Globigerinoides higginsi	Bolli, 1957	9.6	50.5	40.9	2		I	K
300	Haeuslerina	helevetojurassica	Globigerina helvetojurassica	Haeusler, 1881	5.3	159.4	154.1	1		?	
301		parva	Globuligerina parva	Kuznetsova, 1985	1.7	154.1	152.4	1		?	
302	Hantkenina	alabamensis	Hantkenina alabamensis	Cushman, 1925	7.6	40.9	33.3	2		I	B
303		dumblei	Hantkenina dumblei	Wienzierl & Applin, 1929	6.6	46.9	40.3	2		D	B,K
304		liebusi	Hantkenina liebusi	Shokhina, 1937	8.2	46.9	38.7	2		D	B,K
305		mexicana	Hantkenina mexicana	Cushman, 1925	7.3	47.6	40.3	2		D	B
306		nanggulanensis	Hantkenina nanggulanensis	Hartono, 1969	1.7	**36.9**	35.2	Coxall, pers. comm.	Mid P15-P16	I	B,O
307		nuttalli	Hantkenina nuttalli	Toumarkine, 1981	3.2	49	45.8	2		D	B
308		primitiva	Hantkenina alabamensis var. primitiva	Cushman & Jarvis, 1929	6.7	40.4	33.7	7		D	B
309	Hastigerina	pelagica	Nonionina pelagica	d'Orbigny, 1839	8.2	8.2	0	5		D	
310	Hastigerinoides	alexanderi	Hastigerinella alexanderi	Cushman, 1931	3.5	87	83.5	7		S	
311		subdigitata	Globigerina subdigitata	Carmen, 1929	16.7	85.6	68.9	7		S	
312		watersi	Hastigerinella watersi	Cushman, 1931	13.7	85	71.3	7		S	U
313	Hastigerinopsis	riedeli	Hastigerinella riedeli	Rogl & Bolli, 1973	2	2	0	5		?	
314	Hedbergella	bizonae	Hastigerinella bizonae	Chevalier, 1961	4.4	116.6	112.2	1		S	G
315		delrioensis	Hedbergella delrioensis (Carsey)	Carsey, 1926	32.1	117.5	85.4	1		S	G,U
316		flandrini	Hedbergella flandrini	Porthault, 1970	4.7	89.7	85	1		S	G
317		gorbachikae	Hedbergella gorbachikae	Longoria, 1974	15.4	121	105.6	1		S	G
318		hoelzli	Hedbergella hoelzli	Hagn & Zeil, 1954	5.5	93.9	88.4	1		S	G
319		holmdelensis	Hedbergella holmdelensis	Olsson, 1964	24	89	65	1		S	G,O
320		maslakovae	Hedbergella maslakovae	Longoria, 1974	3.5	117.5	114	1		S	G
321		monmouthensis	Globorotalia monmouthensis	Olsson, 1960	22.1	87	64.9	1		S	G
322		planispira	Globigerina planispira	Tappan, 1940	29.5	118.1	88.6	1		S	G
323		sigali	Hedbergella sigali	Moullade, 1966	6	127	121	7		S	G
324		simplex	Hastigerinella simplex	Morrow, 1934	21.7	110.3	88.6	1		S	G
325		sliteri	Hedbergella sliteri	Huber, 1990	6.3	71.3	65	24		S	G
326		trocoidea	Hedbergella trocoidea (Gandolfi)	Gandolfi, 1942	4.8	115.9	111.1	1		S	G
327	Heterohelix	globulosa	Heterohelix globulosa (Ehrenberg)	Ehrenberg, 1840	14.2	83.5	69.3	7		S	U
328		moremani	Guembelina moremani	Cushman, 1938	10.9	101.6	90.7	7		S	U

329		navarroensis	Heterohelix navarroensis	Loeblich, 1941	4.8	69.8	65	7		S	
330		planata	Heterohelix planata (Cushman)	Cushman, 1938	8	75.3	67.3	21		S	
331		punctulata	Heterohelix punculata (Cushman)	Cushman, 1938	18	83	65	21		S	
332		reussi	Gumbelina reussi	Cushman, 1938	8.3	91.8	83.5	7		S	
333		semicostata	Heterohelix semicostata (Cushman)	Cushman, 1938	12.4	80.8	68.4	21		S	
334		striata	Heterohelix striata	Ehrenberg, 1840	16.2	81.2	65	7		S	
335	Hirsutellla	bermudezi	Globorotalia bermudezi	Rogl & Bolli, 1973	2	2	0	5		D	
336		challengeri	Globorotalia challengeri	Srinivasan & Kennett, 1981	5.1	15.1	10	5		D	
337		cibaoensis	Globorotalia cibaoensis	Bermudez, 1949	2.8	7.2	4.4	5		D	
338		hirsuta	Rotalina hirsuta	d'Orbigny, 1839	2.7	2.7	0	5	canariensis/patagonica - jnr. Syn.	D	
339		juanai	Globorotalia juanai	Bermudez & Bolli, 1969	3.5	9.2	5.7	5		D	
340		margaritae	Globorotalia margaritae	Bolli & Bermudez, 1965	2.4	5.7	3.3	5	praehirsuta - jnr. Syn.	D	
341		scitula	Pulvinulina scitula	Brady, 1882	15	15	0	5		D	Q,R
342		theyeri	Globorotalia theyeri	Fleisher, 1974	3.5	3.5	0	5	eastropica - jnr. Syn.	D	
343	Igorina	albeari	Globorotalia albeari	Cushman & Bermudez, 1949	4.9	59.7	54.8	2		S	
344		broedermanni	Globorotalia (Truncorotalia) broedermanni	Cushman & Bermudez, 1949	9.5	50.8	41.3	2		S	O
345		convexa	Globorotalia convexa	Subbotina, 1953	10.4	55.5	45.1	2		S	
346		pusilla	Globorotalia pusilla pusilla	Bolli, 1957	2.4	60.9	58.5	2		S	
347		tadjikistanensis	Globorotalia tadjikistanensis	Bykova, 1953	4.7	59.7	55	2		S	
348	Jenkinsella	acrostoma	Globorotalia acrostoma	Wezel, 1966	10.7	23.3	12.6	5		I	
349		bella	Jenkinsella bella (Jenkins)	Jenkins, 1967	4.7	18.6	13.9	12		I	
350		mayeri	Globorotalia mayeri	Cushman & Ellisor, 1939	16.5	28	11.5	5		I	L
351		semivera	Globigerina semivera	Hornibrook, 1961	13.9	29.4	15.5	5		I	
352		siakensis	Globorotalia siakensis	LeRoy, 1939	20.6	32	11.4	5		I	L
353	Jenkinsina	columbiana	Guembelitria columbiana	Howe, 1939	21.3	49.5	28.2	2		S	
354		triseriata	Jenkinsina triseriata	Jenkins, 1967	4.7	18.6	13.9	17		S	
355	Leupoldina	cabri	Schackoina cabri	Sigal, 1952	11	116.6	105.6	1		?	
356		protruberans	Leupoldina protruberans	Bolli, 1957	13.2	121.8	108.6	1		?	
357	Lilliputianella	globulifera	Clavihedbergella globulifera	Kretchmar & Gorbachik, 1971	9.6	121.8	112.2	1		?	
358		kuhryi	Hedbergella kuhryi	Longoria, 1974	6.1	118.3	112.2	1		?	
359		roblesae	Lilliputianella roblesae	Obregon de la Parra, 1959	4.4	116.6	112.2	1		?	
360	Lilliputianelloides	eocretaceus	Clavihedbergella eocretacea	Neagu,1975	4	125	121	1		?	
361	Marginotruncana	canaliculata	Rosalina canaliculata	Reuss, 1854	6.4	93	86.6	21		D	
362		coronata	Globotruncata lapparenti Brotzen, subsp. coronata	Bolli, 1945	8.6	90.7	82.1	9		D	
363		marginata	Rosalina marginata	Reuss, 1845	6.8	90.3	83.5	9		D	
364		marianosi	Globotruncana marianosi	Douglas, 1969	1.3	91	89.7	9		D	
365		paraconcavata	Marginotruncana paraconcavata/renzi	Porthault, 1970	4.8	89.8	85	9		D	
366		pseudolinneiana	Marginotruncana pseudolinneiana	Pessagno, 1967	7.2	90.7	83.5	9		D	
367		renzi	Globotruncana renzi	Gandolfi, 1942	6.6	92	85.4	9		D	
368		schneegansi	Globotruncana schneegansi	Sigal, 1952	7.6	91.7	84.1	9		S	U
369		sigali	Globotruncana (Globotruncana) sigali	Reichel, 1950	6.5	91.7	85.2	9		D	
370		sinuosa	Marginotruncana sinuosa	Porthault, 1970	4.6	89.3	84.7	9		D	
371		tarfayaensis	Marginotruncana tarfayaensis	Lehmann, 1963	6.1	89	82.9	9		D	
372		undulata	Marginotruncana undulata	Lehmann, 1963	6.5	89.7	83.2	9		D	
373	Menardella	archeomenardii	Globorotalia archeomenardii	Bolli, 1957	1.4	15.6	14.2	5		S	R
374		exilis	Globorotalia (Globorotalia) cultrata exilis	Blow, 1969	3.8	5.8	2	5		I	
375		limbata	Rotalia limbata	Fornasini, 1902	8.3	10.6	2.3	5	praemiocenica - jnr Syn.	I	R
376		menardii	Rotalia menardii	Parker, Jones & Brady, 1865	12.3	12.3	0	5	cultrata/fimbriata - likely ecophenotypes	I	Q,R
377		miocenica	Globorotalia menardii (d'Orbigny) var. miocenica	Palmer, 1945	1.8	3.3	1.5	5		I	
378		multicamerata	Globorotalia menardii	Cushman & Jarvis, 1930	4.3	6.5	2.2	5		I	R
379		pertenuis	Globorotalia pertenius	Beard, 1969	1.5	3.2	1.7	5		I	
380		praemenardii	Globorotalia praemenardii	Cushman & Stainforth, 1945	2.3	14.6	12.3	5		D	R
381		pseudomiocenica	Globorotalia pseudomiocenica	Bolli and Bermudez, 1965	3.9	6.3	2.4	7		I	R
382	Morozovella	acuta	Globorotalia wilcoxensis Cushman & Ponton var. acuta	Toulmin, 1941	3	57.8	54.8	2		S	B,O
383		acutispira	Globorotalia acutispira	Bolli & Cita, 1960	2.4	59.2	56.8	2		S	B,O
384		aequa	Globorotalia crassata (Cushman) var.aequa	Cushman & Renz, 1942	6.7	57.7	51	2		S	B,O
385		angulata	Globigerina angulata	White, 1928	2.4	60.9	58.5	2		S	B,O
386		apanthesma	Globorotalia apanthesma	Loeblich & Tappan, 1957	4	59.9	55.9	2		S	B,O
387		aragonensis	Globorotalia aragonensis	Nuttall,1930	7.9	51.5	43.6	2		S	B,O
388		caucasia	Globorotalia aragonensis Nutall var. caucasica	Glaessner, 1937	3.4	49.6	46.2	2		S	B,O
389		conicotruncata	Globorotalia conicotruncata	Subbotina, 1947	2.3	60.8	58.5	2		S	B,O
390		crater	Globorotalia crater	Finlay, 1939	4.4	50.6	46.2	2		S	B,O
391		dolabrata	Globorotalia dolbrata	Jenkins, 1966	0.8	51.5	50.7	2		S	B,O
392		edgari	Globorotalia edgari	Premoli Silva & bolli, 1973	2.1	55.5	53.4	7		S	B,O
393		formosa	Globorotalia formosa formosa	Bolli, 1957	1	51.6	50.6	2		S	B,O
394		gracilis	Globorotalia formosa gracilis	Bolli, 1957	4.5	55.3	50.8	2		S	B,O
395		lehneri	Globorotalia lehneri	Cushman & Jarvis, 1929	6.1	44.6	38.5	2		S	B,O

396		lensiformis	Globorotalia lensiformis	Subbotina, 1953	2.6	51.6	49	2		S	B,O
397		marginodentata	Globorotalia margiodentata	Subbotina, 1953	3.6	55.2	51.6	7		S	B,O
398		occlusa	Globorotalia occlusa	Loeblich & Tappan, 1957	4.4	59.2	54.8	2		S	B,O
399		pasionensis	Psuedogloborotalia pasionensis	Bermudez, 1961	4.6	59.4	54.8	4		S	B,O
400		praeangulata	Globorotalia (Acarinina) praeangulata	Blow, 1979	1.2	61.2	60	2		S	B,O
401		praecursoria	Acarinina praecursoria	Morozova, 1957	0.2	61.3	61.1	4		S	B,O
402		spinulosa	Globorotalia spinulosa	Cushman, 1927	12.1	50.6	38.5	2		S	B,O
403		subbotinae	Globorotalia subbotinae	Morozova, 1939	5.1	55.9	50.8	2		S	B,O
404		trinidadensis	Globorotalia trinidadensis	Bolli, 1957	1.4	62.5	61.1	7		S	B,O
405		velascoensis	Pulvinulina velascoensis	Cushman, 1925	4.4	59.2	54.8	2		S	B,O
406	Mutabella	praecipua	Mutabella praecipua	Pearson, Norris & Empson, in press.	4.7	18.5	13.8	Pearson et. al. 2001		S	O*
407	Neogloboquadrina	acostaensis	Globorotalia acostaensis	Blow, 1959	6.8	10	3.2	5		I	F
408		asanoi	Neogloboquadrina asanoi	Mayia et.al.,1976	1.1	3.3	2.2			I	
409		continuosa	Neogloboquadrina opima Bolli subsp. continuosa	Blow, 1959	15.4	23.2	7.8	5		I	F
410		dutertrei	Globigerina dutertrei	d'Orbigny, 1839	2.4	2.4	0	5		I	Q
411		humerosa	Globorotalia humerosa	Takayanagi & Saito, 1962	4.4	5.8	1.4	5		I	
412		inglei n.sp.	Neogloboquadrina ingei n.sp.	Kucera & Kennett, 2000	0.8	1.5	0.7			I	
413		nympha	Neogloboquadrina mayeri nympha (Jenkins)	Jenkins, 1967	0.8	12	11.2	12		I	
414		pachyderma	Aristospira pachyderma	Ehrenberg, 1861	10	10	0	5		I	F
415	Orbulina	bilobata	Orbulina bilobata (d'Orbigny)	d'Orbigny, 1864	3.7	5.4	1.7	7		S	L
416		suturalis	Orbulina sutralis	Bronnimann, 1951	15.1	15.1	0	5		S	L
417		universa	Orbulina universa	d'Orbigny, 1839	15.1	15.1	0	5		S	F,L,Q
418	Orbulinoides	beckmanni	Porticulasphaera beckmanni	Saito, 1962	0.9	40.6	39.7	7		S	
419	Paragloborotalia	bolivariana	Globigerina wilsoni bolivariana	Petters, 1954	12	50.5	38.5	2		D	
420		continuosa	Globorotalia opima subsp. continuosa	Blow, 1959	9.1	**24.2**	**15.1**	6		D	
421		eoclavia	Hantkenina eoclavia	Coxall, in press	0.7	50.7	50	Coxall, pers. comm.		D	
422		griffinae	Globorotalia (Turborotalia) griffinae	Blow, 1979	12.5	55.4	42.9	7		D	
423		kugleri	Globorotalia kugleri	Bolli, 1957	2.3	23.8	21.5	6		S	F
424	Paragloborotalia?	laccadivensis	Globanomalina laccadivensis	Fleisher, 1974	14.3	**29.4**	**15.1**	29		D	
425		mendacis	Globorotalia (Turborotalia) mendacis	Blow, 1969	3.8	27.6	**23.8**	7	kugleri syn?	D	
426		nana	Globorotalia opima nana	Bolli, 1957	32.2	47.3	15.1	2		D	
427		opima	Globorotalia opima opima	Bolli, 1957	4	30.3	26.3	2		D	
428		pseudocontinuosa	Globorotalia nana pseudocontinuosa	Jenkins, 1967	11	**30.3**	**19.3**	6		D	
429		pseudokugleri	Globorotalia (Turborotalia) pseudokugleri	Blow, 1969	2.3	26.1	23.8	6		S	N
430		pseudomayeri	Globorotalia pseudomayeri	Bolli, 1957	1.6	41.8	40.2	Pearson, unpublished.		S	O
431	Parasubbotina	inaequispira	Globigerina inaequispira	Subbotina, 1953	11.4	52	40.6	2		D	O
432		prolata (lozanoi)	Globigerina lozanoi	Colom, 1954	4.5	51	46.5	7		D	O
433		pseudobulloides	Globigerina pseudo-bulloides	Plummer, 1926	4.3	64.9	60.6	2		D	O
434		quadrilocula	Parasubbotina quadrilocula (Blow)	Blow, 1979	3.2	**62.4**	**59.2**	14	Late P1b-Late P3	D	O
435		varianta	Globigerina varianta	Subbotina, 1953	6.9	62.4	55.5	2		D	O
436		variospira	Globorotalia (Turborotalia) variospira	Belford, 1984	2	60.9	58.9	2		D	O
437	Parvularugoglobigerina	alabamensis	Guembelitria? alabamensis	Liu & Olsson, 1992	4.6	65	60.4	2		S	
438		eugubina	Globigerina eugubina	Luterbacher & Premoli Silva, 1964	0.05	64.95	64.9	2		S	
439		extensa	Eoglobigerina? extensa	Blow, 1979	0.1	65	64.9	2		S	
440	Planoglobulina	acervulinoides	Planoglobulina acervulinoides (Lehmann)	Lehmann, 1963	4.3	69.3	65	21		S	C
441		carseyae	Planoglobulina carseyae (Plummer)	Plummer, 1931	3.2	68.2	65	21		?	
442		multicamerata	Planoglobulina multicamerata (De Klasz)	De Klasz, 1953	6.5	74.7	68.2	21		I	C
443	Planomalina	buxtorfi	Planulina buxtorfi	Gandolfi, 1942	12.1	105.6	93.5	1		S	I
444		cheniourensis	Planulina cheniourensis	Sigal, 1952	1.5	113.7	112.2	1		S	
445		praebuxtorfi	Planomalina praebuxtorfi	Wonders, 1975	6.7	105.6	98.9	1		S	
446	Planorotalites	palmerae	Globorotalia palmerae	Cushman & Bermudez, 1937	1.2	50.2	49	2		S	
447		pseudoscitula	Globorotalia pseudoscitula	Glaessner, 1937	12.6	51.1	38.5	2		S	O
448	Plummerita	hantkeninoides	Ruglobigerina (Plummerella) hantkeninoides	Bronnimann, 1952	4.2	69.3	65.1	9		?	
449	Praeglobotruncana	aumalensis	Praeglobotruncana aumalensis	Sigal, 1952	4.3	95.5	91.2	8		D	
450		delrioensis	Globorotalia delrioensis	Plummer, 1931	8.7	103	94.3	8		D	
451		gibba	Praeglobotruncana stephani (Gandolfi) var.gibba	Klaus 1960	7.1	97.4	90.3	8		D	
452	Helvetoglobotruncana?	helvetica	Globotruncana helvetica	Bolli, 1945	1.5	91.8	90.3	8		D	
453	Helvetoglobotruncana?	praehelvetica	Rogoglobigerina praehelvetica	Trujillo, 1960	3.2	93.9	90.7	8		D	
454		stephani	Globotruncana stephani	Gandolfi, 1942	10.3	101.3	91	8		D	
455	Praehedbergella	handousi	Caucasella handousi	Salaj, 1984	2.5	132	129.5	1		S	
456		pseudosigali	Praehedbergella pseudosigali	Banner, Copestake & White, 1993	3	124	121	1		S	
457		tuschepsensis s.s.	Globigerina tuschepensis	Antonova, 1964	3	127	124	1		S	
458	Praemurica	inconstans	Globigerina inconstans	Subbotina, 1953	1.9	62.4	60.5	2		S	
459		pseudoinconstans	Globorotalia (Turborotalia) pseudoinconstans	Blow, 1979	3.6	64.9	61.3	2		S	
460		taurica	Globigerina (Eoglobigerina) taurica	Morozova, 1961	1.2	65	63.8	2		S	
461		uncinata	Globorotalia uncinata	Bolli, 1957	0.6	61.3	60.7	2		S	
462	Praeorbulina	circularis	Globigerinoides glomerosa circularis	Blow, 1956	0.5	15.4	14.9	5		S	M

463		curva	Globigerinoides glomerosa curva	Blow, 1956	0.9	15.9	15	5		S	M
464		glomerosa	Globigerinoides glomerosa glomerosa	Blow, 1956	0.8	15.8	15	5		S	M
465		sicana	Praeorbulina sicana	Di Stefani, 1950	1.6	16.6	15	7		S	M
466		transitoria	Globigerinoides transitoria	Blow, 1956	0.5	15.4	14.9	5		S	M
467	Protentella	clavaticamerata	Protentella clavaticamerata	Jenkins, 1977	2.1	25.4	23.3	6		D	
468		navazuelensis	Protentella navazuelensis	Molina, 1979	3.8	26.3	22.5	6		D	
469		nicobarensis	Protentella nicobarensis	Srinivasan & Kennett, 1974	8.7	28.2	19.5	6		D	
470		prolixa	Protentella prolixa	Lipps, 1966/4	11.6	26.6	15	5		D	
471	Pseudoguembelina	costulata	Guembelina costulata	Cushman, 1938	22	87	65	7		I	
472		excolata	Guembelina excolata	Cushman, 1926	4.8	69.8	65	7		I	O
473		kempensis	Pseudoguembelina kempensis	Esker, 1968	4.3	69.3	65	22		I	
474		palpebra	Pseudoguembelina plapebra	Bronnimann & Brown, 1953	4.8	69.8	65	7		I	
475	Pseudohastigerina	kerisensis	Biglobigerinella kerisensis	Suleymanov, 1966	10.6	49.6	39	2		S	
476		micra	Nonion micrus	Cole, 1927	16.8	50.6	33.8	2		S	O
477		naguewichiensis	Globigerinella naguewichiensis	Myatliuk, 1950	2.7	34.5	31.8	2	Jnr. Syn. - barbadoensis	S	
478		wilcoxensis	Nonion wilcoxensis	Cushman & Ponton, 1932	13.2	54.8	41.6	2		S	
479	Pseudotextularia	elegans	Cuneolina elegans	Rzehak, 1891	14.4	79.4	65	7		I	O
480		intermedia	Pseudotextularia intermedia	De Klasz, 1953	2.3	67.3	65	21		I	C
481	Pulleniatina	finalis	Pulleniatina obliquiloculata (Parker & Jones) finalis	Banner & Blow, 1967	2.1	2.1	0	19		I	
482		obliquiloculata	Pulleniatina sphaeroides (d'Orbigny) var. obliquiloculata	Banner & Blow, 1967	3.6	3.6	0	5		I	Q
483		praecursor	Pulleniatina obliquiloculata (Parker & Jones) praecursor	Banner & Blow, 1967	2.9	5.2	2.3	5		I	
484		primalis	Pulleniatina primalis	Banner & Blow, 1967	3.7	7.1	3.4	5		I	
485		spectabilis	Pulleniatina spectabilis	Parker, 1965	2.2	5.8	3.6	5		I	
486	Racemiguembelina	fructicosa	Guembelina fructicosa	Egger, 1899	2.7	67.7	65	7		S	D
487		powelli	Racemiguembelina powelli	Smith & Pessagno, 1973	4.3	69.3	65	22		S	
488	Rectogumbelina	cretacea	Rectogumbelina cretacea	Cushman, 1932	10.4	**71.3**	60.9	8	Overestimate - Upper Maas	?	
489	Rotalipora	appenninica	Globotruncana appenninica	Renz, 1936	7	101.3	94.3	8		S	
490		cushmani	Globorotalia cushmani	Morrow, 1934	1.7	95.2	93.5	8		S	
491		deeckei	Rotalipora deeckei	Franke, 1925	1	95.1	94.1	8		S	
492		gandolfii	Rotalipora appenninica gandolfii	Luterbacher & Premoli-Silva, 1962	2.1	99.1	97	8		S	
493		globotruncanoides	Thalmanninella brotzeni	Sigal, 1948	4.6	98.9	94.3	7		S	
494		greenhornensis	Globorotalia greenhornensis	Morrow, 1934	1.5	95.2	93.7	8		S	
495		micheli	Roatlipora micheli	Sacal & Debourle, 1957	2.2	99	96.8	8		S	
496		montsalvensis	Globotruncana (Rotalipora) montsalvensis	Mornod, 1949-50	3.4	97.7	94.3	8		S	
497		reichleli	Globotruncana (Rotalipora) reicheli	Mornod, 1949-50	1.8	97	95.2	7		S	
498		subticiensis	Globotruncana (Thalmanninella) ticinensis	Gandolfi, 1957	4.6	106.2	101.6	8		S	I,O
499		ticiensis	Globotruncana ticinensis	Gandolfi, 1942	4.4	103.8	99.4	8		S	
500	Rugoglobigerina	hexacamerata	Rugoglobigerina reicheli hexacamerata	Bronnimann, 1952	4.8	69.8	65	9		I	O
501		macrocephala	Rugoglobigerina (Rugoglobigerina) macrocephala	Bronnimann, 1952	4.8	69.8	65	9		I	O
502		milamensis	Rugoglobigerina milamensis	Smith & Pessagno, 1973	4.3	69.3	65	9		I	
503		pennyi	Rugoglobigerina (Rugoglobigerina) rugosa pennyi	Bronnimann, 1952	5.4	70.4	65	9		I	
504		pilula	Rugoglobigerina (Rugoglobigerina) pilula	Belford, 1960	6.5	84.5	78	9		I	
505		reicheli	Rugoglobigerina (Rugoglobigerina) reicheli	Bronnimann, 1952	3.2	68.2	65	9		I	
506		rotundata	Rugoglobigerina (Rugoglobigerina) rugosa rotundata	Bronnimann, 1952	4.3	69.3	65	9		S	D
507		rugosa	Globigerina rugosa	Plummer, 1926	15.3	80.3	65	9		I	
508		scotti	Trinitella scotti	Bronnimann, 1952	4.8	69.8	65	9		I	
509	Rugotruncana	subcircumnodifer	Globotruncana (Rugoglobigerina) circum. subcircumnodifer	Gandolfi, 1955	7.4	73.1	65.7	7		?	
510		subpennyi	Globotruncana (Rugoglobigerina) pennyi subpennyi	Gandolfi, 1955	3.3	69.8	66.5	7		?	
511	Schackoina	cenomana	Siderolina cenomana	Schacko, 1897	17.7	116.6	98.9	1		?	
512		cepedai	Hastigerinelloides cepedai	Obregon de la Parra, 1959	4.4	116.6	112.2	1		?	
513		multispinata	Schakoina multispinata (Cushman & Wickenden)	Cushman & Wickenden, 1930	18.4	98.1	79.7	7		?	
514	Sigalia	decoratissima	Ventilabrella decoratissima (De Klasz)	De Klasz, 1953	1.5	**86**	**84.5**	21		?	
515	Sphaeroidinella	dehiscens	Sphaeroidina bulloides d'Orbigny var. dehiscens	Parker & Jones, 1865	5.7	5.7	0	5		I	Q
516	Sphaeroidinellopsis	disjuncta	"Sphaeroidinellopsis" disjuncta	Finlay, 1940	10.9	23.4	**12.5**	5		S	
517		kochi	Globigerina kochi	Caudri, 1934	10.8	14.4	3.6	5		S	
518		paenedehiscens	Sphaeroidinellopsis paenedehiscens	Blow, 1969	3.8	7.1	3.3	5		S	L
519		seminulina	Sphaeroidinellopsis seminulina (Ellis & Messina, 1949)	Schwager, 1866	14.6	16.4	**1.8**	5	unreliable datums?	S	
520	Streptochilus	pristinum	Streptochilus pristinum	Bronnimann & Resig, 1971	14.2	**29.4**	**15.2**	5		S	
521		globigerum	Textularia globigera	Schwager,1866	6.9	10.9	4	5		S	
522		tokelauae	Streptochilus tokelauae	Bronnimann & Resig, 1971	3.6	3.6	0	5		S	
523	Subbotina	angiporoides	Globigerina angiporoides	Hornibrook, 1965	13.6	39.6	26	2		D	B
524		cancellata	Subbotina triangularis cancellata	Blow, 1979	3.7	61.3	57.6	2		D	B
525		eocaena	Globigerina eocaena	Gumbel, 1868	18.5	47.9	29.4	2		I	B,S
526		frontosa	Globigerina frontosa	Subbotina, 1953	5.4	48.3	42.9	2	Snr. syn. of boweri	D	B,O
527		gortanii	Catapsydrax gortanii	Borsetti, 1959	10	33.8	23.8	2		D	B
528		hornibrooki	Subbotina hornibrooki (Bronnimann)	Bronnimann, 1952	10.2	56	45.8	14		D	B
529		lonzanoi	Globigerina lonzanoi	Colom, 1954	4.2	50.7	46.5	2		D	B

530		linaperta	Globigerina linaperta	Finlay, 1939	19.7	53.5	33.8	2		D	B
531		minima	Subbotina angiporoides minima (Jenkins)	Jenkins, 1966/5	8.9	**47.4**	38.5	14	Mid P10-P14	D	B
532		praeturritilina	Globigerina turritilina	Blow & Banner, 1962	13	38.6	25.6	2		D	B
533		triangularis	Globigerina triangularis	White, 1928	9.3	61.3	52	2		D	B
534		triloculinoides	Globigerina triloculinoides	Plummer, 1926	4.9	63.6	58.7	2		D	B
535		trivialis	Globigerina trivialis	Subbotina, 1953	3.6	64.9	61.3	2		D	B
536		utilisindex	Globigerina utilisindex	Jenkins & Orr, 1973	6.7	33.8	27.1	10		D	B
537		velascoensis	Globigerina velascoensis	Cushman, 1925	6.1	59.2	53.1	2		D	B
538	Tenuitella	anfracta	Globorotalia anfracta	Parker, 1967	5.8	5.8	0	5		S	
539		clemenciae	Turborotalia clemenciae	Bermudez, 1961	25.3	32	6.7	5		S	
540		gemma	Globorotalia gemma	Jenkins, 1965	7.7	33.7	26	6		S	
541		insolita	Tenuitella insolita (Jenkins)	Jenkins, 1966	0.9	21.7	20.8	12		S	
542		iota	Globigerinita iota	Parker, 1962	3.5	3.5	0	19		S	
543		jamesi	Tenuitella jamesi	Li, Radford & Banner, 1990	3.3	17.1	13.8	18		S	
544		minutissima	Tenuitella minutissima (Bolli)	Bolli, 1957	8	21.8	13.8	18		S	
545		munda	Tenuitella munda	Jenkins, 1966	7.9	31.1	23.2	5		S	
546		neoclemenciae	Tenuitella neoclemenciae	Li, 1987	17.2	**32**	**14.8**	6		S	
547		postcretacea	Globigerina postcretacea	Mjatliuk, 1950	0.9	34.6	**33.7**	31		S	
548		pragemma	Praetenuitella praegemma	Li, 1987	1.9	35.6	33.7	31		S	
549		pseudoedita	Tenuitella pseudoedita (Subbotina)	Subbotina, 1960	9.6	23.4	13.8	18		S	
550		selleyi	Tenuitella selleyi	Li, Radford & Banner, 1992	5.6	19.4	13.8	18		S	
551	Tenuitellinata	angustiumbilicata	Globigerina ciperoensis angustiumbilicata	Bolli, 1957	23.1	27.1	4	2+5		S	F
552		juvenilis	Globigerina juvenilis	Bolli, 1957	15.5	**30.3**	**14.8**	6		S	
553		praestainforthi	Tenulitellinata praestainforthi	Blow, 1979	14.6	**29.4**	**14.8**	6		S	
554	Ticinella	bejaouensis	Ticinella roberti var. bejaouensis	Sigal, 1966	12.7	113	100.3	7		S	
555		madecassiana	Ticinella madecassiana	Sigal, 1966	3.3	102.2	98.9	7		S	
556		praeticinensis	Ticinella praeticinensis	Sigal, 1966	6	109.2	103.2	7		S	I
557		primula	Ticinella primula	Luterbacher & Schneider, 1963	9.5	110.8	101.3	7		S	T
558		raynaudi	Ticinella raynaudi	Sigal, 1966	6.5	107.3	100.8	7		S	I
559	Truncorotalia	cavernula	Globorotalia cavernula	Be, 1967	0.9	0.9	0	5		D	
560		crassaformis	Globigerina crassaformis	Galloway & Wissler, 1927	3.5	3.5	0	5	crassacrotonensis - jnr. Syn.	D	R
561		crassula	Globorotalia crassula	Cushman & Stewart, 1930	4	5.8	1.8	5	aemiliana/crotonensis - variants	D	Q
562		tosaensis	Globorotalia tosaensis	Takayangi & Saito, 1962	2	3.2	1.2	5		D	Q
563		truncatulinoides	Rotalia truncatulinoides	d'Orbigny, 1839	2	2	0	5		D	Q
564	Truncorotaloides	haynesi	Truncorotaloides haynesi	Samanta, 1970	8.5	47	38.5	7		S	
565		libyaensis	Truncorotaloides libyaensis	El Khoudary, 1977	8.9	47.4	38.5	7		S	
566	Turborotalia	altispiroides	Turborotalia altispiroides	Bermudez, 1961	3.3	40.1	**36.8**	25		D	
567		ampliapertura	Globigerina ampliapertura	Bolli, 1957	3.6	33.8	30.2	2		D	
568		cerroazulensis	Globigerina cerro-azulensis	Cole, 1928	8.3	41.6	33.3	2		D	O
569		cocoaensis	Globorotalia cocoaensis	Cushman, 1928	4.1	37.4	33.3	2		D	O
570		cunialensis	Globorotalia cerroazulensis cunialensis	Toumarkine & Bolli, 1970	1.8	35.1	33.3	2		D	
571		increbescens	Globorotalia (Turborotalia) increbescens	Bandy, 1949	8.2	38.9	30.7	7		D	
572		pomeroli	Globorotalia cerroazulensis pomeroli	Toumarkine & Bolli, 1970	10.5	44.2	33.7	7		D	
573		possagnoensis	Globigerina cerroazulensis possagnoensis	Toumarkine & Bolli, 1970	5.3	45.8	40.5	Pearson, pers.comm.		D	
574		pseudoampliapertura	Globigerina psuedoampliapertura	Blow & Banner, 1962	11.8	42.3	30.5	2		D	O
575	Turborotalita	cristata	Globigerina cristata	Heron-Allen & Earland, 1929	2	2	0	5		S	
576		humilis	Truncatulina humilis	Brady, 1884	5.9	5.9	0	5		S	
577	Whiteinella	aprica	Whiteinella aprica	Loeblich & Tappan, 1961	5.2	94	88.8	9		S	J
578		archaeocretacea	Whiteinella archaeocretacea	Pessagno, 1967	7.2	93.5	86.3	9		S	J
579		baltica	Whiteinella baltica	Douglas & Rankin, 1969	9.5	94.7	85.2	9		S	J
580		brittonensis	Whiteinella brittonensis	Loeblich & Tappan,	11.6	96	84.4	9		S	J
581		inornata	Whiteinella inornata	Bolli, 1957	8	92.7	84.7	7		S	J
582		paradubia	Globigerina paradubia	Sigal, 1952	6.2	94.3	88.1	9		S	J
583	Wondersella	athersuchi	Wondersella athersuchi	Banner & Strank, 1987	3.5	113.5	110	1		?	
584	Woodringina	claytonensis	Woodringina claytonensis	Loeblich & Tappan, 1957	1.9	64.9	63	2		?	
585		hornerstownensis	Woodringina hornerstownensis	Olsson, 1960	5.7	64.9	59.2	2		?	
586	Zeaglobigerina/	apertura	Globigerina apertura	Cushman, 1918	8	10	2	5		I	
587	(Globoturborotalita)	brazieri	Globigerina brazieri	Jenkins, 1961	14.8	30.3	15.5	5		I	
588		connecta	Globigerina connecta	Jenkins, 1964	7.1	23.6	16.5	5		I	
589		decoraperta	Globigerina druryi Akers decoraperta	Takayanagi & Saito, 1962	13	15	2	5		I	
590		druryi	Globigerina druryi	Akers, 1955	12.2	24.9	12.7	5		I	G
591		labiacrassata	Globigerina labiacrassata	Jenkins, 1966	12.7	28.9	16.2	6		I	
592		nepenthes	Globigerina nepenthes	Todd, 1957	7.5	10.9	3.4	5		I	G
593		rubescens	Globigerina rubescens	Hofker, 1956	3.5	3.5	0	5		S	Q
594		tenella	Globigerinoides tenellus	Parker, 1958	2.2	2.2	0	5		I	
595		woodi	Globigerina woodi	Jenkins, 1960	23.8	25.6	1.8	2		I	G
596	Zeauvigerina	aegyptiaca	Zeauvigerina aegyptiaca	Said & Kenawy, 1956	2.6	57.4	54.8	2		S	

597		teuria	Zeauvigerina teuria	Finlay, 1947	5.1	62.2	57.1	2		S	
598		virgata	Heterohelix virgata	Khalihov, 1967	8	62.8	54.8	2		S	
599		waiparaensis	Chiloguembelina waiparaensis	Jenkins, 1965	14.5	**69.3**	**54.8**	2		S	
600		zealandica	Zeavigerina zealandica	Finlay, 1939	16.4	55.5	39.1	12		S	
	Source references (1-33) and depth habitat (A-U) refereces are listed in Appendix 2.2. Depth divisions are S (surface mixed layer), I (intermediate subsurface mixed layer) and D (deep).										

Appendix 2.2 – References for Plankrange database

Range references

1. Boudagher-Fadel, M.K., Banner, F.T., Whittaker, J.E., 1997. *The Early Evolutionary History of Planktonic Foraminifera.* British Micropalaeontological Society publication. Chapman and Hall, London.

2. Pearson, N.P., 1998. Speciation and extinction asymmetries in palaeontological phylogenies: evidence for evolutionary progress. *Palaeobiology*, 24(3):305-335.

3. Hemleben, C., Spindler, M., Anderson, O.R., 1989. *Modern Planktonic Foraminifera.* Springer-Verlag, New York, p.363.

4. Olsson, R.K., Hemleben, C., Berggren, W.A., Huber, B.T., 1999. *Atlas of Palaeocene Planktonic Foraminifera.* Smithsonian Contributions To Palaeobiology, 85.

5. Kennet, J.P., Srinivasen, S., 1983. *Neogene Planktonic Foraminifera: A Phylogenetic Atlas.* Hutchinson Ross Publishing Company, Stroudsburg, Pennsylvania.

6. Spezzaferi, S., 1994. *Planktonic foraminiferal biostratigraphy and taxonomy of the Oligiocene and lower Miocene in the oceanic record. An overview.* Palaeontographica Italica, Pubblicata a cura della societa toscana di scienze naturali, Vol. LXXXI.

7. Bolli, H.M., Saunders J.B., Perch-Nielsen, K., 1985. *Plankton Stratigraphy.* Cambridge University Press, Cambridge.

8. Robaszynski, F., Caron, M., 1979. *Atlas de Foraminiferes Planctoniques du Cretace Moyen (Mer Boreale et Tethys).* Cahiers de Micropaleontologie, 1. Editions du Centre National de le Recherche Scientifique, Paris.

9. Robaszynski, F., Caron, M., Gonzalez Donoso, J.M., Wonders, A.A.H., 1984. E.W.G.P.F. *Atlas of Late Cretaceous Globotruncanids. Revue de Micropaleontologie,* 26(3-4):145-305.

10. Jenkins, D.G., Orr, W.N., 1973. *Globigerina utilisindex n. sp.* from the Upper Eocene-Oligocene of the eastern equatorial pacific. *Journal of Foraminiferal Research,* 3(3):113-136.

11. Li, Q., Radford, S.S., Banner, T., 1992. Distribution of Microperforate Tenuitellid Planktonic Foraminifers in Holes 747A and 747B, Kerguelen Plateau. Wise, S., Jnr., Schlich, R., *et. al.*, (eds.) *Proceedings of the Ocean Drilling Program Scientific Results*, 120. College Station, TX (Ocean Drilling Program).

12. Jenkins, D.G., 1971. *New Zealand Cenozoic Planktonic Foraminifera.* Paleontological Bulletin 42, New Zealand Geological Survey. New Zealand Department of Scientific and Industrial Research.

13. Eames, F.E., Banner, F.T., Blow, W.H., Clarke, W.J., 1962. *Mid-Tertiary Stratigraphic Correlation.* Cambridge University Press, Cambridge.

14. Blow, W.H., 1979. *The Cainozoic Globigerinida: A study of the Morphology, Taxonomy and Evolutionary relationships and the Stratigraphical Distribution of some Globigerinida (mainly Globigerinacea).* Brill E.J., (ed.), Leiden. 3 vols., pp. 1413.

15. Hornibrook, N.D., 1984. *Globorotalia* (Planktic Foraminifera) at the Miocene Pliocene boundary in New Zealand. *Palaeogeography, Palaeoclimatology, Palaeoecology*, 46(1-3):107-117.

16. Parker, F.L., 1967. Late Tertiary Biostratigraphy (Planktonic Foraminifera) of Tropical Indo-Pacific Deep Sea Cores. *Bulletin of American Palaeontology*, 52 (235):115-187.

17. Jenkins, D.G., Whittaker, J.E., Curry, D., 1998. Palaeogene triserial planktonic foraminifera. *Journal of Micropalaeontology*, 17:61-70.

18. Li, Q., Radford, S.S., Banner, F.T., 1992. Distribution of Microperforate Tenuitellid Planktonic Foraminifers in Holes 747A and 747B, Kerguelen Plateau. *Proceedings of the Ocean Drilling Program, Scientific Results*, 120:569-602. College Station, TX (Ocean Drilling Program).

19. Pearson, P.N., 1995. Planktonic foraminifer biostratigraphy and the development of pelagic caps on guyots in the Marshall Island group. *Proceedings of the Ocean Drilling Program Scientific Results*, 144:21-59. College Station, TX (Ocean Drilling Program).

20. Leoblich, A.R. Jnr. *et. al.* 1957. Studies in Foraminifera. *United States National Museum Bulletin* 215. Smithsonian Institution, Washington DC.

21. Pessagno, E.A. Jnr., 1967. Upper Cretaceous Planktonic Foraminifera from the Western Gulf coastal plain. *Palaeontographica Americana*, V(37). *Paleontological Research Institution* Ithaca, NY, USA.

22. Smith, C.C., Pessagno, E.A. Jnr., 1973. Planktonic Foraminifera and Stratigraphy of the Corsican Formation (Maestrichtian), North-Central Texas. *Cushamn Foundation for Foraminiferal Research,* Special Publication, 12.

23. Longoria, J.F., Vonfeldt, A.E., 1991. Taxonomy, Phylogenetics and Biochronology of Single-keeled Globotruncanids (Genus *Globotruncanita* Reiss). *Micropalaeontology*, 37(3):197-243.

24. Huber, B., 1990. Ontogenetic Morphometrics of some Late Cretaceous Trochospiral Planktonic Foraminifera from Austral Realm. *Smisthonian Contributions to Palaeobiology*, 77.

25. Bermudez, P.J., 1960/1. Contribucion al estudio de las Globigerindea de la region Caribe ñ Antillana (Paleoceno ñ Reciente). *Venezuela, Min. Minas Hidrocarb., Bol. Geol., Publ. Espec.*, 3, pp 1316.

26. Jenkins, D.G., 1964. A History of the Holotype, Ontogeny and Dimorphism of *Globotruncanoides turgida* (Finlay). *Contributions from the Cushman Foundation of Foraminiferal Research*, XV(3).

27. Li, Q., Radford, S.S., 1992. Morphology and Affinity of the Planktonic Foraminifer *Cassigerinelloita amekiensis* Stolk and Reclassification of *Cassigerinelloita* Stolk. *Proceedings of the Ocean Drilling Program*, Scientific Results, 120:595-602. College Station, TX (Ocean Drilling Program).

28. Fleisher, R.L., 1974. Cenozoic Planktonic Foraminifera and Biostratigraphy, Arabian Sea, Deep Sea Drilling Project Leg 23A. *Initial Reports of the Deep Sea Drilling Project*, 23:1001-1072.

29. Chaisson, W.P., Pearson, P.N., 1997. Planktonic Foraminifer Biostratigraphy at Site 925: Middle Miocene-Pleistocene. *Proceedings of the Ocean Drilling Program*, Scientific Results, 154:3-31. College Station, TX (Ocean Drilling Program).

30. Li, Q, 1987. Origin, Phylogenetic development and systematic taxonomy of the *Tenuitella plexus* (Globigerinitidae, Globigerinina). *Journal of Foraminiferal Research*, 17(4):298-320.

31. Bronnimann, P., Brown, N.K.Jr., 1955. Taxonomy of the Globotruncanidae. *Scweizerische Palaeontologische Geselleschaft, Eclogae geol. Helv.*, 48.

32. Solakius, N. 1982. Description of a New Species, *Globotruncana pseudoconica* and Remarks on its Relation to *Globotruncana conica* White and *Globotruncana falsostuarti* Sigal. *Geobios*, 15(6):873-889.

Depth habitat references

A. Boersma, A., Premoli-Silva, I.P., 1991. Distribution of Paleogene planktonic foraminifera – analogies with the Recent. *Palaeogeography, Palaeoclimatology, Palaeoecology*, 83 (1-3):29-47.

B. Coxall, H. K, Pearson, P.N., Shackleton, N.J., Hall, M. A., 2000. Hantkeninid depth adaptation: An evolving life strategy in a changing ocean. *Geology*, 28(1):87-90.

C. D'Hondt, S., Zachos, J.C., 1998. Cretaceous foraminifera and the evolutionary history of planktic photosymbiosis. *Paleobiology*, 24 (4):512-523.

D. D'Hondt, S., Arthur, M.A., 2002. Deep water in the late Maastrichtian ocean. *Paleoceanography*, 17 (1): article 1008.

E. Hodell, D.A., Vayavananda, A., 1993. Middle Miocene paleoceanography of the western equatorial pacific (DSDP 289) and the evolution of the *Globorotalia (Fohsella). Marine Micropaleontology*, 22 (4):279-310.

F. Keller, G., 1985. Depth stratification of planktonic foraminifers in the Miocene Ocean. *In*, Kennett, J.P., (ed.), *The Miocene Ocean: Paleoceanography and Biogeography*. GSA Memoir 163. The Geological Society of America, Boulder, Colorado, U.S., pp. 337.

G. Keller, G., Adatte, T., Stinnesbeck, W., *et. al.*, 2002. Paleoecology of the Cretaceous-Tertiary mass extinction in planktonic foraminifera. *Palaeogeography, Palaeoclimatology, Palaeoecology*, 178 (3-4):257-297.

H. Norris, R.D., Corfield, R.M., Cartlidge, J.E., 1993. Evolution of depth ecology in the planktic foraminifera lineage *Globorotalia (Fohsella). Geology*, 21:975-978.

I. Norris, R.D., Wilson, P.A., 1998. Low-latitude sea-surface temperatures for the mid-Cretaceous and the evolution of planktic foraminifera. *Geology* 26, 823-826.

J. Norris, R.D., Bice, K.L., Magno, E.A., Wilson, P.A., 2002. Jiggling the tropical thermostat in the Cretaceous hothouse. *Geology*, 30(4):299-302.

K. Pearson, P.N., Shackleton, N.J., Hall, M.A., 1993. Stable isotope palaeoecology of middle Eocene planktonic foraminifera and multi-species isotope stratigraphy, DSDP Site 523, South Atlantic. *Journal of Foraminiferal Research*, 23:123-140.

L. Pearson, P.N., Shackleton, N.J., 1995. Neogene multispecies planktonic foraminifer stable isotope record, Site 871, Limalok Guyot. *Proceedings of the Ocean Drilling Program Scientific Results*, 144:401-410. College Station, TX (Ocean Drilling Program).

M. Pearson, P.N., Shackleton, N.J., Hall, M.A., 1997a. Stable isotopic evidence for the sympatric divergence of *Globigerinoides trilobus* and *Orbulina universa* (planktonic foraminifer). *Journal of the Geological Society of London*, 154:295-302.

N. Pearson, P.N., Shackleton, N.J., Weedon, G.P., Hall, M.A., 1997b. Multispecies planktonic foraminifer stable isotope stratigraphy through Oligo/Miocene boundary climatic cycles, Site 926. *Proceedings of the Ocean Drilling Program, Scientific Results*, 154:441-449.

O. Pearson, P.N., Ditchfield, P.W., Singano, J., Harcourt-Brown, K.G., Nicholas, C.J., Shackleton, N.J., Hall, M.A., 2001. Warm Late Cretaceous and Eocene tropical sea-surface temperatures. *Nature*, 413:481-487.

O*. Pearson, P.N., Norris, R.D., Empson, A.J., 2001. *Mutabella miriabilis gen. et sp. nov.*, A Miocene microperforate planktonic foraminifer with an extreme level of intraspecific variability. *Journal of Foraminiferal Research*, 31(2):120-132.

P. Schneider, C.E., Kennett, J.P., 1996. Isotopic evidence for interspecies habitat differences during evolution of the Neogene planktonic foraminiferal clade Globoconella. *Paleobiology*, 22 (2):282-303.

Q. Shackleton, N.J., Vincent, E., 1978. Oxygen and carbon isotope studies in the Recent foraminifera populations: *Palaeoceanography, Palaeoclimatology, Palaeoecology*, 48:197-213.

R. Stewart, D.R.M., 2003. *Evolution of Neogene globorotaliid foraminifera and Miocene climate change.* Ph.D. Thesis.

S. Van Eijden, A.J.M., Ganssen, G.M., 1995. An Oligocene multi-species foraminiferal oxygen and carbon isotope record from ODP Hole 758A (Indian Ocean): paleoceanographic and paleo-ecologic implications. *Marine Micropaleontology*, 25:47-65.

T. Wilson, P.A., Norris, R.D., 2001. Warm tropical ocean surface and global anoxia during the mid-Cretaceous period. *Nature*, 412:425-429.

U. Wilson, P.A., Norris, R.D., Cooper, M.J., 2002. Testing the Cretaceous greenhouse hypothesis using glassy foraminiferal calcite from the core of the Turonian tropics on Demerara Rise. *Geology*, 30(7):607-610.

Appendix 2.3 – *Epstein's Test* (Epstein, 1960a, 1960b)

The Survivorship curves presented in Chapter 2 were tested for straightness using Epstein's total-life method. The *total life* of a taxon is the summation of the longevities of all taxa that become extinct before the taxon becomes extinct. That is, if there are n taxa with durations $d_1 \leq d_2 \leq \ldots d_n$, then the total lives ($T_i$) are calculated as follows:

$$T_1 = nd_1$$
$$T_2 = d_1 + (n-1)d_2$$
$$T_i = d_1 + d_2 + \ldots + (n-i+1)d_i$$
$$\cdot$$
$$\cdot$$
$$\cdot$$
$$T_n = d_1 + d_2 + \ldots + (n-r+1)d_n$$

In a linear survivorship situation, the sum of the first $(n-1)$ total lives is normally distributed with a theoretical mean of $(n-1)T_n/2$ and a standard deviation of $[(n-1)T.T_n^2/12]^{1/2}$. In tests for linearity survivorship $\sum_{i-1}^{n-1} T_i$ is compared to a theoretical range which is the mean ± 1.96 times the standard deviation. If $\sum_{i-1}^{n-1} T_i$ is within the range, the hypothesis of linearity is accepted at the 0.05 significance level.

This method tests for straightness only; visual estimation must be used to estimate the degree of departure from linearity. This test does remove the subjectivity of 'fitting a line' to a survivorship curve, however it is not infallible. Hoffman and Kitchell (1984) found that Epstein's Test is sensitive to the lower right hand portion of a survivorship plot. They found that in real and simulated datasets this could result in curves that are linear in all but those last few points being delineated as non-linear.

N.B. misprints occur in Wei and Kennett (1983) and Pearson (1992, 1995, 1996). Either Epstein (1960a; 1960b) or Raup (1975) must be read to obtain the correct formulae. See McGowan and Pearson (1998) for discussion.

Appendix 2.4. Results of Epstein's Test for the survivorship curves presented in Figure 2.12A-F.

DATASET	n	SUM (R-1) LIVES	UPPER LIMIT	LOWER LIMIT	LINEAR?
All PF	600	**204559.6936**	163928.9759	179822.7456	N
Surf	262	**36504.14723**	29442.04216	33877.21996	N
Int	123	**7655.024212**	5934.425946	7289.197268	N
Deep	144	**10681.21082**	8192.162241	9904.658841	N
Neo glob	52	**1323.273673**	977.5420271	1345.670387	Y
Palaeo glob	58	**1802.900542**	1225.708844	1657.921644	N

Appendix 3.1A. Neogene biostratigraphy redrawn from Berggren et. al. (1995), Late Miocene to Pleistocene.

TIME (Ma)	EPOCH	AGE		PLANKTONIC FORAMINIFERA Berggren (1973,1977 & 1995) ATLANTIC			INDO-PACIFIC		
1	PLEISTOCENE	LATE	MIDDLE	PT1	b	 *Gt. truncatulinoides PRZ*	**N23**	*Gd. fistulosus - Gt. truncatulinoides IZ*	N22*
		EARLY	CALABRIAN		a	*Gd. fistulosus - Gt. tosaensis ISZ* 			
2		LATE	GELASIAN	PL6		 ***Gt. miocenica*** *- Gd. fistulosus IZ*	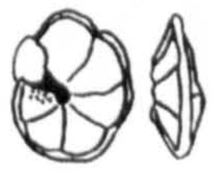 ***Gt. pseudomiocenica*** *- Gd. fistulosus IZ*		
				PL5		*D. altispira - Gt. miocenica IZ*	*D. altispira - Gt. pseudomiocenica IZ*		
3			PIACENZIAN	PL4		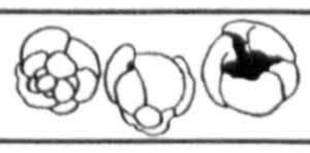 ***D. altispira*** *- Gt. pseudomiocenica IZ*			
				PL3		 *Gr. margaritae - Sph. seminulina IZ* 		
4	PLIOCENE	EARLY	ZANCLEAN	PL2		 ***Glb. nepenthes*** *- Gt. margaritae IZ*			N19
				PL1	b	 ***Gt. cibaoensis*** *- Glb. nepenthes ISZ*		*Gt. tumida - Glb. nepenthes IZ*	
5					a	 ***Gt. tumida*** *- Gt. cibaoensis IRZ*			N18
6	MIOCENE	LATE	MESSINIAN	M14		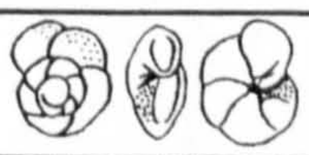 ***Gt. lenguanensis*** *- Gt. tumida IZ*			
				M13	b	  ***Gd. extremus/Gt. plesiotumida*** *- Gt. lenguanensis*			N17
7									
8									

* Variable datum from Spencer-Cervato (1996) & Chaisson (1997)

DRMS2K

Appendix 3.1B. Neogene biostratigraphy redrawn from Berggren et. al. (1995), Middle to Late Miocene.

TIME (Ma)	EPOCH	AGE		PLANKTONIC FORAMINIFERA Berggren (1973,1977 & 1995) (SUB)TROPICAL			Blow (1969)
8	MIOCENE	LATE	TORTONIAN	M13	b	*Gd. extremus/Gt. plesiotumida* - ***Gt. lenguanensis*** *ISZ* 	N17
9					a	 *N. acostaensis - Gd. extremus/ Gt. plesiotumida ISZ* 	N16
10							
11				M12		*N. mayeri - N. acostaensis IZ*	N15
12		MIDDLE	SERRAVALLIAN	M11		*Glb. nepenthes/**N. mayeri** Conc. RZ* 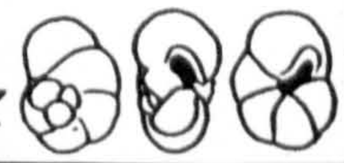	N14
				M10		 ***Gt. f. robusta** - **Glb. nepenthes** IZ* 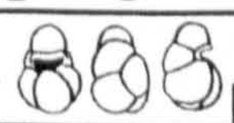	N13
				M9	b	***Gt. f. robusta** Tot. RZ*	*Gt. f. lobata - Gt. f. robusta IZ* — — —
					a	*Gt. f. lobata Lin. RZ*	N12
13				M8		 *Gt. f. fohsi s.s. Lin. Z* 	N11
14				M7		*Gl. peripheroacuta Lin. Z* 	N10
15				M6		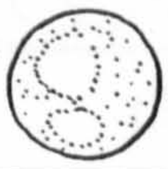 ***O. suturalis** - Gl. peripheroacuta. IZ*	N9

DRMS2K

Appendix 3.1C. Neogene biostratigraphy redrawn from Berggren et. al. (1995), Early to Middle Miocene.

TIME (Ma)	EPOCH	AGE		PLANKTONIC FORAMINIFERA Berggren (1973,1977 & 1995) (SUB)TROPICAL				
16	MIOCENE	MIDDLE	LANGHIAN	M5	b	***Pr. glomerosa*** - *O. suturalis ISZ* 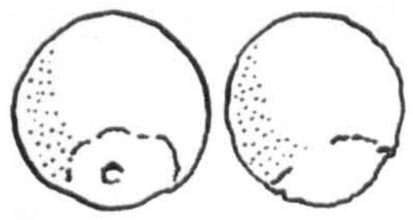	*Pr. sicana - O. suturalis ISZ*	N8
					a	*Pr. sicana - Pr. glomerosa ISZ*		
17			BURDIGALIAN	M4	b	*Gd. bispherica - PRSZ* 	*Cat. dissimilis - Pr. sicana ISZ*	N7
					a	*Cat. dissimilis - **Gt. birnageae** ISZ* 		
18				M3		*Glla. insueta - Cat. dissimilis Conc. RZ* 		N6
19		EARLY		M2		*Catapsydrax dissimilis IZ* 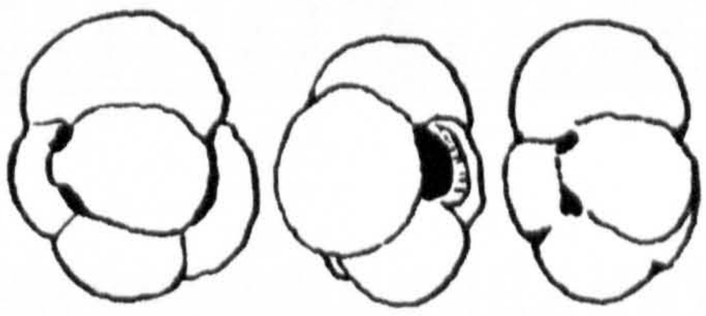		N5
21			AQUITANIAN	M1	b	*Gt. kugleri - Gq. dehiscens Conc. RSZ* 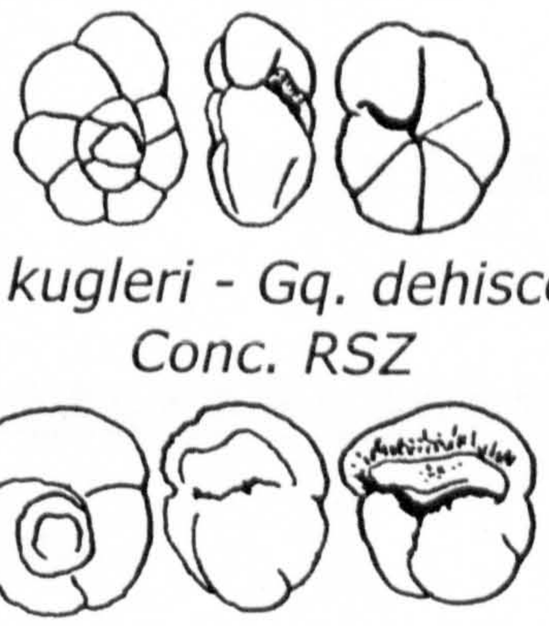	*Gt. kugleri TRZ*	N4
22					a	*Gd. primordius ISZ* 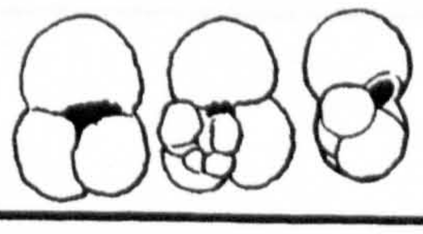		
23								
24	OL	LATE	CHATT-IAN	P22		*G. ciperoensis IZ* 		P22

DRMS2K

Appendix 3.2. Leg 194 planktonic foraminiferal biostratigraphy.

Site	Core	Type	Section	Top Depth (mbsf)	Zone (or age definitive) species	Age assignment
1192A	1	H	CC	9.36	trunc, tosa	N22-N23
	2	H	CC	14.28	trunc, tosa	N22-N24
	3	H	CC	28.49	fist, tosa, no trunc	N21
	4	M	CC		test core	
	5	H	CC	38.48	fist, tosa, no trunc	N21
	6	H	CC	48.79	alti, tosa, mio?	N21
	7	H	CC	58.2	alti, tosa, mio?, pmio?	N21-N22
	8	H	CC	67.87	alti, mio?, semin, marg?	N20
	9	H	CC	76.84	NZF, prim, koch	N19-N20
	10	H	CC	86.58	nep	N19
	11	M	CC		test core	
	12	H	CC	97.28	nep, no Sdeh, ptum	N19-N18
	13	H	CC	106.53	no tum, prim, Gdeh	N18
	14	H	CC	116.28	no tum, acost, ptum	N17-N16
	15	H	CC	125.44	acost, ptum	N17-N16
	16	H	CC	134.52	acost, ptum	N17-N16
	17	H	CC	144.89	acost, ptum	N17-N16
	18	H	CC	154.2	acost, ptum	N17-N16
	19	H	CC	163.73	acost, ptum	N17-N16
	20	H	CC	173.19	acost, ptum	N17-N16
	21	H	CC	182.83	acost, ptum	N17-N16
	22	H	CC	192.25	acost, ptum	N17-N16
	23	M	CC		test core	
	24	H	CC	202.78	acost, ptum	N17-N16
	25	H	CC	212.26	acost R, nep, leng?, ptum, pleng	N16
	26	H	CC	221.82	acost R, nep, ptum, pleng, cont?	N16
	27	H	CC	231.33	ptum, nep, leng, pleng	N16
	28	H	CC		no core	
	29	H	CC	241.71	ptum	N16?

1192B	1	H	CC	2.31	trunc, crassf, Sdeh, prim	N22-N23
	2	H	CC		test core	
	3	H	CC		test core	
	4	H	CC	191.35	alti, pmio, no tum, no trunc, no tosa	N17
	5	H	CC	201.2	pmio, ptum, no tum	N17
	6	H	CC	210.72	ptum, no tum, marg, leng, no prim	N17b
	7	H	CC	211.2	ptum, pmio?, prim R, leng	N17
	8	H	CC	229.79	ptum, no acost	N17
	9	X	CC	236.72	ptum, no acost	N17
	10	X	CC	245.38	ptum, leng	N17
	11	X	CC	248.6	ptum, marg?	N17
	12	X	CC	263.11	no ptum, may?, marg?	Top N14?
	13	X	CC	267.8	leng, barren	
	14	X	CC	277.5	may?	N14?
	15	X	CC	291.53	siak?	N14?
	16	X	CC	301.08	barren	
	17	X	CC	313.4	curva?, clem	N8?
	18	X	CC	322.02	barren	
	19	X	CC	333.12	bisph, curva?	N7b-N8
	20	X	CC	335.2	sic-bisph, curva?, no diss	N7-N8
	21	X	CC	343.86	sic-bisph, no curva	N7-N8
	22	X	CC	346.71	sic-bisph, no curva	N7-N8

1193A	1	H	1, 20cm	0.2	fin, trunc, no tosa	N22-N23
	1	H	1, 100cm	1	trunc, no tosa, fin	N22-N23
	1	H	3, 20cm	3.2	trunc, crassf, obliquil, tosa, tum, no fist, Sdeh	N22
	1	H	5, 18cm	6.18	fist, extr LO, pmio, no trunc	Top N21
	1	H	CC	6.45	alti, pmio, Sdeh, ptum, obliquil	N19
	2	H	2, 10cm	8.2	no fist, Sdeh, tum, alti, prim, pmio, no nep	Base N20
	2	H	5, 20cm	12.8	acost, no nep, no marg	Base N20
	2	H	CC	15.74	extr, prim, tum, ptum, pmio	N18-N19
	3	H	2, 10cm	17.7	punct, marg LO	N19
	3	H	5, 100cm	23.1	alti, marg, pmio, acost, semin, no nep	N19
	3	H	CC	25.82	tum, alti, multi, prim, no S. deh, no nep	N18-N19
	4	H	2, 10cm	27.2	alti, acost, pmio, prim, semin, punct, nep	N19
	4	H	5, 100cm	32.6	semin, acost, alti, pmio, punct	N19
	4	H	CC	35.25	tum, ptum, cib, paen	N18
	5 to 42	Lithified carbonate platform - unsuitable samples				
	43	X	CC	233.35	barren	
	44	X	CC	239.23	woodi, drur?	
	45	X	CC	245.39	Gdeh, woodi, conn?, primor?	N4-7
	46	X	CC	249.48	sic?, fal?	
	47	X	CC	261.52	barren	
	48	X	CC	266.06	barren	
	49	X	CC	275.43	barren	
	50	X	CC	285.08	trilo, woodi, prbull	N4-N5
	51	X	CC	296.14	primor?	N4-N5
	52	X	CC	303.02	trilo, pwoodi	N4b-N7
	53	X	CC	312.66	barren	
	54	X	CC	316.89	barren	
	55	X	CC	320.4	nothing diagnostic	
	56	X	CC	325.2	nothing diagnostic	
	57	X	CC	332.27	Gdeh	N4b-N8
	58	X	CC	348.95		
	59	X	CC	357.93	prbull, bull, altiap, quad	N4b-N7
	60	X	CC	366.92	trilo, imm, primor?	N4a-N5
	61-83	X	CC	377.17-503.30	barren	

1194A	1	H	2, 45cm	1.95	fin, Sdeh, trunc, no tosa	N22-N23
	1	H	CC	4.38	semin, extr, crassf, pmio, Sdeh	N19
	2	H	CC	14.14	tum, pmio, acost, alti, Sdeh, semin	N19
	3	H	CC	23.53	tum, acost, prim, no Sdeh	N19
	4	H	CC	33.49	ptum, tum, Sdeh, pmio, punct, no nep, acost	lower N19
	5	H	2, 80	35.5	extr, ptum, acost, marg, cib, tum, punct	N19
	5	H	5, 80	40	punct, pmio, ptum, acost, Sdeh, nep	N19
	5	H	CC	42.82	tum, marg, ptum, Sdeh	N19
	6	H	2, 80	45	tum, punct, nep, extr, nit	N19
	6	H	5, 80	49.5	ptum, nep, tum, extr, no Sdeh, no punct	N18
	6	H	CC	52.29	tum, ptum, no Sdeh	N18-N19
	7	H	CC	61.85	tum, ptum, no Sdeh	N18-N19
	8	H	CC	71.32	ptum, tum, acost, nep, no Sdeh	N18-N19
	9	H	CC	80.5	no tum, marg, ptum, cib	base N18
	10	H	CC	90.42	acost, ptum, prim, LO leng	top N17a
	11	H	CC	100.02	ptum, nep, extr, cib, leng	N17a
	12	H	CC	109.36	extr, ptum, leng	N17a
	13	H	CC	116.99	extr, ptum	N17a
	14	X	CC	119.32	barren	
	15	X	CC		no core	
	16	X	CC	132.72	barren	
	17	X	CC		no core	
	18	X	CC	160.3	barren	

1194B	3	R	CC	119.6	aper, woodi	non diagnostic
	4	R	CC		no core	
	5	R	CC	138.8	woodi	non diagnostic
	6	R	CC	149.65	prbull? bull?	non diagnostic
	7	R	CC	158	barren	
	8	R	CC	169.76	barren	
	9	R	CC	177.2	drur, may, trilo	N4-N14
	10	R	CC	191.4	primor?, Gdeh, prsiph, imm-quad, trilo	N4-N5?
	11	R	CC	197.79	trilo, glom, prsiph, may	N8?
	12	R	CC	206	trilo, sic, conn?, braz, prbull	N4a-N8
	13	R	CC	215.7	prbull?, trilo	non diagnostic
	14	R	CC	225.3	prbull, fal?	non diagnostic
	15	R	CC		no core	
	16	R	CC	244.5	sic, trilo	N8-N9?
	17	R	CC	256.57	may	N4-N14
	18	R	CC		no core	
	19	R	CC		no core	
	20	R	CC	283	obesa, may	N4-N14
	21	R	CC	292.6	Gdeh, sic, trilo, cip?	N5?
	22	R	CC	303.67	quad, trans?, cip, uni	N5?/N8-N9
	23	R	CC	313.07	nothing diagnostic	
	24	R	CC	323.91	imm, quad	non diagnostic
	25	R	CC	340.45	Gdeh, trilo	non diagnostic
	26	R	CC	347.8	imm, Gdeh, trilo-sic	non diagnostic
	27	R	CC	353.52	prsiph, Gdeh	N4b-N5
	28	R	CC		no core	
	29	R	CC	374.77	trilo, cip	N4-N5
	30	R	CC	384.7	Gdeh	non diagnostic
	31	R	CC	390.8	barren	
	32	R	CC	400.03	barren	
	33	R	CC	411.86	barren	

1195A	1	H	CC	4.59	trunc, cal, no tosa	N22-N23
	2	H	CC	14.09	tum, tosa, crassf, trunc, no fin, no fist, no extr	Middle N22
	3	H	CC	23.5	fist, crassl, trunc, tosa, no extr, pert	N22
	4	H	CC	32.99	fist, extr, tosa, no mio	Top N21
	5	H	CC	42.29	alti, semin, pmio, no fist	N20
	6	H	CC	51.35	lim, tum, pmio, acost, marg, no nep	Base N20
	7	H	CC	60.6	marg, acost, punct, nep	N19
	8	H	CC	70.97	tum, marg, Sdeh	N19
	9	H	CC	80.75	tum, Sdeh	N18

	1	H	CC	8.26	trunc, fin, tosa	N22-N23
	2	H	CC	17.4	trunc, tosa, fin	N22-N23
	3	H	CC	27.11	fist, extr, Sdeh, tum, no trunc	N21-N22
	4	H	CC	36.74	semin, tum, Sdeh, fist, multi	N19-N21
	5	H	CC	45.7	Sdeh, tum, mio, semin	N19-N21
	6	H	CC	55.39	tum, alti, no fist, marg, nep, pmio	Base N20
	7	H	CC	65.6	tum, pmio, Sdeh	N19
	8	H	CC	74.24	tum, nep, Sdeh	N19
	9	H	CC	84.41	Sdeh, nep, no tum	Top N18-N19
	10	H	CC	93.97	cib, no tum, no Sdeh	Top N17
	11	H	CC	103.32	no tum, acost, ptum, cib, extr, nit, no prim	N17a
	12	H	CC	112.89	ptum, extr, nit	N17a
	13	H	CC	122.7	ptum, leng, extr	N17a
	14	H	1, 80cm	123.2	extr, pmio, ptum, acost, scit, leng, cib	N17b?
	14	H	5, 80cm	129.2	extr, ptum, pmio?, leng, cib	N17a?
	14	H	CC	132.05	ptum, extr, nep	N17a
	15	H	2, 80cm	134.2	ptum, acost, nep, leng	N17
	15	H	5, 80cm	138.7	acost, lim, ptum, extr, nit, cont	N17a
	15	H	CC	141.48	no core	
	16	H	CC	150.8	nep, acost, ptum, no extr, no hum	N16-N17
	17	H	CC	160.54	ptum, acost, no extr, hum	N16-N17
	18	H	CC	170.24	ptum, acost, no extr	N16
	19	H	CC	179.68	ptum, acost	N16
	20	H	CC	189.2	acost, no ptum	N16
	21	H	CC	198.76	siak-may, ptum, acost	N16
	22	H	CC	207.36	nep, bilob, ptum, clem	N16
	23	X	CC	210.27	siak, ptum, bilob	N16
	24	X	CC	226.56	alti, nep, ptum	N16
	25	X	CC	236.65	siak, alti, bilob, no ptum	N16
	26	X	2, 43cm	238.6	nep, siak, may, Gdeh, no ptum	Top N14
	26	X	5, 20cm	242.87	may, siak, no nep, perac?	N11-N14
	26	X	CC	243.06	alti, siak, bilob	N14-N15?

1195B	27	X	2, 80cm	248.6	may, siak, lob, uni	N12
	27	X	5, 80cm	253.1	uni, prmen	N12?
	27	X	CC	255.59	alti, bilob, siak, lob?, no nep	N12
	28	X	CC	263.33	lob, foh, alti	N11-N12
	29	X	CC	274.43	alti, perac/perron, Gdeh	N11
	30	X	CC	280.49	alti	non diagnostic
	31	X	CC	284.6	prsiph, may, perron	N10?
	32	X	CC	298.99	may, siak, no Fohsella	N10?
	33	X	CC	309.75	trilo, may, Gdeh	non diagnostic
	34	X	CC	320.72	curva, uni, Gdeh, sic?	N9-N10
	35	X	CC	330.01	bilob, curva, sic	N9
	36	X	CC	338.31	sic, alti, scit	N9
	37	X	CC	350.03	sic, curva, may	N8-N9
	38	X	CC	354.76	sic, no curva	N8-N9
	39	X	CC	365.33	sic, curva, trans, ins?	N8-N9
	40	X	CC	377.16	sic, curva, ins?, trans	N8-N9
	41	X	CC	381.99	barren	
	42	X	CC	394.3	barren	
	43	X	CC	401.06	bisph, glom	N8?
	44	X	CC	418.94	perron, birn	N7-N8
	45	X	CC	428.05	sic, diss?	N7?
	46	X	CC	437.48	barren	
	47	X	CC	445.74	barren	
	48	X	CC	457.69	Cat?, bella, ven, no sic	N7-N8
	49	X	CC	463.33	Gdeh, sic, bella, ven, no sic	N7-N8
	50	X	CC	469.42	barren	
	51	X	CC	479.87	no sample	
	52	X	CC	487.77	barren	
	53	X	CC	496.6	barren	
	54	X	CC	512.7	may, no sic	non diagnostic
	55	X	CC	517.5	barren	
	56	X	CC		no sample	
	57	X	CC		cip, may	N4-N5?

1197A	1	H	2, 136cm	2.86	tosa, trunc, fin, pink rub	N22-N23
	1	H	CC	5.95	trunc, crassf, tum, no fist, no tosa, pink rub	N22-N23
	2	H	CC	15.5	trunc, fin, no fist, dut, tosa?	N22
	3	H	CC	25.04	tosa, trunc, fin, no fist	N22
	4	H	3, 12cm	28.22	tosa, crassf, trunc, no fist, no extr, Sdeh, dut	N22
	4	H	CC	34.74	tosa, trunc, Sdeh, pach, no fist, no extr	N22
	5	H	CC	44.04	fist, trunc, extr, dut	Base N22
	6	H	CC	53.61	lim, Sdeh, crassf, tosa, pmio, no alti, no semin	Top N21-N22
	7	H	1, 28cm	53.88	Sdeh, crassf, multi, tum, dut, Sdeh, no fist, no extr	N22
	7	H	CC	54.44	tum, crassf, Sdeh, extr, pmio, no fist, no semin	N20-N21
	9	X	CC	59.6	barren	
	10	X	CC	69.2	nothing diagnostic	
	11	X	CC	78.8	barren	
	17	X	CC	136.6	bull, bulloid, ptum, obliq	N17b-N19
	20	X	CC	165.4	uni, trilo, alti, ptum, mtum, obliq, lim, baroe	N17

	3	R	CC	69.2	alti, extr, ptum, mtum, sut, no Sdeh	N17-N18
	5	R	CC	88.5	alti, ptum, Gdeh, bull, tum?	N17-N18
	6	R	CC	98.2	nothing diagnostic	
	8	R	CC	117.4	woodi, aper, ven, baroe, alti, ptum, men	N16-N18
	9	R	CC	127	baroe, nothing diagnostic	
	11	R	CC	146.2	obliq, alti, baroe, Gdeh, ptum, obesa, vari, bulloi	N18?
	12	R	CC	155.8	bulloi, obliq, baroe	N17-N18
	13	R	CC	165.4	semin, ptum, quad, obliq, glob, baroe, Gdeh	N17-N18
	14	R	1, 14cm	175.14	barren	
	14	R	CC	?	barren	
	15	R	1, 4cm	184.64	men, Foh sp, O sp	N9-N12?
	15	R	1, 31cm	184.91	men, Gdeh, ven, siak	<N14
	15	R	CC	?	siak, uni, men, Gdeh, rob?	N13-N14
	16	R	CC	194.2	barren	
	17	R	CC	203.8	baroe, alti, obliq?, Gdeh	non diagnostic
	18	R	CC	213.4	nothing diagnostic	
	19	R	CC	223	Gdeh, ven, bilob	non diagnostic
	20	R	CC	232.7	no sample	
	21	R	CC	242.3	Gdeh, ptum, alti, nep, baroe, Fohsella?	N10-N12?
	22	R	CC	251.9	no sample	
	23	R	CC	261.5	Gdeh, alti	non diagnostic
	24	R	CC	271.2	nothing diagnostic	
	25	R	CC	280.8	nothing diagnostic	
	27	R	CC	300	nothing diagnostic	
	28	R	CC	311.2	nothing diagnostic	
	30	R	CC	328.9	barren	
1197B	31	R	CC	340.06	barren	

1197B	32	R	CC	348.2	barren		
	33	R	CC	357.8	barren		
	34	R	CC	367.4	lithified sample		
	35	R	CC	381.57	O spp, alti, Gq sp, trilo	>N9	
	36	R	CC	391.3	lithified sample		
	37	R	CC	397.77	may, siak, Gdeh, trilo, baroe	<N14	
	38	R	CC	411.37	siak, O sp, Gq sp, obesa, alti, Foh sp, panda	N9-N14	
	39	R	CC	424.28	barren		
	40	R	CC	431.35	barren		
	41	R	CC	438.83	barren		
	42	R	CC	448.26	barren		
	46	R	CC	492.29	barren		
	47	R	CC	499.41	trilo, baroe, Gdeh, alti	non diagnostic	
	48	R	CC	509.28	nothing diagnostic		
	49	R	CC	514.34	nothing diagnostic		
	50	R	CC	530.9	glut, scit, ven, Gq sp	>N9	
	51	R	CC	536.27	nothing diagnostic		
	52	R	CC	550.17	nothing diagnostic		
	53	R	CC	557.14	nothing diagnostic		
	54	R	CC	568.66	nothing diagnostic		
	55	R	CC	579.2	nothing diagnostic		
	56	R	CC	585	nothing diagnostic		
	57	R	CC	598.27	nothing diagnostic		
	58	R	CC	606.7	nothing diagnostic		
	59	R	CC	612.34	nothing diagnostic		
	60	R	CC	621.2	nothing diagnostic		
	61	R	CC	631.02	altiap, obesa, Gdeh	N4-N7?	

1198A	1	H	2, 80cm	2.3	cal, digi, rubesc, trunc, no pink rub	<120Kyr N22-N23
	1	H	4, 20cm	4.7	pert, trunc, no pink rub	<120Kyr N22-N23
	1	H	CC	4.87	crassf, trunc, Sdeh, fin, infl, tum, Sdeh, pink rub, no tosa	N22-N23
	2	H	CC	14.39	fin, tum, dut, trunc, tosa	N22
	3	H	CC	23.67	trunc, fin, crassf, tum, flex, no tosa	N22
	4	H	CC	33.71	trunc, crassf, tum, no tosa	N22
	5	H	CC	43.17	tum, trunc, ung, Sdeh, crassf, dut, obliquil	N22
	6	H	CC	52.09	obliquil, tum, crassf, trunc, tosa, dut, ung	N22
	7	H	CC	62.25	dut, obliquil, Sdeh, multi, ung, tosa, trunc, no fist, no extr	N22
	8	H	CC	71.11	tosa, Sdeh, ung, dut, crassf, no fist, no extr	N22
	9	H	CC	81.26	tosa, Sdeh, trunc?, ung, fim, cul	N22
	10	H	CC	89.69	tum, tosa, ung, trunc, no fist, no extr	N22
	11	H	CC	100.21	tum, ung, tosa, obliquil, no fist, no extr	N21-N22
	12	H	CC	109.56	tum, tosa, ung, trunc, crassf, obliquil, fist, no extr	N21-N22
	13	H	CC	119.14	tum, Sdeh, fist, tosa, dut, trunc, no extr	N21-N22
	14	H	CC	128.67	crassf, trunc, tum, fist, tosa	N21-N22
	15	H	3, 85cm	132.35	trunc, no extr	N21-N22
	15	H	CC	137.62	tum, obliquil, multi, pmio?, fist, tosa, extr	N21
	16	H	CC	147.69	pmio, crassf, multi, ung, mio, no alti, no fist, no extr	N21
	17	H	CC	157.03	multi, extr, pmio, tosa, no alti, no fist, no semin	N21
	18	H	CC	166.75	fist, crassf, pmio, extr, no alti, no semin	N21
	19	H	CC	176.19	extr, nit, fist, hum, pmio, tosa, crassf, no alti, no semin	N21
	20	H	CC	185.78	alti, extr, pmio, no tosa, no semin, no marg	N20-N21
	21	H	CC	194.71	alti, extr, pmio, tum, no semin, no marg	N20-N21
	22	H	3, 85cm	198.85	semin, Sdeh, paen	N19-N20
	22	H	CC	202.81	alti, Sdeh, pmio, tum, semin, no nep, no ptum	N19?
	23	X	1, 25cm	203.25	tum, alti, extr, semin, multi, marg, ptum, pmio, semin	N18-N19
	23	X	CC	205.74	alti, ptum, Sdeh, pmio, no nep, no punct	N18-N19

1198B	1	R	CC	199.3	alti, extr, pmio, multi, tum, ptum	N18-N19
	2	R	CC	205.2	obliquil, tum, alti	N19-N20
	3	R	CC	214.8	extr, ptum, alti	N17-N19
	4	R	CC	224.4	lithified sample	
	5	R	CC	234	lithified sample	
	6	R	CC	243.6	alti, ptum, no tum	N17?
	7	R	CC	253.3	lithified sample	
	8	R	CC	262.9	lithified sample	
	9	R	CC	no core		
	10	R	CC	292.2	alti, cul, lim, acost, koch, no tum, no extr, no pmio	N16-N17?
	11	R	CC	291.8	ptum, cul, lim, alti, no extr, no tum, no hum	N16?
	12	R	CC	301.4	no core	
	13	R	CC	311	Gdeh, acost, semin	N16
	14	R	CC	320.6	no core	no core
	15	R	CC	330.3	no core	no core
	16	R	CC	339.9	alti, semin, acost, no nep	N16?
	17	R	CC	350.24	alti, Foh sp.	N12-N15?
	18	R	CC	363.42	Gdeh, alti, trilo, may, siak, prsiph, siph, Foh sp.	N13
	19	R	CC	369.63	semin, may, siak, uni, arch-prmen	N10-N12
	20	R	CC	381.69	arch-prmen	N10-N12
	21	R	CC	390.58	alti, Gdeh, curva, may, siak, prmen	N9?
	22	R	CC	407.31	nothing diagnostic	
	23	R	CC	415.68	sic, prsiph, siak, may, alti, obesa, siph, no uni	N8-N9
	24	R	CC	425.25	imm, alti, prsiph, siak, curva, prscit, sic, trans, no uni	N8-N9
	25	R	CC	436.08	alti, drur, Gdeh, obesa, trilo, sic	N8-N9?
	26	R	CC	442	barren	
	27	R	CC	453.76	nothing diagnostic	
	28	R	CC	463.56	nothing diagnostic	
	29	R	CC	464.9	nothing diagnostic	
	30	R	CC	484.3	nothing diagnostic	
	31	R	CC	489.62	nothing diagnostic	
	32	R	CC	500.99	nothing diagnostic	
	33	R	CC	504.82	no sample	
	34	R	CC	517.22	no sample	

Appendix 3.2 Symbol Key

acost	*N. acostaensis*
alti	*D. altispira*
altiap	*G. altiapertura*
arch	*Gr. archeomenardii*
baroe	*D. baroemoenensis*
bella	*J. bella*
bilob	*O. bilobata*
birn	*Gr. birnageae*
bisph	*Gds. bisphericus*
braz	*G. brazieri*
bulloid	*G. bulloideus*
cal	*Ge. calida*
Cat	*Catapsydrax*
cib	*Gr. cibaoensis*
cip	*G. ciperoensis*
clem	*Te. clemenciae*
conn	*G. connecta*
crassf	*Gr. crassaformis*
crassl	*Gr. crassula*
cul	*Gr. cultrata*
curva	*Pr. curva*
digi	*B. digitata*
diss	*C. dissimilis*
drur	*G. druryi*
dut	*N. dutertrei*
extr	*Gds. extremus*
fal	*G. falconensis*
fim	*Gr. fimbriata*
fin	*P. finalis*
fist	*Gds. fistulosus*
flex	*Gr. flexuosa*
foh	*F. fohsi*
Gdeh	*Gq. dehiscens*
glut	*Ga. glutinata*
hum	*N. humerosa*
imm	*Gds. immaturus*
ins	*Gt. Insueta*
koch	*Ss. Kochi*
leng	*Gr. lenguanensis*
lim	*Gr. limbata*
lob	*F. lobata*
marg	*Gr. margritae*
may	*J. mayeri*
men	*Gr. menardii*
mio	*Gr. miocenica*
multi	*Gr. multicamerata*
nep	*G. nepenthes*
nit	*C. nitida*
obesa	*Ge. obesa*
obliq	*Gds. obliquus*
obliquil	*P. obliquiloculata*
paen	*Ss. paenedehiscens*
panda	*Gr. panda*
perac	*F. peripheroacuta*
perron	*F. peripheroronda*
pert	*Gr. pertenuis*
pleng	*Gr. paralenguanensis*
pmio	*Gr. pseudomiocenica*
prbull	*G. praebulloides*
prim	*P. primalis*
primor	*Gds. primordius*
prmen	*Gr. praemenardii*
prscit	*Gr. praescitula*
prsiph	*Ge. praesiphonifera*
ptum	*Gr. plesiotumida*
punct	*Gr. puncticulata*
pwoodi	*Gds. parawoodi*
quad	*Gds. quadrilobatus*
rob	*F. robusta*
rub	*Gds. ruber*
rubesc	*G. rubescens*
scit	*Gr. scitula*
Sdeh	*Sa. Dehiscens*
semin	*Ss. Seminulina*
siak	*J. siakensis*
sic	*Gds. sicanus*
siph	*Ge. siphonifera*
tosa	*T. tosaensis*
trans	*Pr. transitoria*
trilo	*Gds. trilobatus*
trunc	*T. truncatulinoides*
ung	*Gr. ungulata*
uni	*O. universa*
vari	*Gd. Variabilis*
ven	*G. venezuelana*
woodi	*G. woodi*

Comments

R	Rare
LO	Last Occurence
no	none present
sp	species (singular)
spp	species (plural)
CC	Core catcher

Drill type

H	APC
M	
R	RCB
X	XCB

Appendix 3.3

Datum	Core, section, interval (cm)	Depth of first absence or presence (mbsf)	Depth of last presence or absence (mbsf)	Mean depth (mbsf)	Age (Ma)
Hole 1193A					
FO *Emiliania huxleyi*	1H-1, 90cm, to 1H-2, 80cm	0.90	2.3	1.60	0.26
LO *Pseudoemiliania lacunosa*	1H-2, 80cm to 1H-3, 10cm	2.30	3.1	2.70	0.46
LO *Calcidiscus macintyrei*	1H-3,30cm, to 1H-5,30cm	3.30	6.3	4.80	1.7
LO *Discoaster brouweri*	1H-3,30cm, to 1H-5,30cm	3.30	6.3	4.80	2
LO *Discoaster pentaradiatus*	1H-3,30cm, to 1H-5,30cm	3.30	6.3	4.80	2.5
LO *Discoaster surculus*	1H-3,30cm, to 1H-5,30cm	3.30	6.3	4.80	2.6
LO *Discoaster tamalis*	1H-3,30cm, to 1H-5,30cm	3.30	6.3	4.80	2.8
LO *Dentoglobigerina altispira*	1H-5, 18cm, to 1H-CC	6.18	6.58	6.38	3.09
LO *Sphaeroidinellopsis*	1H-CC to 2H-2, 10cm	6.58	8.2	7.39	3.12
LO *Reticulofenestra pseudoumbilica*	2H-5,90cm, to 2H-6,98	13.50	15.08	14.29	3.7
LO *Globorotalia margaritae*	2H-CC, to 3H-2, 10cm	15.97	17.7	16.84	3.8
LO *Glogigerina nepenthes*	4H-1, 80cm, to 4H-2, 10cm	26.40	27.2	26.80	4.18
FO *Sphaeroidinella dehiscens*	3H-CC to 4H-CC	26.06	35.39	30.73	5.30
FO *Globorotalia tumida*	4H-CC to 5H-CC	35.39	36.06	35.73	5.60
LO *Discoaster quinqueramus*	4H-6, 80cm, to 4H-CC	33.90	35.39	34.65	5.6
FO *Discoaster surculus*	5H-CC to 39X-CC	36.06	211.27	123.67	7.5
LO *Cyclicargolithus floridanus*	5H-CC to 39X-CC	36.06	211.27	123.67	11.9
LO *Globigerina connecta*	43X-CC to 44X-CC	233.74	239.58	236.66	16.40
LO *Globigerinoides parawoodi*	51X-CC to 52X-CC	296.42	303.38	299.90	16.80
FO *Sphenolithus heteromorphus*	60X-CC to 73X-CC	367.31	445.7	406.51	18.2
LO *Sphenolithus belemnos*	73X-CC to 75X-CC	445.70	455.54	450.62	18.5
FO *Sphenolithus belemnos*	78X-CC to 79X-CC	470.03	478.02	474.03	20.6
LO *Zygrhablithus bijugatus*	81X-CC to 82X-CC	486.92	494.7	490.81	22.5

Biostratigrphic datums from Site 1193, adapted from Shipboard Scientific Party, 2002a.

Appendix 4.1

ODP Sample	Depth (mbsf)	Planktonic foraminifera species	d18O	d13C	ODP Sample	Depth (mbsf)	Planktonic foraminifera species	d18O	d13C
871A 9H4 123	79.73	*Gr. praescitula*	-0.16	1.31	1195B 4HCC	36.74	*Gr. cultrata*	-0.35	0.98
871A 9H4 123	79.73	*Gr. praescitula*	-0.59	1.21	1195B 4HCC	36.74	*Gr. menardii 'B'*	-0.79	1.65
871A 9H4 59	79.09	*Gr. praescitula*	-0.58	1.13	1195B 4HCC	36.74	*Gr. pseudomiocenica*	-0.71	1.47
871A 9H2 124	76.74	*Gr. praescitula*	-0.88	1.19	1195B 4HCC	36.74	*Gr. limbata*	-0.88	1.46
871A 8H5 125	71.75	*Gr. archeomenardii*	-2.32	1.44	1195B 4HCC	36.74	*Gr. menardii s.s.*	-1.06	1.53
871A 8H5 125	71.75	*Gr. praescitula*	-2.01	1.54	1195B 4HCC	36.74	*Gr. multicamerata s.l.*	-0.57	1.69
871A 8H5 59	71.09	*Gr. archeomenardii*	-2.32	1.48	1195B 4HCC	36.74	*Gr. tumida*	0.29	1.77
871A 8H4 125	70.25	*Gr. archeomenardii*	-1.31	2.24	1195B 3HCC	27.11	*Gr. menardii s.l.*	-0.44	1.70
871A 8H4 125	70.25	*Gr. praescitula*	-2.15	1.44	1195B 3HCC	27.11	*Gr. limbata*	-0.68	1.54
871A 8H3 59	68.09	*Gr. archeomenardii*	-2.34	1.57	1195B 3HCC	27.11	*Gr. cultrata*	-0.64	1.51
871A 8H3 59	68.09	*Gr. praescitula*	-2.16	1.68	1195B 3HCC	27.11	*Gr. multicamerata s.l.*	-0.70	1.82
871A 8H2 125	67.25	*Gr. archeomenardii*	-2.16	1.62	1195B 3HCC	27.11	*Gr. tumida*	0.07	1.97
871A 8H2 125	67.25	*Gr. praescitula*	-1.92	1.55	1195B 3HCC	27.11	*Gr. crassaformis*	0.06	1.06
871A 8H1 125	65.75	*Gr. archeomenardii*	-2.16	1.56	1195B 2HCC	17.4	*Gr. cultrata*	-0.58	1.03
871A 8H1 125	65.75	*Gr. praescitula*	-2.23	1.56	1195B 2HCC	17.4	*Gr. menardii s.s.*	0.72	1.57
871A 7HCC	62.5	*Gr. archeomenardii*	-2.15	1.50	1195B 2HCC	17.4	*Gr. tumida*	0.63	1.75
871A 7HCC	62.5	*Gr. praescitula*	-2.08	1.55	1195B 2HCC	17.4	*Gr. crassaformis*	0.33	0.80
871A 7H5 125	62.25	*Gr. praescitula*	-2.19	1.80	1195B 1HCC	8.26	*Gr. cultrata*	-0.59	1.15
871A 7H4 124	60.74	*Gr. archeomenardii*	-2.16	1.65	1195B 1HCC	8.26	*Gr. menardii s.s.*	0.48	1.76
871A 7H4 124	60.74	*Gr. praescitula*	-2.02	1.58	1195B 1HCC	8.26	*Gr. tumida*	0.20	1.69
871A 7H3 59	58.59	*Gr. praescitula*	-2.06	1.64	1195B 1HCC	8.26	*Gr. crassaformis*	0.51	1.18
871A 7H2 59	57.09	*Gr. archeomenardii*	-2.14	1.45	1195A 9H-1, 85-87	72.05	*Gds. ruber*	-2.1	1.06
871A 7H2 59	57.09	*Gr. praemenardii*	-2.05	1.37	1195A 8H-4, 85-87	67.05	*Gds. ruber*	-2.05	1.28
871A 7H1 59	55.59	*Gr. archeomenardii*	-2.17	1.25	1195A 8H-3, 85-87	65.55	*Gds. ruber*	-2.09	1.02
871A 7H1 59	55.59	*Gr. praemenardii*	-1.96	1.57	1195A 8H-2, 85-87	64.05	*Gds. ruber*	-1.81	1.22
871A 6H5 124	52.74	*Gr. archeomenardii*	-1.77	1.70	1195A 7H-6, 85-87	60.55	*Gds. ruber*	-1.71	1.6
871A 6H5 124	52.74	*Gr. praemenardii*	-1.86	1.56	1195A 7H-5, 85-87	59.05	*Gds. ruber*	-2.17	1.23
871A 6H4 124	51.24	*Gr. praemenardii*	-1.96	1.43	1195A 7H-4, 85-87	57.55	*Gds. ruber*	-2.16	0.96
871A 6H3 124	49.74	*Gr. praemenardii*	-1.96	1.55	1195A 7H-3, 85-87	56.05	*Gds. ruber*	-2.04	1.25
871A 6H2 124	48.24	*Gr. praemenardii*	-2.01	1.53	1195A 7H-2, 85-87	54.55	*Gds. ruber*	-2.2	1.4
871A 6H1 124	46.74	*Gr. praemenardii*	-1.92	1.61	1195A 7H-1, 85-87	53.05	*Gds. ruber*	-1.95	1.32
871A 5H4 124	41.74	*Gr. praemenardii*	-2.14	1.51	1195A 6H-6, 85-87	51.05	*Gds. ruber*	-1.91	1.65
871A 5H3 59	39.59	*Gr. praemenardii*	-1.06	1.54	1195A 6H-5, 85-87	49.55	*Gds. ruber*	-1.78	1.28
871A 5H2 59	38.09	*Gr. praemenardii*	-0.82	1.12	1195A 6H-4, 85-87	48.05	*Gds. ruber*	-1.78	1.45
871A 5H2 124	38.74	*Gr. praemenardii*	-0.99	1.39	1195A 6H-2, 85-87	45.05	*Gds. ruber*	-1.89	1.36
871A 5H1 59	36.59	*Gr. praemenardii*	-1.33	1.30	1195A 6H-1, 85-87	43.55	*Gds. ruber*	-2.19	1.47
871A 5H1 124	37.24	*Gr. praemenardii*	-0.98	1.43	1195A 5H-6, 85-87	41.55	*Gds. ruber*	-1.62	1.03
871A 4H5 124	33.74	*Gr. praemenardii*	-0.27	1.24	1195A 5H-5, 85-87	40.05	*Gds. ruber*	-1.51	1.49
871A 4H4 124	32.24	*Gr. praemenardii*	-0.46	1.15	1195A 5H-4, 85-87	38.55	*Gds. ruber*	-1.5	1.17
1195B 10HCC	93.97	*Gr. menardii 'A'*	-0.99	0.86	1195A 5H-3, 85-87	37.05	*Gds. ruber*	-1.22	1.3
1195B 10HCC	93.97	*Gr. menardii 'B'*	-1.19	0.99	1195A 5H-2, 85-87	35.55	*Gds. ruber*	-1.62	1.53
1195B 10HCC	93.97	*Gr. limbata*	-0.95	1.06	1195A 5H-1, 85-87	34.05	*Gds. ruber*	-1.37	1.44
1195B 10HCC	93.97	*Gr. sciutla*	-0.33	0.62	1195A 4H-CC	32.99	*Gds. ruber*	-1.58	1.82
1195B 10H1 10-12	84.5	*Gr. menardii 'A'*	-1.10	0.91	1195A 4H-6 85-87	32.05	*Gds. ruber*	-0.99	1.62
1195B 10H1 10-12	84.5	*Gr. menardii 'B'*	-1.76	0.86	1195A 4H-5, 85-87	30.55	*Gds. ruber*	-1.24	1.52
1195B 10H1 10-12	84.5	*Gr. pseudomiocenica*	-1.19	1.01	1195A 4H-4, 85-87	29.05	*Gds. ruber*	-1.24	1.36
1195B 10H1 10-12	84.5	*Gr. limbata*	-1.19	1.05	1195A 4H-3, 85-87	27.55	*Gds. ruber*	-1.11	1.41
1195B 10H1 10-12	84.5	*Gr. sciutla*	-0.87	0.47	1195A 4H-2, 85-87	26.05	*Gds. ruber*	-0.74	1.55
1195B 9H1 10-12	75	*Gr. menardii 'A'*	-1.03	1.42	1195A 4H-1, 85-87	24.55	*Gds. ruber*	-0.83	1.29
1195B 9H1 10-12	75	*Gr. menardii 'B'*	-1.07	1.38	1195A 3H-CC	23.5	*Gds. ruber*	-0.7	1.45
1195B 9H1 10-12	75	*Gr. pseudomiocenica*	-1.13	1.43	1195A 3H-6, 85-87	22.55	*Gds. ruber*	-0.85	1.63
1195B 9H1 10-12	75	*Gr. limbata*	-1.17	1.39	1195A 3H-5, 85-87	21.05	*Gds. ruber*	-0.57	1.77
1195B 9H1 10-12	75	*Gr. tumida*	-0.77	0.98	1195A 3H-4, 85-87	19.55	*Gds. ruber*	-1.08	1.3
1195B 9H1 10-12	75	*Gr. sciutla*	-0.25	0.75	1195A 3H-3, 85-87	18.05	*Gds. ruber*	-0.49	1.06
1195B 7HCC	65.6	*Gr. menardii 'A'*	-1.33	0.98	1195A 3H-2, 85-87	16.55	*Gds. ruber*	-1.14	0.95
1195B 7HCC	65.6	*Gr. menardii 'B'*	-1.29	1.09	1195A 3H-1, 85-87	15.05	*Gds. ruber*	-1.26	1.19
1195B 7HCC	65.6	*Gr. pseudomiocenica*	-1.02	1.21	1195A 2H-7, 10-12	13.8	*Gds. ruber*	-0.92	1.24
1195B 7HCC	65.6	*Gr. limbata*	-1.34	1.08	1195A 2H-6, 85-87	13.05	*Gds. ruber*	-0.86	1.04
1195B 7HCC	65.6	*Gr. multicamerata s.l.*	-0.72	1.64	1195A 2H-6, 10-12	12.3	*Gds. ruber*	-0.97	1.2
1195B 7HCC	65.6	*Gr. tumida*	-0.36	1.57	1195A 2H-5, 85-87	11.55	*Gds. ruber*	-1.07	0.7
1195B 7HCC	65.6	*Gr. sciutla*	-0.99	0.45	1195A 2H-5, 10-12	10.8	*Gds. ruber*	-0.78	0.71
1195B 6HCC	55.39	*Gr. multicamerata s.l.*	-1.76	1.42	1195A 2H-4, 85-87	10.05	*Gds. ruber*	-1.2	1.12
1195B 6HCC	55.39	*Gr. menardii 'B'*	-1.45	1.23	1195A 2H-4, 10-12	9.3	*Gds. ruber*	-0.94	0.92
1195B 6HCC	55.39	*Gr. pseudomiocenica*	-1.33	1.10	1195A 2H-3, 85-87	8.55	*Gds. ruber*	-1.09	1.39
1195B 6HCC	55.39	*Gr. limbata*	-1.59	1.28	1195A 2H-3, 10-12	7.8	*Gds. ruber*	-0.83	0.98
1195B 6HCC	55.39	*Gr. tumida*	-0.67	1.57	1195A 2H-2, 85-87	7.05	*Gds. ruber*	-0.76	1.68
1195B 6HCC	55.39	*Gr. sciutla*	-0.82	0.43	1195A 2H-2, 10-12	6.3	*Gds. ruber*	-0.86	0.94
1195B 5HCC	45.7	*Gr. multicamerata s.l.*	-1.41	1.38	1195A 2H-1, 85-87	5.55	*Gds. ruber*	-0.07	1.14
1195B 5HCC	45.7	*Gr. menardii 'B'*	-1.61	1.33	1195A 2H-1, 10-12	4.8	*Gds. ruber*	-0.39	0.6
1195B 5HCC	45.7	*Gr. pseudomiocenica*	-1.26	1.26	1195A 1H-4, 10-12	4.1	*Gds. ruber*	-0.33	1.2
1195B 5HCC	45.7	*Gr. limbata*	-1.18	1.46	1195A 1H-3, 85-87	3.85	*Gds. ruber*	0.17	1.31
1195B 5HCC	45.7	*Gr. cultrata*	-0.91	1.25	1195A 1H-3, 9-11	3.09	*Gds. ruber*	-0.33	1.12
1195B 5HCC	45.7	*Gr. tumida*	-0.41	1.66	1195A 1H-2, 85-87	2.35	*Gds. ruber*	-0.88	0.89
1195B 5HCC	45.7	*Gr. sciutla*	-0.93	2.25	1195A 1H-2, 10-12	1.6	*Gds. ruber*	-0.43	0.61
					1195A 1H-1, 85-87	0.85	*Gds. ruber*	-0.32	0.52

List of all new stable isotopic results from ODP sites 871 and 1195 with relevent depths (mbsf) and sample numbers.

Appendix 4.2

Sample	Species	$d^{18}O$ (‰)	$d^{13}C$ (‰)	Palaeotemperature (°C)
RAS99-42	*D. globularis*	-2.34	0.41	25.9
	D. baroemoenensis	-2	0.72	24.3
	D. euapertura/prasaepis	-2.26	0.5	25.5
	Gq. venezuelana	-2.22	0.57	25.3
	Gq. tapuriensis	-1.86	0.03	23.7
	G. praebulloides	-3.16	-0.65	29.7
	G. occlusa	-2.26	0.37	25.5
	G. gnauki	**-3.29**	**-0.55**	**30.3**
	G. angulisuturalis	-2.65	-0.16	27.3
	G. ciperoensis	-3.05	0.21	29.2
	Globoturborotalita sp. 1	-2.13	0.38	24.9
	Globoturborotalita sp. 2	-2.96	-0.63	28.8
	Uvigerina spp.	-1.35	0	21.3
	Cibicidoides spp.	-0.95	-0.4	19.5
RAS99-38	*D. altispira*	-1.8	0.8	23.4
	D. globosa	-2.08	1.62	24.7
	D. baroemoenensis	-1.91	0.86	23.9
	Gds. quadrilobatus	-2.52	1.43	26.7
	Gds. trilobus	-2.55	1.01	26.9
	Gds. ruber-subquadratus	**-2.56**	**1.24**	**26.9**
	Gds. sacculifer	-2.33	1.65	25.8
	Gds. quad-immaturus	-2.46	1.73	26.4
	Ga. obesa-praesiphonifera	-1.26	-0.47	20.9
	Ga. praebulloides	-2.16	-0.47	25
	Gq. venezuelana	-1.54	0.42	22.2
	P. mayeri	-1.97	0.29	24.2
	O. suturalis	-2.35	2.07	25.9
	Ss. seminulina	-1.6	0.8	22.5
	Uvigerina spp.	0.63	-0.37	12.4
	Cibicidoides spp.	0.04	0.44	15
180906/1	*D. altispira*	-1.89	0.99	23.8
	O. suturalis	-2.16	1.06	25
	Gds. quadrilobatus	-2.62	2.07	27.2
	Gds. sacculifer	-2.38	1.63	26.1
	Ss. seminulina	-1.56	1.12	22.3
	Ga. obesa-praesiphonifera	-1.05	-0.17	20
	P. mayeri	-1.8	0.73	23.4
	P. siakensis	-2.15	0.52	25
	G. nepenthes	**-2.94**	**-0.05**	**28.7**
	Cibicidoides spp.	0.2	0.19	14.3
	Uvigerina spp.	0.82	-0.12	11.5

Species from the three Tanzanian samples with the carbon, oxygen and calculated temperature data for the species assemblages. The most negative $d^{18}O$ for each assemblage is highlighted. The last two measurements in each sample are from benthic genera.

Appendix 4.3

Time slice	Sites	Latitude	Surface dwelling species	del18O (‰)	Deep dwelling species	del18O (‰)	References
M1b	14	28°19.89'S	*Gds. praebulloides*	0.28	*Gq. dehiscens*	1.08	Savin *et. al.*, 1985
	18	27°58.72'S	*Gds. trilobus-sacculifer*	-1.00	*Gq. dehiscens*	-0.40	Savin *et. al.*, 1985
	55	09°18.11'N	*Gds. trilobus*	0.06	*Gq. venezuelana*	0.20	Savin *et. al.*, 1985
	71	04°28.28'N	*T. angustiumbilicata*	-0.24	*Gq. venezuelana*	-0.21	Savin *et. al.*, 1985
	77B	00°28.90'N	*P. siakensis*	0.50	*Gq. venezuelana*	0.99	Barrera *et. al.*, 1985
	206	32°00.75'S	*Gds. praebulloides*	-0.11	*Catapsydrax spp.*	0.67	Savin *et. al.*, 1985
	208	26°06.61'S	*Gds.*	-0.70	*Gq. dehiscens*	-0.14	Savin *et. al.*, 1985
	214	11°20.21'S	*P. kugleri*	-0.15	*Catapsydrax spp.*	1.30	Savin *et. al.*, 1985
	216	01°27.73'N	[redacted]		*G. venezuelana*	1.22	Vincent *et. al.*, 1985
	237	07°49.99'S			*G. venezuelana*	0.88	Vincent *et. al.*, 1985
	238	11°09.21'S			*G. venezuelana*	0.78	Vincent *et. al.*, 1985
	279A	51°20.14'S			*Catapsydrax spp.*	1.79	Savin *et. al.*, 1985
	289	00°29.92'S	*P. kugleri*	-1.32	*Gq. dehiscens-praedehiscens*	-0.52	Savin *et. al.*, 1985
	292	15°39.11'N	*P. kugleri*	-0.44	*Gq. venezuelana*	0.16	Savin *et. al.*, 1985
	296	29°20.41'N	[redacted]		*Gq. venezuelana*	0.52	Savin *et. al.*, 1985
	317B	12°00.09'S	*P. kugleri*	-0.31	*Gq. venezuelana*	1.48	Savin *et. al.*, 1985
	357	30°00.25'S	*P. kugleri*	-0.40	*Gq. dehiscens*	0.54	Savin *et. al.*, 1985
	360	35°50.75'S	*Gds. praebulloides*	0.82	*Gq. dehiscens*	0.96	Savin *et. al.*, 1985
	362	19°45.45'S	[redacted]		*Catapsydrax spp.*	0.75	Savin *et. al.*, 1985
	366A	05°40.70'N	*P. kugleri*	-1.37	*Gq. praedehiscens*	0.17	Savin *et. al.*, 1985
	407	63°56.32'N	*Gds. praebulloides*	0.43	*Catapsydrax spp.*	1.16	Savin *et. al.*, 1985
	448	16°20.46'N	*P. kugleri*	-0.31	*G. tripartita*	0.78	Savin *et. al.*, 1985
	495	12°02.26'N	*P. siakensis*	-0.19	*Gq. venezuelana*	0.40	Barrera *et. al.*, 1985
	526A	30°07.40'S	*Gds.praebulloides*	0.98	*Catapsydrax spp.*	1.38	Savin *et. al.*, 1985
	758A	05°64.03'N	*T. angustiumbilicata*	-1.3	*Catapsydrax spp..*	1.48	Van Eijden and Ganssen, 1995
	871A	05°33.43'N	*Gds. trilobus*	-1.40	*Gq. venezuelana*	-0.70	Pearson *et. al.*, 1997a
	926B	03°43.15'N	*Gds. praebulloides*	-1.52	*C. dissimilis*	0.33	Pearson *et. al.*, 1997b
	RAS99-42	**09°57.04'S**	***G. gnauki***	**-3.29**	***G. sellii***	**-1.86**	This study
M9	151	15°01.00' N	*D. altispira*	-1.15	*Gq. venezuelana*	0.45	Norris *et. al.*, 1993
	167	07°04.10'N	*Gds. sacculifer*	-0.99	*Gq. venezuelana*	-0.60	Savin *et. al.*, 1985
	173	39°57.71'N	*G. bulloides-praebulloides*	0.12	[redacted]		Barrera *et. al.*, 1985
	214	11°20.21'S	*D. altispira*	-0.55	*Gq. venezuelana*	1.03	Vincent *et. al.*, 1985
	216A	01°27.73'N	*D. altispira*	-0.28	*Gq. venezuelana*	1.66	Vincent *et. al.*, 1985
	289	00°29.92'S	[redacted]		*Fohsella. spp*	0.18	Norris *et. al.*, 1993
	470	28°54.56'N	*G. bulloides*	-0.24	[redacted]		Barrera *et. al.*, 1985
	495	12°29.78'N	*D. altispira*	-1.59	*Gq. venezuelana*	0.80	Savin *et. al.*, 1985
	806B	00°19.00'N	*D. altispira*	-1.25	*Gq. venezuelana*	-0.70	Norris *et. al.*, 1993
	871A	05°33.43'N	*Gds. trilobus*	-1.88	*Gq. venezuelana*	-0.82	Pearson *et. al.*, 1997†
	RAS99-38	**09°57.08'S**	***Gds. trilobus***	**-2.55**	***Gq. venezuelana***	**-1.54**	This study
M11-M12	173	39°57.71'N	*G. bulloides-praebulloides*	-0.19	[redacted]		Barrera *et. al.*, 1985
	214	11°20.21'S	*D. altispira*	-0.64	*Gq. venezuelana*	1.10	Savin *et. al.*, 1985
	216A	01°27.73'N	*D. altispira*	-0.46	*Gq. venezuelana*	1.93	Vincent *et. al.*, 1985
	238	11°09.21'S	*Gds. sacculifer*	-0.86	[redacted]		Savin *et. al.*, 1985
	470	28°54.56'N	*G. bulloides-praebulloides*	-0.51			Barrera *et. al.*, 1985
	180906/1	**09°94.99'S**	***G. nepenthes***	**-2.94**	***G. obesa-siphonifera***	**-1.05**	This study

Oxygen isotope data from DSDP/ODP sites used to plot against the values used for the Tanzanian samples. For each site the most negative surface dwelling species was chosen with the most positive thermocline species to give the maximum range of palaeotemperature. The Tanzanian sample data is highlighted in bold.

Appendix 5.1 – method details

Extended eigenshape software

The extended eigenshape analysis software package used in this study is available on the world wide web as freeware from: http://www.nhm.ac.uk/hosted_sites/paleonet/ftp/ftp.html, or upon request from Dr Norman MacLeod. It is available for Macintosh and Windows formats. It contains four programs and the results from a worked example to test the how each program functions. The programs within the software package perform specific functions within the analysis procedure, discussed below:

X, Y →Ext. Phi

This program reads the *x, y* coordinate data and transforms them into extended phi functions that are later used to compare the original objects using the Extended eigenshape program. The whole software package limits the dimensions of the object outline data to <500 objects, defined by 200 or less *x,y* coordinate pairs per object and any number of landmarks per object. This program treats the starting position as the first landmark so it is vital that the outline is digitised from the same inter-specimen relative point. It should be noted that the total number of outline coordinates used in the shape functions should be smaller than the total number originally used to digitise the outline.

Ext. Eigenshape

This program uses the phi shape functions to calculate the eigenshapes, mean shapes, eigenvalues and projections of the object outlines within eigenshape space (scores or covariances). The eigen scores can be used to graphically represent the eigenspace occupied by each set of objects.

Ext. Phi → X, Y

This program will convert the extended phi shape functions back into their 'equivalent' *x, y* coordinate pairs (subject to a rounding error) to enable the original object outlines to be read into spreadsheet or graphics software (e.g., Excel or KaleidaGraph) to produce plots of the shapes.

Ext. Eshape Models

This program can be used to determine where a set of shapes not in the original eigenshape study and ascertain where they plot within the original eigenshape space. It will read a series of *a priori* extended phi shape functions and extended eigenshapes and use these to calculate the covariances of the shape functions to give the coordinate positions of the eigenshape outlines within eigenshape space.

This program is of great use in assessing exactly what each of the eigenshape axes actually equates to in terms of along axis-shape change within the context of the data set being analysed. These models can be effective heuristic devices for explaining the results of eigenshape analysis in a qualitative manner.

File manipulation

The output data file from *tpsDIG32* can be set as excel format (.xls) or as a data text file (.tps). Saving the coordinate data in the excel format speeds up the file manipulation when preparing the data for analysis, so this is recommended.

Shape 1		Shape 2	
3.97E+02	2.97E+02	4.20E+02	2.39E+02
3.97E+02	3.00E+02	4.20E+02	2.42E+02
3.96E+02	3.03E+02	4.19E+02	2.45E+02
3.95E+02	3.06E+02	4.19E+02	2.48E+02
3.95E+02	3.09E+02	4.18E+02	2.51E+02
3.93E+02	3.12E+02	4.16E+02	2.54E+02
3.93E+02	3.15E+02	4.16E+02	2.56E+02
3.92E+02	3.18E+02	4.15E+02	2.59E+02
3.91E+02	3.21E+02	4.13E+02	2.62E+02
3.91E+02	3.23E+02	4.12E+02	2.65E+02
3.89E+02	3.26E+02	4.10E+02	2.68E+02
3.87E+02	3.29E+02	4.08E+02	2.71E+02
3.85E+02	3.32E+02	4.06E+02	2.74E+02
3.83E+02	3.35E+02	4.04E+02	2.77E+02
3.80E+02	3.37E+02	4.01E+02	2.80E+02
3.79E+02	3.40E+02	3.99E+02	2.82E+02
3.76E+02	3.42E+02	3.97E+02	2.85E+02
3.74E+02	3.45E+02	3.96E+02	2.88E+02
3.73E+02	3.48E+02	3.95E+02	2.90E+02
3.73E+02	3.50E+02	3.94E+02	2.93E+02
3.72E+02	3.53E+02	3.94E+02	2.96E+02
3.72E+02	3.56E+02	3.93E+02	2.99E+02
3.72E+02	3.59E+02	3.93E+02	3.02E+02
3.71E+02	3.61E+02	3.93E+02	3.05E+02
3.71E+02	3.62E+02	3.92E+02	3.08E+02
3.70E+02	3.65E+02	3.92E+02	3.11E+02
3.70E+02	3.68E+02	3.91E+02	3.14E+02
3.70E+02	3.71E+02	3.90E+02	3.17E+02
3.70E+02	3.73E+02	3.89E+02	3.20E+02
3.70E+02	3.76E+02	3.88E+02	3.23E+02
3.70E+02	3.79E+02	3.87E+02	3.25E+02
3.70E+02	3.82E+02	3.86E+02	3.28E+02
3.70E+02	3.85E+02	3.84E+02	3.31E+02
3.69E+02	3.88E+02	3.83E+02	3.34E+02
3.68E+02	3.91E+02	3.81E+02	3.37E+02
3.67E+02	3.94E+02	3.79E+02	3.40E+02
3.66E+02	3.97E+02	3.77E+02	3.43E+02
3.65E+02	4.00E+02	3.75E+02	3.46E+02
3.64E+02	4.03E+02	3.73E+02	3.49E+02
3.63E+02	4.06E+02	3.71E+02	3.52E+02
3.61E+02	4.09E+02	3.69E+02	3.55E+02
3.60E+02	4.12E+02	3.68E+02	3.57E+02
3.58E+02	4.15E+02	3.66E+02	3.60E+02
3.56E+02	4.18E+02	3.64E+02	3.63E+02
3.54E+02	4.21E+02	3.61E+02	3.66E+02
3.53E+02	4.23E+02	3.59E+02	3.69E+02
3.51E+02	4.26E+02	3.57E+02	3.72E+02
3.49E+02	4.29E+02	3.55E+02	3.75E+02
3.47E+02	4.32E+02	3.53E+02	3.77E+02
3.97E+02	2.96E+02	4.20E+02	2.38E+02
Landmarks		Landmarks	
3.27E+02	4.67E+02	3.33E+02	4.04E+02
3.40E+02	1.92E+02	3.47E+02	1.32E+02

→

Shape 1	
3.97E+02	2.97E+02
3.97E+02	3.00E+02
3.96E+02	3.03E+02
3.95E+02	3.06E+02
3.95E+02	3.09E+02
3.93E+02	3.12E+02
3.93E+02	3.15E+02
3.92E+02	3.18E+02
3.91E+02	3.21E+02
3.91E+02	3.23E+02
3.89E+02	3.26E+02
3.87E+02	3.29E+02
3.85E+02	3.32E+02
3.83E+02	3.35E+02
3.80E+02	3.37E+02
3.79E+02	3.40E+02
3.76E+02	3.42E+02
3.74E+02	3.45E+02
3.73E+02	3.48E+02
3.73E+02	3.50E+02
3.72E+02	3.53E+02
3.72E+02	3.56E+02
3.72E+02	3.59E+02
3.71E+02	3.61E+02
3.71E+02	3.62E+02
3.70E+02	3.65E+02
3.70E+02	3.68E+02
3.70E+02	3.71E+02
3.70E+02	3.73E+02
3.70E+02	3.76E+02
3.70E+02	3.79E+02
3.70E+02	3.82E+02
3.70E+02	3.85E+02
3.69E+02	3.88E+02
3.68E+02	3.91E+02
3.67E+02	3.94E+02
3.66E+02	3.97E+02
3.65E+02	4.00E+02
3.64E+02	4.03E+02
3.63E+02	4.06E+02
3.61E+02	4.09E+02
3.60E+02	4.12E+02
3.58E+02	4.15E+02
3.56E+02	4.18E+02
3.54E+02	4.21E+02
3.53E+02	4.23E+02
3.51E+02	4.26E+02
3.49E+02	4.29E+02
3.47E+02	4.32E+02
Landmarks	
3.27E+02	4.67E+02
3.40E+02	1.92E+02
Shape 2	
4.20E+02	2.39E+02
4.20E+02	2.42E+02
4.19E+02	2.45E+02
4.19E+02	2.48E+02
4.18E+02	2.51E+02
4.16E+02	2.54E+02
4.16E+02	2.56E+02
4.15E+02	2.59E+02
4.13E+02	2.62E+02
4.12E+02	2.65E+02
4.10E+02	2.68E+02
4.08E+02	2.71E+02
4.06E+02	2.74E+02
4.04E+02	2.77E+02
4.01E+02	2.80E+02
3.99E+02	2.82E+02
3.97E+02	2.85E+02
3.96E+02	2.88E+02
3.95E+02	2.90E+02
3.94E+02	2.93E+02
3.94E+02	2.96E+02
3.93E+02	2.99E+02
3.93E+02	3.02E+02
3.93E+02	3.05E+02
3.92E+02	3.08E+02
3.92E+02	3.11E+02
3.91E+02	3.14E+02
3.90E+02	3.17E+02
3.89E+02	3.20E+02
3.88E+02	3.23E+02
3.87E+02	3.25E+02
3.86E+02	3.28E+02
3.84E+02	3.31E+02
3.83E+02	3.34E+02
3.81E+02	3.37E+02
3.79E+02	3.40E+02
3.77E+02	3.43E+02
3.75E+02	3.46E+02
3.73E+02	3.49E+02
3.71E+02	3.52E+02
3.69E+02	3.55E+02
3.68E+02	3.57E+02
3.66E+02	3.60E+02
3.64E+02	3.63E+02
3.61E+02	3.66E+02
3.59E+02	3.69E+02
3.57E+02	3.72E+02
3.55E+02	3.75E+02
3.53E+02	3.77E+02
Landmarks	
3.33E+02	4.04E+02
3.47E+02	1.32E+02

Figure 5.1A. Desired data format for each object data file required to enter data for extended eigenshape analysis. Data manipulation is easiest if the object data is arranged side-by-side horizontally (left figure), however, to allow reading by the eigenshape software the data must be arranged sequentially below each other (right figure).

For the outline data to be compatible with the extended eigenshape software it must be presented in a format compatible with the analysis software.

- Both the *x* and *y* coordinates must be in a separate column within an Excel spreadsheet, and must be sequentially organised down the first two columns (Figure 5.1A).

File manipulation

The output data file from *tpsDIG32* can be set as excel format (.xls) or as a data text file (.tps). Saving the coordinate data in the excel format speeds up the file manipulation when preparing the data for analysis, so this is recommended.

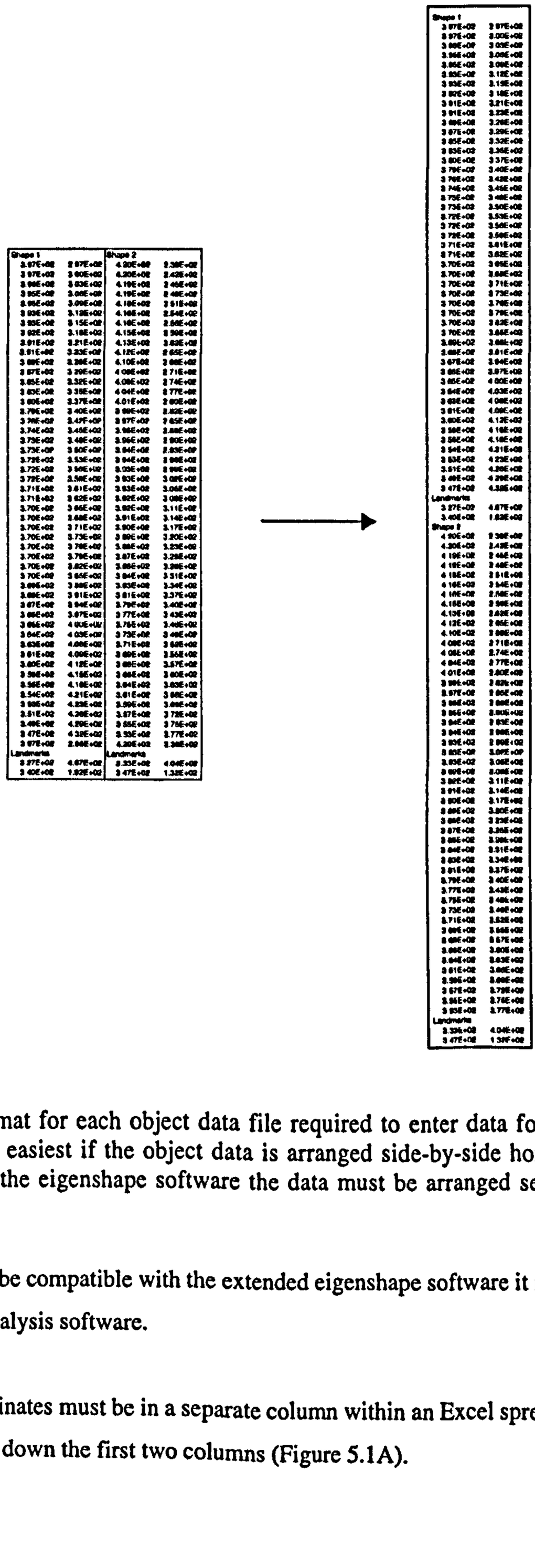

Figure 5.1A. Desired data format for each object data file required to enter data for extended eigenshape analysis. Data manipulation is easiest if the object data is arranged side-by-side horizontally (left figure), however, to allow reading by the eigenshape software the data must be arranged sequentially below each other (right figure).

For the outline data to be compatible with the extended eigenshape software it must be presented in a format compatible with the analysis software.

- Both the *x* and *y* coordinates must be in a separate column within an Excel spreadsheet, and must be sequentially organised down the first two columns (Figure 5.1A).

- The first row above the data should contain the shape number in the format 'Shape *x*'.
- The landmark data should be placed at the end of the outline data with a row before them containing the word 'Landmarks'.
- All coordinate data must be in the 'exponent' form ('scientific', in *Excel*), i.e. *x* coordinate 397 in exponent form is 3.97E+02.
- Any other text or data in the file is not required and should be discarded.

When dealing with large numbers of object outlines it is more efficient to have all the data (for 1 species) on one worksheet side by side filling up the columns from left to right. This way data manipulation can be done quickly to all of the files at once rather than separately. However, all data for each object must be sequentially below each other occupying the first two columns of the worksheet for the data to be read, as in Figure 5.1A. To manually input all data in the same two columns sequentially below each other can be very time consuming, however, an Excel macro was used to do this much faster (see below).

The numbers in bold indicate how many rows each object occupies. In this case each object occupied 206 rows composed of 1 row with a shape number in, 200 coordinate pairs, 1 row with 'landmarks' in, and 4 rows with the landmark coordinates. Both numbers in bold (see macro) can be altered to a new figure using the 'Step into' Excel function, i.e. if multiple columnised objects needed to be moved quickly.

The data must be in text format only without any of the program-specific formatting that comes with the standard *.xls* or *.doc* file. A quick way to transport data from Excel to a text only program is to save the excel file as Formatted text (Space delimited), then open it in a text editor program and save it as a text file. When using the PC platform; Notepad seems to offer an adequate function. When using the Macintosh platform; Simpletext is not compatible for the larger data files so Word can be used. The procedure is to open up the space-delimited Excel file and save as a 'Text only' file. The data are then compatible with the extended eigenshape software package referred to above.

Macro used to program file manipulation.

```
Sub ()
i = 1
l = 0
While Cells(1, i).Value <> ""
For k = 1 To 203
j = l * 203 + k
Cells(j, 1).Value = Cells(k, i).Value
Cells(j, 2).Value = Cells(k, i + 1).Value
If i > 1 Then
Cells(k, i).Value = ""
Cells(k, i + 1).Value = ""
End If
Next
l = l + 1
i = i + 2
Wend
End Sub
```

Appendix 5.2

Eigenshape	Eigenvalues	Total variance %	Total variance cumulative %
1	1805.326	97.963	97.963
2	6.001	0.326	98.289
3	1.916	0.104	98.393
4	1.332	0.072	98.465
5	1.208	0.066	98.53
6	0.953	0.052	98.582
7	0.941	0.051	98.633
8	0.852	0.046	98.679
9	0.664	0.036	98.715
10	0.64	0.035	98.75
11	0.596	0.032	98.783
12	0.558	0.03	98.813
13	0.532	0.029	98.842
14	0.501	0.027	98.869
15	0.446	0.024	98.893
16	0.421	0.023	98.916
17	0.413	0.022	98.938
18	0.392	0.021	98.96
19	0.39	0.021	98.981
20	0.376	0.02	99.001
21	0.353	0.019	99.02
22	0.348	0.019	99.039
23	0.333	0.018	99.057
24	0.329	0.018	99.075
25	0.318	0.017	99.092
26	0.31	0.017	99.109
27	0.3	0.016	99.126
28	0.293	0.016	99.141
29	0.276	0.015	99.156
30	0.265	0.014	99.171

Eigenvalues of the analysis of 25 specimens of 19 taxa from ODP sites 926 and 1195. The first 30 are listed here to show the decreasing significance of the higher eigenshapes on the % variance in morphology of the objects within the dataset. Only the covariance with the first 3 eigenshapes are used to represent the shape variability within the sample. For this dataset, 235 eigenshapes can be used to account for 100% of the variation. Note the significant majority (98%) of variation is described by the first eigenshape alone.

Appendix 6.1A

	Characters	Gr. prs	Gr. ar	Gr. prm	Gr. m	Gr. m 'A'	Gr. m 'B'	Gr. cul	Gr. fim	Gr. lim	Gr. mul	Gr. ex	Gr. mio	Gr. pmio	Gr. per	Gr. mt	Gr. pt	Gr. tum	Gr. flex	Gr. ung	Gr. berm
1	Surface honeycomb texture	0	1	1	1	1	1	1	1	1	1	1	1	1	1	1	1	1	1	1	1
2	Depression around pores	0	0	0	1	1	1	1	1	0	1	1	1	1	1	1	1	1	1	1	1
3	Umbilical pustules	0	0	0	0	0	0	0	0	0	0	1	0	0	0	1	0	0	0	0	0
4	Umb pust morph	1	1	2	2	1	1	0	0	1	1	0	1	1	1	0	1	2	2	2	0
5	Umb pust position	1	0	0	0	0	0	0	0	0	0	0	1	1	1	0	0	0	0	0	0
6	Pustulate shoulders	1	1	1	1	1	1	1	1	1	1	1	1	1	1	1	0	0	0	0	1
7	Pustule fusing	1	1	1	1	1	1	1	1	1	1	1	1	1	1	1	1	1	1	1	1
8	Spiral pustules	1	1	1	1	1	1	1	1	1	1	1	1	1	1	1	1	1	1	1	1
9	Pustulate keel	?	0	0	0	0	0	0	1	0	0	0	0	1	0	0	0	0	0	0	0
10	Test perforation	1	1	1	1	1	1	0	0	1	1	0	0	1	0	0	0	1	1	0	1
11	Imperforate band	0	0	1	1	1	1	1	1	1	1	1	1	1	1	1	1	1	1	1	1
12	Keel	2	1	0	0	0	0	0	0	0	0	0	0	0	0	0	0	0	0	0	0
13	Edge morphology	0	1	2	3	3	3	3	3	3	3	3	3	3	3	3	3	3	3	3	3
14	Keel thickness	?	0	0	2	1	2	0	0	1	2	0	0	0	0	1	2	2	2	2	0
15	Keel curvature	?	2	2	1	1	1	2	1	1	2	1	0	0	1	1	2	2	3	3	2
16	Radially flared pustules along keel	?	1	1	1	1	1	1	0	1	1	1	1	1	1	1	1	1	1	1	1
17	Test coil	0	0	0	0	0	0	0	0	0	0	2	1	1	1	1	0	2	0	0	1
18	Coiling direction	2	2	2	0	2	2	0	?	2	1	1	1	2	1	1	2	2	0	0	2
19	No. test whorls	1	2	1	1&2	1	1	2	1	2	2	2	1	2	1	2	2	2	0	0	0
20	No. chambers final whorl	0	0	1	1	1	2	1	1	2	3	2	2	1&2	2	2	2	2	1	1	1
21	Chamber size incr. cont.	0	0	0	0	0	0	0	0	0	0	0	0	0	0	0	0	1	1	1	1
22	Tumidosity	2	2	2	2	2	2	2	2	2	2	2	2	2	2	2	1	1	0	0	0
23	Edge view aperture linearity	1	0	0	0	0	0	1	1	0	1	1	1	1	1	1	1	1	1	1	1
24	Edge view trunc aperture arch	1	1	1	1	1	1	1	1	1	0	1	0	0	0	1	1	1	1	1	0
25	Edge view aperture semicircularity	1	1	1	1	1	1	0	0	1	0	0	0	0	0	0	0	0	1	1	0
26	Apertural lip shape	0	0	0	1	1	1	0	1	0	2	2	0	0	0	2	1	1	1	1	1
27	Lip symmetry	0	0	0	1	0	0	0	0	0	1	1	0	0	0	1	1	1	1	1	1
28	Umbilicus	0	0	0	2	2	2	1	1	1	2	1	1	1	1	2	1	1	1	1	1
29	Test biconvexity	0	0	0	1	0	1	0	0	0	0	0	0	0	0	1	0	0	0	0	0
30	Spiral side geometry	1	2	2	1	1	2	2	1	1	1	1	0	0	1	1	1	2	3	3	3
31	Equatorial periphery	3	1	2	2	1	0	2	2	2	0	2	0	2	1	0	1	3	3	3	3
32	Axial periphery	2	0	0	0	0	0	0	0	0	0	0	3	3	3	0	0	1	2	0	1
33	Conical test	1	1	1	1	1	1	1	1	1	1	1	1	1	1	1	1	1	1	1	1
34	Final chamber edge view point	1	1	1	1	1	1	1	1	1	1	1	1	1	1	1	1	1	1	1	1
35	Spiral sutures	0	1	1	1	1	1	1	1	1	1	1	1	1	1	1	1	1	1	1	1
36	Spiral suture curve	1	1	1	1	1	1	1	1	2	2	2	1	1	1	0	0	0	0	0	0
37	Sp suture peripheral continuity	1	1	0	0	0	0	1	0	0	1	0	2	2	2	0	2	2	2	2	2
38	Sprial suture overlap	1	1	1	1	1	1	1	1	1	1	0	1	1	1	0	1	1	1	1	1
39	Downstepping spiral sutures	1	1	1	1	1	1	1	1	1	1	1	1	1	1	1	1	1	1	1	1
40	Umbilical sutures	0	0&1	0	0	0&1	0&2	0&1	0	2	0	0&1	0	1&2	0&1	2	0	0	0	0	0
41	Umbilical suture overplap	1	1	1	1	1	1	1	1	1	0	0	1	1	1	0	1	1	1	1	1
42	Fin (umb) chamb elong	2	2	2	2	2	2	2	2	2	2	2	2	2	2	2	1	1	1	0	1
43	Final sprial chamber shape	1	1	1	1	1	1	1	1	1	1	1	1	1	1	1	2	2	2	3	2
44	Final umb chamber shape	0	0	0	0	0	0	0	0	0	0	0	0	0	0	0	0	0	0	0	0
45	Chamber inflation globose morp	2	2	2	2	2	2	2	2	2	2	2	2	2	2	2	2	2	2	2	2
46	Chamber flaring	1	1	1	1	1	1	1	1	1	1	1	1	1	1	1	1	1	1	1	1
47	Larger penult than last chamber	1	1	1	1	1	1	1	1	1	1	1	0	1	1	0	1	1	1	1	1
48	Edge view final chamber width	1	1	1	1	1	1	1	1	1	1	1	1	1	1	1	1	1	1	1	1
49	Final chamber embracing test	1	1	2	2	2	2	2	2	2	2	2	2	2	2	2	2	2	2	2	2
50	Stratigraphy	0&1&2	1&2	2&3&4	3-9 inc.	3&4&5&6	5&6&7	6&7&8&9	9	4&5&6&7	7&8	6&7	7&8	6	6&7&8	7&8	5&6	6	6&7&8&9	7&8	8&9

Data matrix of taxa in cladistic analyses and characters coded, see text for explanation of characters.

Appendix 6.1B (continuation of data matrix)

	Characters	Gr. cav	Gr. chall	Gr. cib	Gr. crcon	Gr. crasf	Gr. cr hes	Gr. cr oc	Gr. cr ron	Gr. cr vio	Gr. crsu	Gr. hir	Gr. juan	Gr. marg	Gr. nuprim	Gr. m ev	Gr. primar	Gr. scit	Gr. sc gig	Gr. thev	Gr. tosa	Gr. to ten	Gr. trunc	Gr. tr pach	Gr. tr ex
1	Surface honeycomb texture	1	1	1	1	1	1	1	1	1	1	1	1	1	1	1	1	1	1	1	1	1	1	1	1
2	Depression around pores	1	0	1	1	1	1	1	1	1	1	1	0	0	0	0	0	0	0	1	1	1	1	1	1
3	Umbilical pustules	0	0	0	0	0	0	0	0	0	0	0	0	0	0	0	0	0	0	0	0	0	0	0	0
4	Umb pust morph	0	1	1	1	2	2	2	2	2	2	2	2	1	1	1	1	1	1	0	0	0	0	2	2
5	Umb pust position	1	1	1	2	2	2	2	2	2	2	2	2	1	2	2	2	2	1	1	1	?	1	2	2
6	Pustulate shoulders	1	0	0	0	0	0	0	0	0	0	0	1	1	1	1	1	1	1	1	1	1	1	0	0
7	Pustule fusing	1	1	1	1	1	1	0	1	0	1	1	1	1	1	1	1	1	1	1	1	0	1	0	1
8	Spiral pustules	1	0	1	0	0	0	0	1	0	1	1	1	1	1	1	0	0	1	1	1	1	1	0	0
9	Pustulate keel	?	0	?	?	0	?	?	?	?	1	0	0	?	0	0	?	1	?	0	0	?	1	?	?
10	Test perforation	0	0	1	0	0	0	0	0	0	0	0	0	1	0	0	1	1	1	1	1	1	1	0	0
11	Imperforate band	0	1	0	1	1	0	0	0	0	1	1	1	0	1	1	0	1	0	0	0	0	1	1	0
12	Keel	2	1	2	2	2	2	2	2	2	1	1	1	2	0	0	2	2	2	1	1	2	0	2	2
13	Edge morphology	0	4	5	5	4	4	4	4&5	4	4	4	2	5	2	3	3	1	1	1	1	5	3	4	4
14	Keel thickness	?	0	?	?	1	?	?	?	?	0	0	0	?	1	0	?	0	?	0	0	?	0	?	?
15	Keel curvature	?	0	?	?	0	?	?	?	?	0	0	3	?	3	2	?	2	?	1	1	?	0	?	?
16	Radially flared pustules along keel	?	1	?	?	1	?	?	?	?	1	1	1	?	1	1	?	1	?	1	1	?	1	?	?
17	Test coil	0	0	0	0	0	0	1	0	0	0	1	3	1	0	0	0	0	0	0	0	0	0	0	0
18	Coiling direction	2	0	0	2	0	0	0	2	2	0	2	2	1	2	0	0	0	2	1	2	2	0	2	2
19	No. test whorls	1	1	2	0	1	1	0	0	0	0	0	1	1	1	0&1	1	0&1	1&2	2	2	1	2	1	1
20	No. chambers final whorl	0	1	1	0	0	0	0	0	0	0	0	0	0	0	0	0	0	0	0	0	1	0	0	0
21	Chamber size incr. cont.	0	0	0	1	0	0	1	0	0	0	0	0	0	0	0	0	0	0	0	0	0	0	0	0
22	Tumidosity	2	2	2	2	2	2	2	2	2	2	0	1	0	0	0	0	0	0	0	0	0	0	0	0
23	Edge view aperture linearity	1	1	1	1	0	0	0	0	0	0	0	0	1	1	1	2	2	2	2	2	2	2	2	2
24	Edge view trunc aperture arch	1	1	1	1	1	1	1	1	0	0	1	1	1	1	1	1	1	1	1	1	1	1	1	1
25	Edge view aperture semicircularity	0	0	0	0	1	1	1	1	1	1	1	1	0	0	0	0	0	0	0	0	0	0	0	0
26	Apertural lip shape	0	0	0	0	0	0	0	0	0	0	0	0	0	0	0	0	0	0	0	0	0	0	0	0
27	Lip symmetry	0	1	0	0	0	0	0	0	0	0	0	0	0	0	0	0	0	0	0	0	1	4	1	1
28	Umbilicus	4	4	4	1	1	1	1	1	1	1	1	1	1	0	0	0	0	0	0	1	0	0	0	0
29	Test biconvexity	0	0	0	0	0	0	0	0	0	0	0	3	1	3	2	2	2	2	1	1	1	1	4	0
30	Spiral side geometry	1	0	1	1	0	0	0	0	0	0	0	1&3	1	1	1	1	0&1	1	1	2	1	2	0	1
31	Equatorial periphery	1	3	2	4	5	5	5	5	5	5	5	1	2	0	0	2	0	1	2	2	2	0	2	2
32	Axial periphery	2	3	2	2	3	3	2	3	3	3	2	1	1	1	1	1	1	1	1	1	1	1	0	0
33	Conical test	1	0	1	1	0	0	0	0	0	0	1	1	1	1	1	1	1	1	1	1	1	1	1	1
34	Final chamber edge view point	1	1	1	1	1	1	1	1	1	1	0	0	0	1	1	0	1	0	0	0	0	0	2	0
35	Spiral sutures	0	0	0	0	0	0	0	2	0	1	0	1	0	1	1	1	1	0	1	1	0	1	3	3
36	Spiral suture curve	1	2	1	1	1	1	1	1	1	1	1	1	0	1	1	0	0	0	0	0	0	0	2	2
37	Sp suture peripheral continuity	0	2	0	0	1	1	1	1	1	1	1	1	0	1	0	1	0	0	0	0	0	0	1	1
38	Sprial suture overlap	1	1	1	1	1	1	1	1	1	1	1	0	0	1	0	1	0	0	0	0	0	0	1	1
39	Downstepping spiral sutures	0	0	0	0	0	0	0	0	0&1	0	0&1	0&1	0	0	2	0&1	0	0&1	0&1	0&2	0&2	0&1	0&1	0&1
40	Umbilical sutures	1	0	0&1	0	0&2	0	5	1	1	1	1	1	1	1	1	1	1	1	1	1	1	1	2	2
41	Umbilical suture overplap	1	1	1	1	1	1	1	2	2	2	2	2	2	2	2	2	2	2	2	2	2	2	4	4
42	Fin (umb) chamb elong	2	2	2	2	2	2	2	4	4	0	0	0	0	2	0	0	2	2	0	0	0	0	1	1
43	Final sprial chamber shape	2	2	2	0	0	0	4	1	1	1	1	0	0	0	0	0	0	1	2	2	1	2	2	2
44	Final umb chamber shape	0	1	0	0	1	1	1	1	2	2	2	2	0	2	2	2	2	1	1	1	1	0	1	1
45	Chamber inflation globose morp	1	2	0	1	2	2	1	1	1	1	1	1	1	1	1	1	1	1	1	1	1	1	1	1
46	Chamber flaring	1	1	1	1	1	1	0	1	1	1	1	1	1	1	1	1	1	1	1	1	1	1	0	0
47	Larger persit than last chamber	1	1	1	1	1	0	1	1	1	1	1	1	1	1	1	1	1	1	1	1	1	2	1	2
48	Edge view final chamber width	1	1	1	1	0	1	1	1	1	1	2	0	1	1	1	1	1	1	2&3&4&5&					
49	Final chamber embracing test	1	2	2	0	1	1	1	1	1	1	1	1	1	1&2&3&4&	1	1	1	1	6&7&8&9	2&3&4&5	5&6	7&8&9	8	7&8
50	Stratigraphy	8&9	8&9	2&3&4&5	6&7	7	7&8&9	8	6&7&8&9	6&7&8&9	8	6&7&8	8&9	5&6	5&6	7	6	7	5&6						

Appendix 6.2

		archeomenardii	*cultrata*	*exilis A*	*exilis sl*	*exilis ss*	*flexuosa*	*limbata*	*menardii A*	*menardii B*	*menardii sl*	*menardii ss*	*miocenica*	*multicamerata*	*pertenuis*	*mero/plesiotumida*	*praemenardii*	*praescitula*	*pseudomiocenica*	*tumida*	*ungulata*
2H-1, 120-122	1195A Pt		0.67									0.67								0.00	
5H-5, 10-12	1195A LP		19.33					100.00		100.00		94.67		98.67					100.00	2.67	94.67
7H-6, 10-12	1195A EP							100.00		100.00		3.33		98.67					99.33	0.00	
9H-1/10H-1, 10-12	1195B LM							6.00	100.00	9.33				17.33		45.33			77.33	10.67	
4H-1, 126-128/4H-2, 59-61	871A MM N12																7.33				
8H2,3,4,5, 59-61	871A MM N8	52.00																50.00			
2H-2, 70-72	926A Pt		0.00				0.00				0.00									0.00	0.00
8H-4, 68-70	926A LP N21					98.00							98.00		100.00						
11H-4, 70-72	926A EP N19					99.33								98.67					99.33		
16H-6, 60-62	926A LM N18			98.00	100.00			96.67	98.67	100.00									99.33		

Coiling ratios of 150 specimens of taxa from the menardine and *Gr. tumida* lineages. Figures represent percentage of specimens that coil dextrally. Figures in grey were calculated from only 50 specimens due to rareity.